JONIX

pure living

DOSSIER SCIENTIFICO

JONIX
pure living

I dispositivi **Jonix** utilizzano generatori **“Non Thermal Plasma”** coperti da brevetto industriale “APPARECCHIO IONIZZATORE PROVVISTO DI UN TUBO IONIZZANTE PER RIMUOVERE PARTICELLE INQUINANTI/CONTAMINANTI PRESENTI IN UN FLUIDO E RELATIVO METODO DI FUNZIONAMENTO” - numero concessione 0001429908 - numero domanda 102015902351864

JONIX
pure living

Applicazione della tecnologia NTP Jonix per la sanificazione indoor e ambientale

1 INDICE

2 I DISPOSITIVI JONIX

Tutti i I dispositivi JONIX utilizzano la tecnologia NTP (Non Thermal Plasma o Plasma Freddo) che produce specie ossidanti, e quindi sanificanti, attraverso i "generatori JONIX" (o "attuatori"), costituiti da tubi cilindrici con lamine in metallo.

3 PRINCIPIO DI FUNZIONAMENTO

Il *plasma non termico (NTP – Non Thermal Plasma)* produce varie specie reattive che prendono nel loro insieme il nome di ROS (*Reactive Oxygen Species*) e che permettono il **potere sanificante** dei sistemi Jonix.

In base a quanto noto sul plasma freddo, è possibile ipotizzare che i processi di sanitizzazione possano avvenire per diretta interazione fra il plasma (superficie dell'attuatore) ed il contaminante e per interazione con le specie prodotte dal passaggio dell'aria nel plasma, che vengono allontanate nella corrente gassosa.

I dispositivi Jonix, se correttamente utilizzati secondo le specifiche tecniche, permettono la **riduzione di batteri, muffe e virus** sia nell'aria ambiente che sulle superfici.

Nei dispositivi della famiglia MATE (MiniMate, Mate, MaxiMate) la presenza di filtri aria aumentano l'efficienza sanificante delle macchine.

4 CERTIFICAZIONI

Tutti i dispositivi a marchio Jonix hanno le seguenti certificazioni e riconoscimenti.

Marcatura CE

Prodotti conformi alle direttive Europee

Direttiva comunitaria, di un prodotto regolamentato nell'Unione europea, il quale dichiara, per mezzo della dichiarazione di conformità o di prestazione per i prodotti da costruzione, che il prodotto è conforme ai requisiti di sicurezza previsti dalle direttive o dai regolamenti comunitari applicabili.

TÜV PROFiCERT

Certificazione della qualità dei dispositivi

TÜV PROFiCERT certifica la qualità dei processi di produzione dei dispositivi Jonix attraverso audit in sede, dove sono esaminate: la gestione dell'azienda, le qualifiche dei dipendenti, la soddisfazione del cliente, l'ispezione interna dei processi aziendali e l'esatta definizione di tutte le procedure.

Prodotti validati e continuamente monitorati. Il logo TÜV, per i dispositivi Jonix, certifica la veridicità dei dati e delle performances dichiarate nei dossier scientifici e nei cataloghi prodotti.

Ongreening e ProductMAP

La piattaforma per il Green Building

Ongreening® è una piattaforma digitale indipendente dedicata alla filiera dell'edilizia green che supporta la diffusione delle migliori pratiche sostenibili rendendo il green building accessibile a tutti. Include il database innovativo, ProductMAP®, che consente la selezione di materiali e prodotti edilizi sulla base di criteri prestazionali e di sostenibilità e fornisce la conformità dei prodotti, materiali e componenti edilizi ai più diffusi sistemi di rating della sostenibilità negli edifici, come il LEED, WELL, BREEAM, BRE Home Quality Mark, Estidama e HK BEAM Plus.

I dispositivi Jonix per la purificazione dell'aria contribuiscono a soddisfare i requisiti di valutazione degli edifici ecologici: Leed®, Breeam®, Estidama®, HK Beam®, Well®.

Bio-Safe

La Certificazione Bio-Safe® è marchio di garanzia per la salute ed il benessere abitativo all'interno dei luoghi confinati.

I dispositivi Jonix sono stati testati, secondo il protocollo brevettato Bio-Safe® che ha verificato e certificato la loro capacità di riduzione dei contaminanti attraverso analisi di laboratorio con camera di prova (UNI EN 16000) capaci di verificare le loro potenzialità emissive e attraverso rilievi ambientali (UNI EN 14412) in grado di restituire il livello di purificazione d'aria raggiunto dagli stessi all'interno dei locali di utilizzo.

Lo specifico percorso d'analisi e controllo intrapreso in ognuno dei seguenti casi ha portato questi prodotti all'ottenimento del Sigillo di Validazione Bio-Safe®: marchio di garanzia per la salute ed il benessere abitativo all'interno dei luoghi confinati.

5 Plasma freddo (NTP – Non Thermal Plasma)

Esistono varie tipologie di plasma; in generale viene definito tale un gas completamente o parzialmente ionizzato, costituito da varie particelle come elettroni, ioni, atomi e molecole, che nell'insieme risulta elettricamente neutro. Fra questi, il plasma non termico (NTP – Non Thermal Plasma) è caratterizzato dal fatto di non trovarsi in equilibrio termodinamico: a causa della loro piccola massa, gli elettroni possono essere facilmente accelerati sotto l'influenza di un campo elettrico e possono quindi raggiungere alte temperature, mentre le altre particelle non accelerate rimangono a temperatura ambiente. Complessivamente la temperatura raggiunta è di poche decine di gradi centigradi, e proprio per questo motivo tale plasma viene detto, appunto, "freddo". Poiché pressoché tutta l'energia impartita viene convertita in elettroni ad alta energia piuttosto che in calore risulta avere una elevata efficienza energetica rispetto al plasma convenzionale, e questo rende la tecnologia interessante per svariate applicazioni ambientali (Hao Zhang, 2017). Gli elettroni accelerati inducono ionizzazione, eccitazione e dissociazione delle molecole del gas, portando alla formazione di molecole eccitate, atomi, ioni e radicaliche che, se in presenza di ossigeno, prendono nel loro insieme il nome di ROS (*Reactive Oxygen Species*) e sono responsabili del potere ossidativo acquisito dal flusso gassoso. Quest'insieme risulta altamente reattivo ed in grado di attaccare una grande varietà di composti inquinanti con meccanismi di vario genere che saranno illustrati più avanti.

La generazione di NTP si basa sull'utilizzo di appositi attuatori, responsabili della ionizzazione del flusso gassoso.

5.1 Produzione plasma tramite DBD (Dielectric Barrier Discharge)

La produzione di plasma freddo avviene attraverso degli attuatori che possono avere una grande varietà di configurazioni geometriche e principi di funzionamento. Essi possono avere svariate tipologie di geometria e alimentazione elettrica, che di solito prevede corrente alternata (con frequenza da 50 fino a vari kHz) ed una differenza di potenziale di alcuni kVolt. In questo modo si creano delle scariche all'interno delle quali avviene il processo di ionizzazione per impatto elettronico (Figura 1) (U. Kogelschatz, 1997). Uno dei più diffusi e consolidati, adottato da Jonix in quanto abbina una discreta efficienza di produzione di plasma ad aspetti costruttivi non eccessivamente complessi, si basa sul principio della scarica a barriera di dielettrico, o DBD (Dielectric Barrier Discharge). Si definisce in tal modo perché è presente, tra gli elettrodi, un materiale dielettrico che impedisce lo sviluppo di correnti elevate.

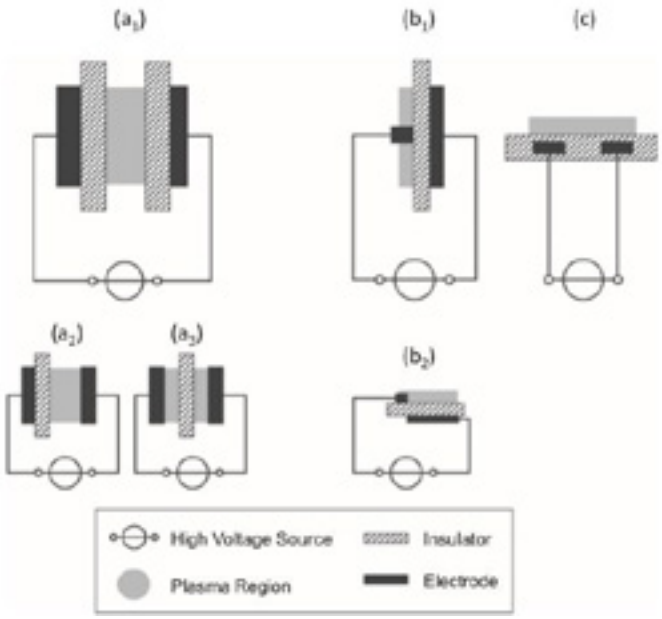

Figura 1 – esempi di configurazioni di reattori DBD: (a) volume DBD (1-symmetric, 2-asymmetric, 3-floated dielectric); (b) surface DBD (1symmetric, 2-asymmetric 'actuator' design); (c) coplanar discharge (Brandenburg R. , 2017)

Nella maggior parte delle applicazioni il dielettrico limita la densità di corrente media nello spazio gassoso, agendo come una resistenza che, in caso ideale, non consuma energia, evitando la transizione della scarica ad arco. Quando uno "streamer", ovvero una scarica elettrica transiente, si propaga fino alla barriera, esso crea una carica di superficie che si contrappone al campo elettrico applicato, schermandolo. Perciò lo streamer si interrompe (se la forza dielettrica della barriera è sufficiente). Per rimuovere la carica superficiale la tensione viene invertita. Questo tipo di scarica opera solo in corrente alternata, in quanto il dielettrico tra gli elettrodi, essendo un isolante, non può essere attraversato da una corrente continua. I materiali preferenziali per la barriera dielettrica sono vetro o vetro di silice, in casi speciali anche materiali ceramici, e sottili vernici e strati polimerici. In alcune applicazioni sono utilizzati rivestimenti protettivi o funzionali aggiuntivi. A frequenze molto alte la limitazione della corrente da parte del dielettrico diventa meno efficace. Per questa ragione normalmente le scariche DBD operano a frequenze comprese tra la frequenza di linea della rete elettrica e circa 1 MHz.

5.2 Jonix e il plasma freddo

Gli attuatori di plasma Jonix (tubi ionizzanti) sono costituiti da un cilindro in quarzo rivestito da una maglia metallica (elettrodo esposto) nella quale sono presenti numerosi fori, in numero che varia da 30 a 45 per centimetro quadrato, ed un elettrodo coassiale posto all'interno (elettrodo incapsulato) (Figura 2).

Figura 2 – attuatore al plasma DBD Jonix

Il sistema è alimentato da una corrente elettrica alternata con frequenza di rete (50Hz) e voltaggio di 2850V (tensione nominale). La scarica si genera grazie alla corrente sinusoidale con tale elevata differenza di potenziale, portando alla generazione di micro-archi sull'elettrodo esposto che hanno luogo grazie all'accumulo di elettroni sullo strato del dielettrico, ovvero sulla maglia metallica (Figura 3), dove si genera il plasma freddo (surface discharge): il flusso gassoso che lambisce tale superficie viene quindi ionizzato (CL Enloe, 2008).

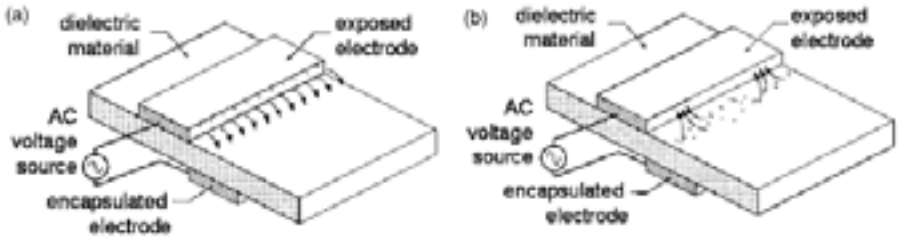

Figura 3 - Funzionamento del DBD: (a) semiciclo negativo e (b) semiciclo positivo.

L'elettrodo interno, essendo posto dentro al tubo in quarzo, risulta quindi incapsulato e pertanto su esso non si ha la formazione di plasma.

5.3 La chimica del plasma non-termico in effluente gassoso

La chimica delle reazioni che avvengono nel plasma non termico è estremamente complessa e varia in funzione del gas che si va ad ionizzare, i tempi di contatto, le caratteristiche di alimentazione elettrica e la geometria del reattore. In linea generale, poiché il principale meccanismo di ionizzazione nelle scariche elettriche è la ionizzazione per impatto elettronico, le reazioni che iniziano i processi possono essere genericamente descritte come segue:

$X + e^- \rightarrow X^{+\bullet} + 2e^-$

$XY + e^- \rightarrow XY^{+\bullet} + 2e^-$

$XY + e^- \rightarrow X^\bullet + Y^\bullet + e^-$

Nel caso in cui il gas ionizzato sia aria le principali reazioni che possono avvenire sono:

$O_2 + e^- \rightarrow O_2^{+\bullet} + 2e^-$ (Ea = 12,5 eV)

$N_2 + e- \rightarrow N_2^{+\bullet} + 2e^-$ (Ea = 15,5 eV)

La ionizzazione in aria è accompagnata da processi di frammentazione con formazione di radicali liberi:

$XY^{+\bullet} \rightarrow X^\bullet + Y^+$

Altri processi che avvengono nel plasma sono l'eccitazione di specie atomiche o molecolari; sempre nel caso dell'aria:

$O_2 + e^- \rightarrow O_2^\bullet + e^-$ (Ea = 1 eV)

$N_2 + e^- \rightarrow N_2^\bullet + e^-$

$N_2 + e^- \rightarrow 2N^\bullet + e^-$ (Ea = 9 eV)

$O_2 + e^- \rightarrow 2O + e^-$

I prodotti di queste reazioni primarie sono specie molto reattive che possono successivamente ricombinarsi per dare ossidi di azoto, NO e NO_2 e ozono. Un'altra specie generata nei plasmi non termici, estremamente importante per il suo grande potere ossidante, è il radicale idrossilico, $^\bullet OH$. Esso si forma solo in presenza di umidità secondo il meccanismo:

$H_2O + e^- \text{ -> } H^\bullet + HO^\bullet + e^-$

In conclusione, quindi, **le principali specie generate nel plasma non-termico in aria** sono:

- ioni $O_2^{+\bullet}$, $N_2^{+\bullet}$, NO^+, $O^{-\bullet}$, $O_2^{-\bullet}$, $O_3^{-\bullet}$;
- la specie atomica O e il radicale $^\bullet OH$;
- specie eccitate dell'ossigeno molecolare e atomico ($O_2^\bullet$) e dell'azoto molecolare ($N_2^\bullet$);
- le specie neutre O_3 e NOx.

Le reazioni che queste specie possono dare sono numerose e ancora oggetto di studio in letteratura a causa della notevole complessità che un insieme così eterogeneo di specie comporta. A reazioni di decomposizione radicaliche si affiancano reazioni di ossidazione, come l'attacco secondo Criegee dell'ozono, il quale reagisce anche con piccole particelle di carbonio (2,5 micron) producendo rimozione del particolato sottile. Le stesse molecole inquinanti, a contatto con l'eccitazione elettronica del plasma, posso a loro volte essere ionizzate e generare quindi iniziatori di reazione. I meccanismi di ossidazione sono generalizzati e possono coinvolgere anche molecole inorganiche trasportate all'interno del plasma.

6 EFFETTI SUGLI INQUINANTI CHIMICI

La trattazione è stata opportunamente suddivisa secondo la tipologia di molecola: inorganiche e organiche (VOCs).

6.1 Azione su molecole inorganiche

Le tecnologie NTP costituiscono uno scenario promettente per il trattamento delle tipiche molecole inorganiche inquinanti dell'aria, come gli ossidi dello zolfo e dell'azoto, ma anche dell'acido solfidrico nel caso di applicazioni su emissioni industriali (Bratislav M. Obradović, 2011), questo perché l'NTP è in grado di agire anche sugli inquinanti inorganici (Zulfam Adnana, 2017): i radicali dell'ossigeno reagiscono con monossido di carbonio (CO) per formare anidride carbonica (CO_2), anidride solforosa (SO_2) per formare triossido di zolfo (SO_3) e ossido di azoto (NOx), che può per formare acido nitrico in presenza di umidità. Gli ossidi di azoto e l'ozono, in quanto persistenti, posso anche essere considerati sottoprodotti indesiderati.

Le nuove applicazioni appaiono interessanti e sono oggetto di studi in quanto un trattamento al plasma permette la rimozione simultanea degli inquinanti e, attraverso una gestione della potenza applicata proporzionata alla necessità, ottenere bassi consumi, come evidenziato da autori in vari studi (Wen-Jun Liang, 2011).

6.2 Meccanismi di reazioni con le VOC's

Esistono varie applicazioni industriali del plasma freddo, ormai consolidate (packaging, funzionalizzazione polimeri etc.). Altre sono ancora oggetto di studio, e fra queste vi è l'abbattimento dei VOC nelle emissioni come alternativa ai sistemi a carboni attivi, scrubber, biofiltri o combustori, in quanto gli inquinati volatili organici possono essere ossidati a CO_2 in questi plasmi già a temperatura ambiente, con un'efficienza che dipende dal tipo di molecola, dai tempi di contatto e altri fattori (Arne M. Vandenbroucke, 2011) (Kim, 2004).

Questo è possibile poiché, nel caso in cui l'aria (formata da azoto e ossigeno quasi esclusivamente) si trovi sottoposta al bombardamento di questi elettroni ad alta energia, le molecole dallo stato stabile (N2, O2)) diventano metastabili, (N2m, O2m) o eccitate (N2*, O2*). Queste forme collidono fra loro o con altre rimaste a livello base, o vengono nuovamente bombardare da elettroni eccitati. Il risultato è una sommatoria di processi di ionizzazione (anche tipo Penning), anche se i percorsi di reazione più accreditati prevedono comunque la formazione di radicali (Seinfeld & Pandis, 1998):

- $R^{\bullet} + O_2 \rightarrow ROO^{\bullet}$
- $ROO^{\bullet} + NO \rightarrow RO^{\bullet} + NO_2$
- $2\ ROO^{\bullet} \rightarrow 2\ RO^{\bullet} + O_2$
- $RO^{\bullet} \rightarrow$ composti carbonilici + radicali ($Cl^{\bullet}$, R'•, etc.)

Il risultato di queste reazioni a step è la formazione di ioni e radicali liberi ad altissimo potere ossidante che, in contatto con i contaminanti, conducono teoricamente a prodotti come anidride carbonica e vapor acqueo, analogamente a quanto possa avvenire nei sistemi a combustione ad alta temperatura. Tuttavia, sperimentalmente occorre ipotizzare una efficienza parziale, che si verifica quando alcuni inquinanti vengono ossidati solo parzialmente (Oda, 2003), nonché la formazione di intermedi di decomposizione come sottoprodotti (K. Urashima, 2000). Tali limitazioni devono essere valutate caso per caso, per stabilire la convenienza del processo e possibili altre interferenze.

In ultima analisi, la tecnologia NTP costituisce una soluzione promettente per il trattamento di qualsiasi VOC, anche in condizioni particolari o per molecole inerti e persistenti, come gli alogeno alcani, sia in condizioni di bassa concentrazione (<100 ppm_v) di inquinanti che alta (>1000 ppm_v) (Penetrante, 2011) (S. Schmid, 2010) e pertanto dimostra una notevole flessibilità di utilizzo. Ad esempiom può essere applicata al caso di composti maleodoranti, che spesso causano disturbi già al livello di ppb. In comparazione con le varie tecnologie ad oggi disponibili per la purificazione dell'aria da VOCs, i sistemi NTP mostrano il loro punto di forza quando si verificano le condizioni di medio- bassa concentrazione(<1000 ppmv) (J. Karuppiaha, 2012), di contaminanti scarsamente solubili in acqua (Schiavon M. T., 2017). Per le applicazioni industriali risultano interessanti le prospettive legate all'aumento della solubilità dei sottoprodotti dei trattamenti, soprattutto sei in abbinamento con catalizzatori, in quanto migliorano il funzionamento di biolfitri e colonne di assorbimento. Per applicazioni legate all'indoor risultano interessanti soprattutto per la bassa concentrazione attesa dei sottoprodotti.

6.3 Focus sulle applicazioni indoor

In questo quadro, i sistemi a plasma non termico (NTP) offrono interessanti opportunità nel campo dei sistemi di depurazione dell'aria indoor poiché, come è stato detto, risultano particolarmente vantaggiosi nelle condizioni di utilizzo tipiche per gli ambienti destinati alla presenza umana, ovvero:

- Basse concentrazioni;
- Numerosità della tipologia di inquinanti
- Temperatura e pressione ambiente

Rispetto alle alternative, l'NTP si dimostra flessibile ed una tecnica più rispettosa dell'ambiente e promettente per rimozione di numerosi inquinanti atmosferici (Stasiulaitiene et al., 2015; Thevenet et al., 2014). Fra le numerose tipologie di plasma, e di modi per generarlo, i più studiati per la pulizia aerea, in relazione agli scopi proposti, sono quelli generati dagli scarichi della corona e da scariche dielettriche di barriera (DBD) (Moscosa-Santillan et al.,2008).

Gli abbattimenti non sono uguali per tutte le tipologie di inquinanti e genericamente, nelle condizioni di bassa concentrazione indicate oscillano tra il 50 e il 90 % [1] (per un NTP generato con DBD) (Osman Karatum, A comparative study of dilute VOCs treatment in a non-thermal, 2016). Le percentuali più elevate si hanno nel caso di strutture molecolari più ricche di idrogeno. In questi casi si registra l'assenza di prodotti di ossidazione parziale e si può ipotizzare che una volta iniziata una catena di reazioni la cui entalpia genera calore che permette di completare l'ossidazione ad anidride carbonica (Carlos M. Nunez, 2012)!!

[1] Es. specific input energy (SIE) of 350 J L: _1,methyl ethyl ketone (50%), benzene (58%), toluene (74%), 3-pentanone (76%), methyl tert-butyl ether (80%), ethylbenzene (81%), and n-hexane (90%)

7 EFFETTI SANITIZZANTI: MECCANISMI DI AZIONE CONTRO VIRUS, MUFFE E BATTERI

In letteratura sono presenti numerosi studi che dimostrano che il plasma non termico è in grado di inattivare molti tipi diversi di microrganismi, come muffe, virus e batteri (Michael J. Gallagher, 2004), sia su superfici che in aria. In quest'ultimo caso esiste un interesse particolare su questa tecnologia in quando i filtri antiparticolato ad alta efficienza (HEPA), comunemente impiegati per rimuovere gran parte dei microrganismi, sono efficaci per particelle di dimensioni fino a 0,5 micron, ma perdono di efficacia nei confronti dei virus presenti nell'aria (tramite droplets), poiché sono tra i microrganismi più piccoli (20-300 nm) (Harstad, 1969).

Per quanto riguarda i trattamenti superficiali, fra le applicazioni più interessanti oggetto di studio si citano le applicazioni biomediche, grazie agli effetti di inattivazione microbica, sterilizzazione e disinfezione verificati dagli autori. In questo caso i vantaggi sono l'ampio spettro di azione, l'uso di gas non tossici e l'assenza di residui tossici (Kong M.G., 2009).

Visti i vantaggi rispetto alle altre tecnologie di sanificazione, molti studi si sono occupati di individuare i meccanismi di azioni nei confronti delle varie tipologie di virus anche in considerazione dell'incrementare della resistenza ai trattamenti. (Chulkyoon, Non-thermal plasmas (NTPs) for inactivation of viruses in abiotic environment, 2016). Diversi ricercatori hanno affermato che le specie neutre chimicamente reattive come O, O2 *, O3, OH •, NO e NO2 possono contribuire in modo significativo al processo di sterilizzazione del plasma, in particolare alle pressioni atmosferiche (Laroussi, 2005) e gli effetti più consistenti dal punto di vista dell'effetto germicida (Herrmann H.W., 1999) si sono visti nei casi di ionizzazione dei gas contenenti ossigeno, nei quali è presente l'ozono (noto battericida) ed i radicali idrossilici (OH) che possono attaccare chimicamente le strutture esterne delle cellule batteriche, il potere ossidante agisce quindi sull'integrità del virus sia a livello strutturale che genomico, influenzando sia le proteine che gli acidi nucleici. Si cita che altri autori attribuiscono alcuni effetti virucida ad altri meccanismi concernenti l'azoto (Wu Y., 2015).Quasi tutti gli autori concordano invece sul ritenere che la componente di radiazione UV, nonché quella termica, seppur presenti nel plasma freddo, siano ininfluenti sugli effetti di sanificazione (Arijana Filipić, 2020) (M. Laroussi, 2004) (Leipold, 2004).

Occorre ricordare che esistono numerose tipologie di NTP che si differenziano per densità di energia, metodo di produzione ed altri parametri. Anche se tutti gli studi concordano chiaramente sugli effetti virucidi, il grado di inattivazione dipende dalla categoria dei virus e dal tipo di plasma, oltre ovviamente a parametri sperimentali come il tempo di esposizione.

8 STUDI DEL CENTRO RICERCA&SVILUPPO JONIX

Nel corso degli anni sono stati condotti, dal Centro Ricerca&Sviluppo di Jonix, numerosi studi su scala di laboratorio al fine di aumentare le conosce sugli effetti prodotti dai sistemi NTP Jonix in varie applicazioni. Vengono qui di seguito riportati i principali risultati e descritte le attività in forma riassuntiva.

8.1 Studio di laboratorio sull'attività biocida delle specie ossidanti formate via NTP

SCOPO: verifica la capacità battericida dell'aria ionizzata su piastre di coltura.

RISULTATO: NTP risulta efficace già a partire dai primissimi minuti di utilizzo. Infatti, dopo appena 5 minuti, tutte le specie testate sono completamente eradicate dalla superficie delle piastre. Un ulteriore elemento che caratterizza positivamente il successo della sperimentazione consiste nel fatto che, contrariamente a quanto previsto da alcune metodiche che prevedono l'esecuzione delle sperimentazioni su superfici di acciaio inox, le prove sopra descritte sono state eseguite in condizioni ottimali per i microrganismi sia dal punto di vista ecologico.

I dettagli della sperimentazione sono riportati in ALLEGATO 1.

8.2 Studio di laboratorio sugli effetti sanificanti prodotti da un MATE - Jonix

SCOPO: verificare la riduzione spontanea di contaminazione microbica in un ambiente di lavoro in presenza e in assenza del trattamento NTP prodotto da un dispositivo MATE.

RISULTATO: dopo circa 30 minuti di trattamento la percentuale di riduzione microbica è molto vicina al 100%. Questo conferma l'efficacia del MATE nella sanitizzazione degli ambienti di vita o lavorativi.

I dettagli della sperimentazione sono riportati in ALLEGATO 2.

8.3 Utilizzo della tecnologia NTP nei confronti delle maleodoranze che si associano all'utilizzo delle calzature

SCOPO: testare la capacità del sistema NTP Jonix di abbattere la concentrazione di molecole chimiche (VOCs) responsabili delle maleodoranze che si associano all'utilizzo delle calzature.

RISULTATO: la sperimentazione condotta ha portato a concludere che trattamenti mediante aria NTP per tempi sufficientemente lunghi (dalle 6 ore in poi) risultano EFFICACI e in grado di abbattere e distruggere completamente le molecole in questione

I dettagli della sperimentazione sono riportati in ALLEGATO 3

8.4 Sanificazione di sonde ecografiche non critiche

SCOPO: confrontare la capacità di sanificazione di sonde ecografiche "non critiche", utilizzando un flusso di aria arricchito via NTP, rispetto alla sanificazione realizzata da device commerciali.

RISULTATO: I test hanno evidenziato una efficacia dell'NTP assolutamente comparabile a quella dei device commercializzati allo scopo.

I dettagli della sperimentazione sono riportati in ALLEGATO 4.

8.5 Studi di laboratorio sull'abbattimento di VOC via NTP: review

SCOPO: sintesi di alcune prove di laboratorio condotte internamente allo scopo di razionalizzare i risultati ottenuti e valutare possibili applicazioni.

RISULTATO: Le percentuali di abbattimento, generalmente superiori al 95%; indicano la capacità del sistema di agire su determinati composti, per lo più odorigeni. Emergono interessanti scenari per le applicazioni di riduzione dell'impatto odorigeno su impianti di depurazione o trattamento rifiuti.

I dettagli della sperimentazione sono riportati in ALLEGATO 5.

8.6 Prova per la valutazione dell'efficacia di riduzione di microrganismi intenzionalmente inoculati in piastre utilizzando il sistema di ionizzazione di aria Mate di Jonix

SCOPO: verificare la riduzione di microrganismi intenzionalmente inoculati in terreni culturali ed esposti per tempi prestabiliti all'effetto di aria ionizzata. Per ogni prova è stato effettuato un test di controllo utilizzando gli stessi terreni inoculati non soggetti a trattamento.

RISULTATO: l'abbattimento microbico che si ottiene in presenza del sistema di ionizzazione dell'aria Jonix Mate su superfici di simulanti materiale organico inoculato con diverse specie microbiche è elevato e permette di inibire completamente entro le 12 24 ore gran parte delle specie inoculate. In molti casi l'abbattimento ottenuto è superiore al 95%. L'effetto di riduzione microbica dell'aria ionizzata è analogo sia

su Gram positivi, su Gram negativi e che lieviti e muffe, anche se l'efficacia risulta spesso dipendente dalla specie considerata.

I dettagli della sperimentazione sono riportati in ALLEGATO 6.

8.7 Studio del potere sanificante di un dispositivo Jonix applicato ad un fan coil commerciale

SCOPO: verificare l'efficacia sanificante a livello biologico di un dispositivo NTP Jonix installato all'interno di un ventilatore convettore per installazione a parete. Lo scopo della prova è testare se la produzione di specie ossidanti sia o meno in grado di risolvere il problema dell'inquinamento di alcune parti delle apparecchiature da parte di muffe, nonché di sanificare l'aria del locale nel quale viene installato.

RISULTATO: risultati ottenuti mostrano come l'adozione di un dispositivo di sanificazione Jonix consenta di ottenere nel tempo una marcata riduzione della contaminazione microbica ambientale sia in termini di batteri che di muffe e lieviti.

I dettagli della sperimentazione sono riportati in ALLEGATO 7.

8.8 Sperimentazione per la verifica della capacità sanitizzante di dispositivi Fotocatalitici in confronti a sistemi Jonix NTP

SCOPO: l'obiettivo è stato quantificare e quindi confrontare l'eventuale effetto sanitizzante svolto da due tipologie di dispositivi commerciali (NTP-Jonix ed un dispositivo Fotocatalitico SHU900X) , all'interno di una condotta in acciaio da 30 cm di diametro e lungo 12 m, dove viene fatta passare aria (attraverso un ventilatore) a differenti velocità/portate, simulando cosa accade all'interno di una condotta di areazione in caso di contaminazione microbiologica e nel caso fossero o meno presenti dei dispositivi "sanitizzanti" tipo quelli testati. A tale scopo, ARCHA ha progettato e condotto una serie di esperimenti nei quali, in modo controllato, differenti tipologie e quantità di microrganismi sono stati esposti all'interno del tubo, a flussi di aria con differenti tipologie di dispositivi sanitizzanti attivati.

RISULTATO: Sia il sistema Jonix NTP che quello Fotocatalitico si dimostrano efficaci nell'abbattimento totale dei lieviti. Il sistema Fotocatalitico risulta più efficiente del sistema Jonix nell'effetto di sanitizzazione sulle muffe su piastra ma è inefficiente su bioaereosol al contrario di Jonix. In conclusione i sistemi Jonix hanno una azione ad ampio spettro che permette di sanificare sia le superfici che l'aria.

I dettagli della sperimentazione sono riportati in ALLEGATO 8.

8.9 Studio sugli effetti antimicrobici della Jonix NTP technology

JONIX
pure living

JONIX S.p.A.
Società Benefit

Sede Legale
viale Spagna 31-33.
35020 Tribano (PD) - Italy

Sede Centrale
via dell'Artigianato 1.
35020 San Pietro
Viminario (PD) - Italy

STUDIO SUGLI EFFETTI ANTIMICROBICI DELLA JONIX NTP TECHNOLOGY

maggio-giugno 2021

Laboratori ARCHA S.r.l. unipersonale
Via di Tegulaia 10/a - 56121 - PISA - ph. +39 050 985165 - fax +39 050 985233 - www.archa.it - archainf@archa.it
C.F., P.IVA, Iscr. Reg. Impr. di Pisa n. 01115340505 - Rep. Econ. Amm. di Pisa n°101169 - Capitale Sociale 101.400,00 i.v.

1 SOMMARIO

Laboratori ARCHA S.r.l. unipersonale
Via di Tegulaia 10/a - 56121 - PISA - ph. +39 050 985165 - fax +39 050 985233 - www.archa.it - archainf@archa.it
C.F., P.IVA, Iscr. Reg. Impr. di Pisa n. 01115340505 - Rep. Econ. Amm. di Pisa n°101169 - Capitale Sociale 101.400,00 i.v.

Laboratori ARCHA S.r.l. unipersonale
Via di Tegulaia 10/a - 56121 - PISA - ph. +39 050 985165 - fax +39 050 985233 - www.archa.it - archainf@archa.it
C.F., P.IVA, Iscr. Reg. Impr. di Pisa n. 01115340505 - Rep. Econ. Amm. di Pisa n°101169 - Capitale Sociale 101.400,00 i.v.

2 PREMESSA e GLOSSARIO

Il seguente report descrive i risultati dei principali esperimenti condotti su incarico di JONIX S.p.A. al fine di valutare l'effetto antimicrobico (batteriostatico o battericida) dei dispositivi, anche in relazione a effetti simili che si hanno in natura.

Per questo sono state condotte prove sperimentali esponendo colonie batteriche sia all'aria emessa da dispositivi Jonix che all'aria naturale in una giornata di bel tempo.

Di seguito la definizione dei termini utilizzati nel report:

Antimicrobico	Sostanza o prodotto in grado di uccidere i microrganismi (biocida) oppure di rallentarne la crescita (biostatico)
Battericida	Sostanza o prodotto in grado di uccidere i batteri (biocida)
Batteriostatico	Sostanza o prodotto in grado di inibire o rallentare la replicazione batterica senza uccidere il microorganismo (biostatico)
Enterococco	Batteri gram positivi, catalasi negativi, dalla forma rotondeggiante od ovaliforme, spesso disposti in catenelle
Escherichia Coli	Batteri Gram-negativi che risiedono normalmente nell'intestino delle persone sane; tuttavia, alcuni ceppi possono causare infezioni a carico del tratto digerente, delle vie urinarie o di molte altre parti del corpo.
Gram Negativi	Batteri che rimangono colorati di rosa dopo aver subito la colorazione di Gram. I gram negativi hanno una parete costituita da una struttura più semplice, sempre a base di peptidoglicano e presentano inoltre una membrana lipidica esterna.
Gram Positivi	Batteri che rimangono colorati di blu o viola dopo aver subito la colorazione di Gram. I batteri gram positivi presentano una parete con una struttura complessa, rigida e spessa a base di peptidoglicano.
Ozono	Forma allotropica dell'ossigeno con formula O_3, dal caratteristico odore agliaceo. Presente in natura per effetto della radiazione solare. Forte ossidante utilizzato per operazioni di disinfezione.
Pseudomonas	Batteri Gram-negativi, aerobi obbligati, ossidasi positivi, catalasi positivi ed hanno flagelli polari che permettono loro di muoversi. Si trovano nel terreno e nelle acque ma anche sulle piante.
ROS	Le specie reattive dell'ossigeno, i ROS, sono i radicali liberi a maggior diffusione. I più importanti ROS sono l'anione superossido O2-, il perossido d'idrogeno H2O2 e il radicale ossidrilico •OH.
Stafilococco	Batteri Gram-positivi di forma sferica aerobi (cioè in grado di vivere solo in presenza di ossigeno) o anaerobi facoltativi (cioè che richiedono normalmente ossigeno, ma che in caso di necessità possono sopravvivere anche in sua assenza). Questi microbi

sono normalmente presenti sulla pelle e nel naso di individui sani, dove nella maggior parte dei casi non causano alcun problema o danno luogo a infezioni della pelle non gravi. In alcune circostanze possono scatenare infezioni anche molto pericolose.

3 TECNICI INCARICATI DELLA SPERIMENTAZIONE

Le sperimentazioni sono state condotte dai seguenti tecnici qualificati:

Dott.ssa Francesca Gambineri	Laureata in Chimica Industriale, 20 anni di esperienza nel settore della ricerca chimica, in scienze dei materiali e tecnologie innovative 10 anni di esperienza nello studio dell'NTP e dei suoi effetti su sostanze chimiche e materiali Co-inventore di 3 brevetti Co-autore in numerose pubblicazioni scientifiche di cui 6 riguardanti le potenziali applicazioni dell'NTP Coordinatrice degli esperimenti
Dott. Fabrizio Cervelli	Laureato in Biologa, Dottore di Ricerca in Patologia Cellulare e Molecolare Esperto in Igiene degli ambienti di vita e di lavoro e delle risorse idriche 10 di esperienza in Ricerca biologica di base 20 anni di esperienza in microbiologia e ricerca applicata Coordinatore e esecutore delle sperimentazioni microbiologiche nello studio dell'NTP e dei suoi effetti sui microrganismi Coautore di numerose pubblicazioni in riviste scientifiche nazionali e internazionali
Dott. Lamberto Cursi	Laureato in Chimica 20 anni di esperienza in conduzione di progetti di ricerca Coordinatore e esecutore delle misure chimico-fisiche

4 STRUMENTAZIONE E DISPOSITIVI JONIX

4.1 Strumentazione di misura

La tecnologia NTP di JONIX si basa sul Non Thermal Plasma e produce specie ossidanti all'intorno dei generatori che vengono anche veicolati nell'ambiente attraverso la ventilazione dei dispositivi stessi e l'ausilio della umidità dell'aria.

Tra le specie ossidanti che vengono generate c'è anche l'ozono che risulta essere l'unica specie misurabile. La concentrazione di ozono ambientale è quindi non solo un riferimento importante e necessario da misurare per garantire il rispetto di tutte le normative che prevedono limiti di esposizione in ambienti di vita, ma anche un riferimento sulla "potenzialità" dei dispositivi nel generare specie ossidanti.

Per la misura delle concentrazioni ambientali di ozono è stato utilizzato un analizzatore Horiba.

HORIBA è leader nel settore della strumentazione per analisi ambientali, e lo strumento utilizzato è il modello APOA 370.

Si basa sul metodo NDUV (Principle Non dispersive ultra-violet-absorption) e permette di rilevare concentrazioni tra 0 e 100 ppb utilizzando il range basso e fino a 1.000 ppb utilizzando il range più alto, con una rilevabilità di 0,1 ppb.

Ha una ripetibilità di ±1.0% del fondo scala ed una linearità del ±1.0% del fondo scala.

Lo strumento viene periodicamente sottoposto a taratura e a fianco si riporta l'ultimo rapporto:

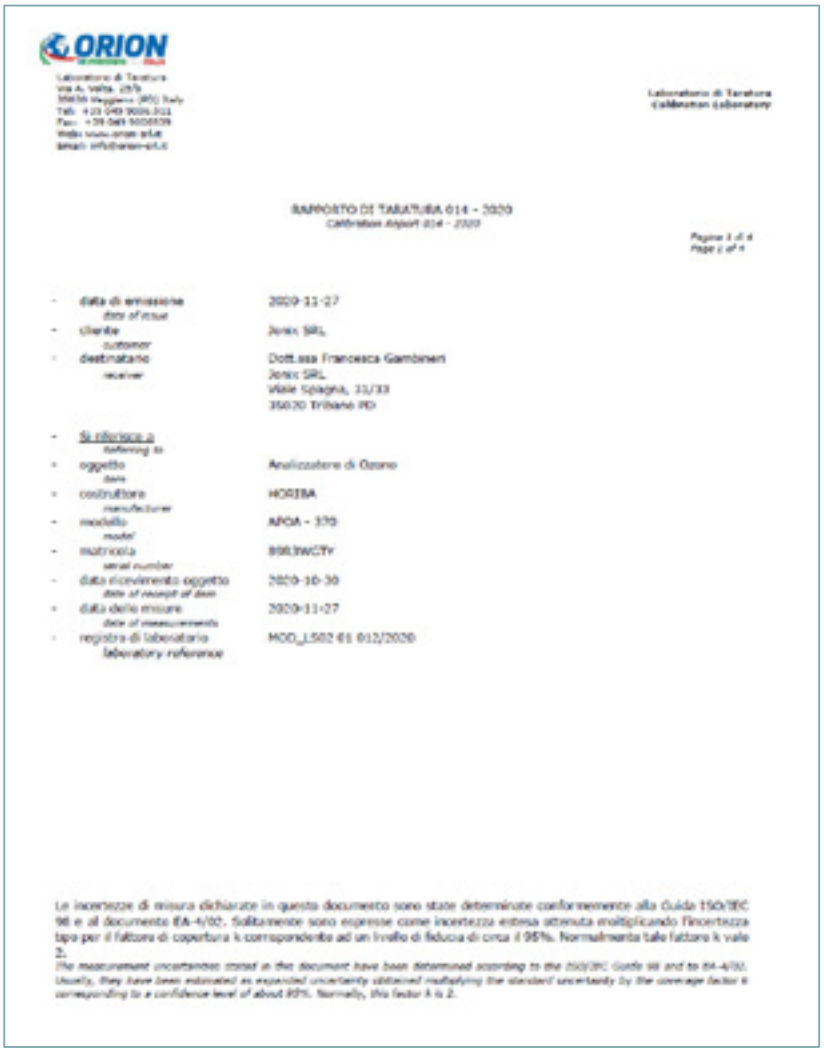

ORION

RAPPORTO DI TARATURA 014 - 2020

- data di emissione / date of issue: 2020-11-27
- cliente / customer: Jonix SRL
- destinatario / receiver: Dott.ssa Francesca Gambinieri, Jonix SRL, Viale Spagna, 31/33, 35020 Tribano PD
- Si riferisce a / referring to
- oggetto / item: Analizzatore di Ozono
- costruttore / manufacturer: HORIBA
- modello / model: APOA - 370
- matricola / serial number: 898JNWCTV
- data ricevimento oggetto / date of receipt of item: 2020-10-30
- data delle misure / date of measurements: 2020-11-27
- registro di laboratorio / laboratory reference: MOD_LS02 01 012/2020

Le incertezze di misura dichiarate in questo documento sono state determinate conformemente alla Guida ISO/IEC 98 e al documento EA-4/02. Solitamente sono espresse come incertezza estesa ottenuta moltiplicando l'incertezza tipo per il fattore di copertura k corrispondente ad un livello di fiducia di circa il 95%. Normalmente tale fattore k vale 2.

The measurement uncertainties stated in this document have been determined according to the ISO/IEC Guide 98 and to EA-4/02. Usually, they have been estimated as expanded uncertainty obtained multiplying the standard uncertainty by the coverage factor k corresponding to a confidence level of about 95%. Normally, this factor k is 2.

4.2 Dispositivi Jonix utilizzati per i test

Per i test di seguito descritti sono stati utilizzati dispositivi commerciali Jonix MiniMate e Jonix Cube, in alcuni casi modificati elettricamente per simulare il dimensionamento corretto all'interno dei locali di sperimentazione.

L'uso, il dimensionamento e la gestione dei dispositivi sono stati quindi tale da mantenere i livelli di ozono ambientali al di sotto di 50 ppb che risulta essere il target per il corretto dimensionamento dei dispositivi nei locali.

Laboratori ARCHA S.r.l. unipersonale
Via di Tegulaia 10/a - 56121 - PISA - ph. +39 050 985165 - fax +39 050 985233 - www.archa.it - archainf@archa.it
C.F., P.IVA, Iscr. Reg. Impr. di Pisa n. 01115340505 - Rep. Econ. Amm. di Pisa n°101169 - Capitale Sociale 101.400,00 i.v.

5 PROVE EFFETTUATE

Sono state condotte le seguenti prove sperimentali, oltre ad altre non documentate che sono state propedeutiche per la messa a punto dei metodi:

PROVA	CODICE	DESCRIZIONE	OBIETTIVO
A	S20/005800001	Esposizione di piastre con microorganismi Escherichia coli e Stafilococco aureo, a diverse distanze dal dispositivo JONIX	Valutare l'effetto antimicrobico dell'NTP a diverse distanze dal dispositivo
B	S20/005800003	Esposizione di piastre con microorganismi Enterococco fecale e Pseudomonas aeruginosa, a diverse distanze dal dispositivo JONIX	Valutare l'effetto antimicrobico dell'NTP a diverse distanze dal dispositivo
C	S20/005800004	Esposizione di piastre con microorganismi Stafilococco aureo, Enterococco fecale, Escherichia coli e Pseudomonas aeruginosa in box di piccole dimensioni (teca), mantenendo l'umidità interna a circa il 50%	Valutare l'effetto antimicrobico dell'NTP a condizioni di umidità controllate
D	S20/005800009	Esposizione di piastre con microorganismi Stafilococco aureo, Enterococco fecale, Escherichia coli e Pseudomonas aeruginosa in box di piccole dimensioni (teca), mantenendo l'umidità interna a circa il 80%	Valutare l'effetto antimicrobico dell'NTP a condizioni di elevata umidità
E	S20/005800008	Esposizione di piastre con microorganismi Stafilococco aureo, Enterococco fecale, Escherichia coli e Pseudomonas aeruginosa in ambiente naturale	Valutare l'effetto dell'aria esterna, contenente specie ossidanti di formazione naturale

5.1 PROVA A

5.1.1 Sintesi della prova

Codice prova	S20/005800001
Data	21 aprile 2021
Descrizione della prova	Esposizione di piastre con microorganismi Escherichia coli e Stafilococco aureo, a diverse distanze dal dispositivo JONIX
Obiettivo della prova	Valutare l'effetto antimicrobico dell'NTP a diverse distanze dal dispositivo
Dispositivo Jonix utilizzato	JONIX MiniMate
Ambiente di prova	Locale di dimensioni in pianta pari a 9,2 m x 6,8 m x 2,8 m (h) per una superficie in pianta di 62,6 mq e un volume di 175 m^3
Sintesi dei risultati	Abbattimento della carica microbica fino al 100% per lo Stafilococco aureo e fino al 9 % sull'Escherichia coli

5.1.2 Descrizione della prova

Per questa prova sono state utilizzate colture di microrganismi rappresentativi dei batteri gram negativi (Escherichia coli) e gram positivi (Stafilococco aureo), poiché è nota una sensibilità agli agenti biocidi differente tra le due tipologie di batteri.

I microrganismi sono stati seminati, in doppio, su piastre petri a doppio settore riempite con agar PCA (terreno non selettivo) ad una densità di circa 200 UFC/settore. Successivamente le piastre sono state esposte, scoperte, all'NTP mantenendole ad una distanza di 1, 2 e 4 metri dal dispositivo generatore per un tempo complessivo di 24 ore. Le piastre di controllo sono state mantenute all'interno del laboratorio, chiuse con il proprio coperchio, evitando così ogni possibile esposizione all'NTP.

Dopo l'esposizione le piastre sono state fotografate e quindi mantenute in incubatore a 37°C per 24+24 ore.

5.1.3 Concentrazioni di ozono nell'ambiente

Le misurazioni dell'ozono a cui sono state esposte le piastre durante le 24 ore di trattamento hanno rilevato un valore medio di 45 ppb durante il periodo di prova come raffigurato nel seguente grafico:

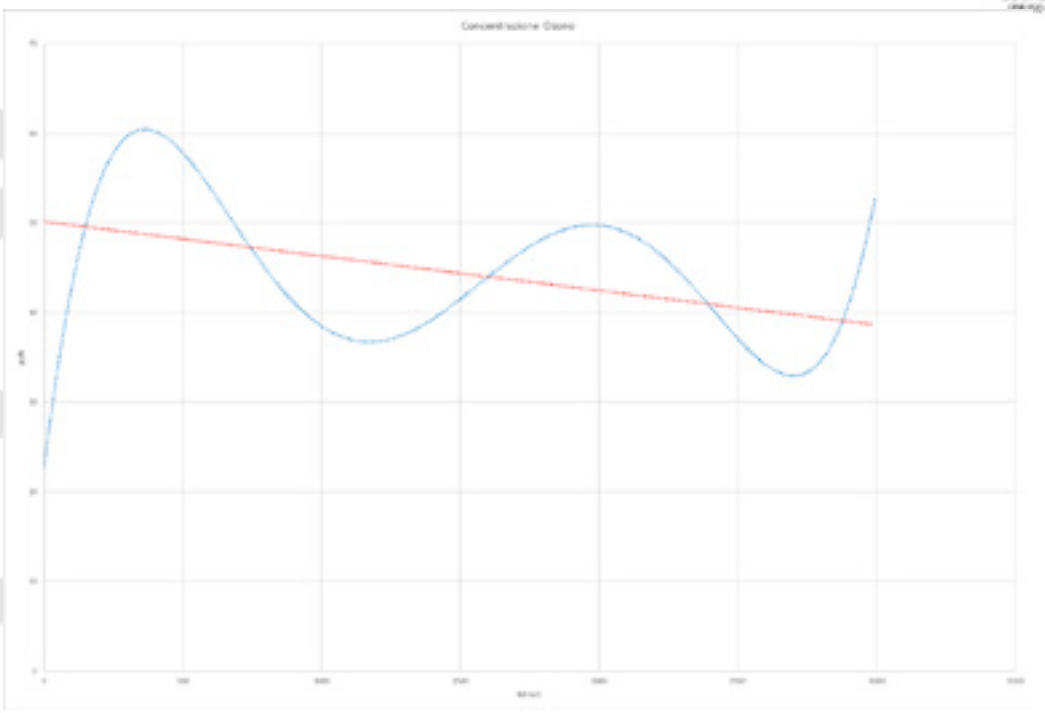

Concentrazione di Ozono nell'ambiente di prova durante la Prova A (linea rossa = media)

5.1.4 Evidenze fotografiche

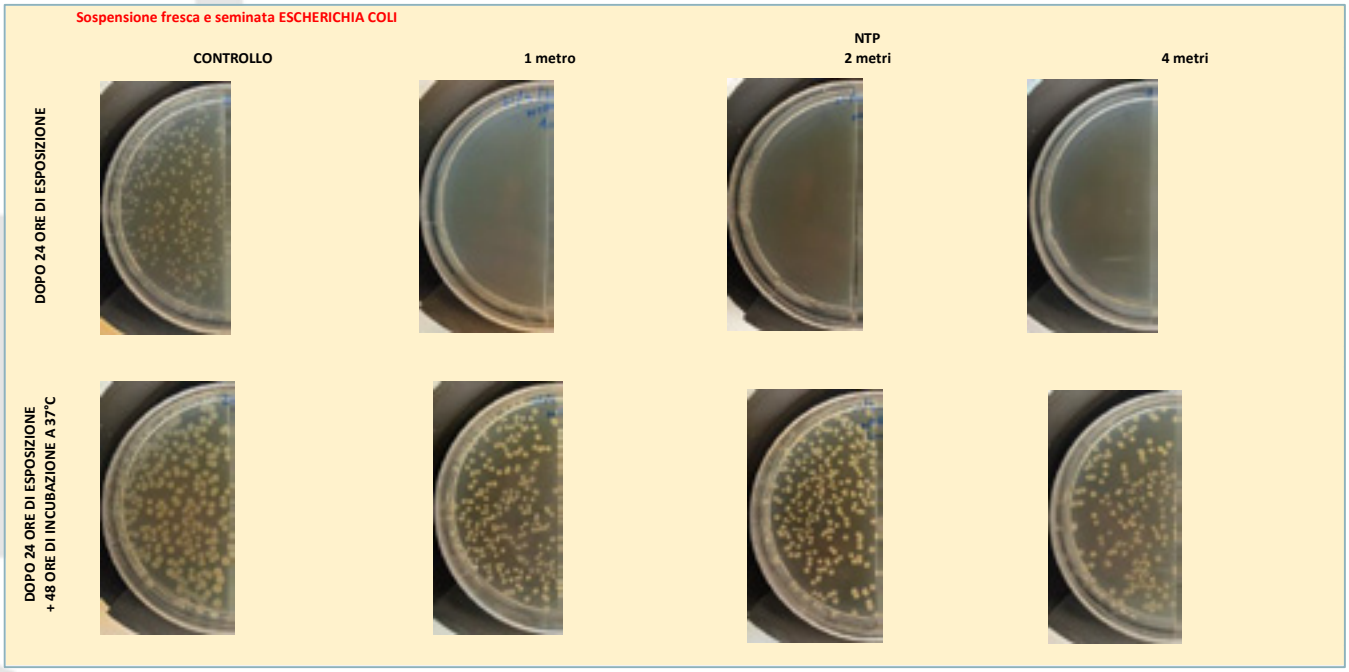

Effetti antimicrobici: particolare dei settori contenenti Escherichia coli
Riga superiore: aspetto delle piastre di coltura dopo l'esposizione di 24 ore all'NTP (confronto con il controllo non esposto) al variare della distanza dal generatore
Riga inferiore: stesse piastre ma dopo 48 ore di incubazione a 37°C

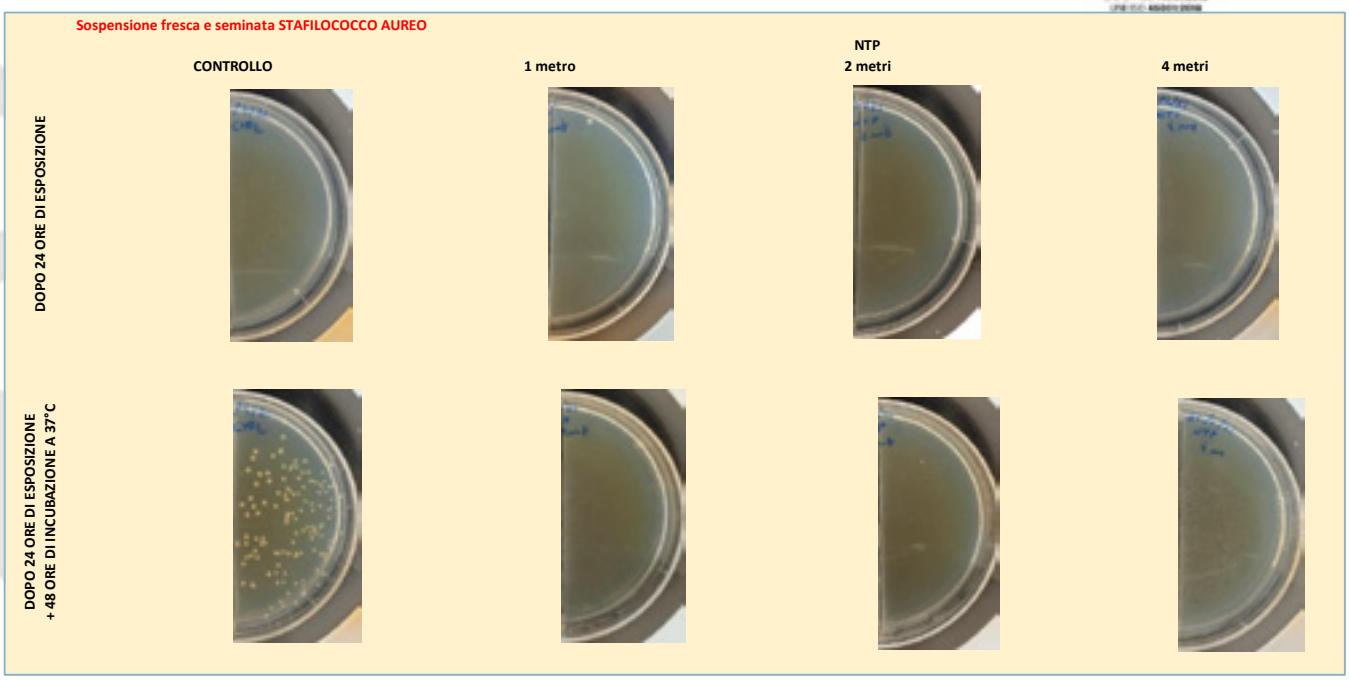

Effetti antimicrobici: particolare dei settori contenenti Stafilococco aureo
Riga superiore: aspetto delle piastre di coltura dopo l'esposizione di 24 ore all'NTP (confronto con il controllo non esposto) al variare della distanza dal generatore
Riga inferiore: stesse piastre ma dopo 48 ore di incubazione a 37°C

5.1.5 Risultati

Dall'immagine precedente è facile osservare come esista una differenza sostanziale degli effetti esercitati dall'NTP sui due diversi tipi di batteri. In particolare si osserva, per tutte e tre le distanze di esposizione, un effetto di pressoché totale inibizione della crescita nei confronti di Stafilococco aureo (settori di destra) ed una limitata azione verso Escherichia coli.

Interessante inoltre osservare come al termine delle 24 ore di esposizione all'NTP, non fosse possibile apprezzare alcuna crescita microbica in tutti i settori, compresi quelli contenenti Escherichia coli, cosa che invece non si verifica dopo la successiva incubazione, in cui colonie di Escherichia coli compaiono anche nelle piastre esposte all'NTP. Questo dato, unitamente alle minori dimensioni delle colonie batteriche sono a dimostrazione dell'effetto batteriostatico prodotto dall'NTP.

Diverso è invece il discorso relativo allo Stafilococco aureo che invece ha evidenziato un effetto quasi assoluto di abbattimento microbico dopo l'esposizione all'NTP.

La conta microbica delle colonie cresciute in piastra ha riportato i seguenti valori:

Concentrazione microbica in ciascun settore delle piastre utilizzate.

			piastra 1	piastra 2	media	Dev St
Ecoli	**UFC/settore**	**Ctrl**	291	272	**281,5**	13
		NTP 1 mt	263	260	**262**	2
		NTP 2 mt	259	257	**258**	1
		NTP 4 mt	178	170	**174**	6
	Log UFC/settore	**Ctrl**	2,45	2,43	**2,45**	0,02
		NTP 1 mt	2,42	2,41	**2,42**	0,00
		NTP 2 mt	2,41	2,41	**2,41**	0,00
		NTP 4 mt	2,25	2,23	**2,24**	0,01

			piastra 1	piastra 2	media	Dev St
Saureo	**UFC/settore**	**Ctrl**	108	134	**121**	18
		NTP 1 mt	0	0	**0**	0
		NTP 2 mt	0	2	**1**	1
		NTP 4 mt	0	0	**0**	0
	Log UFC/settore	**Ctrl**	2,03	2,13	**2,08**	0,07
		NTP 1 mt	0,00	0,00	**0,00**	0,00
		NTP 2 mt	0,00	0,30	**0,15**	0,21
		NTP 4 mt	0,00	0,00	**0,00**	0,00

5.1.6 Conclusioni sintetiche dei risultati della prova

La trasposizione grafica dei dati permette di meglio mettere in evidenza i risultati ottenuti:

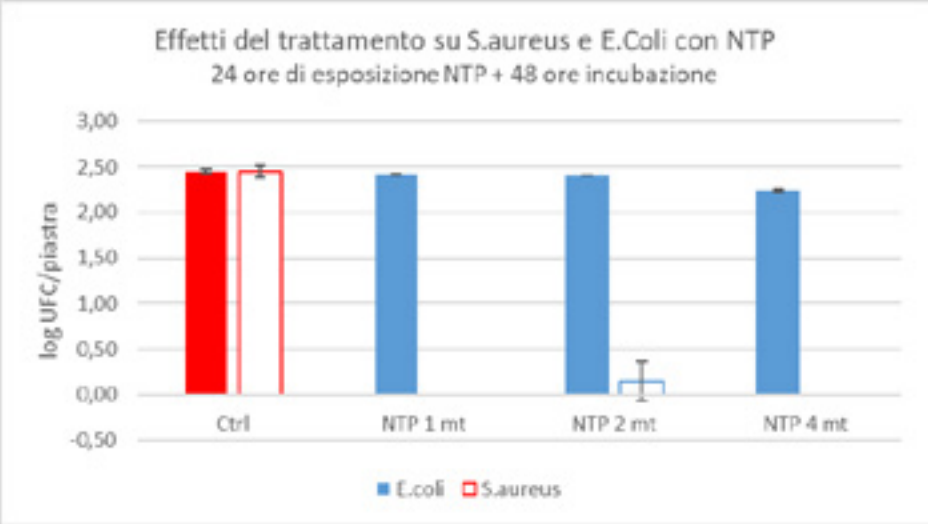

Confronto degli effetti del trattamento con NTP, valori espressi come media di due piastre

Esprimendo invece i dati ottenuti in termini di riduzione percentuale di crescita rispetto ai controlli, si può bene evidenziare come questa sia stata altissima esclusivamente per lo Stafilococco aureo e presente solamente alla distanza di 4 metri dal generatore per quanto riguarda Escherichia coli.

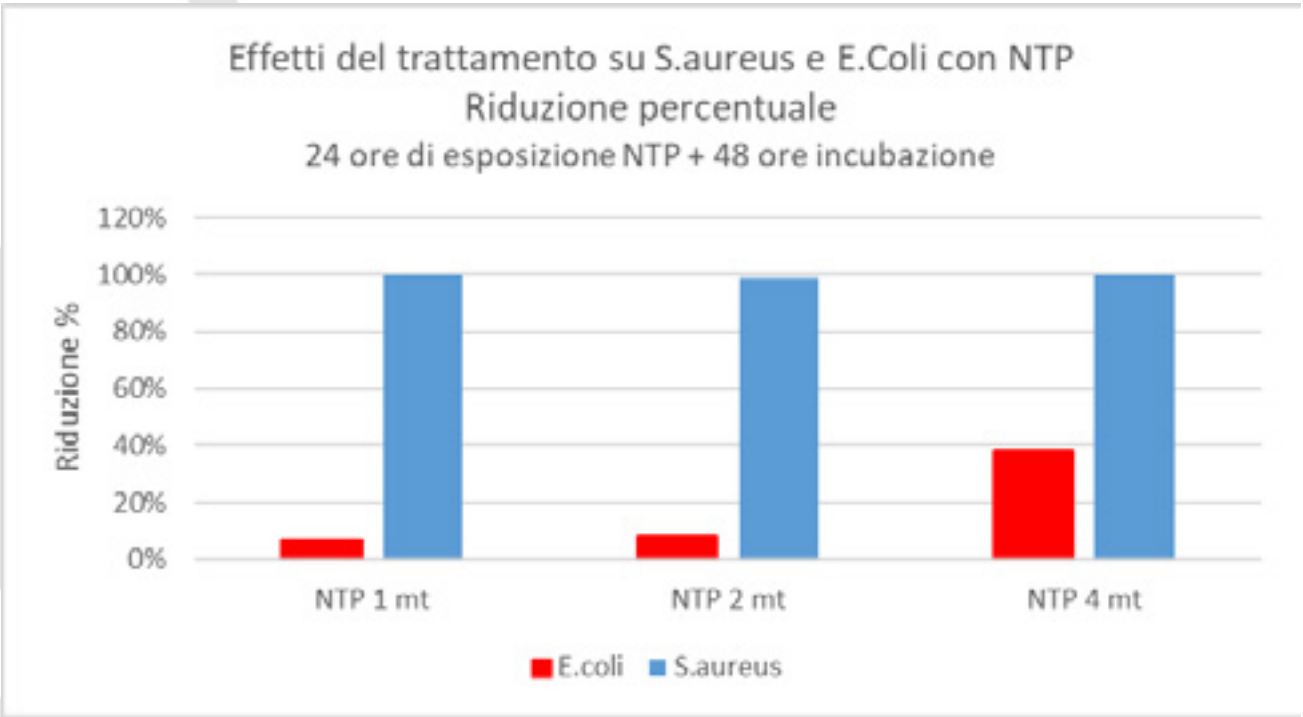

Confronto tra le riduzioni percentuali della crescita microbica tra i due microrganismi testati

La distanza dal generatore NTP non ha evidenziato delle differenze significative.

5.2 PROVA B

5.2.1 Sintesi della prova

Codice prova	S20/005800003
Data	29/04/2021
Descrizione della prova	Esposizione di piastre con microorganismi Enterococco fecale e Pseudomonas aeruginosa, a diverse distanze dal dispositivo JONIX
Obiettivo della prova	Valutare l'effetto antimicrobico dell'NTP a diverse distanze dal dispositivo
Dispositivo Jonix utilizzato	JONIX MiniMate
Ambiente di prova	Locale di dimensioni in pianta pari a 9,2 m x 6,8 m x 2,8 m (h) per una superficie in pianta di 62,6 mq e un volume di 175 m^3
Sintesi dei risultati	Abbattimento della carica microbica fino al 56% per Enterococco, 7% Pseudomonas

5.2.2 Descrizione della prova

Appurato il differente effetto sui due microrganismi Escherichia coli e Stafilococco aureo (Prova A), si è voluto verificare se questo fosse un tratto distintivo dei gruppi microbici di appartenenza.

Si sono così esposti all'NTP altri due microrganismi appartenenti ai Gram positivi (Enterococco fecale) e ai Gram negativi (Pseudomonas aeruginosa).

Come per la prova precedente i batteri sono stati seminati, in doppio, su piastre petri a doppio settore riempite con agar PCA (terreno non selettivo) ad una densità di circa 200 UFC/settore. Successivamente le piastre sono state esposte, scoperte, all'NTP mantenendole ad una distanza di 1, 2 e 4 metri dal dispositivo generatore per un tempo complessivo di 24 ore. Le piastre di controllo sono state mantenute all'interno del laboratorio, chiuse con il proprio coperchio, evitando così ogni possibile esposizione all'NTP.

Dopo l'esposizione le piastre sono state fotografate e quindi mantenute in incubatore a 37°C per 24+24 ore.

5.2.3 Concentrazioni di ozono nell'ambiente

Le misurazioni dell'ozono a cui sono state esposte le piastre durante le 24 ore di trattamento hanno rilevato un valore medio di 24 ppb durante il periodo di prova come raffigurato nel seguente grafico:

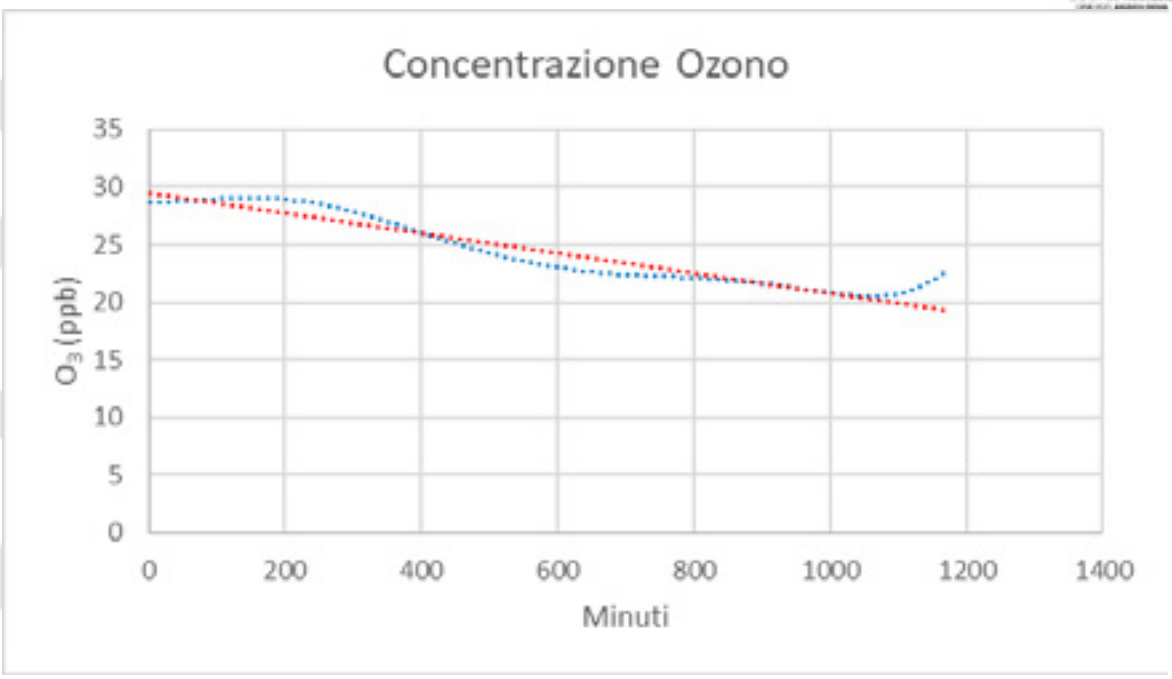

Concentrazione di Ozono nell'ambiente di prova durante la Prova B. (Linea rossa = media)

5.2.4 Evidenze fotografiche

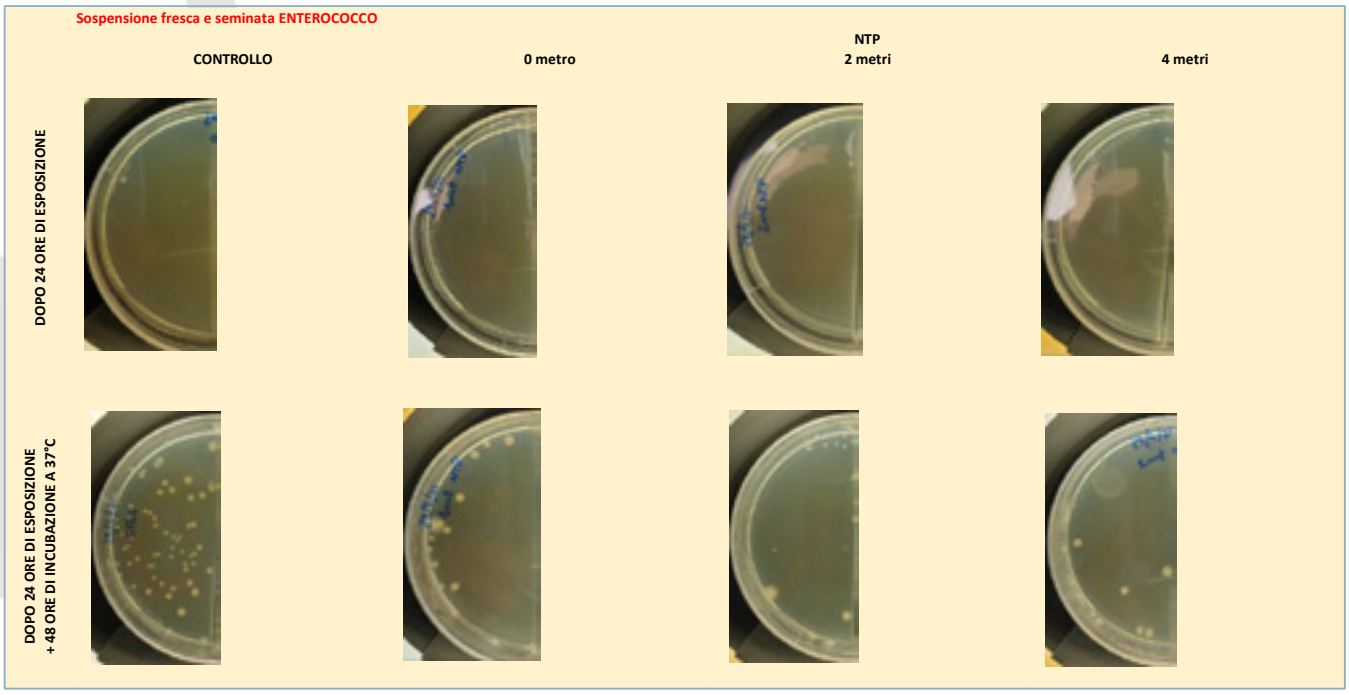

Effetti antimicrobici: particolare dei settori contenenti Enterococco fecale
Prima riga: aspetto delle piastre di coltura dopo l'esposizione di 24 ore all'NTP (confronto con il controllo non esposto) al variare della distanza dal generatore
Seconda riga: stesse piastre ma dopo 48 ore di incubazione a 37°C

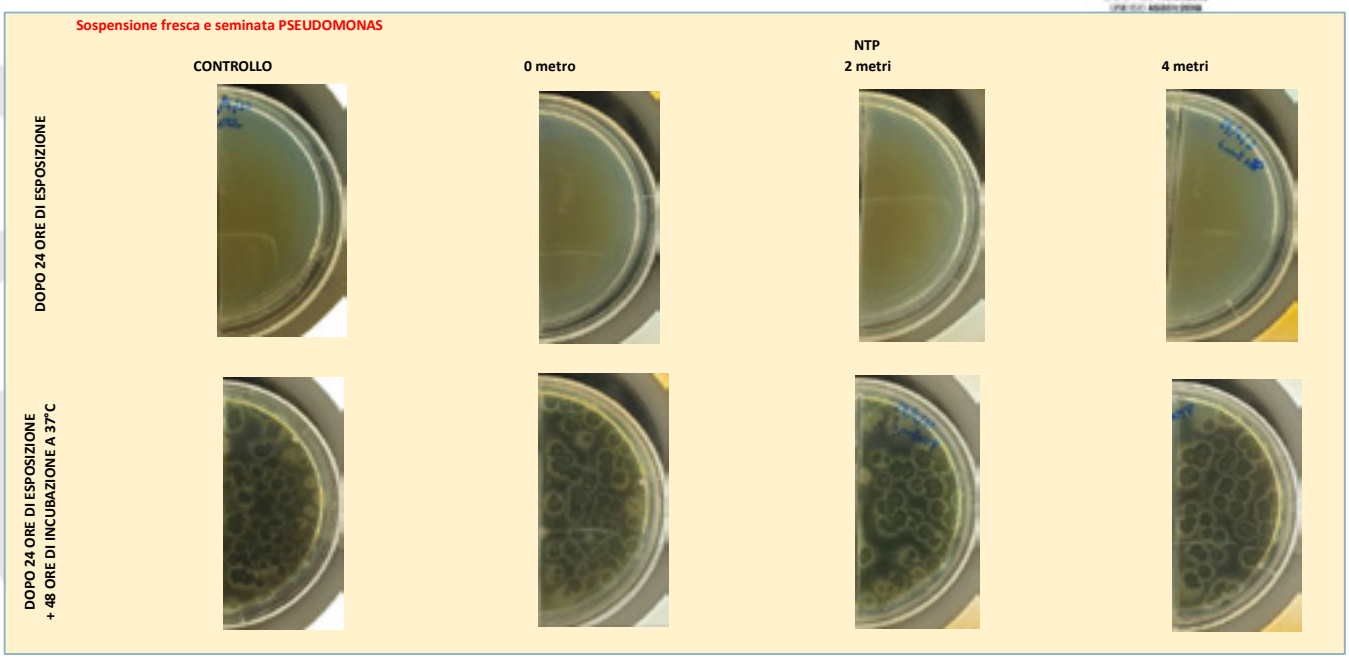

Effetti antimicrobici: particolare dei settori contenenti Pseudomonas aeruginosa
Prima riga: aspetto delle piastre di coltura dopo l'esposizione di 24 ore all'NTP (confronto con il controllo non esposto) al variare della distanza dal generatore
Seconda riga: stesse piastre ma dopo 48 ore di incubazione a 37°C

5.2.5 Risultati

Anche in questo caso è possibile osservare un importante effetto inibitorio nei confronti dei gram positivi (Enterococco f.) a differenza di quanto accade per i gram negativi (Pseudomonas a.).

Di nuovo si apprezza inoltre una totale assenza di crescita nelle piastre dopo 24 ore di esposizione, sia nei settori dei gram positivi che in quelli dei gram negativi, cosa che invece viene meno dopo l'incubazione a 37°C, confermando l'effetto batteriostatico dell'NTP.

La conta microbica delle colonie cresciute in piastra ha riportato i seguenti valori:

Concentrazione microbica in ciascun settore delle piastre utilizzate.

			piastra 1	piastra 2	media	Dev.St.
Enterococco fecale	**UFC/settore**	**Ctrl**	66	61	**63,5**	4
		NTP 1 mt	11	14	**13**	2
		NTP 2 mt	5	8	**7**	2
		NTP 4 mt	4	10	**7**	4
	Log UFC/settore	**Ctrl**	1,82	1,79	**1,80**	0,02
		NTP 1 mt	1,04	1,15	**1,09**	0,07
		NTP 2 mt	0,70	0,90	**0,80**	0,14
		NTP 4 mt	0,60	1,00	**0,80**	0,28

			piastra 1	piastra 2	media	Dev.St.
Pseudomonas aureog.	**UFC/settore**	**Ctrl**	65	54	**59,5**	8
		NTP 1 mt	56	44	**50**	8
		NTP 2 mt	38	53	**46**	11
		NTP 4 mt	45	43	**44**	1
	Log UFC/settore	**Ctrl**	1,81	1,73	**1,77**	0,06
		NTP 1 mt	1,75	1,64	**1,70**	0,07
		NTP 2 mt	1,58	1,72	**1,65**	0,10
		NTP 4 mt	1,65	1,63	**1,64**	0,01

5.2.6 Conclusioni sintetiche dei risultati della prova

La trasposizione grafica dei dati permette di meglio mettere in evidenza i risultati ottenuti:

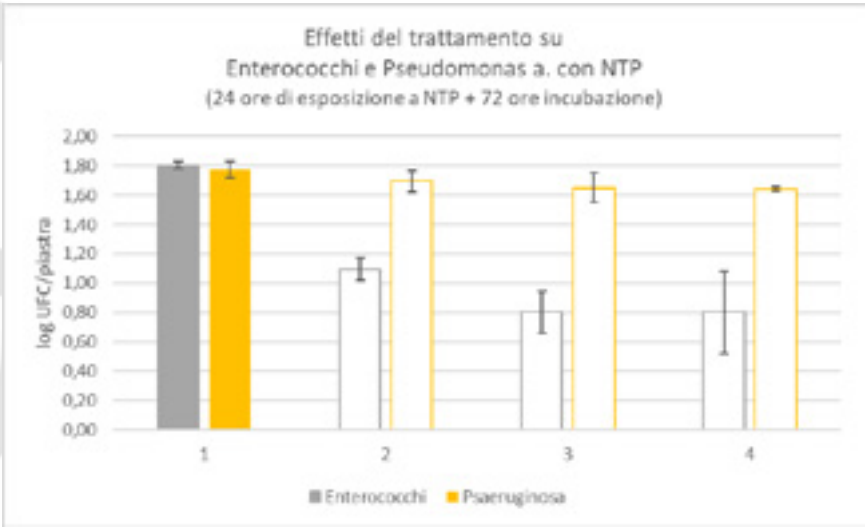

Confronto degli effetti del trattamento con NTP, valori espressi come media di due piastre

Esprimendo invece i dati ottenuti in termini di riduzione percentuale di crescita rispetto ai controlli, si può notare come questa sia stata evidenziata ancora una volta per i batteri gram positivi (Enterococco), estremamente limitata per i gram negativi, rappresentati in questo caso da Pseudomonas.

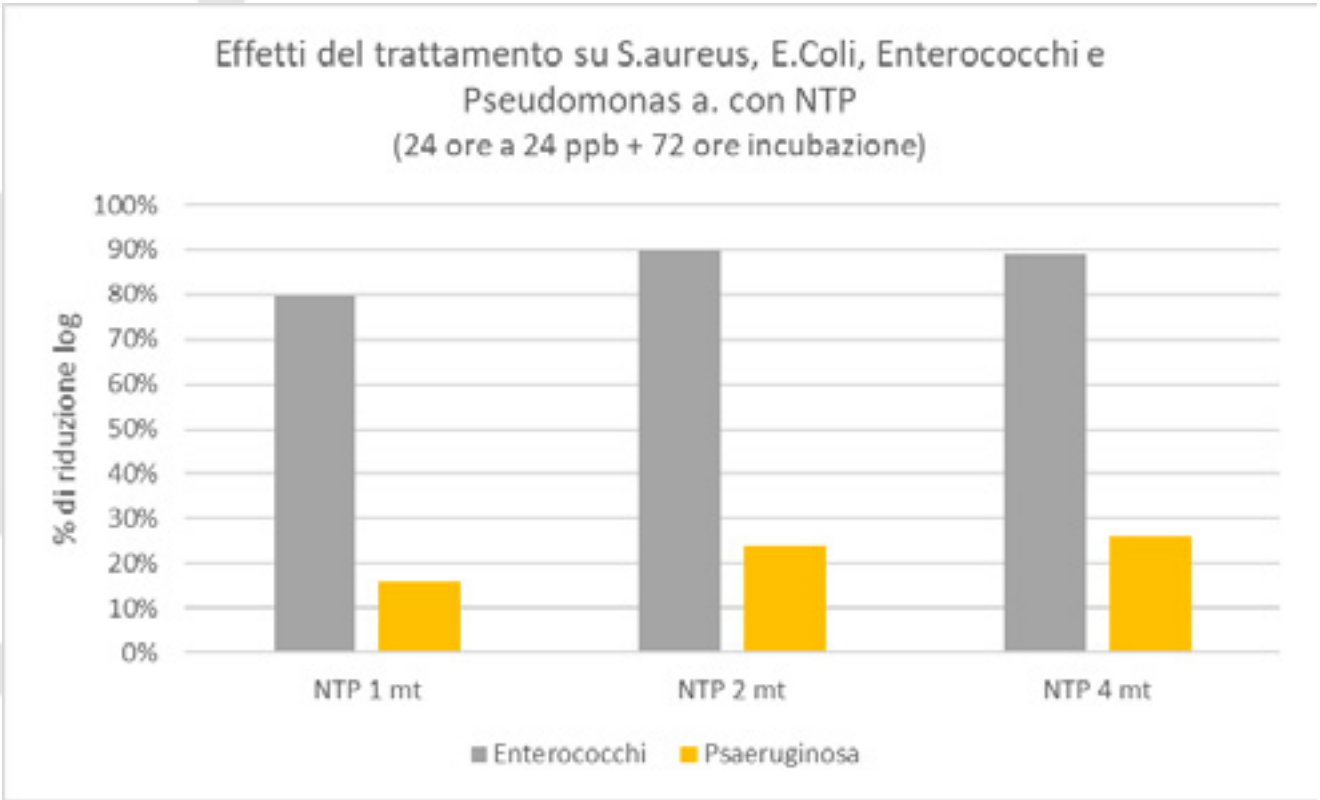

Confronto tra le riduzioni percentuali della crescita microbica tra i vari microrganismi testati

5.3 PROVA C

5.3.1 Sintesi della prova

Codice prova	S20/005800004
Data	11 maggio 2021
Descrizione della prova	Esposizione di piastre con microorganismi Stafilococco aureo, Enterococco fecale, Escherichia coli e Pseudomonas aeruginosa in box di piccole dimensioni (teca), mantenendo l'umidità interna a circa il 50%
Obiettivo della prova	Valutare l'effetto antimicrobico dell'NTP a condizioni di umidità controllate
Dispositivo Jonix utilizzato	JONIX Cube modificato
Ambiente di prova	Box in materiale plastico di dimensioni 100 cm x 50 cm x 50 cm per un volume di 0,250 m^3
Sintesi dei risultati	Abbattimento della carica microbica fino al 3% per Escherichia, 20% Stafilococco aureo, 30% Enterococco. Non rilevato su Pseudomonas

5.3.2 Descrizione della prova

In questa prova, e nella successiva, si è cercato di replicare quanto osservato in un ambiente di dimensioni maggiori, all'interno di un piccolo ambiente confinato in cui sia più agevole controllarne le condizioni ambientali.

Per questo scopo è stata utilizzata un'apposita teca (50 cm x 50 cm x 100 cm) all'interno della quale inserire un generatore di NTP (CUBE) alimentato con una tensione regolata appositamente per mantenere l'esposizione il più possibile sotto i 50 ppb, appunto per simulare il comportamento di un dispositivo Jonix in condizioni reali. Prove preliminari hanno permesso di stabilire che le migliori condizioni di alimentazione per questo scopo erano di 850 volts a 50 Hz.

La prova di esposizione è stata condotta utilizzando sia batteri Gram positivi (Stafilococco aureo e Enterococco fecale) che Gram negativi (Escherichia coli e Pseudomonas aeruginosa).

Come per le altre prove i batteri sono stati seminati, in doppio, su piastre petri a doppio settore riempite con agar PCA (terreno non selettivo) ad una densità di circa 200 UFC/settore. Successivamente le piastre sono state esposte, scoperte, all'NTP all'interno della teca nella quale è stato posizionato un generatore di NTP (CUBE) mantenuto costantemente acceso per tutto il tempo della prova. Le piastre di controllo sono state mantenute all'interno del laboratorio, chiuse con il proprio coperchio, evitando così ogni possibile esposizione all'NTP.

Dopo l'esposizione le piastre sono state fotografate e quindi mantenute in incubatore a 37°C per 24+24 ore.

5.3.3 Concentrazioni di ozono nell'ambiente

L'ozono prodotto è stato misurato per mezzo dell'HORIBA con acquisizione dei dati ogni tre minuti.

I valori di ozono che si sono mantenuti all'interno della teca sono stati piuttosto variabili con una tendenza continua all'aumento e, in media, leggermente superiori a quanto atteso. La media della concentrazione nell'intero test è stata di 64 ppb.

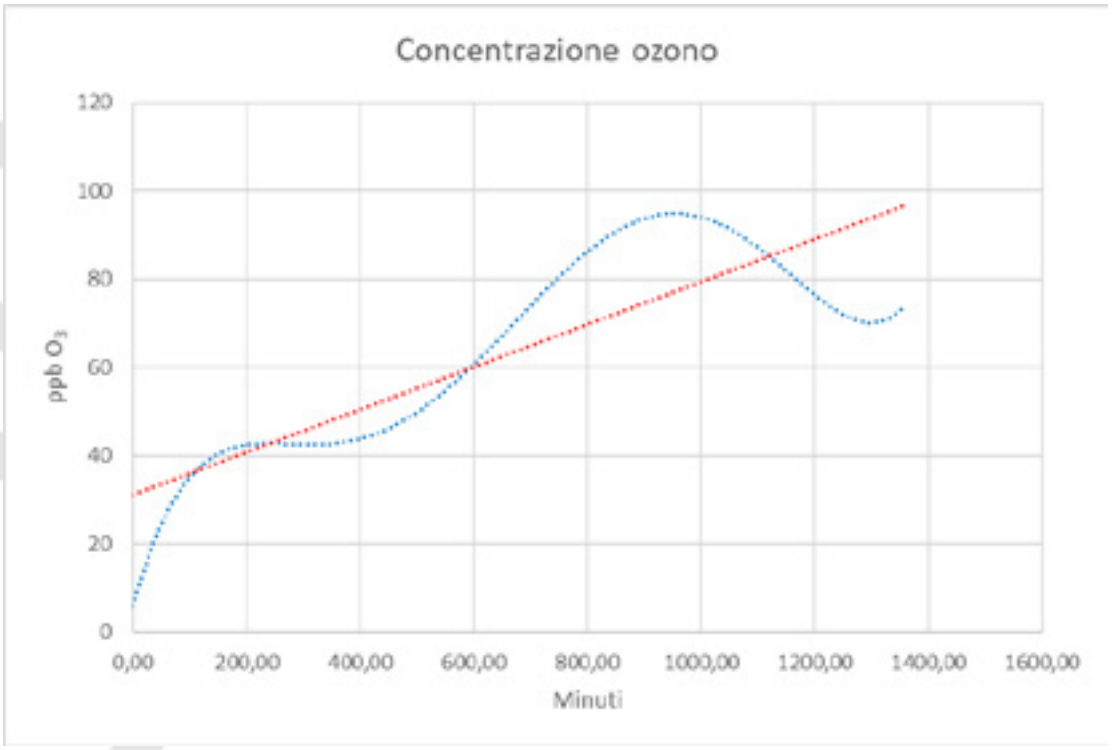

Andamento della concentrazione di ozono (linea rossa = media)

All'interno della teca è stata misurata un'umidità media di circa il 54%.

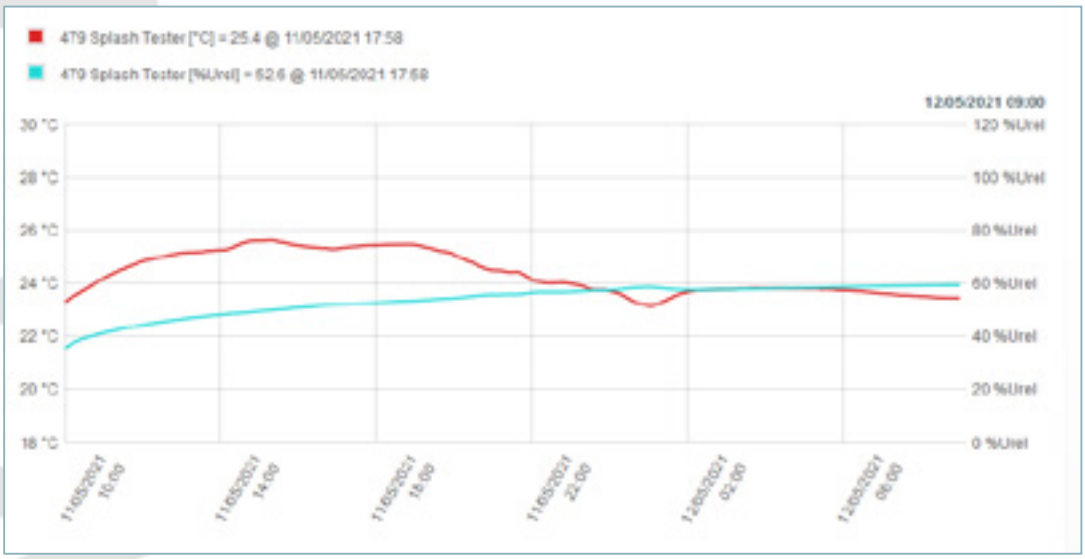

Andamento della temperatura (curva rossa) e umidità (curva celeste) in teca

5.3.4 Evidenze fotografiche

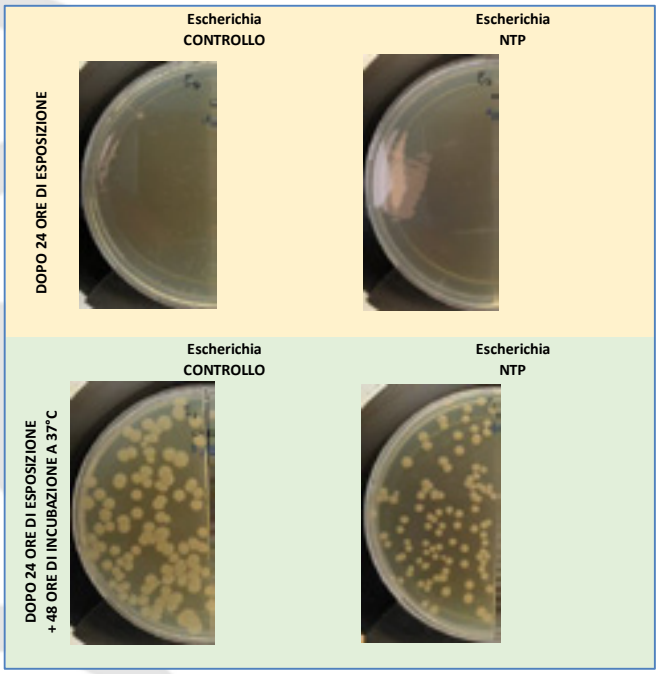

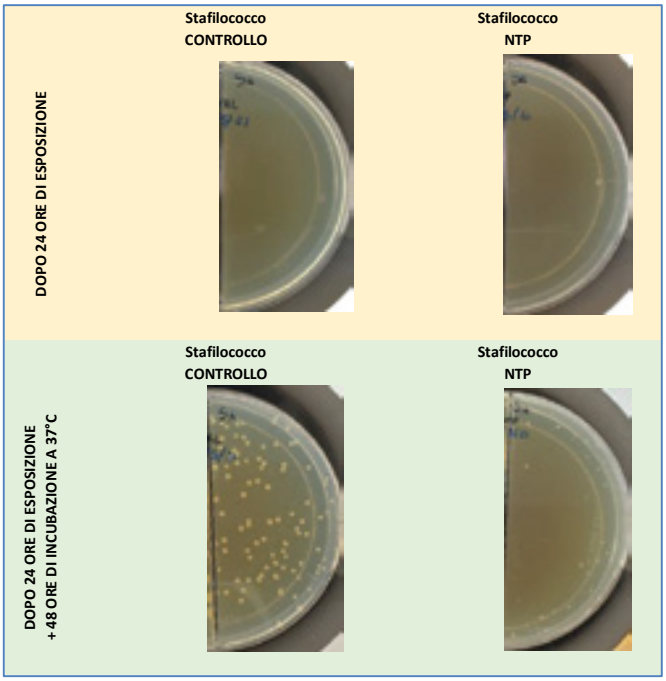

Riga superiore: aspetto delle piastre di coltura dopo l'esposizione di 24 ore all'NTP (confronto con il controllo non esposto)
Riga inferiore: stesse piastre ma dopo 48 ore di incubazione a 37°C

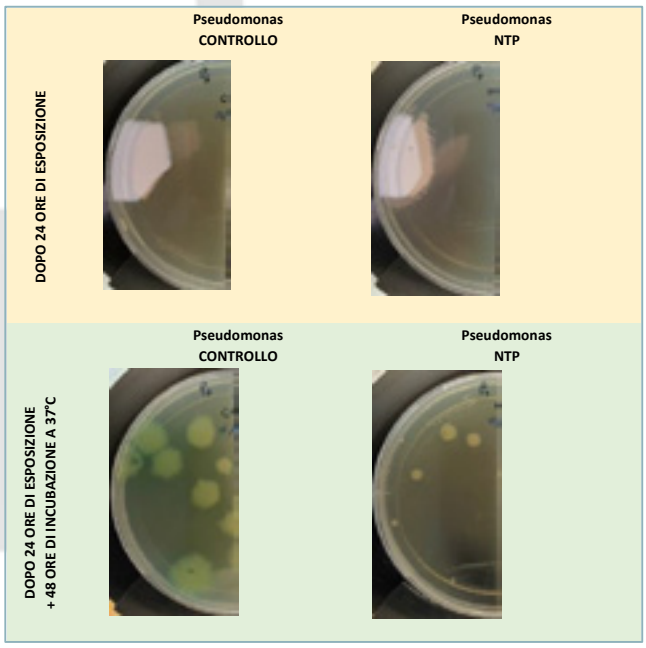

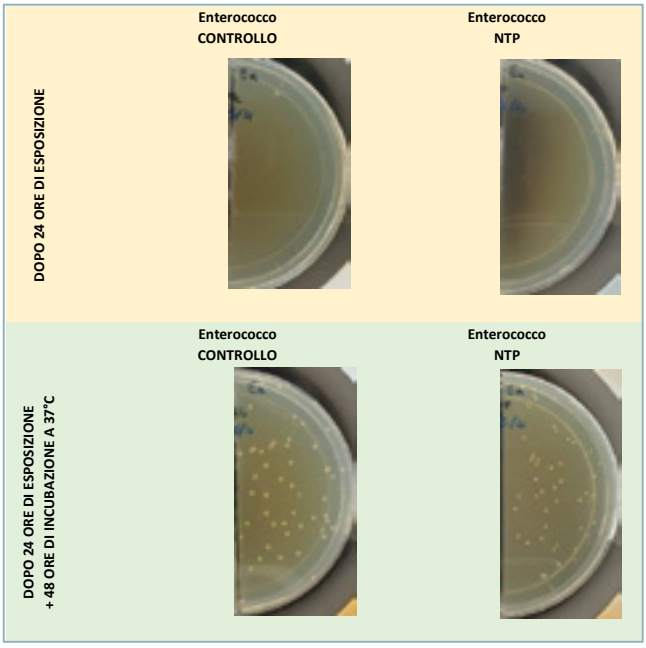

Riga superiore: aspetto delle piastre di coltura dopo l'esposizione di 24 ore all'NTP (confronto con il controllo non esposto)
Riga inferiore: stesse piastre ma dopo 48 ore di incubazione a 37°C

5.3.5 Risultati

Ancora una volta risulta confermato l'effetto "differenziale" nei confronti dei Gram positivi contro una modesta efficacia verso i Gram negativi.

Nuovamente si apprezza molto bene il "fenomeno" Batteriostatico, cioè del ritardo della crescita microbica delle colture esposte all'NTP rispetto a quelle di controllo.

La conta microbica delle colonie cresciute in piastra ha riportato i seguenti valori:

Concentrazione microbica in ciascun settore delle piastre utilizzate.

			piastra 1	piastra 2	media	Dev.St.
Ecoli	**UFC/settore**	**Ctrl**	**113**	*n.e.*	*n.a*	*n.a.*
		NTP	**108**	*n.e.*	*n.a*	*n.a.*
	Log UFC/settore	**Ctrl**	**2,05**	*n.e.*	*n.a*	*n.a.*
		NTP	**2,03**	*n.e.*	*n.a*	*n.a.*

			piastra 1	piastra 2	media	Dev.St.
Saureo	**UFC/settore**	**Ctrl**	**97**	*n.e.*	*n.a*	*n.a.*
		NTP	**38**	*n.e.*	*n.a*	*n.a.*
	Log UFC/settore	**Ctrl**	**1,99**	*n.e.*	*n.a*	*n.a.*
		NTP	**1,58**	*n.e.*	*n.a*	*n.a.*

			piastra 1	piastra 2	media	Dev.St.
Efecale	**UFC/settore**	**Ctrl**	**10**	*n.e.*	*n.a*	*n.a.*
		NTP	**5**	*n.e.*	*n.a*	*n.a.*
	Log UFC/settore	**Ctrl**	**1**	*n.e.*	*n.a*	*n.a.*
		NTP	**0,7**	*n.e.*	*n.a*	*n.a.*

			piastra 1	piastra 2	media	Dev.St.
Paureog	**UFC/settore**	**Ctrl**	**48**	*n.e.*	*n.a*	*n.a.*
		NTP	**51**	*n.e.*	*n.a*	*n.a.*
	Log UFC/settore	**Ctrl**	**1,68**	*n.e.*	*n.a*	*n.a.*
		NTP	**1,71**	*n.e.*	*n.a*	*n.a.*

5.3.6 Conclusioni sintetiche dei risultati della prova

La trasposizione grafica dei dati permette di meglio mettere in evidenza i risultati ottenuti:

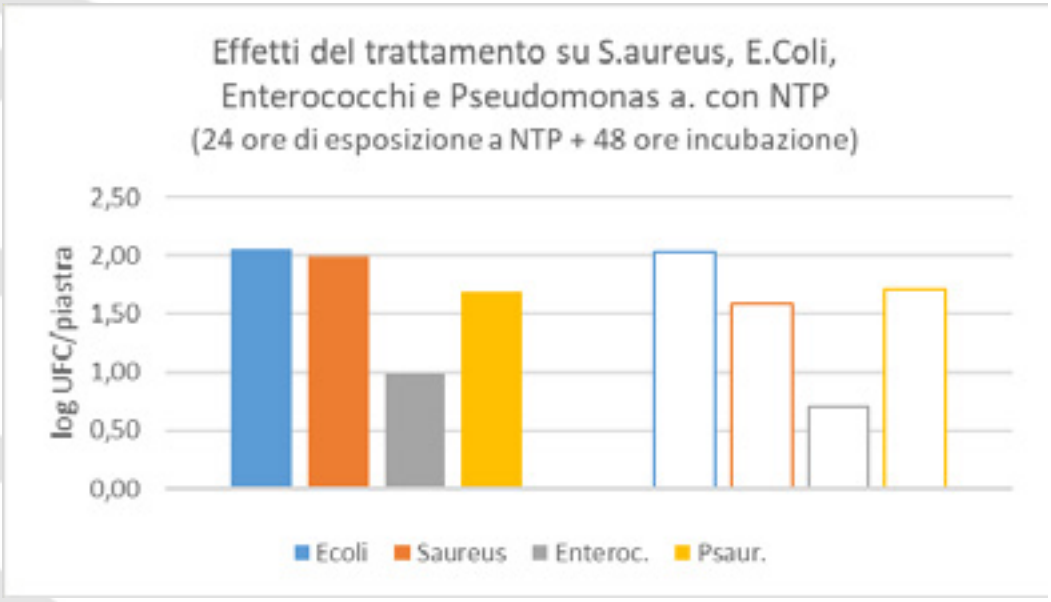

Confronto degli effetti del trattamento con NTP

Mentre esprimendoli in termini di riduzione percentuale di crescita rispetto ai controlli, si può notare nuovamente come questa sia stata evidente praticamente solo per i batteri gram positivi (Stafilococco ed Enterococco).

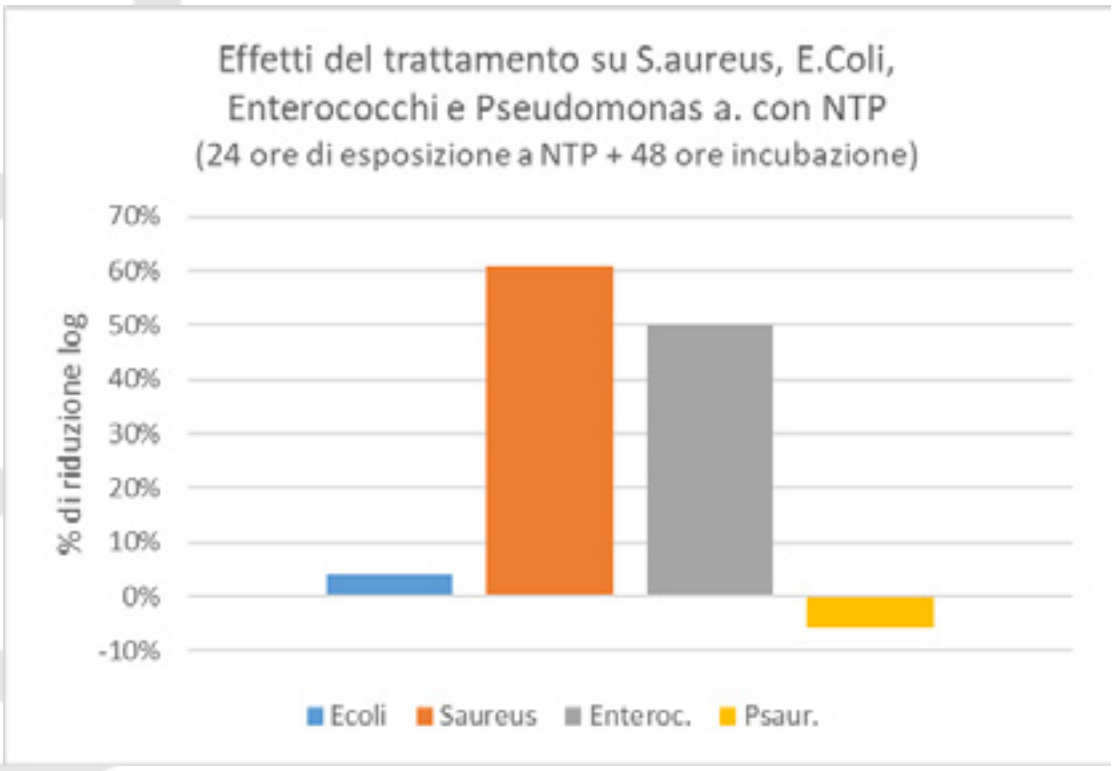

Confronto tra le riduzioni percentuali della crescita microbica tra i vari microrganismi testati

5.4 PROVA D

5.4.1 Sintesi della prova

Codice prova	S20/005800009
Data	27 maggio 2021
Descrizione della prova	Esposizione di piastre con microorganismi Stafilococco aureo, Enterococco fecale, Escherichia coli e Pseudomonas aeruginosa in box di piccole dimensioni (teca), mantenendo l'umidità interna a circa il 80%
Obiettivo della prova	Valutare l'effetto antimicrobico dell'NTP a condizioni di elevata umidità
Dispositivo Jonix utilizzato	JONIX Cube modificato
Ambiente di prova	Box in materiale plastico di dimensioni 100 cm x 50 cm x 50 cm per un volume di 0,250 m^3
Sintesi dei risultati	Abbattimento della carica microbica fino al 51% per Enterococco, 59% Stafilococco aureo

5.4.2 Descrizione della prova

Come per la prova precedente sono stati utilizzati sia batteri Gram positivi (Stafilococco aureo e Enterococco fecale) che Gram negativi (Escherichia coli e Pseudomonas aeruginosa) seminati, in doppio, su piastre petri a doppio settore riempite con agar PCA (terreno non selettivo) ad una densità di circa 200 UFC/settore. Successivamente le piastre sono state esposte, scoperte, all'NTP all'interno della teca nella quale è stato posizionato un generatore di NTP (CUBE) mantenuto costantemente acceso per tutto il tempo della prova. Le piastre di controllo sono state mantenute all'interno del laboratorio, chiuse con il proprio coperchio, evitando così ogni possibile esposizione all'NTP.

All'interno della teca è stata creata, grazie all'impiego di una soluzione sovrasatura di NaCl, un ambiente con valori di umidità relativa superiori all'80%.

5.4.3 Concentrazioni di ozono nell'ambiente

Al fine di evitare danno strumentale, le misurazioni dell'Ozono in teca non sono avvenute di continuo come nelle altre prove, ma in maniera discontinua e puntuale, interrompendole solamente durante le ore notturne. Ad ogni modo i valori rilevati hanno permesso di stabilire un "trend" sostanzialmente sovrapponibile ai precedenti. Il valore medio riscontrato è stato di 47 ppb, inferiore a quello della prova precedente.

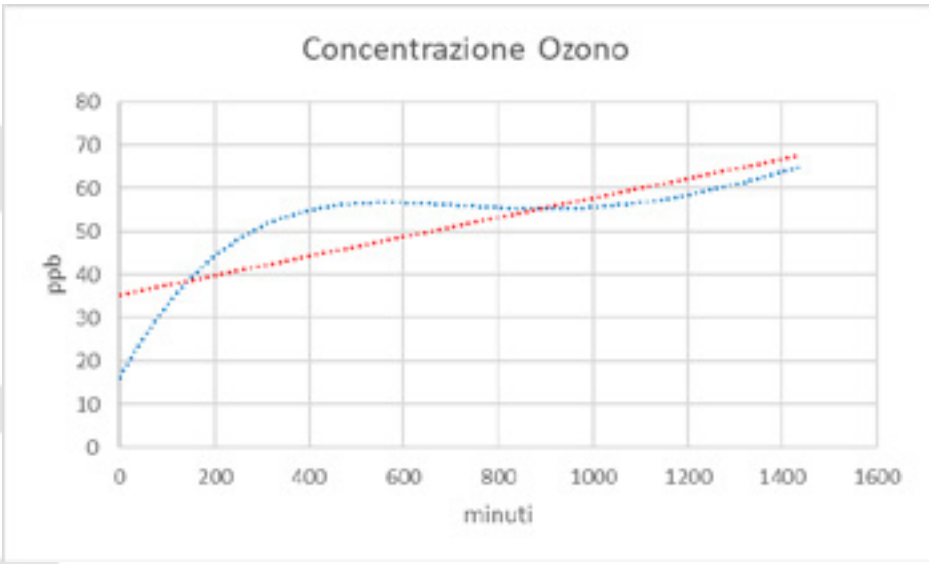

Andamento della concentrazione di ozono. Linea rossa = media

Poiché le condizioni di alimentazione del generatore sono state identiche (850 volts a 50 Hz), la minore quantità di Ozono rilevata potrebbe essere dovuta proprio alla presenza di una maggiore umidità dell'aria che, veicolando acqua, avrebbe funzionato come agente "sequestrante" l'Ozono diffuso in forma gassosa dando luogo a specie chimiche differenti (es. H_2O_2) che peraltro spiegherebbero anche la maggiore efficacia del trattamento.

La temperatura in teca e quella dell'ambiente dei controlli è risultata essere sostanzialmente poco influente con un solo grado di differenza ($T°_{media}$ NTP: 24,7; $T°_{media}$ CTRL: 23,7).

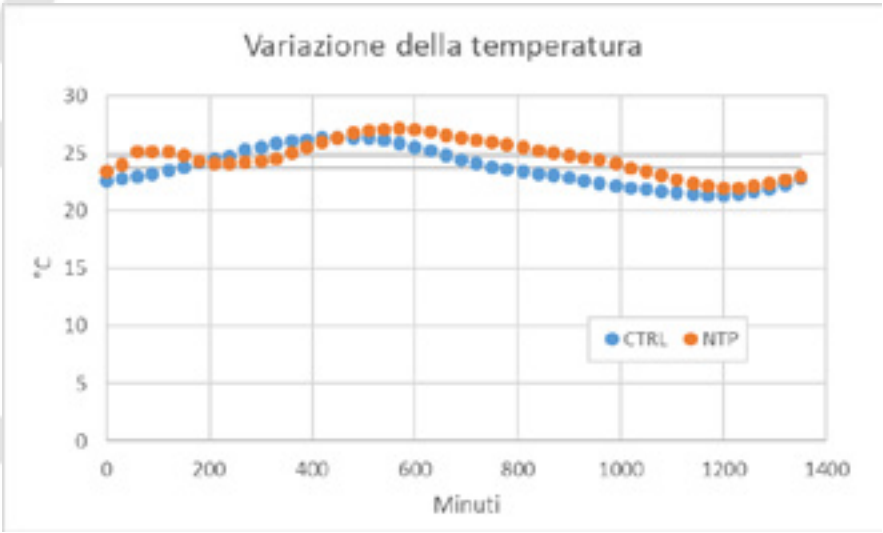

Confronto tra le due temperature di esposizione nelle 24 ore. CTRL: piastre conservate nella cappa a flusso laminare; NTP: piastre conservate in teca.

All'interno della teca, inoltre, è stata misurata un'umidità media di circa 80%.

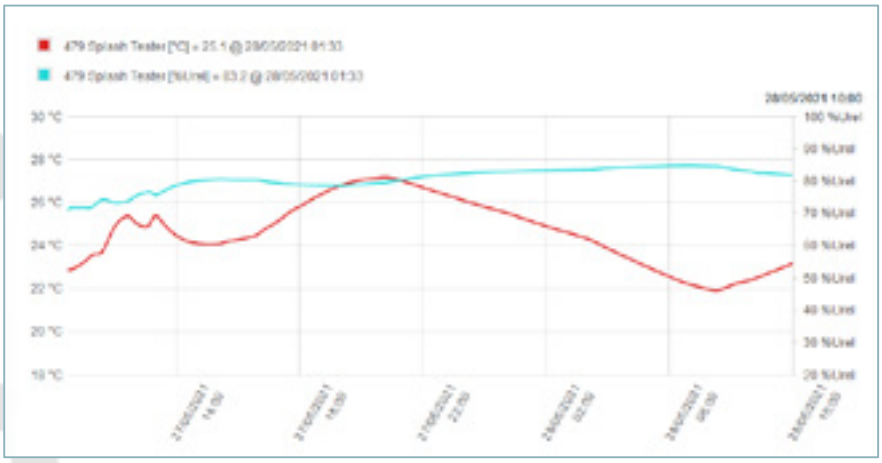

Andamento della temperatura (curva rossa) e umidità (curva celeste) in teca

5.4.4 Evidenze fotografiche

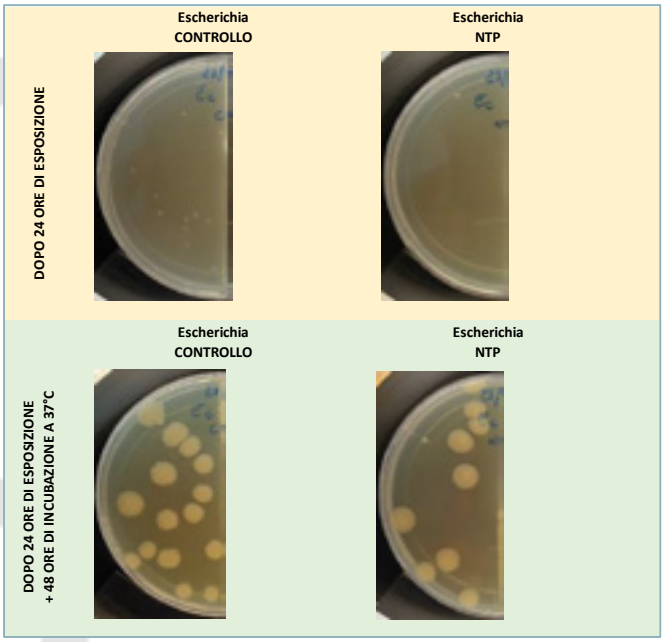

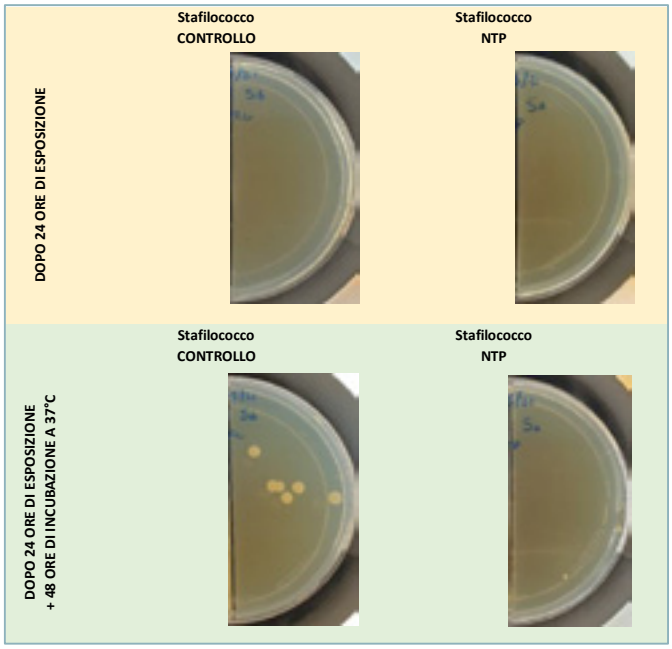

Riga superiore: aspetto delle piastre di coltura dopo l'esposizione di 24 ore all'NTP (confronto con il controllo non esposto)
Riga inferiore: stesse piastre ma dopo 48 ore di incubazione a 37°C

Laboratori ARCHA S.r.l. unipersonale
Via di Tegulaia 10/a - 56121 - PISA - ph. +39 050 985165 - fax +39 050 985233 - www.archa.it - archainf@archa.it
C.F., P.IVA, Iscr. Reg. Impr. di Pisa n. 01115340505 - Rep. Econ. Amm. di Pisa n°101169 - Capitale Sociale 101.400,00 i.v.

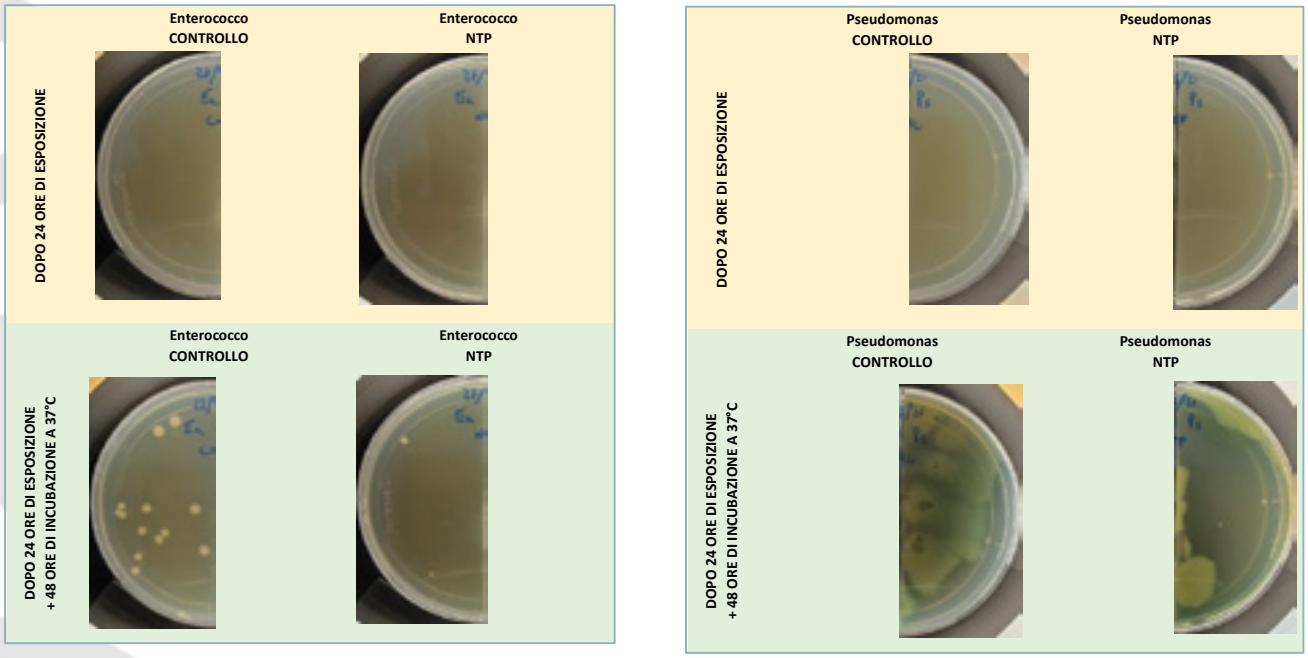

Riga superiore: aspetto delle piastre di coltura dopo l'esposizione di 24 ore all'NTP (confronto con il controllo non esposto)
Riga inferiore: stesse piastre ma dopo 48 ore di incubazione a 37°C

5.4.5 Risultati

In questo caso la prova ha messo in evidenza un effetto inibitorio (biocida) anche nei confronti dei batteri Gram negativi (Escherichia coli e Pseudomonas aeruginosa), fenomeno non osservato nel test ad umidità inferiore.

La conta microbica delle colonie cresciute in piastra ha riportato i seguenti valori:

Concentrazione microbica in ciascun settore delle piastre utilizzate.

			piastra 1	piastra 2	media	Dev.St.
Ecoli	**UFC/settore**	**Ctrl**	15	16	**15,5**	1
		NTP	13	9	**11**	3
	Log UFC/settore	**Ctrl**	-	-	**1,19**	0,02
		NTP	-	-	**1,04**	0,11

			piastra 1	piastra 2	media	Dev.St.
Saureo	**UFC/settore**	**Ctrl**	7	6	**6,5**	1
		NTP	3	1	**2**	1
	Log UFC/settore	**Ctrl**	-	-	**0,81**	0,05
		NTP	-	-	**0,30**	0,34

			piastra 1	piastra 2	media	Dev.St.
Efecale	**UFC/settore**	**Ctrl**	18	15	**16,5**	2
		NTP	2	0	**1**	1
	Log UFC/settore	**Ctrl**	-	-	**1,22**	0,06
		NTP	-	-	**0,02**	0,92

			piastra 1	piastra 2	media	Dev.St.
Paureog	**UFC/settore**	**Ctrl**	4	15	**9,5**	8
		NTP	4	2	**3**	1
	Log UFC/settore	**Ctrl**	-	-	**0,98**	0,41
		NTP	-	-	**0,48**	0,21

5.4.6 Conclusioni sintetiche dei risultati della prova

La trasposizione grafica dei dati permette di meglio mettere in evidenza i risultati ottenuti:

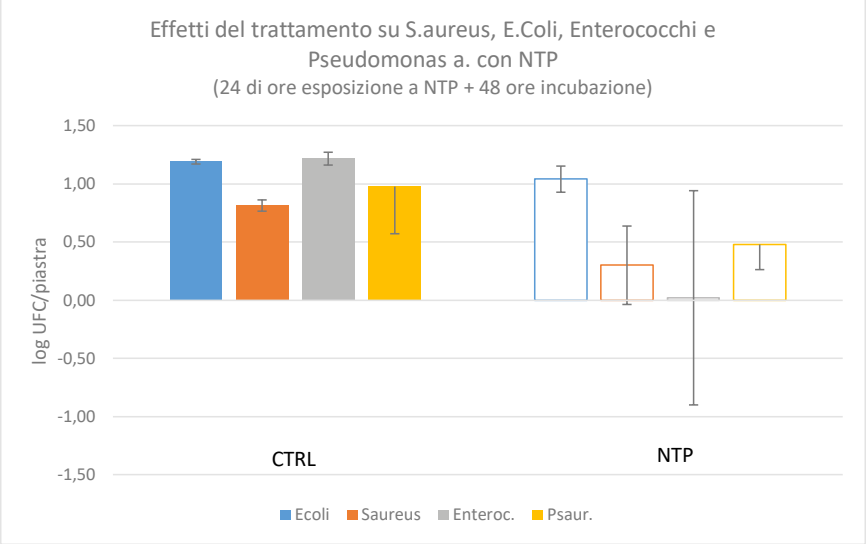

Confronto degli effetti del trattamento con NTP

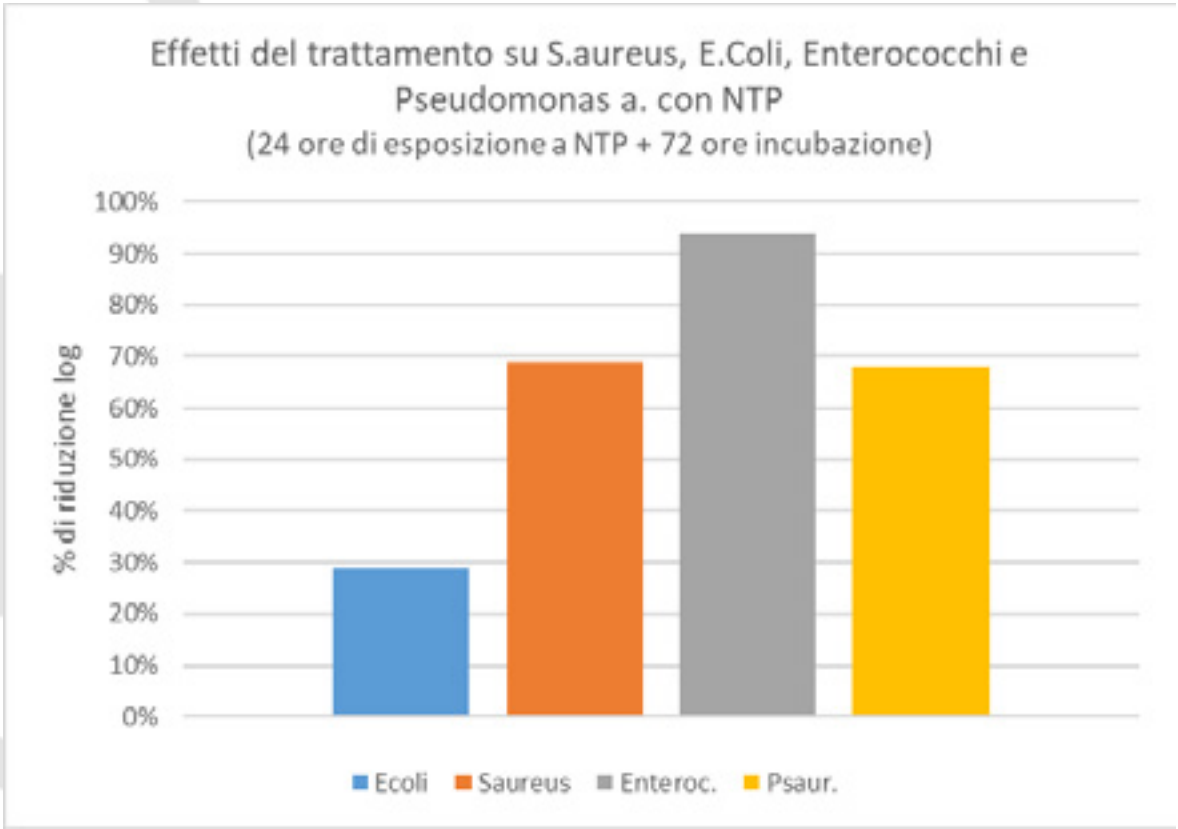

Confronto tra le riduzioni percentuali della crescita microbica tra i vari microrganismi testati

Il confronto delle riduzioni percentuali mette bene in evidenza un fenomeno nuovo.

L'avere esposto i microrganismi all'NTP in un ambiente ad alta umidità relativa, ha aumentato considerevolmente la capacità biocida esercitata dal trattamento.

Mettendo infatti a confronto i risultati della prova C condotta ad Umidità Relativa pari a circa 54% e quelli della prova D condotta ad Umidità Relativa di circa l'80% si rileva come il tenore di umidità influenza l'efficacia dell'NTP, come era ipotizzabile in quanto il droplet naturale agisce come veicolo per le specie ossidanti.

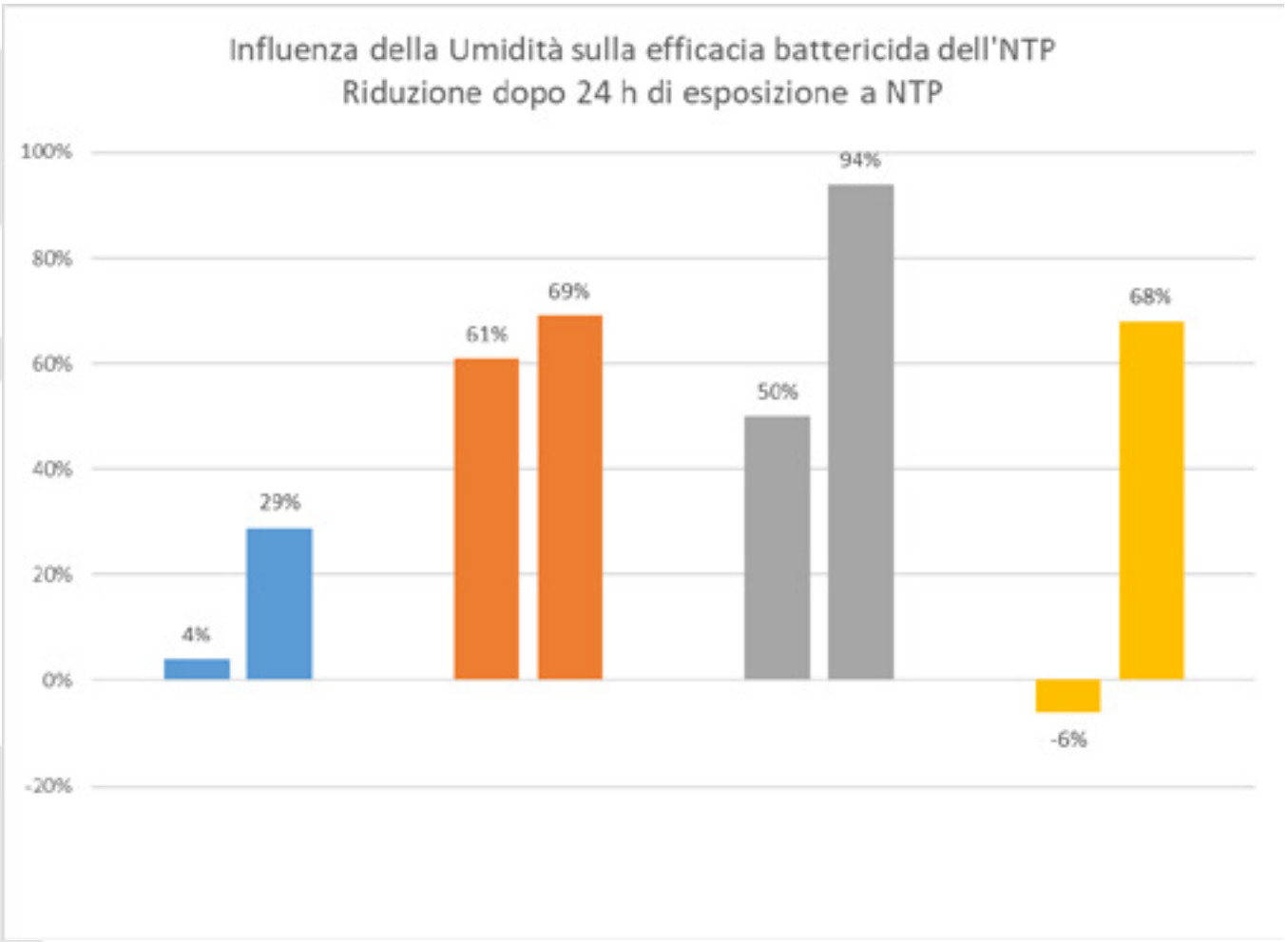

Confronto fra le percentuali di riduzione batterica in diverse condizioni di Umidità

5.5 PROVA E

5.5.1 Sintesi della prova

Codice prova	S20/005800008
Data	24 maggio 2021
Descrizione della prova	Esposizione di piastre con microorganismi Stafilococco aureo, Enterococco fecale, Escherichia coli e Pseudomonas aeruginosa in ambiente naturale
Obiettivo della prova	Valutare l'effetto dell'aria esterna, contenente specie ossidanti di formazione naturale
Dispositivo Jonix utilizzato	NESSUNO
Ambiente di prova	Locale interno con affaccio verso l'esterno
Sintesi dei risultati	Abbattimento della carica microbica fino al 51% per Enterococco, 59% Stafilococco aureo

5.5.2 L'ozono nell'aria esterna

E' noto che l'Ozono si ritrova anche nell'atmosfera per effetto dell'interazione della radiazione solare che, interagendo con l'ossigeno atmosferico, porta alla produzione del gas.

Tipicamente, come è facile constatare dai dati di monitoraggio ambientale rilevati dalle centraline delle varie ARPA sparse sul territorio nazionale, la concentrazione di Ozono aumenta sensibilmente nelle giornate di bel tempo, quando la radiazione solare può liberamente esplicare i propri effetti.

Come indicato anche nel rapporto del Sistema nazionale per la Protezione dell'Ambiente "La qualità dell'aria in Italia edizione 2020", nelle zone di pianura o a livello del mare, le concentrazioni di O3 seguono abbastanza bene il profilo dell'intensità della radiazione solare (tendendo quindi ad aumentare nelle ore di massima insolazione e a diminuire nella notte).

Sempre lo stesso rapporto riporta la statistica media delle concentrazioni di Ozono rilevata da 224 stazioni di monitoraggio indicando una media di circa 35 ppb (da ricordare che i $\mu g/m^3$ sono il doppio dei ppb) con punte che superano anche i 50-60 ppb.

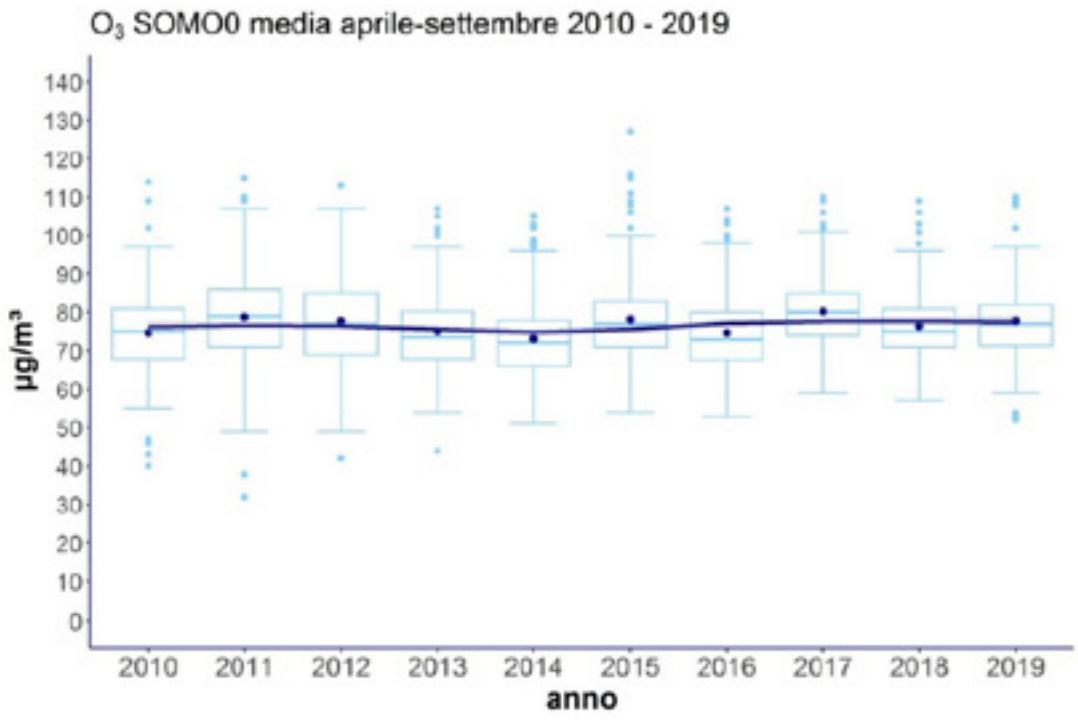

Figura 6.4. Ozono (SOMO0), 2010 – 2019. - Statistiche descrittive calcolate su una selezione di 224 stazioni di monitoraggio distribuite sul territorio nazionale.

Fonte: Elaborazioni ISPRA su dati ARPA/APPA

Interessante è anche il grafico che riporta la statistica media in relazione alla posizione delle stazioni da cui si rileva che le concentrazioni più elevate, 40-45 ppb, si hanno nelle zone rurali, quindi quelle che tutti noi reputiamo con “aria pulita”. Ed in effetti è proprio l’inquinamento delle zone urbane che “sottrae” l’ozono facendolo reagire con gli inquinanti presenti per il traffico veicolare, riscaldamento, ecc.

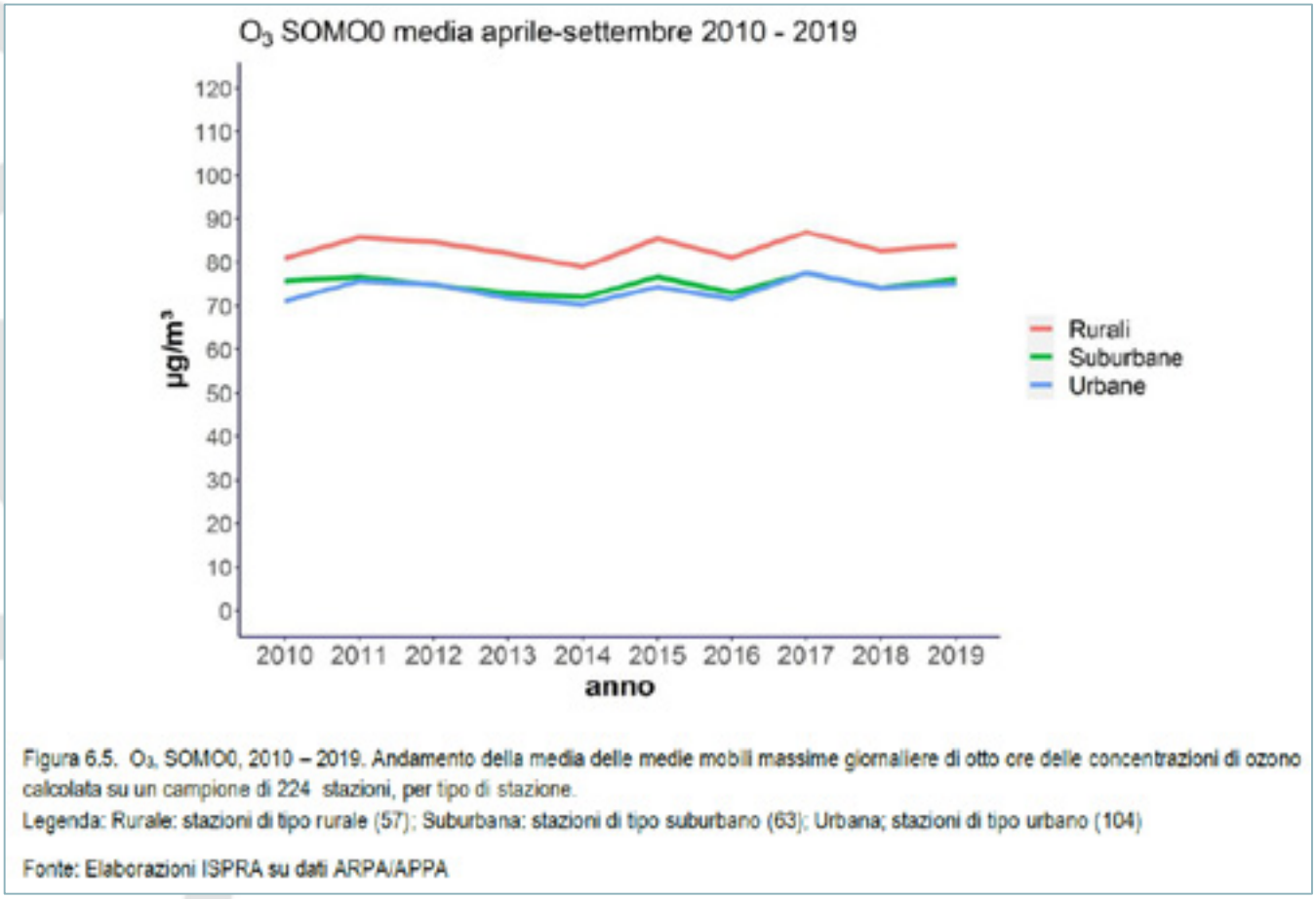

Figura 6.5. O_3, SOMO0, 2010 – 2019. Andamento della media delle medie mobili massime giornaliere di otto ore delle concentrazioni di ozono calcolata su un campione di 224 stazioni, per tipo di stazione.
Legenda: Rurale: stazioni di tipo rurale (57); Suburbana: stazioni di tipo suburbano (63); Urbana; stazioni di tipo urbano (104)

Fonte: Elaborazioni ISPRA su dati ARPA/APPA

Da considerare inoltre che laddove è presente ozono sono presumibilmente presenti anche altre specie ossidanti, radicali liberi, ossidrili, ecc. che intervengono nei meccanismi di formazione della molecola O_3.

5.5.3 Descrizione della prova

Questa prova sperimentale aveva l'obiettivo di verificare se gli effetti dell'esposizione delle colonie batteriche su piastre a concentrazioni di ozono (e presumibilmente di altre specie ossidanti naturali) presenti naturalmente nell'aria ambiente esterna fosse analoga e paragonabile a quelli rilevati all'interno della teca.

Per questo scopo, come per le precedenti prove, sono stati utilizzati sia batteri Gram positivi (Stafilococco aureo e Enterococco fecale) che Gram negativi (Escherichia coli e Pseudomonas aeruginosa) seminati, in doppio, su piastre petri a doppio settore riempite con agar PCA (terreno non selettivo) ad una densità di circa 200 UFC/settore.

L'esposizione all'Ozono atmosferico è avvenuta posizionando le piastre in un locale con affaccio all'esterno, lasciano la finestra completamente aperta per permettere all'aria atmosferica di saturare il locale. E' stato così riprodotta l'esposizione ad aria esterna ma senza avere irraggiamento solare né turbolenze dovute a venti e brezze.

5.5.4 Concentrazioni di ozono nell'ambiente

Layout della prova.
A) collocazione dell'Horiba e delle piastre rispetto alla finestra aperta;
B) particolare delle piastre esposte con il tubo di prelievo dell'aria dell'Horiba (freccia rossa)

Il valore di Ozono misurato dall'HORIBA è stato confrontato con quello registrato dalla più vicina centralina ARPAT collocata nel quartiere "I Passi" di Pisa, a circa 6 km di distanza dalla sede della prova.

Collocazione della centralina ARPAT rispetto alla sede di esecuzione della prova

Prove precedenti hanno infatti permesso di stabilire che esiste un'ottima corrispondenza tra i valori registrati dalla centralina ARPAT e quelli misurati nell'ambiente esterno alla sede di prova con l'HORIBA, nonostante l'apprezzabile distanza che separa i due punti di misura.

Contestualmente al valore di Ozono atmosferico è stata misurata la temperatura e l'umidità ambientale.

Anche in questo caso, come in tutte le altre sperimentazioni, l'ozono è da considerarsi l'indicatore delle "specie ossidanti" perché è sicuramente la specie più longeva e soprattutto l'unica sostanza misurabile.

Le piastre di controllo sono state mantenute all'interno del laboratorio, chiuse con il proprio coperchio, evitando così ogni possibile esposizione all'ozono ambientale. Come consueto, dopo 24 ore di esposizione tutte le piastre sono state posizionate all'interno dell'incubatore a 37°C per agevolare la crescita dei microrganismi.

Per confrontare i valori di Ozono ambientali misurati dalla centralina ARPAT e dall'Horiba, si è reso necessaria una parziale elaborazione dei dati rilevati da quest'ultimo, poiché dal sito dell'ARPAT sono mostrati solamente i valori in $\mu g/m^3$ espressi come media oraria. Di conseguenza si è reso necessario eseguire una media oraria di tutte le misure effettuate dall'Horiba e convertire i dati ARPAT in ppb (dividendo per 2).

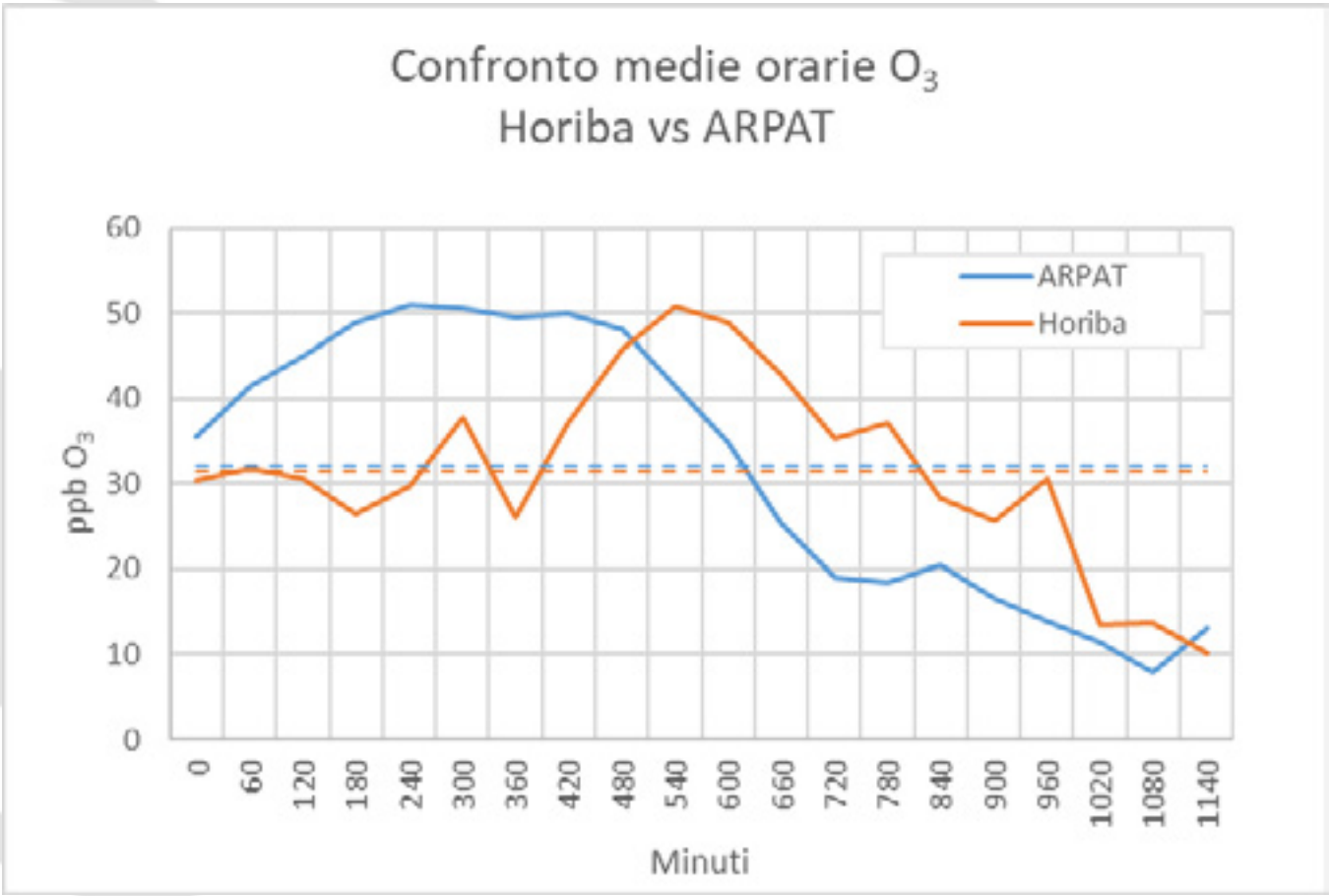

Valori di Ozono ambientale a cui sono state esposte le piastre. Confronto tra le misure ARPAT e HORIBA

Come si può osservare dal grafico precedente, le curve sono abbastanza simili ma soprattutto il valore medio rilevato (linee tratteggiate) risulta praticamente identico: 32,2 ppb (valore ARPAT) contro 31,6 ppb (valore HORIBA).

Di conseguenza è possibile concludere che le piastre siano state esposte a valori di Ozono (e presumibilmente di altre specie ossidanti) che, in media, sono assolutamente simili ad altri precedentemente testati con i trattamenti NTP.

Per quanto concerne infine i valori di temperatura e umidità ambientale, il grafico seguente mostra i dati registrati dal data logger di monitoraggio.

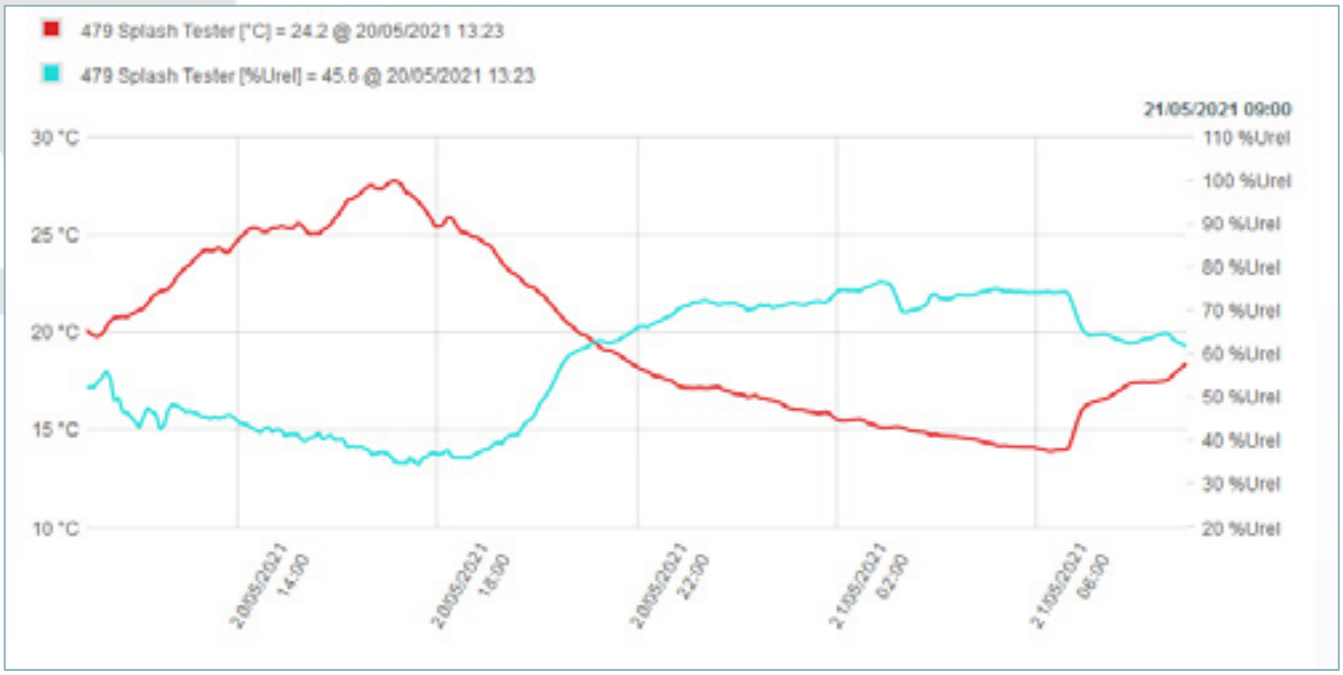

Andamento della temperatura (curva rossa) e umidità (curva celeste) nell'ambiente di prova

In questo caso si sono registrati dei valori (medi) di umidità del 57,9% e di temperatura di 19,9°C.

5.5.5 Evidenze fotografiche

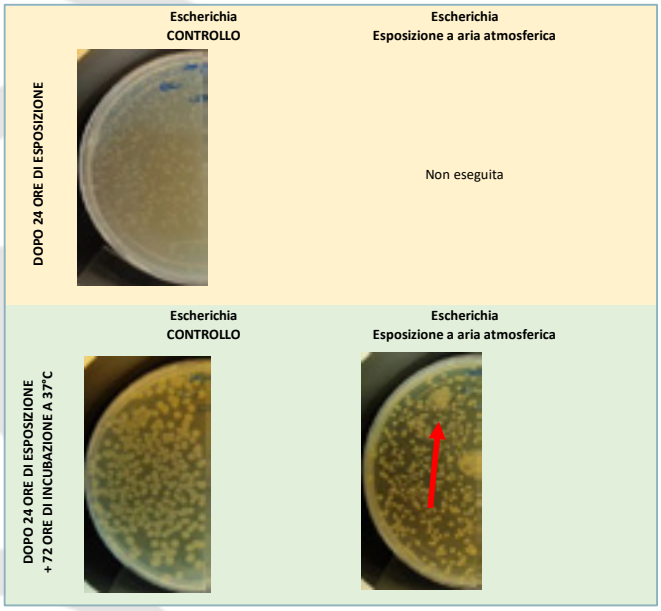

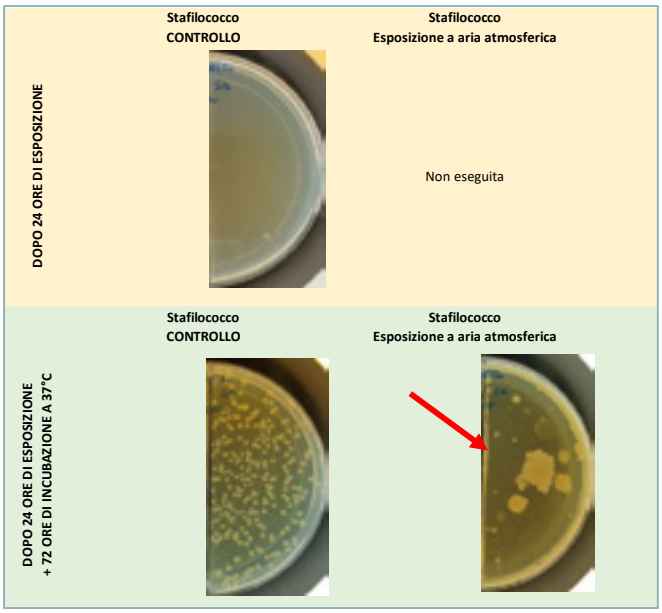

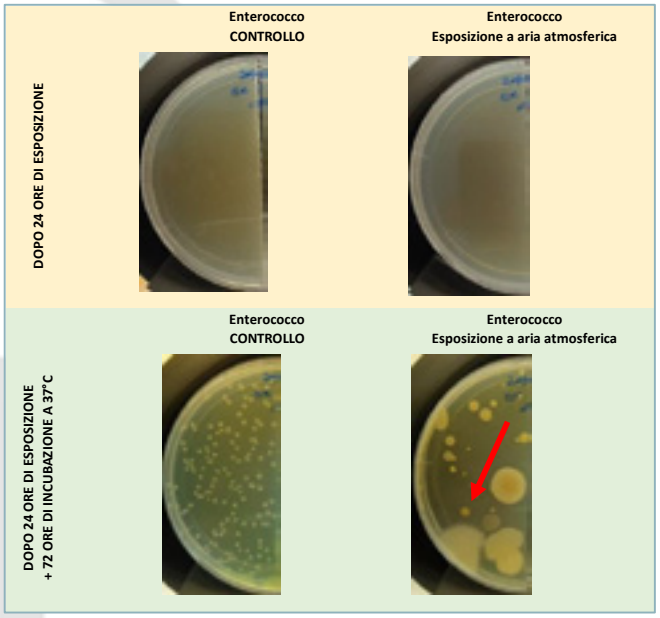

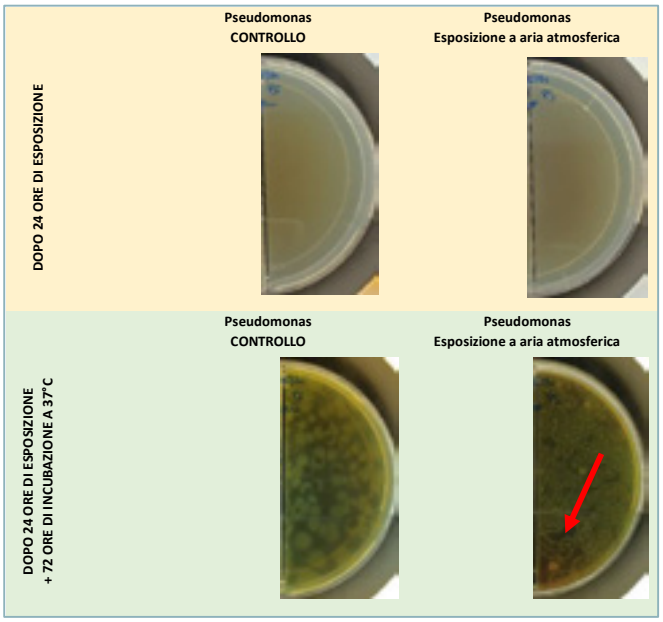

Riga superiore: aspetto delle piastre di coltura dopo l'esposizione di 24 ore all'Ozono ambientale (confronto con il controllo non esposto).
Riga inferiore: stesse piastre ma dopo 72 ore di incubazione a 37°C.
Le frecce indicano la presenza di colonie di microrganismi ambientali contaminanti.

Laboratori ARCHA S.r.l. unipersonale
Via di Tegulaia 10/a - 56121 - PISA - ph. +39 050 985165 - fax +39 050 985233 - www.archa.it - archainf@archa.it
C.F., P.IVA, Iscr. Reg. Impr. di Pisa n. 01115340505 - Rep. Econ. Amm. di Pisa n°101169 - Capitale Sociale 101.400,00 i.v.

5.5.6 Risultati

Come si può ben apprezzare dalle figure precedenti, gli effetti alla “semplice” esposizione all’aria ambientale (contenente ozono naturale) ha replicato quanto osservato relativamente all’azione dell’NTP in un ambiente confinato (stanza o teca) con un effetto significativo di inibizione della crescita nei confronti dei batteri Gram positivi e nessun effetto verso i batteri Gram negativi.

Dall’osservazione delle piastre si può notare una presenza di microrganismi contaminanti di provenienza ambientale che si sono sviluppati sulla superficie dell’agar di coltura, presenza tanto maggiore quanto minore era quella dei microrganismi di prova. Questo fatto trova un’ovvia spiegazione nei comuni fenomeni di competizione ecologica che si instaurano quando un comune ambiente (con le relative sostanze nutritive) è condiviso da più specie; in questo caso la più forte e/o numerosa prende il sopravvento impedendo o limitando lo sviluppo delle altre.

Inoltre appare chiaro ancora una volta come ci sia stato un effetto inibitorio (biocida) della crescita differenziale in funzione del tipo di microrganismo.

La conta microbica delle colonie cresciute in piastra ha riportato i seguenti valori:

Concentrazione microbica in ciascun settore delle piastre utilizzate.

			piastra 1	piastra 2	media	Dev.St.
Ecoli	**UFC/settore**	**Ctrl**	369	355	**362**	10
		O_3	438	318	**378**	85
	Log UFC/settore	**Ctrl**	-	-	**2,56**	0,01
		O_3	-	-	**25,58**	0,1

			piastra 1	piastra 2	media	Dev.St.
Saureo	**UFC/settore**	**Ctrl**	220	301	**260,5**	57
		O_3	14	6	**10**	6
	Log UFC/settore	**Ctrl**	-	-	**2,42**	0,1
		O_3	-	-	**1**	0,26

			piastra 1	piastra 2	media	Dev.St.
Efecale	**UFC/settore**	**Ctrl**	164	110	**137**	38
		O_3	9	13	**11**	3
	Log UFC/settore	**Ctrl**	-	-	**2,14**	0,12
		O_3	-	-	**1,04**	0,11

			piastra 1	piastra 2	media	Dev.St.
Paureog	**UFC/settore**	**Ctrl**	82	145	**113,5**	45
		O_3	164	174	**169**	7
	Log UFC/settore	**Ctrl**	-	-	**2,05**	0,18
		O_3	-	-	**2,23**	0,02

5.5.7 Conclusioni sintetiche dei risultati della prova

La trasposizione grafica dei dati permette di meglio mettere in evidenza questi risultati:

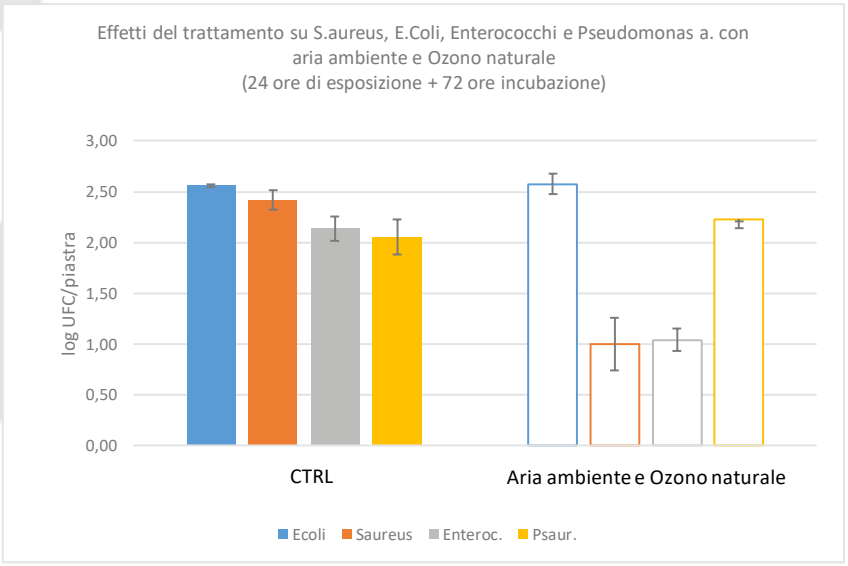

Confronto degli effetti della esposizione ad aria ambiente e ozono naturale

La consueta conversione dei dati in valori di riduzione percentuale evidenzia gli effetti ottenuti sui due principali ceppi batterici.

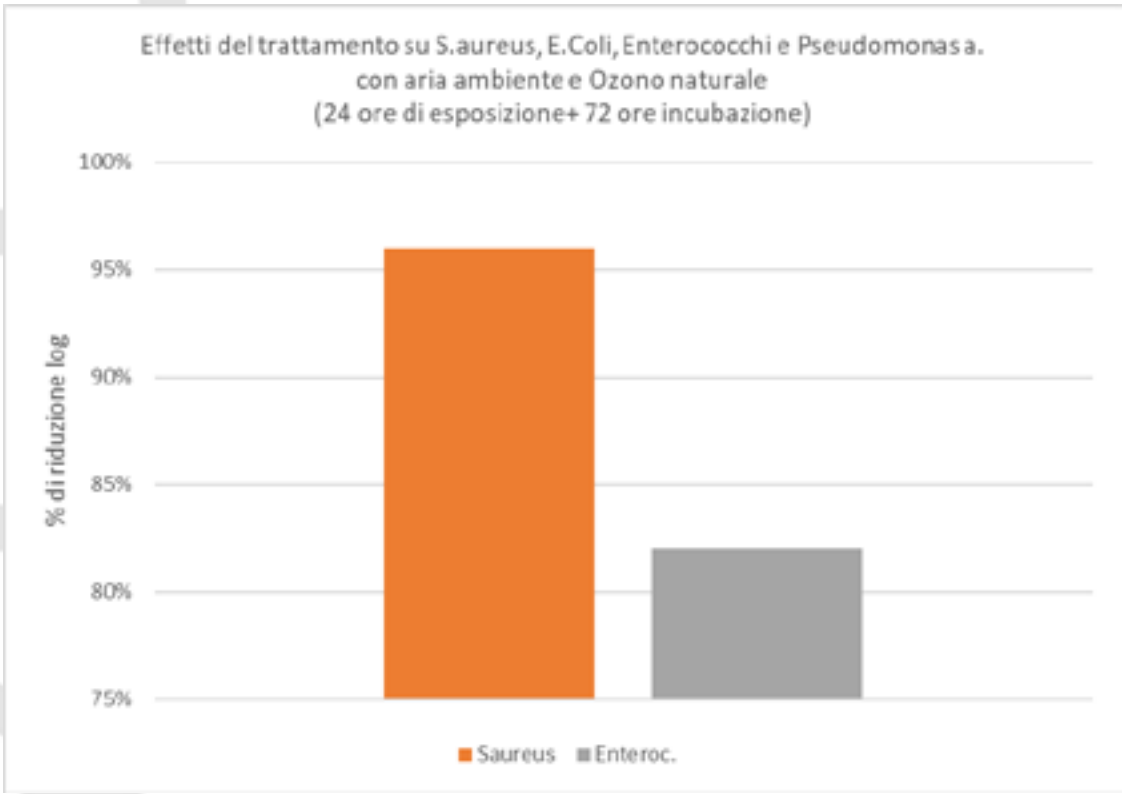

Confronto tra le riduzioni percentuali della crescita microbica tra i vari microrganismi testati

6 RIEPILOGO E CONCLUSIONI

La tabella seguente mette a confronto i risultati ottenuti con le varie prove. Sono riportati, quando disponibili, i dati ambientali di temperatura e umidità relativa (sia dell'ambiente in cui è avvenuto il trattamento che quello di controllo), oltre alla concentrazione di Ozono (naturale o generato dall'NTP) e il valore di riduzione percentuale di crescita microbica (R). Quest'ultimo valore nel caso delle prime due prove A e B è indicato come valore medio di quello rilevato alle tre distanze valutate.

Tabella riepilogativa dei risultati. N.r. non rilevato

i.d. prova	T°		UR (%)	O_3 (ppb)	R (%)			
	NTP	CTRL			GRAM NEGATIVI		GRAM POSITIVI	
					E. coli	P. aeruginosa	S. aureo	E. fecale
Prova A	19,7	25,2	42	45	7		100	
Prova B	n.r.	n.r.	58	24		26		90
Prova C	24,4	22,4	54	64			61	50
Prova D	24,7	23,7	80	47	29	68	69	94
Prova E	19,9	23,9	58	32			96	92

Come si rileva dalle celle colorate le % di Riduzione della carica microbica sono pressoché analoghe nel caso di esposizione a NTP "artificiale=Jonix" e di esposizione a NTP "naturale".

9 I CASE STUDY: STUDI SU APPLICAZIONI PRATICHE DEI SISTEMI SANIFICANTI INDOOR JONIX

9.1 Case study 1: riduzione impatti odorigeni su impianto gestione rifiuti

SCOPO: lo studio e l'analisi degli aspetti ambientali legati alle misure di impatto odorigeno correlate alla gestione dei rifiuti e alla realizzazione di una sperimentazione su scala pilota, relativamente al trattamento di effluenti gassosi al fine di ridurne efficacemente il carico odorigeno presente.

RISULTATI: Dai risultati presentati appare evidente come la tecnologia NTP abbia un effetto positivo nell'abbattimento delle specie presenti nel flusso gassoso generato da un rifiuto, con percentuali variabili tra il 25 e il 40%. Questo risultato è stato ottenuto mediante l'esecuzione di una complessa sperimentazione eseguita su un impianto pilota dotato di tecnologia NTP, effettuando il trattamento su differenti rifiuti e miscele degli stessi, ed impiegando come tecniche analitiche per la "quantificazione" dell'efficienza sia il Naso Elettronico che la Gascromatografia con rivelatore di Massa. I risultati così ottenuti offrono ampie prospettive di impiego di questa tecnologia come sistema di abbattimento, sia degli inquinanti di natura organica presenti in una emissione che per quanto concerne più nello specifico l'obiettivo del progetto, ovvero l'abbattimento delle molecole odorigene. Le molecole organiche, come è stato verificato in modo particolare sulle catene alifatiche e aromatiche attraverso le analisi condotte con la GC-MS, vengono abbattute fino a circa il 40%. Le sostanze odorigene, come è stato possibile verificare tramite l'impiego del Naso Elettronico, subiscono un decremento della loro concentrazione fino a percentuali pari al 30%. Un eventuale ulteriore sviluppo dello studio e della tecnologia proposta, potrebbe riguardare differenti matrici di rifiuti caratterizzati da impatti olfattivi dovuti a composti inorganici, quali ad esempio l'ammoniaca e l'acido solfidrico. In questi casi, le metodiche analitiche da applicare potrebbero essere il Naso Elettronico e tecniche specifiche per la determinazione di tali composti.

I dettagli della sperimentazione sono riportati in ALLEGATO 9.

9.2 Case study 2: Studio della sanificazione dell'aria in una clinica veterinaria

SCOPO: verificare l'efficacia della tecnologia Non Thermal Plasma in sanità Veterinaria. La sperimentazione è stata condotta presso una Clinica Veterinaria con l'obiettivo di ottenere una riduzione degli odori percepiti e riduzione della contaminazione microbica aero-trasportata in locali dove le concentrazioni potrebbero risultare significative e avere un impatto negativo su animali e persone. La sperimentazione ha previsto una

serie di campionamenti prima dell'installazione dei dispositivi, durante la normale attività della clinica per valutare le condizioni inziali, da comparare le misurazioni effettuate dopo l'accensione dei dispositivi Jonix.

RISULTATI: Nella sala degenza la tendenza rilevata indica una riduzione nel contenuto microbico totale e degli stafilococchi mentre i miceti vedono una leggera tendenza all'aumento, imputabile alle frequenti aperture delle porte che danno sull'esterno dell'edificio, circondato da siepi e piante. I punti di campionamento erano a circa 50 cm dalle aperture, di conseguenza l'aria aspirata era miscelata con quella proveniente dall'esterno. Nella sala di attesa si è avuta una linea di tendenza generale di leggero aumento nei parametri rilevati inizialmente per le promiscuità con la l'aria proveniente dall'aperura e chiusa delle porte. Risulta evidente l'effetto di riduzione batterica nel tempo, l'apporto prolungato all'aria di molecole ionizzanti fa si che l'aria diventi inospitale per i contaminanti. **L'effetto di deodorizzazione dell'aria è stato sensorialmente apprezzabile in entrambe le sale controllate**: l'odore presente si era ridotto in modo sensibile. Gli utenti hanno infatti percepito un'aria quasi priva di odori nella sala di attesa dopo l'accensione dei dispositivi Jonix. Al fine di poter condurre una valutazione più approfondita dell'affetto antimicrobico della ionizzazione, già documentato in bibliografia e con gli stessi dispositivi in altri ambiti, è necessario impostare un protocollo di ricerca in locali con un maggiore controllo delle variabili o con degli indicatori ambientali che risentano meno delle variabili in atto.

I dettagli della sperimentazione sono riportati in ALLEGATO 10.

9.3 Case study 3: Effetti sanitizzanti del dispositivo MATE nel settore della Grande Distribuzione Alimentare

SCOPO: valutare gli effetti di sanificazione presso un Ipermercato dove è stato installato un sistema di ionizzazione e filtrazione dell'aria modello JONIX MINIMATE, dispositivo di filtrazione sanificazione dell'aria. Il dispositivo è stato posizionato nella zona di confezionamento del reparto lavorazione carni.

RISULTATI: è risultato che il dispositivo Jonix Minimate ha ridotto le contaminazioni presenti in aria in modo significativo, nonostante l'influenza dell'aria proveniente dai locali adiacenti.

I dettagli della sperimentazione sono riportati in ALLEGATO 11.

9.4 Case study 4: Effetti sanitizzanti del dispositivo MATE nelle sale operatorie ospedaliere

SCOPO: studiare l'azione dell'armadio MATE sui livelli di contaminazione di due sale operatorie in una casa di cura privata.

RISULTATI: per le **superfici di lavoro**, i dati raccolti hanno evidenziato una sostanziale bassa contaminazione microbica, **l'impiego continuativo del MATE ha esercitato un'importante e significativa azione coadiuvante alle operazioni di detersione**, senza alcun impiego di ulteriori composti chimici da nebulizzare nell'ambiente.

Per quanto riguarda **l'aria ambiente**, è stato possibile rilevare una bassa contaminazione microbica contaminazione microbica aerodispersa, con la stesso tipologia di microrganismi isolati (esclusivamente CBT37 e sporadicamente SC+). Anche in questo caso l'aria ha mostrato la stessa tendenza in diminuzione, come se risultasse nel tempo sempre più protetta durante gli interventi (anche se il mate è spento) e la sua bonifica durante le ore notturne diventasse via via più efficace.

I dettagli della sperimentazione sono riportati in ALLEGATO 12.

9.5 Case study 5: Effetti sanitizzanti del dispositivo MATE nelle corsie di degenza ospedaliere

SCOPO: stabilire le potenzialità d'azione della tecnologia NTP anche nei confronti dei microrganismi potenzialmente rinvenibili all'interno delle corsie di degenza. Per questo scopo sono stati utilizzati dei sistemi ionizzanti di ridotte dimensioni appositamente disegnati per una loro collocazione meno "invasiva" e più facilmente inseribile in un contesto di vita abituale. Le attrezzature sono state collocate in diversi punti di una corsia e lasciate in funzione in maniera pressoché costante durante tutto il periodo di studio. Il confronto degli effetti è stato eseguito valutando i livelli di contaminazione in una corsia di "controllo" priva di sistemi NTP. In questo modo lo studio ha potuto risponde in modo efficace e estremamente pertinente all'esigenza di valutazione di sistemi innovativi per la prevenzione delle infezioni in sala operatoria in particolare, e delle infezioni ospedaliere in generale, permettendo di individuare una tecnologia in grado di affiancare le consuete attività di bonifica ambientale, massimizzandone l'efficacia e contribuendo a creare ambienti più sicuri e con minore rischio infettivo.

RISULTATI: In corsia è stato verificato un ABBATTIMENTO MEDIO* pari all'86% (* valori riferiti alla Carica Batterica totale aerodispersa L'uso della tecnologia NTP, con la sua capacità dimostrata in corsia di ridurre nel tempo la contaminazione microbica aerodispersa e di facilitare le operazione di sanificazione delle superfici, può con ogni probabilità contribuire anche al raggiungimento e mantenimento di migliori condizioni igienico-sanitarie, aiutando il management nella gestione del rischio clinico.

I dettagli della sperimentazione sono riportati in ALLEGATO 13.

10 CONCLUSIONI

In conclusione, **il plasma non termico può essere impiegato per inattivare una vasta gamma di microrganismi come batteri, spore, funghi, virus e prioni**.

Il meccanismo di interazione del plasma con i sistemi viventi è decisamente complesso e non è ben noto, sia a causa alla complessità della biologia che del plasma. In linea generale si ritiene che le specie cariche, in particolare gli ioni, svolgano un ruolo chiave nell'interazione tra cellule viventi (Dobrynin D., 2009), interagendo chimicamente e non attraverso fenomeni fisici come stress da taglio, danni da bombardamento ionico, effetti termici o da irraggiamento UV. Le particelle cariche potrebbero svolgere un ruolo significativo nella rottura delle membrane cellulari esterne, *specialmente nei batteri gram-negativi* che possiedono membrane esterne più sottili.

Anche i meccanismi specifici che portano all'inattivazione del virus da parte degli NTP non sono chiari. Studi hanno dimostrato che l'esposizione agli NTP provoca la modifica e / o la degradazione delle proteine virali e degli acidi nucleici e anche dei lipidi nei virus avvolti (Yasuda H., 2010). Inoltre, le specie reattive possono danneggiare l'RNA virale, portando a una riduzione dell'espressione genica e all'eliminazione dell'RNA virale.

L'uso dell'NTP nei processi di sanificazione appare interessante, a prescindere dall'interpretazione dei fenomeni, in quanto attivo ad ampio spettro. La tecnologia risulta quindi flessibile e facilmente applicabile a numerosi contesti, ed in particolare per la sanificazione degli ambienti indoor da particelle disperse in aria, per le quali le altre tecnologie risultano inadatte o inefficaci.

11 BIBLIOGRAFIA CITATA NEL TESTO

Alex Lindsay, B. B. (2014). Fertilization of Radishes, Tomatoes, and Marigolds Using a Large-Volume Atmospheric Glow Discharge. *Plasma Chem Plasma Process*, 34 1271 - 1290.

Arijana Filipić, I. G.-A. (2020). Cold plasma, a new hope in the field of virus inactivation . *Trends in Biotechnology*.

Arne M. Vandenbroucke, R. M. (2011). Non-thermal plasmas for non-catalytic and catalytic VOC abatement. *Journal of Hazardous Materials, 195*, 30 - 54.

Brandenburg, R. (2017). Dielectric barrier discharges: progress on plasma sources and on the understanding of regimes and single filaments. *Plasma Sources Sci. Technol. 26*, 053001 (29pp).

Brandenburg, R. K.-D. (2014). Plasma based pollutant degradation in gas streams: status, examples and outlook. *Contrib. Plasma Phys. 54,*, 202 - 214.

Bratislav M. Obradović, G. B. (2011). A dual-use of DBD plasma for simultaneous NOx and SO2 removal from coal-combustion flue gas. *Journal of Hazardous Materials volume 185, Issues 2–3*, 1280-1286.

Carlos M. Nunez, G. H. (2012). Corona Destruction: An Innovative Control Technology for VOCs and Air Toxics. *Waste*, 242-247.

Chulkyoon, P. P. (2016). Non-thermal plasmas (NTPs) for inactivation of viruses in abiotic environment. *Research Journal of Biotechnology* , Vol. 11 (6) .

Chulkyoon, P. P. (2016). Non-thermal plasmas (NTPs) for inactivation of viruses in abiotic environments. *Research Journal of Biotechnology*, Vol. 11 (6) .

CL Enloe, M. M. (2008). Time-correlated force production measurements of the dielectric barrier discharge plasma aerodynamic actuator. *Journal of applied physics, 103(7)*, 073302-073302.

Dayonna P. Park, K. D.-A. (2013). Reactive nitrogen species produced in water by non-equilibrium plasma increase plant growth rate and nutritional yield. *Current Applied Physics*, 13 S19 - S29.

Dobrynin D., F. G. (2009). Physical and biological mechanisms of direct plasma interaction with living tissue. *New J. Phys., 11*.

Hao Zhang, D. M. (2017). Non-thermal plasma technology for organic contaminated soil remediation: A review. *Chemical Engineering Journal (313)*, 157-170.

Harstad, J. (1969). Evaluation of air filters with submicron viral aerosols and bacterial aerosols. *American Industrial Hygiene Association Journal*.

Herrmann H.W., H. I. (1999). Decontamination of chemical and biological warfare, (CBW) agents using an atmospheric pressure plasma jet (APPJ). *Phys. Plasmas, 6*, 2284-2289 .

J. Han, B. P. (July 5-10, 2015). Non-equilibrium plasmas in agriculture. *22nd International Symposium on Plasma Chemistry*.

J. Karuppiaha, E. L. (2012). Abatement of mixture of volatile organic compounds (VOCs) in a catalytic non-thermal plasma reactor. *Journal of Hazardous Materials (2012)* , 283– 289.

K. Urashima, J. C. (2000). Removal of volatile organic compounds from air streams and industrial flue gases by non-thermal plasma technology. *IEEE Transactions on Dielectrics and Electrical Insulation (Volume: 7, Issue: 5)*, 602 - 614.

Kim, H. (2004). Nonthermal plasma processing for air-pollution control: a historical review, current issues, and future prospects. *Plasma Processes and Polymers*, 91-110.

Kong M.G., K. G. (2009). Plasma medicine: an introductory review. *New J. Phys., 11*.

Laroussi, M. (2005). Low temperature plasma-based sterilization: Overview and state-of-the-art. *Plasma Process Polym.*, 391-400.

Leipold, M. L. (2004). Evaluation of the roles of reactive species, heat, and UV radiation in the inactivation of bacterial cells by air plasmas at atmospheric pressure. *nternational Journal of Mass Spectrometry, 233 (1–3)*, 81-86.

M. Laroussi, F. (2004). Evaluation of the roles of reactive species, heat, and UV radiation in theinactivation of bacterial cells by air plasmas at atmospheric pressure. *International Journal of Mass Spectrometry 233*, 81–86.

Marco Schiavon, M. S. (2015). Potential of non-thermal plasmas for helping the biodegradation of volatile organic compounds (VOCs) released by waste management plants. *Journal of Cleaner Production 104*, 211 - 219.

Marco Schiavon, M. S. (2017). Non-thermal plasma assisting the biofiltration of volatile organic compounds. *Journal of Cleaner Production 148*, 498-508.

Michael J. Gallagher, A. G. (2004). Non-thermal plasma application in air sterilization. *Conference Paper in IEEE International Conference on Plasma Science*.

Mráz, P. B. (2014). EFFECT OF LOW-TEMPERATURE PLASMA TREATMENT ON THE GROWTH AND REPRODUCTION RATE OF SOME PLANT PATHOGENIC BACTERIA. *Journal of Plant Pathology*, 96 (1), 63-67.

Oda, T. (2003). Non-thermal plasma processing for environmental protection: decomposition of dilute VOCs in air. *J. Electrostat 57*, 293-311.

Osman Karatum, M. A. (2016). A comparative study of dilute VOCs treatment in a non-thermal. *Chemical Engineering Journal 294*, 308-315.

Osman Karatum, M. A. (2016). A comparative study of dilute VOCs treatment in a non-thermal plasma reactor. *Chemical Engineering Journal 294*, 308–315.

Penetrante, B. S. (2011). Non-thermal plasma techniques for pollution control: Part A-overview, fundamentals and supporting technologies and part B-electron beam and electrical discharge processing. *NATO ASI Ser Ser G 84*, 1296–1300.

S. Schmid, M. J. (2010). Degradation of volatile organic compounds in a non-thermal plasma air purifier. *Chemosphere*, 124 - 130.

Sang-Hye Ji, K.-H. C.-H. (2016). Effects of high voltage nanosecond pulsed plasma and micro DBD plasma on seed germination, growth development and physiological activities in spinach. *Archives of Biochemistry and Biophysics 605*, 117 - 128.

Schiavon, M. R. (2016). Comparison between conventional biofilters and biotrickling filters applied to waste bio-drying in terms. *Environ. Technol. 37*, 975-982.

Schiavon, M. T. (2017). Non-thermal Plasma as an Innovative Option for the Abatement of Volatile Organic Compounds: a Review. *Water Air Soil Pollut* , 228,388.

Seinfeld, J., & Pandis, S. (1998). Atmospheric Chemistry and Physics. From Air Pollution to. In *John Wiley & sons, inc.* .

U. Kogelschatz, B. E. (1997). Dielectric-Barrier Discharges. Principle and Applications . *Journal de Physique IV Colloque, 07*, C4-47-C4-66.

Wen-Jun Liang, H.-P. F.-X.-Q. (2011). Performance of non-thermal DBD plasma reactor during the removal of hydrogen sulfide. *Journal of Electrostatics Volume 69, Issue 3*, 206-213.

Wu Y., L. Y. (2015). MS2 virus inactivation by atmospheric-pressure cold plasma using different gas carriers and power levels. *Appl. Environ. Microbiol., 81*, 996-1002.

Yasuda H., M. T. (2010). A., Biological evaluation of DNA damage in bacteriophages inactivated by atmospheric pressure cold plasma. *Plasma Process Polym., 7*, 301–308 .

Zulfam Adnana, S. M. (2017). Exhaust gases depletion using non-thermal plasma (NTP). *Atmospheric Pollution Research (volume 8 issue 2)*, 338-343.

12 ALLEGATI

12.0 ALLEGATO 0 – Report Test di Efficacia Battericida nei confronti di batteri MDR

12.1 ALLEGATO 1 – Report efficacia virucida “Prova quantitativa in sospensione per la valutazione dell’attività virucida del virus SARS-CoV-2” Dip. di Medicina Molecolare, Università degli studi di Padova

12.2 ALLEGATO 2 - Studio di laboratorio sull’attività biocida delle specie ossidanti formate via NTP

12.3 ALLEGATO 3 - Studio di laboratorio sugli effetti sanificanti prodotti da un MATE - Jonix

12.4 ALLEGATO 4 - Utilizzo della tecnologia NTP nei confronti delle maleodoranze che si associano all’utilizzo delle calzature

12.5 ALLEGATO 5 - Sanificazione di sonde ecografiche non critiche

12.6 ALLEGATO 6 - Studi di laboratorio sull’abbattimento di VOC via NTP: review

12.7 ALLEGATO 7 - Prova per la valutazione dell’efficacia di riduzione di microrganismi intenzionalmente inoculati in piastre utilizzando il sistema di ionizzazione di aria Mate di Jonix

12.8 ALLEGATO 8- Studio del potere sanificante di un dispositivo Jonix applicato ad un fan coil commerciale

12.9 ALLEGATO 9 - Sperimentazione per la verifica della capacità sanitizzante di dispositivi Fotocatalitici in confronti a sistemi Jonix NTP

12.10 ALLEGATO 10 - Case study 1: riduzione impatti odorigeni su impianto gestione rifiuti

12.11 ALLEGATO 11 - Case study 2: Studio della sanificazione dell’aria in una clinica veterinaria

12.12 ALLEGATO 12 - Case study 3: Effetti sanitizzanti del dispositivo MATE nel settore della Grande Distribuzione Alimentare

12.13 ALLEGATO 13 - Case study 4: Effetti sanitizzanti del dispositivo MATE nelle sale operatorie ospedaliere

12.14 ALLEGATO 14 - Case study 5: Effetti sanitizzanti del dispositivo MATE nelle corsie di degenza ospedaliere

Allegato 0

Report Test di Efficacia Battericida nei confronti di batteri MDR

DMM Dipartimento di Medicina Molecolare

1222·2022 800 ANNI

UNIVERSITÀ DEGLI STUDI DI PADOVA

Via A. Gabelli 63 - 35121 Padova
C.F. 80006480281 - P.IVA 00742430283

REPORT TEST DI EFFICACIA BATTERICIDA

Prova quantitativa in sospensioneper la valutazione dell'attività biocida nei confronti di batteri MDR

PRODOTTO:

JONIX CUBE
un dispositivo di purificazione dell'aria

COMMITTENTE

Jonix S.r.l.. Indirizzo: Viale Spagna, 31/33 - 35020 Tribano (PD)
P.Iva e C.F. 04754080283

RESPONSABILE SCIENTIFICO

Prof. Andrea Crisanti

Collaboratori: dott.ssa Claudia Del Vecchio, dott.ssa Manuela Sciro e dott. Giuseppe Di Pietra

Data Report: 28/05/2021

Sede di *Microbiologia e Virologia*
Via A. Gabelli 63 - 35121 Padova, Italy · Tel. 049 8212545 - Fax 049 8272355

Via A. Gabelli 63 - 35121 Padova
C.F. 80006480281 - P.IVA 00742430283

INDICE

Sede di *Microbiologia e Virologia*
Via A. Gabelli 63 - 35121 Padova, Italy - Tel. 049 8212545 - Fax 049 8272355

Via A. Gabelli 63 - 35121 Padova
C.F. 80006480281 - P.IVA 00742430283

1. SCOPO

Il seguente report ha la finalità di definire in modo chiaro e dettagliato le modalità di esecuzione dell'analisi in maniera da garantire massima precisione e accuratezza in conformità alla norma europea UNI EN 17272:2020. Tale norma, impiegata per la validazione di disinfettanti chimici e antisettici, è stata impiegata per la verifica dell'attività battericida di strumentazione che utilizza la tecnologia Non Thermal-Plasma, o plasma freddo. L'attività battericida è stata eseguita impiegando un ceppo di controllo di *Escherichia coli* e in successione dei ceppi di microorganismi MDR (MultiDrug Resistant).

2. TERMINI E DEFINIZIONI

Attività battericida: capacità di un prodotto di produrre una riduzione del numero di colonie batteriche tramite procedure sperimentali che comprendono precise e definite condizioni di prova.

Unità Formanti Colonie (UFC): numero di colonie per mL.

Airborne disinfection contact (ADC) time: tempo che intercorre dal primo rilascio del prodotto al punto in cui i carriers sono recuperati.

Microrganismo sensibile: microrganismo in cui l'essiccamento causa una riduzione logaritmica maggiore di 1,5.

3. INTRODUZIONE

Il metodo di prova per verificare l'attività battericida del dispositivo Jonix Cube (prodotto test) nei confronti di batteri MDR è stata condotta in conformità alla norma Europea UNI EN 17272:2020 disinfettanti chimici e antisettici- Metodo per la disinfezione ambientale mediante processi automatici. Il plasma freddo in aria produce un cocktail di specie reattive primarie (ioni, elettroni, specie radicaliche, molecole ossidanti) responsabili di numerosi processi chimici e fisici (tra cui l'ossidazione) e innescano reazioni a catena producendo a loro volta altre molecole eccitate, radicali liberi e particelle reattive (specie reattive secondarie). Tali specie reattive prodotte complessivamente dal plasma freddo (specie reattive primarie e secondarie) possono esplicare una azione biocida nei confronti di microrganismi.

Via A. Gabelli 63 - 35121 Padova
C.F. 80006480281 - P.IVA 00742430283

4. CARATTERIZZAZIONE DEL CAMPIONE

Prodotto: Dispositivo Non Thermal-Plasma Jonix Cube (di seguito denominata Jonix Cube)

Descrizione del prodotto: Jonix CUBE è un dispositivo di purificazione dell'aria; di design che sfrutta una tecnologia avanzata chiamata a plasma freddo per eliminare batteri, muffe, virus, inquinanti e odori

Condizioni di stoccaggio: temperatura ambiente

Istruzioni strumentazione: vedasi allegato

5. CONDIZIONI SPERIMENTALI

Temperatura test: 20 ± 2 °C

Umidità relativa (RH): 50-75%

Tempo di contatto: 12 h - 14 h - 16 h

Periodo di Analisi: data inizio del test: 25-05-2020 ÷ Data fine test 28-05-2021

6. MATERIALI E REAGENTI

Microrganismi usati in fase sperimentale:

- ***Ceppo di Escherichia coli* ATCC 10536**: *Escherichia coli* è un bacillo Gram-negativo. Costituisce parte integrante della normale flora intestinale dell'uomo e di altri animali. Nonostante la maggior parte dei ceppi di E. coli siano innocui, ne esistono tuttavia alcuni che mettono a rischio la salute umana.
- ***Ceppo di Acinetobacter baumannii* MDR:** ceppo produttore di carbapenemasi tipo OXA-23. *Acinetobacter baumanni* è un bacillo Gram-negativi ubiquitario. Presenta una sopravvivenza di circa un mese sulle superfici asciutte.
- ***Klebsiella pneumoniae* MDR:** ceppo produttore di carbapenemasi tipo KPC. *Klebsiella pneumoniae* è un bacillo Gram-negativo in grado di provocare polmonite batterica, sebbene sia più comunemente coinvolta in infezioni acquisite in ospedale nel tratto urinario. *Klebsiella pneumoniae* è diventata una infezione nosocomiale in crescita dato che continuano ad apparire ceppi antibiotico-resistenti.
- ***Pseudomonas aeruginosa* MDR:** ceppo produttore di carbapenemasi tipo OXA-48. *Pseudomonas aeruginosa* è un bacillo Gram-negativo ubiquitario. È causa di numerosi tipi di infezioni.

Via A. Gabelli 63 - 35121 Padova
C.F. 80006480281 - P.IVA 00742430283

*ATCC (American Type Culture Collections)

MEZZI DI COLTURA E REAGENTI

I reagenti utilizzati sono puri per analisi e/o adatti per applicazioni microbiologiche.

Terreno di coltura per conta batterica

Il terreno di coltura utilizzato per la conta delle cellule è il TSA (Tryptone Soya Agar).

Diluente per sospensioni microbiche

Il diluente per le sospensioni microbiche, preparato come da norma UNI EN 17272:2020, è stato utilizzato per preparare la sospensione microbica e per effettuare le diluizioni previste dalla norma sopra indicata.

7. APPARECCHIATURE

- Carriers in acciaio
- DensiCheck Plus Biomerieux
- Cronometro
- Agitatore Vortex
- Incubatore a temperatura controllata di 36°C ± 1°C.
- Cappa a flusso laminare verticale "BioHazard" classe II
- pHmetro
- Frigorifero a temperatura controllata di 4°C
- Pipette graduate
- Piastre Petri
- Bilancia
- Becker
- Scrapers

Via A. Gabelli 63 - 35121 Padova
C.F. 80006480281 - P.IVA 00742430283

8. TEST DI EFFICACIA

PREPARAZIONE DELLA SOSPENSIONE BATTERICA

Sospensione batterica

Dalla coltura madre è stata preparata una subcultura in TSA incubata a 37 ± 1 °C per 18-24 ore. È stato ripetuto il passaggio e incubato per altre 24 ore. Infine, è stata generata una terza subcultura dalla seconda (II e III subcultura sono considerate working colture). Dalla working colture è stata prelevata un'ansata ed è stata trasferita all'interno di una provetta contenente il diluente per le sospensioni microbiche fino ad ottenere 0,5 McF con DensiCheck Plus Biomerieux corrispondente a 1 x 10^8 ufc/mL.

Sostanza interferente

Alla sospensione è stata aggiunta la sostanza interferente (BSA 3g/l) in modo da ottenere una diluizione 1/10, e, in seguito è stato eseguito un adattamento per microrganismi sensibili, addizionando il latte scremato (100g/l) in concentrazione 1:20.

DETERMINAZIONE DEL TITOLO

Per determinare il titolo della sospensione madre, sono state allestite delle diluizioni seriali fino a 10^{-8}. 1 ml della diluizione 10^{-6}, 10^{-7} e 10^{-8} è stata inclusa in agar TSA. Inoltre, 1 ml della diluizione 10^{-6}, 10^{-7} e 10^{-8} è stata filtrata attraverso l'uso di membrane filtranti.

Tutte le prove sono state condotte in doppio.

VALUTAZIONE DEL PROCESSO DI DISINFEZIONE

Sopravvivenza del microrganismo test nei carriers di controllo

I carriers di controllo sono stati inseriti all'interno di piastre Petri senza coperchio e contaminati con 50 µl di sospensione microbica, la quale è stata poi ben distribuita e sottoposta ad asciugatura. Al termine

Via A. Gabelli 63 - 35121 Padova
C.F. 80006480281 - P.IVA 00742430283

del periodo di asciugatura è stato applicato il coperchio della piastra corrispondente. Ogni piastra, contente il carrier di controllo, è stata lasciata in laboratorio per tutta la durata del periodo di esposizione. Al termine del periodo di esposizione i carriers di controllo sono stati trasferiti all'interno di un becker contenente 100 ml di diluente per sospensioni microbiche. A una prima fase di scraping, durata 1 minuto, è seguita una seconda fase di agitazione meccanica per permettere il distacco di eventuali microrganismi rimasti adesi al carrier. Dalla soluzione ottenuta sono state eseguite le diluizioni seriali fino a 10^{-3}. 1 ml della diluizione 10^{-2} e 1 ml della diluizione 10^{-3} sono state seminate in terreno TSA con la tecnica dell'inclusione; tali prove sono state condotte in doppio. Le piastre sono state riposte in incubatore a 37 ± 1 °C per 24 ore, per la prima conta, e reincubate altre 24 ore per la seconda conta.

Test preparatori per valutare l'assenza di effetti residui

Per valutare l'assenza di effetti residui, 50 µl di sostanza interferente sono stati depositati in altri carriers. A completa asciugatura i carriers sono stati inseriti nella teca per essere esposti all'azione dell'NTP. Al termine del periodo di esposizione i carriers sono stati trasferiti all'interno di un becker contenente 100 ml di diluente per sospensioni microbiche. A una prima fase di scraping, durata 1 minuto, è seguita una seconda fase di agitazione meccanica per permettere il distacco di eventuali microrganismi rimasti adesi al carrier, ottenendo così una soluzione, definita S.

È stato poi effettuato uno screening per valutare eventuali effetti inibitori in agar, pertanto, 1 ml della soluzione S è stata inclusa in agar TSA insieme ad 1 ml di sospensione batterica nota. La piastra è stata incubata a 37 ± 1 °C per 24 ore, per la prima conta, e reincubata altre 24 ore per la seconda conta. È stato eseguito un ulteriore screening per valutare eventuali effetti inibitori con le membrane filtranti. Per farlo 98 ml di soluzione S sono stati filtrati con membrane filtranti da 0,45 µm a cui sono seguiti 3 lavaggi con 50 ml di diluente per sospensioni microbiche. Successivamente 1 ml di diluizione della sospensione microbica nota è stato filtrato. La membrana è stata trasferita su una piastra contenente agar TSA ed è stata incubata a 37 ± 1 °C per 24 ore, per la prima conta, e reincubata altre 24 ore per la seconda conta. Infine, per valutare un possibile effetto inibitorio correlato al carrier è stato trasferito 1 ml di sospensione microbica nota insieme al carrier esposto in una piastra Petri. È stato aggiunto l'agar e la piastra è stata incubata a 37 ± 1 °C per 24 ore, per la prima conta, e reincubata altre 24 ore per la seconda conta.

I test preliminari sono stati condotti per ogni microrganismo testato.

Sede di *Microbiologia e Virologia*
Via A. Gabelli 63 - 35121 Padova, Italy · Tel. 049 8212545 - Fax 049 8272355

Via A. Gabelli 63 - 35121 Padova
C.F. 80006480281 - P.IVA 00742430283

Test di efficacia

Esposizione dei carriers al prodotto test

I carriers sono stati posizionati all'interno di piastre Petri vuote. Sono stati depositati 50 µl di sospensione microbica (carriers contaminati), in seguito ben distribuita sul carrier tramite l'utilizzo di un'ansa, e sono stati tenuti sotto cappa fino a completa asciugatura della sospensione microbica.

Quando la sospensione microbica si è asciugata completamente i carriers da esporre all'NTP sono stati inseriti nella teca fornita con il coperchio aperto, in posizione opposta alla localizzazione del dispositivo test, per permettere l'esposizione dei carriers al prodotto test. La durata dell'esposizione è stata ponderata in funzione dei risultati ottenuti.

Recupero dei carriers

I carriers esposti sono stati depositati all'interno di un becker contenente 100 ml di diluente per sospensioni microbiche. A una prima fase di scraping, durata 1 minuto, è seguita una seconda fase di agitazione meccanica per permettere il distacco di eventuali microrganismi rimasti adesi al carrier, ottenendo così una soluzione. 1 ml di soluzione è stata utilizzata per eseguire una semina diretta per inclusione in TSA; successivamente la piastra è stata incubata a 37 ± 1 °C per 24 ore, per la prima conta, e reincubata altre 24 ore per la seconda conta. 10 ml di soluzione sono stati filtrati con membrane filtranti da 0,45 µm a cui sono seguiti 3 risciacqui con liquido di recupero. La membrana è stata poi traferita in una piastra TSA che è stata incubata a 37 ± 1 °C per 24 ore, per la prima conta, e reincubata altre 24 ore per la seconda conta. Infine, il carrier è stata trasferito in una piastra TSA a cui è stata poi aggiunto altro agar TSA per coprire completamente il carrier. La piastra è stata incubata a 37 ± 1 °C per 24 ore, per la prima conta, e reincubata altre 24 ore per la seconda conta.

9. RISULTATI

Via A. Gabelli 63 - 35121 Padova
C.F. 80006480281 - P.IVA 00742430283

Escherichia coli ATCC 10536

Nella prima fase sperimentale è stato effettuato il test di efficacia su *E. coli* ATCC 10536 come richiesto dalla norma UNI EN 17272:2020 per valutare l'efficacia del prodotto test su un microrganismo noto.

Microrganismo test	Titolo della sospensione iniziale (ufc/mL)	Test di validazione	Titolo della sospensione del carrier di controllo (ufc/mL)	Riduzione Logaritmica (R)
E. coli ATCC 10536 12 h	$4{,}55 \cdot 10^8$	Valido	$1{,}46 \cdot 10^6$	6.2
E. coli ATCC 10536 14 h		Valido	$1{,}45 \cdot 10^6$	5.9
E. coli ATCC 10536 16 h		Valido	$1{,}44 \cdot 10^6$	6.2

Tabella 1 - E. coli - Esposizione all'NTP per 12, 14 e 16 ore.

Dimostrato che i requisiti della norma con *E. coli* ATCC 10536 vengono rispettati, si è proseguita la fase sperimentale testando dei ceppi di microorganismi Gram Negativi multiresistenti (MDR): *K. pneumoniae* KPC, *A. baumannii* OXA-23 e *P. aeruginosa* OXA-48.

Klebsiella pneumoniae MDR

Microrganismo test	Titolo della sospensione iniziale (ufc/mL)	Test di validazione	Titolo della sospensione del carrier di controllo (ufc/mL)	Riduzione Logaritmica (R)
K. pneumoniae KPC 12 h	$4{,}45 \cdot 10^8$	Valido	$1{,}61 \cdot 10^6$	6.2
K. pneumoniae KPC 14 h		Valido	$1{,}38 \cdot 10^6$	6.1

Sede di *Microbiologia e Virologia*
Via A. Gabelli 63 - 35121 Padova, Italy · Tel. 049 8212545 - Fax 049 8272355

Via A. Gabelli 63 - 35121 Padova
C.F. 80006480281 - P.IVA 00742430283

K. pneumoniae KPC 16 h		Valido	1,83· 10^6	6.3

Tabella 2. – K. pneumoniae - Esposizione all'NTP per 12, 14 e 16 ore.

Acinetobacter baumanii MDR

Microrganismo test	Titolo della sospensione iniziale (ufc/mL)	Test di validazione	Titolo della sospensione del carrier di controllo (ufc/mL)	Riduzione Logaritmica (R)
A. baumanni OXA-23 12 h	4,93 · 10^8	Valido	3,93 · 10^6	3.1
A. baumanni OXA-23 14 h		Valido	2,45· 10^6	4.1
A. baumanni OXA-23 16 h		Valido	2,56· 10^6	6.4

Tabella 3. A. baumannii - Esposizione all'NTP per 12, 14 e 16 ore.

Pseudomonas aeruginosa MDR

Microrganismo test	Titolo della sospensione iniziale (ufc/mL)	Test di validazione	Titolo della sospensione del carrier di controllo (ufc/mL)	Riduzione Logaritmica (R)
P. aeruginosa OXA-48 12 h	2,59 · 10^8	Valido	1,17 · 10^6	4.1
P. aeruginosa OXA-48 14 h		Valido	1,13 · 10^6	4.8
P. aeruginosa OXA-48 16 h		Valido	1,15· 10^6	6.1

Tabella 4. P. aeruginosa - Esposizione all'NTP per 12, 14 e 16 ore.

Via A. Gabelli 63 - 35121 Padova
C.F. 80006480281 - P.IVA 00742430283

10. EFFICACIA BATTERICIDA

Il prodotto in esame è considerato **battericida** quando, dopo il tempo di contatto, si assiste ad una **riduzione della vitalità di almeno 10^5,** corrispondenti a una riduzione pari a 5 logaritmi nei confronti del ceppo batterico test in base al metodo e ai criteri di accettabilità della UNI EN 17272:2020.

Per ottenere la riduzione della carica batterica (R) è stato effettuato il logaritmo del rapporto tra i microrganismi presenti sul carrier di controllo e i microrganismi sopravvissuti nel carrier dopo esposizione all'NTP.

11. CONCLUSIONI

I risultati ottenuti hanno dimostrato che il dispositivo è efficace già a partire dalle 12 ore, determinando una riduzione della carica batterica totale sia per il ceppo di *E. coli* ATCC 10536 (R>5) che per il ceppo di *K. pneumoniae* KPC (R>5).

Per i ceppi di *A. baumannii* OXA-23 e *P. aeruginosa* OXA-48 la riduzione della carica batterica non è sufficiente a dimostrare l'efficacia del dispositivo dopo 12 ore (rispettivamente R=3,1 e R=4,1) e 14 ore (rispettivamente R=4,1 e R=4,8) di esposizione. Tuttavia dopo 16 ore di esposizione per entrambi i microrganismi la riduzione della carica batterica è totale, dimostrando l'efficacia del dispositivo, con R>5.

I risultati ottenuti dimostrano che il dispositivo Jonix Cube presenta un'efficace attività batterica nei confronti di diversi microrganismi multidrug resistant dopo una fase di esposizione microrganismo-correlata.

12. RIFERIMENTI

Sede di *Microbiologia e Virologia*
Via A. Gabelli 63 - 35121 Padova, Italy · Tel. 049 8212545 - Fax 049 8272355

Via A. Gabelli 63 - 35121 Padova
C.F. 80006480281 - P.IVA 00742430283

- NORMA EUROPEA UNI EN 17272:2020 Disinfettanti chimici e antisettici –Metodo per la disinfezione ambientale mediante processi automatici
- NORMA EUROPEA EN 14476:2019 Disinfettanti chimici e antisettici -Prova quantitativa in sospensione per la valutazione dell'attività virucida in area medica
- ISO 15189:2012 Medical laboratories — Requirements for quality and competence

Si ricorda che:

- ***1. Il sigillo istituzionale dell'Università è di proprietà esclusiva dell'Università di Padova.***
- ***2. Ai sensi dell'art.12 del Regolamento per le attività eseguite dall'Università degli Studi di Padova a fronte di contratti o di accordi con soggetti pubblici o privati, l'eventuale utilizzo del nome o dei segni distintivi dell'Università da parte di terzi deve essere oggetto di specifici accordi approvati dal Consiglio di amministrazione e dal Senato Accademico compatibili con la tutela dell'immagine dell'Ateneo.***
- ***3. Qualora il Committente, intenda immettere in commercio o comunque utilizzare a scopi commerciali, i risultati o parte di essi, il Committente medesimo dovrà intendersi come unico responsabile degli eventuali danni, diretti o indiretti, a qualunque titolo derivanti dalle attività connesse alla immissione in commercio o, comunque, all'utilizzazione commerciale da parte di terzi dei suddetti Risultati, senza che alcuna pretesa possa essere avanzata nei confronti dell'Università.***

Il Responsabile Scientifico
(dott.ssa Claudia Del Vecchio)

Il Direttore del Dipartimento
(Prof Andrea Crisanti)

Sede di *Microbiologia e Virologia*
Via A. Gabelli 63 - 35121 Padova, Italy · Tel. 049 8212545 - Fax 049 8272355

Escherichia coli

Klebsiella pneumoniae

Acinetobacter baumannii

Pseudomonas aeruginosa

Allegato 1

Report efficacia virucida "Prova quantitativa in sospensione per la valutazione dell'attività virucida del virus SARS-CoV-2" Dip. di Medicina Molecolare, Università degli studi di Padova

DMM Dipartimento di Medicina Molecolare

1222·2022 800 ANNI

UNIVERSITÀ DEGLI STUDI DI PADOVA

Via A. Gabelli 63 - 35121 Padova
C.F. 80006480281 - P.IVA 00742430283

REPORT EFFICACIAVIRUCIDA

Prova quantitativa in sospensioneper la valutazione dell'attività virucida nei confronti del virus *SARS-CoV-2*

PRODOTTO:

JONIX CUBE
un dispositivo di purificazione dell'aria

COMMITTENTE
Jonix S.r.l.. Indirizzo: Viale Spagna, 31/33 - 35020 Tribano (PD)
P.Iva e C.F. 04754080283

RESPONSABILE SCIENTIFICO:
Prof. Andrea Crisanti
Collaboratori: dott.ssa Claudia Del Vecchio, dott.ssa Manuela Sciro, dott. Di Pietra Giuseppe

Data Report: 22/09/2020

Via A. Gabelli 63 - 35121 Padova
C.F. 80006480281 - P.IVA 00742430283

INDICE

Via A. Gabelli 63 - 35121 Padova
C.F. 80006480281 - P.IVA 00742430283

1. SCOPO

Il seguente report ha la finalità di definire in modo chiaro e dettagliato le modalità di esecuzione e i risultati dello studio svolto per la verifica dell'attività virucida su superfici di strumentazione che utilizza la tecnologia del plasma freddo (Non Thermal Plasma) emettendo specie ossidanti.

2. TERMINI E DEFINIZIONI

Attività virucida o antivirale: capacità di un prodotto di produrre una riduzione del numero di particelle virali infettanti tramite procedure sperimentali che comprendono precise e definite condizioni di prova.

Unità Formanti Placche (PFU): numero di particelle virali infettanti per mL.

ID_{50}: dose infettante il 50% di sospensione virale o della diluizione della sospensione virale che induce nelle colture cellulare il 50% di effetto citotossico virale (CPE).

Effetto citotossico virale (CPE): alterazione morfologica delle cellule e/o la loro distruzione conseguente alla moltiplicazione del virus.

Inattivazione dei virus: riduzione dell'infettività di un virus nei confronti del prodotto in esame.

3. INTRODUZIONE

Al fine di garantire la massima precisione e accuratezza il test è stato eseguito in conformità alla norma EN 14476:2019 "Disinfettanti chimici e antisettici- prova quantitativa in sospensione per la valutazione dell'attività virucida in area medica- Metodo di prova e requisiti (Fase2/Stadio1)" e alla norma EN 17272:2020 "Disinfettati chimici e antisettici: metodi di disinfezione dell'aria indoor attraverso processi automatizzati – Determinazione delle attività battericida, micobattericida, sporicida, fungicida, lievicida , virucida e fagocita" (limitatamente all'utilizzo dei supporti metallici descritti).

L'attività virucida è stata testata impiegando il ceppo di SARS-CoV-2. Tutti gli esperimenti sono stati condotti in Laboratorio di Biosicurezza livello 3 (BSL3).

Via A. Gabelli 63 - 35121 Padova
C.F. 80006480281 - P.IVA 00742430283

4. CARATTERIZZAZIONE DEL CAMPIONE

Prodotto: Dispositivo Non thermal Plasma Jonix Cube (di seguito denominata Jonix Cube)

Descrizione del prodotto: Jonix CUBE è un dispositivo di purificazione dell'aria; di design che sfrutta una tecnologia avanzata chiamata a plasma freddo per eliminare batteri, muffe, virus, inquinanti e odori

Condizioni di stoccaggio: temperatura ambiente

Istruzioni strumentazione: vedasi allegato

5. CONDIZIONI SPERIMENTALI

Temperatura test: è stato eseguito a +20°C ± 1°C.

Tempo di contatto: 30'-60'-120'-240'

Periodo di Analisi: data inizio del test: 01-08-2020 ÷ Data fine test 01-09-2020

6. MATERIALI E REAGENTI

Microrganismi di prova:

SARS-CoV 2

Linea cellulare:

VERO E 6 (ATCC CCL-81)*

*ATCC (American Type Culture Collections)

Sospensione stock virale

Via A. Gabelli 63 - 35121 Padova
C.F. 80006480281 - P.IVA 00742430283

Ogni sospensione virale è stata preparata e amplificata su larga scala in colture cellulari in monostrato. Dopo l'infezione e la moltiplicazione del virus, i detriti cellulari sono stati allontanati mediante doppia centrifugazione a bassa velocità (2500 rpm per 10 min), ed il surnatante, contenente il virus, è prelevato per determinare il titolo virale. È stato suddiviso in aliquote a titolo noto di 2 ml di volume in eppendorf e conservato alla temperatura di - 80°C in congelatore.

Colture cellulari

Cellule VERO E6, cellule di origine epiteliale, provenienti da rene di scimmia (linea continua).

Supporti (carriers)

Sono stati impiegati dischi di acciaio INOX AISI 316 da 35 mm di diametro, preventivamente sterilizzati in autoclave.

MEZZI DI COLTURA E REAGENTI

I reagenti devono essere puri per analisi e/o adatti per applicazioni microbiologiche.

Terreno di coltura delle colture cellulari

Ogni linea cellulare è mantenuta in un termostato a 37°C con il 5% (v/v) di CO_2 in terreno DMEM (Dulbecco's Modified Eagle Medium) addizionate con il 10% (v/v) di siero fetale bovino (FBS) e 1% (p/v) di penicillina - streptomicina (pen- strep).

Phosphate Buffered Saline (PBS)

Soluzione contenente: 8 g di NaCl, 0,2 g di KCl, 2,89 g Na_2HPO_4 12 H_2O, 0,20 g KH_2PO_4 in 1000 ml di H_2O distillata.

7. APPARECCHIATURE

- Microscopio invertito per l'osservazione delle colture cellulari
- Cronometro
- Agitatore Vortex

Via A. Gabelli 63 - 35121 Padova
C.F. 80006480281 - P.IVA 00742430283

- Centrifuga
- Incubatore a CO2 (5% v/v) in grado di mantenere la temperatura a 37°C ± 1°C.
- Cappa a flusso laminare verticale "BioHazard" classe II
- Congelatori

8. PROVE PRELIMINARI

PREPARAZIONE DELLA SOSPENSIONE VIRALE - TITOLO VIRALE

0,2 ml di sospensione virale (soluzione madre) + 1,8 ml di DMEM serum-free sono stati miscelati e preparate diluizioni seriali da 10^{-2} a 10^{-9} (diluizioni 1:10).

250 µl di ogni diluizione è stato trasferito in piastre a 24 pozzetti contenenti il monostrato cellulare a confluenza (>90%) dopo aspirazione del terreno di coltura. Ogni diluizione della sospensione virale è stata piastrata in sestuplo. Sono stati lasciati senza inoculo 12 pozzetti, (controllo della linea cellulare). Dopo 1 ora di incubazione a 37°C (tempo di adsorbimento virale), l'inoculo è stato rimosso, effettuato un lavaggio con PBS e aggiunti 500 µl di DMEM addizionati di 2% (v/v) FBS e 0,75% (v/v) di carbossimetilcellulosa.

Condizioni di incubazione in termostato

Le infezioni sono state poste in incubatore con il 5% (v/v) di CO_2 a 37°C ± 1°C e osservate al microscopio invertito per rilevare la formazione di placche di lisi, causate dall'effetto citopatico (CPE) della sospensione virale. Sono state contate al microscopio invertito le placche presenti nei pozzetti alla diluizione contabile dopo la fissazione con formaldeide e colorazione con una soluzione di cristalvioletto.

I risultati di CPE (prova quantitativa) di ogni diluizione sono espressi con la percentuale di risultati positivi compresa tra 100% e 0% e registrate come "0" per nessuna CPE e da "1" (25% CPE) a "4" (100% CPE) a seconda del grado di danno cellulare.

Il titolo virale è stato calcolato utilizzando il metodo Spaerman – Karber (valutazione ID_{50}).

Via A. Gabelli 63 - 35121 Padova
C.F. 80006480281 - P.IVA 00742430283

9. VERIFICA INATTIVAZIONE – PROVA CON FORMALDEIDE

2 mL di sospensione virale sono stati miscelati con 8 mL di PBS e 10 mL di soluzione di formaldeide al 1,4 % (p/v) per controllare la validità del sistema. Immediatamente dopo un contatto di 30 min. e 60 minuti, 0,2 mL di questa soluzione sono stati miscelati a 1,8 mL di DMEM + 2% FBS in ghiaccio. Sono state eseguite le diluizioni seriali da 10^{-2} a 10^{-6} (diluizioni 1:10) con PBS + 2% FBS. Per ogni diluizione sono stati distribuiti 250 µl in 6 pozzetti della micropiastra da 24 pozzetti e poste incubatore a 37°C per 1 ora. Dopo 1 ora di incubazione a 37°C (tempo di adsorbimento virale), l'inoculo è stato rimosso, effettuato un lavaggio con PBS e aggiunti 500 µl di DMEM addizionati di 2% (v/v) FBS e 0,75% (v/v) di carbossimetilcellulosa

La coltura cellulare è stata posta in incubatore al 5%(v/v) di CO_2 a 37°C ± 1°C, e osservate al microscopio invertito per la rilevazione dell'effetto citopatico (CPE) della sospensione virale. Sono state contate le placche presenti nei pozzetti alla diluizione contabile dopo la fissazione e la colorazione con la soluzione di cristalvioletto - metanolo. I risultati di CPE (prova quantitativa) di ogni diluizione sono espressi con la percentuale di risultati positivi compresa tra 100% e 0% e registrate come "0" per nessuna CPE e da "1" (25% CPE) a "4" (100% CPE) a seconda del grado di danno cellulare.

Il titolo virale è stato calcolato utilizzando il metodo Spaerman – Karber (valutazione ID_{50}).

Citotossicità della soluzione test della formaldeide

1 ml di formaldeide 1,4% (p/v) è stato aggiunto a 1 ml di PBS. Da questa diluizione sono state preparate le diluizioni seriali da 10^{-2} a 10^{-4} (diluizioni 1:10) prelevando 0.2 ml della miscela ottenuta + 1.8 ml DMEM serum-free.

0.1 ml di ogni diluizione è stata piastrata in sestuplo nelle colture cellulari in monostrato a confluenza (>90%). A 6 pozzetti non è stata aggiunto la miscela (controllo della linea cellulare). Dopo 1 ora a 37°C ± 1°C sono stati aggiunti 100 µl di DMEM + 10% FBS e la coltura cellulare è stata posta in incubatore a 37°C ± 1°C, 5% di CO_2 ed osservata al microscopio invertito costantemente per i successivi 9 giorni per la rilevazione dell'effetto citopatico (CPE), causato dall'azione citotossica della soluzione di formaldeide.

Via A. Gabelli 63 - 35121 Padova
C.F. 80006480281 - P.IVA 00742430283

10.VERIFICA DELL'ATTIVITA' VIRUCIDA DEI DISPOSITIVI

Il test virucida è stato eseguito a 20°C.

50 µl di sospensione virale sono stati inoculati su ogni carrier e lasciati asciugare sotto cappa a flusso laminare. I dischi così inoculati sono stati impiegati per la verifica dell'attività virucida esponendoli all'azione della strumentazione Jonix Cube, oppure lasciati all'interno di capsule petri usandoli come dischi di controllo. I dischi trattati sono stati collocati all'interno di un apposito box contenente il dispositivo Jonix ed esposti alla sua azione per un tempo pari a 30'-60'-120'-240'. Successivamente, i dischetti (trattati e di controllo) sono stati eluiti con 1 ml di terreno di coltura e preparate diluizioni seriali da 10^{-2} a 10^{-9} (diluizioni 1:10). 250 µl di ogni diluizione è stato trasferito in piastre a 24 pozzetti contenenti il monostrato cellulare a confluenza (>90%) dopo aspirazione del terreno di coltura. Ogni diluizione della sospensione virale è stata piastrata in sestuplo. Sono stati lasciati senza inoculo 12 pozzetti (controllo della linea cellulare). Dopo 1 ora di incubazione a 37°C (tempo di adsorbimento virale), l'inoculo è stato rimosso, effettuato un lavaggio con PBS e aggiunti 500 µl di DMEM addizionati di 2% (v/v) FBS e 0,75% (v/v) di carbossimetilcellulosa.

11. CALCOLO DELL'ESPRESSIONE DEI RISULTATI

Determinazione del titolo di infettività (ID_{50}).

L'attività infettante è stata determinata con il metodo Spaerman - Kärber, che utilizza la seguente formula per il calcolo del valore ID_{50}:

$$-\text{Log}_{10}\, ID_{50} = -(x_0) - \{ [R/100] - 0{,}5 \} \times \log_{10} \text{fattore di diluizione}$$

Dove:

x_0 = $\log_{10}$ della diluizione più bassa con il 100% di reazione positiva

(CPE) R = sommatoria (%) delle colture positive

Via A. Gabelli 63 - 35121 Padova
C.F. 80006480281 - P.IVA 00742430283

Il test dell'attività virucida è valido quando nelle prove preliminari si verifica tale condizione: la sospensione test virale deve presentare una concentrazione virale per determinare la riduzione di almeno 4 lg del titolo virale iniziale: **$ID_{50} = 10^7$ /mL.**

12. EFFICACIA VIRUCIDA

Il prodotto in esame è considerato **VIRUCIDA** quando a 20°C, dopo il tempo di contatto preso in esame, dimostra una **riduzione della vitalità di almeno 10^4,** corrispondenti a una riduzione pari 4 logaritmi (99,99%) nei confronti del ceppo virale test (EN 14476:2019 e EN 17272:2020).

13. RISULTATI ED ATTIVITA' VIRUCIDA

I risultati ottenuti sono riportati nella seguente tabella

Tabella 1 – Effetti del trattamento con Jonix CUBE. I valori di riduzione della carica virale sono espressi sia in termine di unità logaritmiche che in termini percentuali.

Tempo di esposizione (minuti)	Controlli		Trattati		Riduzione	
	PFU/ml	$log_{(PFU/ml)}$	PFU/ml	$log_{(PFU/ml)}$	$U_{logaritmiche}$	%
0	10.000.000	7	10.000.000	7	0	0
30	10.000.000	7	1,07	0,03	6,97	99,99999
60	10.000.000	7	1,02	0,01	6,99	99,99999
120	10.000.000	7	1,02	0,01	6,99	99,99999
240	10.000.000	7	1,02	0,01	6,99	99,99999

15. CONCLUSIONE

I risultati ottenuti dimostrano che il dispositivo Jonix Cube (tecnologia Non Thermal Plasma (NTP)) presenta una **efficace attività antivirale nei confronti di SARS-CoV-2 con un abbattimento della carica virale pari al 99,99999% (circa 7 unità logaritmiche) dopo soli 30 minuti di esposizione; ciò lascia supporre che il raggiungimento del livello di abbattimento richiesto dalle norme tecniche (4 unità logaritmiche) possa occorrere anche per tempi considerevolmente minori.**

Via A. Gabelli 63 - 35121 Padova
C.F. 80006480281 - P.IVA 00742430283

16. RIFERIMENTI

- NORMA EUROPEA EN 17272:2020 Disinfettanti chimici e antisettici –Metodo per la disinfezione ambientale mediante processi automatici
- NORMA EUROPEA EN 14476:2019 Disinfettanti chimici e antisettici -Prova quantitativa in sospensione per la valutazione dell'attività virucida in area medica
- ISO/IEC 17025:2017 General requirements for the competence of testing and calibration laboratories
- ISO 15189:2012 Medical laboratories— Requirements for quality and competence

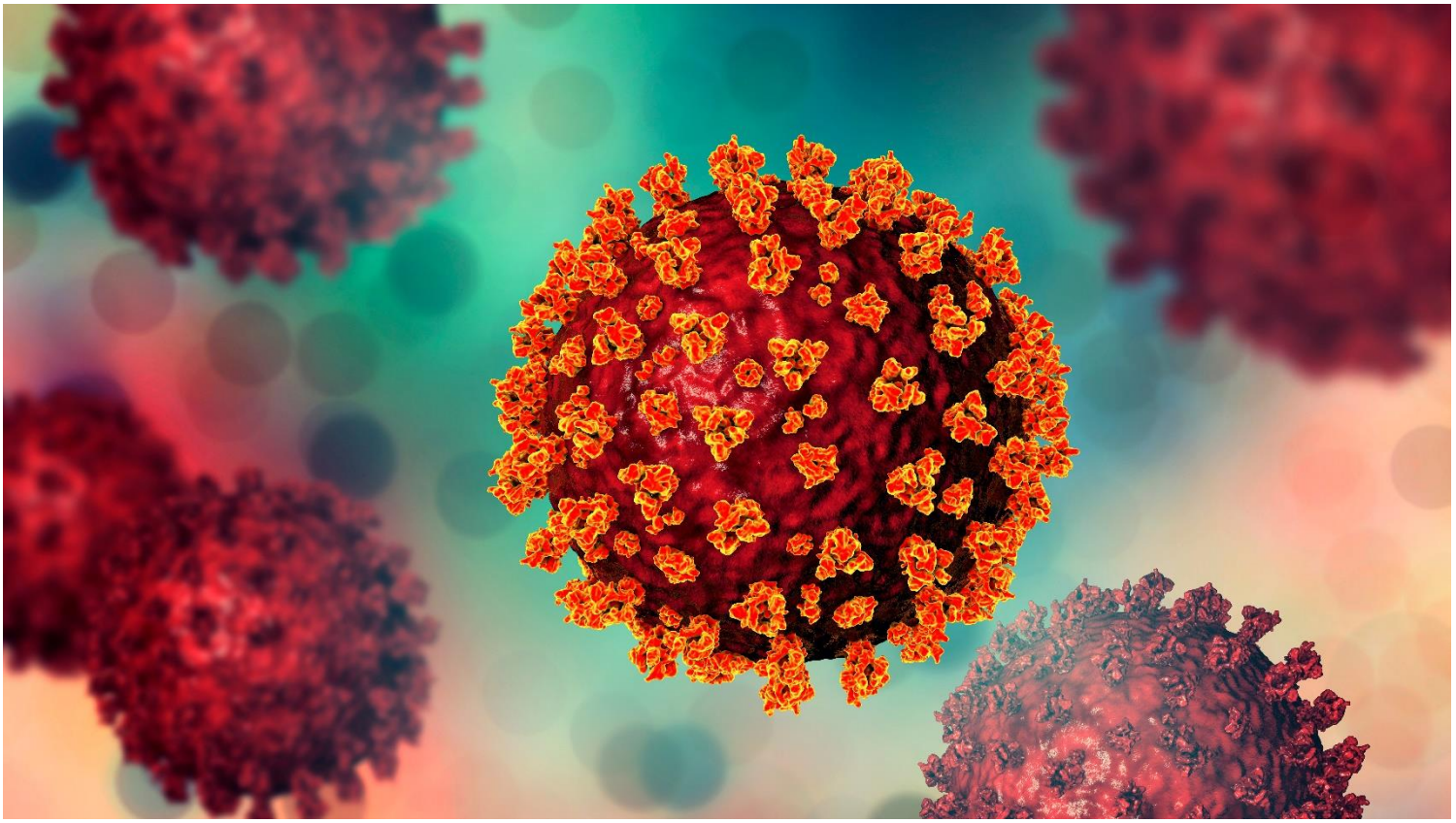

virus SARS-CoV-2

ALLEGATO 12.2

Studio di laboratorio sull'attività biocida delle specie ossidanti formate via NTP

SCOPO DEL LAVORO
Attestare l'attività biocida di aria NTP (ionizzata mediante Non Thermal Plasma) su diversi ceppi batterici.

PROCEDURA
Le piastre Petri sono state contaminate con Salmonella spp., Escherichia Coli, Listeria monocytogenes, Staphylococcus aureus e Pseudomonas aeruginosa e poi esposte per differenti tempi (2,5 e 10 minuti) a flussi di aria ambiente oppure aria trattata via NTP. In questo modo è possibile avere un confronto diretto fra la crescita o meno dei microorganismi.

RISULTATI

Le foto sottostanti mostrano il confronto nei vari casi

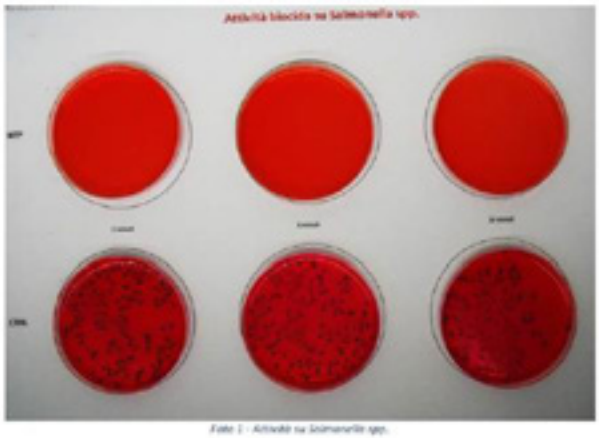

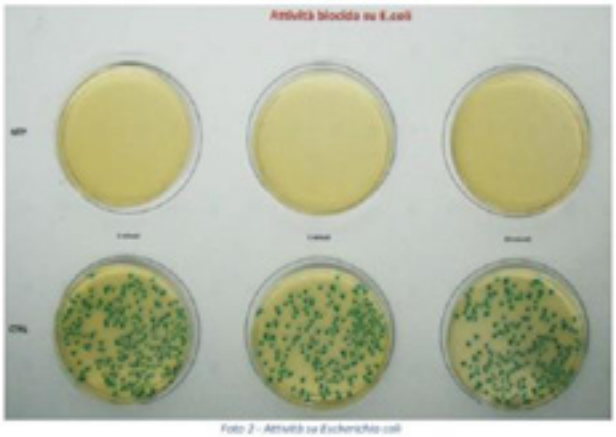

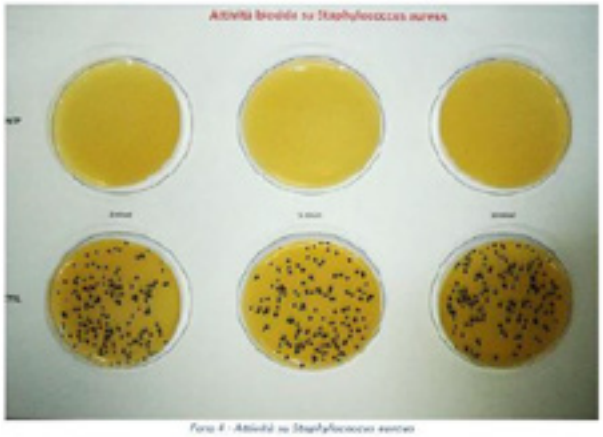

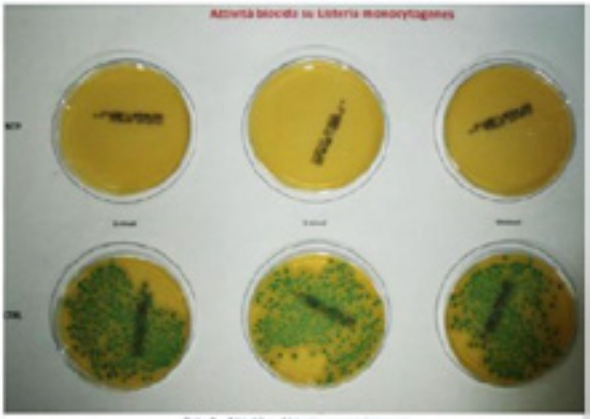

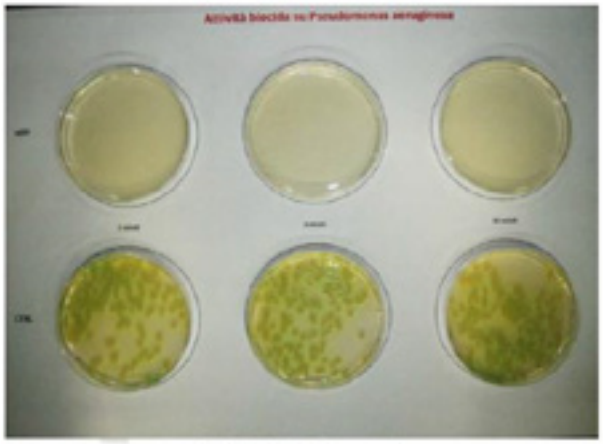

La successiva tabella riassume le medie dei risultati ottenuti.

Tabella 1. Risultati delle prove di trattamento

	Tempo di trattamento (minuti)						
	0	**1**	**3**	**5**	**10**	**15**	**30**
Ceppo\ trattamento							
Escherichia coli \ aria	~ 500	~ 500	~ 500	~ 500	~ 500	~ 500	~ 500
Escherichia coli \ NTP	~ 500	0	0	0	0	0	0
Candida albicans \ aria	~ 600	~ 600	~ 600	~ 600	~ 600	~ 600	~ 600
Candida albicans \ NTP	~ 600	38	20	0	0	0	0
Staphylococcus aureus \ aria	~ 300	~ 300	~ 300	~ 300	~ 300	~ 300	~ 300
Staphylococcus aureus \ NTP	~ 300	78	1	0	0	0	0

Risultati in forma grafica

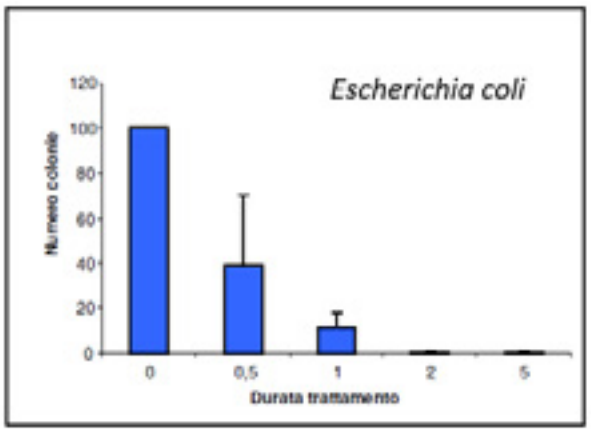

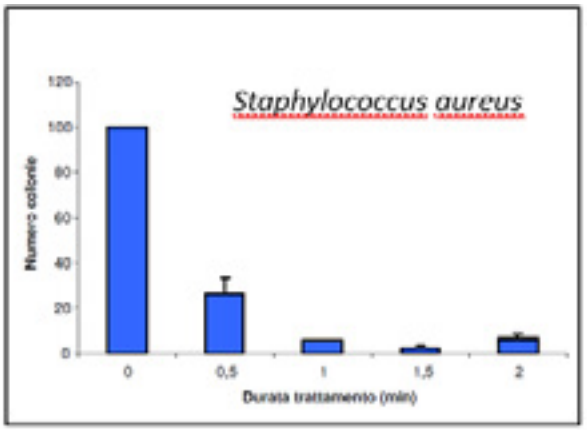

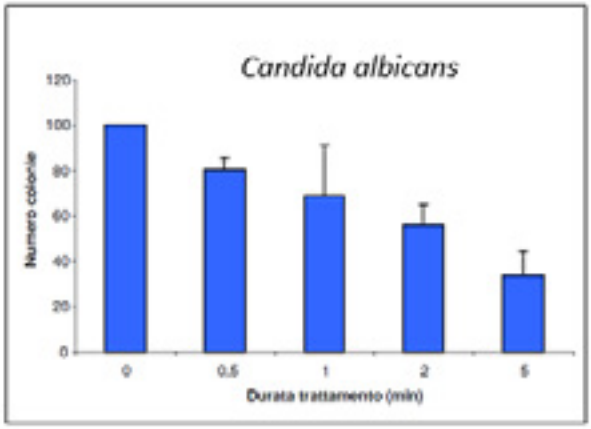

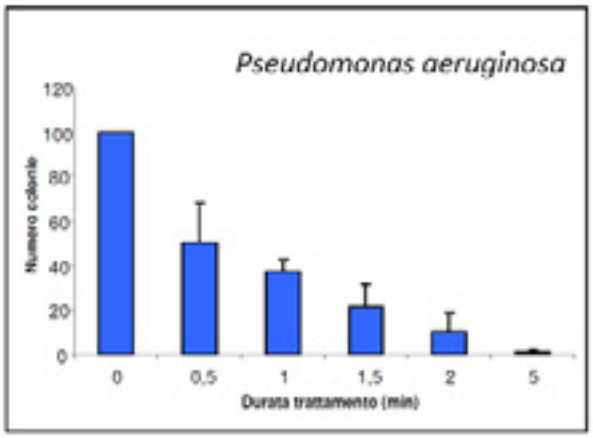

Dalle fotografie, risulta evidente come già a brevi tempi di contatto (2 minuti), l'attività biocida dell'aria NTP risulta totale: le piastre esposte a aria NTP non mostrano alcuna crescita dei ceppi microbici testati, che invece si sono normalmente sviluppati sulle piastre esposte semplicemente all'aria

Come mostrato dalle foto il trattamento NTP risulta efficace già a partire dai primissimi minuti di utilizzo. Infatti, dopo appena 5 minuti, tutte le specie testate sono completamente eradicate dalla superficie delle piastre. Un ulteriore elemento che caratterizza positivamente il successo della sperimentazione consiste nel fatto che, contrariamente a quanto previsto da alcune metodiche che prevedono l'esecuzione delle sperimentazioni su superfici di acciaio inox, le prove sopra descritte sono state eseguite in condizioni ottimali per i microrganismi sia dal punto di vista ecologico(umidità, pH ottimale, presenza di nutrienti, etc.), sia per la presenza di grandi quantità di sostanza organica che notoriamente interferisce con i biocidi di tipo classico.

ALLEGATO 12.3

Studio di laboratorio sugli effetti sanificanti prodotti da un MATE marca Jonix

Sanificazione ambienti con il MATE JONIX

Il dispositivo MATE prodotto dalla JONIX srl è un sistema sanificante ad armadio il cui funzionamento sfrutta la tecnologia a plasma freddo NTP, utilizzata per la ionizzazione dell'aria. L'utilizzo è rivolto alla sanificazione di ambienti industriali, medici e ambulatoriali, ed è estendibile anche a molti altri campi, tra cui quello agroalimentare (coltivazione e la conservazione dei cibi).

La Laboratori ARCHA srl ha confrontato la riduzione spontanea di contaminazione microbica in un ambiente di lavoro in presenza e in assenza del trattamento NTP (rispettivamente MATE in funzione e non in funzione). I risultati sono esposti nel grafico seguente.

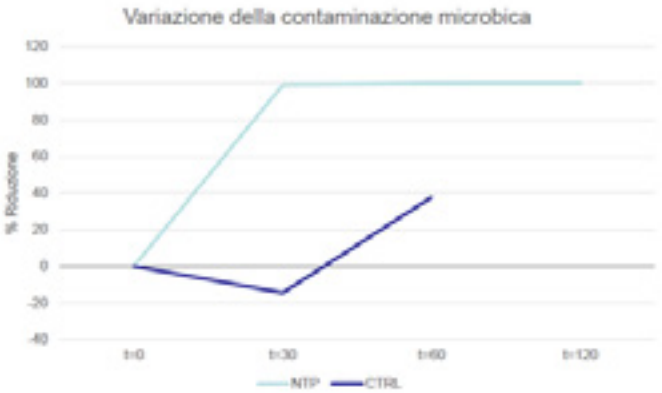

Confronto tra la riduzione spontanea della contaminazione microbica aerodispersa (CTRL) e quella determinata dal trattamento (NTP). Valori negativi indicano un aumento della contaminazione rispetto al tempo zero (fine nebulizzazione)

Dal grafico si osserva come, in presenza del dispositivo, dopo 30 minuti di trattamento la percentuale di riduzione microbica sia molto vicina al 100%. Questo conferma l'efficacia del MATE nella sanitizzazione degli ambienti di vita o lavorativi.

ALLEGATO 12.4

Utilizzo della tecnologia NTP nei confronti delle maleodoranze che si associano all'utilizzo delle calzature

Introduzione

E' stata testata l'efficacia dell'aria NTP nei confronti dell'abbattimento di molecole chimiche e nei confronti della sanificazione microbiologica relativamente all'abbattimento delle maleodoranze che si associano all'utilizzo delle calzature.

In particolare è stata verificata l'efficacia dell'aria NTP nell'abbattimento delle seguenti specie:

- Molecole chimiche responsabili dell'odore;
- Microrganismi responsabili della produzione dell'odore.

Per quanto riguarda l'abbattimento delle molecole chimiche la sperimentazione condotta ha portato a concludere che trattamenti mediante aria NTP per tempi sufficientemente lunghi (dalle 6 ore in poi) risultano EFFICACI e in grado di abbattere e distruggere completamente le molecole in questione, come mostrato nella tabella seguente.

molecola chimica	**Abbattimento % delle molecole rispetto alla concentrazione iniziale, mediante aria NTP**		
	60 min	**6 h**	**17 h**
Acido Acetico	69%	100%	100%
Acido Propionico	45%	100%	100%
Acido Iso-butirrico	31%	100%	100%
Acido Butirrico	21%	100%	100%
Acido Iso-valerico	0%	100%	100%
Acido Valerico	10%	100%	100%
Acido Caproico	6%	100%	100%
Acido Caprilico	6%	99%	99%
Acido Caprico	6%	88%	95%

ALLEGATO 12.5

Sanificazione di sonde ecografiche non critiche

Scopo del test

Sono state condotte delle prove di sanificazione di sonde ecografiche “non critiche”, utilizzando ARIA NTP, in comparazione alla sanificazione realizzata da device commerciali.

I test hanno evidenziato una efficacia dell’NTP assolutamente comparabile a quella dei device commercializzati allo scopo.

Risultati

Nelle figure di seguito riportate si visualizza l’abbattimento di specie microbiche associata all’aria NTP e Ai dispositivi commerciali, nel corso della medesima procedura di disinfezione.

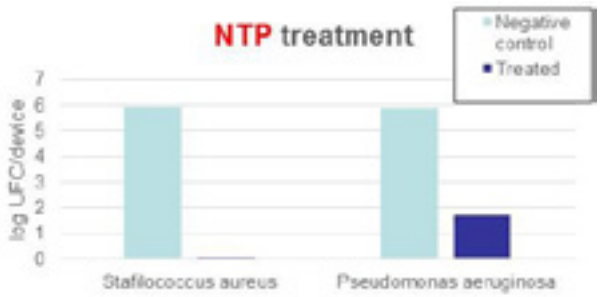

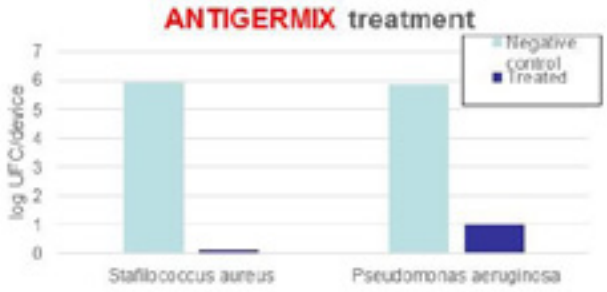

ALLEGATO 12.6

Studi di laboratorio sull'abbattimento di VOC via NTP: review

Studi di laboratorio sull'abbattimento di VOC via NTP: review

Uno fra i campi più indagati è quello dell'abbattimento dei VOC (o COV, Composti Organici Volatili – Volatile Organic Compounds - ovvero una vasta gamma di inquinanti in fase gas) in quanto possono essere ossidati a CO2 in questi plasmi già a temperatura ambiente, con un'efficienza che dipende dal tipo di VOC e dai tempi di contatto. E' da segnalare il fatto questi plasmi siano in grado di trattare anche l'Halon (un alogenoalcano) notoriamente molto inerte.

Oltre che su molecole di natura organica, l'NTP è in grado di agire anche sugli inquinanti inorganici, come gli ossidi di azoto (NOx), diossido di zolfo (SO_2), l'acido solfidrico (H_2S) etc…, ad esempio come quelli provenienti dai gas di scarico dei motori degli autoveicoli.

La tecnologa NTP è quindi efficace ad ampio raggio e può essere applicata tal quale in numerosi campi poiché è facilmente scalabile sia per piccole che grandi applicazioni.

I fattori che influenzano l'efficacia dell'abbattimento degli inquinanti con i sistemi NTP sono davvero molti. Dalla geometria dei sistemi di produzione del plasma ai sistemi di alimentazione elettrica, dalla concentrazione degli inquinanti all'umidità dell'aria, e così via.

I Case Study che la laboratori ARCHA1 ha sperimentato rappresentano ambiti applicativi nei quali è stato testato il sistema di produzione di plasma freddo Jonix e hanno tutti avuto l'obiettivo di mettere a punto le condizioni migliori di trattamento nonché di individuare e misurare con opportune metodiche analitiche l'efficacia di abbattimento delle molecole contaminanti indesiderate. Questi casi rappresentano quindi solo un esempio ed uno spunto non esaustivo delle possibilità applicative della tecnologia NTP, e forniscono una serie di dati robusti ed attendibili che indicano quali siano le potenzialità di tale tecnologia.

---

[1] ARCHA, acronimo di **A**nalisi e **R**icerche di **CH**imica **A**pplicata, nato nel 1989 a Pisa, su iniziativa di un pool di professionisti chimici. Rappresenta un laboratorio chmico all'avanguardia, dotato di attrezzature e personale qualificato.

Negli anni la società è cresciuta sotto ogni profilo: competenze scientifiche, efficienza di servizio e risultati di mercato.

Oggi il gruppo ARCHA è organizzato in **tre settori** (Tecnico – ICT- Industrializzazione), all'interno dei quali fanno riferimento diverse aree di competenza e/o diverse società del gruppo.

Nella tabella sottostante si riportano i composti organici ed inorganici che sono stati trattati nel corso dei vari casi di studio e l'efficacia di abbattimento di ognuno ottenuta mediante trattamento NTP Jonix.

La percentuale di abbattimento è relativa ai singoli casi studio, ma è comunque indicativa della capacità del sistema di agire sul determinato composto.

VOC – Volatile Organic Compounds	Abbattimento % post trattamento NTP Jonix
Toluene	> 95
TBA (tribomanisolo)	> 95
Acetati di etile	> 95
Acetato di butile	> 95
Acetaldeide	> 95
Butanale	> 95
Dicloroetilene	> 95
TCE	> 95
1,2 DCP	> 95
Metilcicloesano	> 95
Ottano	> 95
PCE	> 95
Xileni	> 95
Aromatici C9	> 95
Acido Acetico	> 95
Acido Propionico	> 95
Acido Iso-butirrico	> 95
Acido Butirrico	> 95
Acido Iso-valerico	> 95
Acido Valerico	> 95
Acido Caproico	> 95
Acido Caprilico	> 95
Composti alifatici (C5-12)	> 95
Composti aromatici (C7-C10)	> 95

Composti Inorganici Volatili/Gassosi	Abbattimento % post trattamento NTP Jonix
NOx	> 95
SOx	> 95
H_2S	> 95
CO	> 95
NH_3	> 95

Composti organici volatili	> 95

La definizione di VOC è ampia e vi rientrano anche i composti cosiddetti “odorigeni”, e spesso in modo improprio anche i composti di natura inorganica.

I contesti applicativi in cui è stata testata la tecnologia NTP Jonix e nei quali sono state valutate le efficacie di abbattimento di VOC riportati nelle precedenti tabelle sono i seguenti:
Impianti pilota NTP per l’abbattimento delle emissioni odorigene di rifiuti solidi pericolosi (VOC vari e composti inorganici - H2S, NOx, NH3, …)
Impianti pilota NTP per l’abbattimento delle emissioni odorigene negli impianti di depurazione di acque reflue civili ed industriali (VOC vari e composti inorganici - H2S, NOx, NH3, …)
Sistemi di trattamento NTP di sostanze organiche fortemente odorigene/moleste (acidi carbossilici: acido acetico, acido propionico, acido butirrico….)
Impianti pilota NTP di abbattimento di VOC in sistemi di verniciatura industriale (toluene, acetato di etile, acetato di butile, …)
Sistemi di trattamento NTP di gas di scarico post combustione (gas di scarico di motori a scoppio diesel): SOx, NOx, CO, …

ALLEGATO 12.7

Studio di laboratorio sull'attività biocida delle specie ossidanti formate via NTP

Relazione tecnica

Protocollo di prova per la valutazione dell'efficacia di riduzione di microrganismi intenzionalmente inoculati in piastre utilizzando il sistema di ionizzazione di aria Mate di Jonix .

Prof. Giuseppe Comi
Dipartimento di Scienze Agro-Alimentari, Ambientali e Animali, Università degli Studi di Udine, via Sondrio 2/a, 33100 Udine.

28 Febbraio 2016

Indice

Introduzione

Il presente protocollo è stato implementato per verificare la riduzione di microrganismi intenzionalmente inoculati in terreni culturali ed esposti per tempi prestabiliti all'effetto di aria ionizzata. Per ogni prova è stato effettuato un test di controllo utilizzando gli stessi terreni inoculati non soggetti a trattamento.

Ceppi inoculati

I microrganismi testati sono di seguito riportati:

- *Staphylococcus aureus* (Gram + , asporigeno, aerobio – anaerobio facoltativo)
- *Listeria monocytogenes* (Gram + , asporigeno, aerobio – anaerobio facoltativo)
- *Aspergillus niger* (fungo - Muffa)
- *Kluyveromyces marxianus* (forma perfetta di *Candida pseudotropicalis*)
- Microrganismi vari in associazione (Enterobacteriaceae – Conta batterica totale)

Materiali e metodi

Diversi microrganismi erano direttamente inoculati in piastre di Plate Count agar (Oxoid, Italia) e di Agar Malto (lieviti e muffe) (Oxoid, Italia), trattati per diversi tempi 0 (controllo), 30, 60, 90, 120 min e 12 e 24 h con lo ionizzatore. Dopo il trattamento le piastre erano incubate a 25 °C per 2-5 giorni. Quindi si procedeva alla conta delle colonie sopravvissute al trattamenti. I risultati erano espressi in % di inattivazione/decadimento.100 – (Numero iniziale/Numero finale %)

Preparazione della sospensione microbica e inoculo

Staphylococcus aureus

L'inoculo era costituito da 2 ceppi di *Staphylococcus aureus* derivanti da collezioni internazionali (DSMZ 4910) e da Collezione del Dipartimento di Scienze degli Alimenti della Facoltà di Agraria dell'Università degli Studi di Udine (DIAL). Le singole sospensioni erano preparate con un'ansata di *St. aureus* aggiunto ad acqua peptonata sterile (0.8% NaCl). Allo spettrofotometro era valutata una densità ottica pari a 0.1 a 600 nm. Ai fini di valutare la carica di ogni sospensione, erano eseguite diluizioni delle stesse in acqua peptonata sterile. Quindi 0.1 ml di ogni diluizione era inoculata in

piastre contenenti Plate Count Agar (Oxoid, Italia). Le piastre erano incubate a 37 °C per 48 ore e le colonie cresciute erano contate. Ogni sospensione conteneva mediamente circa 10^7 CFU/ml. Venivano eseguite diluizioni decimali e 0.1 ml della diluizione 10^{-3} CFU/ml era spatolata in Plate Count Agar. Le piastre erano poste aperte nella camera con lo ionizzatore acceso 24 ore prima. Ai tempi sopracitati le piastre erano recuperate e poste ad incubare a 37 °C per 48 ore. Ad ogni tempo erano analizzate 5 repliche (campioni).

Listeria monocytogenes

L'inoculo era costituito da 2 ceppi di *Listeria monocytogenes*: L. monocytogenes , L. monocytogenes derivanti da Collezioni Internazionali e da vegetali e conservate nella Collezione del Dipartimento di Scienze degli Alimenti della Facoltà di Agraria dell'Università degli Studi di Udine (DIAL). Le singole sospensioni erano preparate con un'ansata di *L. monocytogenes* aggiunta ad acqua peptonata sterile (0.8% NaCl). Allo spettrofotometro era valutata una densità ottica pari a 0.1 a 600 nm. Ai fini di valutare la carica di ogni sospensione, erano eseguite diluizioni delle stesse in acqua peptonata sterile. Quindi 0.1 ml di ogni diluizione era inoculata in piastre contenenti Plate Count Agar (Oxoid, Italia). Le piastre erano incubate a 37 °C per 48 ore e le colonie cresciute erano contate. Ogni sospensione conteneva mediamente circa 10^7 CFU/ml. Cinque ml di ogni sospensione erano miscelate e diluite in acqua peptonata sterile e 0.1 ml della diluizione 10^{-3} CFU/ml era spatolata in Plate Count Agar. Le piastre erano poste aperte nella camera con lo ionizzatore acceso 24 ore prima. Ai tempi sopracitati le piastre erano recuperate e poste ad incubare a 37 °C per 48 ore. Ad ogni tempo erano analizzate 5 repliche (campioni).

Kluyveromyces marxianus

Kluyveromyces marxianus era seminato in agar malto (Oxoid, Italia), incubato a 25 °C per 3 giorni, quindi una colonia era diluita in acqua peptonata (NaCl 0.1%, Peptone 0.8%, Acqua 1000 ml). Allo spettrofotometro era valutata una densità ottica pari a 0.1 a 600 nm. Ai fini di valutare la carica della sospensione, erano eseguite diluizioni delle stesse in acqua peptonata sterile. Quindi 0.1 ml di ogni diluizione era inoculata in piastre contenenti Agar Malto (Oxoid, Italia). Le piastre erano incubate a 25 °C per 3-5 giorni e le colonie cresciute erano contate. La sospensione conteneva mediamente circa 10^7 CFU/ml. Venivano eseguite diluizioni decimali e 0.1 ml della diluizione 10^{-4} CFU/ml era spatolata in Agar Malto. Le piastre erano poste aperte nella camera con lo ionizzatore acceso 24 ore prima. Ai tempi sopracitati le piastre erano recuperate e poste ad incubare a 25 °C per 3-5 giorni. Ad ogni tempo erano analizzate 5 repliche (campioni).

***Coliformi* ed *Escherichia coli* (contaminazione ambientale/fecale)**

L'inoculo era costituito da 2 ceppi di *E. coli* isolati da farine e conservati nella Collezione del Dipartimento di Scienze degli Alimenti della Facoltà di Agraria dell'Università degli Studi di Udine (DIAL), un ceppo di *Pantoea (Enterobacter) agglomerans* di origine ambientale. Le singole sospensioni erano preparate con un'ansata di ogni microrganismo aggiunta ad acqua peptonata sterile (0.8% NaCl).

Allo spettrofotometro era valutata una densità ottica pari a 0.1 a 600 nm. Ai fini di valutare la carica di ogni sospensione, erano eseguite diluizioni delle stesse in acqua peptonata sterile. Quindi 0.1 ml di ogni diluizione era inoculata in piastre contenenti Plate Count Agar (Oxoid, Italia). Le piastre erano incubate a 37 °C per 48 ore e le colonie cresciute erano contate. Ogni sospensione conteneva mediamente circa 10^7 CFU/ml. Cinque ml di ogni sospensione erano miscelate e diluite in acqua peptonata sterile e 0.1 ml della diluizione 10^{-3} CFU/ml era spatolata in Plate Count Agar. Le piastre erano poste aperte nella camera con lo ionizzatore acceso 24 ore prima. Ai tempi sopracitati le piastre erano recuperate e poste ad incubare. Ad ogni tempo erano analizzate 5 repliche (campioni).

Aspergillus niger

Spore, prodotte da colonie di *Aspergillus niger,* seminate in agar malto (Oxoid, Italia) incubato a 25 °C per 5 giorni, sono state diluite in acqua peptonata (NaCl 0.1%, Peptone 0.8%, Acqua 1000 ml). Dopo omogenizzazione le spore, previa diluizione, sono state contate in piastre di agar malto (Oxoid, Italia) e 0.1 ml della diluizione 10^{-3} erano spatolate in piastre di Malto Agar. Le piastre erano poste aperte nella camera con lo ionizzatore acceso 24 ore prima. Ai tempi sopracitati le piastre erano recuperate e poste ad incubare a 25 °C per 3-5 giorni. Ad ogni tempo erano analizzate 5 repliche (campioni).

E' stata misurata anche la concentrazione dell'ozono durante il trattamento ai fini di valutare la salubrità della metodica.

Modello di ionizzatore utilizzato

E' stato utilizzato uno ionizzatore di aria modello dello ionizzatore Jonix Mate della Ditta Jonix srl. Viale Spagna 31-33, 31020 Tribano (PD). Lo ionizzatore, posto in una cella frigorifera di tipo alimentare di circa 60 m^3 (6x3.6x 2.70 m) mantenuta ad una temperatura media di 15 °C., era stato acceso 2 giorni prima dell'inizio della sperimentazione ai fini di eliminare interferenze dovute alla contaminazione dell'aria della cella. Le piastre erano posizionate aperte su scaffali metallici e soggette a trattamento lasciando lo ionizzatore acceso per tutta la durata delle prove.


JONIX mate

Risultati

Di seguito sono riportati i risultati ottenuti dalle prove. I numeri sono il valore medio approssimato di cinque piastre; il dato è espresso in UFC/ml in piastra da 90 mm.

Tabella 1: Variazione concentrazione di *Staphylococcus. Aureus*

Tempo min/h	Media UFC/ml	dev. st.	% abbattimento
0	58400000	10822199,41	
30	31320000	7121235,84	37,1
60	34100000	3090307,42	31,5
90	21640000	3710525,56	56,5
120	4600000	854400,37	90,8
12 h	40000	89442,71	99,9
24 h	0	0	100,0

Legenda: dev. st.: deviazione standard

Tabella 2: Variazione della concentrazione di *Listeria monocytogenes*

Tempo min/h	Media UFC/ml	dev. st.	% abbattimento
0	65280000	1752712,18	
30	65080000	7150314,67	0,3
60	51360000	25677772,49	21,3
90	3520000	1605303,71	94,6
120	2006000	1080823,76	96,9
12 h	980000	752994,02	98,5
24 h	960000	409878,03	98,5

Legenda: dev. st.: deviazione standard

Tabella 3: Variazione della concentrazione di *Kluyveromyces marxianus*

Tempo min/h	Media UFC/ml	dev. st.	% abbattimento
0	2184480	505268,19	
30	2292400	622791,13	4,9
60	2336000	782642,95	6,9
90	2266000	979938,77	3,7
120	2158000	864823,68	1,2
12 h	0	0	100,0
24 h	0	0	100,0

Legenda: dev. st.: deviazione standar

Tabella 4: Variazione della Conta betterica totale

Tempo min/h	Media UFC/ml	dev. st.	% abbattimento
0	70240000	7029082,44	
30	63420000	3692153,84	9,7
60	82480000	16818799,01	17,4
90	54800000	10471867,07	21,9
120	57960000	16288277,99	17,5
12 h	0	0	100,0
24 h	0	0	100,0

Legenda: dev. st.: deviazione standard

Tabella 5: Variazione della concentrazione di *Aspergillus niger*

Tempo min/h	Media UFC/ml	dev. st.	% abbattimento
0	1300000	200000	
30	740000	54772,25	43,1
60	1000000	519615,24	23,1
90	1000000	353553,39	23,1
120	1260000	421900,46	30,8
12 h	360000	207364,41	72,3
24 h	180000	130384,04	82,7

Legenda: dev. st.: deviazione standard

Commento ai risultati

Come si può evincere dai risultati delle prove sopra indicate, l'abbattimento microbico che si ottiene in presenza del sistema di ionizzazione dell'aria Jonix Mate su superfici di simulanti materiale organico inoculato con diverse specie microbiche è elevato e permette di inibire completamente entro le 12 24 ore gran parte delle specie inoculate. Infatti in molti casi l'abbattimento ottenuto è superiore al 95%. L'effetto di riduzione microbica dell'aria ionizzata è analogo sia su Gram positivi, su Gram negativi e che lieviti e muffe, anche se l'efficacia risulta spesso dipendente dalla specie considerata, e in particolare:.

1) *Staphylococcus aureus* (Tabella 1). Questo è un microrganismo tipico delle mucose umane ed animali. E' un potenziale patogeno presentando all'interno della specie ceppi produttori di enterotossine (A, B, C, D, E, F). L'enterotossina A sembra la più diffusa a livello alimentare. Infatti è risultata responsabile di numerose intossicazioni essendo prodotta, come del resto anche le altre enterotossine nell'alimento conservato in abuso termico. Gli alimenti possono essere naturalmente contaminati da *Staphylococcus aureus* o ne vengono a contatto a causa di manipolazioni umane e di ambienti e attrezzature contaminati. In caso di sviluppo la tossina permane essendo termostabile e conseguentemente non viene eliminata con la pastorizzazione

e/o cottura. L'impiego del trattamento ionizzante permette la completa inibizione di tale microrganismo. Infatti si osserva (Tabella 1) una continua inattivazione nel tempo. Infatti dopo 2 ore l'abbattimento è del 90% e a 12 e 24 del 99.9-100%.

2) *Listeria monocytogenes* (Tabella 2). Questo è un microrganismo psicrotrofo di origine ambientale. Contamina ogni ambiente e conseguentemente ogni alimento sia come materia prima che prodotto finito (Cocolin et al., 2005). La sua presenza nei prodotti alimentari (ready to eat) viene regolamentata da criteri microbiologici riportati nel Reg. CE 2073/05 e 1414/08, essendo patogena e altamente virulenta. Ogni anno vengono, infatti, denunciati numerosi casi di listeriosi (0.4/100.000 abitanti) in seguito al consumo di alimenti. Conseguentemente l'industra alimentare utilizza numerose tecnologie sia per eradicare o impedire la sua presenza negli alimenti, sia per impedirne la crescita. Il sistema Jonix permette di abbattere già dopo 90 min il 94% delle *L. monocytogenes* presenti, e a 12-24 ore l'abbattimento risulta superiore al 98%. Per arrivare alla eradicazione totale (100%) occorre operare trattamenti prolungati (36 ore).
3) *Kluyveromyces marxianus* (Tabella 3). *K. marxianus* è un lievito innocuo, considerato la forma perfetta della *Candida pseudotropicalis*; specie, invece, riconosciuta patogena, seppur meno virulenta della *Candida albicans*, tipico patogeno delle mucose umane e animali. E' largamente diffuso in natura, in particolare in latte e latti fermentati (i.e. Kefir). Viene utilizzato per la produzione di bioetanolo. Tale lievito è particolarmente resistente brevi trattamenti ionizzanti (< 120 min). Tuttavia è possibile eradicare la sua presenza da substrati organici dopo 12/24 ore di trattamento, come viene efficacemente riportato in tabella 3.
4) Conta batterica totale (Tabella 4). Per la valutazione dell'effetto del trattamento ionizzante sulla conta batterica totale sono stati impegati diversi microrganismi tipici di cantaminazione fecale (*Escherichia coli*) e ambientale (*Pantoea agglomerans*). Anche in questo caso trattamenti con tempi inferiori ai 120 minuti, non portano ad abbattimenti significativi, mentre trattamenti di 12 e 24 ore portano alla completa eradicazione delle 2 specie considerate.
5) *Aspergillus niger* (Tabella 5). Muffa (fungo) di origine ambientale e tipica di vegetali, anche se spesso isolata su superfici di salumi. Presenta ceppi micotossinogeni. Infatti i black aspergilli possono produrre Ocratossina A e B; largamente diffusa in semi, vegetali e talvolta in farine di cereali. L'Ocratossina A indesiderabile negli alimenti perché è stata classificata dallo IARC (International Agency for Research of Cancer) nel gruppo "2B" come un possibile carcinogeno. Parecchi studi, infatti, hanno dimostrato che ha proprietà teratogenica, neurotossica, genotossica, immunotossica e nefrotosica (IARC, 1993; JEFCA, 2001). Infatti, in Italia sono è stato suggerito il limite di 1 µg/Kg per la sua presenza in prodotti carnei e a

base di carne (Circolare Ministero Sanità n° 10-09/06/1999). La ionizzazione permette un abbattimento variabile di tale microrganismo; abbattimento legato al tempo di trattamento. Infatti occorrono tempi di 12 o 24 ore per abbattere il 72 e 82 % della carica di *A. niger* inoculato in terreno organico. Per arrivare alla completa inattivazione delle spore inoculate occorre operare un trattamento pari a 36-48 ore.

Conclusione

Il sistema Jonix Mate basato sulla ionizzazione dell'aria permette di inattivare popolazioni microbiche intenzionalmente inoculate in terreni di cultura organici. La percentuale di abbattimento è strettamente legata alla specie microbica considerata e al tempo di trattamento.

Bibliografia

Abarca, M.L., Bragulat, M.R., Castellà, G., Cabanes, F.J. (1994) Ochratoxin A production by strain of *Aspergillus niger* var. niger. Appl. Eniviron. Microbiol., 60 (7), 2650-2652.

Cocolin, L., Stella, S., Nappi, R., Bozzetta, E., Cantoni, C., Comi, G. (2005) Analysis of PCR-based methods for characterization of *Listeria monocytogenes* strains isolated from different sources. Int. J. Food Microbiol., 103, 167-178.

Comi, G., Iacumin, L. (2013) Ecology of moulds during the pre-ripening and ripening of San Daniele dry cured ham. Food Research Int. 54, 1113-1119.

Comi, G., Lovo, A., Bortolussi, N., Paiani, M., Berton, A., Bustreo, G. (2005) Ionizzatori per decontaminare l'aria nei locali di produzione del prosciutto crudo di San Daniele. Ind. Alim., XLIV, ottobre, 1-9.

Comi, G., Osualdini, M., Manzano, M., Lovo, A., Bortolussi, N., Berton, A., Bustreo, G. (2006) Decontaminazione di superfici di strutture e attrezzature utilizzate in aziende alimentari attraverso l'impiego di ionizzatori. Ind. Alim., XLV, giugno, 661-669.

JEFCA, 2001. Ochratoxin A. First Draft 47 series.

Iacumin, L., Manzano, M., Comi, G. (2012) Prevention of *Aspergillus ochraceus* growth on and Ochratoxin A contamination of Sausages using ozonated air. Food Microbiol., 29 (2), 229-232.

I.A.R.C., 1993. Ochratoxin A. In Some naturally occurring substances: Food items and constituents, heterocyclic aromatic amines and mycotoxins. IARC Monograph on the evolution of carcinogenic risks to humans, vol. 56, pp. 489-521. Geneva: International Agency for Research on Cancer.

ALLEGATO 12.8

Studio del potere sanificante di un dispositivo Jonix applicato ad un fan coil commerciale

Studio del potere sanificante di un dispositivo Jonix applicato ad un fan coil commerciale

Pisa, Febbraio 2017

Laboratori ARCHA S.r.l. unipersonale
Via di Tegulaia 10/a - 56121 - PISA - ph. +39 050 985165 - fax +39 050 985233 - www.archa.it - archainf@archa.it
C.F., P.IVA, Iscr. Reg. Impr. di Pisa n. 01115340505 - Rep. Econ. Amm. di Pisa n°101169 - Capitale Sociale 101.400,00 i.v.

1. Sommario

2. Introduzione

Nella sperimentazione di seguito descritta è stata eseguita una serie di test volti a verificare l'efficacia sanificante a livello biologico di un dispositivo NTP Jonix installato all'interno di un ventilatore convettore per installazione a parete.

Lo scopo della prova è testare se la produzione di specie ossidanti sia o meno in grado di risolvere il problema dell'inquinamento di alcune parti delle apparecchiature da parte di muffe, nonché di sanificare l'aria del locale nel quale viene installato.

2.1. Impostazione della prima prova

Il test è stato eseguito utilizzando due apparecchiature gemelle poste in due stanze di uguale dimensione. Nella prima stanza è stato alloggiato un fan coil dotato del sistema NTP, nella seconda stanza è stato alloggiato un fan coil del tutto identico ma senza nessun dispositivo sanificante. Entrambi i dispositivi sono stati avviati alla minima portata possibile e sono stati inquinati artificialmente con muffe, dopo di che sono stati attivati e lasciati lavorare per un tempo pari a 7 giorni.

L'inquinamento è stato applicato sulla girante, prima dell'attuatore NTP. La girante è infatti una delle componenti dove è stata riscontrata, in sistemi simili, la formazione di muffe ed il deposito di sporco in genere.

Il campionamento è stato eseguito al termine del periodo di prova misurando l'abbattimento in due punti:

1) **Direttamente sulle alette della girante**, sia perché è il punto più critico, che per verificare l'effetto di rilascio di molecole sanificanti nell'ambiente che poi vengono convogliate nuovamente dentro l'apparecchio, sanificando anche le parti prima del generatore NTP;
2) **Alla bocca di uscita**, per verificare, per differenza rispetto alle concentrazioni di inquinanti in entrata, se vi sia abbattimento diretto:

Parametri sperimentali:

- Dimensione locale: 25 m^3 (2,7x3,8x2,5)
- Modello fan coil: ESTRO_GT FL 7 – Marca Galletti
- Dispositivo sanificante: Jonix Modello "C/2"
- Portata aria di ricircolo: 320 m^3/h

2.2. Impostazione della seconda prova

Il test è stato eseguito utilizzando due apparecchiature gemelle poste in 2 punti di una sola grande stanza. Entrambi i fan coil erano dotati del sistema NTP, con la ventilazione impostata alla massima portata possibile.

I due fan coil sono stati inquinati artificialmente con muffe, dopo di che sono stati attivati e lasciati lavorare per un tempo pari a 15 giorni.

L'inquinamento è stato applicato nell'area posta a valle del pacco refrigerante, a valle dell'attuatore NTP, in modo da poter valutare la capacità auto-sanificante in un'altra delle componenti a rischio di inquinamento microbico.

Il campionamento è stato eseguito al termine del periodo di prova misurando l'abbattimento in due punti:

3) **Direttamente sull'area contaminata con muffe**, per valutare la sanificazione nella parte a valle del generatore NTP;
4) **Al centro del locale**, per valutare il grado di contaminazione ambientale.

Parametri sperimentali:

- Dimensione locale: circa 250 m^3 (2,7x3,8x2,5)
- Modello fan coil: ESTRO_GT FL 7 – Marca Galletti
- Dispositivo sanificante: Jonix Modello "C/2"
- Portata aria di ricircolo: 640 m^3/h per ciascun dispositivo

3. Materiali e metodi

3.1. Microrganismi impiegati

Dal momento che le due macchine impiegate per la sperimentazione erano nuove di fabbrica, per assicurare la presenza di microrganismi contaminanti all'interno dei dispositivi, La contaminazione è stata effettuata con una soluzione contenente 10^6 UFC/ml di spore di *Aspergillus brasiliensis* applicata mediante tampone di cotone.

Il microrganismo selezionato, l'*Aspergillus brasiliensis (ex niger)*, è una muffa tipica degli ambienti domestici, soprattutto dei luoghi più umidi ed è uno dei principali responsabili delle macchie nere che si formano sulle pareti di alcuni locali. Durante esperienze precedenti, questa muffa è stata rilevata in grandi quantità all'interno dei rotori di ventilazione di fan coil utilizzati per molte ore al giorno.

Le spore fungine sono strutture di resistenza che resistono per lungo tempo nell'ambiente anche in condizioni sfavorevoli quali la mancanza d'acqua; **l'impiego di spore ha garantito la permanenza pressoché costante dei livelli di contaminazione per tutta la durata della sperimentazione e, inoltre, ha consentito di valutare gli effetti sanificanti su forme microbiche difficilmente eradicabili**.

3.2. Campionamento ed analisi microbiologiche

3.2.1. Metodi di campionamento

Ai fini della determinazione delle cariche microbiche sono stati impiegati i seguenti metodi di campionamento:

1) SAS (*Surface Air System*) Super 100 (International PBI): il metodo consente la determinazione della quantità di microrganismi aerodispersi e di poter valutare eventuali cinetiche di abbattimento nel tempo. La figura 1 mostra una fase di campionamento eseguita durante la sperimentazione. Lo strumento SAS è stato posto di fronte al fan coil a 50 cm di distanza dalle bocchette di ventilazione.

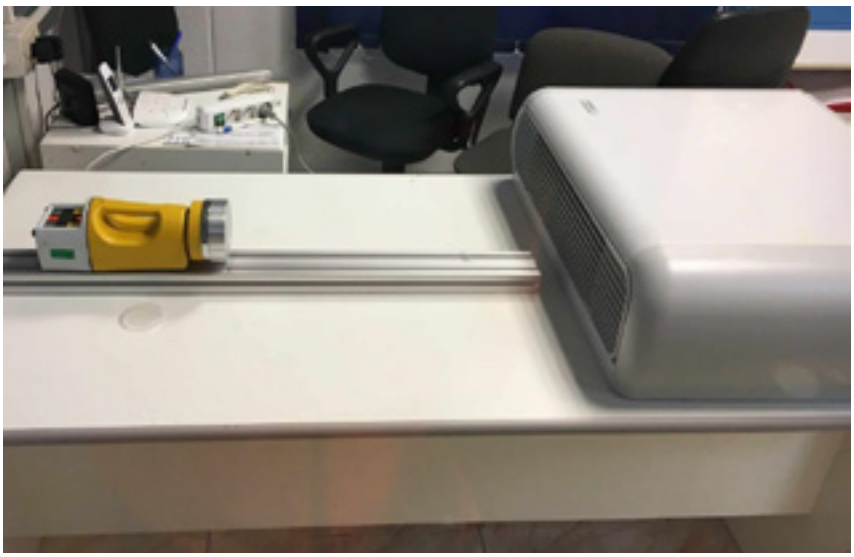

Figura 1 – prelievo di aerosol mediante SAS Super 100

2) Tampone di superficie: permette di valutare il grado di contaminazione delle superfici, nel caso in della prima sperimentazione le lamelle dell'impianto di ventilazione dei fan coil: il prelievo (figura 2) è stato effettuato su entrambe le facce di una singola aletta, successivamente marcata in modo da evitare di ripetere il prelievo dalla stessa aletta durante le sessione successive.

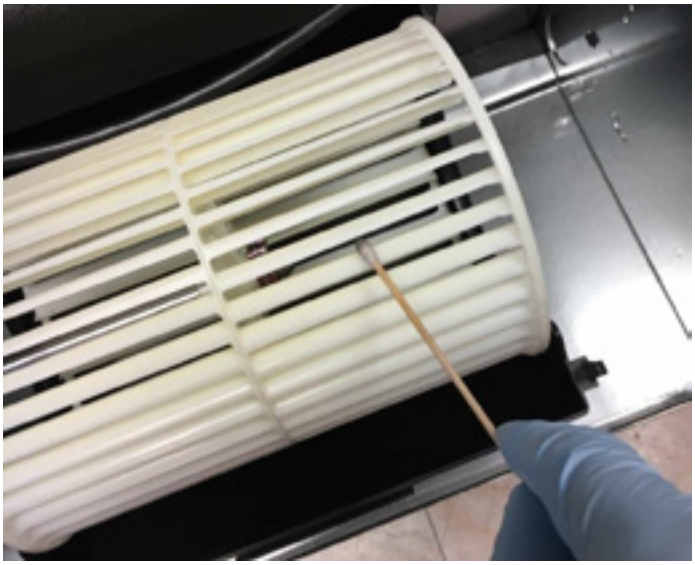

Figura 2 – prelievo dei microrganismi mediante tampone di superficie

3.2.2. Metodi analitici

Per la determinazione delle specie microbiche sono stati utilizzati i seguenti metodi analitici ufficiali:

Aerosol:

- Carica batterica totale: Metodo Unichim 1962-2:2006
- Muffe e Lieviti: Metodo Unichim 1962-2:2006

Superfici:

- Muffe e Lieviti: ISO 18593:2004 + ISO 21527-1:2008

3.3. Misura del livello di ozono

Contestualmente alla prova è stato misurato il livello di ozono prodotto all'interno del locale dove era installato il dispositivo Jonix.

La lettura del valore di concentrazione è avvenuta tramite un misuratore marca Horiba – modello APOA-370. Il range di lettura dello strumento varia da 10 ppb a 3 ppm.

Al fine di valutare la cinetica di accumulo ed i livelli di saturazione dell'ozono, la misura è stata avviata al tempo zero e proseguita per le successive 24 ore.

4. Risultati e discussione

4.1. Prima sperimentazione

4.1.1. Camere di sperimentazione

Le camere gemelle in cui è stata effettuata la sperimentazione erano due locali ad uso ufficio collocati all'interno di un capannone in cui sono effettuate prove pilota di varia natura, comprese prove su matrici naturalmente contaminate, quali compost e acque di scarico, per cui ci si attendeva la presenza di una significativa contaminazione microbica ambientale, evidenza confermata dai prelievi effettuati a inizio sperimentazione.

Al fine di evitare interferenze dovute alla contaminazione dell'ambiente esterno, le stanze sono state mantenute chiuse per tutta la durata delle prove. Per effettuare i campionamenti periodici, l'operatore entrava rapidamente nella stanza e richiudeva immediatamente la porta di ingresso. Durante le operazioni di prelievo, l'addetto indossava camice, guanti e mascherina respiratoria, in modo da minimizzare il contributo microbico legato alla sua presenza nella stanza.

4.1.2. Contaminazione dei dispositivi

Nel caso della prima sperimentazione sono state contaminate con muffe le lamelle dei rotori di ventilazione (figura 3).

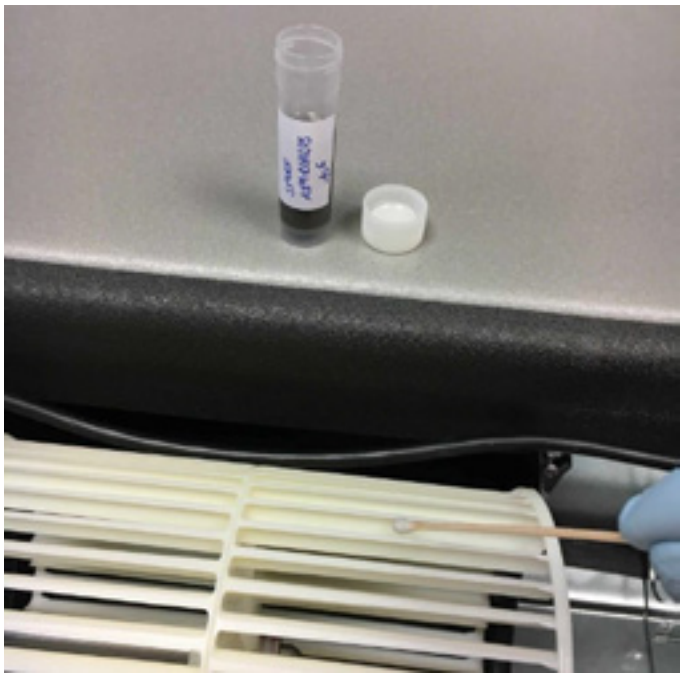

Figura 3 – contaminazione con spore fungine delle alette di ventilazione

Tutte le lamelle di ventilazione sono state contaminate su entrambe le facce, il che ha comportato un consumo di circa 3 ml di soluzione di spore per ciascun apparato, per un totale di circa 3 milioni di spore fungine per ciascun fan coil.

4.1.3. Analisi degli aerosol

La successiva tabella 1 mostra l'andamento delle cariche batteriche (CBT) rilevate negli aerosol prelevati ai vari intervalli di tempo nelle due camere di sperimentazione. La camera di "controllo" conteneva il fan coil privo del dispositivo sanificante, la camera "dispositivo" aveva al proprio interno il dispositivo dotato del sistema sanificante Jonix.

Tabella 1 – Carica batterica totale aerodispersa rilevata ai vari tempi

	Carica batterica totale a 30 °C (UFC/m³)	
Tempo (ore)	Controllo	Dispositivo NTP
0	520	620
3	540	600
6	470	540
24	450	190
48	400	30
72	380	20
120	260	50
144	260	20
168	240	50

Il grafico successivo (figura 4) riporta la rappresentazione grafica dei risultati ottenuti.

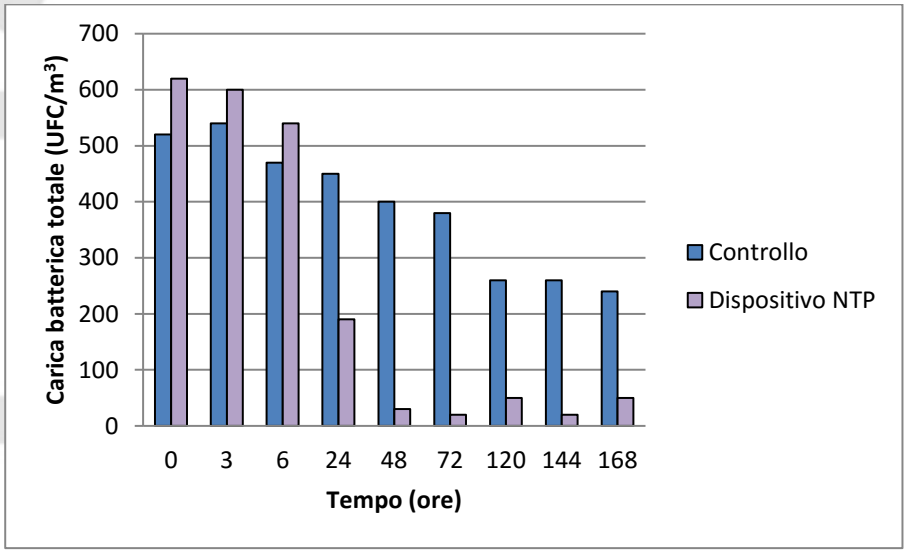

Figura 4 – Andamento della CBT aerodisperse nelle due camere di prova

Dal grafico è possibile osservare come la carica batterica totale aerodispersa tenda a diminuire all'interno della camera contenente il fan coil equipaggiato col dispositivo Jonix. Il lieve calo rilevato nella camera di controllo è da imputare al fatto che la camera veniva mantenuta chiusa e, quindi, isolata dall'ambiente esterno fonte di contaminazione

ambientale. I microrganismi aerodispersi, soprattutto i batteri, tendono a perdere vitalità a causa di fenomeni quali la disidratazione oppure a sedimentare insieme al materiale particolato che spesso li veicola per cui, in assenza di fonti di nuova contaminazione tendono a ridurre la propria concentrazione.

La successiva tabella 2 riassume i dati relativi alla contaminazione da funghi (muffe e lieviti) rilevata ai vari tempi di prelievo.

Tabella 2 – Muffe rilevate nell'aria ai vari tempi

	Muffe (UFC/m³)	
Tempo (ore)	Controllo	Dispositivo NTP
0	250	280
3	260	250
6	230	260
24	190	180
48	200	40
72	170	20
120	160	50
144	140	30
168	160	50

Il grafico successivo (figura 5) riporta la rappresentazione grafica dei risultati ottenuti.

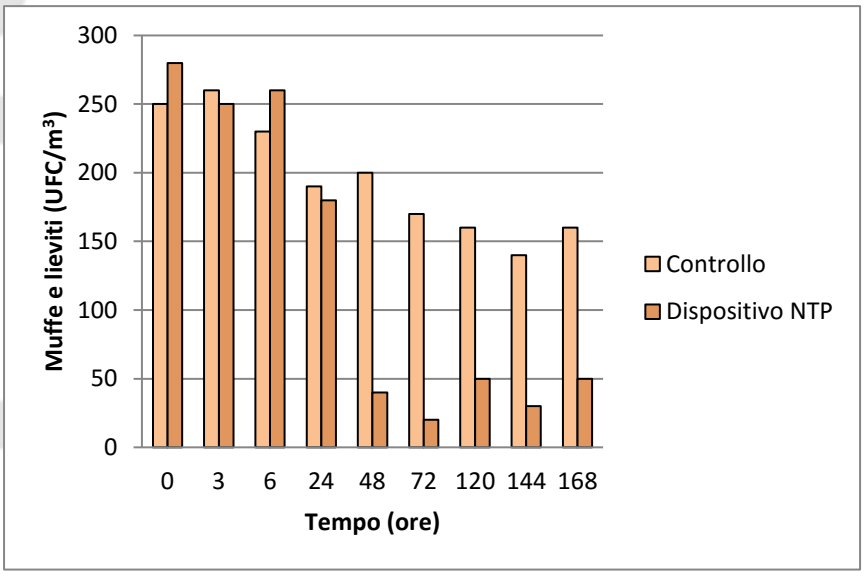

Figura 5 – Muffe e lieviti aerodispersi nelle due camere di prova

Dal grafico è possibile osservare come le muffe tendano a diminuire nell'aria della camera contenente il fan coil equipaggiato col dispositivo Jonix con una cinetica diversa rispetto a quella rilevata per i batteri.

Infatti, nel caso delle muffe, il tempo necessario a rilevare un abbassamento significativo è più lungo, probabilmente a causa della maggiore resistenza delle spore fungine rispetto alle cellule batteriche.

Il lieve calo rilevato nella camera di controllo è da imputare al fatto che la camera veniva mantenuta chiusa e, quindi, isolata dall'ambiente esterno fonte di contaminazione ambientale, per cui nel tempo si può assistere ad una "sedimentazione" dei contaminanti aerodispersi oppure ad una loro perdita di vitalità, un fenomeno che, nel caso delle muffe, è decisamente meno evidente di quanto rilevato per i batteri.

Da rilevare che le muffe utilizzate per contaminare le alette, benché rilevabili sulla superficie del rotore anche dopo giorni dall'inizio della prova (vd. paragrafo 3.1.4.), rappresentino una piccolissima percentuale di quelle rilevate nell'aria ambientale.

Le foto successive mostrano i livelli di contaminazione da muffe rilevati dopo 48 ore nella camera di controllo ed in quella contenente il dispositivo Jonix. Le foto illustrano ancor più dei numeri come sia marcata la differenza di contaminazione tra i due ambienti, sulla superficie delle piastre è possibile osservare il numero di funghi rilevati in 100 litri d'aria, praticamente la quantità d'aria respirata in circa 15 minuti da una persona adulta a riposo.

Figura 6 –Muffe e lieviti aerodispersi nelle due camere di prova (a sinistra la camera di controllo)

4.1.4. Misura dei livelli di contaminazione delle alette della girante

La successiva tabella riporta i livelli di contaminazione fungina di una singola aletta presente nel fan coil di controllo e in quello dotato di generatore NTP. La contaminazione teorica introdotta al momento della contaminazione era di circa 38.000 spore per aletta, ma essendo stata effettuata manualmente il valore può subire qualche variazione dovuta alla manualità ed alla quantità di liquido depositata sulla singola aletta. I livelli di contaminazione microbica introdotti sulle alette erano volutamente molto elevati, in modo da valutare gli effetti del sistema sanificante in condizioni estreme.

Tabella 3 – Muffe rilevate su una aletta ai singoli tempi di prelievo

	Muffe (UFC/aletta)	
Tempo (giorni)	Controllo	Dispositivo NTP
0	35000	40000
3	34000	32000
5	30000	21000
7	27000	11000

Il grafico successivo (figura 7) riporta la rappresentazione grafica dei risultati ottenuti.

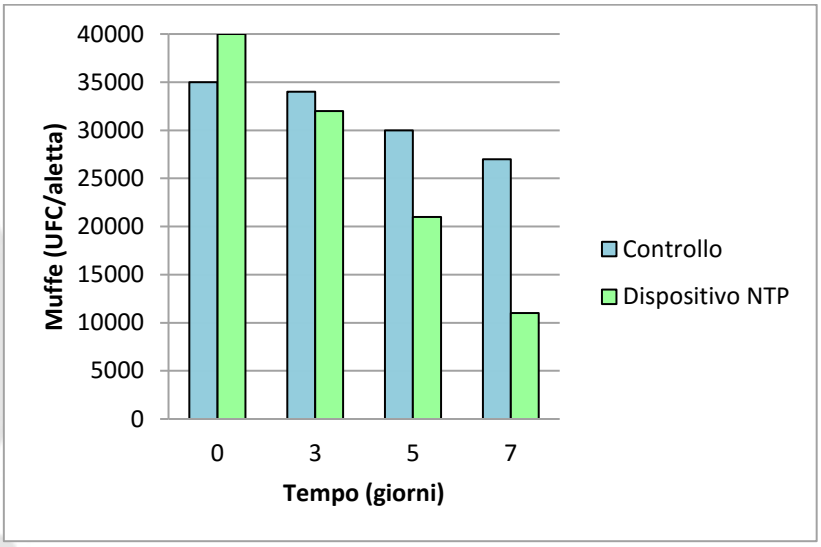

Figura 7 – Muffe rilevate su una singola aletta ai vari tempi di prelievo

I livelli di muffe presenti sulle alette del dispositivo di controllo tendono a scendere a causa dell'azione meccanica dovuta al moto vorticoso del rotore di ventilazione ma, dopo 7 giorni il numero di spore si riduce di circa un 20% soltanto, mentre nel dispositivo dotato di generatore NTP la riduzione osservata supera il 70%. Da questi dati si può dedurre che circa un 50% delle spore fungine è stato ucciso dalle specie ossidanti prodotte dal generatore NTP.

Nell'interpretare i risultati occorre considerare che il rotore è posto a monte del generatore NTP per cui, a causa del flusso d'aria generato dal rotore stesso, l'effetto sanificante è dovuto prevalentemente alle specie ossidanti che rientrano nel dispositivo dopo essere state liberate nell'ambiente, per cui il risultato ottenuto in una sola settimana è sicuramente incoraggiante.

4.2. Seconda sperimentazione

4.2.1. Camera di sperimentazione

La grande stanza in cui è stata effettuata la sperimentazione è un locale di servizio adiacente ad altri ad uso ufficio, per cui ci si attendeva la presenza di una contaminazione microbica ambientale relativamente bassa, evidenza confermata dai prelievi effettuati a inizio sperimentazione.

Trattandosi di un grande locale, al fine di garantire un sufficiente numero di ricambi/ora (almeno 5) sono stati impiegati 2 fan coil dotati di dispositivo NTP settati ad una portata di 640 m^3/ora. I due dispositivi sono stati collocati in 2 aree differenti del locale, in modo da garantire un trattamento ottimale dell'aria ambiente.

Al fine di evitare interferenze dovute alla contaminazione dell'ambiente esterno, la stanza è stata tenuta chiusa per tutta la durata delle prove. Per effettuare i campionamenti periodici, l'operatore entrava rapidamente nella stanza e richiudeva immediatamente la porta di ingresso. Durante le operazioni di prelievo, l'addetto indossava camice, guanti e mascherina respiratoria, in modo da minimizzare il contributo microbico legato alla sua presenza nella stanza.

4.2.2. Contaminazione dei dispositivi

In questo caso la contaminazione ha riguardato una superficie piana posta a valle del generatore NTP (figura 8).

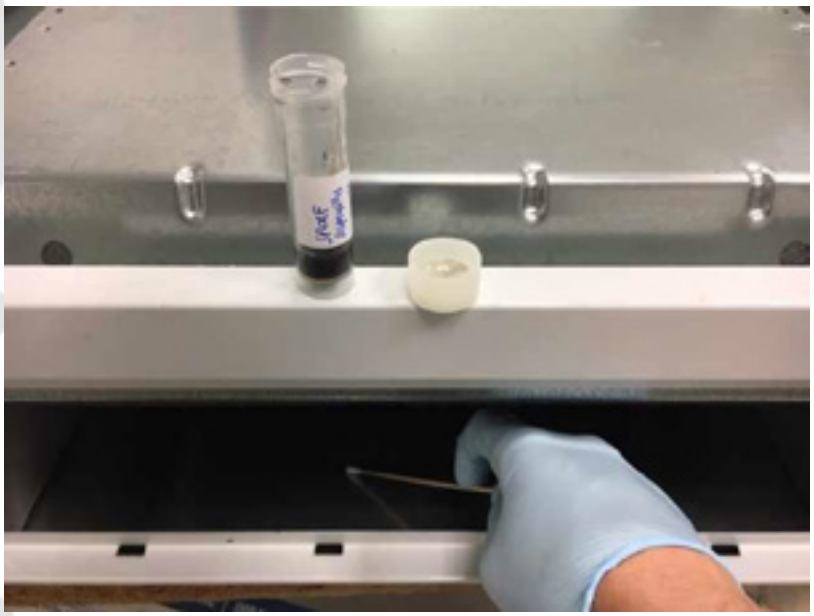

Figura 8 – contaminazione del dispositivo con spore fungine

L'area è stata contaminata con circa 30.000 spore di *Aspergillus brasiliensis* per centimetro quadrato di superficie.

4.2.3. *Analisi degli aerosol*

La successiva tabella 4 mostra l'andamento delle cariche batteriche (CBT) e delle Muffe rilevate negli aerosol prelevati ai vari intervalli di tempo nella camera di sperimentazione.

Tabella 4 – Contaminazione microbica aerodispersa rilevata ai vari tempi

Tempo (giorni)	CBT 30°C (UFC/m³)	Muffe (UFC/m³)
0	100	50
1	40	30
4	10	20
5	40	10
6	20	20
7	40	30
8	20	20
10	20	30
11	20	30
12	20	30

I grafici successivi (figure 9 e 10) riportano la rappresentazione grafica dei risultati.

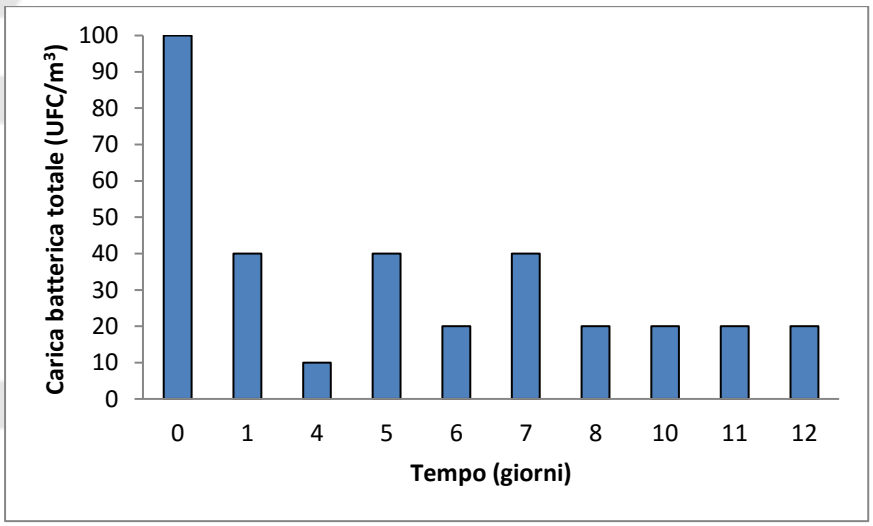

Figura 9 –CBT aerodisperse nella camera di prova

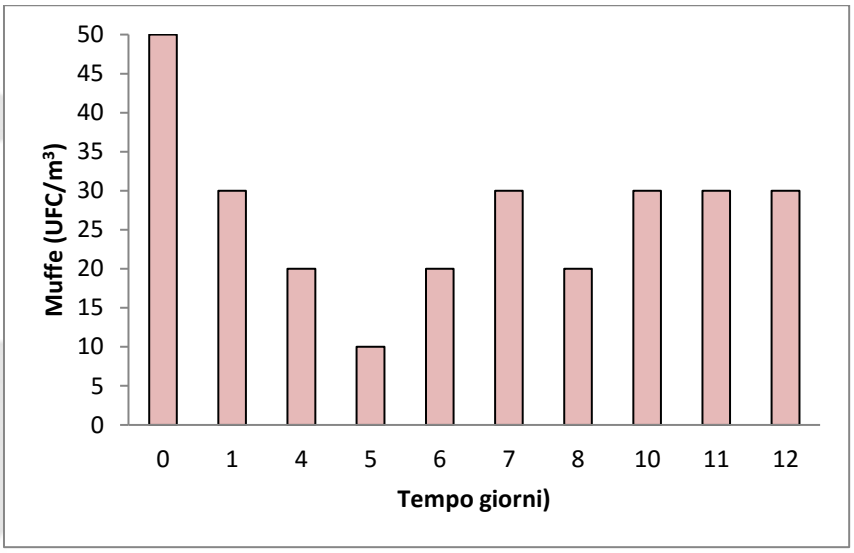

Figura 10 – Muffe aerodisperse nella camera di prova

Contrariamente a quanto rilevato nel corso della prima prova, i valori di contaminazione ambientale sono molto bassi già all'inizio della sperimentazione. Sia le CBT che le Muffe diminuiscono nel tempo per stabilizzarsi su un "rumore di fondo" sotto il quale è praticamente impossibile scendere, dal momento che non si può ipotizzare di raggiungere una condizione di sterilità assoluta.

4.2.4. Misura dei livelli di contaminazione dell'interno del dispositivo

La Tabella successiva contiene i valori medi dei prelievi effettuati in 2 diverse aree della superficie interna al dispositivo contaminata artificialmente con spore fungine.

Tabella 5 – Muffe rilevate nel dispositivo ai singoli tempi di prelievo

Tempo (giorni)	Muffe interno dispositivo (UFC/cm²)
0	28800
1	26000
4	15000
5	9900
6	6900
7	5900
8	5200
10	4600
11	4000
12	3500

La successiva figura 11 mostra i dati riportati in forma grafica.

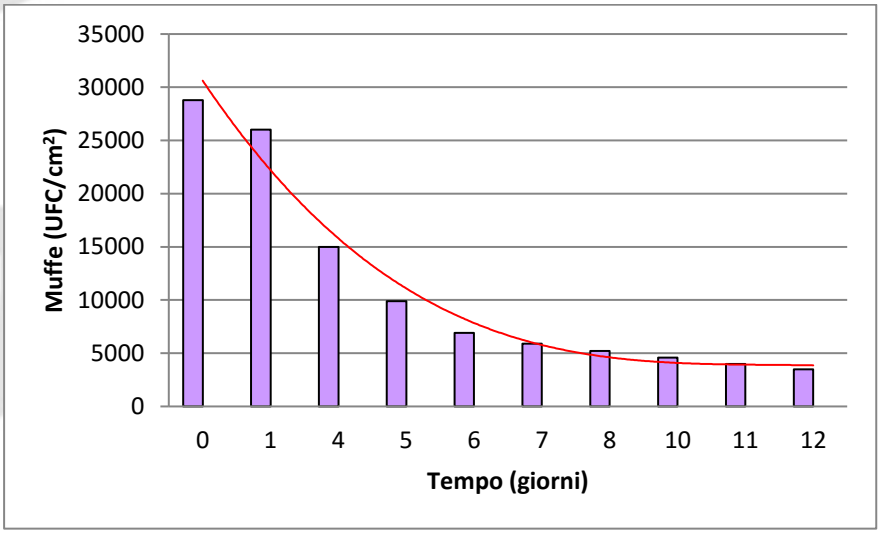

Figura 11 – Muffe rilevate all'interno del dispositivo

La contaminazione fungina cala costantemente, ma la curva di abbattimento (linea rossa) sembra tendere a ridurre la propria pendenza nel tempo. I valori di contaminazione a 12 giorni dall'inizio della sperimentazione sono comunque un decimo di quelli iniziali.

4.3. Breve sperimentazione finalizzata all'ottimizzazione del processo di auto-sanificazione

La seconda sperimentazione è stata prolungata per ulteriori 2 giorni (dal 12° al 14°) al fine di individuare un potenziale miglioramento tecnico/impiantistico che consentisse di ottimizzare il processo di auto-sanificazione del dispositivo contenente la sonda Jonix.

In pratica, i fan coil ancora contaminati sono stati lasciati in funzione per altri 2 giorni con le stesse modalità previste dalla sperimentazione descritta al punto 3.2, con una sola variazione sperimentale:

- per 3 volte al giorno il dispositivo di ventilazione di uno dei fan coil veniva spento per 2 minuti lasciando il generatore NTP acceso;
- durante i 2 minuti di spegnimento della ventola, ogni 20 secondi veniva dato un impulso di accensione e spegnimento al rotore di ventilazione (totale 6 impulsi).

In questo modo, durante i 20 secondi di fermo ventilazione le sostanze ossidanti si accumulavano nelle immediate vicinanze del generatore per poi venire convogliate nelle aree adiacenti grazie all'impulso di accensione del rotore; l'immediato spegnimento di quest'ultimo impediva di far fuoriuscire la maggior parte delle specie ossidanti dal fan coil e permetteva a queste ultime di agire sulle muffe ancora presenti nell'area contaminata artificialmente.

Questa strategia ha consentito di accelerare il processo di abbattimento delle muffe residue che, ricordiamo, al 12° giorno erano ancora 3500 UFC/cm^2 .

Il successivo diagramma mostra l'andamento delle cariche fungine all'interno del dispositivo nei 3 giorni di sperimentazione.

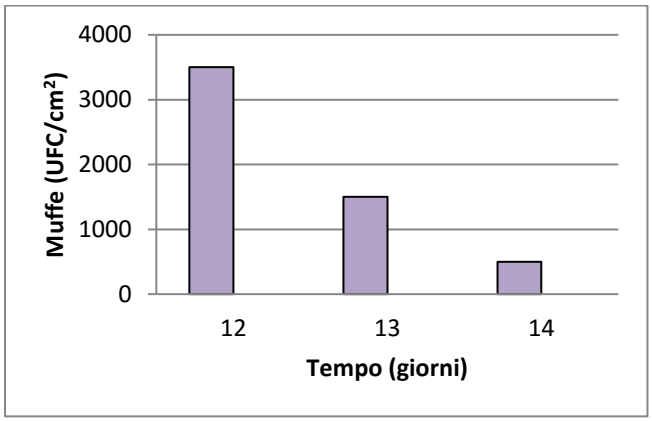

Figura 12 – Muffe rilevate all'interno del dispositivo

Dal diagramma è possibile osservare come in soli 2 giorni le muffe contaminanti siano scese da 3500 a 500 UFC/cm^2.

La successiva figura mostra i risultati ottenuti messi "in coda" al grafico relativo alle muffe contaminanti rilevate nel corso della sperimentazione descritta al punto 3.2.

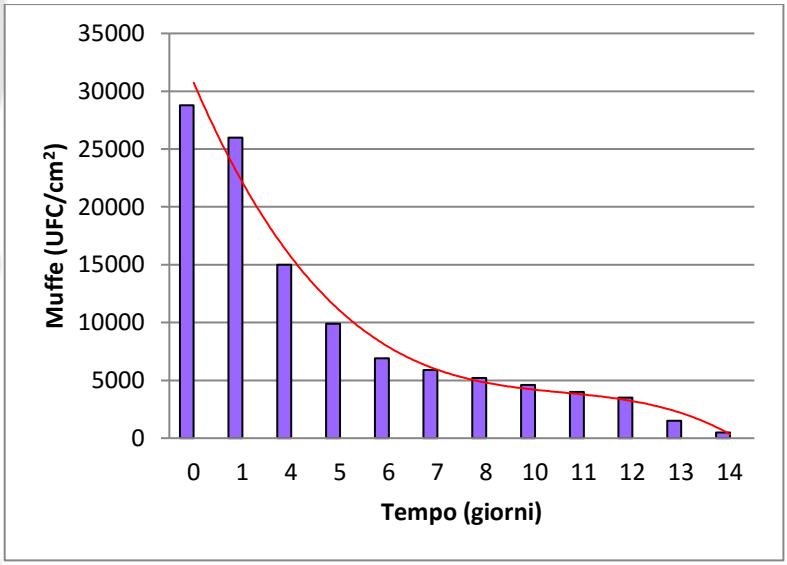

Figura 13 – Muffe rilevate all'interno del dispositivo

I dati fino al 12° giorno sono relativi alla prova descritta al paragrafo 3.2, mentre gli ultimi 2 dati (giorno 13 e 14) sono relativi ai risultati ottenuti dalla prova descritta nel presente paragrafo. È interessante vedere come la linea di tendenza cambi nettamente la propria pendenza, dimostrando una forte accelerazione del processo di abbattimento dei microrganismi.

Questa semplice strategia si è dimostrata in grado di accelerare ed ottimizzare il processo di auto-sanificazione dello strumento: da misure effettuate con un misuratore Horiba è stato rilevato che, nei 2 minuti di durata del processo di

spegnimento del rotore, all'interno dello strumento (e soltanto in questo micro-ambiente) si raggiungono concentrazioni di ozono di circa 200 ppb, ovvero 10 volte superiori a quelle rilevate in condizioni di normale operatività.

4.4. . Misura del livello di ozono ambientale ed in uscita dal condizionatore

4.4.1. Misura della concentrazione di ozono ambientale

Contestualmente alla prova è stato misurato il livello di ozono prodotto all'interno del locale dove era installato il dispositivo Jonix.

L'analizzatore Horiba è stato posto al centro dell'area di prova al fine di acquisire il valore del livello di ozono durate la prova. In Figura 14 viene riportato il grafico dei valori acquisiti, ogni punto rappresenta la media di 30 minuti di acquisizione.

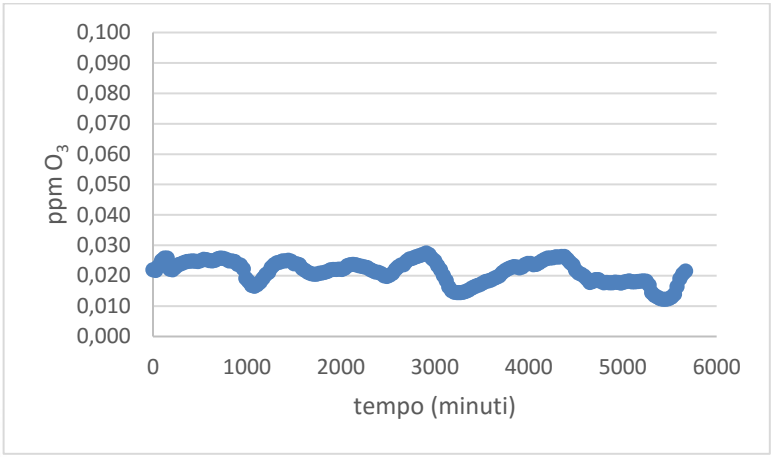

Figura 14 - curva di concentrazione ozono

Dal grafico riportato è possibile osservare che non vi è alcuna variazione significativa del livello di ozono, che rimane costantemente sotto al valore di 30ppb e comunque prossimo al valore minimo rilevabile.

Le leggere oscillazioni che si osservano possono essere attribuite a fattori ambientali (temperatura etc..).

4.4.2. Misura livello di ozono uscita fan coil

Il test è stato condotto per verificare l'uniformità nella distribuzione dell'ozono all'interno del fan coil, in quanto essendo il tubo posizionato lateralmente rispetto al flusso d'aria che lo investe, è ragionevole ipotizzare che possa verificarsi una condizione di disomogeneità come quella illustrata.

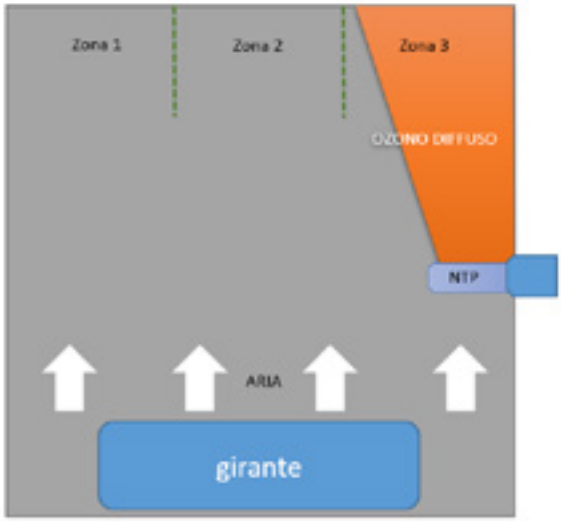

Figura 15 – ipotesi diffusione ozono all'interno del fan coil

La bocca di uscita è stato pertanto suddivisa in tre zone, come in figura, ed in ognuna è stata eseguita la misura di ozono per circa 40 minuti. I risultati sono riportati in Figura 16, ogni punto è relativo ad una media su tre minuti di acquisizioni.

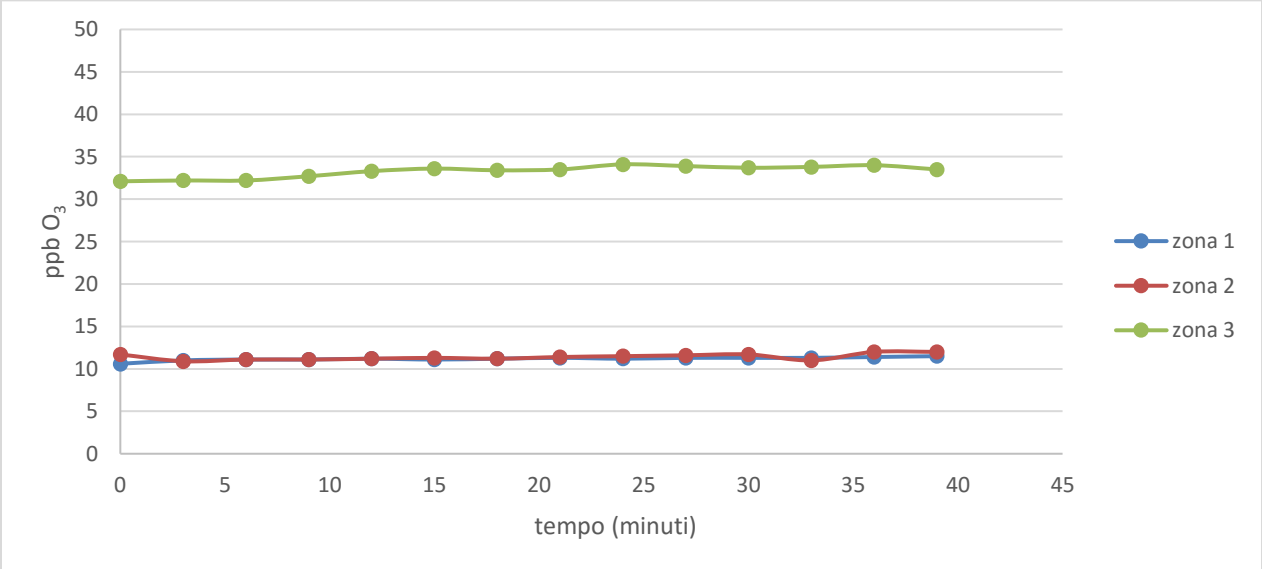

Figura 16 – livelli di ozono in uscita dal fan coil

Dai grafici riportati è possibile osservare chiaramente come vi sia una netta concentrazione dell'ozono nella Zona 3.

5. Conclusioni

L'ambiente utilizzato per la prima sperimentazione è stato selezionato perché caratterizzato da una contaminazione microbica che può essere definita di media entità, sicuramente più elevata di quella rilevabile in un ambiente domestico - oppure in un ufficio - pulito e areato con regolarità. Infatti, nel programmare le prove sperimentali si è voluto inizialmente valutare l'efficacia del dispositivo in condizioni "sfavorevoli" e, per tale motivo, la situazione è stata ulteriormente "aggravata" contaminando artificialmente le giranti di ventilazione degli apparati con muffe tipiche di ambienti umidi e malsani.

I risultati ottenuti mostrano come l'adozione di un dispositivo di sanificazione Jonix consenta di ottenere nel tempo una marcata riduzione della contaminazione microbica ambientale sia in termini di batteri che di muffe e lieviti.

La cinetica di abbattimento dei contaminanti microbici, siano essi batteri, muffe o lieviti, richiede almeno 48 ore di utilizzo continuativo dell'apparato, mantenendo chiuso il locale in cui esso è attivo, per cui c'è da attendersi che, in caso di utilizzo del dispositivo per qualche ora al giorno, i tempi necessari al raggiungimento di bassi livelli di contaminazione ambientale siano più lunghi. D'altro canto, a parziale compensazione di quest'ultima affermazione, occorre anche considerare che le condizioni ambientali in cui è stata svolta la sperimentazione erano volutamente peggiori di quelle normalmente presenti in un ambiente "domestico".

Quando il dispositivo viene introdotto in un ambiente a bassa contaminazione ambientale, quale quello di un ufficio, i livelli di contaminazione vengono rapidamente abbattuti a valori molto bassi che abbiamo definito "rumore di fondo", al di sotto dei quali è possibile scendere soltanto mediante l'adozione di strategie impiantistiche necessarie solo per ambienti particolari, quali le camere bianche di confezionamento dei farmaci (filtri HEPA, ambiente con pressione positiva dotato di anticamera, etc.).

Riguardo alla capacità auto-sanificante del dispositivo, la contaminazione artificiale da muffe adottata in entrambe le sperimentazioni era volutamente elevata, in modo da valutare le potenzialità del dispositivo anche in condizioni molto sfavorevoli.

Tali condizioni si potrebbero verificare dopo lunghi tempi di funzionamento in un fan coil privo di generatore NTP, mentre è inimmaginabile che si verifichino nel caso in cui un dispositivo nuovo di fabbrica presenti al suo interno un generatore NTP che consenta di prevenire l'instaurarsi ed il proliferare di una contaminazione microbica così elevata.

L'adozione di una semplice strategia impiantistica, come quella descritta al punto 3.3 potrebbe migliorare decisamente il processo di auto-sanificazione dello strumento, senza che sia necessario introdurre costose modifiche tecniche.

I dati riportati al paragrafo 3.4, relativi alla distribuzione dei livelli di ozono all'interno del fan coil, fanno pensare che potrebbe essere valutato, per una eventuale e successiva ottimizzazione, un diverso posizionamento del generatore NTP all'interno del condizionatore, in modo da favorire una più omogenea diffusione delle specie ossidanti al suo interno ed in uscita da esso. In ogni caso l'attuale situazione risulta comunque ampiamente cautelativa circa l'effetto sanificante o "autosanificante" dell'apparecchio con il sistema JONIXinside.

In conclusione, sulla base di quanto constatato durante la sperimentazione, è possibile affermare che l'adozione di un generatore NTP all'interno di un apparato fan coil può presentare il duplice vantaggio di mantenere a bassi livelli

la quantità di microrganismi aerodispersi - anche in aree caratterizzate da consistente contaminazione ambientale - e di prevenire la contaminazione dello strumento da parte di microrganismi indesiderati, in particolare le muffe.

Pisa, 13 marzo 2017

Laboratori ARCHA S.r.l. unipersonale
Via di Tegulaia 10/a - 56121 - PISA - ph. +39 050 985165 - fax +39 050 985233 - www.archa.it - archainf@archa.it
C.F., P.IVA, Iscr. Reg. Impr. di Pisa n. 01115340505 - Rep. Econ. Amm. di Pisa n°101169 - Capitale Sociale 101.400,00 i.v.

ALLEGATO 12.9

Sperimentazione per la verifica della CAPACITÀ SANITIZZANTE dei dispositivi Fotocatalitici vs Condensatori Jonix NTP

ARCHA

ACCREDIA
LAB N° 0522

Sperimentazione per la verifica della

CAPACITÀ SANITIZZANTE

dei dispositivi

Fotocatalitici vs Condensatori Jonix NTP

Laboratori ARCHA S.r.l. unipersonale
Via di Tegulaia 10/a - 56121 - PISA - ph. +39 050 985165 - fax +39 050 985233 - www.archa.it - archainf@archa.it
C.F., P.IVA, Iscr. Reg. Impr. di Pisa n. 01115340505 - Rep. Econ. Amm. di Pisa n°101169 - Capitale Sociale 101.400,00 i.v.

Sommario

Premesse

La Laboratori ARCHA ha impostato uno studio sperimentale, con l'obiettivo di verificare e quantificare l'eventuale effetto sanitizzante svolto da due tipologie di dispositivi commerciali (NTP-Jonix ed un dispositivo Fotocatalitico SHU900X) , all'interno di una condotta in acciaio da 30 cm di diametro e lungo 12 m, dove viene fatta passare aria (attraverso un ventilatore) a differenti velocità/portate.

L'obiettivo era quello di simulare cosa accade all'interno di una condotta di areazione in caso di contaminazione microbiologica e nel caso fossero o meno presenti dei dispositivi "sanitizzanti" tipo quelli testati.

A tale scopo, ARCHA ha progettato e condotto una serie di esperimenti nei quali, in modo controllato, differenti tipologie e quantità di microrganismi sono stati esposti all'interno del tubo, a flussi di aria con differenti tipologie di dispositivi sanitizzanti attivati.

Riguardo a questa tipologia di test, non esistendo delle norme tecniche di riferimento, ARCHA ha dovuto procedere alla messa a punto di procedure di test adeguate, andando a verificare sperimentalmente le condizioni operative più opportune/funzionali per lo studio dei fenomeni e andando ad individuare i settaggi da adottare in termini di:

- Portate di aria del ventilatore
- Tipologie e concentrazioni di microrganismi da testare
- Tempi e modalità di contatto coi sistemi sanitizzanti

In merito alla portata di aria all'interno del tubo- test, sono state condotte delle prove preliminari ed è stato verificato che non era possibile agire in modo controllato e riproducibile con microrganismi e piastre di coltura in presenza di flussi di aria elevati come quelli tipicamente segnalati dal Dr.Marangon (2.000 m^3/h).

Per questo motivo i test sono stati messi a punto e condotti con flussi di aria più bassi (130 m^3/h e 800 m^3/h) ed i test sono stati condotti tutti in modo COMPARATIVO "NTP-Jonix vs. Fotocatalitico", in modo da avere una lettura relativa dei fenomeni (i.e. quale dei 2 dispostivi funziona meglio a parità di condizioni operative?) e potersi così svincolare dalla "realisticità" delle condizioni operative adottate.

L'impianto di prova sul quale sono stati condotti i test è costituito da un plenum quadrato all'interno del quale è installato un ventilatore a portata regolabile, il cui range può essere regolato da 100 a 2000 m^3/h. Da esso l'aria viene convogliata in una condotta circolare avente diametro 30 cm. Per garantire che i dispositivi lavorino in regime di flusso lineare i sistemi di sanificazione sono stati installati subito a valle di un tratto lineare di due metri, che sono stati considerati sufficienti per garantire la stabilizzazione dei flussi eliminando eventuali turbolenze dovute al pescaggio dell'aria. Il tratto dell'impianto nel quale sono stati effettuati i test, in coda ai dispositivi, è costituito da una condotta di 10 m. Lo schema generale dell'impianto viene riportato in Figura 1.

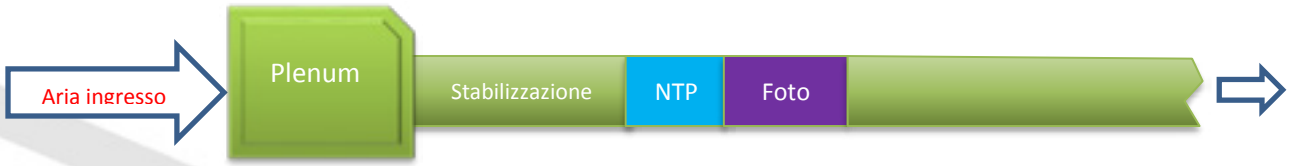

Figura 1 - configurazione impianto pilota

I dispositivi sanitizzanti testati negli esperimenti condotti da ARCHA sono i seguenti:

- JONIX – NTP, allestito con N° 2 tubi Modello C;
- SHU - Modello 900X;

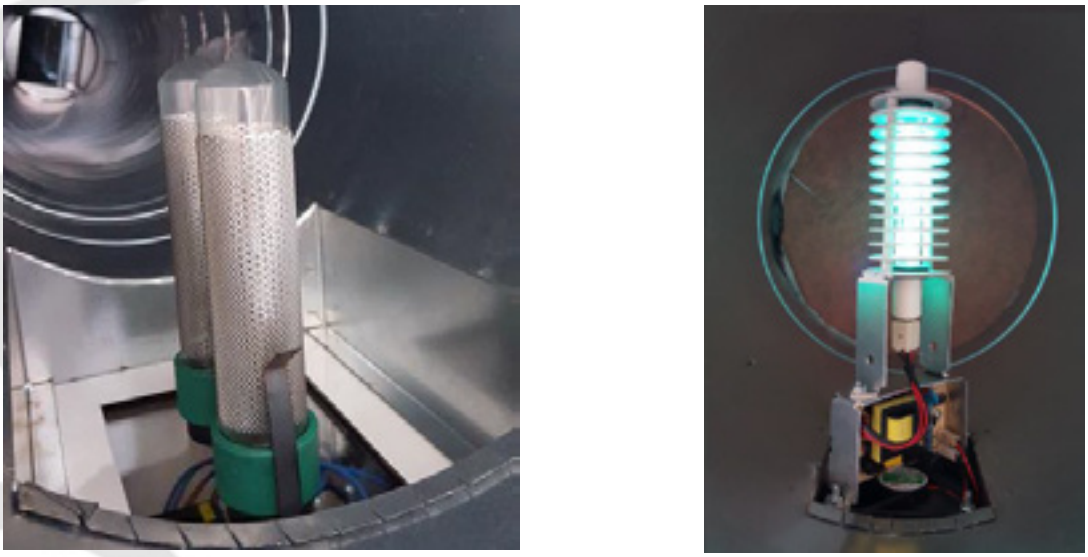

Figura 2 - JONIX-NTP (sinistra), SHU 900X (destra)

Il sistema **JONIX NTP** si basa sull'utilizzo di un sistema barrier discharge per la generazione di plasma freddo (NTP) che a sua volta è in grado di produrre le specie attive (Figura 2 – sinistra).

Il sistema **SHU** si base su un sistema di ossidazione catalitico promosso su una superficie di drogata con un catalizzatore al nano Nichel ed attivata da una sorgente luminosa costituita da una lampada UVC (Figura 2 – destra).

Misure di ozono e numero di ioni

Sono state condotte delle misure per quantificare la concentrazione di ozono e di ioni presenti nell'aria nel momento in cui vengono attivati i dispositivi sanitizzanti oggetto del presente studio.

Le misure sono state condotte alla fine del tubo di 12m, secondo quanto illustrato nella seguente figura:

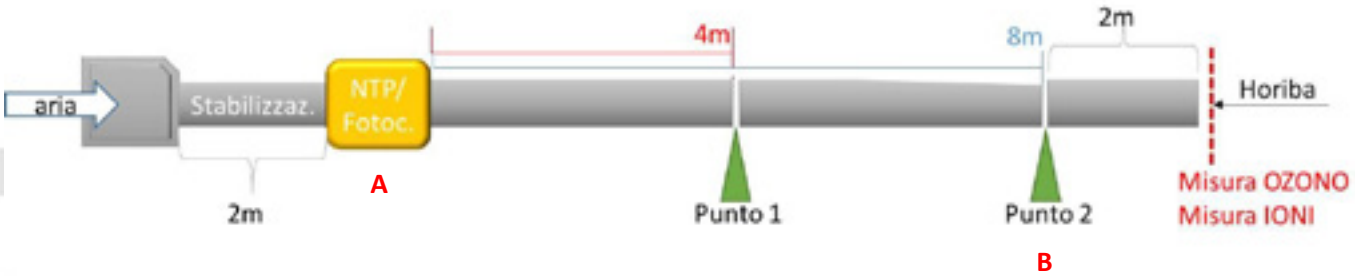

La misura della **concentrazione di ozono** è stata fatta mediante un analizzatore in continuo **HORIBA – APOA – 370**, equipaggiato con sonda di aspirazione posta al punto di uscita dell'aria e nel centro della tubazione. Il range di lettura dello strumento varia da 0,0001 ppm a 3 ppm.

Le misure sono state effettuate impostando una portata di 130m^3/h (portate superiori comportano eccessiva diluizione). Considerata la natura instabile dell'ozono, nonché le basse concentrazioni prossime al limite di quantificazione dello strumento, le misure sono state ripetute in quintuplo e quindi mediate.

Gli assetti dei dispositivi sanitizzanti testati sono stati i seguenti (si faccia riferimento alla figura sopra riportata):

- Dispositivo Jonix NTP, posizionato nel punto A;
- Dispositivo fotocatalitico, posizionato nel punto A;
- Fotocatalitico + NTP JONIX "vicini" , posizionati entrambi nel punto A;
- Fotocatalitico + NTP JONIX "lontani": il dispositivo NTP posizionato nel punto A, mentre il sistema Fotocatalitico è posizionato nel punto B.

La Tabella 1 riporta i risultati numerici mentre in Figura 3 un grafico illustra i risultati ottenuti.

Tabella 1 - media aritmetica misure di ozono

	Media (ppb)	Dev. stand
Jonix	43	± 12
Fotocatalitico	8	± 2
Jonixi - foto (vicini)	54	± 7
Jonixi - foto (lontani)	68	± 3

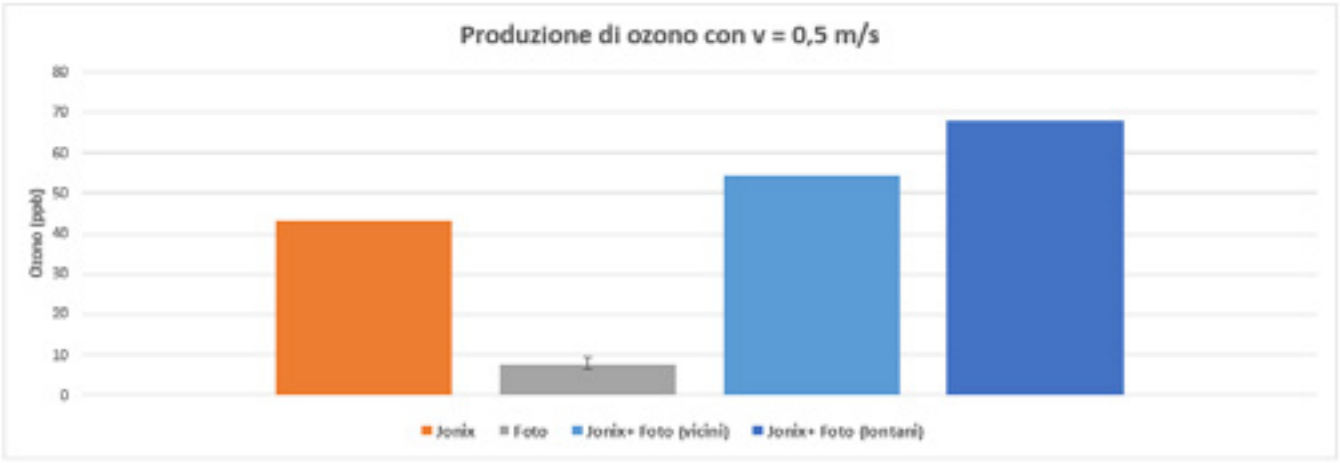

Figura 3 – valori di ozono rilevati

La misura del **numero di ioni** nel flusso di aria è stata condotta con un contaioni della AlphaLab Inc. Mod. AIC, che è in grado di misurare la densità di ioni presente nell'aria con una range di lettura che parte da 10 ioni/cm^3 (concentrazione di fondo naturale) ed arriva fino a 2x10^6 ioni/cm^3. La misura è stata effettuata nel medesimo punto di campionamento utilizzato per le misure di ozono. Occorre precisare che la naturale instabilità degli ioni rende le misure affette da notevole incertezza. Il produttore riporta una accuratezza del 25% rispetto al valore letto.

	Jonix	**Δ**	**Foto**	**Δ**	**Jonix+ Foto**	**Δ**
Ioni positivi	15.000	± 3750	400	± 100	15.000	± 3750
Ioni negativi	10.000	± 2500	10.000	± 2500	23.000	± 5750
Ioni totali	500	± 125	600	± 150	300	± 75

Figura 4 - concentrazione ionica (Ioni/cm3) in uscita

I valori di ioni rilevati sono conformi con quanto ragionevolmente attendibile dai dispositivi elettrici impiegati.

Dalle misure effettuate si possono fare le seguenti considerazioni:

- Il sistema fotocatalitico produce ozono in basse quantità (< 10 ppb)
- Il sistema fotocatalitico produce leggermente più ozono senza fotocatalizzatore (solo lampada UV)
- Il dispositivo Jonix a 2 tubi C produce 4 volte più ozono del sistema Fotocatalitico (> 40 ppb)
- Mettendo in serie i due sistemi (Jonix + Foto oppure Foto + Jonix), vicini o lontani, l'ozono formato è la somma dell'ozono prodotto dai due dispositivi: il Foto non è in grado di abbattere l'ozono formato da Jonix, anzi lo forma a sua volta
- A valori di portata di aria solitamente utilizzati su impianti reali (500-2.000 m^3/h) la concentrazione di ozono risulta ampiamente sotto i limiti (50 ppb) anche col sistema Jonix
- Il sistema Fotocatalitico forma molti meno ioni (+) del sistema Jonix.
- Il sistema Fotocatalitico forma lo stesso numero di ioni, anche se «nudo» (senza fotocatalizzatore)
- La combinazione dei 2 sistemi (Jonix + Foto) forma un numero di ioni che è la somma degli ioni prodotti dai singoli sistemi (effetto ADDITIVO, come per OZONO)
- Sia il sistema Jonix che quello fotocatalitico formano «pochi» ioni se confrontati con un "tipico" generatore di ioni (si veda la figura sotto riportata):

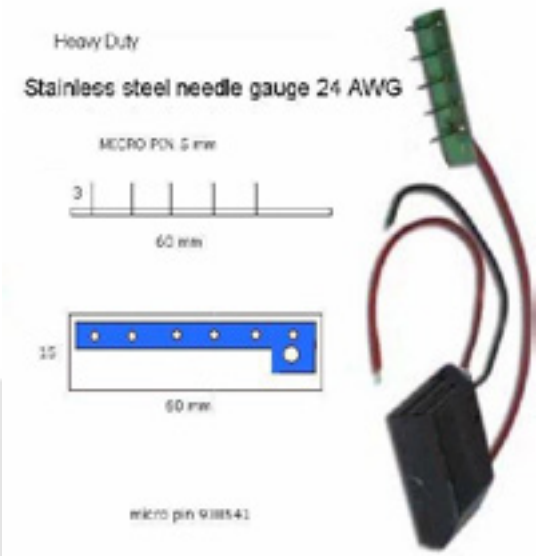

Performance:
• Ion density: $3.1x10^{12}$ ions/cm^3 at 2.9 cm from emitter
• High voltage output 9.5 Kv.
• Power use: less than 1 watt
• Power requirements: 12VDC

Tipico generatore di ioni basato sull'effetto "punta" e sue performance caratteristiche

Sono state anche fatte misure per quantificare i consumi elettrici dei due dispositivi di sanitizzazione: la seguente tabella riporta i valori rilevati.

	Jonix	Foto
Consumi elettrici (Watt)	13	11

I consumi elettrici dei 2 dispositivi sono assolutamente confrontabili.

Test di verifica dell'effetto sanitizzante dei dispositivi

La Laboratori ARCHA ha impostato uno studio sperimentale, con l'obiettivo di verificare e quantificare l'eventuale effetto sanitizzante svolto da due tipologie di dispositivi commerciali (NTP-Jonix ed un dispositivo Fotocatalitico SHU900X), all'interno di una condotta in acciaio da 30 cm di diametro e lungo 12 m, dove viene fatta passare aria (attraverso un ventilatore) a differenti velocità/portate.

L'obiettivo era quello di simulare cosa accade all'interno di una condotta di areazione in caso di contaminazione microbiologica e nel caso fossero o meno presenti dei dispositivi "sanitizzanti" tipo quelli testati.

A tale scopo, ARCHA ha progettato e condotto una serie di esperimenti nei quali, in modo controllato, differenti tipologie e quantità di microrganismi sono stati esposti all'interno del tubo, a flussi di aria con differenti tipologie di dispositivi sanitizzanti attivati.

In particolare, il tubo simulante il condotto di areazione dove sono stati condotti i test è rappresentato nella seguente figura:

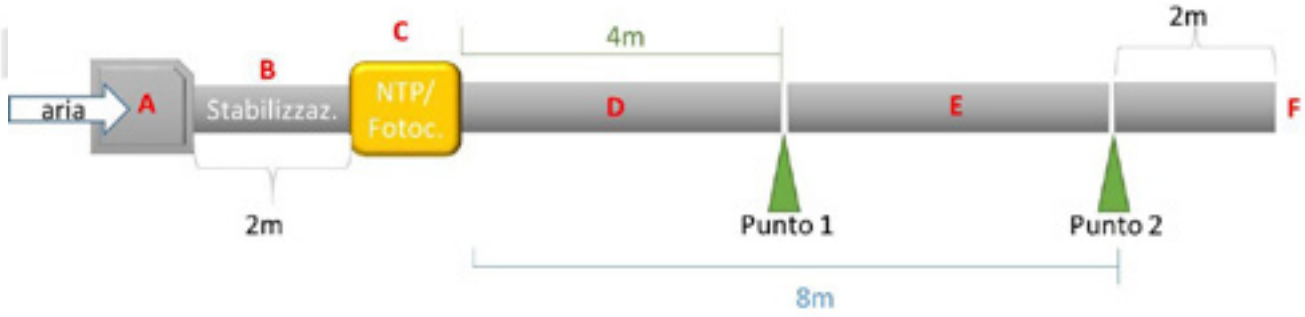

Un ventilatore (**A**) è in grado di generare flussi di aria a diversa portata, e quindi a diversa velocità, all'interno del tubo.

Dopo un tratto di 2m (**B**) necessario a stabilizzare il flusso di aria, sono stati alloggiati i dispositivi sanitizzanti testati (**C**).

Le verifiche della contaminazione microbiologica presente nell'aria sono state condotte in differenti punti lungo il tubo: nel Punto 1 (dopo 4m dai dispositivi di sanitizzazione – tratto **D**), nel Punto 2 (dopo 8m dai dispositivi di sanitizzazione – tratto **E**), e all'uscita del tubo (**F**).

Nei test condotti, sono state eseguite due tipologie di esperimenti di tipo microbiologico:

- Test su piastre Petri contaminate, esposte a flussi di aria all'interno del tubo;
- Test mediante bio-aerosl, nebulizzato in continuo all'interno del tubo.

Tali tipologie di test sono strutturalmente diverse e permettono di fornire informazioni diverse sui fenomeni in gioco:

- **Test su piastre Petri contaminate, esposte a flussi di aria all'interno del tubo (PROVE SU PIASTRA ESPOSTA)**: in questo caso, delle piastre di coltura microbiologica, contaminate da differenti tipologie di microrganismi a concentrazione nota, sono state esposte all'interno del tubo ad un flusso di aria definito, attivando o meno i diversi dispositivi di sanitizzazione. In questa tipologia di esperimento, le variabili indagate sono state:

- La distanza delle piastre dal dispositivo sanitizzante (i campionamenti microbiologici sono stati condotti nei seguenti punti: Punto 1 e Punto 2)
- Il tempo di esposizione all'aria e al dispositivo sanitizzante (i.e. misure protratte per differenti tempi di esposizione): maggiore è il tempo che le piastre Petri rimangono esposte all'azione dell'aria, e migliore/maggiore è l'effetto che dovrei aspettarmi da una eventuale sanificazione

Con questa tipologia di test, i microrganismi si trovano in un "ambiente" a loro estremamente favorevole, con grandi quantità di nutrimento a disposizione (i.e. terreno di coltura), nelle condizioni ottimali di pH, in una sorta di "culla" che ne favorisce la sopravvivenza e la crescita, costituita da enormi quantità di sostanza organica che potrebbe essere un "interferente"/"competitor" ai microrganismi nelle reazioni con le specie "attive" generate dai dispositivi di sanitizzazione testati. Tale test è quindi da considerarsi come "conservativo" (*worst case*) nei confronti della verifica dell'effetto dei dispositivi oggetto di studio.

- **Test mediante bio-aerosl, nebulizzato in continuo all'interno del tubo**: in questo caso, un aerosol di microrganismi di diversa natura, a concentrazione nota, vengono nebulizzati in modo continuo all'interno del tubo, nel punto indicato nella seguente figura, in concomitanza all'attivazione del flusso di aria.

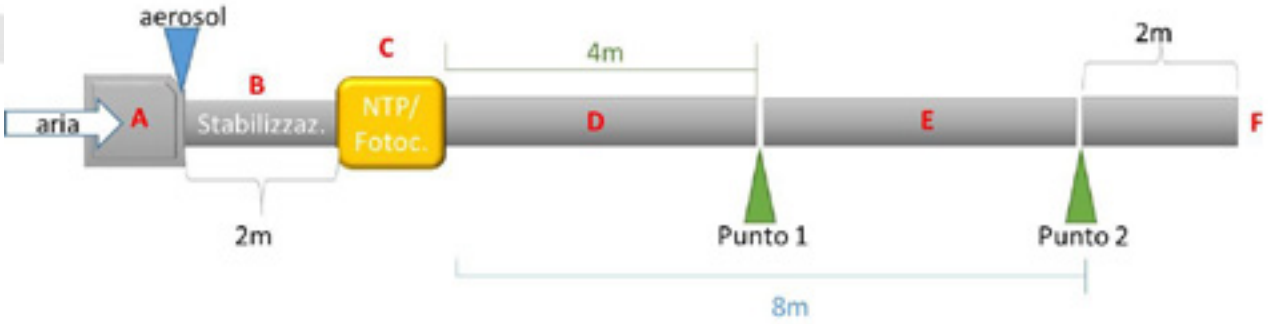

In questo caso, il tempo di permanenza dei microrganismi all'interno del tubo è funzione della velocità del flusso di aria e della lunghezza del tubo. Il campionamento microbiologico per la verifica della contaminazione microbiologica dell'aria, in questa tipologia di assetto è stata condotta alla fine del tubo, nel punto F.
In questo caso, dallo "start" temporale dell'esperimento, il tempo di campionamento non costituisce una variabile del sistema: il tempo che il bio-aerosol impiega ad arrivare alla fine del tubo e solo funzione della velocità dell'aria, variando la velocità dell'aria varia anche il tempo di contatto del bio-aerosol con le specie generate dal sistema sanitizzante.

Nei successivi paragrafi vengono illustrati i risultati ottenuti nelle differenti tipologie di esperimento condotte.

Prove su piastra esposta

I test su piastre Petri contaminate, esposte a flussi di aria all'interno del tubo, sono stati condotti secondo lo schema rappresentato in figura:

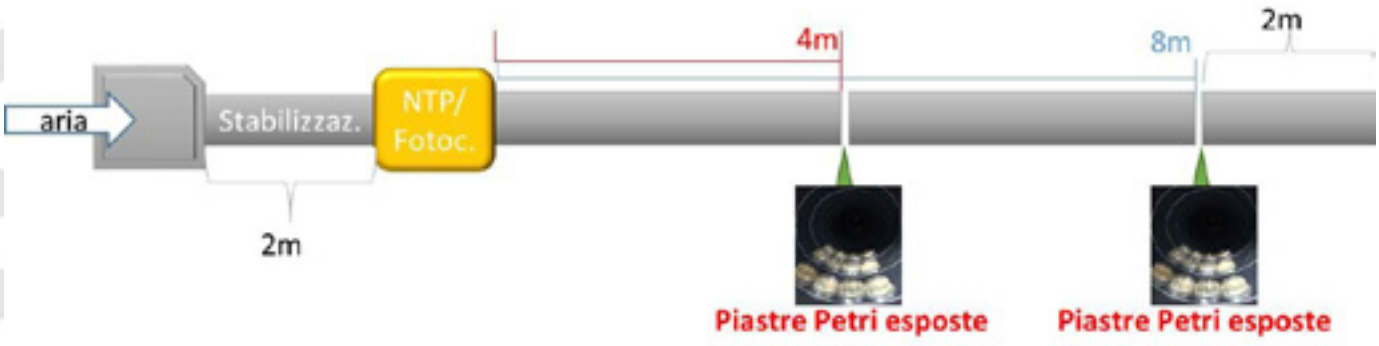

Gli esperimenti sono stati condotti nelle seguenti condizioni sperimentali:

- portata di aria = 130 m^3/h (velocità = 0,5 m/sec)
- concentrazione microbica sulle piastre Petri: 500 UFC/piastra
- tempo di esposizione delle piastre Petri: 30', 1h, 90', 4h

I microrganismi testati sono i seguenti:

- batteri di 2 diverse tipologie: Escherichia coli [gram (-)] e Stafilococco aureus [gram (+)]
- muffe: Aspergillus brasiliensis
- lieviti: Saccharomyces cerevisiae

Rispetto ai dispositivi sanitizzanti studiati, gli assetti testati negli esperimenti sono i seguenti:

- nessun dispositivo sanitizzante acceso (test di controllo, "Ctrl");
- dispositivo fotocatalitico acceso;
- dispositivo fotocatalitico "nudo": lampada UV accesa senza il supporto di nano-catalizzatore;
- dispositivo NTP acceso
- entrambi i sistemi (Fotocatalitico e NTP) accesi

Nelle seguenti tabelle si riportano i risultati ottenuti dai test condotti utilizzando tempi di esposizione di 4h: i test condotti a tempi di contatto minori (30', 1h, 90') non hanno dato effetti significativi rilevabili con nessuno dei dispositivi testati.

Ciascuna prova è stata condotta in triplicato. I risultati analitici mostrati sono quindi la media di 3 diverse determinazioni microbiologiche.

test sui BATTERI:

EFFETTO a 4h di esposizione con 130 m³/h	Concentrazione microbica adottata: 500 UFC/piastra	Riduzione % della crescita microbica	
dispositivo di trattamento sanitizzante	Distanza dal dispositivo sanitizzante (m)	Batterio gram (-) *E. coli*	Batterio gram (+) *S. aureus*
Nessuno (Ctrl)	4	0	0
	8	0	0
Fotocatalitico	4	56	15
	8	0	0
Fotocatalitico «nudo»	4	62	74
	8	8	52
NTP	4	0	71
	8	0	75
Fotocatalitico+NTP	4	0	78
	8	0	79

Il dispositivo **Fotocatalitico** è:

- Mediamente attivo sui batteri solo «vicino» al dispositivo: allontanandosi da esso si perdono gli effetti.
- Più attivo sui gram (-) rispetto al dispositivo Jonix
- Se si toglie il fotocatalizzatore (solo lampada UV), l'attività biocida aumenta, soprattutto nel caso dei gram (+)

Il dispositivo **JONIX** è:

- Non attivo sui gram (-)
- Attivo sui gram (+) indipendentemente dalla distanza dal dispositivo

Non sembra ci sia sinergia tra i due sistemi (NTP + Fotocatalitico)

test su MUFFE e LIEVITI:

EFFETTO a 4h di esposizione con 130 m³/h	Concentrazione microbica adottata: 500 UFC/piastra	Riduzione % della crescita microbica	
dispositivo di trattamento sanitizzante	Distanza dal dispositivo sanitizzante (m)	lievito *S. cerevisiae*	muffa *A. brasiliensis*
Nessuno (Ctrl)	4	0	0
	8	0	0
Fotocatalitico	4	0	59
	8	0	57
Fotocatalitico «nudo»	4	-	56
	8	-	48
NTP	4	18	35
	8	17	47
Fotocatalitico + NTP	4	0	42
	8	0	51

Il dispositivo **Fotocatalitico** è:

- Non attivo sui lieviti
- Attivo sulle muffe
- Se si toglie il fotocatalizzatore e si usa solo la lampada UV si ha sostanzialmente lo stesso effetto del fotocatalizzatore integro

Il dispositivo **JONIX** è:

- Debolmente attivo sui lieviti, indipendentemente dalla distanza dal dispositivo
- Mediamente attivo sulle muffe, indipendentemente dalla distanza dal dispositivo

Non sembra ci sia sinergia tra i due sistemi (NTP + Fotocatalitico)

OSSERVAZIONI sui TEST su PIASTRA:

Nel corso della conduzione degli esperimenti su PIASTRA, è stato osservato un effetto di protezione delle colonie batteriche da parte del bordo della piastra, rispetto al flusso di aria sanitizzante, secondo lo schema illustrato nella seguente figura:

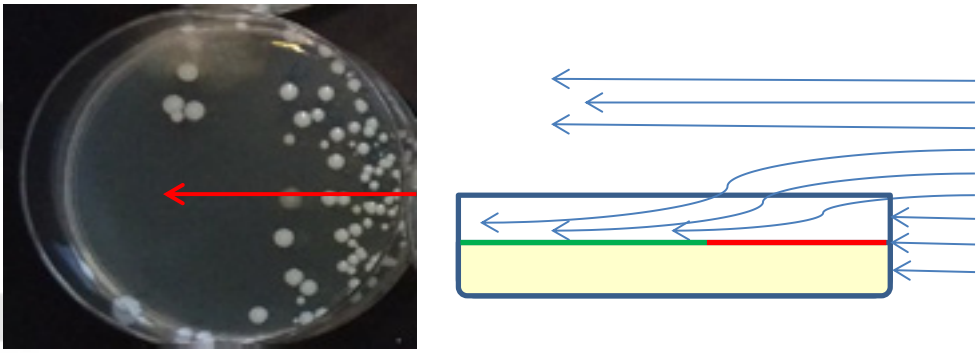

Nelle seguenti fotografie si illustra tale effetto nelle prove i cui risultati sono sopra riportati.

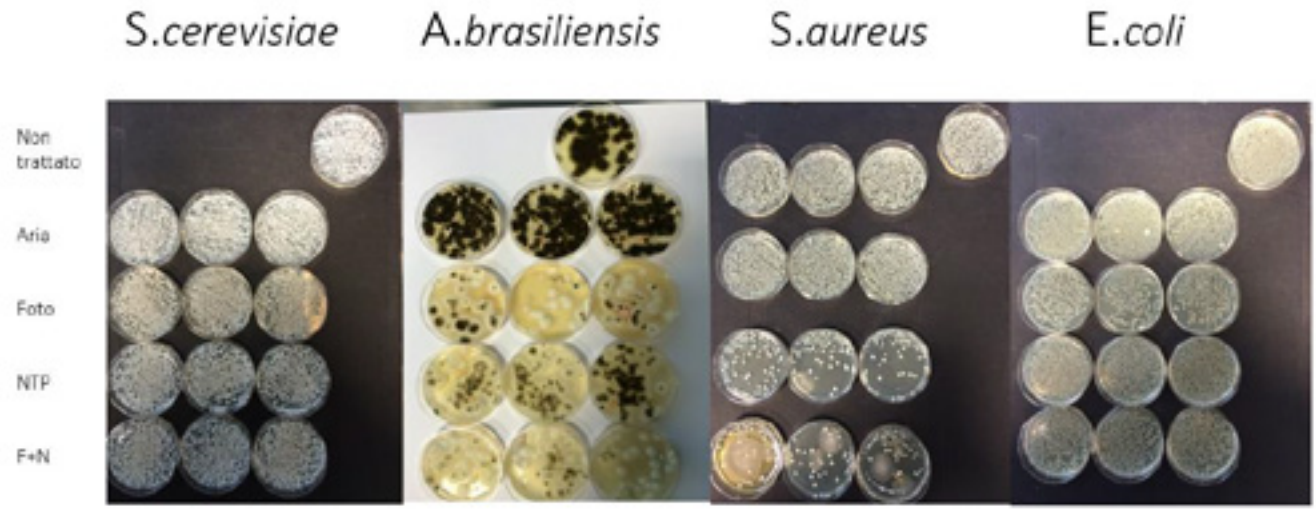

APPROFONDIMENTO dei TEST su PIASTRA: prove su piastre inclinate di 30°

A seguito dell'osservazione del così detto "effetto bordo" provocato dalle piastre sulle colture batteriche esposte ai flussi di aria sanitizzante, i test di esposizione su PIASTRA sono stati replicati inclinando di 30° le piastre esposte.

Nella seguente tabella vengono illustrati i risultati ottenuti. Ciascuna prova è stata condotta in triplicato. I risultati analitici mostrati sono quindi la media di 3 diverse determinazioni microbiologiche

EFFETTO a 4h di esposizione con 130 m³/h	Concentrazione microbica adottata: 500 UFC/piastra	Riduzione % della crescita microbica					
dispositivo di trattamento sanitizzante	Distanza dal dispositivo sanitizzante (m)	Batterio gram (-) *E. coli*		Batterio gram (+) *S. aureus*		Muffa *A. brasiliensis*	
		Piastre «sdraiate» con «effetto bordo»	*Piastre inclinate di 30°*	*Piastre «sdraiate» con «effetto bordo»*	*Piastre inclinate di 30°*	*Piastre «sdraiate» con «effetto bordo»*	*Piastre inclinate di 30°*
NTP	4	0	0	71	79	35	35
	8	0	0	75	74	47	48
Foto + NTP	4	0	0	78	93	42	48
	8	0	0	79	82	51	64

Dai risultati ottenuti si osserva che una debole inclinazione delle piastre (30°) comporta, in qualche caso, un debole incremento della capacità sanitizzante del flusso di aria, ma le differenze non sono grandi.

Prove con bio-aerosol microbico

I test mediante bio-aerosol microbico, generato in modo continuo mediante una apparecchiatura biomedicale e introdotto all'interno della tubazione subito a valle del ventilatore, sono stati condotti secondo lo schema rappresentato in figura:

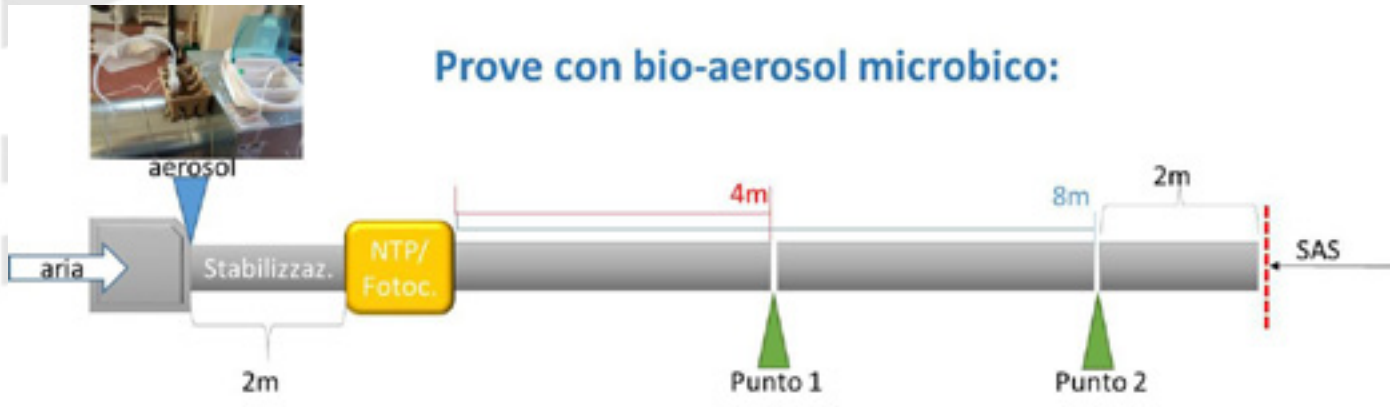

Gli esperimenti condotti sono i seguenti:

PROVA 1:

- portata di aria = 130 m^3/h (velocità = 0,5 m/sec)
- bio-aersol:
  - batteri = 70.000 UFC/min = 30 UFC/L aria
  - muffe e lieviti: 7.000 UFC/min = 3 UFC/L aria
- tempo di campionamento: 30', 60', 90'

PROVA 2:

- portata di aria = 130 m^3/h (velocità = 0,5 m/sec)
- bio-aersol:
  - batteri = 700.000 UFC/min = 300 UFC/L aria
  - muffe e lieviti: 70.000 UFC/min = 30 UFC/L aria
- tempo di campionamento: 30', 60', 90'

PROVA 3:

- portata di aria = 800 m^3/h (velocità = 3 m/sec)
- bio-aersol:
  - batteri = 700.000 UFC/min = 300 UFC/L aria
  - muffe e lieviti: 70.000 UFC/min = 30 UFC/L aria
- tempo di campionamento: 30', 60', 90'

Rispetto ai dispositivi sanitizzanti studiati, gli assetti testati negli esperimenti sono i seguenti:

- nessun dispositivo sanitizzante acceso (test di controllo, "Ctrl");
- dispositivo fotocatalitico acceso;
- dispositivo NTP acceso
- entrambi i sistemi (Fotocatalitico e NTP) accesi

OSSERVAZIONE: nella conduzione degli esperimenti sopra descritti, si è osservato un recupero di microrganismi (mediante campionatore SAS) in fondo a tubo di 12m, veramente molto bassi: i recuperi microbici sono inferiori al 10% dei microrganismi nebulizzati.

Quindi i risultati analitici delle Prove 2 e 3, condotte con concentrazioni microbiche più elevate rispetto alla prova 1, sono da considerarsi più "affidabili" rispetto a quelli ottenuti dalla Prova 1 stessa.

Nelle seguenti tabelle si riportano i risultati ottenuti dai test condotti le seguenti concentrazioni microbiche (Prove 2 e 3):

- batteri = 700.000 UFC/min = 300 UFC/L aria
- muffe e lieviti: 70.000 UFC/min = 30 UFC/L aria

Ciascuna prova è stata condotta in triplicato. I risultati analitici mostrati sono quindi la media di 3 diverse determinazioni microbiologiche.

⇒ Si osservi che mediante campionatore SAS, non è possibile distinguere i batteri gram (+) da quelli gram (-): lo sviluppo avviene in modo non distinto sulla medesima piastra Petri. Il risultato del test è quindi espresso come risultato totale "gram (+) + gram (-)".

⇒ Si osservi che per la struttura dell'esperimento, in questo caso il tempo al quale viene condotto il monitoraggio microbiologico non costituisce una variabile del sistema: il tempo di permanenza dei microrganismi all'interno del tubo è funzione solo della velocità del flusso di aria e della lunghezza del tubo. Quindi campionamenti a tempi diversi mediante SAS sono da intendersi solo come repliche di misure condotte nelle stesse condizioni sperimentali di test.

PROVA 2 - test sui BATTERI:

Prova 2	Riduzione % del numero di microrganismi			
130 m^3/h		Batteri TOT (gram + e gram -)		
Dispositivo sanitizzante	TEMPO di campionamento (min)	Misure singole	MEDIA	Dev.Std
Foto	30	50	68	16
	60	82		
	90	72		
NTP	30	100	98	2
	60	97		
	90	96		
Foto + NTP	30	84	90	6
	60	95		
	90	92		

Il sistema **Jonix NTP** risulta **più efficiente (+30-40%)** del sistema Fotocatalitico nell'effetto di sanitizzazione sui BATTERI TOT [gram (+) + gram (-)]

Nel seguente diagramma vengono visualizzati i risultati ottenuti coi differenti dispositivi sanitizzanti testati.

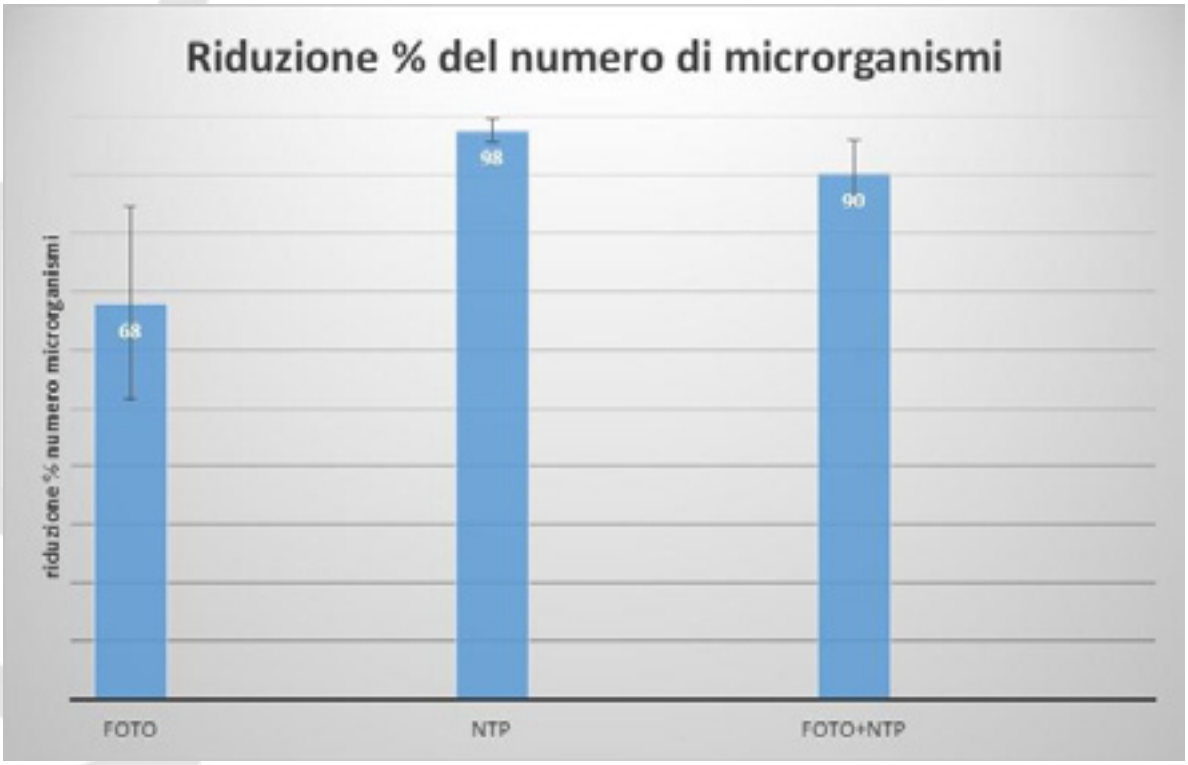

Non c'è sinergia tra il sistema Jonix e il sistema Fotocatalitico nell'effetto di sanitizzazione sui BATTERI TOT.

Laboratori ARCHA S.r.l. unipersonale
Via di Tegulaia 10/a - 56121 - PISA - ph. +39 050 985165 - fax +39 050 985233 - www.archa.it - archainf@archa.it
C.F., P.IVA, Iscr. Reg. Impr. di Pisa n. 01115340505 - Rep. Econ. Amm. di Pisa n°101169 - Capitale Sociale 101.400,00 i.v.

PROVA 2 - test sui LIEVITI:

Prova 2	Riduzione % del numero di microrganismi	
130 m^3/h		*S. cerevisiae*
Dispositivo sanitizzante	TEMPO di campionamento (min)	Misure singole
Foto	30	100
	60	100
	90	100
NTP	30	100
	60	100
	90	100
Foto + NTP	30	100
	60	100
	90	100

Sia il sistema **Jonix NTP** che quello **Fotocatalitico** si dimostrano **efficaci** nell'abbattimento totale dei lieviti.

I lieviti non sono microrganismi discriminanti per capire quale dei 2 sistemi di sanificazione sia il più efficace.

PROVA 2 - test sulle MUFFE:

Prova 2	Riduzione % del numero di microrganismi
130 m^3/h	*A. brasiliensis*
Dispositivo sanitizzante	Misure singole
Foto	50
	50
NTP	25
	25
Foto + NTP	25
	25

Il sistema **Fotocatalitico** risulta **più efficiente** del sistema Jonix nell'effetto di sanitizzazione sulle muffe.

Non c'è sinergia tra il sistema Jonix e il sistema Fotocatalitico nell'effetto di sanitizzazione sulle MUFFE.

PROVA 3 - test sul Bioaerosol:

Prova 3	Riduzione % del numero di microrganismi	
800 m^3/h	*Batteri (gram+ e gram-)*	*A. brasiliensis*
Foto	0	0
NTP	100	100
Foto + NTP	86	100

Per portate di aria alte (800m^3/h) il sistema **JONIX risulta efficiente (+100%)** sia nei confronti di batteri che di muffe.

Il sistema Fotocatalitico risulta totalmente **inefficiente** anche nei confronti delle muffe, sulle quali (dalla prova 2) sembrava esplicasse una azione migliore dell'NTP.

Non c'è sinergia tra il sistema Jonix e il sistema Fotocatalitico nell'effetto di sanitizzazione.

Test di verifica dell'effetto sanitizzante dei dispositivi su muffe accresciute

L'obiettivo del test è verificare se, e dopo quanto tempo dall'istallazione del dispositivo sanitizzante, all'interno di una conduttura esistente (e ormai contaminata da tempo), si possa osservare una azione sanitizzante attiva anche su microrganismi cresciuti e sviluppati. Le prove sono state effettuate sulle muffe (*Aspergillus brasiliensis*), quali rappresentanti della categoria microbica ecologicamente più adatta alla colonizzazione di questa tipologia di impianto.

Le muffe a piena maturazione sono state poste all'interno del tubo e attivato il flusso di aria (130 m^3/h): viene quindi verificato l'effetto dell'aria sanitizzante, prodotta da entrambe le tecnologie, sulle muffe sviluppate, a diversi tempi di esposizione (1, 2 e 4 giorni di esposizione) .

I microrganismi sono stati inoculati circa 4 giorni prima dell'inizio delle prove, in modo tale da fare sviluppare le colonie e consentire ai microrganismi di maturare i corpi fruttiferi contenenti le spore. Al fine di prevenire gli effetti di protezione dovuti al bordo delle piastre, le muffe sono state inoculate al centro delle piastre in modo da sviluppare una sola grande struttura centrale. Nella immagine successiva è possibile osservare una delle piastre impiegate per le prove: la colonia si è sviluppata lontano dai bordi, la parte centrale più scura è rappresentata dalla porzione di micelio che ha sviluppato i corpi fruttiferi, mentre la corona bianca periferica è costituita da una porzione di micelio composta da ife ma priva di corpi fruttiferi.

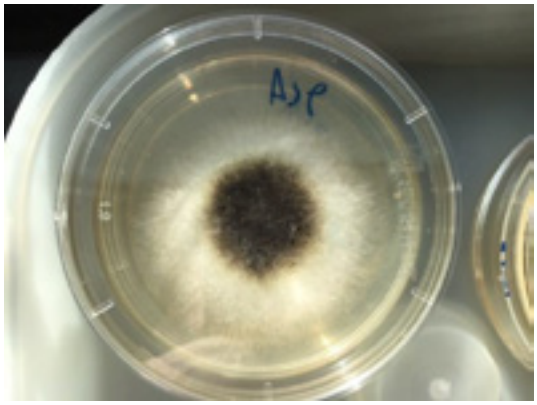

Le piastre sono state collocate in 1 punto intermedio del tubo, a circa 4 metri dai dispositivi sanificanti, ed estratte ai 3 tempi previsti dalla prova.

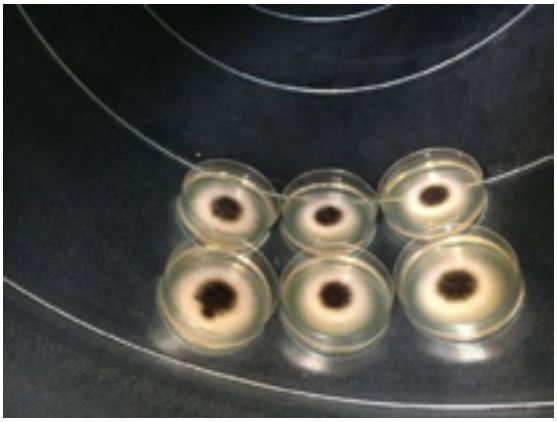

Laboratori ARCHA S.r.l. unipersonale
Via di Tegulaia 10/a - 56121 - PISA - ph. +39 050 985165 - fax +39 050 985233 - www.archa.it - archainf@archa.it
C.F., P.IVA, Iscr. Reg. Impr. di Pisa n. 01115340505 - Rep. Econ. Amm. di Pisa n°101169 - Capitale Sociale 101.400,00 i.v.

La vitalità dei microrganismi veniva valutata sia per i corpi fruttiferi che per le ife, andando a prelevare con un'ansa sterile porzioni di micelio dall'area pigmentata contenente le spore e da quella chiara che ne era priva. Questo accorgimento era finalizzato a valutare se l'attività antimicrobica si esplicasse sulle porzioni vegetative – teoricamente più facili da aggredire – sulle strutture di resistenza (spore), su entrambe le forme o su nessuna di esse.

Le porzioni di micelio venivano inoculate su Sabouraud Agar ed incubate a 25°C per 5 giorni. Trattandosi di un test qualitativo, finalizzato a valutare la presenza o meno di microrganismi vitali, al termine dell'incubazione non veniva determinato il numero esatto di microrganismi cresciuti, ma valutata la presenza o meno di colonie fungine.

La tabella successiva riassume gli effetti ottenuti dal trattamento con il dispositivo fotocatalitico.

	Porzione del micelio	
Tempo di esposizione	**Spore**	**Ife**
1 giorno	Vitali	Vitali
2 giorni	Vitali	Vitali
4 giorni	Vitali	Vitali

Mentre la tabella seguente mostra gli effetti rilevati con il trattamento mediante dispositivo NTP.

	Porzione del micelio	
Tempo di esposizione	**Spore**	**Ife**
1 giorno	Vitali	Non vitali
2 giorni	Vitali	Non vitali
4 giorni	Vitali	Non vitali

Nessuno dei due dispositivi è risultato in grado di inattivare completamente le spore presenti nella porzione pigmentata del micelio, probabilmente a causa delle capacità di resistenza di queste strutture fungine ma, sicuramente, anche per l'elevato numero di spore presenti: infatti, le prove effettuate in precedenza con tempi di esposizione più brevi (massimo 4 ore), sebbene eseguite su un numero contenuto di spore hanno mostrato una percentuale di sopravvivenza che al minimo si attestava intorno al 30%. Pur volendo ammettere un incremento esponenziale degli effetti nei 4 giorni di prova, bisogna considerare che all'interno dell'area pigmentata si ritrovano centinaia di milioni di spore, per cui era prevedibile la sopravvivenza di un certo numero di queste.

Molto più interessante è il risultato ottenuto sulla porzione vegetativa del micelio. Infatti, nel caso delle ife, il trattamento col dispositivo NTP è risultato in grado di inattivare i microrganismi, sebbene i filamenti prelevati fossero sicuramente numerosi e quasi certamente "contaminati" da un certo numero di spore sollevate dal flusso d'aria e

ricadute su questa porzione del micelio. Quest'ultimo risultato significa che, in presenza di impianti già colonizzati, il trattamento con NTP potrebbe svolgere un triplice effetto positivo, andando a:

- uccidere la parte vegetativa delle muffe già cresciute nelle condotte, impedendone l'ulteriore accrescimento;
- a tempi più lunghi ridurre e gradualmente azzerare il numero di spore vitali;
- prevenire la colonizzazione di nuove porzioni dell'impianto, poiché le ife germinate dalle eventuali spore sopravvissute sarebbero comunque rapidamente inattivate.

ALLEGATO 12.10

Studio sulla riduzione degli impatti odorigeni

Laboratori ARCHA S.r.l.
Via di Segalaia, 10/A - 56121 Loc. Ospedaletto (PI)
Tel. +39 050 985165 (4 linee ricerca automatica)
Fax +39 050 985233 - www.archa.it - archa@archa.it
C.F., P.IVA, Iscr. Reg. Imp. di Pisa n. 01115340505
Reparto Economico Amministrativo di Pisa n. 130169
Capitale Sociale € 101.400,00 i.v.

RIDUZIONE IMPATTI ODORIGENI

Laboratori ARCHA S.r.l.
Via di Tegulaia, 10/A - 56121 Loc. Ospedaletto (PI)
Tel. +39 050 985165 (4 linee ricerca automatica)
Fax +39 050 985233 - www.archa.it - archainfo@archa.it
C.F., P.IVA, Iscr. Reg. Imp. di Pisa n. 01115340505
Reparto Economico Amministrativo di Pisa n. 101169
Capitale Sociale € 101.400,00 i.v.

INDICE

Laboratori ARCHA S.r.l.
Via di Segalaia, 10/A - 56121 Loc. Ospedaletto (PI)
Tel. +39 050 985165 (4 linee ricerca automatica)
Fax +39 050 985233 - www.archa.it - archa@archa.it
C.F., P.IVA, Iscr. Reg. Imp. di Pisa n. 01115340505
Reparto Economico Amministrativo di Pisa n. 130169
Capitale Sociale € 101.400,00 i.v.

Laboratori ARCHA S.r.l.
Via di Segalaia, 10/A - 56121 Loc. Ospedaletto (PI)
Tel. +39 050 985165 (4 linee ricerca automatica)
Fax +39 050 985233 - www.archa.it - archa@archa.it
C.F., P.IVA, Iscr. Reg. Imp. di Pisa n. 01115340505
Reparto Economico Amministrativo di Pisa n. 130169
Capitale Sociale € 101.400,00 i.v.

Laboratori ARCHA S.r.l.
Via di Segalaia, 10/A - 56121 Loc. Ospedaletto (PI)
Tel. +39 050 985165 (4 linee ricerca automatica)
Fax +39 050 985233 - www.archa.it - archa@archa.it
C.F., P.IVA, Iscr. Reg. Imp. di Pisa n. 01115340505
Reparto Economico Amministrativo di Pisa n. 130169
Capitale Sociale € 101.400,00 i.v.

1. INTRODUZIONE

Il presente documento descrive lo studio e l'analisi degli aspetti ambientali legati alle misure di impatto odorigeno correlate alla gestione dei rifiuti e alla realizzazione di una sperimentazione su scala pilota, relativamente al trattamento di effluenti gassosi al fine di ridurne efficacemente il carico odorigeno presente.

2. INQUADRAMENTO DELLA PROBLEMATICA ODORI

Il presente lavoro ha riguardato una indagine di screening volta ad individuare le migliori modalità attraverso cui affrontare la delicata tematica delle emissioni odorigene generate da un impianto di trattamento rifiuti.

Il tema affrontato è quanto mai attuale e urgente. E' noto, infatti, come la dispersione di odori poco gradevoli si manifesti a partire da attività industriali o, comunque, da impianti produttivi che implichino la presenza di sorgenti odorigene: tra l'ampia gamma di attività che possono essere considerate – oltre ad impianti industriali specifici – rientrano anche categorie ampie quali gli impianti di trattamento delle acque reflue, impianti di trattamento e selezione dei rifiuti, discariche, etc.

Nonostante la rilevanza di tali criticità, manca allo stato attuale una metodologia integrata per il "controllo" di tali fenomeni, comprendendo con tale termine non solo la "misura" dei fenomeni – peraltro assai complessa – ma una vera strategia per affrontare il problema secondo la precisa gerarchia: interventi alla fonte – confinamento – mitigazione.

Nell'ambito di contesti industriali-commerciali, che vedono la presenza di un elevato numero di possibili "sorgenti" odorigene, diventa particolarmente complicato andare a determinare, dimostrare e controllare, quale sia l'esatta fonte del problema, che spesso viene evidenziata da lamentele – talora caratterizzate da una non completa affidabilità – da parte della popolazione presente nell'area interessata alle cosiddette "ricadute".

Di fatto, la complessità di questa problematica scaturisce da tre ragioni fondamentali:

- ✓ la difficoltà di analizzare sostanze odoranti le cui concentrazioni nell'ambiente siano al di sotto di una soglia di rilevabilità analitica (pur provocando, alle suddette concentrazioni, fenomeni di "molestia");
- ✓ la variabilità dell'intensità e delle caratteristiche dell'inquinamento odorigeno in funzione del tempo e delle condizioni meteorologiche;
- ✓ la grande soggettività che caratterizza la percezione delle sostanze odorigene.

In bibliografia, sono assai scarsi gli studi condotti in materia di identificazione delle sostanze odoranti provenienti da matrici odorigene e di valutazione degli effetti di specifici sistemi di trattamento sulle sostanze odorigene.

A questo si aggiunge la mancanza di una legislazione specifica di riferimento, sia a livello internazionale, che italiano. Infatti, a livello nazionale, solo poche Regioni hanno definito, e solo recentemente, delle Linee Guida in materia, per lo più applicabili solo a specifici settori. Questa "carenza normativa" risulta ancora più critica considerando che, al contrario, vi è una crescente presa di coscienza della società nei confronti delle questioni legate all'ambiente, di cui gli impatti odorigeni costituiscono, allo stato attuale, uno degli aspetti più subdoli e sfuggenti.

Laboratori ARCHA S.r.l.
Via di Tegulaia, 10/A - 56121 Loc. Ospedaletto (PI)
Tel. +39 050 985165 (4 linee ricerca automatica)
Fax +39 050 985233 - www.archa.it - archa@archa.it
C.F., P.IVA, Iscr. Reg. Imp. di Pisa n. 01115340505
Reparto Economico Amministrativo di Pisa n. 130169
Capitale Sociale € 101.400,00 i.v.

3. 5.4. ABBATTIMENTO DELLE COMPONENTI ODORIGENE SU IMPIANTO PILOTA-LABORATORIO NTP (BA-TEST SCALA PILOTA-INDUSTRIALE)

L'attività svolta riguarda l'impiego di un impianto pilota-industriale (applicabile quindi anche su scala industriale) utilizzato su scala di laboratorio, applicato al trattamento di specifici flussi di rifiuti (i più critici) e a miscele degli stessi.

Per la realizzazione di questa attività sperimentale è stata quindi progettata una modalità per "gestire" un flusso di sostanze odorigene di entità ben maggiore.

In Figura successiva è rappresentato schematicamente il contenitore che è stato impiegato per le prove da effettuare con il BA-TEST industriale, che ha una portata modulabile tra 150 e 600 m^3/h.

Il sistema è costituito da un fusto in PP da 100 L sul cui fondo sono praticati una serie di fori, mentre sul coperchio è realizzato un raccordo per il collegamento con il ventilatore del BA-TEST.

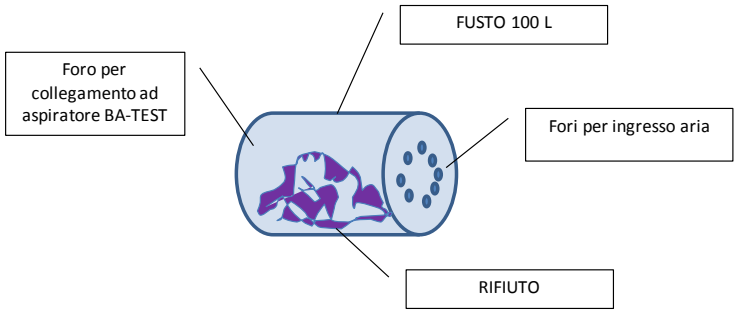

Schema contenitore per prove con BA-TEST

Il rifiuto (30-50 kg) viene collocato all'interno del fusto e questo è collegato al ventilatore del BA-TEST. Il fusto è posizionato orizzontalmente, e può essere smosso periodicamente per rinnovare la superficie esposta della massa di rifiuto. Il sistema di trattamento delle molecole (odorigene e non) emesse dal rifiuto contenuto nel fusto è presentato nella foto seguente.

Laboratori ARCHA S.r.l.
Via di Tegulaia, 10/A - 56121 Loc. Ospedaletto (PI)
Tel. +39 050 985165 (4 linee ricerca automatica)
Fax +39 050 985233 - www.archa.it - archa@archa.it
C.F., P.IVA, Iscr. Reg. Imp. di Pisa n. 01115340505
Reparto Economico Amministrativo di Pisa n. 130169
Capitale Sociale € 101.400,00 i.v.

Foto impianto BA-TEST pilota impiegato nelle prove.

LEGENDA:

A. Aspirazione emissioni
B. Selettore di by-pass
C. Generatore NTP®
D. Uscita emissioni
E. Punti di campionamento (1: in alto a monte del sistema di abbattimento; 2: in basso a valle del trattamento; 3 a valle del sistema di trattamento, prima dell'emissione finale

Attraverso l'uso di tale sistema, sono state effettuate prove e test per verificare il migliore assetto impiantistico, cioè quello che garantisce i migliori risultati in termini di abbattimento delle sostanze odorigene sviluppate da specifici rifiuti selezionati in seguito all'attività sperimentale condotta nell'ambito dei precedenti obiettivi operativi.

Messa a punto delle condizioni sperimentali

Questa parte dell'attività sperimentale è stata piuttosto complessa, dato che sono state valutate con attenzione le singole risposte e la loro la variabilità, dipendente dalla tipologia dei rifiuti in gioco e dalla condizione di prova impiegata.

Le condizioni delle varie prove (schematicamente riportate in Tabella 5) sono state impostate facendo uso di tecniche di Disegno Sperimentale (DoE). I risultati degli esperimenti ottenuti attraverso il NE e la GC-MS sono stati elaborati al fine di individuare le migliori condizioni operative.

Laboratori ARCHA S.r.l.
Via di Tegulaia, 10/A - 56121 Loc. Ospedaletto (PI)
Tel. +39 050 985165 (4 linee ricerca automatica)
Fax +39 050 985233 - www.archa.it - archa@archa.it
C.F., P.IVA, Iscr. Reg. Imp. di Pisa n. 01115340505
Reparto Economico Amministrativo di Pisa n. 130169
Capitale Sociale € 101.400,00 i.v.

Tabella 5. Condizioni di prova testate.

		Livelli		
		1	2	3
Settaggi studiate	Quantità rifiuto (kg)	30	50	
	Tipologia di rifiuto	LO	LA	MIX
	Temperatura rifiuto (°C)	50		
	Portata aspirazione (m^3/h)	150	300	600
	By-pass	0	0,5	1
	Voltaggio sonda 1 (V)	3000		
	Voltaggio sonda 2 (V)	3000		
	Voltaggio sonda 3 (V)	3200		
	Punti di prelievo	1	2	3

Le prove hanno quindi riguardato 3 differenti tipologie di rifiuti (già noti per le caratteristiche critiche in termini di impatti odorigeni prodotti): LO (CER 19 01 05*), LA (CER 19 02 05*) e MIX (costituito da una miscela di differenti rifiuti, compresi LO e LA, al fine di simulare la condizione media dell'impianto con presenza di rifiuti "odorigeni" e non). Tali rifiuti sono stati messi all'interno del fusto bucato, posto su una piastra scaldante a circa 50°C, e dopo 5 minuti di condizionamento sono iniziate le prove, effettuando i prelievi dai 3 punti di campionamento con le sonde spente e, successivamente, accese.

Per poter valutare le migliori condizioni di prova sono state eseguiti differenti test, andando a variare uno o più dei settaggi riportati in Tabella 5.

Il confronto tra la sommatoria delle aree ottenute mediante GC-MS e la sommatoria dei segnali registrati dai 10 sensori del NE, ha fornito le risposte ricercate per l'individuazione delle migliori condizioni operative, relativamente alle prove di trattamento dei flussi odorigeni prodotti dai rifiuti in esame, impiegando il BA-Test su scala pilota-laboratorio.

Le migliori condizioni di prova, ottenute impiegando il rifiuto LO (e poi confermate con gli altri rifiuti testati), sono risultate:

1. Quantità di rifiuto = 30 kg
2. Temperatura rifiuto = 50°C
3. Portata aspirazione = 150 m^3/h
4. By-pass = chiuso (0)
5. Voltaggio condensatori = 3000, 3000, 3200 V
6. Punti di prelievo = 1 e 3

Risultati ottenuti con il rifiuto LO CER 19 01 05*

Le prove condotte perl'abbattimento delle molecole odorigene contenute nel rifiuto LO hanno permesso di ottenere i risultati sinteticamente presentati nel grafico di Figura 25. I punti di campionamento considerati sono il punto 1 (a monte del sistema di trattamento NTP) che rappresenta l'emissione gassosa non trattata e il punto 3 (a valle della sonda NTP) che rappresenta, a sonda accesa, l'emissione dopo trattamento con sonda. In tal modo, è necessario considerare anche i contributi dei bianchi ed in particolar modo il contributo negativo che ha la sonda sulla lettura del NE, come è possibile osservare dalla prova SA_SR nel grafico a

Laboratori ARCHA S.r.l.
Via di Segalaia, 10/A - 56121 Loc. Ospedaletto (PI)
Tel. +39 050 985165 (4 linee ricerca automatica)
Fax +39 050 985233 - www.archa.it - archa@archa.it
C.F., P.IVA, Iscr. Reg. Imp. di Pisa n. 01115340505
Reparto Economico Amministrativo di Pisa n. 130169
Capitale Sociale € 101.400,00 i.v.

sinistra della Figura 26: la sommatoria dei segnali dei sensori del NE diminuisce di circa l'11% a seguito dell'accensione della sonda stessa. Analogamente è possibile registrare un decremento (circa il 7% con il NE e 6% con la GC) dovuto, quasi sicuramente, a fenomeni di adsorbimento delle molecole lungo il condotto dell'impianto pilota. Tali percentuali di decremento sono state considerata ai fini della valutazione dell'efficienza di abbattimento del sistema NTP nei confronti delle molecole odorigene, sottraendole dalla percentuale di abbattimento complessiva determinata come differenze di segnali registrati nei punti 1 e 3, durante la prova che ha impiegato il rifiuto e la sonda accesa.

In conclusione, per il rifiuto LO sono state rilevate percentuali di abbattimento delle molecole odorigene presenti, variabili tra il 34% (con il Naso Elettronico) e il 28% (con la Gas-cromatografia).

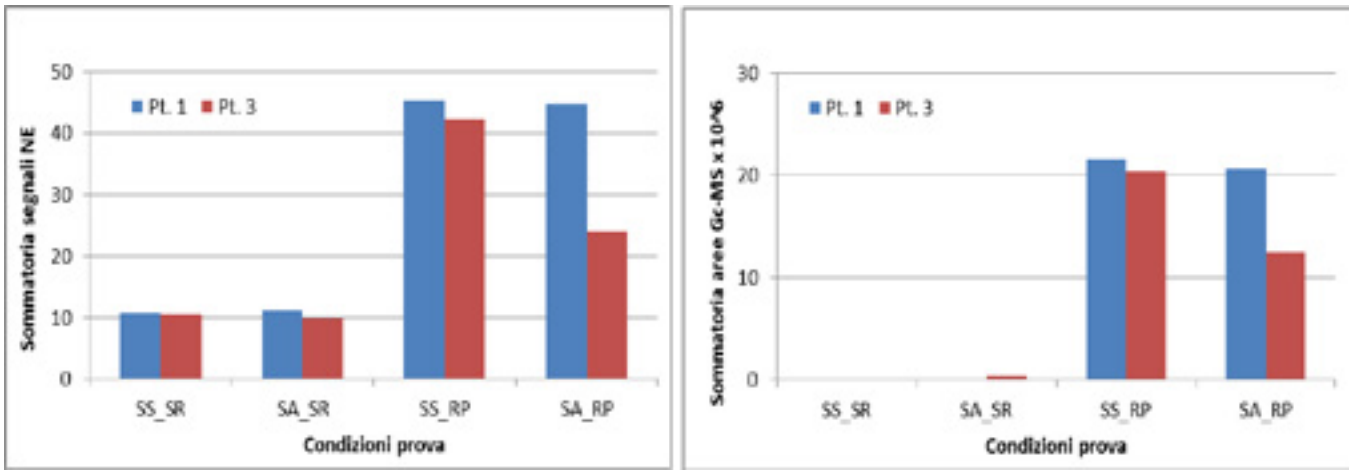

Figura 25. Risultati prove condotte sul rifiuto LO (NE a sinistra; GC-MS a destra).

Legenda: SS_SR = sonda spenta - senza rifiuto (bianco prova); SA_SR = sonda accesa - senza rifiuto (bianco sonda); SS_RP = sonda spenta – rifiuto su piastra (emissioni rifiuto scaldato a 50°C); SA_RP = sonda accesa – rifiuto su piastra (emissioni rifiuto scaldato a 50°C + trattamento NTP)

Laboratori ARCHA S.r.l.
Via di Tegulaia, 10/A - 56121 Loc. Ospedaletto (PI)
Tel. +39 050 985165 (4 linee ricerca automatica)
Fax +39 050 985233 - www.archa.it - archa@archa.it
C.F., P.IVA, Iscr. Reg. Imp. di Pisa n. 01115340505
Reparto Economico Amministrativo di Pisa n. 130169
Capitale Sociale € 101.400,00 i.v.

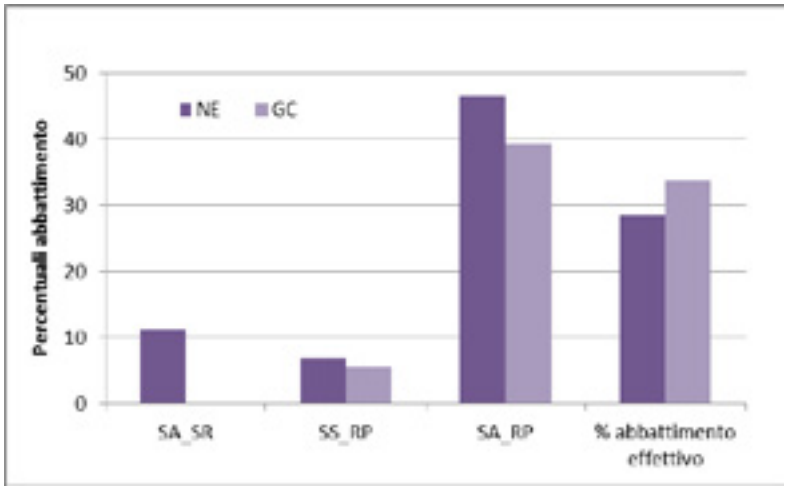

Figura 26. Risultati prove condotte sul rifiuto LO espresse come percentuali di abbattimento, valutate nei punti di campionamento 1 e 3.

Legenda: SA_SR = % contributo sonda; SS_RP = % diminuzione per perdite dell'emissione del rifiuto lungo il camino; SA_RP = % abbattimento sonda non corretta; % abbattimento effettivo = SA_RP – SS_RP – SA_SR

Risultati ottenuti con il rifiuto LA CER 19 02 05*

Analogamente a quanto effettuato con il rifiuto LO, sono state effettuate le prove di trattamento delle molecole odorigene prodotte dal rifiuto LA.

I grafici dei risultati sperimentali ottenuti sono riportati in Figura 27, a sinistra i valori delle sommatorie dei segnali registrati dal Naso Elettronico, a destra i risultati ottenuti mediante l'analisi SPME-GC-MS.

Le percentuali di abbattimento definite come descritto nel Paragrafo 5.4.3. sono rappresentate in Figura 28: l'abbattimento effettivo sulle molecole odorigene effettuato attraverso la sonda NTP è calcolato pari al 40% mediante analisi GC e al 26% mediante NE.

Tale differenze può essere facilmente spiegata attraverso la differente composizione del rifiuto LA rispetto a LO, ottenute mediante analisi GC-FID, sul campione solido (Figura 29): il primo è infatti esclusivamente composto da Sostanze Organiche Volatili alifatiche a catena corta (C5 – C12), mente nel rifiuto LO sono presenti anche composti aromatici più complessi, a numero di carboni C8-C10 (toluene, xileni…), più difficilmente degradabili da parte delle specie emesse dalla sonda NTP.

Laboratori ARCHA S.r.l.
Via di Segalaia, 10/A - 56121 Loc. Ospedaletto (PI)
Tel. +39 050 985165 (4 linee ricerca automatica)
Fax +39 050 985233 - www.archa.it - archa@archa.it
C.F., P.IVA, Iscr. Reg. Imp. di Pisa n. 01115340505
Reparto Economico Amministrativo di Pisa n. 130169
Capitale Sociale € 101.400,00 i.v.

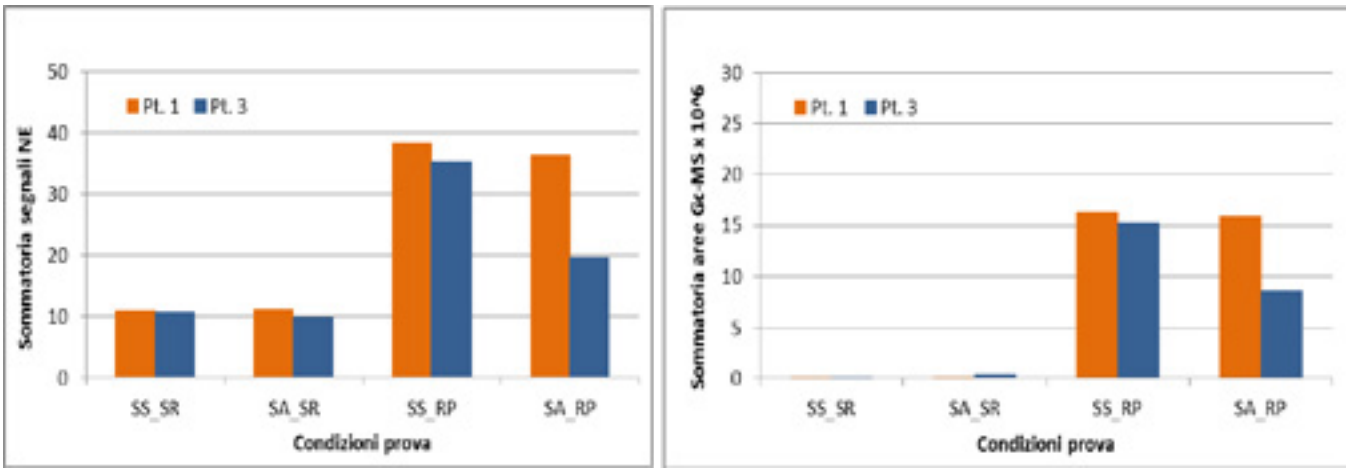

Figura 27. Risultati prove condotte sul rifiuto LA (NE a sinistra; GC-MS a destra).

Legenda: SS_SR = sonda spenta - senza rifiuto (bianco prova); SA_SR = sonda accesa - senza rifiuto (bianco sonda); SS_RP = sonda spenta – rifiuto su piastra (emissioni rifiuto scaldato a 50°C); SA_RP = sonda accesa – rifiuto su piastra (emissioni rifiuto scaldato a 50°C + trattamento NTP)

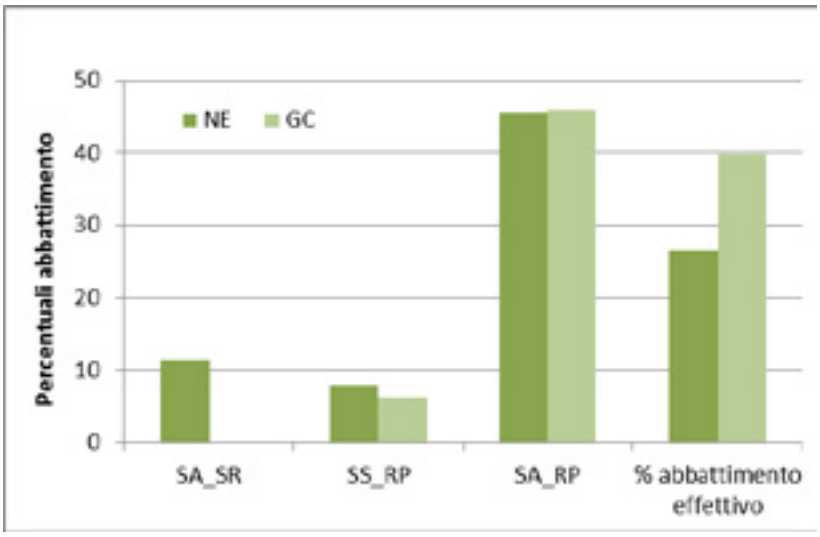

Figura 28. Risultati prove condotte sul rifiuto LA espresse come percentuali di abbattimento, valutate nei punti di campionamento 1 e 3.

Legenda: SA_SR = % contributo sonda; SS_RP = % diminuzione per perdite dell'emissione del rifiuto lungo il camino; SA_RP = % abbattimento sonda non corretta; % abbattimento effettivo = SA_RP – SS_RP – SA_SR

Laboratori ARCHA S.r.l.
Via di Segalaia, 10/A - 56121 Loc. Ospedaletto (PI)
Tel. +39 050 985165 (4 linee ricerca automatica)
Fax +39 050 985233 - www.archa.it - archa@archa.it
C.F., P.IVA, Iscr. Reg. Imp. di Pisa n. 01115340505
Reparto Economico Amministrativo di Pisa n. 130169
Capitale Sociale € 101.400,00 i.v.

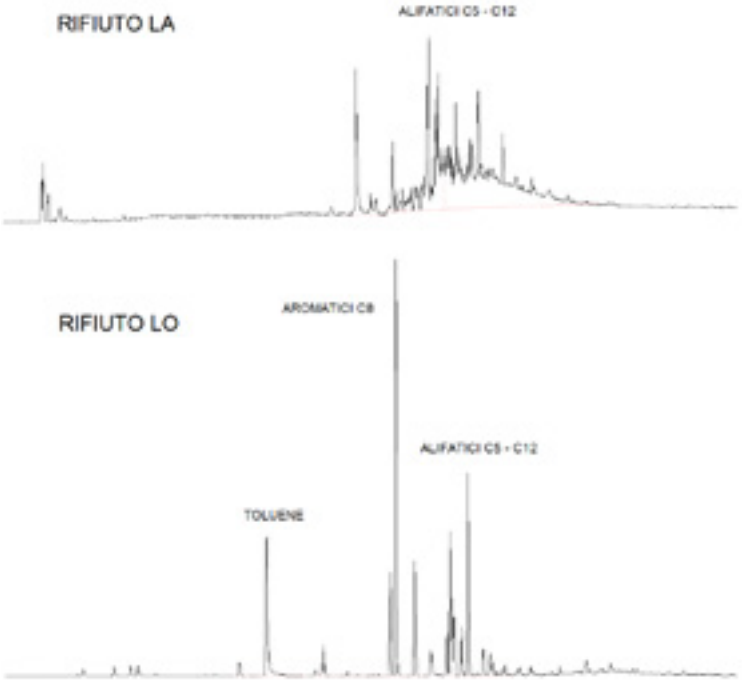

Figura 29. Cromatogrammi relativi all'analisi dei campioni di rifiuto LA (in alto) e LO (in basso).

Risultati ottenuti con la miscela di rifiuti (MIX)

Per la validazione finale delle prove di trattamento mediante tecnologia NTP, sono state condotte ulteriori sperimentazioni, impiegando una miscela di rifiuti (denominata MIX), costituita dai due precedenti LO e LA, unitamente ad altri 4 rifiuti, non particolarmente critici, ma di natura pericolosa e ricchi comunque di composti organici volatili.

Le analisi condotte sui campioni di aria prelevati nei punti 1 e 3, nelle condizioni sperimentali già descritte nei precedenti paragrafi, hanno fornito gli andamenti riportati nel grafico di Figura 30 (NE, a sinistra; GC-MS, a destra).

In generale, i valori rilevati sia al NE che alla GC, sono inferiori rispetto a quanto riscontrato con i singoli rifiuti presenti nei precedenti paragrafi. Le percentuali di abbattimento riscontrabili nel corso delle prove condotte raggiungono circa il 30% del carico di sostanze presenti nel flusso gassoso in uscita al BA-TEST (Figura 31).

Laboratori ARCHA S.r.l.
Via di Segalaia, 10/A - 56121 Loc. Ospedaletto (PI)
Tel. +39 050 985165 (4 linee ricerca automatica)
Fax +39 050 985233 - www.archa.it - archa@archa.it
C.F., P.IVA, Iscr. Reg. Imp. di Pisa n. 01115340505
Reparto Economico Amministrativo di Pisa n. 130169
Capitale Sociale € 101.400,00 i.v.

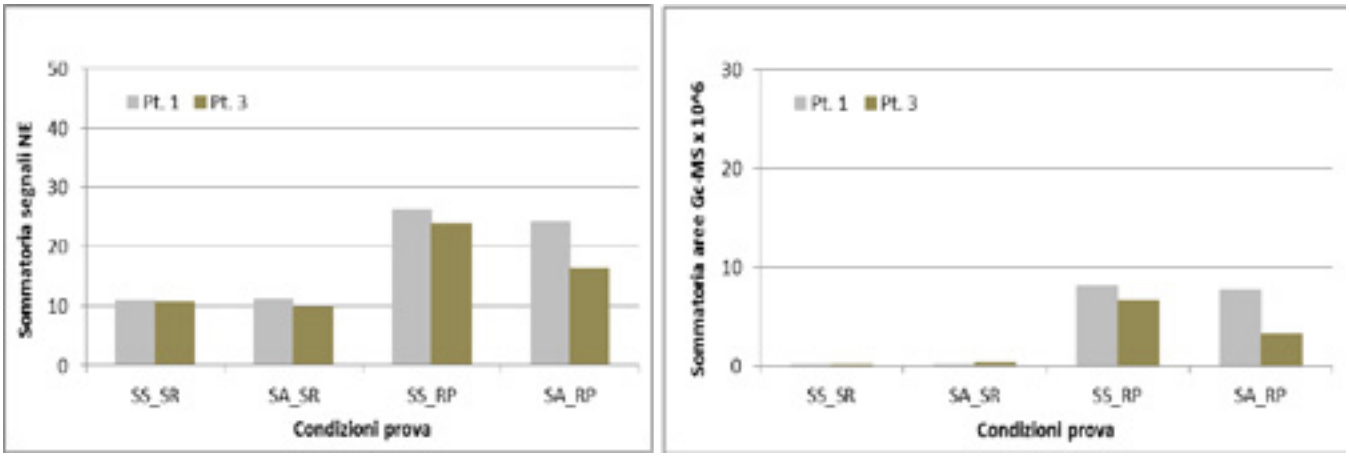

Figura 30. Risultati prove condotte sulla miscela di rifiuti MIX (NE a sinistra; GC-MS a destra).

Legenda: SS_SR = sonda spenta - senza rifiuto (bianco prova); SA_SR = sonda accesa - senza rifiuto (bianco sonda); SS_RP = sonda spenta – rifiuto su piastra (emissioni rifiuto scaldato a 50°C); SA_RP = sonda accesa – rifiuto su piastra (emissioni rifiuto scaldato a 50°C + trattamento NTP)

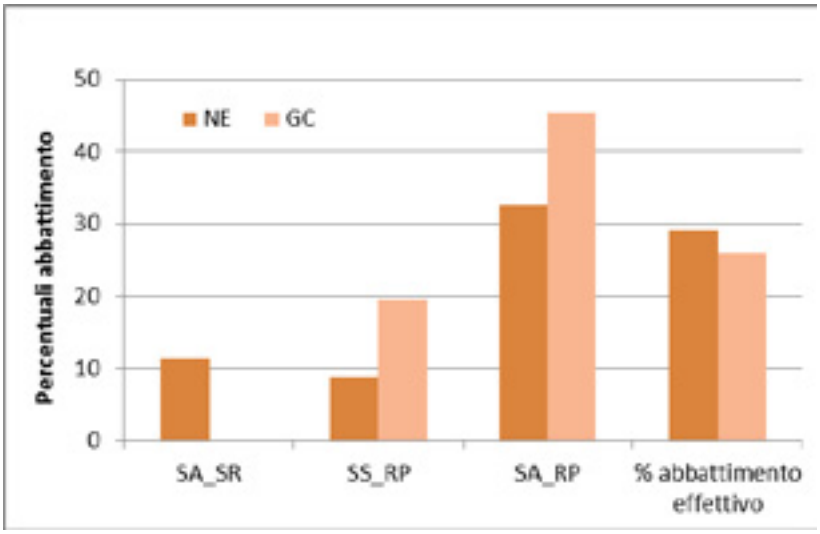

Figura 31. Risultati prove condotte su MIX espresse come percentuali di abbattimento, valutate nei punti di campionamento 1 e 3.

Legenda: SA_SR = % contributo sonda; SS_RP = % diminuzione per perdite dell'emissione del rifiuto lungo il camino; SA_RP = % abbattimento sonda non corretta; % abbattimento effettivo = SA_RP – SS_RP – SA_SR

Laboratori ARCHA S.r.l.
Via di Tegulaia, 10/A - 56121 Loc. Ospedaletto (PI)
Tel. +39 050 985165 (4 linee ricerca automatica)
Fax +39 050 985233 - www.archa.it - archa@archa.it
C.F., P.IVA, Iscr. Reg. Imp. di Pisa n. 01115340505
Reparto Economico Amministrativo di Pisa n. 130169
Capitale Sociale € 101.400,00 i.v.

Considerazioni conclusive

Dai risultati presentati appare evidente come la tecnologia NTP abbia un effetto positivo nell'abbattimento delle specie presenti nel flusso gassoso generato da un rifiuto, con percentuali variabili tra il 25 e il 40%.

Questo risultato è stato ottenuto mediante l'esecuzione di una complessa sperimentazione eseguita su un impianto pilota dotato di tecnologia NTP, effettuando il trattamento su differenti rifiuti e miscele degli stessi, ed impiegando come tecniche analitiche per la "quantificazione" dell'efficienza sia il Naso Elettronico che la Gascromatografia con rivelatore di Massa.

I risultati così ottenuti offrono ampie prospettive di impiego di questa tecnologia come sistema di abbattimento, sia degli inquinanti di natura organica presenti in una emissione che per quanto concerne più nello specifico l'obiettivo del progetto, ovvero l'abbattimento delle molecole odorigene.

Le molecole organiche, come è stato verificato in modo particolare sulle catene alifatiche e aromatiche attraverso le analisi condotte con la GC-MS, vengono abbattute fino a circa il 40%. Le sostanze odorigene, come è stato possibile verificare tramite l'impiego del Naso Elettronico, subiscono un decremento della loro concentrazione fino a percentuali pari al 30%.

Un eventuale ulteriore sviluppo dello studio e della tecnologia proposta, potrebbe riguardare differenti matrici di rifiuti caratterizzati da impatti olfattivi dovuti a composti inorganici, quali ad esempio l'ammoniaca e l'acido solfidrico. In questi casi, le metodiche analitiche da applicare potrebbero essere il Naso Elettronico e tecniche specifiche per la determinazione di tali composti.

ALLEGATO 12.11

Studio della sanificazione dell'aria in una clinica veterinarie

Sanificazione dell’aria nelle cliniche veterinarie

JONIX
pure living

Sommario

Introduzione

L'inquinamento "indoor" delle abitazioni e dei luoghi di lavoro rappresenta un problema di natura chimica e microbiologica che può risultare significato per la salute delle persone e degli animali che vivono in questi ambienti. La problematica è tale da avere una branca di studio dedicata: l'Aerobiologia.
Si tratta di una nuova scienza multidisciplinare che studia le particelle presenti in atmosfera, le fonti che le producono, le modalità con cui queste vengono trasportate dall'aria, i loro effetti sia in ambienti chiusi che all'aperto.

Le tecniche utilizzate per migliorare la "salubrità" degli ambienti, in particolare gli ambienti di lavoro, sono molteplici, possono fare parte degli impianti di trattamento dell'aria o essere dispositivi mobili indipendenti. Si utilizzano la filtrazione, le lampade UV o l'ozono, questi ultimi non sono compatibili con la presenza delle persone.
Nell'ultimo decennio le ricerche si sono orientate verso la ionizzazione dell'aria, un fenomeno naturale riproducibile artificialmente che si è dimostrato capace di agire su molte particelle presenti in aria (microbiologiche e chimiche).

Sugli effetti della ionizzazione dell'aria esistono molte pubblicazioni, nazionali e internazionali, che dimostrano, oltre agli effetti terapeutici sulle patologie dell'apparato respiratorio, anche un'efficace riduzione del contenuto microbio in aria e sulle superfici.
Sono state svolte numerosissime ricerche e sperimentazioni nel settore alimentare e sanitario ospedaliero.

Le applicazioni nel settore delle cliniche ed ambulatori veterinari sono molto recenti.
L'esigenza di sanitizzazione constante è emersa contestualmente a quella degli interventi di chirurgia, generale ed ortopedica in particolare.
Analogamente a quanto accade infatti nella chirurgia "umana" le infezioni post chirurgiche trovano tra le loro cause anche le infezioni aero-trasportate. Pur non essendovi, in ambito veterinario, sperimentazioni cliniche vere e proprie, i fattori sulla qualità dell'aria indoor del settore inducono a stimare una percentuale significativa.

Vi è inoltre la tendenza ad una visione olistica del servizio di medicina veterinaria, con un approccio saluto-genetico ed eco-sostenibile; focalizzato sul paziente e sul suo nucleo familiare; con il minimo uso possibile di medicinali di sintesi ed invece l'adozione, ove possibile, di protocolli omeopatici.
Questi nuovi scenari, per coerenza, debbono necessariamente vivere all'interno di ambienti con un fattore di qualità dell'aria adeguato, microbiologicamente controllati, privi di sostanze organiche volatili e odori; aspetto questo direttamente correlato alla qualità percepita del servizio clinico offerto.

Scopo

Jonix S.r.l. ha voluto verificare l'efficacia della tecnologia Nono Thermal Plasma in sanità Veterinaria.
Questa prima sperimentazione è stata condotta presso la prestigiosa Clinica Veterinaria San Marco

L'obiettivo era quello di ottenere una riduzione degli odori percepiti e riduzione della contaminazione microbica aero-trasportata in locali dove le concentrazioni potrebbero risultare significative e avere un impatto negativo su animali e persone.

La sperimentazione, effettuata nei mesi di marzo e aprile 2018, ha previsto una serie di campionamenti prima dell'installazione dei dispositivi, durante la normale attività della clinica per valutare le condizioni inziali, da comparare le misurazioni effettuate dopo l'accensione dei dispositivi Jonix.
I prelievi e le analisi sono state condotte da tecnici qualificati e da istituto indipendente in seguito indicato, utilizzando un dispositivo SAS-Super 180 della PBI.
Valutazioni iniziali:
Nell'ambito delle cliniche veterinarie non è stata individuata bibliografia a supporto della valutazione iniziale.

La clinica veterinaria ove ha avuto luogo la sperimentazione ha un affluenza elevata di animali sia per le prestazioni ambulatoriale che nel reparto degenza che offre 30 gabbie, con conseguente tour-over elevato di animali.
Questi possono variare per specie, taglia, patologia e numero complessivo di occupazione in contemporanea. Ciò comporta un altissima variabilità delle particelle rilasciate in aria dagli animali stessi e dal movimento di operatori all'interno della sala.

La struttura è priva di impianti di trattamento aria se non per la immissione di aria primaria, questo comporta una ulteriore fonte di variabilità al contenuto microbico dell'aria degli ambienti. Le condizioni descritte hanno creato delle condizioni interessanti per la sperimentazione, si è quindi deciso di effettuare le rilevazioni negli ambienti con maggiore variabilità di affluenza e conseguenti variazioni delle concentrazioni batteriche aero disperse:
la Sala di attesa in ingresso (fig.1) e la Sala degenza animali (vedi fig 2).

In questi locali infatti troviamo il maggior numero di variabili legate alla movimentazione dell'aria: l'apertura e chiusura delle porte d'ingresso e di accesso agli ambulatori e l'estrema mutevolezza delle presenze umane hanno offerto la possibilità di "fotografare" la contaminazione microbica dell'aria in una situazione di attività regolare.
La clinica è operativa 24 ore su 24.
Per una migliore comprensione sui fattori di variabilità dell'aria è stato calcolato il contributo di aria esterna proveniente dall'apertura delle porte, sia quelle rivolte verso l'interno dell'edificio che quelle rivolte verso l'esterno.
Nella sala degenza si è calcolato che l'aria proveniente dalla porta rivolta verso il giardino esterno è di circa 1.300 mc/h; mentre dalla porta risvolta verso il corridoio centrale circa 1.700 mc/h.

Nella sala di attesa si è calcolato che, complessivamente, dalle tre porte, entrata, ingresso zona ambulatori e uscita il volume d'aria aria che si miscela all'aria ambiente è di orientativamente di 4.500 mc/h.

I calcoli sono basati sul numero medio di aperture orarie osservate durante i campionamenti.
Ciò nonostante si è deciso di effettuare delle misurazioni per comprendere il livello di contaminazione presente e se, nelle condizioni attuali, il sistema di ionizzazione dell'aria proposto potesse arrivare agli obiettivi desiderati di riduzione degli odori e del contenuto microbico.

Per definire il contributo d'aria proveniente dalle aperture è stato utilizzato un apposito sistema di calcolo, usato abitualmente nei calcoli tecnici specifici del settore; nella tabella sottostante sono visibili i fattori utilizzati.

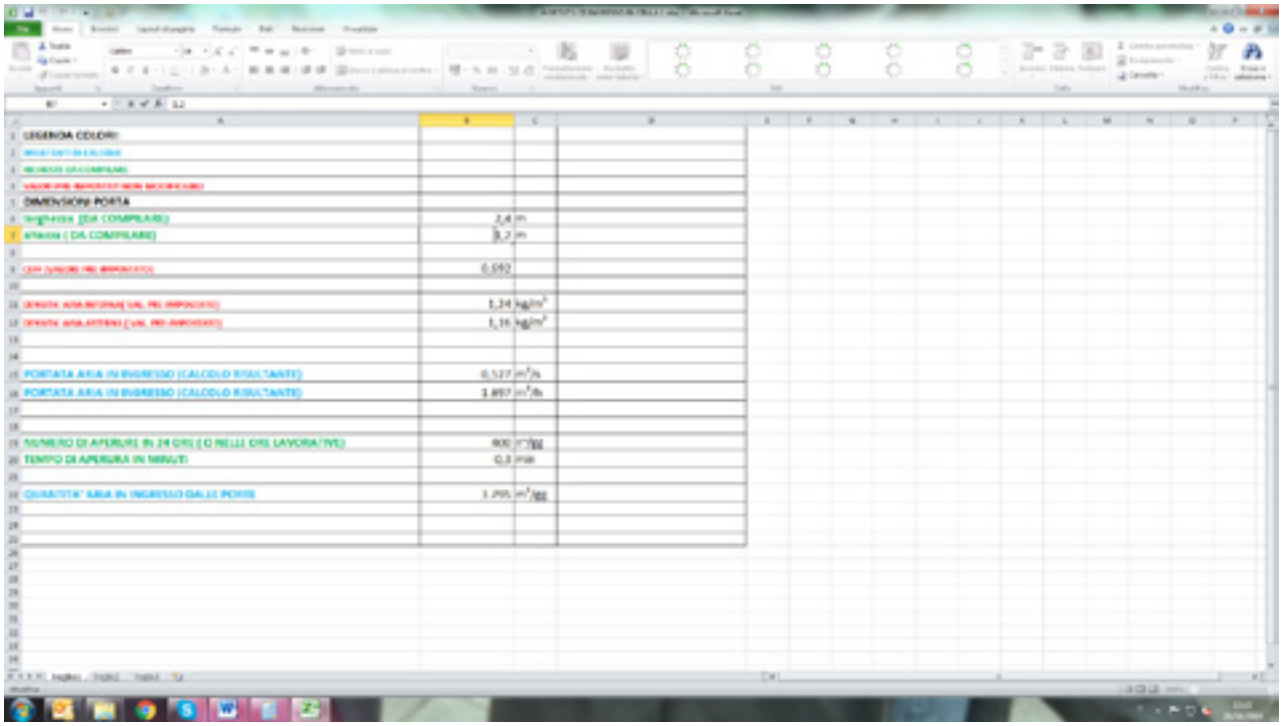

Fig. 1 – Sala di attesa

Fig. 2 – Sala degenza animali clinica veterinaria San Marco

Teoria della ionizzazione con plasma non termico

Con il termine plasma non termico, detto anche plasma freddo, si indica una forma evoluta miscela di gas ionizzati composta da una gran quantità di particelle caricate, come ioni o elettroni, radicali liberi, ros, molecole e anche atomi neutri.
La ionizzazione di un atomo si manifesta quando un elettrone acquisisce sufficiente energia per superare le forze attrattive del nucleo dell'atomo. Quando questo risultato si ottiene con processi che generano un plasma in cui la temperatura degli ioni e degli atomi neutri è sensibilmente minore di quella degli elettroni, si parla di plasma freddo o Non-Thermal Plasma (NTP).
Il plasma freddo emette luce con lunghezze d'onda sia nella parte visibile che nella parte ultravioletta dello spettro. Oltre all'emissione di radiazioni UV, un'importante proprietà del plasma a bassa temperatura è la presenza di elettroni ad alta energia, fortemente reattivi, che generano numerosi processi chimici e fisici come l'ossidazione, l'eccitazione di atomi e molecole, la produzione di radicali liberi e di altre particelle reattive. Un plasma si può generare artificialmente fornendo ad un gas un'energia sufficientemente alta, applicando cioè energia a un gas in modo tale da riorganizzare la struttura elettronica delle specie (atomi, molecole) e produrre specie eccitate e ioni. Uno dei più comuni modi per creare artificialmente e mantenere un plasma è attraverso una scarica elettrica in un gas. Nella tecnologia JONIX NTP, si utilizzano le cosiddette scariche non termiche con metodo a barriera di dielettrico. Le potenzialità di ionizzazione e la densità delle specie cariche generate dal plasma con scarica elettrica a barriera (DBD) sono maggiori rispetto a quelle presenti nel plasma non termico generato da altri sistemi.

Descrizione della attrezzatura Jonix

JO**NIX** steel è un unità di sanitizzazione, con tecnologia a plasma freddo per la purificazione e decontaminazione dell'aria.
Ideale per sale degenza, ambulatori, sale chirurgiche, di attesa e dove sia necessario prevenire e ridurre le contaminazioni batteriche aerotrasportate. Facilmente installabile a parete o in appoggio su piano orizzontale. Il dispositivo è studiato per consentire la propagazione dell'aria purificata in modo uniforme grazie al sistema di ventilazione frontale in entrata e agli spiragli ai lati che garantiscono l'uscita ottimale dell'aria. Compatto e silenzioso, il modulo JO**NIX** steel abbatte rapidamente le cariche batteriche e i contaminanti chimici.
JO**NIX** steel è semplice ed essenziale. In ottica di gestione integrata degli impianti, il controllo e le funzioni possono essere gestite da remoto.
ECOLOGICO E COMPATIBILE CON LA PRESENZA DI PERSONE
Nessun prodotto chimico e zero impatto ambientale. Sanitizza l'aria in modo continuativo, elimina gli odori migliorando così il comfort ambientale. Garantisce agli operatori la salubrità dell'aria come previsto dalle normative per la sicurezza dei lavoratori.

Fig. 2 – Flusso aria ionizzata

Fig. 3 – Dispositivo utilizzato

Materiali e metodi

Sono stati effettuati prelievi in due punti in due locali definiti: Sala Degenza e Sala Attesa. Nella sala degenza sono presenti degli animali in gabbie in attesa di interventi/controlli o dopo gli interventi. Nella sala di attesa sono presenti da un lato gli operatori della segreteria e dall'altro i clienti con i loro animali (foto 1 e 2).
I tempi di stazionamento nella sala degenza e la variabilità degli animali è molto elevata poiché variano durante il periodo delle prove il numero, la tipologia e lo stato generale di ogni singolo animale. Inoltre è presente un flusso di persone che accede direttamente dall'esterno alla sala comportando una significativa variazione dell'aria.
Anche nella sala di attesa la variabilità è molto elevata: il numero di persone, il numero la tipologia e la taglia degli animali cambia in continuazione come anche la frequenza di apertura delle porte.

I campionamenti sono stati eseguiti con un dispositivo SAS-Super 180 della PBI, che consente di prelevare una quantità d'aria prestabilita dall'operatore, questa viene a diretto contatto con una piastra contenente un specifico terreno di cultura per i microrganismi che si intendono monitorare. Nel test sono stati campionati per ciascun prelievo 100 lt d'aria.
Tali piastre vengono quindi trasferite all'interno di un contenitore refrigerato in laboratorio che provvederà all'incubazione delle piastre alla temperatura previste per la metodica specifica.

I parametri misurati sono:

Parametro	Terreno utilizzato	Temperatura e tempi di incubazione
Carica batterica mesofila	Plate count agar	30°C per 48 ore
Miceti	Sabouroud Dextrose Agar	30°C per 5 giorni
Pseusomonas ss	Pseusomonas cetrimide agar	35°C per 18-72 ore
Stafilococchi spp	Baird Parker Medium E.Y.T.E.	37°C per 24-48 ore

Le prove sono state condotte in collaborazione con l'Istituto Zooprofilattico Sperimentale delle Venezie, sezione di Treviso – Laboratorio di Diagnostica. I prelievi sono stati condotti con la collaborazione di Alimentaria S.r.l..

Sono inoltre state condotte delle **valutazioni sull'odore** percepito sia nella sala di attesa che nella sala degenza. La prova è stata condotta mediante valutazione dei tecnici intervenuti per i prelievi e del personale presente nei locali sopra indicati.

Risultati delle prove

Risultati delle analisi microbiologiche in aria

Sono state condotte delle analisi microbiologiche in aria campionando una quantità nota di aria con lo strumento denominato SAS. Il prelievo è stato effettuato in due punti per sala, a circa 1,5 metri di altezza dal pavimento.

Tab. 1 – Andamento risultati analitici sala Degenza punto 1

Degenza 1	Data	CBT Ufc/m^3	Miceti Ufc/m^3	*Pseudomonas spp* Ufc/m^3	*Stafilococco Spp* Ufc/m^3
Senza ionizzazione	26/03/18	120	110	10	210
	27/03/18	270	80	10	10
	28/03/18	340	110	10	220
	29/03/18	80	190	10	50
Con ionizzazione	04/04/18	100	100	10	150
	09/04/18	160	210	30	140
	17/04/18	190	160	10	180
	18/04/18	150	200	10	40
	20/04/18	50	40	10	80

(*) Carica batterica mesofila

Tab. 2 – Andamento risultati analitici sala Degenza punto 2

Degenza 2	Data	CBT Ufc/m^3	Miceti Ufc/m^3	*Pseudomonas spp* Ufc/m^3	*Stafilococco Spp* Ufc/m^3
Senza ionizzazione	26/03/18	1180	60	10	300
	27/03/18	180	170	10	10
	28/03/18	340	140	10	150
	29/03/18	320	110	40	240
Con ionizzazione	04/04/18	1050	120	10	320
	09/04/18	160	430	40	260
	17/04/18	350	150	20	170
	18/04/18	300	120	10	20
	20/04/18	<10	40	10	10

Tab. 3 – Andamento risultati analitici sala attesa punto 1

Attesa 1	Data	CBT Ufc/m^3	Miceti Ufc/m^3	*Pseudomonas spp* Ufc/m^3	*Stafilococco Spp* Ufc/m^3
Senza ionizzazione	26/03/18	30	100	<10	50
	27/03/18	10	30	<10	10
	28/03/18	160	120	50	40
	29/03/18	50	160	20	120
Con ionizzazione	04/04/18	70	50	<10	160
	09/04/18	220	130	<10	100
	17/04/18	10	150	<10	130
	18/04/18	160	240	<10	10
	20/04/18	30	10	<10	40

Tab. 2 – Andamento risultati analitici sala attesa punto 2

Attesa 2	Data	CBT Ufc/m^3	Miceti Ufc/m^3	*Pseudomonas spp* Ufc/m^3	*Stafilococco Spp* Ufc/m^3
Senza ionizzazione	26/03/18	30	100	<10	50
	27/03/18	40	40	<10	<10
	28/03/18	120	40	<10	90
	29/03/18	30	130	10	50
Con ionizzazione	04/04/18	170	80	<10	60
	09/04/18	180	190	10	210
	17/04/18	170	90	<10	70
	18/04/18	280	180	<10	<10
	20/04/18	40	<10	<10	40

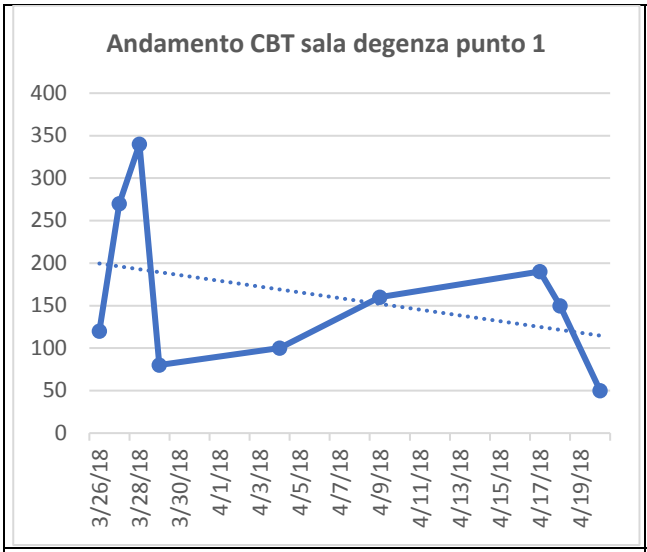
Andamento CBT sala degenza punto 1
400
350
300
250
200
150
100
50
0
3/26/18
3/28/18
3/30/18
4/1/18
4/3/18
4/5/18
4/7/18
4/9/18
4/11/18
4/13/18
4/15/18
4/17/18
4/19/18

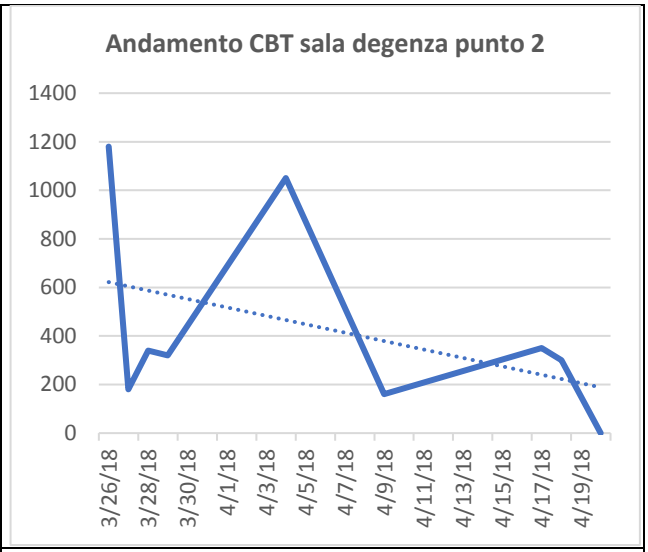
Andamento CBT sala degenza punto 2
1400
1200
1000
800
600
400
200
0
3/26/18
3/28/18
3/30/18
4/1/18
4/3/18
4/5/18
4/7/18
4/9/18
4/11/18
4/13/18
4/15/18
4/17/18
4/19/18

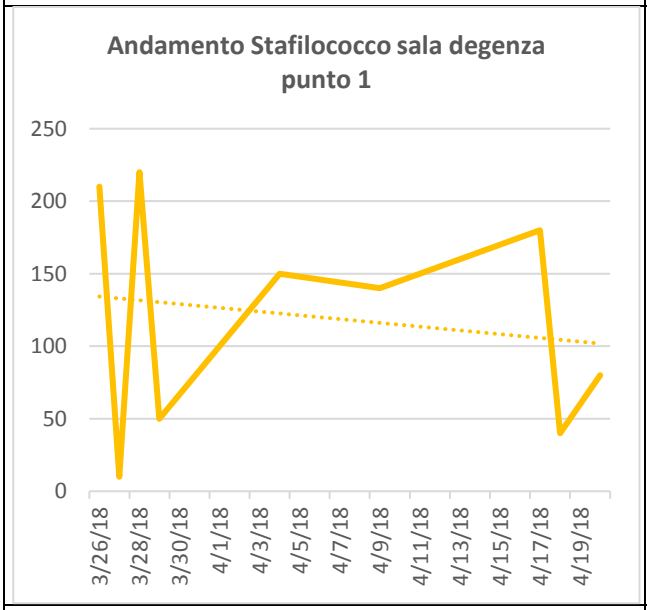
Andamento Stafilococco sala degenza punto 1
250
200
150
100
50
0
3/26/18
3/28/18
3/30/18
4/1/18
4/3/18
4/5/18
4/7/18
4/9/18
4/11/18
4/13/18
4/15/18
4/17/18
4/19/18

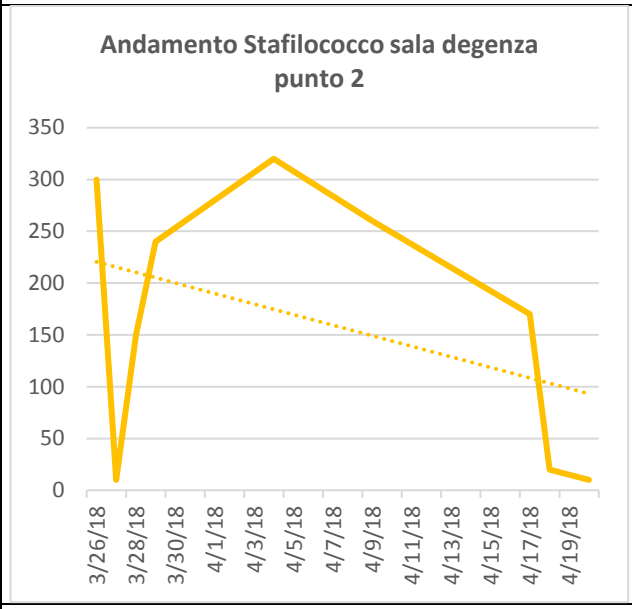
Andamento Stafilococco sala degenza punto 2
350
300
250
200
150
100
50
0
3/26/18
3/28/18
3/30/18
4/1/18
4/3/18
4/5/18
4/7/18
4/9/18
4/11/18
4/13/18
4/15/18
4/17/18
4/19/18

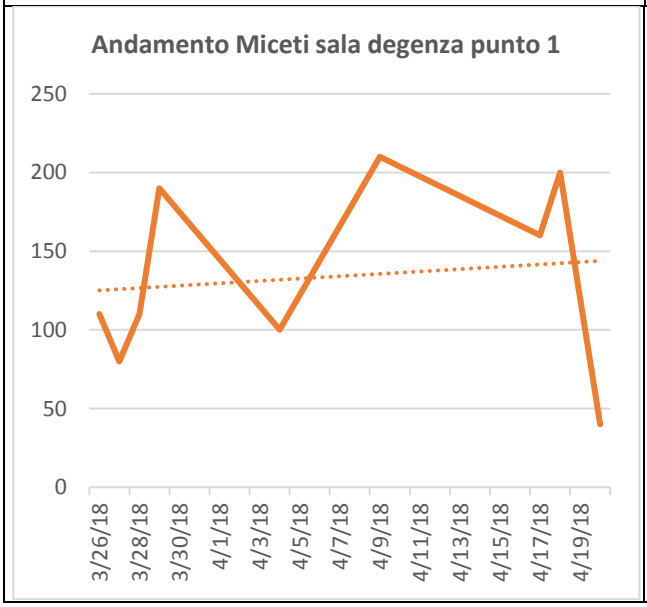
Andamento Miceti sala degenza punto 1
250
200
150
100
50
0
3/26/18
3/28/18
3/30/18
4/1/18
4/3/18
4/5/18
4/7/18
4/9/18
4/11/18
4/13/18
4/15/18
4/17/18
4/19/18

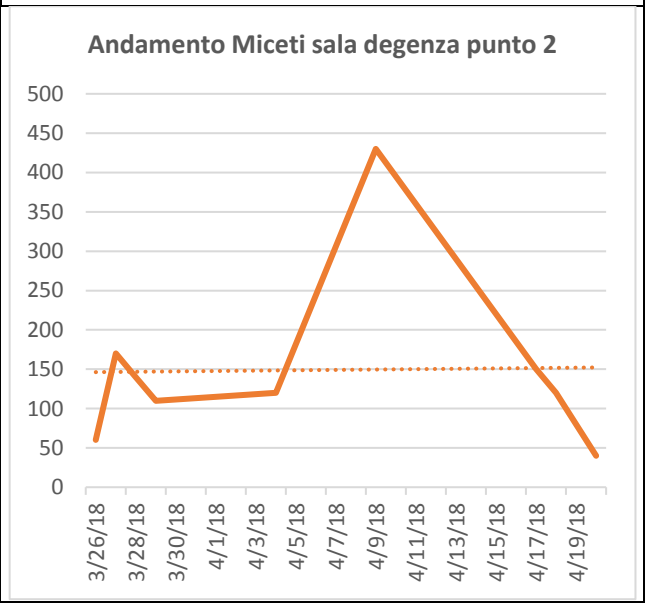
Andamento Miceti sala degenza punto 2
500
450
400
350
300
250
200
150
100
50
0
3/26/18
3/28/18
3/30/18
4/1/18
4/3/18
4/5/18
4/7/18
4/9/18
4/11/18
4/13/18
4/15/18
4/17/18
4/19/18

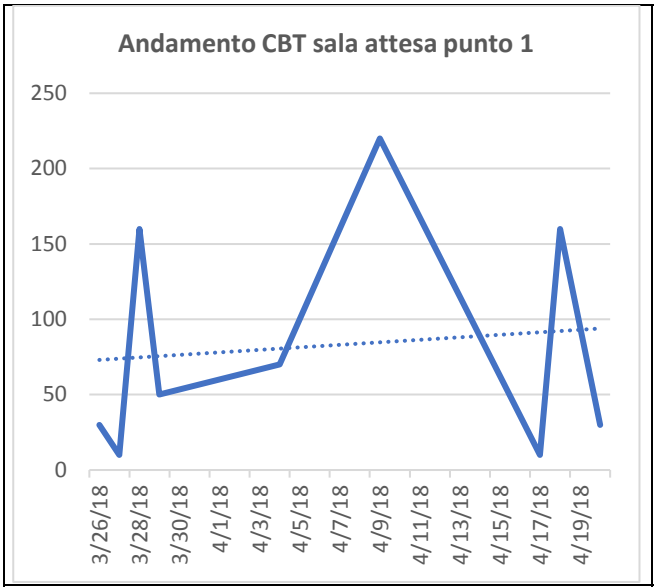
Andamento CBT sala attesa punto 1
250
200
150
100
50
0
3/26/18
3/28/18
3/30/18
4/1/18
4/3/18
4/5/18
4/7/18
4/9/18
4/11/18
4/13/18
4/15/18
4/17/18
4/19/18

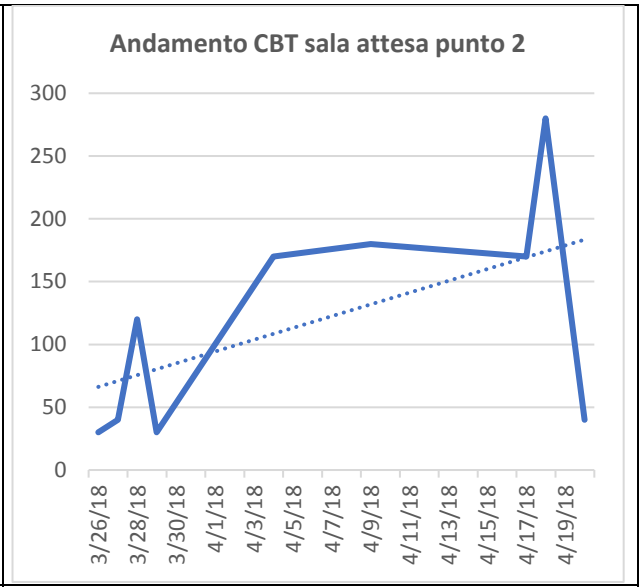
Andamento CBT sala attesa punto 2
300
250
200
150
100
50
0
3/26/18
3/28/18
3/30/18
4/1/18
4/3/18
4/5/18
4/7/18
4/9/18
4/11/18
4/13/18
4/15/18
4/17/18
4/19/18

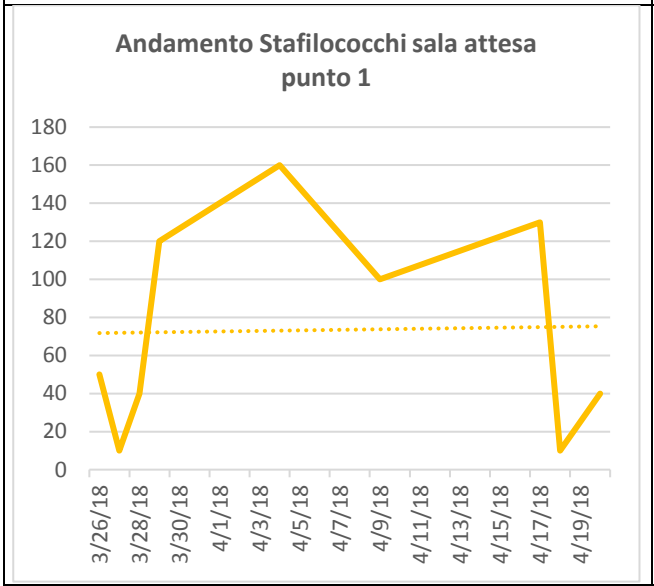
Andamento Stafilococchi sala attesa punto 1
180
160
140
120
100
80
60
40
20
0
3/26/18
3/28/18
3/30/18
4/1/18
4/3/18
4/5/18
4/7/18
4/9/18
4/11/18
4/13/18
4/15/18
4/17/18
4/19/18

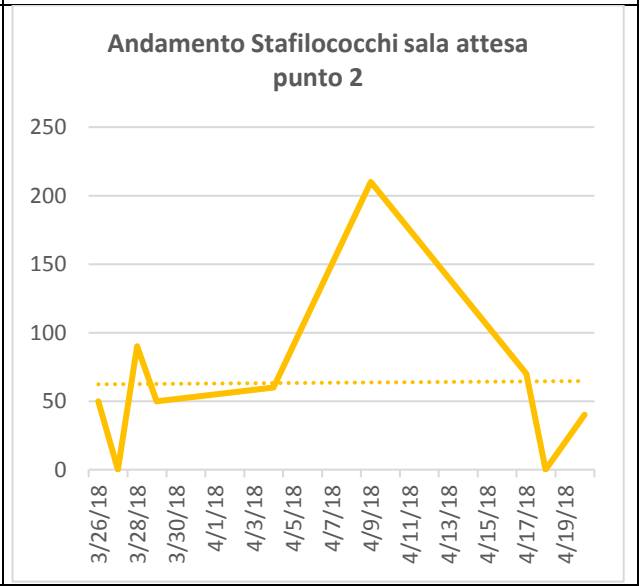
Andamento Stafilococchi sala attesa punto 2
250
200
150
100
50
0
3/26/18
3/28/18
3/30/18
4/1/18
4/3/18
4/5/18
4/7/18
4/9/18
4/11/18
4/13/18
4/15/18
4/17/18
4/19/18

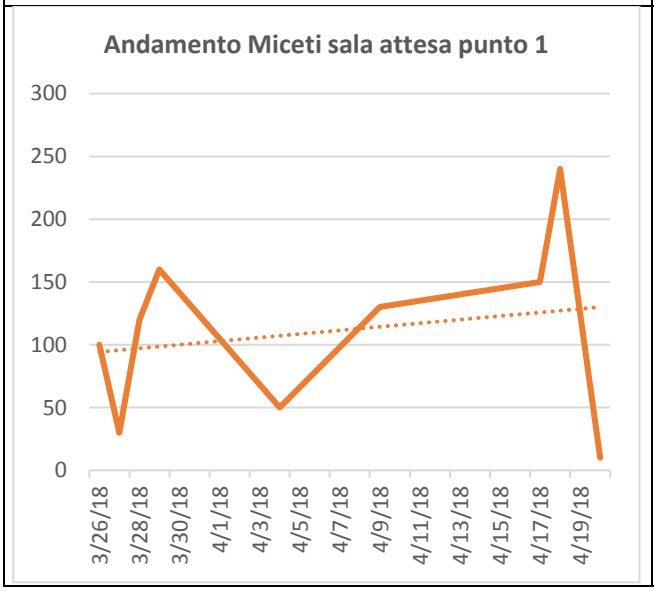
Andamento Miceti sala attesa punto 1
300
250
200
150
100
50
0
3/26/18
3/28/18
3/30/18
4/1/18
4/3/18
4/5/18
4/7/18
4/9/18
4/11/18
4/13/18
4/15/18
4/17/18
4/19/18

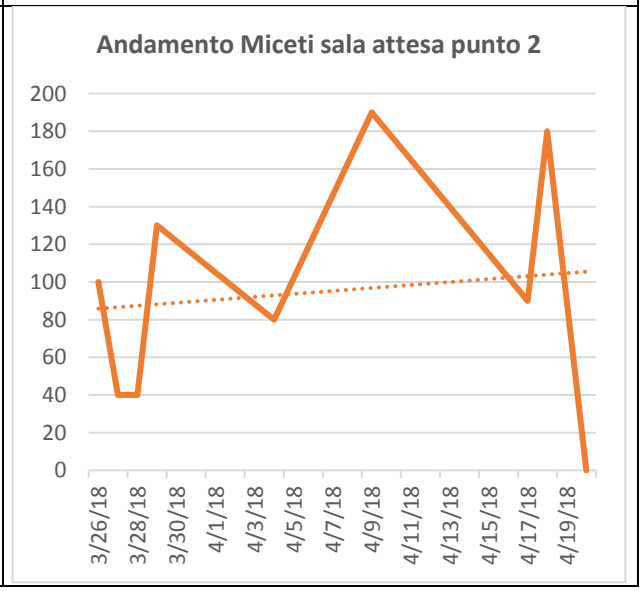
Andamento Miceti sala attesa punto 2
200
180
160
140
120
100
80
60
40
20
0
3/26/18
3/28/18
3/30/18
4/1/18
4/3/18
4/5/18
4/7/18
4/9/18
4/11/18
4/13/18
4/15/18
4/17/18
4/19/18

Risultati della valutazione sull'odore percepito

I locali sopra indicati presentano un odore tipico derivante dagli animali che sono ospitati nella struttura. Tale odore risulta "normale" per chi lavora quotidianamente nella struttura per un elevato numero di ore. Cosi invece non è per gli operatori e per le persone (clienti) che occasionalmente entrano nella clinica.

L'effetto sull'odore ha avuto un effetto apprezzabile e percepibile sin dalla prima rilevazione.

Data	Presenza ionizzazione	Sala attesa	Degenza
26/03/18	Senza ionizzazione	5	5
27/03/18		5	5
28/03/18		5	5
29/03/18		5	5
04/04/18	Con ionizzazione	1	3
09/04/18		1	3
17/04/18		1	3
18/04/18		1	3
20/04/18		1	3

La scala utilizzata durante l'intervista andava da 5 odore alto ad 1 poco odore.

Il test è stato condotto intervistando le persone (5 persone per ogni intervista) in sala di attesa nel periodo precedente e quello successivo all'accensione dei dispositivi Jonix.

Il personale operativo non era adeguato al pannel test poiché tali persone sono assuefatte all'odore.

Non potendo introdurre persone esterne per effettuare la verifica, la valutazione è stata effettuata intervistando i tecnici addetti ai prelievi.

Considerazioni

L'utilizzo della ionizzazione dell'aria per la riduzione degli odori e del contenuto microbico dell'aria e delle superfici a contatto con questa è stato più volte dimostrato e documentato (vedi rif. bibliografia).

Tutte le prove riportate in bibliografia sono state condotte avendo un limitato numero di variabili ambientali che potessero influire sui risultati.

Nel caso specifico, durante la sperimentazione, è emerso che le variabili sono molteplici e queste hanno un impatto significativo sull'andamento dei risultati.

La sala degenza che presenta le seguenti variabili:

a) Numero operatori da 2 a oltre 10 contemporaneamente presenti,
b) Tempi di permanenza del personale variabili
c) Numero di animali variabile
d) Taglia degli animali, specie e patologie diverse, con grado di igiene dell'animale variabile.
e) Porta verso l'esterno con apertura casuale variabile nella giornata

La sala di attesa presenta le seguenti variabili:

a) Numero di clienti variabile da nessuno a più di 10 in tempi brevi
b) Numero di animali variabile di conseguenza
c) Apertura verso l'esterno frequente per il passaggio di persone

La struttura dove sono state condotte le prove presenta un sistema di gestione dell'aria basato su UTA che immettono aria primaria, del quale però non sono noti i volumi delle portate aria, né complessive, né di eventuale ricircolo.
Il tipo di prelievo utilizzato effettua un campionamento istantaneo di una quantità nota di aria. Questa modalità di prelievo ha una durata di alcuni minuti (3-5 minuti). In questo periodo nei punti di prelievo si svolgono le normali attività che però, ovviamente, variano ad ogni prelievo.
Nella sala degenza, ad ogni prelievo cambiava il numero di animali, la loro taglia, il numero di persone che entrava e il loro tempo di permanenza, oltre al fatto che vi è una porta verso l'esterno che veniva aperta secondo necessità.
Nella sala di attesa la situazione ha previsto variabili analoghe anche se superiori poiché l'aria è influenzata anche dall'operato della segreteria oltre che dal numero di clienti e di animali; in alcuni casi vi erano 1 o 2 persone mentre in altri la sala presentava anche 10 o 15 persone presenti con i rispettivi animali.
L'andamento del contenuto microbico dell'aria è esposto ad un numero di variabili elevato e imprevedibile (apertura porte, numero clienti e di animali, influenza aria esterna, numero di passaggi, etc). Per avere dei risultati sull'effettivo apporto da parte della ionizzazione sarà necessario ridurre il numero di variabili e/o modificare gli indicatori utilizzati per la verifica dell'efficacia del sistema di ionizzazione in ambienti ad alta variabilità.
Dalla bibliografia risulta che il sistema di ionizzazione è efficace la ricerca deve essere condotta con un protocollo che dovrà essere rivisto per poter effettuare delle misurazioni attendibili.

Conclusioni

Nella sala degenza la tendenza rilevata indica una riduzione nel contenuto microbico totale e degli stafilococchi mentre i miceti vedono una leggera tendenza all'aumento, imputabile alle frequenti aperture delle porte che danno sull'esterno dell'edificio, circondato da siepi e piante. I punti di campionamento erano a circa 50 cm dalle aperture, di conseguenza l'aria aspirata era miscelata con quella proveniente dall'esterno.
Nella sala di attesa si è avuta una linea di tendenza generale di leggero aumento nei parametri rilevati inizialmente per le promiscuità con la l'aria proveniente dall'aperura e chiusa delle porte.
La modalità di prelievo utilizzata è quindi una "fotografia puntale" del momento in analisi.
Risulta evidente l'effetto di riduzione batterica nel tempo, l'apporto prolungato all'aria di molecole ionizzanti fa si che l'aria diventi inospitale per i contaminanti.

L'effetto di deodorizzazione dell'aria è stato sensorialmente apprezzabile in entrambe le sale controllate: l'odore presente si era ridotto in modo sensibile.
Gli utenti hanno infatti percepito un'aria quasi priva di odori nella sala di attesa dopo l'accensione dei dispositivi Jonix.
Al fine di poter condurre una valutazione più approfondita dell'affetto antimicrobico della ionizzazione, già documentato in bibliografia e con gli stessi dispositivi in altri ambiti, è necessario impostare un protocollo di ricerca in locali con un maggiore controllo delle variabili o con degli indicatori ambientali che risentano meno delle variabili in atto.
Viste le condizioni ambientali rilevate, dove il contenuto microbico è legato anche a particelle aero-disperse, può essere anche condotta una prova utilizzando dispositivi dotati di sistemi di filtrazione abbinati alla ionizzazione dell'aria, sistema analogo a quello utilizzato in ambito ospedaliero umano.

Test condotto in collaborazione con :

Alimentaria S.r.l. Dipartimento sicurezza e ambiente
Sede legale: Parco Scientifico & Tecnologico di Venezia – Via delle Industrie 19/B/11-30175 Venezia Marghera Tel. 041.5382629 – e-mail: info@alimentariavenezia.it
C.F. e P.IVA 03089520278 – Capitale sociale € 58.000,00 i.v.– R.E.A. VE 281802 – Reg. Imp. VE 03089520278

Istituto Zooprofilattico Sperimentale delle Venezie.
SCT2 Struttura complessa territoriale di Treviso, Belluno e Venezia
Vicolo Mazzini, 4 31020 Villorba (TV) Tel. 0422 302302

Bibliografia

Comi, G., Lovo, A., Bortolussi, N., Paiani, M., Berton, A., Bustreo, G. (2005) Ionizzatori per decontaminare l'aria nei locali di produzione del prosciutto crudo di San Daniele. Ind. Alim., XLIV, ottobre, 1-9.
Comi, G., Osualdini, M., Manzano, M., Lovo, A., Bortolussi, N., Berton, A., Bustreo, G. (2006) Decontaminazione di superfici di strutture e attrezzature utilizzate in aziende alimentari attraverso l'impiego di ionizzatori. Ind. Alim., XLV, giugno, 661-669.
JEFCA, 2001. Ochratoxin A. First Draft 47 series.

ALLEGATO 12.12

Reparto macelleria Ipermercato

Valutazione dell'effetto dei dispositivi di sanificazione dell'aria Jonix Minimate in un ipermercato

Presso un Ipermercato è installato un sistema di ionizzazione e filtrazione dell'aria modello JONIX MINIMATE, dispositivo di filtrazione sanificazione dell'aria. Il dispositivo è stato posizionato nella zona di confezionamento del reparto lavorazione carni.
Il locale è chiuso su tre lati e aperto sul lato che si affaccia sul punto vendita.

Il lato libero permette la miscelazione con l'aria della zona vendita.

L'aria della zona vendita è stata campionata in prossimità dei banchi frigo, per valutarne la concentrazione batterica.

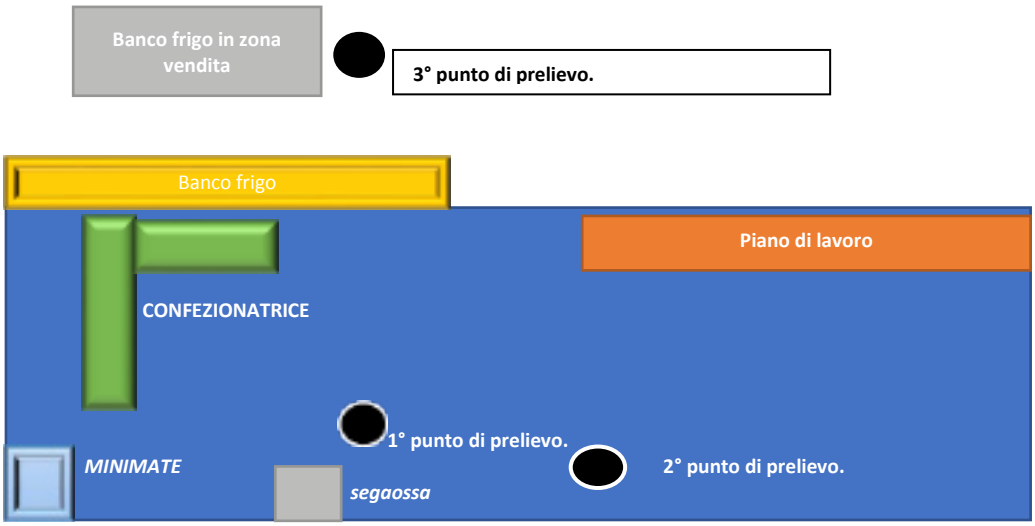

Figura 1. Vista in pianta del locale Dimensioni : mt 15x5x4h = 75 mq--300 mc. Lato aperto verso il punto vendita, dimensioni mt. 13 x 2.5 ca .superficie aperta di 32,5 mq. Ne risulta una miscelazione per un volume aria di 30.904 mc/h ca.

La soffittatura della zona indicata ha una apertura grigliata a soffitto. L'apertura permette l'entrata dell'aria proveniente della parte sovrastante al locale. Come indicato nella figura . Il locale subisce quindi le contaminazioni provenienti dalla zona vendita e dal soffitto.

Figura 2 Vista frontale del locale. Griglia superiore, dimensioni : mt 0,5 x 13 = 6.5 mq. superficie dell'apertura. Aperta in modo continuativo, ne risulta un volume di aria in ingresso paria 2.764mc/h .

Materiali e metodi

Il dispositivo JONIX MINIMATE è stato avviato nelle settimane precedenti al periodo di test e fatto funzionare con portate aria variabili dai 1000 ai 2000 metri cubi ora.

Per valutare gli effetti di sanificazione dell'aria del dispositivo sono stati eseguiti due campionamenti, in orari diversi e con portate aria differenti, a dieci 10 gironi di distanza l'uno dall'altro.

Il primo campionamento è stato effettuato il 19.09.18 alle 9.30, erano presenti 4 addetti, il prelevatore, ed il direttore del punto vendita. Da circa 10 gg la portata di aria era impostata a 1000 mc/h ed erano attivi i 4 generatori di plasma in dotazione al dispositivo.

Il secondo campionamento dell'aria è stato effettuato il 28/09/2018 alle 20.00. Dai 2 giorni precedenti la portata aria del dispositivo era impostata a 2000 mc/h. Erano presenti due addetti, il prelevatore ed il direttore del punto vendita.

Per i campionamenti è stato utilizzato un dispositivo SAS-Super 180 della PBI, sono stati campionati 100 lt aria su ciascun punto di prelievo. Sono state utilizzate piastre Petri con terreno di coltura PCA per la CBT e Ros Bengal Agar per muffe e lieviti.

Nelle tabelle sottostanti sono riportati i risultati dei due campionamenti.

Campionamento del 19.09.18

Area reparto macelleria	Carica batterica totale UFC/m3	Muffe e Lieviti UFC/m3
Punto 1 prelievo vicino a segaossa	330	210
Punto 2 prelievo vicino cella avicolo	310	297
Punto 3 davanti a reparto macelleria	>370	//

Campionamento del 28.09.18

Area	Carica batterica totale UFC/m3	Muffe e Lieviti UFC/m3
Punto 1 prelievo vicino a segaossa	150	57
Punto 2 prelievo vicino cella avicolo	90	63
Punto 3 davanti a reparto macelleria	310	//

Grafico 1 – Confronto andamento primo prelievo e secondo prelievo – carica batterica totale /mc

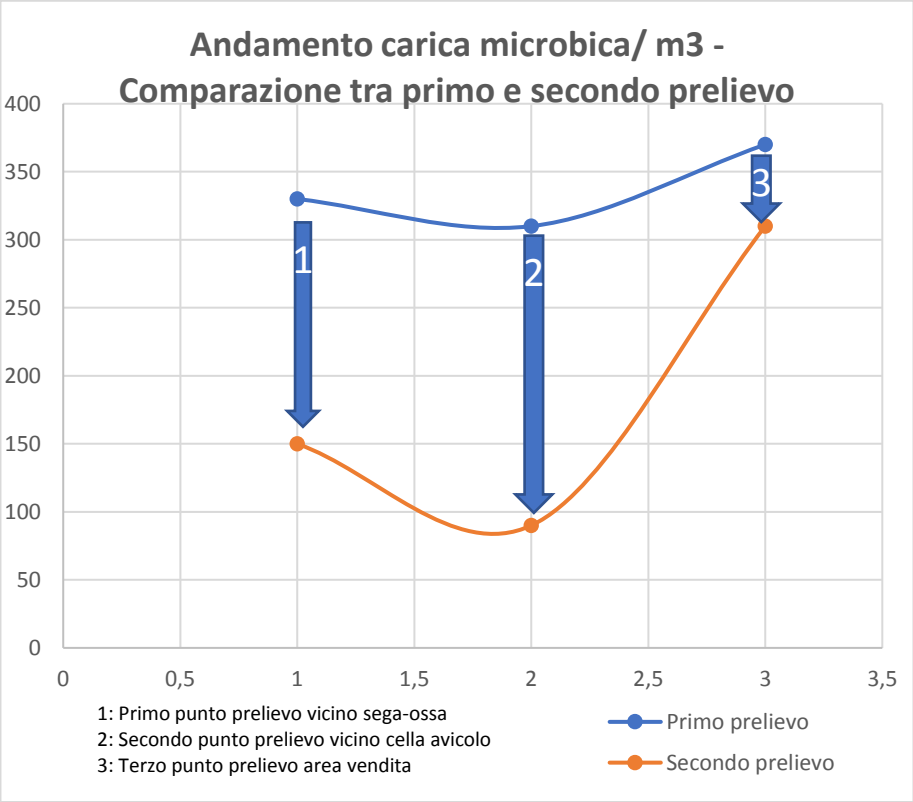

Il volume del locale è di circa 300 m. cubi, che subiscono la miscelazione con l'aria proveniente dalla zona vendita per circa 30.900 mc/h e con quella proveniente dalla griglia superiore per circa 2.700 mc/h.

Non conosciamo né le caratteristiche di filtrazione fornite dall'impianto trattamento aria centralizzato, né le percentuali di rinnovo. In ogni caso l'ambiente ne viene inevitabilmente influenzato.

Il dispositivo Jonix Minimate in uso nella zona analizzata è un sistema di sanificazione dell'aria, che unisce filtrazione e sanitizzazione. È dotato di tre filtri in successione (G4+F7+F9) a valle dei quali sono posti i 4 generatori di plasma freddo, come si può vedere nella figura 3

Figura 3. Vista frontale del dispositivo Jonix Minimate

La tecnologia Non Thermal Plasma https://jonixair.com/tecnologia (plasma freddo) è una forma evoluta di ionizzazione, che genera specie ossidanti in grado di ridurre il contenuto microbico presente in aria. Questo sistema consente il controllo continuativo dei contaminati, una sorta di "lavaggio" continuo dell'aria che riduce al minimo le contaminazioni aerotrasportate.

Jonix Minimate ha una portata aria modulabile dai 300 ai 2.000 mc/h. il dispositivo deve essere dimensionato in funzione del volume dell'aria da trattare. Nel locale in questione, alla portata massima di 2.000 mc/h il dispositivo effettua il "lavaggio" dell'aria 6, 6 volte ogni ora. Alla portata di 1.000 mc/h 3,3 volte per ora.

I valori di concentrazione batterica totale negli ambienti ad uso supermercato, possono variare da 500 a 1000 unità formanti colonia per metro cubo, in funzione dell'affluenza, della stagionalità e dello stato di manutenzione dell'impianto di trattamento aria.

Conclusioni

Dal grafico 1 è visibile come già al primo prelievo la concentrazione batterica per metro cubo sia inferiore ai valori medi di riferimento, risulta migliorata in modo significativo all'aumentare della portata aria. I valori raggiunti sono compatibili con un locale dotato di impianto di filtrazione per ambienti protetti, rispondente alla classe microbiologica D. come indicato nell'immagine sottostante.

Risulta quindi evidente che il dispositivo Jonix Minimate ha ridotto le contaminazioni presenti in aria in modo significativo, nonostante l'influenza dell'aria proveniente dai locali adiacenti.

Volendo ulteriormente migliorare i risultati suggeriamo due interventi infrastrutturali:

a) Chiusura della grata a soffitto con materiale trasparente, consentendo pertanto il passaggio della luce ma impedendo il passaggio incontrollato di aria e polveri da una zona non filtrata;
b) Chiusura del lato che si affaccia sull'area vendita al pubblico, evitando così l'ingresso di polveri e altri contaminanti, migliorando sensibilmente il contenuto microbico dell'aria del reparto che non avrebbe più influenze incontrollabili dall'esterno.

A disposizione per ulteriori chiarimenti.

Λimentaria
Dr. Andrea Lovo

ALLEGATO 12.13

Effetti sanitizzanti del dispositivo MATE nelle sale operatorie ospedaliere

ARCHA

ACCREDIA
LAB N° 0522

Effetti sanitizzanti del dispositivo MATE nelle sale operatorie ospedaliere

(Mate: sistema di trattamento aria mediante tecnologia NTP)

Studio condotta nel periodo
Febbraio – Marzo 2017

Laboratori ARCHA S.r.l. unipersonale
Via di Tegulaia 10/a - 56121 - PISA - ph. +39 050 985165 - fax +39 050 985233 - www.archa.it - archainf@archa.it
C.F., P.IVA, Iscr. Reg. Impr. di Pisa n. 01115340505 - Rep. Econ. Amm. di Pisa n°101169 - Capitale Sociale 101.400,00 i.v.

Sommario

Premessa

Il presente documento riporta i risultati ottenuti nella prima campagna di studio dell'azione dell'armadio MATE sui livelli di contaminazione di due sale operatorie in una casa di cura privata.
Lo studio si riferisce al primo periodo di sperimentazione svolto nel periodo 27 febbraio-23 marzo 2017.

Impostazione dello studio

Armadi MATE

I due armadi MATE sono stati posizionati uno per ciascuna delle due sale operatorie della casa di cura, denominate Sala operatoria A e Sala operatoria B.
L'esatta collocazione è stata scelta assieme agli operatori cercando di soddisfare le seguenti esigenze:

- Presenza di un punto di alimentazione elettrica;
- Minimo disturbo alle attività routinarie di sala;
- Adeguata distanza da elementi che potevano ostacolare il regolare flusso di aria attraverso il MATE.

Gli armadi sono stati così posizionati come risulta dalle seguenti immagini.

Foto 1 – Collocazione dei MATE all'interno delle sale operatorie

L'accensione dei MATE, avvenuta esclusivamente durante le ore notturne, è stata lasciata in manuale (nonostante la possibilità di programmarla attraverso il software interno) per garantire una certa flessibilità di utilizzo.
Il programma di studio è stato impostato in maniera tale da cercare di valutare al meglio gli effetti del MATE il cui impiego si doveva inserire nelle consuete attività svolte all'interno della sala operatoria che prevedono,

al termine degli interventi, delle approfondite operazioni di sanificazione ambientale. Inoltre, come previsto dalle normative di settore, l'aria di ciascuna sala operatoria è stata costantemente filtrata dall'impianto di trattamento presente.
L'azione del MATE doveva perciò essere di aiuto alle regolari e consuete attività di bonifica ambientale, andando a sostituire/integrare il sistema finora utilizzato che prevedeva la nebulizzazione di una soluzione disinfettante a base di perossido d'idrogeno e ioni argento (GLOSAIR 400).

Piano di controllo

E' stato stabilito di eseguire il monitoraggio dell'azione del MATE mediante l'esecuzione di mirate campagne di analisi volte alla caratterizzazione in ciascuna sala operatoria di:

- 3 tamponi di superficie;
- 1 campione di aria ambiente.

In ciascun campione sono stati ricercati i seguenti parametri:

Carica batterica totale a 37°C (CBT37)	*Rappresenta la somma di tutti i microrganismi in grado di crescere a 37°C. Sono perciò generici indicatori di contaminazione, anche di germi potenzialmente patogeni. La loro presenza non restituisce alcuna informazione sulla presenza di patogeni ma indica esclusivamente la possibilità di rilevarli.*
Muffe e lieviti (M&L)	*Microrganismi indicatori di contaminazione generalmente di origine ambientale. Permettono, assieme alla CBT37, di stabilire il livello di pulizia di un dato campione.*
Stafilococchi coagulasi positivi (SC+)	*Microrganismi patogeni opportunisti, in grado di provocare infezioni nell'uomo. Normalmente impiegati come indici di contaminazione antropica, spesso associati a pericolose infezioni in ambiente nosocomiale.*

Il piano di campionamento è stato predisposto sulla base delle consuete attività lavorative di entrambe le sale, cercando di valutare momenti sia di intensa che bassa attività (figura 1) rispettando il flusso lavorativo indicato dalla figura 2.

1° INTERVENTO		2° INTERVENTO		3° INTERVENTO		4° INTERVENTO		5° INTERVENTO		6° INTERVENTO		7° INTERVENTO		8° INTERVENTO	
TEMPO DI UTILIZZO LUNGO		TEMPO DI UTILIZZO BREVE		TEMPO DI UTILIZZO LUNGO		TEMPO DI UTILIZZO BREVE		TEMPO DI UTILIZZO LUNGO		TEMPO DI UTILIZZO BREVE		TEMPO DI UTILIZZO LUNGO		TEMPO DI UTILIZZO BREVE	
27-feb	28-feb	01-mar	02-mar	06-mar	07-mar	08-mar	09-mar	13-mar	14-mar	15-mar	16-mar	20-mar	21-mar	22-mar	23-mar
L	Ma	Me	G	L	Ma	Me	G	L	Ma	Me	G	L	Ma	Me	G

Figura 1 – programma di campionamento

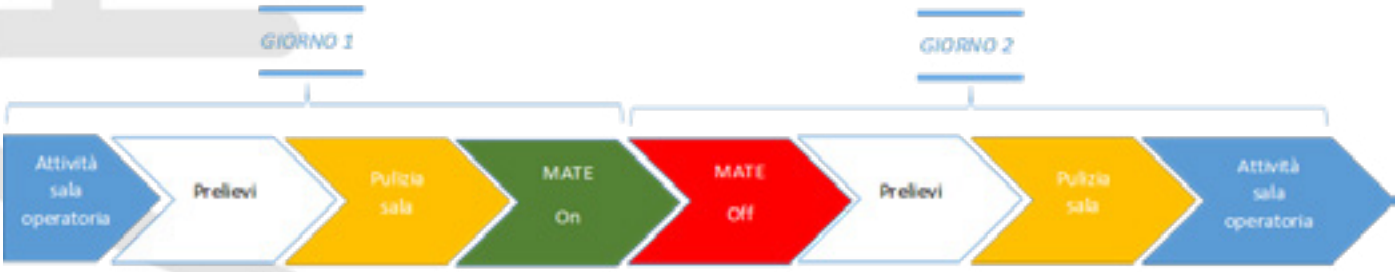

Figura 2-Flusso delle attività durante il periodo di studio

Sulla base di quanto stabilito è stato quindi possibile valutare il livello di contaminazione nelle condizioni di massima contaminazione (worst-case) al termine della giornata di lavoro in sala, confrontandolo con quello rilevabile nelle condizioni di massima pulizia mediante prelievi eseguiti il giorno successivo, dopo gli interventi di bonifica manuale e un periodo di utilizzo ininterrotto del MATE durate le ore notturne.
Le superfici scelte per il prelievo sono state le medesime per entrambe le sale operatorie, cercando di privilegiare quelle maggiormente esposte alla contaminazione, perché più frequentemente manipolate dagli operatori o per la loro particolare conformazione che le rendevano meno facilmente sanificabili con le operazioni manuali. L'aria ambiente è stata invece prelevata costantemente al centro di ciascuna sala, in prossimità del lettino operatorio.

Tutti campionamenti ed analisi sono state eseguite da laboratorio qualificato e accreditato. Contestualmente al prelievo dei campioni sono stati rilevati anche i tempi di accensione e spegnimento di ciascun MATE.

Risultati conseguiti

Superfici di lavoro

I dati raccolti, presentati in allegato 1, hanno evidenziato una sostanziale bassa contaminazione microbica.

Le muffe e lieviti non sono stati mai isolati dai campioni analizzati in entrambe le condizioni valutate (sala sporca/pulita). Gli stafilococchi invece sono stati occasionalmente trovati in alcuni campioni prelevati al termine delle attività lavorative, ma esclusivamente durante i primi giorni di monitoraggio.

Considerazioni a parte devono invece essere fatte per la CBT37.
Innanzitutto la carica microbica a 37°C è stata sempre isolata esclusivamente nei campioni prelevati in sala sporca e mai dopo il trattamento con il MATE; in quest'ultimo caso quindi **i campioni si sono rilevati assolutamente puliti e privi di livelli rilevabili dei microrganismi ricercati**, testimoniando una ideale condizione di pulizia.

Durante le attività invece le superfici, come è ovvio che sia, tendono a contaminarsi indipendentemente dal tipo di superficie valutata.
La cosa interessante emersa è che però il livello di sporcamento medio (valutato cioè come media di quanto rilevato nelle sei superfici campionate in entrambe le sale operatorie) tendeva nel tempo a diminuire, mano a mano che il MATE veniva impiegato, come se questo fornisse loro una sorta di refrattarietà alla contaminazione durante le consuete attività operatorie.

Il grafico seguente evidenzia quanto appena descritto.

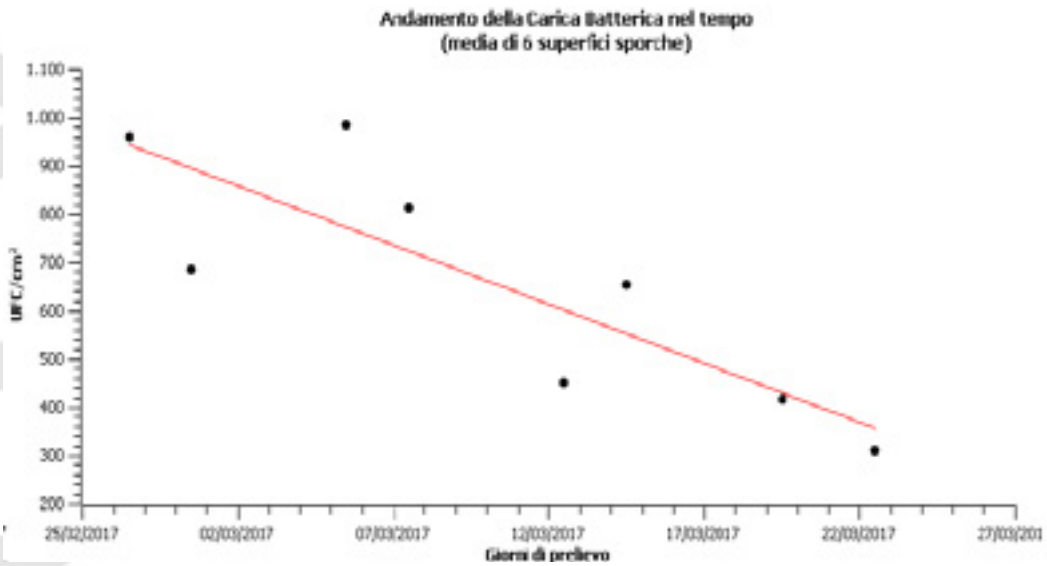

Figura 3 – Contaminazione microbica media; andamento durante il periodo di sperimentazione. I Dati rappresentano le medie delle contaminazioni rilevate sulle 6 superfici campionate in entrambe le sale (3 per sala).

Come si può osservare dalla figura, la CBT37 tende indiscutibilmente a ridursi, passando da un valore medio di oltre 900 unità formanti colonia per centimetro quadrato (UFC/cm^2) a poco più di 300 UFC/cm^2 con una andamento di riduzione in buona approssimazione lineare.

Analizzando i risultati ottenuti nelle singole sale operatorie è possibile verificare se questo comportamento era presente in tutte e due le sale.

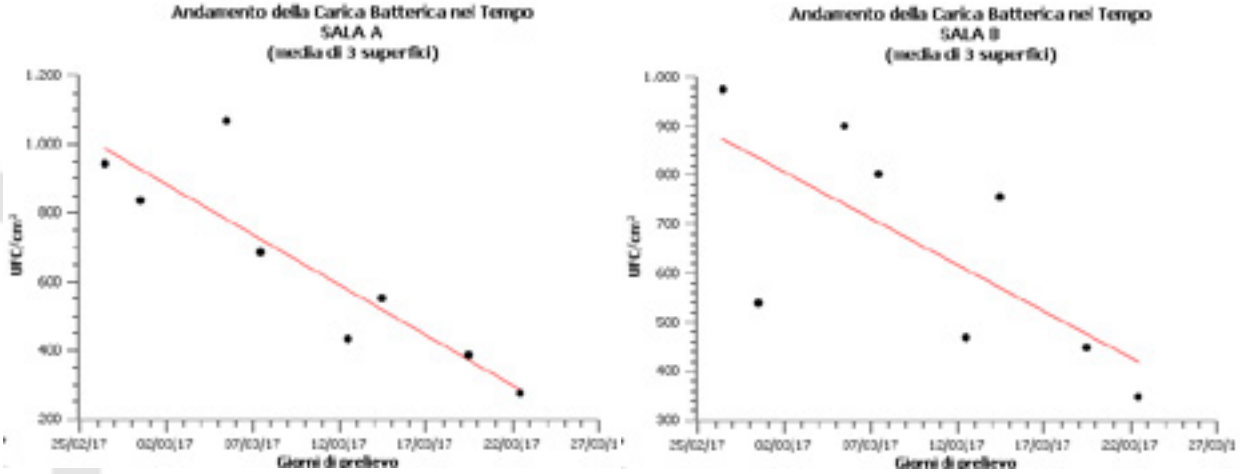

Figura 4 - Contaminazione microbica media nelle due sale operatorie: a sinistra Sala A; a destra Sala B

In questo caso si può osservare come il fenomeno osservato sia ripetibile in tutte e due le sale operatorie.

Poiché la contaminazione avviene durante il regolare utilizzo della sala operatoria con il MATE spento, il fenomeno sembrerebbe dovuto ad un "qualcosa" che tende a proteggere le superfici dalle contaminazioni, come se nel tempo l'azione del MATE le rendesse meno ospitali per i microrganismi.

In linea di massima una superficie risulta meno contaminata perché:

a) Viene sporcata meno

oppure

b) I microrganismi, a parità di sporcamento, sopravvivono peggio sulla superficie.

In quest'ultimo caso ciò può essere dovuto a:
b') presenze di elementi ad azione biocida (che in questo caso si accumulerebbero nel tempo);
b'') mancanza di elementi favorenti l'insediamento/sopravvivenza microbica (acqua libera, nutrienti come sostanza organica)

Con ogni probabilità si può escludere che le superfici vengano sporcate di meno (non si vede il perché) e quindi deve essere vera la seconda ipotesi di una minore sopravvivenza microbica. In questo caso è probabile che ciò non sia dovuto alla permanenza/accumulo di elementi ad azione biocida (le specie reattive generate dal MATE hanno una emivita brevissima) né ad una riduzione dell'acqua libera (non appare correlabile con l'azione del MATE). L'ipotesi più probabile è che grazie all'impiego del MATE, le operazioni di pulizia eseguite diventano più efficaci non solo ad eliminare i microrganismi (obiettivo sempre raggiunto fin dall'inizio della sperimentazione) ma anche e soprattutto a rimuovere più efficacemente la sostanza organica fonte di nutrimento microbico (sporco) che si deposita sulle superfici.
Indipendentemente però dalla spiegazione scientifica dell'origine del fenomeno osservato, appare comunque evidente che **l'impiego continuativo del MATE possa esercitare un'importante e significativa azione coadiuvante alle operazioni di detersione**, senza alcuna impiego di ulteriori composti chimici da nebulizzare nell'ambiente.

Aria ambiente

Anche per la contaminazione microbica aerodispersa è stato possibile rilevare una bassa contaminazione microbica, con lo stesso tipologia di microrganismi isolati (esclusivamente CBT37 e sporadicamente SC+).
Anche in questo caso l'aria ha mostrato la stessa tendenza in diminuzione, come se risultasse nel tempo sempre più protetta durante gli interventi (anche se il mate è spento) e la sua bonifica durante le ore notturne diventasse via via più efficace.

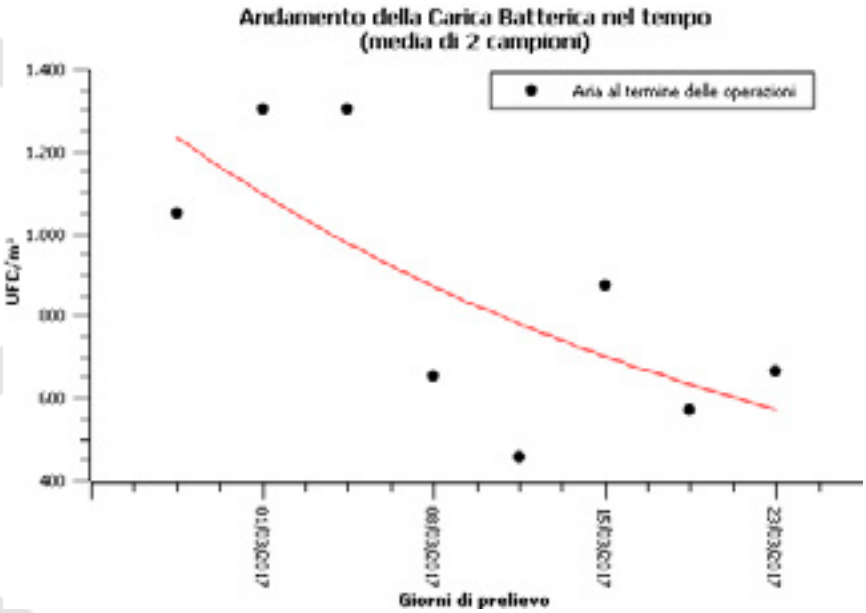

Figura 5 – Andamento della contaminazione aerodispersa al termina delle attività operatorie (sala sporca). Media dei valori rilevati nelle due sale operatorie

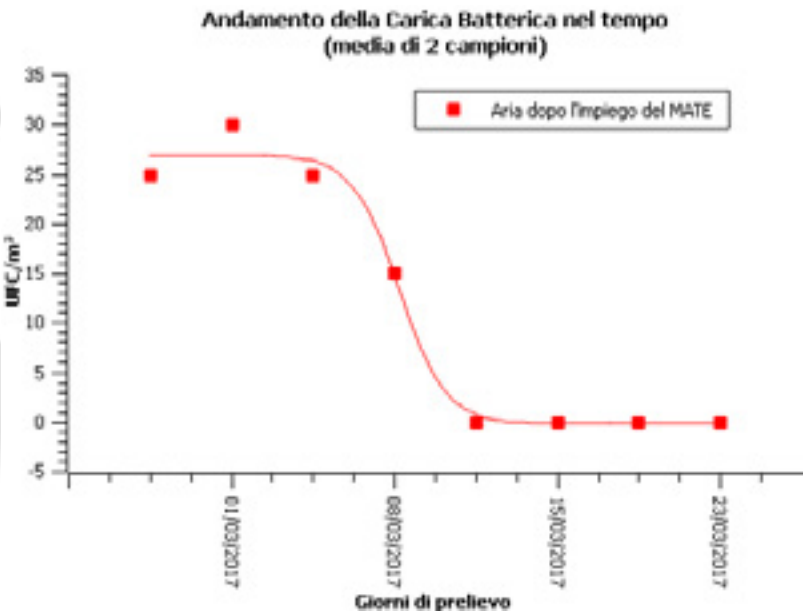

Figura 6 - Andamento della contaminazione aerodispersa al termina dell'impiego notturno del MATE (sala pulita). Media dei valori rilevati nelle due sale operatorie

Come si può osservare la riduzione di carica microbica è evidente sia nella sala sporca che in quella pulita. In quest'ultimo caso poi si è evidenziato un fenomeno particolare per cui all'inizio della sperimentazione, dopo l'impiego notturno del MATE, restava in aria un minimo livello di contaminazione (circa 30 UFC/m^3) per poi improvvisamente scomparire del tutto nella seconda metà del periodo di prova (andamento sigmoidale).

La spiegazione di quanto osservato è in questo caso più complicata che per le superfici non essendo assolutamente facile capire il motivo per cui, mano a mano che viene utilizzato il MATE, l'aria si contamini in misura minore anche durante le attività operatorie, quando il sistema di ionizzazione è spento.

Nel caso della contaminazione aerodispersa non si può invocare una permanenza di attività biocida (come già detto estremamente breve) né altri fattori ipotizzati per le superfici. Un'ipotesi potrebbe essere stata quella di una possibile correlazione tra il livello di sporcamento delle superfici e la contaminazione aerodispersa (vale a dire meno sono sporche le superfici meno i microrganismi si ritrovano nell'aria).

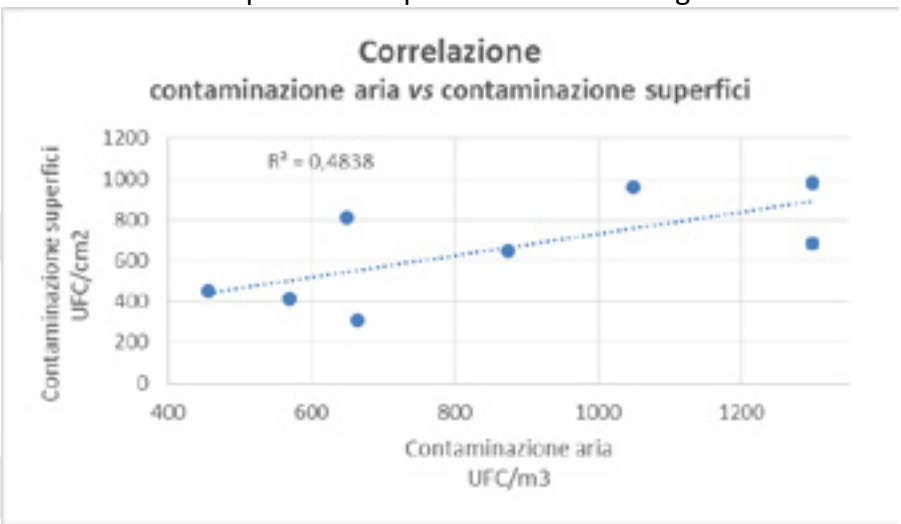

Figura 7 – Correlazione tra contaminazione superficiale e aerodispersa

L'analisi dei dati purtroppo evidenzia una scarsa correlazione tra questi fattori (r^2= 0,49) facendo cadere quindi anche questa ipotesi.

Un'altra possibilità, attualmente impossibile da verificare con i dati disponibili, è che le specie reattive prodotte durante la notte dal MATE, combinandosi con il vapore acqueo presente nell'aria, diano luogo a molecole di perossido d'idrogeno caratterizzato da una netta maggiore persistenza in aria. L'uso prolungato del MATE avrebbe perciò permesso di accumulare nel tempo dei composti ad azione biocida in grado di contrastare la presenza di microrganismi aerodispersi.

Anche in questo caso, comunque, indipendentemente dalla spiegazione scientifica rigorosa del fenomeno osservato, si può concludere che **l'impiego del MATE migliora la qualità dell'aria ambiente**, portando ad una graduale diminuzione della contaminazione microbica dell'aria, a netto vantaggio delle condizioni igienico sanitarie.

Allegato 1

- Risultati analitici -

Laboratori ARCHA S.r.l. unipersonale
Via di Tegulaia 10/a - 56121 - PISA - ph. +39 050 985165 - fax +39 050 985233 - www.archa.it - archainf@archa.it
C.F., P.IVA, Iscr. Reg. Impr. di Pisa n. 01115340505 - Rep. Econ. Amm. di Pisa n°101169 - Capitale Sociale 101.400,00 i.v.

Superfici

						Sala A					
Ora del prelievo	***Sporca***	*17:30*	*Orario MATE*	***Mate ON***	*17:51*	**Sportello mobile porta fili sutura**		**Soffietto lettino operatorio**		**Lampada scialitica lato dx**	
	Pulita	*07:35*		***Mate OFF***	*7:30*	**27/02/17**	**28/02/17**	**27/02/17**	**28/02/17**	**27/02/17**	**28/02/17**
Tempo funzionamento MATE (ore:minuti)					*13:39*	**Sporca**	**Pulita**	**Sporca**	**Pulita**	**Sporca**	**Pulita**
CBT a 37°						1300	<1	1500	<1	30	<1
Muffe						<10	<10	<10	<10	<10	<10
Lieviti						<10	<10	<10	<10	<10	<10
Stafilococco						15	<10	<10	<10	<10	<10
						Sala B					
Ora del prelievo	***Sporca***	*17:55*	*Orario MATE*	***Mate ON***	*18:13*	**Sportello mobile porta fili sutura**		**Soffietto lettino operatorio**		**Lampada scialitica lato dx**	
	Pulita	*08:00*		***Mate OFF***	*07:32*	**27/02/17**	**28/02/17**	**27/02/17**	**28/02/17**	**27/02/17**	**28/02/17**
Tempo funzionamento MATE (ore:minuti)					*13:19*	**Sporca**	**Pulita**	**Sporca**	**Pulita**	**Sporca**	**Pulita**
CBT a 37°						1400	<1	1500	<1	20	<1
Muffe						<10	<10	<10	<10	<10	<10
Lieviti						<10	<10	<10	<10	<10	<10
Stafilococco						<10	<10	<10	<10	<10	<10

						Sala A					
Ora del prelievo	***Sporca***	*20:00*	*Orario MATE*	***Mate ON***	*20:15*	**Tubo corrugato**		**Macchina anestesia zona pulsanti**		**Piano inox carrello ferri**	
	Pulita	*08:10*		***Mate OFF***	*07:40*	**01/03/17**	**02/03/17**	**01/03/17**	**02/03/17**	**01/03/17**	**02/03/17**
Tempo funzionamento MATE (ore:minuti)					*11:25*	**Sporca**	**Pulita**	**Sporca**	**Pulita**	**Sporca**	**Pulita**
CBT a 37°						900	<1	1000	<1	600	<1
Muffe						<10	<10	<10	<10	<10	<10
Lieviti						<10	<10	<10	<10	<10	<10
Stafilococco						15	<10	<10	<10	<10	<10
						Sala B					
Ora del prelievo	***Sporca***	*19:30*	*Orario MATE*	***Mate ON***	*19:49*	**Tubo corrugato**		**Macchina anestesia zona pulsanti**		**Piano inox carrello ferri**	
	Pulita	*07:45*		***Mate OFF***	*07:42*	**01/03/17**	**02/03/17**	**01/03/17**	**02/03/17**	**01/03/17**	**02/03/17**
Tempo funzionamento MATE (ore:minuti)					*11:53*	**Sporca**	**Pulita**	**Sporca**	**Pulita**	**Sporca**	**Pulita**
CBT a 37°						700	<1	110	<1	800	<1
Muffe						<10	<10	<10	<10	<10	<10
Lieviti						<10	<10	<10	<10	<10	<10
Stafilococco						<10	<10	<10	<10	<10	<10

						Sala A					
Ora del prelievo	***Sporca***	*18:15*	*Orario MATE*	***Mate ON***	*18:34*	**Carrello portafarmaci cassetto lato dx**		**Maniglia carrello assistente paziente**		**Sportello mobile porta fili di sutura**	
	Pulita	*11:20*		***Mate OFF***	*11:15*	**06/03/17**	**07/03/17**	**06/03/17**	**07/03/17**	**06/03/17**	**07/03/17**
Tempo funzionamento MATE (ore:minuti)					*16:41*	**Sporca**	**Pulita**	**Sporca**	**Pulita**	**Sporca**	**Pulita**
CBT a 37°						1300	<1	1000	<1	900	<1
Muffe						<10	<10	<10	<10	<10	<10
Lieviti						<10	<10	<10	<10	<10	<10
Stafilococco						<10	<10	<10	<10	<10	<10
						Sala B					
Ora del prelievo	***Sporca***	*17:10*	*Orario MATE*	***Mate ON***	*17:31*	**Carrello portafarmaci cassetto lato dx**		**Maniglia carrello assistente paziente**		**Sportello mobile porta fili di sutura**	
	Pulita	*10:55*		***Mate OFF***	*10:52*	**06/03/17**	**07/03/17**	**06/03/17**	**07/03/17**	**06/03/17**	**07/03/17**
Tempo funzionamento MATE (ore:minuti)					*17:21*	**Sporca**	**Pulita**	**Sporca**	**Pulita**	**Sporca**	**Pulita**
CBT a 37°						900	<1	700	<1	1100	<1
Muffe						<10	<10	<10	<10	<10	<10
Lieviti						<10	<10	<10	<10	<10	<10
Stafilococco						<10	<10	<10	<10	<10	<10

						Sala A					
Ora del prelievo	***Sporca***	*20:30*	*Orario MATE*	***Mate ON***	*20:46*	**Soffietto lettino operatorio**		**Lampada scialitica lato sx**		**Tubo corrugato**	
	Pulita	*11:20*		***Mate OFF***	*07:47*	**08/03/17**	**09/03/17**	**08/03/17**	**09/03/17**	**08/03/17**	**09/03/17**
Tempo funzionamento MATE (ore:minuti)					*11:01*	**Sporca**	**Pulita**	**Sporca**	**Pulita**	**Sporca**	**Pulita**
CBT a 37°						1100	<1	840	<1	530	<1
Muffe						<10	<10	<10	<10	<10	<10
Lieviti						<10	<10	<10	<10	<10	<10
Stafilococco						<10	<10	<10	<10	<10	<10
						Sala B					
Ora del prelievo	***Sporca***	*20:10*	*Orario MATE*	***Mate ON***	*20:28*	**Soffietto lettino operatorio**		**Lampada scialitica lato sx**		**Tubo corrugato**	
	Pulita	*07:40*		***Mate OFF***	*07:41*	**08/03/17**	**09/03/17**	**08/03/17**	**09/03/17**	**08/03/17**	**09/03/17**
Tempo funzionamento MATE (ore:minuti)					*11:13*	**Sporca**	**Pulita**	**Sporca**	**Pulita**	**Sporca**	**Pulita**
CBT a 37°						1300	<1	650	<1	450	<1
Muffe						<10	<10	<10	<10	<10	<10
Lieviti						<10	<10	<10	<10	<10	<10
Stafilococco						<10	<10	<10	<10	<10	<10

						Sala A					
Ora del prelievo	***Sporca***	*14:50*	*Orario MATE*	***Mate ON***	*15:13*	**Macchina anestesia zona pulsanti**		**Carrello portafarmaci cassetto lato sx**		**Piano inox carrello ferri**	
	Pulita	*12:45*		***Mate OFF***	*12:46*	**13/03/17**	**14/03/17**	**13/03/17**	**14/03/17**	**13/03/17**	**14/03/17**
Tempo funzionamento MATE (ore:minuti)					*21:33*	**Sporca**	**Pulita**	**Sporca**	**Pulita**	**Sporca**	**Pulita**
CBT a 37°						400	<1	400	<1	500	<1
Muffe						<10	<10	<10	<10	<10	<10
Lieviti						<10	<10	<10	<10	<10	<10
Stafilococco						<10	<10	<10	<10	<10	<10

						Sala B					
Ora del prelievo	***Sporca***	*15:40*	*Orario MATE*	***Mate ON***	*16:07*	**Macchina anestesia zona pulsanti**		**Carrello portafarmaci cassetto lato sx**		**Piano inox carrello ferri**	
	Pulita	*13:10*		***Mate OFF***	*13:06*	**13/03/17**	**14/03/17**	**13/03/17**	**14/03/17**	**13/03/17**	**14/03/17**
Tempo funzionamento MATE (ore:minuti)					*20:59*	**Sporca**	**Pulita**	**Sporca**	**Pulita**	**Sporca**	**Pulita**
CBT a 37°						640	<1	410	<1	350	<1
Muffe						<10	<10	<10	<10	<10	<10
Lieviti						<10	<10	<10	<10	<10	<10
Stafilococco						<10	<10	<10	<10	<10	<10

						Sala A					
Ora del prelievo	***Sporca***	*19:10*	*Orario MATE*	***Mate ON***	*19:33*	**Maniglia carrello assistente paziente**		**Sportello mobile porta fili di sutura**		**Soffietto lettino operatorio**	
	Pulita	*07:40*		***Mate OFF***	*07:37*	**15/03/17**	**16/03/17**	**15/03/17**	**16/03/17**	**15/03/17**	**16/03/17**
Tempo funzionamento MATE (ore:minuti)					*12:04*	**Sporca**	**Pulita**	**Sporca**	**Pulita**	**Sporca**	**Pulita**
CBT a 37°						540	<1	710	<1	400	<1
Muffe						<10	<10	<10	<10	<10	<10
Lieviti						<10	<10	<10	<10	<10	<10
Stafilococco						<10	<10	<10	<10	<10	<10

						Sala B					
Ora del prelievo	***Sporca***	*19:40*	*Orario MATE*	***Mate ON***	*19:53*	**Maniglia carrello assistente paziente**		**Sportello mobile porta fili di sutura**		**Soffietto lettino operatorio**	
	Pulita	*08:10*		***Mate OFF***	*07:54*	**15/03/17**	**16/03/17**	**15/03/17**	**16/03/17**	**15/03/17**	**16/03/17**
Tempo funzionamento MATE (ore:minuti)					*12:01*	**Sporca**	**Pulita**	**Sporca**	**Pulita**	**Sporca**	**Pulita**
CBT a 37°						730	<1	1100	<1	430	<1
Muffe						<10	<10	<10	<10	<10	<10
Lieviti						<10	<10	<10	<10	<10	<10
Stafilococco						<10	<10	<10	<10	<10	<10

						Sala A					
Ora del prelievo	***Sporca***	*17:30*	*Orario MATE*	***Mate ON***	*17:55*	**Lampada scialitica zona centrale**		**Tubo corrugato**		**Macchina anestesia zona pulsanti**	
	Pulita	*12:40*		***Mate OFF***	*12:37*	**20/03/17**	**21/03/17**	**20/03/17**	**21/03/17**	**20/03/17**	**21/03/17**
Tempo funzionamento MATE (ore:minuti)					*18:42*	**Sporca**	**Pulita**	**Sporca**	**Pulita**	**Sporca**	**Pulita**
CBT a 37°						430	<1	310	<1	410	<1
Muffe						<10	<10	<10	<10	<10	<10
Lieviti						<10	<10	<10	<10	<10	<10
Stafilococco						<10	<10	<10	<10	<10	<10

						Sala B					
Ora del prelievo	***Sporca***	*18:15*	*Orario MATE*	***Mate ON***	*18:37*	**Lampada scialitica zona centrale**		**Tubo corrugato**		**Macchina anestesia zona pulsanti**	
	Pulita	*13:05*		***Mate OFF***	*13:00*	**20/03/17**	**21/03/17**	**20/03/17**	**21/03/17**	**20/03/17**	**21/03/17**
Tempo funzionamento MATE (ore:minuti)					*18:23*	**Sporca**	**Pulita**	**Sporca**	**Pulita**	**Sporca**	**Pulita**
CBT a 37°						510	<1	310	<1	520	<1
Muffe						<10	<10	<10	<10	<10	<10
Lieviti						<10	<10	<10	<10	<10	<10
Stafilococco						<10	<10	<10	<10	<10	<10

						Sala A					
Ora del prelievo	***Sporca***	*19:05*	*Orario MATE*	***Mate ON***	*19:45*	**Piano inox carrello porta ferri**		**Cassetto basso carrello portafarmaci**		**Maniglia carrello assistente pazienti**	
	Pulita	*09:48*		***Mate OFF***	*09:40*	**23/03/17**	**24/03/17**	**23/03/17**	**24/03/17**	**23/03/17**	**24/03/17**
Tempo funzionamento MATE (ore:minuti)					*13:55*	**Sporca**	**Pulita**	**Sporca**	**Pulita**	**Sporca**	**Pulita**
CBT a 37°						210	<1	70	<1	540	<1
Muffe						<10	<10	<10	<10	<10	<10
Lieviti						<10	<10	<10	<10	<10	<10
Stafilococco						<10	<10	<10	<10	<10	<10

						Sala B					
Ora del prelievo	***Sporca***	*19:30*	*Orario MATE*	***Mate ON***	*19:33*	**Piano inox carrello porta ferri**		**Cassetto basso carrello portafarmaci**		**Maniglia carrello assistente pazienti**	
	Pulita	*09:20*		***Mate OFF***	*09:15*	**23/03/17**	**24/03/17**	**23/03/17**	**24/03/17**	**23/03/17**	**24/03/17**
Tempo funzionamento MATE (ore:minuti)					*13:42*	**Sporca**	**Pulita**	**Sporca**	**Pulita**	**Sporca**	**Pulita**
CBT a 37°						530	<1	100	<1	410	<1
Muffe						<10	<10	<10	<10	<10	<10
Lieviti						<10	<10	<10	<10	<10	<10
Stafilococco						<10	<10	<10	<10	<10	<10

Aria ambiente

						Sala A	
Ora del prelievo	***Sporca***	*17:30*	*Orario MATE*	***Mate ON***	*17:51*	**Aria lettino operatorio**	
	Pulita	*07:35*		***Mate OFF***	*7:30*	**27/02/17**	**28/02/17**
Tempo funzionamento MATE (ore:minuti)					*13:39*	**Sporca**	**Pulita**
CBT a 37°						1200	50
Muffe						assente	assente
Lieviti						assente	assente
Stafilococco						70	assente
						Sala B	
Ora del prelievo	***Sporca***	*17:55*	*Orario MATE*	***Mate ON***	*18:13*	**Aria lettino operatorio**	
	Pulita	*08:00*		***Mate OFF***	*07:32*	**27/02/17**	**28/02/17**
Tempo funzionamento MATE (ore:minuti)					*13:19*	**Sporca**	**Pulita**
CBT a 37°						900	<1
Muffe						assente	assente
Lieviti						assente	assente
Stafilococco						assente	assente

						Sala A	
Ora del prelievo	***Sporca***	*20:00*	*Orario MATE*	***Mate ON***	*20:15*	**Aria lettino operatorio**	
	Pulita	*08:10*		***Mate OFF***	*07:40*	**01/03/17**	**02/03/17**
Tempo funzionamento MATE (ore:minuti)					*11:25*	**Sporca**	**Pulita**
CBT a 37°						1400	30
Muffe						assente	assente
Lieviti						assente	assente
Stafilococco						35	assente
						Sala B	
Ora del prelievo	***Sporca***	*19:30*	*Orario MATE*	***Mate ON***	*19:49*	**Aria lettino operatorio**	
	Pulita	*07:45*		***Mate OFF***	*07:42*	**01/03/17**	**02/03/17**
Tempo funzionamento MATE (ore:minuti)					*11:53*	**Sporca**	**Pulita**
CBT a 37°						1200	30
Muffe						assente	assente
Lieviti						assente	assente
Stafilococco						assente	assente

						Sala A	
Ora del prelievo	***Sporca***	*18:15*	*Orario MATE*	***Mate ON***	*18:34*	**Aria lettino operatorio**	
	Pulita	*11:20*		***Mate OFF***	*11:15*	**06/03/17**	**07/03/17**
Tempo funzionamento MATE (ore:minuti)					*16:41*	**Sporca**	**Pulita**
CBT a 37°						1400	30
Muffe						assente	assente
Lieviti						assente	assente
Stafilococco						assente	assente
						Sala B	
Ora del prelievo	***Sporca***	*17:10*	*Orario MATE*	***Mate ON***	*17:31*	**Aria lettino operatorio**	
	Pulita	*10:55*		***Mate OFF***	*10:52*	**06/03/17**	**07/03/17**
Tempo funzionamento MATE (ore:minuti)					*17:21*	**Sporca**	**Pulita**
CBT a 37°						1200	20
Muffe						assente	assente
Lieviti						assente	assente
Stafilococco						40	assente

						Sala A	
Ora del prelievo	***Sporca***	*20:30*	*Orario MATE*	***Mate ON***	*20:46*	**Aria lettino operatorio**	
	Pulita	*11:20*		***Mate OFF***	*07:47*	**08/03/17**	**09/03/17**
Tempo funzionamento MATE (ore:minuti)					*11:01*	**Sporca**	**Pulita**
CBT a 37°						500	30
Muffe						assente	assente
Lieviti						assente	assente
Stafilococco						assente	assente
						Sala B	
Ora del prelievo	***Sporca***	*20:10*	*Orario MATE*	***Mate ON***	*20:28*	**Aria lettino operatorio**	
	Pulita	*07:40*		***Mate OFF***	*07:41*	**08/03/17**	**09/03/17**
Tempo funzionamento MATE (ore:minuti)					*11:13*	**Sporca**	**Pulita**
CBT a 37°						800	<1
Muffe						assente	assente
Lieviti						assente	assente
Stafilococco						assente	assente

						Sala A	
Ora del prelievo	***Sporca***	*14:50*	*Orario MATE*	***Mate ON***	*15:13*	**Aria lettino operatorio**	
	Pulita	*12:45*		***Mate OFF***	*12:46*	**13/03/17**	**14/03/17**
Tempo funzionamento MATE (ore:minuti)					*21:33*	**Sporca**	**Pulita**
CBT a 37°						340	<1
Muffe						assente	assente
Lieviti						assente	assente
Stafilococco						assente	assente
						Sala B	
Ora del prelievo	***Sporca***	*15:40*	*Orario MATE*	***Mate ON***		**Aria lettino operatorio**	
	Pulita	*13:10*		***Mate OFF***		**13/03/17**	**14/03/17**
Tempo funzionamento MATE (ore:minuti)					*00:00*	**Sporca**	**Pulita**
CBT a 37°						570	<1
Muffe						assente	assente
Lieviti						assente	assente
Stafilococco						assente	assente

						Sala A	
Ora del prelievo	***Sporca***	*19:10*	*Orario MATE*	***Mate ON***	*19:33*	**Aria lettino operatorio**	
	Pulita	*07:40*		***Mate OFF***	*07:37*	**15/03/17**	**16/03/17**
Tempo funzionamento MATE (ore:minuti)					*12:04*	**Sporca**	**Pulita**
CBT a 37°						810	<1
Muffe						assente	assente
Lieviti						assente	assente
Stafilococco						30	assente
						Sala B	
Ora del prelievo	***Sporca***	*19:40*	*Orario MATE*	***Mate ON***	*19:53*	**Aria lettino operatorio**	
	Pulita	*08:10*		***Mate OFF***	*07:54*	**15/03/17**	**16/03/17**
Tempo funzionamento MATE (ore:minuti)					*12:01*	**Sporca**	**Pulita**
CBT a 37°						940	<1
Muffe						assente	assente
Lieviti						assente	assente
Stafilococco						assente	assente

						Sala A	
Ora del prelievo	***Sporca***	*17:30*	*Orario MATE*	***Mate ON***	*17:55*	**Aria lettino operatorio**	
	Pulita	*12:40*		***Mate OFF***	*12:37*	**20/03/17**	**21/03/17**
Tempo funzionamento MATE (ore:minuti)					*18:42*	**Sporca**	**Pulita**
CBT a 37°						340	<1
Muffe						assente	assente
Lieviti						assente	assente
Stafilococco						assente	assente
						Sala B	
Ora del prelievo	***Sporca***	*18:15*	*Orario MATE*	***Mate ON***	*18:37*	**Aria lettino operatorio**	
	Pulita	*13:05*		***Mate OFF***	*13:00*	**20/03/17**	**21/03/17**
Tempo funzionamento MATE (ore:minuti)					*18:23*	**Sporca**	**Pulita**
CBT a 37°						800	<1
Muffe						assente	assente
Lieviti						assente	assente
Stafilococco						assente	assente

						Sala A	
Ora del prelievo	***Sporca***	*19:05*	*Orario MATE*	***Mate ON***	*19:45*	**Aria lettino operatorio**	
	Pulita	*09:48*		***Mate OFF***	*09:40*	**23/03/17**	**24/03/17**
Tempo funzionamento MATE (ore:minuti)					*13:55*	**Sporca**	**Pulita**
CBT a 37°						1100	<1
Muffe						assente	assente
Lieviti						assente	assente
Stafilococco						assente	assente
						Sala B	
Ora del prelievo	***Sporca***	*19:30*	*Orario MATE*	***Mate ON***	*19:33*	**Aria lettino operatorio**	
	Pulita	*09:20*		***Mate OFF***	*09:15*	**23/03/17**	**24/03/17**
Tempo funzionamento MATE (ore:minuti)					*13:42*	**Sporca**	**Pulita**
CBT a 37°						230	<1
Muffe						assente	assente
Lieviti						assente	assente
Stafilococco						assente	assente

ALLEGATO 12.14

Case study 5: Effetti sanitizzanti del dispositivo MATE nelle corsie di degenza ospedaliere

[redacted]

ASSE I – PROMOZIONE DELLA RICERCA E DELL'INNOVAZIONE

""

Servizi di Innovazione

Report finale

Servizio 1.1.

Inizio: 1 Febbraio 2018

Fine: 30 Aprile 2018

Laboratori ARCHA S.r.l. unipersonale
Via di Tegulaia 10/a - 56121 - PISA - ph. +39 050 985165 - fax +39 050 985233 - www.archa.it - archainf@archa.it
C.F., P.IVA, Iscr. Reg. Impr. di Pisa n. 01115340505 - Rep. Econ. Amm. di Pisa n°101169 - Capitale Sociale 101.400,00 i.v.

Sommario

Riassunto

Nella precedente attività di studio svolta relativamente al [redacted] nel contesto del progetto di ricerca denominato "[redacted]" e finanziato dal [redacted] per il supporto all'adozione di innovazioni e nuove tecnologie, sono emerse interessanti possibilità d'impiego della tecnologia NTP relativamente alla sua capacità di ridurre in maniera estremamente significativa i livelli di inquinamento microbico all'interno delle sale operatorie.

Nell'ottica di agire nella direzione della riduzione del Rischio Clinico connesso alle infezioni ospedaliere, si è cercato di stabilire le potenzialità d'azione della tecnologia NTP anche nei confronti dei microrganismi potenzialmente rinvenibili all'interno delle corsie di degenza.

Per questo scopo sono stati utilizzati dei sistemi ionizzanti di ridotte dimensioni appositamente disegnati per una loro collocazione meno "invasiva" e più facilmente inseribile in un contesto di vita abituale. Le attrezzature sono state collocate in diversi punti di una corsia e lasciate in funzione in maniera pressoché costante durante tutto il periodo di studio. Il confronto degli effetti è stato eseguito valutando i livelli di contaminazione in una corsia di "controllo" priva di sistemi NTP.

In questo modo lo studio ha potuto risponde in modo efficace e estremamente pertinente all'esigenza di valutazione di sistemi innovativi per la prevenzione delle infezioni in sala operatoria in particolare, e delle infezioni ospedaliere in generale, permettendo di individuare una tecnologia in grado di affiancare le consuete attività di bonifica ambientale, massimizzandone l'efficacia e contribuendo a creare ambienti più sicuri e con minore rischio infettivo.

Introduzione

Il Rischio clinico: le infezioni acquisite in ambiente nosocomiale

Il Ministero della Salute nel suo "Manuale per la formazione degli operatori sanitari - Sicurezza dei pazienti e gestione del rischio clinico"(1) definisce il Rischio Clinico come "la possibilità che un paziente subisca un danno o disagio involontario, imputabile, alle cure sanitarie, che causa un prolungamento del periodo di degenza, un peggioramento delle condizioni di salute o la morte"

Tale possibilità è strettamente correlata all'insorgenza di errori nel trattamento sanitario dai quali possono derivare danni differenti per il paziente. In sanità tali errori sono generalmente classificati in errori attivi (l'infermiere che sbaglia la dose di farmaco), facilmente individuabili nel tempo e nello spazio, e in errori latenti (un sistema manuale di prescrizione e trascrizione della terapia) viceversa più complessi da individuare ma che possono generare a catena tutta una serie di errori attivi.

E' riconosciuto che tali errori, da cui derivano gli incidenti sanitari, sono generati dall'interazione fra le diverse componenti del sistema sanitario: tecnologica, umana ed organizzativa, ciascuna in grado di funzionare da barriera protettiva contro l'insorgenza degli errori ma che talvolta presentano delle "falle" che in particolare condizioni possono portare al verificarsi dell'evento avverso.

Ciascun sistema sanitario è quindi caratterizzato da un proprio "grado di rischiosità" al quale concorrono numerosi fattori:

- fattori strutturali e tecnologici;

- fattori organizzativo-gestionali e condizioni di lavoro;

- fattori umani (individuali e del team);

- caratteristiche dell'utenza.

In base al tipo di evento avverso si prenda in considerazione, uno o più di questi fattori risultano determinante nella sua genesi.

Fra gli eventi avversi più temuti in sanità, sicuramente la possibilità di contrarre infezioni secondarie (oltre cioè a quelle primitive per le quali eventualmente si è ricorso all'assistenza sanitaria) rappresenta uno dei principali temi affrontati nel management del rischio clinico.

Queste infezioni possono derivare dalla contaminazione crociata paziente/paziente o operatore/paziente o ambiente/paziente e possono derivare sia da errori attivi (uso promiscuo di attrezzature sanitarie, mancato impiego di sistemi di protezione da parte del personale sanitario, inosservanza delle norme igieniche, …) che latente (non

corretta formalizzazione di procedure di sicurezza, formazione del personale inadeguata, mancata o insufficiente esecuzione di procedure di igiene ambientale,…).

Se alla fine del secolo scorso le infezioni ospedaliere venivano considerate come “le infezioni contratte durante il ricovero ospedaliero, che si manifestano clinicamente almeno dopo 48 ore dall’ingresso del ricovero, durante la degenza stessa o dopo la dimissione” oggi si è spostata l’attenzione sul concetto di infezione correlate ai processi assistenziali ed all’attività lavorativa in ambiente sanitario anche non strettamente ospedaliero, al punto che il Piano Sanitario Nazionale, fin dal biennio 2002-2004, le identificava come errori nelle pratiche assistenziali. E’ importante comunque sottolineare che tali errori sono insiti nell’attività sanitaria stessa e quindi, seppure prevenibili, non potranno mai essere azzerati, con una incidenza nazionale (in continua ascesa) che si attesta attorno al 5-10%.

In quest’ottica sicuramente riuscire a tenere sotto controllo il livello di contaminazione ambientale presente in sala operatoria rappresenta un elemento imprescindibile di ogni gestione del rischio clinico; in sala operatoria infatti i pazienti sono esposti come non mai alla possibilità di contrarre pericolose infezioni in una misura che è direttamente proporzionale al tipo di invasività dell’intervento e, ovviamente, al livello di contaminazione aerodispersa e presente sulle superfici.

Accanto a questo ambiente “critico” ne esistono però molti altri che necessitano di un attento controllo dei livelli di contaminazione ambientale, dagli ambulatori alle sale di attesa fino ad arrivare alle corsie di degenza. Quest’ultime sono molto spesso fonte di infezione crociata a causa della possibile presenza di pazienti portatori noti ma, molto spesso ignoti, di agenti infettivi in grado di determinare un aumento del rischio clinico. D’altro canto anche la presenza di visitatori può, in alcuni casi, andare a peggiorare il livello di igiene ambientale generale, con conseguente aumento del rischio infettivo per i pazienti.

Studio in corsia

Con questo studio si è cercato di capire se gli eccellenti risultati ottenuti in sala operatoria potevano essere in qualche maniera replicati anche in corsia degenti.

Per questo motivo si è fatto ricorso di una tipologia di attrezzatura differente dal MATE, basato sempre sull'impiego di moduli ionizzanti in grado di generare aria NTP, ma di dimensioni decisamente più contenute e privi del modulo di filtrazione HEPA.

Figura 1 – Unità di trattamento aria impiegata in corsia

Il sistema impiegato, denominato CUBE, sfrutta i medesimi principi alla base dell'armadio MATE e, essendo munito di un sistema temporizzato automatico, è in grado di eseguire dei cicli di trattamento personalizzabili a seconda delle esigenze.

Per gli scopi dello studio sono state individuate due corsie di degenza, perfettamente sovrapponibili per quanto riguarda la tipologia di pazienti ospitati (pazienti ortopedici), il loro numero e la frequenza di visite da parte dei familiari esterni.

Entrambe le corsie hanno le stesse identiche dimensioni e sono sottoposte alle medesime attività di sanificazione da parte del personale ausiliario.

Una delle due corsie è stata attrezzata con tre unità CUBE collocate in maniera tale da coprire tutta l'estensione del corridoio, con particolare attenzione alle zone di più altra frequentazione (zona caffè).

Figura 2 – Collocazione dei tre CUBE nella corsia "trattata". A) zona caffè-sala di aspetto; B) centro corsia; C) fine corsia

I Cube sono stati programmati in maniera tale da garantire un funzionamento continuativo secondo un ciclo che prevedeva 2 minuti di accensione seguiti da 8 minuti di pausa/24 ore al giorno.

Per la valutazione dell'efficacia sono stati previsti dei prelievi ambientali periodici bisettimanali da eseguirsi contemporaneamente sia nella corsia trattata che in quella di controllo.

I punti di prelievo scelti (i medesimi per entrambe le corsie) sono stati:

<u>Superfici</u>

- Pulsantiera distributore caffè	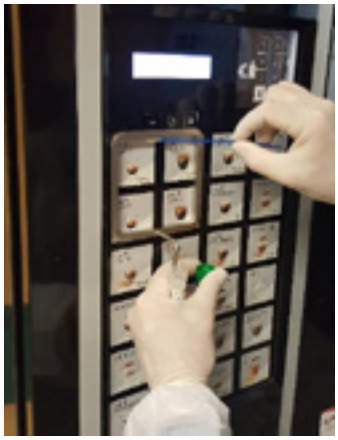

- Passamano	
- Parete sx fine corridoio	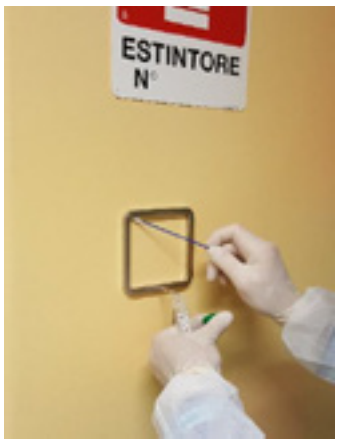

Le superfici sono state selezionate in quanto ritenute a più alto tasso di contaminazione e quindi maggiormente significative per gli scopi dello studio.

Analogamente anche l'aria ambiente, prelevata mediante campionatore attivo SAS, è stata campionata nella sala di attesa, in prossimità dell'ascensore e macchina caffè.

<u>Aria</u>

- Sala di attesa

In ogni campione sono stati ricercati:

- Carica batterica totale a 37°C;

- Muffe e lieviti;

- Stafilococchi coagulasi positivi.

I prelievi sono stati eseguiti per quattro settimane, il martedì e il giovedì, immediatamente al termine delle visite dei familiari e prima di qualunque operazione di pulizia ambientale, in maniera tale da andare a monitorare le peggiori condizioni d'inquinamento che si potessero realizzare.

Risultati conseguiti

Aria ambiente

Di seguito sono presentati i risultati ottenuti relativamente ai valori di contaminazione aerodispersa confrontando i dati ambientali delle due corsie.

t (giorni)	*Corsia Controllo UFC/m³*	*Corsia Trattata CUBE UFC/m³*	Riduzione giornaliera %
0	2100	300	85,71%
2	1100	310	71,82%
7	2000	420	79,00%
9	300	50	83,33%
14	2300	30	98,70%
16	1200	270	77,50%
21	1300	140	89,23%
23	900	100	88,89%
Media	**1400**	**203**	
% Riduzione Tot.	**86%**		

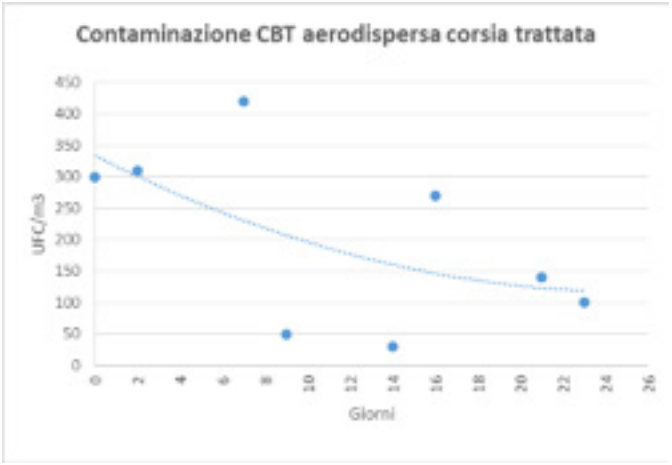

Figura 3 – TABELLA: andamenti della contaminazione da Carica Batterica Totale rilevata nell'aria delle due corsie sottoposte a prova. La riduzione % giornaliera si riferisce ai valori rilevati per giorno di campionamento nelle due corsie in studio; la riduzione % totale invece alle medie dei valori complessivamente rilevati nelle due tipologie di corsie. GRAFICO: andamento della CBT durante la sperimentazione nella sola corsia "trattata".

Dai risultati presentati si può ben apprezzare come la contaminazione microbica tenda progressivamente a diminuire nel tempo nella corsia trattata, andando a ridursi ad un terzo alla fine della sperimentazione. Confrontando poi i dati ottenuti nella corsia di controllo con quella trattata appare ben evidente come l'impiego del CUBE abbia portato fin da subito ad un netto miglioramento, con una riduzione di contaminazione che complessivamente si va ad attestare all'86% (valori medi).

Tabella 1 - Andamenti della contaminazione da Muffe e Lieviti (tabella a sinistra) e Stafilococchi (tabella di destra) rilevata nell'aria delle due corsie sottoposte a prova. La riduzione % giornaliera si riferisce ai valori rilevati per giorno di campionamento nelle due corsie in studio; la riduzione % totale invece alle medie dei valori complessivamente rilevati nelle due tipologie di corsie.

t (giorni)	*Corsia Controllo UFC/m³*	*Corsia Trattata (CUBE) UFC/m³*	Riduzione giornaliera %
0	80	0	100,00%
2	210	0	100,00%
7	150	0	100,00%
9	180	0	100,00%
14	170	0	100,00%
16	210	0	100,00%
21	100	0	100,00%
23	60	0	100,00%
Media	**145**	**0**	
% riduzione	**100%**		

t (giorni)	*Corsia Controllo UFC/m³*	*Corsia Trattata (CUBE) UFC/m³*	Riduzione giornaliera %
0	60	0	100,00%
2	12	0	100,00%
7	19	0	100,00%
9	22	0	100,00%
14	20	0	100,00%
16	24	0	100,00%
21	0	0	100,00%
23	0	0	100,00%
Media	**20**	**0**	
% riduzione	**100%**		

In questo caso si può osservare come la presenza dei CUBE nella corsia trattata abbia di fatto reso l'ambiente assolutamente inospitale per i germi ricercati (Muffe e Lieviti, Stafilococchi coagulasi positivi) quando viceversa nell'altra corsia era praticamente sempre presenti. In questo caso quindi si è osservata una riduzione di contaminazione che complessivamente si va ad attestare al 100% (valori medi).

Superfici di lavoro

Analogamente ai risultati relativi all'aria ambiente, di seguito sono presentati i valori di contaminazione ricavati dall'analisi delle superfici campionate.

Tabella 2 - Andamenti della contaminazione da Carica Batterica Totale rilevata nelle superfici campionate nelle due corsie sottoposte a prova.

CBT	**Corsia Controllo**			**Corsia Trattata (CUBE)**		
t (giorni)	Pulsantiera	Passamano	Parete	Pulsantiera	Passamano	Parete
0	1400	1200	9100	800	400	620
2	1400	9000	3900	140	40	60
7	2100	700	800	400	180	150
9	350	400	1000	60	70	90
14	500	1200	610	290	180	90
16	1400	2300	730	200	210	130
21	900	1000	1600	70	80	120
23	1000	810	1100	80	85	90
Media	**1131**	**2076**	**2355**	**255**	**156**	**169**

In questo caso è possibile evidenziare, rispetto ai valori medi rilevati per ogni tipologia di superficie nelle due corsie, le seguenti percentuali di abbattimento:

Tabella 3 - Riduzione della contaminazione microbica per superficie campionata. Confronto tra superficie da corsia trattata/superficie da corsia controllo

CBT	Pulsantiera	Passamano	Parete
Riduzione %	77%	93%	93%

I grafici seguenti permettono di evidenziare come la contaminazione microbica tenda progressivamente a diminuire nel tempo nella corsia trattata su tutte le superfici campionate, in maniera del tutto analoga a quanto visto per l'aria.

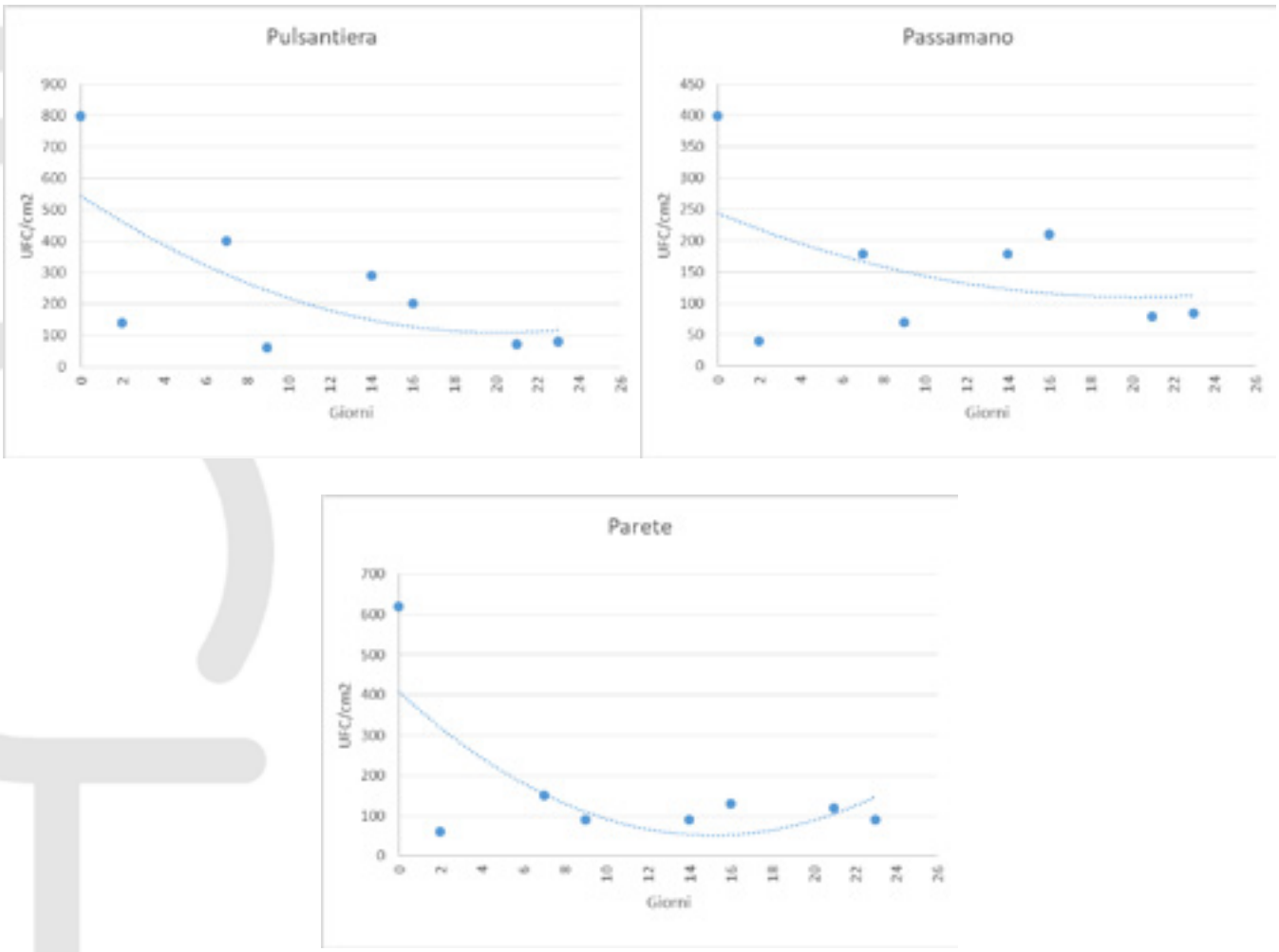

Figura 4 – Andamento della contaminazione da CBT nelle superfici della corsia trattata con CUBE

I risultati presentati evidenziano chiaramente che dal trattamento dell'aria ambiente con il CUBE ne beneficiano anche le superfici rivelando una chiara tendenza alla diminuzione della carica microbica totale presente sulle superfici campionate nel corso della sperimentazione. La riduzione è presente sia confrontando i valori medi delle contaminazioni superficiali nelle due corsie (tabella 18), sia valutandone l'andamento nel tempo nella corsia trattata (figura 45).

In questo caso le percentuali di riduzione osservate sono state:

Tabella 4 - Riduzione della contaminazione microbica per superficie campionata nella corsia trattata. Confronto tra superficie ad inizio trattamento/fine trattamento

CBT	Pulsantiera	Passamano	Parete
Riduzione %	90%	78%	85%

Nel caso degli altri due parametri analizzati i risultati sono stati i seguenti.

Tabella 5 Andamenti della contaminazione da Muffe e Lieviti (tabella superiore) e Stafilococchi coagulasi positivi (tabella inferiore) rilevata nelle superfici campionate nelle due corsie sottoposte a prova.

ML	Corsia Controllo			Corsia Trattata (CUBE)		
t (giorni)	Pulsantiera	Passamano	Parete	Pulsantiera	Passamano	Parete
0	0	0	120	0	0	0
2	0	0	100	0	0	0
7	0	50	140	0	0	0
9	0	0	200	0	0	0
14	0	0	160	0	0	0
16	0	85	180	0	0	0
21	0	0	40	0	0	0
23	0	0	80	0	0	0
Media	**0**	**17**	**128**	**0**	**0**	**0**

SC+	Corsia Controllo			Corsia Trattata (CUBE)		
t (giorni)	Pulsantiera	Passamano	Parete	Pulsantiera	Passamano	Parete
0	40	0	30	0	0	0
2	80	0	0	0	0	0
7	70	0	0	0	0	0
9	130	0	0	0	0	0
14	110	70	0	0	0	0
16	19	45	0	0	0	0
21	0	0	0	0	0	0
23	30	0	0	0	0	0
Media	**60**	**14**	**4**	**0**	**0**	**0**

Con i seguenti valori di riduzione

MF	Pulsantiera*	Passamano	Parete
Riduzione %	0%	100%	100%

** mai rilevata la presenza di muffe e lieviti in entrambe le corsie*

SC+	Pulsantiera	Passamano	Parete
Riduzione %	100%	100%	100%

Dai dati presentati è possibile trarre le seguenti conclusioni:

- L'applicazione dei sistemi CUBE ha determinato una costante migliore della qualità dell'aria per tutti i parametri ricercati, con differenze di contaminazione fra la corsia "trattata" e quella di "controllo" di almeno due ordini di grandezza; differenze evidenti fino dal primo giorno di trattamento e più marcato a mano a mano che il trattamento è proseguito nel tempo;

- La corsia "trattata" ha rilevato una importante diminuzione dei valori di contaminazione fino e ciò si evidenzia in particola modo valutando i valori di Carica Batterica Totale a 37°C; nel caso della corsia "trattata" l'apporto inquinante antropico (rilevato dalla presenza dei Stafilococchi coagulasi positivi) è risultato perfettamente sotto controllo, con costante assenza del germe patogeno in tutti i campioni analizzati. Anche per quanto riguarda i miceti (alcuni dei quali potenzialmente patogeni) sono risultati non rilevabili, a ulteriore testimonianza degli ottimi livelli di salubrità dell'aria ambiente;

- Così come accaduto nelle sale operatorie, l'impiego di aria ionizzata ha determinato una marcata diminuzione dei livelli di contaminazione delle superfici campionate, a diretta testimonianza delle potenzialità d'impiego di questa tecnologia. In particolare appare degno di sottolineatura il risultato ottenuto nella pulsantiera della macchina del caffè. In questo caso siamo di fronte ad una superficie che entra molto spesso in contatto con le mani dei visitatori, del personale e dei pazienti, molto spesso trascurata dalle consuete operazioni di sanificazione, e perciò in grado di trasferire potenziali agenti microbici infettivi da un soggetto all'altro.

Come evidenziato dai risultati presentati questa superficie conferma le sue "potenzialità" nel caso della corsia di controllo, con valori di contaminazione estremamente elevati. Fanno da contraltare a questi dati quelli ottenuti nella macchina collocata nella corsia "trattata" in cui si è assistito alla scomparsa degli stafilococchi e ad una brusca importante diminuzione delle cariche batteriche totali.

Vantaggi del possibile impiego del trattamento NTP per il Rischio Clinico – riduzione del Rischio Infettivo

I risultati mostrati evidenziano che la tecnologia NTP presenta degli effetti interessanti per quanto concerne la sua attività biocida. In particolare è risultata evidente la sua elevata capacita di disinfezione delle superfici in tempi assolutamente contenuti. La possibilità poi di abbinare il trattamento di ionizzazione con quello di filtrazione, crea delle prospettive assolutamente interessanti.

Si potrebbe infatti ipotizzare un dispositivo, mobile, in grado di eseguire il trattamento di disinfezione e filtrazione dell'aria là dove si ritiene al momento più necessario.

Ad esempio in sala operatoria si verrebbe quindi a configurare come una unità che può integrare l'azione di depurazione dell'aria ambiente esercitata dal sistema di trattamento canalizzato. In questo modo l'apparato contribuirebbe ad un'azione di "bonifica" del particolato che viene emesso durante gli interventi in sala operatoria, andando a ricircolare attraverso un ultrafiltro HEPA, aria già di per sé trattata. Questa filtrazione ulteriore, se poi unita alla ionizzazione mediante NTP, garantirebbe la presenza di un aria a livelli di purezza estremamente elevati.

La sua capacità di sanificare le superfici contaminate, introdurrebbe inoltre ulteriori elementi di garanzia, contribuendo a migliorare l'igiene ambientale e a ridurre l'insorgenza di eventuali infezioni.

Un ipotetico scenario "tipo" potrebbe così configurarsi:

- Inizio giornata operatoria. Impianto di trattamento aria standard in funzione + sistema di ricircolo su filtro HEPA;
- Intervallo tra un intervento e l'altro. Entrata in funzione del sistema di ionizzazione dell'aria e disinfezione delle superfici;
- Fine giornata. Pulizia profonda della sala operatoria. Spegnimento del sistema di trattamento aria standard. Entrata in funzione del sistema di ionizzazione dell'aria.

In questo modo si avrebbe il vantaggio non irrilevante di trovare al mattino un ambiente pulito e costantemente disinfettato dal trattamento in continuo, oltre a garantire di avere pronta la sala operatoria in minore tempo nel caso di urgenze notturne.

Accanto ai risultati in sala operatoria lo studio ha ben evidenziato che l'impiago di aria NTP, seppur prodotta con dispositivi di dimensioni più ridotte e semplificati, ha apportato indubbi benefici alla qualità ambientale della corsia di degenza sottoposta al trattamento con un raggiungimento di contaminazione aerodispersa assolutamente contenuta, una netta riduzione dei microrganismi presenti sulle superfici con la contestuale scomparsa degli Stafilococchi patogeni. In questo caso si potrebbe ipotizzare di integrare l'attuale sistema di gestione della sanificazione ambientale con l'istallazione di tre CUBE per corsia, lasciandoli in funzione ininterrottamente con un programma minimo che preveda 2 minuti di funzionamento seguiti da 8 minuti di pausa, con la possibilità di aumentare i tempi di funzionamento in casi particolari (ad esempio presenza di particolari soggetti ad aumentato rischio infettivo).

In conclusione l'uso della tecnologia NTP, con la sua capacità dimostrata in sala operatoria e in corsia di ridurre nel tempo la contaminazione microbica aerodispersa e di facilitare le operazione di sanificazione delle superfici, può con ogni probabilità contribuire anche al raggiungimento e mantenimento di migliori condizioni igienico-sanitarie, aiutando il management nella gestione del rischio clinico.

Indicatori per la verifica finale del servizio

INDICATORI DI RISULTATO

Risultato fisico

Abbattimento % dell'eventuale contaminazione microbica presente:

CORSIA

ABBATTIMENTO MEDIO*: 86%

**** valori riferiti alla Carica Batterica totale aerodispersa***

Questo dato riflette quasi esattamente il risultato ottenuto nella sperimentazione in sala operatoria, così come descritto nel Report conclusivo relativo al Servizio 2.1

SALA OPERATORIA

Prima sperimentazione: **100%;** Seconda sperimentazione: **75%**

ABBATTIMENTO MEDIO*: 87,5%

**** valori riferiti alla Carica Batterica totale aerodispersa***

Assieme, quindi, testimoniano come l'effetto del sistema NTP, indipendentemente dalle sue dimensioni e dagli ambienti in cui viene collocato, se correttamente dimensionato per le esigenze contingenti, è in grado di produrre dei risultati perfettamente riproducibili, ad ulteriore garanzia delle sue potenzialità in termini di riduzione del Rischio Clinico relativamente alle Infezioni Ospedaliere.

(1) “Manuale per la formazione degli operatori sanitari - Sicurezza dei pazienti e gestione del rischio clinico” hiip:// www.salute.gov.it/portale/documentazione/p6_2_2_1.jsp?lingua=italiano&id=640

13 ARTICOLI SCIENTIFICI

ALLEGATO 13.1

ARTICOLI SCIENTIFICI SU
SANIFICAZIONE BATTERICA E VIRALE CON NON THERMAL PLASMA

Leipold, M. L. (2004). Evaluation of the roles of reactive species, heat, and UV radiation in the inactivation of bacterial cells by air plasmas at atmospheric pressure. nternational Journal of Mass Spectrometry, 233 (1–3), 81-86.

Ming Zhang, Jun Kyun Oh, Luis Cisneros-Zevallos, Mustafa Akbulut – (2013) Bactericidal effects of nonthermal low-pressure oxygen plasma on S. typhimurium LT2 attached to fresh produce surfaces. Journal of Food Engineering 119 (2013) 425–432

Michael J. Gallagher, A. G. (2004). Non-thermal plasma application in air sterilization. Conference Paper in IEEE International Conference on Plasma Science.

Puligundla Pradeep and Mok Chulkyoon (2016) -Non-thermal plasmas (NTPs) for inactivation of viruses in abiotic environment. Research Journal of Biotechnology. Vol. 11 (6) June (2016)

Cold plasma, a new hope in the field of virus inactivation (2020) - Arijana Filipić, Ion Gutierrez-Aguirre, Gregor Primc, Miran Mozetič, David Dobnik. PII: S0167-7799(20)30108-6, DOI: https://doi.org/10.1016/j.tibtech.2020.04.003, Reference: TIBTEC 1923

Inattivazione del virus della sindrome riproduttiva e respiratoria dei suini (PRRSv) con tecnologia Non Thermal Plasma generato da scarica di barriera dielettrica.

Journal of Food Engineering 119 (2013) 425–432

Contents lists available at SciVerse ScienceDirect

Journal of Food Engineering

journal homepage: www.elsevier.com/locate/jfoodeng

Bactericidal effects of nonthermal low-pressure oxygen plasma on *S. typhimurium* LT2 attached to fresh produce surfaces

Ming Zhang [a], Jun Kyun Oh [b], Luis Cisneros-Zevallos [c,*], Mustafa Akbulut [a,b,*]

[a] Artie McFerrin Department of Chemical Engineering, Materials Science and Engineering Program, Texas A&M University, College Station, TX 77843-3122, United States
[b] Materials Science and Engineering Program, Texas A&M University, College Station, TX 77843-3122, United States
[c] Department of Horticultural Sciences, Texas A&M University, College Station, TX 77843-2133, United States

ARTICLE INFO

Article history:
Received 25 March 2013
Received in revised form 17 May 2013
Accepted 31 May 2013
Available online 19 June 2013

Keywords:
Oxygen plasma
Bactericidal effect
Sanitization
Fresh produce

ABSTRACT

This work investigates the feasibility of nonthermal low-pressure oxygen plasma on sanitization of spinach, lettuce, tomato and potato surfaces from *Salmonella enterica* subsp. enterica serovar Typhimurium str. LT2 (*Salmonella typhimurium* LT2). It was shown that the time of exposure and plasma power density were two critical parameters influencing the bactericidal efficiency. Surface roughness and hydrophobicity did not influence the sanitization of produce. Oxygen plasma was more effective than washing with 3% H_2O_2 on eliminating *S. typhimurium* LT2 on spinach. Plasma treatment chemically changed a very thin section of tomato wax cuticle layer by oxidation reaction and decomposition of carbon chains, which could readily and completely be removed by water. Overall, this study confirms that nonthermal oxygen plasma can be a new effective method of sanitization for fresh produce.

1. Introduction

Fruits and vegetables play an important role in our diet and health by providing essential vitamins, minerals, and fibers. Human pathogens can reach and attach fruit and vegetable surfaces during growth, harvest, transportation and further handling from animal and human sources. Contaminated fruits and vegetables in particular the ones that are consumed raw can lead to foodborne illnesses. In recent years, the number of documented outbreaks of human infections associated with the consumption of contaminated fruits and vegetables has increased (Berger et al., 2010; Van Boxstael et al., 2013).

Typical approaches for the sanitization of pathogenic microorganisms involve the use of heat, pressure, liquid or gas chemical disinfectants, and ionizing or non-ionizing radiation. However, because of their fragile nature, high temperature methods are not suitable for the decontamination of fresh produce. With outbreaks of foodborne illnesses occurring more frequently, the development of novel nonthermal methods to reduce and eliminate bacterial pathogens from fresh produce has received increasing attention (Parish et al., 2003a,b). To this end; X-rays, ultrasound, ultraviolet light, oscillating magnetic fields, pulsed light, and high voltage arc discharge based methods have recently been considered in the context of fresh produce safety (Zhang et al., 2011; Moosekian et al., 2012; Garcia Loredo et al., 2013; Odriozola-Serrano et al., 2013).

Among novel methods of bacterial sanitization, nonthermal plasma-based sanitization approaches has displayed promising outcomes in decontaminating living tissues and biomaterials from various microorganisms (Ragni et al., 2010; Ermolaeva et al., 2011; Noriega et al., 2011). Effectiveness of nonthermal plasma in decontaminating pathogenic bacteria is attributed to a combination of effects including the formation of electrons, ions, free radicals and excited molecules, as well as UV radiation (Moisan et al., 2001; Laroussi and Leipold, 2004; Kong et al., 2009). The key advantages of nonthermal plasma technologies are their relatively simple and inexpensive design, short processing times, absence of toxicity, and lack of residue formation (Rossi et al., 2009; Roth et al., 2010; Rupf et al., 2010). Its effectiveness against pathogenic bacteria and the above mentioned advantages have prompted an interest in the use of the nonthermal plasma-based approaches in food safety. For instance, Deng et al. (2007) has demonstrated the applicability of nonthermal atmospheric plasma technology for the pasteurization of almonds. The technology was found to effectively reduce *Escherichia coli* on almond by almost a 5 log factor after 30-s treatment at 30 kV and 2000 Hz. Ragni et al. (2010) investigated the efficacy of resistive barrier discharge (RBD) plasma for decontamination of shell egg surfaces and

* Corresponding authors. Address: Materials Science and Engineering Program, Texas A&M University, College Station, TX 77843-3122, United States. Tel.: +1 609 964 6174; fax: +1 979 845 6446 (M. Akbulut).
E-mail addresses: lcisnero@tamu.edu (L. Cisneros-Zevallos), makbulut@mail.che.tamu.edu (M. Akbulut).

0260-8774/$ - see front matter © 2013 Elsevier Ltd. All rights reserved.
http://dx.doi.org/10.1016/j.jfoodeng.2013.05.045

observed reductions up to 2.5 log CFU/eggshell and 4.5 log CFU/eggshell for *Salmonella enteritidis* using air with low and high moisture contents, respectively, after 90 min of RBD plasma treatment. Noriega et al. (2011) investigated the efficiency of nonthermal atmospheric gas plasmas for decontaminating chicken skin and muscle inoculated with *Listeria innocua* and observed a 1 log reduction on skin, and a 3 log reductions on muscle under optimal conditions.

The studies on the efficiency of nonthermal plasma on bacteria responsible for foodborne illnesses when they are attached to fresh produce surfaces is very limited. Niemira and Sites (2008) reported the use of cold air plasma to inactivate human pathogens inoculated on golden delicious apples. The reductions of Salmonella Stanley and *E. coli* O157: H7 ranged from 2.9 to 3.7 and 3.4 to 3.6 respectively, after treatment for 3 min at 30 kV and 60 Hz with flow rate of 40 l/min. Fresh produce surfaces may favor bacterial proliferation specially if rich in nutrients (Thunberg et al., 2002; Johnston et al., 2005), through biofilm formation and protection in crevices (i.e. microscale roughnesses and valleys between the asperities of the produce surface) (Burnett and Beuchat 2000; Burnett et al., 2000). Thus, there is a need to correctly assess the feasibility of nonthermal plasma in sanitizing fresh produce surfaces (Niemira, 2012).

In general, non-thermal plasma is generated from either atmospheric pressures or low pressures. Both atmospheric and low pressure plasma generates same species and same electron densities range (Schutze et al., 1998). Therefore, they have similar plasma sanitization mechanics (Moisan et al., 2001; Laroussi, 2005). The main advantage of the atmospheric-pressure plasmas is that they do not require vacuum systems to operate. However, under atmospheric conditions, higher voltages are required to generate plasma. To be specific, the voltage required to initiate the ionization decreases from ~10,000 V to ~100 V if the pressure reduces from atmospheric pressure to 10^{-3} atm for a 1-cm gap between electrode plates (Lieberman and Lichtenberg, 2005). At higher voltages, often arcing occurs between the electrodes. The arcing may damage and burn fragile surfaces such as fresh produce surfaces. Considering that the low pressure vacuum packaging has been used for packaging of many fresh produces (An et al., 2009) and the abovementioned points, the use of low-pressure plasma sanitization instead of atmospheric-pressure one has certain advantages.

Accordingly, this paper investigated the bactericidal effect of nonthermal low-pressure oxygen plasma on *Salmonella enterica* subsp. enterica serovar Typhimurium LT2 (*S. typhimurium* LT2) attached on fresh lettuce, spinach, tomato, and potato surfaces. This microorganism was selected because data from the US-CDC foodborne outbreak surveillance system show that the most commonly reported microorganisms associated with fresh produce foodborne illness outbreaks are *Salmonella* spp. (Sivapalasingam et al., 2004). Oxygen was selected as the gas source because oxygen was found to be one of the best sanitization agents (Bol'shakov et al., 2004). Furthermore, four possible combinations of surface roughness and hydrophilicity including hydrophobic smooth, hydrophobic rough, hydrophilic smooth, and hydrophilic rough surfaces were covered through the selected produce. This is possible since spinach and potato are relatively rough, while tomato and lettuce are relatively smooth, and spinach and tomato are relatively hydrophobic, while lettuce and potato are relatively hydrophilic. These properties can influence sanitization efficacy in some sanitization methods, especially liquid based methods (Ukuku and Fett, 2006; Fransisca and Feng, 2012). In the present study, the efficiency of a nonthermal oxygen plasma method was compared with that of washing with aqueous solutions of H_2O_2. Associated physicochemical changes upon the plasma treatment were also reported.

2. Materials and methods

2.1. Preparation of produce surface

Spinach, lettuce, tomato and potato were purchased from a local grocery store (Wal-Mart, College Station, TX, USA). After mildly washed for 30 s using 1 L of deionized water, the produce was dried using tissue paper. Then, spinach, lettuce, tomato skin and potato skin were cut into square pieces of 1 cm × 1 cm. The produce pieces were immobilized on a silica wafer using a double sided adhesive carbon tape.

2.2. Preparation of inoculum

Rifampicin-resistant *S. enterica* subsp. enterica serovar Typhimurium str. LT2 (*S. typhimurium* LT2; ATCC 700720) was obtained from the ATCC (Manassas, VA, USA) and maintained on slants of tryptic soy agar (TSA; Becton, Dickinson and Co., Sparks, MD, USA) at 5 °C. Working cultures were obtained by transferring a loop of culture from TSA slants to 9.0 mL of tryptic soy broth (TSB; Becton, Dickinson and Co.) and incubating aerobically without agitation at 37.5 °C for 24 h. After 24 h, a loop of culture was transferred to a fresh 9 mL of TSB and incubated aerobically without agitation at 37.5 °C for 24 h. After incubation, the culture was transferred to a 15 mL conical centrifuge tube (Thermo-Fisher Scientific, Inc.). Bacterial cells were collected by centrifugation at 2191 × g in a Jouan B4i centrifuge (Thermo-Fisher Scientific, Inc.) for 15 min at 22 °C. The resulting pellet was suspended in 9.0 mL of Milli Q (MQ) water and washed by centrifugation for 15 min at 22 °C; the entire centrifugation and washing procedure was repeated identically three times. After the final cycle, the pellet was suspended in 9.0 mL MQ water and used immediately in the inoculation experiments. This resulted in an inoculum concentration of $8 \pm 0.4 \times 10^{10}$ CFU/ml, and determined via selective plating on TSA. Survivors were enumerated following 24 h aerobic incubation at 37.5 °C.

2.3. Nonthermal oxygen plasma treatment

Plasma treatment experiments were performed by March CS-1701 Reactive Ion Etching system (March Plasma Systems, Inc., CA, USA). The system consists of four modules: a reaction chamber/process controller, a solid state radio frequency (RF) power generator, a vacuum pump and an oxygen source (Fig. 1A). By applying a strong RF electromagnetic field to the wafer

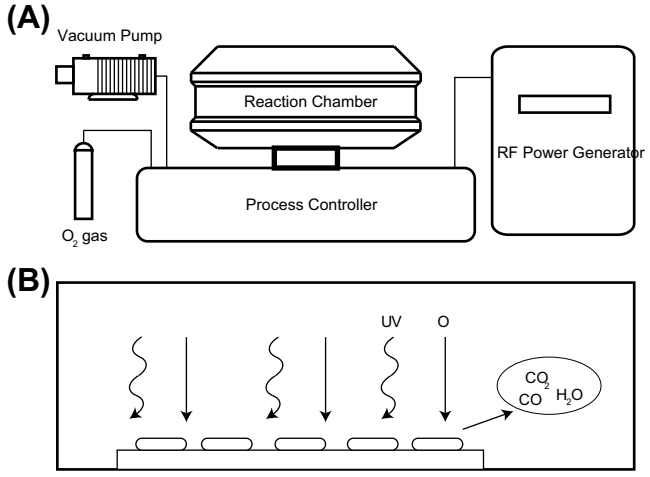

Fig. 1. Schematic illustration of (A) oxygen plasma system, and (B) plasma sanitization in reaction chamber.

platter, plasma is initiated in the system using oxygen gas. The system runs at an RF frequency of 13.56 MHz with a maximum power output of 600 W. The chamber is 15 cm in interior diameter with 2.5 cm spacing between electrodes. When the gas in the chamber is exposed to the oscillating electric field at high frequency and energy, the electrons of the gas start to gain energy, eventually ionizing to atoms. The initial ionization will provide more energy to the system to cause further ionizations in a chain reaction manner, ultimately filling the chamber with plasma, which could react with the treated surface (Fig. 1B). The RF power applied and pressure of the chamber are two main parameters influencing the density and temperature of the plasma (Chen and Chang, 2003). In the present study, we investigated the effect of plasma power and exposure time on the bactericidal properties of the oxygen plasma. To ensure the reproducibility of the results, each experiment was repeated at least three times.

Plasma chemistry of pure oxygen RF plasma has been well identified. Mogul et al. (2003) studied emission spectrum for pure O_2 plasma discharge powered by a 13.56 MHz radio frequency at 100 W and 500 mTorr (67 Pa). They found the presence of excited atomic oxygen, oxygen cation, dioxygen cation, and neutral excited dioxygen in plasma. Bol'shakov et al. (2004) also found the similar results when they studied oxygen plasma generated at 13.56 MHz in the range of 13–67 Pa and pressure and 100–300 W power. These emission spectrum results were also consistent with the previously published oxygen spectra of oxygen plasmas (Carl et al., 1990; Tuszewski et al., 1995). Since the plasma in this paper was generated under similar experiment conditions (13.56 MHz, 34 Pa, 50–350 W), species in plasma in this paper is expected to consist of excited atomic oxygen, oxygen cation, dioxygen cation, and neutral excited dioxygen as well.

2.4. Inoculation of produce surfaces

The experimental protocol for the inoculation of produce surfaces used in plasma treatment studies was as follows: Initially, 100 μl of bacterial inoculum at $8 \pm 0.4 \times 10^{10}$ CFU/ml was added dropwise and distributed evenly onto produce surfaces (1 cm × 1 cm pieces) and the produce surfaces were air-dried at room temperature for ~4 h. After the inoculated surface was placed in the chamber, the chamber was first evacuated at 13 Pa, and then the chamber was filled with O_2 to 30 Pa with a gas flow rate of 10 sccm. After the plasma treatment at room temperature, the chamber was ventilated with air to reach atmospheric pressure. To compare the efficacy of plasma sanitization with that of H_2O_2 washing, some of inoculated surfaces (spinach) were rinsed in 3% H_2O_2 solution for 600 s instead of the plasma treated. Both of the treated produce surfaces were then used for bacterial counting.

2.5. Enumeration of inoculum organisms

The numbers of *S. typhimurium* LT2 cells on the produce surfaces were measured for each exposure time and power density of plasma treatment. Once the treated surfaces were removed from the plasma chamber, these were put in 9 ml test tubes of 0.1% of peptone water. The tubes were shaken on a Mini Shaker (VWR International, LLC) at 900 rpm for 10 min. Serial dilutions of the suspension were made and plated on TSA supplemented with 80 μg/ml rifampicin. Survivors were enumerated following 24 h aerobic incubation at 37.5 °C.

2.6. Water contact angle measurement

The relative hydrophobicity of produce surface was evaluated using water contact angle measurements. One drop of Milli-Q water was placed on a produce surface and allowed to equilibrate for 30 s before making any measurements. A digital camera was used to take the images for angle measurement. For each specimen, at least three contact angle measurements were conducted.

2.7. Scanning electron microscopy (SEM)

SEM (JSM-7500F, JEOL, Peabody, MA, USA) was used for three purposes in this study: to determine morphology (roughness) of the neat produce surfaces; to characterize the physical changes on the produce surface due to oxygen plasma treatment; and to compare the bacterial attachment behavior of the produce surfaces. To study the effect of surface property on bacteria adhesion, produce surfaces rinsed into *S. typhimurium* LT2 solution for 5 min and then dry in a hood at room temperature for overnight. SEM images were obtained from there with or without the above treatment. Prior to the SEM studies, the samples were coated with

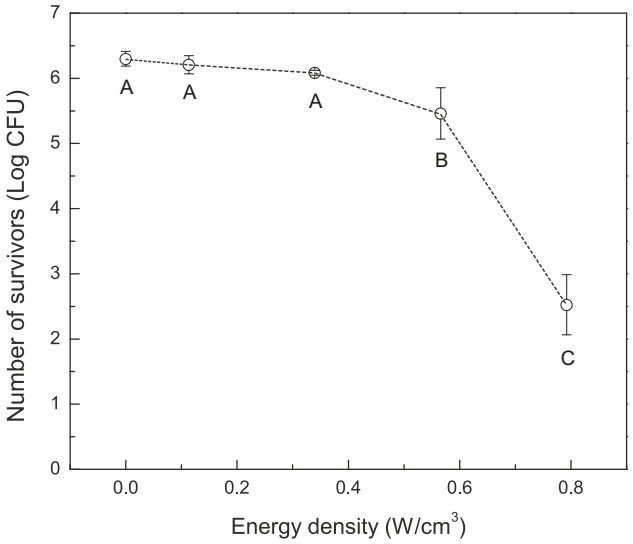

Fig. 2. Survival curve of *S. typhimurium* LT2 on spinach after plasma treatment for 100 s as a function of plasma power density. Treatments with same letters are not significantly different based on Tukey's test ($p \leqslant 0.05$).

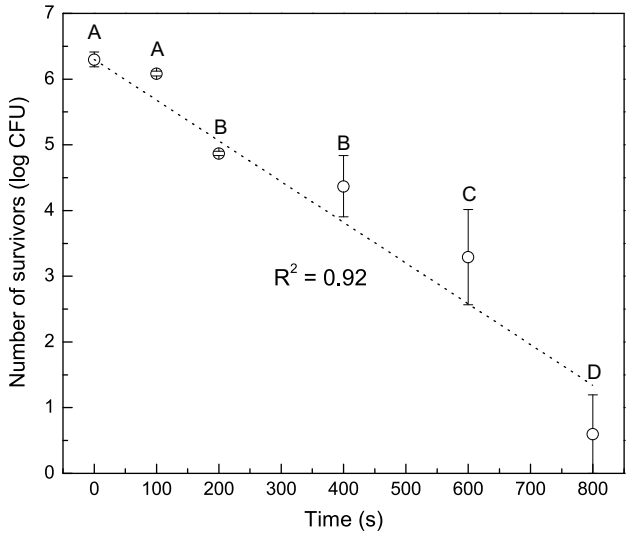

Fig. 3. Survival curve of *S. typhimurium* LT2 on spinach after plasma treatment at 0.34 W/cm^3 for different times of exposures. Treatments with same letters are not significantly different based on Tukey's test ($p \leqslant 0.05$).

a 50-nm layer of Au by sputter coater (Cressington 105HR, Cressington, England) to ensure electrical conductivity.

2.8. Nuclear magnetic resonance (NMR)

Proton nuclear magnetic resonance (H NMR) was used to investigate chemical changes induced by oxygen plasma treatment. Tomato skin with and without exposure to the oxygen plasma was placed in deuterated chloroform ($CDCl_3$) and sonication for 5 min to dissolve non-polar compounds and in deuterated water (D_2O) to dissolve polar ones. The extracted compounds were transferred into 5 mm NMR tubes and analyzed using a Bruker 400 MHz NMR spectrometer (Bruker, Billerica, MA, USA) at 298 K.

2.9. Statistical analysis

All experiments were replicated at least three times. Numbers of survival bacteria were converted to log CFU and means and

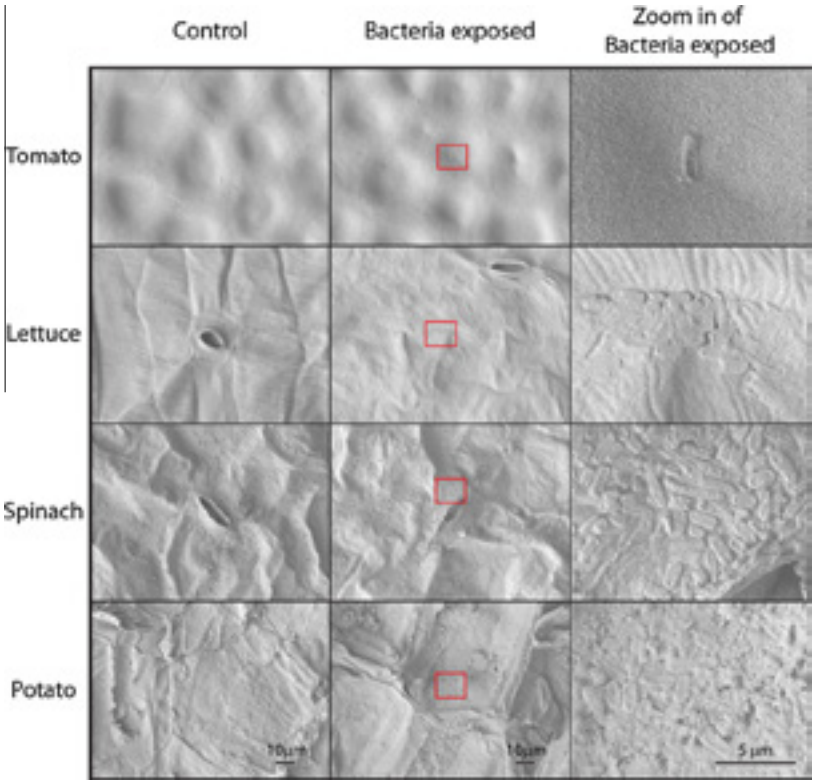

Fig. 4. SEM micrographs of four produce surfaces with or without exposing to bacteria dispersion for 5 min. Red rectangles indicates the areas from which higher magnification images were obtained. (For interpretation of the references to color in this figure legend, the reader is referred to the web version of this article.)

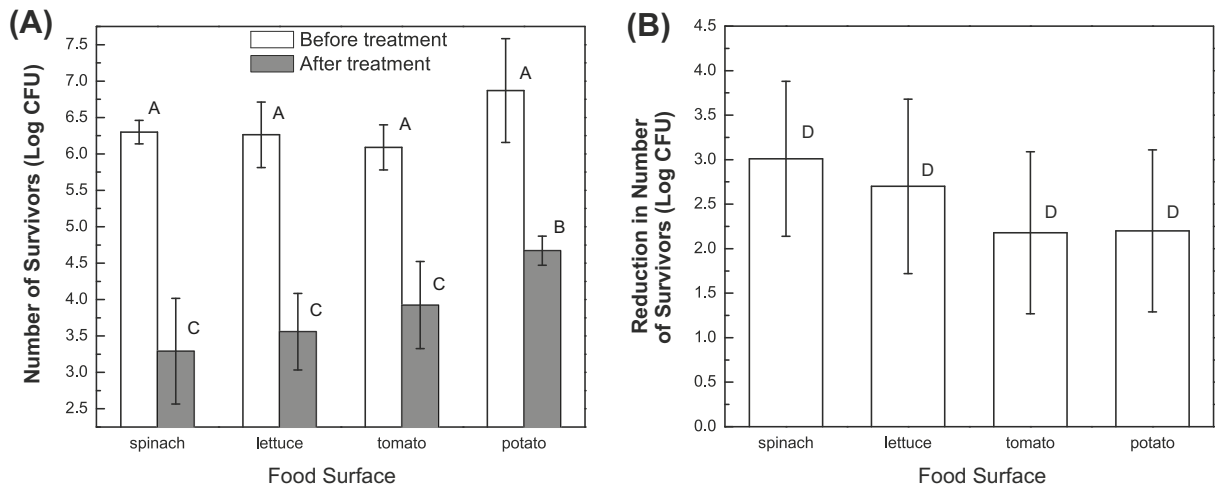

Fig. 5. (A) Number of surviving *S. typhimurium* LT2 on different produce surfaces before and after plasma treatment of 600 s at 0.34 W/cm^3. (B) Corresponding Log reductions in number of surviving *S. typhimurium* LT2 on different food surfaces. Treatments with same letters are not significantly different based on Tukey's test ($p \leqslant 0.05$).

standard deviations were calculated. Analyses of variance were conducted using JMP (SAS Cary, NC, USA) and mean separation tests performed using a post hoc Tukey's test ($p < 0.05$).

3. Results and discussion

3.1. Effect of plasma energy density on bactericidal efficiency

Fig. 2 shows the number of surviving *S. typhimurium* LT2 on spinach surface as a function of actual power output of radio frequency (RF) per unit volume of the reaction chamber (power density) of plasma for a given time ($t = 100$ s). The number of survivors decreased with increasing power density in a nonlinear manner: At low power densities the bactericidal effect increased weakly while at large power densities the bactericidal effect increased strongly ($p < 0.05$). Given higher plasma energy densities give rise to higher intensities of UV irradiation, UV photons, and reactive species such as O, O^*, and O_2^* (Laroussi and Leipold, 2004; Wu et al., 2012), it is reasonable that bactericidal effect increased with increase power density. No visual damage was observed for power densities up to 0.57 W/cm^3. However, the spinach surface showed some signs of etching at a power density of 0.79 W/cm^3 and an exposure time of 100 s. Thus, although higher energy densities can allow better sanitization, care must be taken to prevent damage on the produce surface.

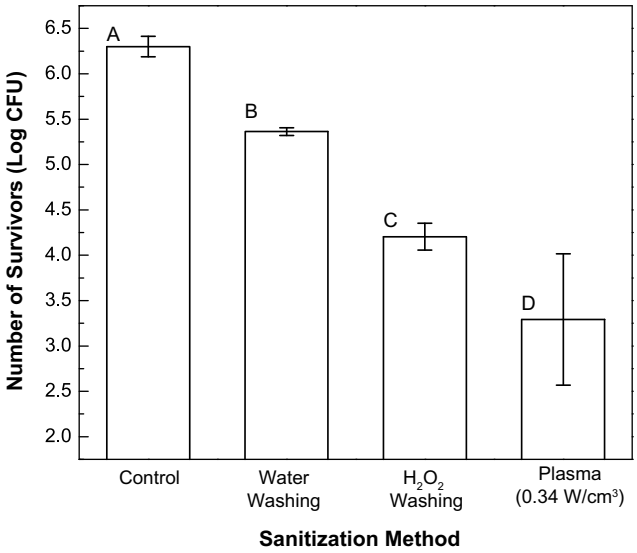

Fig. 6. Number of surviving *S. typhimurium* LT2 for different sanitization methods on spinach surface. Duration of each treatment method was kept constant, i.e. an exposure time of 600 s. Treatments with different letters were significantly different based on Tukey's test ($p \leqslant 0.05$).

3.2. Effect of plasma exposure time on bactericidal efficiency

Fig. 3 shows number of *S. typhimurium* LT2 on spinach surface as a function of time of plasma exposure at a power density of 0.34 W/cm^3 (output power of 150 W). The logarithmic number of surviving bacteria before the exposure ($t = 0$) was 6.3 ± 0.1. The complete sanitization was achieved at 800 s (≤1 log CFU). No visible side effect was observed on the spinach after a plasma treatment of 800 s at 0.34 W/cm^3.The logarithmic numbers of viable bacteria decreased linearly with increasing plasma exposure time. This finding implies the number of surviving microorganisms decreased, as an exponential function of time. This trend is consistent with other plasma sanitization studies involving other types of surfaces (Herrmann et al., 1999; Moisan et al., 2002). The half-life of the bacteria killing reaction is about 48 s at a power density of 0.34 W/cm^3. Accordingly, an exposure time of 317 s decreases the total number of surviving *S. typhimurium* LT2 to 1.0%, and an exposure time of 635 s decreases to 0.01%.

3.3. Effect of food surface on bactericidal efficiency

Tomato, lettuce, spinach, and potato were selected due to their different surface properties. The water contact angles are 107 ± 6 for tomato, 81 ± 7 for spinach, 57 ± 4 for lettuce, and <30 for potato. SEM micrographs showed that tomato and lettuce were relatively smooth while spinach and potato were relatively rough (Fig. 4). Rough and hydrophilic surface (potato) favored for bacteria adhesion, while smooth and hydrophobic surface (tomato) hindered bacterial adhesion (Fig. 4). This behavior is consistent with the previous studies also showing that these surface properties

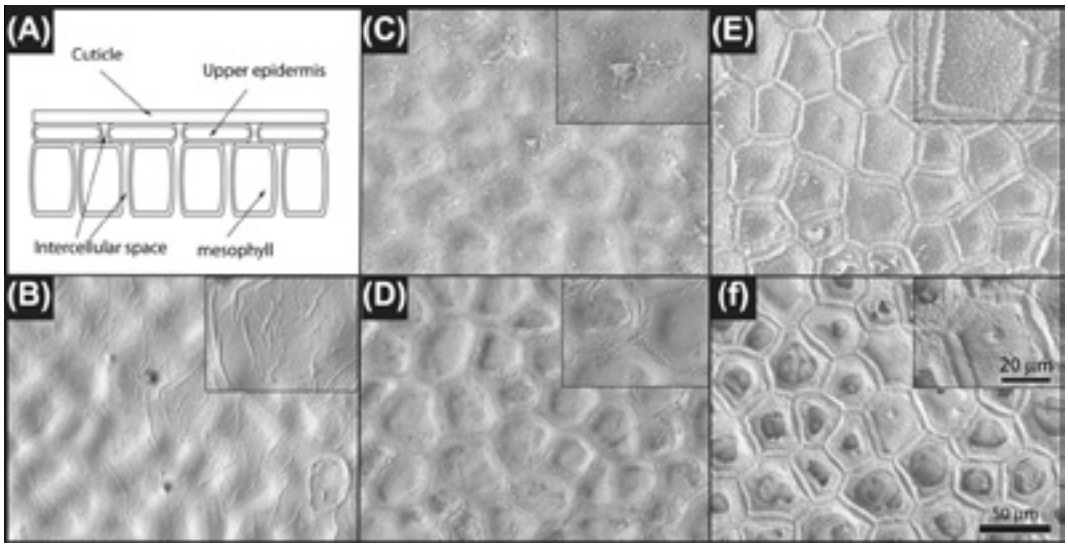

Fig. 7. An illustration of tomato surface (A); SEM images of tomato before plasma treatment (B); after plasma treated for 100 s (C) and then rinsing in MQ water (D); after plasma treated for 600 s (E) and then rinsing in MQ water (F).

(roughness and hydrophobicity) can influence bacterial adhesion (Bruinsma et al., 2001; Wang et al., 2009).

To better understand the effect of produce surface properties on the efficiency of plasma sanitization, we conducted plasma sanitization experiments using four different produce surfaces: tomato (smooth hydrophobic), lettuce (smooth hydrophilic), spinach (rough hydrophobic), and potato (rough hydrophilic). The number of viable bacteria after drying and after plasma treatment for 600 s at 0.34 W/cm^3 is shown in Fig. 5A. Initial viable bacteria were the same for all surfaces ($p < 0.05$); and after treatments, all surfaces showed lower bacteria counts, still the same for all surfaces ($p < 0.05$) with exception of a slight higher value for potatoes. However, when reporting reductions in numbers of the viable bacteria, these were 3.0 ± 0.9, 2.7 ± 1.0, 2.2 ± 0.9 and 2.2 ± 0.9 for spinach, lettuce, tomato and potato, respectively with no significant difference among them ($p < 0.05$). Accordingly, we confirm that surface properties of roughness and hydrophobicity have no impact on oxygen plasma sanitization. Upon 600 s plasma treatment at 0.34 W/cm^3, no visible damage was observed for all produce surfaces.

3.4. Comparison to hydrogen peroxide washing

Hydrogen peroxide treatment is one of the most common sanitization methods for vegetable and fruit surfaces (Parish et al. 2003a,b; Ukuku and Fett, 2006). Therefore, we compared the efficiencies of the nonthermal oxygen plasma treatment method with a hydrogen peroxide treatment and water washing using spinach surface (Fig. 6). Duration of each treatment method was kept constant, i.e. an exposure time of 600 s. The logarithmic number of surviving bacteria decreased from 6.3 ± 0.1 to 5.4 ± 0.1 after water washing. The survival number decreased to 4.2 ± 0.1 upon a 600 s exposure to 3% H_2O_2 while the number further decreased to 3.4 ± 0.4 for the case of 600 s plasma treatment at 0.34 W/cm^3.

When surface characteristics such as roughness and hydrophobicity promote the formation of a physical barrier for aqueous media penetration, the effectiveness of H_2O_2 treatment decreases (Ukuku and Fett, 2006; Fransisca and Feng, 2012). We hypothesize that the barrier is due to micro-air pockets which protect the microorganisms from the sanitizer. On the other hand, the length scale (~angstrom) of gas reactive species is much smaller than the length scale of surface roughness of produce surfaces (several micrometers). Therefore, the crevices and micro-air pockets do not hinder the plasma sanitization. The difference in the efficiency of plasma and peroxide treatment is attributed to this phenomenon.

3.5. Physical changes occurring on produce surfaces after plasma treatment

SEM was used to study the physical changes occurring on produce due to the nonthermal oxygen plasma treatment (Fig. 7). Typical produce surfaces like tomato cuticle are covered by a wax layer followed by a layer of cutin or cutin blends of wax and cell wall substances such as carbohydrates. Bellow the cuticle are the epidermis and mesophyll cells (Fig. 7A). As observed in Fig. 7B, tomato surfaces exhibited regular ridge-and-valley structures. Because the outermost layer is covered with cuticle, it was not possible to directly visualize the upper epidermis. Upon an exposure of 100 s to oxygen plasma at 0.34 W/cm^3 (output power of 150 W), the surface roughness increased slightly and very small amount of debris was observed on the surfaces (Fig. 7C). After rinsing with water, the debris was almost completely removed and intercellular spaces became slightly more apparent (Fig. 7D). There was no sign of damage in epidermis at this point.

Upon an exposure of 600 s to oxygen plasma at 0.34 W/cm^3, intercellular space could be observed through the translucent cuticle layer, indicating removal of the wax cuticle layer (Fig. 7E). In addition, the surface became roughness. When water rinsing follow the plasma treatment, the epidermal cells seem to be damaged, indicating a possible partial removal of the cuticle layer with an exposure of 600 s to oxygen plasma at 0.34 W/cm^3 (Fig. 7F) The damage was more evident after water washing, since the plasma treatment may convert hydrophobic groups from wax to small molecule weight hydrophilic forms and water can dissolve and etch away the hydrophilic groups easier.

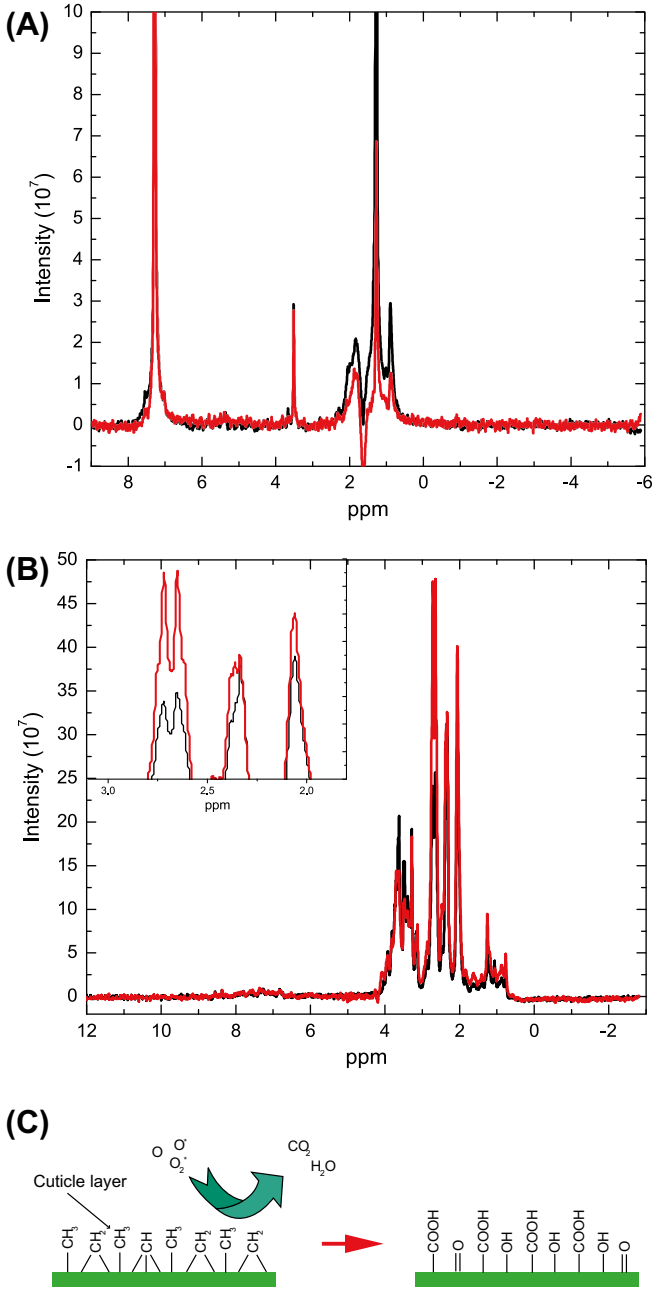

Fig. 8. (A) ^{1}H-NMR spectrum of solution obtained through extraction of tomato skin in CDCl3; (B) ^{1}H-NMR spectrum of solution obtained through extraction of tomato skin in D2O. Black lines indicate "before plasma treatment", and red lines indicate "after the plasma treatment"; and (C) An illustration of potential chemical changes taking place on produce surface upon oxygen plasma treatment. (For interpretation of the references to color in this figure legend, the reader is referred to the web version of this article.)

In general, SEM studies suggest that short exposure times have no major effects on the produce surface while long exposure times may partially damage the cuticle layer and epidermis cells. Depending on the produce type, the removal of the cuticle layer may reduce the storage and shelf life of produce (Kissinger et al., 2005; Saladie et al., 2007). However, given that coating of produce surfaces with edible wax or other coatings is becoming widespread (Park, 1999; Dávila-Aviña et al., 2012), if necessary, the removed cuticle layer can be substituted with an edible wax layer. In essence, the time and power density of nonthermal plasma treatment needs to be optimized for each produce surface to ensure an acceptable level of cuticle/upper epidermis removal and bacterial sanitization.

3.6. Chemical changes occurring on produce surfaces after plasma treatment

To characterize such chemical changes taking place on produce surface upon nonthermal oxygen plasma treatment (e.g., tomato surface, 100 s, 0.34 W/cm^3), we relied on NMR. NMR spectra obtained using $CDCl_3$ extraction indicated that the signal intensity of proton at ~1–2 ppm, which is presumably due to R-CH_2CH_3, R-$CH(CH3)_2$, or R-$C(CH3)_3$ groups, decreased after the plasma treatment (Fig. 8A). NMR spectra obtained using D_2O extraction showed that the signal intensity of proton at ~2–3 ppm, which is presumably due to R-CO-CH_3, R-CO-CH_2CH_3 or R-CH_2COOH groups, increased after plasma treatment (Fig. 8B). These findings are consistent with previous studies focusing on the chemical effects of oxygen plasma on mineral oils (Korzec et al., 1994; Jing et al., 2005), polymers (Hillborg et al., 2000; Calvimontes et al., 2011) and other organic materials (Li and Horita, 2000). Accordingly, NMR results suggest that when tomato surfaces are treated by nonthermal oxygen plasma, the wax cuticle layer can be oxidized to form aldehyde and carboxylic acid groups and/or further oxidized (decomposition of carbon chains) to CO_2 and H_2O, which would be removed from the tomato surface (Fig. 8c).

4. Conclusion

In the present study, we have investigated the efficiency of nonthermal low-pressure oxygen plasma treatment on sanitization of fresh produce surfaces and the associated physicochemical changes taking place on surface cuticle layers. It was shown that the time of exposure and plasma power density were two critical parameters influencing the bactericidal efficiency of nonthermal oxygen plasma treatment. The half-life of the oxygen plasma killing reaction of *S. typhimurium* LT2 was about 48 s at power density of 0.34 W/cm^3. The sanitization method worked equally well for rough hydrophobic (spinach), rough hydrophilic (lettuce), smooth hydrophobic (tomato) and smooth hydrophilic (potato) produce. For a given time, the bactericidal efficacy of nonthermal oxygen plasma was found to be 1 order of magnitude better than that of 3% H_2O_2 treatment for *S. typhimurium* LT2 on spinach surface. It was also shown that oxygen plasma treatment (0.34 W/cm^3) only affects the wax cuticle layer under conditions of short- to intermediate-exposure times. However for long exposure times, wax cuticle layer and upper epidermis cells may be damaged. Oxygen plasma changed the wax surface chemistry through oxidation reactions forming aldehyde and carboxylic acid, and by decomposition of carbon chains. Water rinsing could easily remove these residues from the produce surface. Overall, the nonthermal oxygen plasma treatment shows a potential for the efficient sanitization of fresh produce surfaces.

Acknowledgement

This project was supported by Agriculture and Food Research Initiative Competitive Grant No. 2011-67017-30028 from the USDA National Institute of Food and Agriculture.

References

An, D.S., Park, E., et al., 2009. Effect of hypobaric packaging on respiration and quality of strawberry and curled lettuce. Postharvest Biology and Technology 52 (1), 78–83.
Berger, C.N., Sodha, S.V., et al., 2010. Fresh fruit and vegetables as vehicles for the transmission of human pathogens. Environmental Microbiology 12 (9), 2385–2397.
Bol'shakov, A.A., Cruden, B.A., et al., 2004. Radio-frequency oxygen plasma as a sterilization source. Aiaa Journal 42 (4), 823–832.
Bruinsma, G.M., van der Mei, H.C., et al., 2001. Bacterial adhesion to surface hydrophilic and hydrophobic contact lenses. Biomaterials 22 (24), 3217–3224.
Burnett, S.L., Beuchat, L.R., 2000. Human pathogens associated with raw produce and unpasteurized juices, and difficulties in decontamination. Journal of Industrial Microbiology & Biotechnology 25 (6), 281–287.
Burnett, S.L., Chen, J.R., et al., 2000. Attachment of *Escherichia coli* O157: H7 to the surfaces and internal structures of apples as detected by confocal scanning laser microscopy. Applied and Environmental Microbiology 66 (11), 4679–4687.
Calvimontes, A., Mauersberger, P., et al., 2011. Effects of oxygen plasma on cellulose surface. Cellulose 18 (3), 803–809.
Carl, D.A., Hess, D.W., et al., 1990. Oxidation of silicon in an electron cyclotron resonance oxygen plasma: kinetics, physicochemical, and electrical properties. Journal of Vacuum Science & Technology A: Vacuum, Surfaces, and Films 8 (3), 2924–2930.
Chen, F.F., Chang, J.P., 2003. Lecture Notes on Principles of Plasma Processing. Kluwer Academic/Plenum Publishers, New York.
Dávila-Aviña, J., Villa-Rodríguez, J., et al., 2012. Effect of edible coatings on bioactive compounds and antioxidant capacity of tomatoes at different maturity stages. Journal of Food Science and Technology, 1–7.
Deng, S., Ruan, R., et al., 2007. Inactivation of *Escherichia coli* on almonds using nonthermal plasma. Journal of Food Science 72 (2), M62–M66.
Ermolaeva, S.A., Varfolomeev, A.F., et al., 2011. Bactericidal effects of non-thermal argon plasma in vitro, in biofilms and in the animal model of infected wounds. Journal of Medical Microbiology 60 (1), 75–83.
Fransisca, L., Feng, H., 2012. Effect of surface roughness on inactivation of *Escherichia coli* O157:H7 87-23 by new organic-acid surfactant combinations on alfalfa, broccoli, and radish seeds. Journal of Food Protection 75 (2), 261–269.
Garcia Loredo, A.B., Guerrero, S.N., et al., 2013. Impact of combined ascorbic acid/$CaCl_2$, hydrogen peroxide and ultraviolet light treatments on structure, rheological properties and texture of fresh-cut pear (William var.). Journal of Food Engineering 114 (2), 164–173.
Herrmann, H.W., Henins, I., et al., 1999. Decontamination of chemical and biological warfare, (CBW) agents using an atmospheric pressure plasma jet (APPJ). Physics of Plasmas 6 (5), 2284–2289.
Hillborg, H., Ankner, J.F., et al., 2000. Crosslinked polydimethylsiloxane exposed to oxygen plasma studied by neutron reflectometry and other surface specific techniques. Polymer 41 (18), 6851–6863.
Jing, G.S., Eluru, H.B., et al., 2005. Paraffin surfaces for culture-based detection of mycobacteria in environmental samples. Journal of Micromechanics and Microengineering 15 (2), 270–276.
Johnston, L.M., Jaykus, L.A., et al., 2005. A field study of the microbiological quality of fresh produce. Journal of Food Protection 68 (9), 1840–1847.
Kissinger, M., Tuvia-Alkalai, S., et al., 2005. Characterization of physiological and biochemical factors associated with postharvest water loss in ripe pepper fruit during storage. Journal of the American Society for Horticultural Science 130 (5), 735–741.
Kong, M.G., Kroesen, G., et al., 2009. Plasma medicine: an introductory review. New Journal of Physics 11.
Korzec, D., Rapp, J., et al., 1994. Cleaning of metal parts in oxygen radio-frequency plasma – process study. Journal of Vacuum Science & Technology A: Vacuum Surfaces and Films 12 (2), 369–378.
Laroussi, M., 2005. Low temperature plasma-based sterilization: overview and state-of-the-art. Plasma Processes and Polymers 2 (5), 391–400.
Laroussi, M., Leipold, F., 2004. Evaluation of the roles of reactive species, heat, and UV radiation in the inactivation of bacterial cells by air plasmas at atmospheric pressure. International Journal of Mass Spectrometry 233 (1–3), 81–86.
Li, X., Horita, K., 2000. Electrochemical characterization of carbon black subjected to RF oxygen plasma. Carbon 38 (1), 133–138.
Lieberman, M.A., Lichtenberg, A.J., 2005. Principles of plasma discharges and materials processing. Wiley-Interscience, Hoboken, NJ.
Mogul, R., Bolapos, et al., 2003. Impact of low-temperature plasmas on deinococcusradiodurans and biomolecules. Biotechnology Progress 19 (3), 776–783.
Moisan, M., Barbeau, J., et al., 2001. Low-temperature sterilization using gas plasmas: a review of the experiments and an analysis of the inactivation mechanisms. International Journal of Pharmaceutics 226 (1–2), 1–21.
Moisan, M., Barbeau, J., et al., 2002. Plasma sterilization. Methods mechanisms. Pure and Applied Chemistry 74 (3), 349–358.

Moosekian, S.R., Jeong, S., et al., 2012. X-ray irradiation as a microbial intervention strategy for food. Annual Review of Food Science and Technology 3, 493–510.
Niemira, B.A., 2012. Cold plasma decontamination of foods. Annual Review of Food Science and Technology 3 (3), 125–142.
Niemira, B.A., Sites, J., 2008. Cold plasma inactivates salmonella stanley and *Escherichia coli* O157:H7 inoculated on golden delicious apples. Journal of Food Protection 71 (7), 1357–1365.
Noriega, E., Shama, G., et al., 2011. Cold atmospheric gas plasma disinfection of chicken meat and chicken skin contaminated with *Listeria innocua*. Food Microbiology 28 (7), 1293–1300.
Odriozola-Serrano, I., Aguiló-Aguayo, I., et al., 2013. Pulsed electric fields processing effects on quality and health-related constituents of plant-based foods. Trends in Food Science & Technology 29 (2), 98–107.
Parish, M., Beuchat, L., et al., 2003a. Methods to reduce/eliminate pathogens from fresh and fresh-cut produce. Comprehensive Reviews in Food Science and Food Safety 2, 161–173.
Parish, M.E., Beuchat, L.R., Suslow, T.V., Harris, L.J., Garrett, E.H., Farber, J.N., Busta, F.F., 2003b. Methods to reduce/eliminate pathogens from produce and fresh-cut produce. Comprehensive Reviews in Food Science and Food Safety 2 (Suppl. s1), 161–173.
Park, H.J., 1999. Development of advanced edible coatings for fruits. Trends in Food Science & Technology 10 (8), 254–260.
Ragni, L., Berardinelli, A., et al., 2010. Non-thermal atmospheric gas plasma device for surface decontamination of shell eggs. Journal of Food Engineering 100 (1), 125–132.
Rossi, F., Kylian, O., et al., 2009. Low pressure plasma discharges for the sterilization and decontamination of surfaces. New Journal of Physics 11.
Roth, S., Feichtinger, J., et al., 2010. Characterization of bacillus subtilis spore inactivation in low-pressure, low-temperature gas plasma sterilization processes. Journal of Applied Microbiology 108 (2), 521–531.
Rupf, S., Lehmann, A., et al., 2010. Killing of adherent oral microbes by a non-thermal atmospheric plasma jet. Journal of Medical Microbiology 59 (2), 206–212.
Saladie, M., Matas, A.J., et al., 2007. A reevaluation of the key factors that influence tomato fruit softening and integrity. Plant Physiology 144 (2), 1012–1028.
Schutze, A., Jeong, J.Y., et al., 1998. The atmospheric-pressure plasma jet: a review and comparison to other plasma sources. IEEE Transactions on Plasma Science 26 (6), 1685–1694.
Sivapalasingam, S., Friedman, C.R., et al., 2004. Fresh produce: a growing cause of outbreaks of foodborne illness in the United States, 1973–1997. Journal of Food Protection 67 (10), 2342–2353.
Thunberg, R.L., Tran, T.T., et al., 2002. Microbial evaluation of selected fresh produce obtained at retail markets. Journal of Food Protection 65 (4), 677–682.
Tuszewski, M., Scheuer, J.T., et al., 1995. Composition of the oxygen plasmas from two inductively coupled sources. Journal of Vacuum Science & Technology A: Vacuum, Surfaces, and Films 13 (3), 839–842.
Ukuku, D.O., Fett, W.F., 2006. Effects of cell surface charge and hydrophobicity on attachment of 16 Salmonella serovars to cantaloupe rind and decontamination with sanitizers. Journal of Food Protection 69 (8), 1835–1843.
Van Boxstael, S., Habib, I., et al., 2013. Food safety issues in fresh produce: bacterial pathogens, viruses and pesticide residues indicated as major concerns by stakeholders in the fresh produce chain. Food Control 32 (1), 190–197.
Wang, H., Feng, H., et al., 2009. Effect of surface roughness on retention and removal of *Escherichia coli* O157:H7 on surfaces of selected fruits. Journal of Food Science 74 (1), E8–E15.
Wu, H., Sun, P., et al., 2012. Reactive oxygen species in a non-thermal plasma microjet and water system: generation, conversion, and contributions to bacteria inactivation—an analysis by electron spin resonance spectroscopy. Plasma Processes and Polymers 9 (4), 417–424.
Zhang, H.Q., Barbosa-Cánovas, G.V., et al., 2011. Nonthermal Processing Technologies for Food. Ames, Iowa, Wiley-Blackwell/IFT Press, Chichester, West Sussex, UK.

Available online at www.sciencedirect.com
SCIENCE DIRECT®
International Journal of Mass Spectrometry 233 (2004) 81–86
Mass Spectrometry

Evaluation of the roles of reactive species, heat, and UV radiation in the inactivation of bacterial cells by air plasmas at atmospheric pressure

M. Laroussi*, F. Leipold

Department of Electrical and Computer Engineering, Old Dominion University, 231 Kaufman Hall, Norfolk, VA 23529, USA

Received 2 October 2003; accepted 13 November 2003

Abstract

Recently, non-equilibrium, atmospheric pressure air plasmas have been shown to possess excellent germicidal properties. A number of studies have shown that air plasmas are capable of inactivating a wide range of microorganisms in the matter of few seconds to few minutes. However, until now little information regarding quantitative measurements of the various plasma agents that can potentially participate in the inactivation process has been published. In this paper, emission spectroscopy and gas detection are used to evaluate important plasma inactivation factors such as UV radiation and reactive species. Our measurements show that for non-equilibrium, atmospheric pressure air plasmas, it is the oxygen-based and nitrogen-based reactive species that play the most important role in the inactivation process.

Keywords: Microorganism; Air plasma; Discharge; Reactive species; Sterilization

1. Inroduction

The inactivation of harmful microorganisms such as bacteria can be achieved by chemical and/or physical means, such as heat, chemical solutions and gases, and radiation [1]. Most conventional sterilization techniques are associated with some level of damage to the material or medium supporting the microorganisms. This does not present a problem in cases where material preservation is not an issue. However, in cases where it is imperative not to damage the materials to be sterilized, conventional methods are either not suitable at all or offer very impractical and/or tedious and time consuming solutions. This situation led to the development of new techniques that are at least as effective as established ones, but with added superior characteristics such as short processing times, non-toxicity, and medium preservation. Amongst these new methods, non-equilibrium atmospheric pressure plasmas have been shown to present a great promise [2–5].

In this paper, the identification and potential role of each inactivation agent generated by the plasma is assessed. Generally, various gas mixtures can be used to optimize the production of an agent or another and to optimize the efficiency of the inactivation process. The analysis presented here, however, is for low temperature atmospheric pressure plasmas generated in air. For information on plasma sterilization using other gas mixtures such as O_2/CF_4, or at low pressures, the reader is referred to Refs. [6–8].

2. Identification of the inactivation factors and assessment of their roles

Under plasma exposure, bacterial cells can be inactivated by one of four known factors or by a synergistic combination of these. These factors are the heat, UV radiation, charged particles, and reactive neutral species. The extent of the influence of each factor depends on the plasma operating parameters such as power and gas mixture and flow rate. Here, we present relative, and when possible, absolute measurements of the presence of these agents in an atmospheric pressure air plasma generated by a Dielectric Barrier Discharge (DBD). Since our experiments are conducted with the biological sample placed at some distance from the plasma (remote exposure), the effects of charged particles (electrons and ions) will not be discussed. A comprehensive study of the effects of charging bacterial cells by a plasma can be found in Ref. [9].

* Corresponding author. Tel.: +1-757-683-2416; fax: +1-757-683-3220.
E-mail address: mlarouss@odu.edu (M. Laroussi).

1387-3806/$ – see front matter © 2004 Elsevier B.V. All rights reserved.
doi:10.1016/j.ijms.2003.11.016

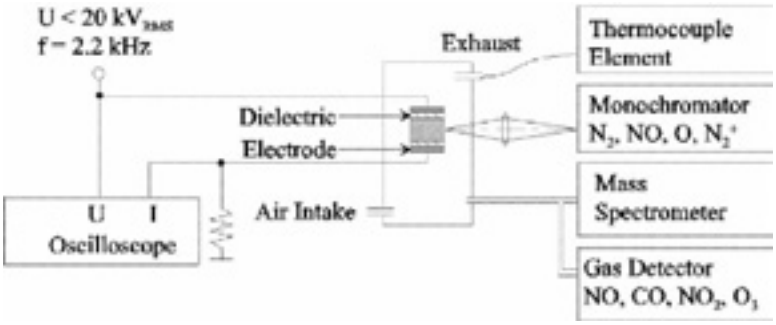

Fig. 1. Experimental setup of DBD air plasma generator and related diagnostics.

A schematic of the experimental setup showing the DBD and the diagnostics used in our evaluations is presented in Fig. 1. The electrodes of our DBD consist of two symmetrical aluminum plates covered by 1 mm thick sheets of alumina (Al_2O_3). The distance between the electrodes is adjustable, up to 1.25 cm. Water cooling of the electrodes allows us to keep the temperature close to room temperature. The applied voltage and the discharge current are monitored by means of a high voltage probe and a current viewing resistor, respectively. The discharge was operated at power levels up to 20 W at an electrode separation of about 7 mm. Optical emission spectroscopy, mass spectroscopy, and gas detection (for NO_2, NO, and O_3) were used to diagnose the plasma contents.

2.1. Heat and its potential effect

It has long been known that heat has detrimental effects on living cells. Therefore, heat-based sterilization techniques were developed and commercially used for applications that do not require medium preservation. In heat-based conventional sterilization methods, both moist heat and dry heat are used. In the case of moist heat, such as in an autoclave, a temperature of 121 °C at a pressure of 15 psi is used [10]. Dry heat sterilization requires temperatures close to 170 °C and treatment times of about 1 h [10].

To assess if heat plays a role in the case of an air plasma, the gas temperature in the discharge was determined by comparing the experimentally measured rotational bands structure of the 0–0 transition of the 2nd positive system of nitrogen with simulated spectra at different temperatures. In addition, the temperature in a sample, placed 2 cm away from the discharge, was measured by a thermocouple probe.

Fig. 2 shows the measured and calculated rotational bands of the 0–0 transition of the 2nd positive system of N_2, for a power of 10 W. It indicates that the gas temperature remains close to room temperature. A variation in power from 2 to 15 W showed no significant change in the relative spectral distribution. This indicates a power-independent temperature in the range between 2 and 15 W at a gas flow rate of 10 l/min. The gas temperature for various gas flow rates at a power consumption of 10 W was also investigated. The results are shown in Fig. 3. For a very low flow (0.5 l/min), a gas temperature of 340 K was found. Increasing the airflow causes the gas temperature to approach room temperature (300 K).

Fig. 4 shows the increase in the temperature of the biological sample under treatment for various dissipated power

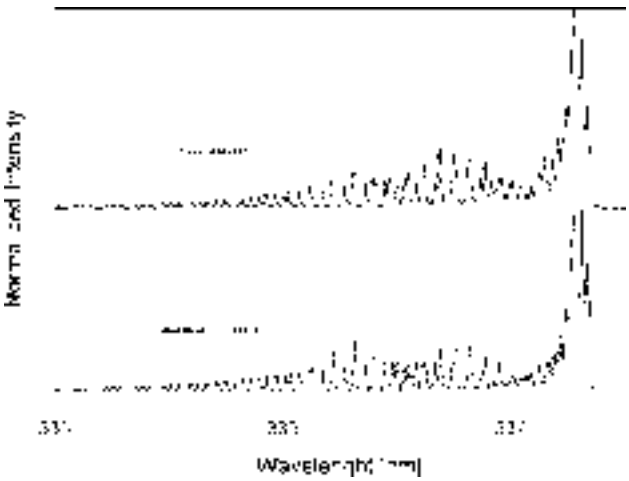

Fig. 2. Measured and calculated rotational bands of the 0–0 transition of the second positive system of nitrogen. The spectra are intentionally shifted vertically for better comparison.

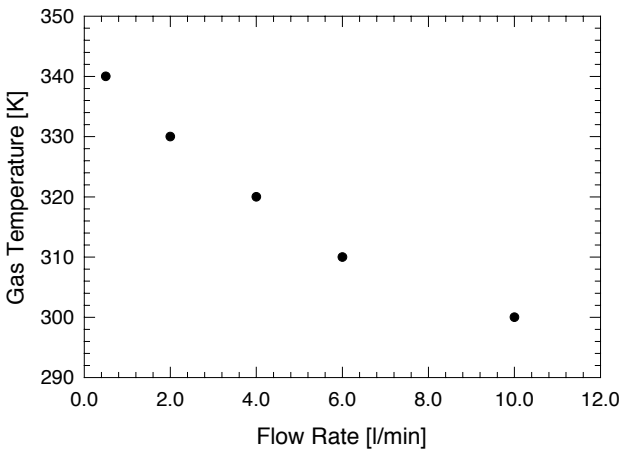

Fig. 3. Gas temperature vs. gas flow rate for a power of 10 W.

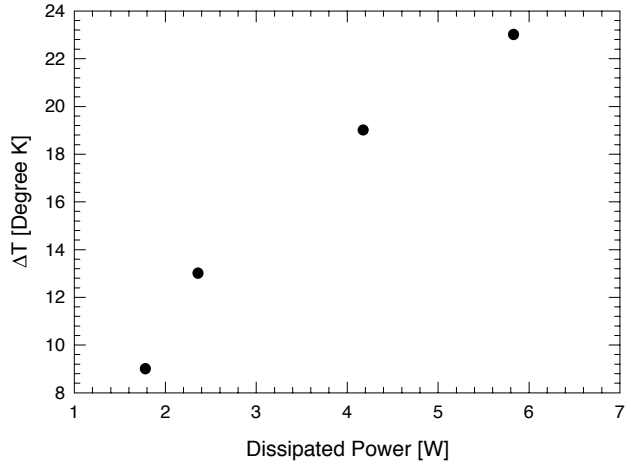

Fig. 4. Increase of sample temperature vs. plasma dissipated power.

levels, as measured by a thermocouple. At our typical running power levels, a maximum increase of 21° was observed. Therefore, based on these measurements no substantial thermal effects on bacterial cells are expected.

2.2. Ultraviolet radiation and its potential role

From early times humans have known that sunlight has beneficial hygienic effects. This is of course due the presence of UV radiation in the sunlight spectrum. Amongst UV effects on cells of bacteria is the dimerization of thymine bases in their DNA strands. This inhibits the bacteria's ability to replicate properly. Wavelengths in the 220–280 nm range and doses of several mW s/cm^2 are known to have the optimum effect [11].

Spectroscopic and absolute power measurements were conducted to quantify the UV contribution to the inactivation process in the case of an air plasma. Our results show that no significant UV emission occurs below 285 nm. This is illustrated in Fig. 5. Power measurements with a calibrated UV detector in the 200–300 nm wavelength region revealed that the power density of the emitted UV radiation is below 50 μW/cm^2 and is essentially independent of the air flow rate. At this power levels we expect the UV not to play a significant direct role in the sterilization process by low temperature air plasmas.

2.3. Reactive species and their role

In high-pressure non-equilibrium plasma discharges, reactive species are generated through various collisional pathways, such as electron impact excitation and dissociation. Reactive species play an important role in all plasma–surface interactions. Air plasmas are excellent sources of reactive oxygen species (ROS) and reactive nitrogen species (RNS), such as atomic oxygen (O), ozone (O_3), hydroxyl (OH), NO, NO_2, etc. Some reaction pathways that lead to the generation of these species in air plasmas are:

$$e + O_2 \rightarrow e + O_2(A^3 \sum_u^+) \rightarrow e + O(^3P) + O(^3P)$$

$$e + O_2 \rightarrow e + O_2(B^3 \sum_u^-) \rightarrow e + O(^1D) + O(^3P)$$

$$O + O_2 + M \rightarrow O_3 + M$$

$$N + O + N_2 \rightarrow NO + N_2$$

$$NO + O_3 \leftrightarrow NO_2 + O_2$$

$$NO_2 + O_2 + hv \rightarrow O_3 + NO$$

$$H_2O + O_3 \leftrightarrow O_2 + 2OH$$

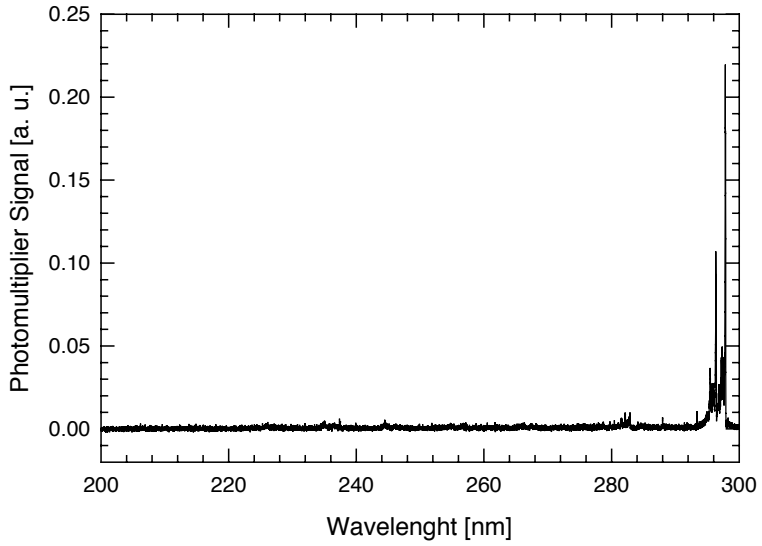

Fig. 5. UV spectrum of a DBD in air in the 200–300 nm wavelength range.

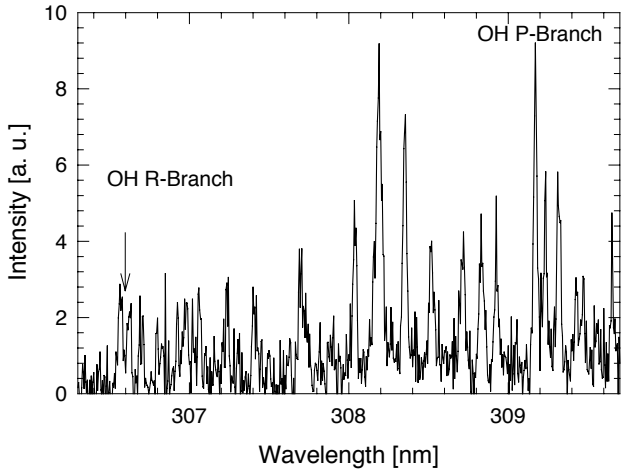

Fig. 6. Emission spectrum from a DBD in air showing OH band heads.

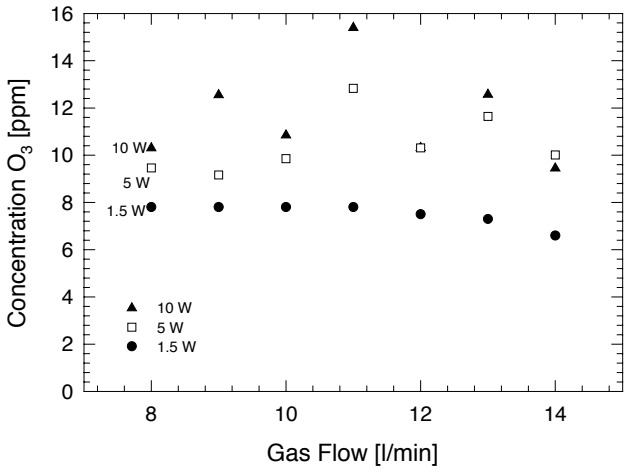

Fig. 8. Ozone concentration generated in a DBD in air as a function of air flow rate and at three power levels (1.5, 5, and 10 W).

$$e + H_2O \rightarrow OH + H + e$$

$$O + H_2O \rightarrow 2OH$$

The following are measurements of oxygen, hydroxyl, ozone, and nitrogen dioxide obtained from a DBD operated in atmospheric pressure air. Relative concentration of atomic oxygen in the DBD, as measured by detecting the oxygen lines at 615.597 and 615.678 nm, showed that the concentration of atomic oxygen decreased less than 20% as the flow rate was increased from 1 to 18 l/min. The presence of OH was measured by means of emission spectroscopy, looking for the rotational band of OH A–X (0–0) transition. This molecular band has a branch at about 306.6 nm (R branch) and another one at 309.2 nm (P branch). Fig. 6 shows the emission spectrum in the range between 306 and 310 nm and it indicates the OH band heads. Fig. 7 shows the relative concentration of OH in the discharge as a function of the air flow rate and dissipated power, assuming that the rotational band intensity represents the OH concentration. The ozone concentration was measured for varying flow rates and at various power levels by a calibrated ozone detector. The results are shown in Fig. 8. Ozone germicidal effects are caused by its interference with cellular respiration. Nitrogen dioxide was measured as a function of the air flow rate and for different power levels by a calibrated gas detecting system and the results are shown in Fig. 9.

The reactive species mentioned above have direct impact on the cells of microorganisms, and especially on their outermost membranes. These membranes are made of lipid bilayers, an important component of which is unsaturated fatty acids. The unsaturated fatty acids give the membrane a gel-like nature. This allows the transport of the biochemical

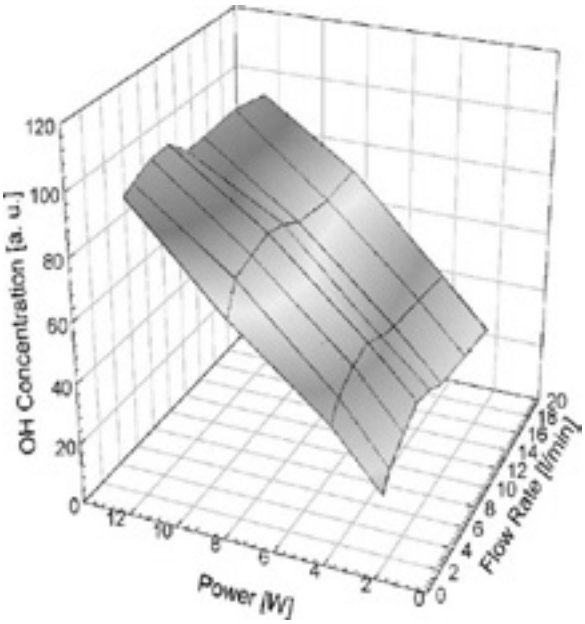

Fig. 7. Relative OH concentration as a function of plasma dissipated power and air flow rate.

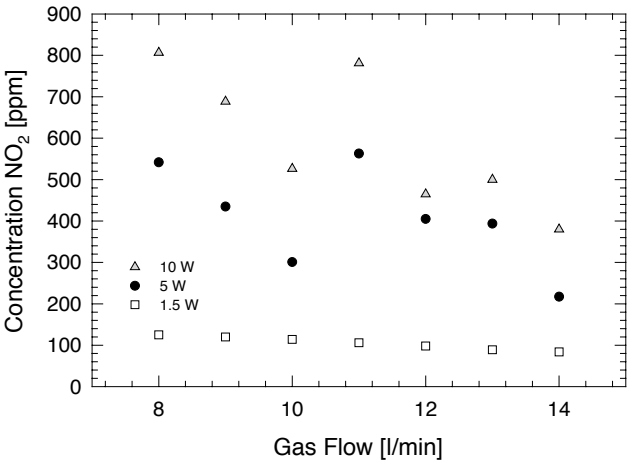

Fig. 9. Concentration of nitrogen dioxide generated in a DBD in air as a function of air flow rate and at three power levels (1.5, 5, and 10 W).

by-products across the membrane. Since unsaturated fatty acids are susceptible to attacks by hydroxyl radical (OH) [12], the presence of this radical can therefore compromise the function of the membrane lipids whose role is to act as a barrier against the transport of ions and polar compounds in and out of the cells [13]. Imbedded in the lipid bilayer are protein molecules which also control the passage of various compounds. Proteins are basically linear chains of aminoacids. Aminoacids are also susceptible to oxidation when placed in the radical-rich environment of the plasma. Therefore, the reactive species generated by air plasmas are expected to greatly compromise the integrity of the cells of microorganisms, leading to their eventual destruction.

3. Correlation between the presence of reactive species and inactivation kinetics

One kinetics measurement parameter, which has been used extensively by researchers studying sterilization by plasma, is what is referred to as the "*D*" value (Decimal value). The *D*-value is the time required to reduce an original concentration of microorganisms by 90%, or if the "kill' curve is plotted on a semi-logarithmic scale, the *D*-value is determined as the time for a one $\log_{10}$ reduction.

To show the effects of reactive species on the destruction of bacteria, kill curves were plotted for three different gaseous conditions: helium only, 97% helium/3% oxygen mixture, and air, all at atmospheric pressure. Spores of the *Bacillus* genus were used since they are hard to kill and are accepted metrics for biological sterilization. When helium is used, only very small concentrations of radicals originating from impurities are expected. When helium is mixed with oxygen, oxygen-based species such as O and O_3 are generated. When air is used, both oxygen-based and nitrogen-based species are generated.

Fig. 10 shows a comparison between the inactivation kinetics in the case of helium and when a 97%–3% helium/oxygen mixture, respectively, was used. After 10 min of treatment time the surviving spore population percentage

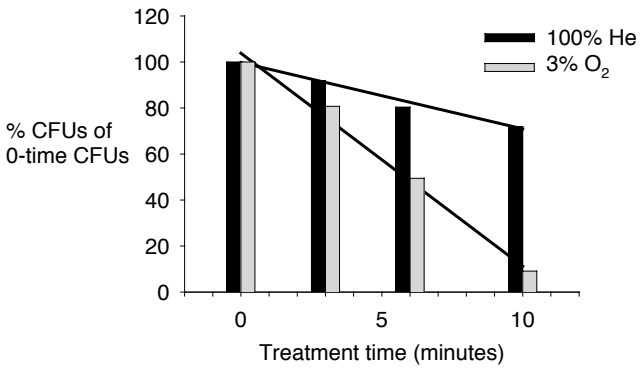

Fig. 10. Percent of surviving *Bacillus* spores vs. plasma treatment time for helium (black) and helium/oxygen mixture (97% He, 3% O_2) (gray).

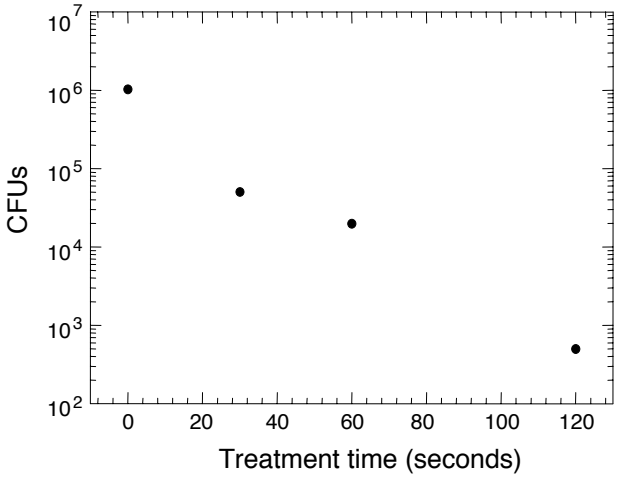

Fig. 11. Colony forming units of *Bacillus* spores vs. treatment time by a low temperature, atmospheric pressure air plasma.

was still much greater than 10%, when only helium was used as the operating gas. In fact the *D*-value in this case was greater than 20 min. When the helium/oxygen mixture was used, as shown in Fig. 10, a *D*-value of 10 min was achieved. Fig. 11 shows the inactivation kinetics of an air plasma. A *D*-value close to 20 s was achieved in this case. This is a 30 times faster inactivation process than the previous case. Since heat and UV radiation were shown not to play an important role for cold air plasmas, the dramatic increase in inactivation efficacy is attributed to the presence of the chemically reactive species such as NO, NO_2, O, O_3, etc. . . . .

4. Conclusion

Low temperature, atmospheric pressure plasmas have been shown to possess very effective germicidal characteristics. Their relatively simple and inexpensive designs, as well as their non-toxic nature, give them the potential to replace conventional sterilization methods in the near future. This is a most welcome technology in the healthcare arena where re-usable, heat sensitive medical tools are becoming more and more prevalent.

In this paper, based mainly on non-intrusive optical diagnostics and gas detection systems, we conclude that in the case of low temperature air plasmas, it is the highly reactive species such as O, OH, and NO_2 that play the most crucial role in the destruction of microorganisms. Heat and UV radiation may play a secondary role, but we expect their effects to be either minimal or indirect.

Acknowledgements

Work supported by a grant from the US Air Force Office of Scientific Research.

References

[1] S.S. Block, Encyclopedia of Microbiology, vol. 4, Academic Press, 1992, p. 87.
[2] M. Laroussi, IEEE Trans. Plasma Sci. 24 (3) (1996) 1188.
[3] H.W. Herrmann, I. Henins, J. Park, G.S. Selwyn, Phys. Plasmas 6 (5) (1999) 2284.
[4] J.G. Birmingham, D.J. Hammerstrom, IEEE Trans. Plasma Sci. 28 (1) (2000) 51.
[5] M. Laroussi, IEEE Trans. Plasma Sci. 30 (4) (2002) 1409.
[6] S. Lerouge, M.R. Werthheimer, R. Marchand, M. Tabrizian, L.'H. Yahia, J. Biomed. Mater. Res. 51 (2000) 128.
[7] S. Moreau, M. Moisan, J. Barbeau, J. Pelletier, A. Ricard, J. Appl. Phys. 88 (2000) 1166.
[8] M. Moisan, J. Barbeau, S. Moreau, J. Pelletier, M. Tabrizian, L.'H. Yahia, Int. J. Pharm. 226 (2001) 1.
[9] M. Laroussi, A. Mendis, M. Rosenberg, New J. Phys. 5 (2003) 41.1.
[10] S.S. Block, Disinfection, Sterilization, and Preservation, Lea & Febiger, Philadelphia, 1983.
[11] A. Norman, J. Cell Comp. Physiol. 44 (1954) 1.
[12] T.C. Montie, K. Kelly-Wintenberg, J.R. Roth, IEEE Trans. Plasma Sci. 28 (1) (2000) 41.
[13] F.A. Bettleheim, J. March, Introduction to General, Organic & Biochemistry, 4th ed., Saunders College Pub., 1995.

Non-thermal plasma application in air sterilization

Conference Paper *in* IEEE International Conference on Plasma Science · January 2004

DOI: 10.1109/PLASMA.2004.1339779

CITATIONS
9

READS
950

5 authors, including:

Michael Gallagher
Drexel University
20 PUBLICATIONS **313** CITATIONS
SEE PROFILE

Alexander F. Gutsol
Actively searching for new opportunity
179 PUBLICATIONS **7,188** CITATIONS
SEE PROFILE

Greg Fridman
AAPlasma LLC
157 PUBLICATIONS **5,721** CITATIONS
SEE PROFILE

Non-Thermal Plasma Applications in Air-Sterilization

Michael J. Gallagher[1], Alexander Gutsol[1], Gary Friedman[2], Alexander Fridman[1]
1 Department of Mechanical Engineering & Mechanics, Drexel University, Philadelphia, PA
2 Department of Electrical & Computer Engineering, Drexel University, Philadelphia, PA
Drexel Plasma Institute, Drexel University, Philadelphia, Pennsylvania, USA

Abstract

In our present study, two non-thermal plasma devices, dielectric barrier discharge and magnetically-rotated gliding arc, are being used to sterilize air containing high concentrations of viral and bacterial bioaerosols. A Pathogen Detection and Remediation Facility was designed for bioaerosol generation, containment, and sampling during plasma sterilization experiments.

Keywords: non-thermal plasma, sterilization; decontamination, airborne virus, bacteria, influenza

1. Introduction

The improvement of indoor air quality has been a challenge since the dawn of heating, ventilation, and air conditioning (HVAC) systems. Incidents like the infamous outbreak of Legionnaires disease in 1976 in Philadelphia and the recent increasing threat of bioterrorism have raised awareness of the dangers of airborne microorganisms in indoor environments. In recent years, non-thermal atmospheric pressure plasma has been the focus of research as an improved method for the sterilization of air from biological contaminates. Non-thermal plasma has been proven to inactivate many different types of microorganisms, such as viruses and bacteria, on surfaces of materials, but there have been few scientific studies of air sterilization using non-thermal plasma. Also, of the few researchers that have been able to use plasma to decontaminate a moving air stream, many rely on high efficiency particulate air (HEPA) filters to remove a large portion of microorganisms. HEPA filters are effective at trapping particles down to 0.5 microns in size; however, studies have shown that they are not as effective at capturing airborne viruses, which are among the smallest (20-300nm) known microorganisms [1]. HEPA filters also cause significant pressure losses in HVAC systems giving rise to higher energy and maintenance costs. There are several alternative methods for air cleaning, which include electrostatic precipitators, Ultraviolet Germicidal Irradiation (UVGI) devices, and some portable negative air ionizers, that are all capable of reducing particulates and even certain levels of microbial contamination in indoor environments. However, many of these methods are not proven as an efficient and cost effective means of eliminating airborne viruses. In this ongoing scientific study, we will examine the sterilization effect of two types of non-thermal plasma; dielectric barrier discharge (DBD) and magnetically-rotated gliding arc on air contaminated with high concentrations of aerosolized Influenza A virus. A non-pathogenic unicellular bacterium known as Synechococcus Elongatus, or Cyanobacteria, was also used in initial trials to demonstrate the decontamination ability of active chemical species generated from dielectric barrier discharge for bacteria in water and to provide benchmark data regarding bioaerosol sampling efficiency.

2. Non-thermal plasma for air sterilization

Although Dielectric Barrier Discharge (DBD) and magnetically-rotated Gliding Arc [2] are quite different in terms of current-voltage characteristics and operational power levels, both devices can provide a high concentration of active chemical species, which are a necessary component of the sterilization process. There are two main sterilization effects that bioaerosols are subjected to as they are passed through each plasma device: the direct interaction with the lethal environment of the discharge itself and the downstream interaction with active chemical species, such as ozone (O_3) and hydroxyl (OH), produced by the discharge. Figure 1 below shows a photo of the DBD device which consists of a thin plane of wires with equally spaced air gaps of 1.5 mm. The high voltage electrodes are coated with a quartz capillary dielectric that has an approximate wall

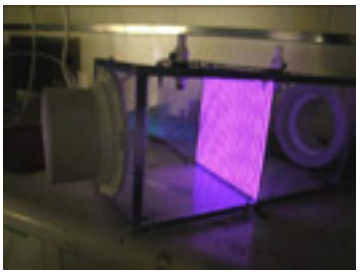

Figure 1. Dielectric Barrier Discharge for air sterilization

thickness of 0.5 mm and the device requires 14 kV for breakdown while consuming less than 200 watts of power. DBD is a low temperature discharge that is very efficient for the production of ozone, which is a strong oxidizer and proven microbial disinfectant [3-6]. The second discharge, magnetically-rotated Gliding Arc, generates a transitional non-thermal plasma and has a relatively low translational gas temperature with a high electron temperature. Gliding Arc uses a strong magnetic field to rotate and elongate an initial thermal arc resulting in rapid convective cooling, keeping the passing air flow near room temperature. This type of discharge has a large power density that can work at atmospheric pressure, but is still very efficient in providing active species. The Gliding Arc device is eight inches in diameter which keeps air velocity low allowing for greater uniformity of treatment. In figure 2, the arc is partially elongated at the center electrode. Additionally, both DBD and gliding arc devices have been designed to prevent an air pressure loss during operation and are capable of retrofit into existing HVAC systems.

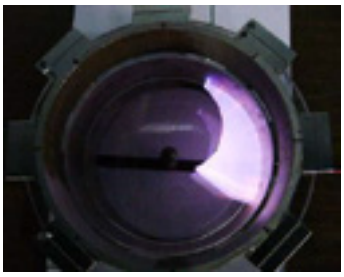

Figure 2. Magnetically Rotated Gliding Arc

3. Preliminary experiments with plasma-water decontamination

To understand the decontamination effectiveness of DBD, we designed a simple experiment to test the effect of active chemical species generated from this discharge on cyanobacteria suspended in liquid growth medium. Approximately 35 ml of liquid with cyanobacteria was placed in a Petri dish at a distance of 30 mm from the surface of the plasma discharge. A small fan forced air through the discharge at a direction normal to the surface of the liquid. Figure 3 shows a diagram of the experimental setup. The DBD discharge produces 0.11 mg of ozone per liter of air, most of which was directed toward the liquid-gas interface as the solution was stirred with a magnetic stir bar. After 3.9 minutes of treatment, we demonstrated more than a 2-log reduction (99.3%) of bacteria in the solution. We attribute ozone as the main active specie responsible for the inactivation of bacteria in this case because of its longer lifetime in comparison to hydroxyl. A similar experiment was performed by Moreau, et al. [7] to demonstrate the lethal effect of a gliding arc discharge on strain of a bacterial plant pathogen, Erwina, suspended in a liquid medium.

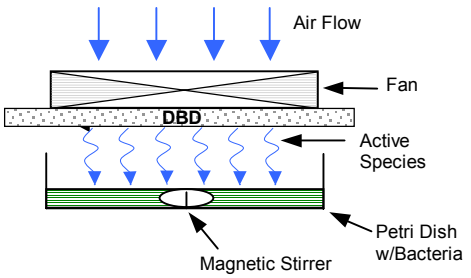

Figure 3. Water decontamination experiment using Dielectric Barrier Discharge (DBD).

4. Air Decontamination / Sterilization

In order to prove that non-thermal plasma is the main factor responsible for sterilization, one must first build a system that is capable of creating, handling, and analyzing dense concentrations of viable bioaerosols. Designing and building an air sterilization system is challenging because there are many factors that contribute to losses of aerosolized microorganisms in moving air streams. These factors include diffusion of aerosol to walls of the air flow system, desiccation stress on the microorganism due to evaporation of bioaerosol droplets in flight, and inertial and gravitational forces which can remove larger droplets from the air stream. The factors causing these losses must be carefully considered in order to avoid misinterpretation of sterilization data and may also be one reason why bioaerosol sterilization studies are limited in comparison to studies involving water or surface sterilization. Careful attention to these potential sources of error will yield greater accuracy and validity in distinguishing non-thermal plasma as the true sterilizing agent. Figure 4 below shows a scheme of the Pathogen Detection and Remediation Facility (PDRF) which is a plug flow reactor that was designed for

bioaerosol generation, containment, and sampling. It was designed to simulate conditions commonly found in an HVAC system: it has an overall volume of 250 liters, and can operate at flow rates up to 25 liters per second. The PDRF houses interchangeable non-thermal plasma devices, DBD and Magnetic Gliding Arc, which are connected to the system with four inch (10 cm) diameter flexible piping. At a flow rate of 25 L/s, the residence time, that is, the time for one droplet to make one revolution through the system, is approximately 10 seconds. An air sampling system is included in the PDRF and was designed to take as large volume air sample as possible (~ 1 liter) in a short period of time (~ 1 second) so that we do not disturb the flow inside the system and can evaluate the viability of the bioaerosol as a function of treatment time.

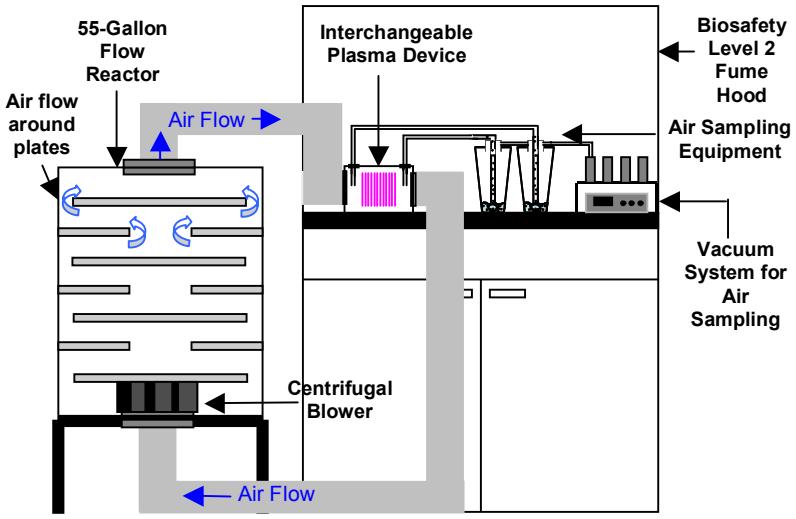

Figure 4. Pathogen Detection and Remediation Facility (PDRF)

Liquid impingement was chosen as the air sampling method for our system, as opposed to filtration or impaction, because it minimizes dessication stress and allows for the direct deposition of the microorganism into growth media. The AGI-30 liquid impinger is a commonly used bioaerosol sampler and it operates by drawing a sample of air through in inlet tube submerged in a solution, thereby causing the air stream to strike the liquid bed trapping aerosols in the solution through forces of inertia [8]. The AGI-30 impinger contains a critical orifice that contains one exit port and limits the maximum air sampling rate to 12.5 liters per minute [9]. To accommodate our desired sampling rate of 1 liter per second, we modified the AGI-30 by increasing its overall volume and replacing the standard critical orifice with a hollow spherical tip with several exit ports. Several calibration experiments performed with our modified AGI-30 impinger demonstrated reproducibility in terms of sampling efficiency. In these experiments, a Collison nebulizer was connected directly to the modified liquid impinger and after five minutes of continuous sampling in each trial, we obtained a stable sampling efficiency rating of 3.5%. Some may not consider this as an optimal efficiency rating, however, when sampling bioaerosols, reproducibility is often considered more important than the efficiency rating because the final conclusions are derived from internal comparisons between various data collected using the same samplers [9].

Several additional calibration experiments were performed in which cyanobacteria aerosol (droplet size: 1.5 micron) was injected into the Pathogen Detection and Remediation Facility (PDRF) not for the purpose of sterilization, but to identify all bioaerosol losses from diffusion, inertia, and evaporation, thereby establishing accurate controls before non-thermal plasma is introduced. In these experiments, a Collison nebulizer was used to generate the bioaerosol, the air flow rate was fixed at 25 liters per second, and the lifetime of droplets was measured by periodic air sampling with two modified liquid impingers. For all experiments described here, the system was prehumidified with sterile de-ionized water until the internal surface of the system walls were wet prior to input of the bioaerosol. Initial results showed a very poor recovery of cyanobacteria bioaerosol from the PDRF in comparison to air sampler calibration experiments. When examining the sources of loss: diffusion, inertia, and evaporation, we ruled out inertial forces because air velocity is relatively low and the aerosol droplets are small (1-2 microns). Also, our estimate of droplet diffusion time to the wall is approximately 40 minutes, well beyond the upper time limit of these trials. The effect of small droplet evaporation, however, can be prominent because the saturation pressure around a small droplet is high in comparison to the saturation pressure near the wet walls of the system. To test the effect of evaporation on the survivability of cyanobacteria, we performed two experiments: the first (Experiment A) in which additional humidity was applied continuously with the bioaerosol using an additional nebulizer with with sterile de-ionized water, and the

second (Experiment B) without additional humidification. Our results, which are described in figure 5 below, show that additional humidification reduces the rate of inactivation of aerosolized cyanobacteria, by dessication stress compared to the results of experiments without additional humidification.

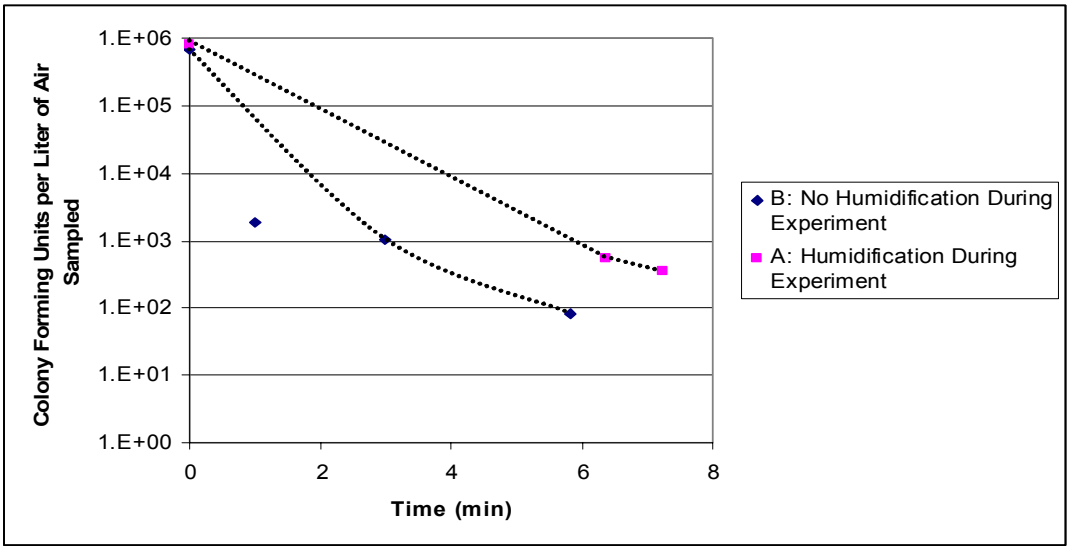

Figure 5. Evaluation of the effect of droplet evaporation on the survivability of aerosolized cyanobacteria. Experiment A minimizes evaporation by providing constant humidity.

The experimentally estimated maximum lifetime of aerosolized Cyanobacteria is 10 minutes, which is far below the estimated diffusion time of droplets to the walls of the system. We desire to have the ability to recover viable cyanobacteria over an extended period of time (tens of minutes) so that when we perform sterilization experiments with non-thermal plasma, we have enough time to take several air samples and thus acquire many data points to accurately describe the rate of inactivation. To determine if the droplets were indeed still present in the air flow after 10 minutes, we added a laser to the system to characterize the optical density of the bacterial aerosol over time. Figure 6 shows an image of the illuminated laser beam at the first minute of the experiment when the concentration of viable Cyanobacteria is high. Illumination from the laser beam slowly decayed over a period of nearly 2 hours indicating that aerosolized bacteria were still present in the flow, however, they were non-viable. Similar results were reported by Ehresmann & Hatch, who described the optical density of aerosolized unicellular bacteria lasting up to four hours at high humidity (92-94%) with viability lasting only minutes [10]. These calibration experiments with Cyanobacteria provided us with a basic understanding of the flow characteristics of the Pathogen Detection and Remediation Facility and efficiency of our air sampling system. This was a necessary step before working with viral bioaerosols because immunoassay detection methods used to quantify viruses are less accurate than the serial dilution methods used to quantify Cyanobacteria in these calibration experiments. Sterilization experiments with Cyanobacteria and Influenza A virus are in progress and we expect to have results in the summer of 2005.

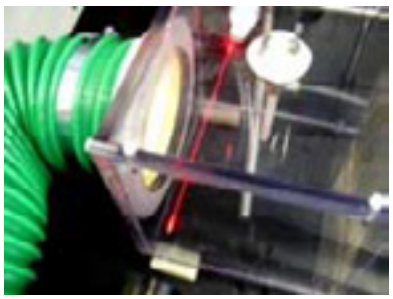

Figure 6. A laser beam illuminates the dense concentration of bioaerosol

5. Plasma chemistry sterilization modeling

The results from our experiments with the PDRF will be used to verify a model of plasma chemical sterilization [11]. We have composed a physiochemical model of the oxidizing effects of the active chemical species

generated by non-thermal plasma on many different types of microorganisms. We are investigating the individual sterilizing effects of hydroxyl radicals (OH), ozone (O_3), ultraviolet radiation (UV) as there is a large amount empirical data regarding the role of each of these components for the sterilization of various bacteria, viruses, and spores in various media. Our model combines this data with the chemical kinetics of non-thermal plasma to predict the rate of destruction of microorganisms under varying conditions.

This research is supported by Telemedicine and Advanced Technology Research Center of the US Department of Defense (TATRC of DoD) through Civilian Medical Response Center (CiMeRC).

References

[1] Harstad, J.B. Evaluation of air filters with submicron viral aerosols and bacterial aerosols. American Industrial Hygiene Association Journal. May-June (1969).
[2] Gangoli, S., Gutsol, A. and Fridman A. Rotating Non-Equilibrium Gliding Arc Plasma Disc for Enhancement in Ignition and Combustion of Hydrocarbon Fuels, ISPC-17, August 7-12, 2005, Toronto, Canada.
[3] Kowalski, W.J., Bahnfleth, W.P., and Whittam, T.S. Bactericidal effects of high airborne ozone concentrations on escherichia coli and staphylococcus aureus. Ozone Sci. Engin. 20 (1998).
[4] Kowalski, W.J., W.P. Bahnfleth, B.A. Striebig, and T.S. Whittam. Demonstration of a hermitic airborne ozone disinfection system: studies on E. coli. American Industrial Hygiene Association Journal. March-April (2003).
[5] Ishizaki, K., Shinriki N., and Matsuyama H. Inactivation of bacillus spores by gaseous ozone. Journal of Applied Bacteriology 60 (1986).
[6] Burleson G.R., Murray T.M., Pollard M. Inactivation of viruses and bacteria by ozone, with and without sonication. Applied Microbiology 29, 3 (1975).
[7] Moreau M., Feuilloley M.G.J., Orange N., and Brisset J.-L. Lethal effect of the gliding arc discharges on Erwinia spp. Journal of Applied Microbiology. 98 (2005).
[8] Perry, J.H. Chemical engineers' handbook, 2nd ed. McGraw-Hill, New York. (1941).
[9] Cown WB, Kethley TW, Fincher EL. The critical-orifice liquid impinger as a sampler for bacterial aerosols. Applied Microbiology 5 (1957).
[10] Ehresmann D.W., Hatch M.T. Effect of relative humidity on the survival of airborne unicellular algae. Applied Microbiology 29:3 (1975).
[11] Gangoli, S., Gallagher, M., Dolgopolsky, A., Gutsol, A. and Fridman A. Sterilization of Microorganisms using Non-Thermal Dielectric Barrier Discharge Plasma – Statistically based Chemical Kinetics Model, ISPC-17, August 7-12, 2005, Toronto, Canada.

Non-thermal plasmas (NTPs) for inactivation of viruses in abiotic environment

Article · June 2016

CITATIONS
9

READS
1,136

2 authors:

Pradeep Puligundla
Gachon University
75 PUBLICATIONS **791** CITATIONS
SEE PROFILE

Chulkyoon Mok
Gachon University
67 PUBLICATIONS **785** CITATIONS
SEE PROFILE

Review Paper:

Non-thermal plasmas (NTPs) for inactivation of viruses in abiotic environment

Puligundla Pradeep and Mok Chulkyoon*
Department of Food Science and Biotechnology, Gachon University, Seongnam 13120, KOREA
mokck@gachon.ac.kr

Abstract

Despite several successful disinfection strategies, process of controlling the environmental survival and transmission of human pathogenic viruses is becoming increasingly more difficult because of their emerging resistance to disinfectants. Therefore, range of non-chemical methods of inactivation is being explored extensively as an alternative. Especially, non-thermal, chemical-free techniques find wide application in the inactivation of air-borne, water and food-borne and surface-borne viruses. Among such methods, the application of non-thermal plasmas (NTPs) for viral inactivation is a relatively new technique and is quite promising. The present review evaluates comprehensively the studies of virucidal effect of NTPs against human pathogenic viruses in abiotic environment.

Keywords: Non-thermal plasma, pathogenic virus, inactivation, disinfection, abiotic environment.

Introduction

Medically-important viruses continue to survive and evolve in abiotic environment despite several successful disinfection strategies to control them. This is primarily due to the resistance of several viruses to disinfectants and sterilants, especially to chemical-based ones and continuous appearance of mutations. Also, the highly related viruses can exhibit different disinfection kinetics when treated with the same biocide which makes virus inactivation complicated [8, 14].

The mode of transmission of several groups of viruses to humans is through contaminated food, water and air, person-to-person transmission via contaminated environmental surfaces or objects and direct person-to-person contact[11, 34]. It is known that viruses pass into the environment from clinically ill or carrier hosts although they do not replicate outside living animals or people; they are maintained and transported to susceptible hosts[33]. Viruses are less tolerant to heat and therefore lose infectivity rapidly on heat treatment. However, heat-induced inactivation is not always suitable and non-thermal sterilization methods may be required to deactivate viruses on thermolabile surfaces or materials and heat-sensitive foodstuffs. Several non-chemical, non-thermal technologies have been developed to combat surface-borne, food- and water-borne viruses. Such methods uses ionizing radiation, UV irradiation, pulsed light, pulsed electric field, supercritical fluids, high hydrostatic pressure processing and gas plasma[7, 13, 16, 20, 38].

The use of atmospheric pressure, nonthermal plasmas (NTPs) is a promising approach for sterilization and disinfection of both viable and nonviable surfaces[5]. NTPs have been used for a range of biomedical applications including microbial inactivation, sterilization and disinfection.[17,23,27] The sterilants produced by the nonthermal plasma killed or inactivated a wide range of organisms, spores and viruses[43]. The potential advantages of NTPs over chemical disinfectants include simplicity of design and operation[47], utilization of nontoxic gases, an absence of toxic residues[36] and production of a large quantity of diverse microbicidal active species. Plasmas are not only capable of inactivating or killing bacteria and viruses; they can also dislodge these dead microorganisms from the surfaces of the objects being sterilized[12].

Fundamentals of non-thermal plasmas: Plasma is defined as a neutral ionized gas with a net neutral charge. It is constituted by different species including ions (both positive and negative), electrons, atoms, free radicals, photons and excited and nonexcited molecules[18]. A neutral gas can be converted to plasma by applying energy in several forms including electric, thermal or magnetic fields and radio or microwave frequencies, thereby resulting in an increase in the kinetic energy of the electrons of constituent gas atoms. This causes interatomic collisions in the gas resulting in the formation of aforementioned plasma constituents. Plasma can be categorized based on the relative energetic levels of electrons and heavy particles of plasma into thermal (equilibrium plasma) and nonthermal or cold (non-equilibrium plasma). Thermal plasmas are generated at high pressure ($\geq 10^5$ Pa) and consume substantial power (up to 50 MW) to be generated.

On the other hand, NTPs can be generated at lower pressures using less power. They are characterized by an electron temperature much higher than that of the gas temperature and thus do not present a local thermodynamic equilibrium. Such plasma can be generated by electric discharges in lower pressure gases[30].

NTPs are further divided into two other categories: low-pressure plasmas (10^{-4} to 10^{-2} kPa) and atmospheric-pressure plasmas. The atmospheric plasma sources can be classified regarding their excitation mode into distinct groups - the DC (direct current) and low frequency

discharges; the plasmas which are ignited by radio frequency waves and the microwave discharges[41]. The DC and low frequency discharges can work, depending on their design either with a continuous or a pulsed mode. The arc plasma torches belong to continuous working mode whereas corona discharge, dielectric barrier discharge (DBD) and microplasma belong to pulsed DC discharges. The NTP technology has potential application for microbial inactivation on surfaces and other thermally-sensitive materials.

Plasma species responsible for inactivation: In general, heat is not a major contributor to the sterilization effect using non-thermal plasmas. In atmospheric pressure plasmas, UV photons are not the main microbicidal agents[22, 28]. On contrary, however, some authors claim that UV photons, under specific operating conditions, can be the dominant inactivation species[10,31]. Several researchers claimed that the chemically reactive neutral species such as O, O_2*, O_3, $OH^{\bullet}$, NO and NO_2 can significantly contribute to the plasma sterilization process, especially at atmospheric pressures[17, 26, 27]. It has been shown that discharges containing oxygen provide a strong germicidal effect[19, 35]. Moreover, discharges containing oxygen also generate ozone (O_3) which is known to have a strong bactericidal effect[27]. Also, the presence of moisture in discharge gas plays a significant role in bactericidal action by generating hydroxyl (OH) radicals in the plasma which can chemically attack the outer structures of bacterial cells. Therefore, the best bactericidal effects were achieved in moistened oxygen and air[24].

Reactive species of low-temperature plasma are believed to play a dominant role in hepatitis B virus deactivation process[39]. Virucidal action of reactive oxygen species (ROS) has been demonstrated. Wu et al[46] reported that the ROS species namely OH radicals and atomic oxygen were associated with the inactivation of MS2 viruses by the atmospheric-pressure cold plasma. In addition, ROS have been shown to be implicated in the inactivation of MS2 coliphage by an in-house-built kilohertz-driven atmospheric pressure, nonthermal plasma jet[5]. In the case of feline calicivirus (FCV) inactivation by cold atmospheric gaseous plasma (CGP), the chemical interaction of ROS and reactive nitrogen species (RNS) such as singlet oxygen (O_2*), ozone (O_3) and superoxide (O_2^-) or peroxynitrous acid, has been shown to play a key role[1]. Sakudo et al[37] found that hydrogen peroxide-like molecules which can create oxidative stress, were predominantly responsible for inactivation of influenza virus by N_2 gas plasma.

Inactivation mechanisms: Nonthermal plasma may be employed to inactivate a wide range of microorganisms such as bacteria, spores, fungi, viruses and prions. The mechanism of interaction of plasma with living systems is complex and is not well known. This is mainly due to the complexity of biology and partly due to the complexity of plasma. The charged species of plasma, especially ions, are believed to play a key role in plasma-living cell interaction[15]. In direct plasma exposure, both positive and negative ions have been reported to possess relatively the same effect. The charged species interact chemically and not through physical phenomena such as shear stress, ion bombardment damage or thermal effects. The charged particles might play a significant role in the rupture of outer cell membranes, especially in gram-negative bacteria which possess thin outer membranes and a thin murein layer[29].

The specific mechanisms that lead to virus inactivation by NTPs are also unclear. Previous studies demonstrated that exposure to NTPs results in modification and/or degradation of viral proteins and nucleic acids and also lipids in enveloped viruses. Yasuda et al[48] attributed inactivation of λ phage by atmospheric pressure DBD to the damage of coat proteins and found DNA damage hardly contributed to the inactivation. It has been shown that singlet oxygen $^1O_2$ can cause inactivation of MS2 phage by rendering the genome nonreplicable and significant genome decay and also through minor effects on host binding and genome injection into the host[45].

It was hypothesized in the case of FCV inactivation by CGP that both ROS and RNS species can potentially react with the capsid protein, leading to protein peroxidation and destruction of the capsid. In addition, reactive species can damage the viral RNA, leading to reduced gene expression and elimination of viral RNA, or both[1]. The degradation of viral proteins including nucleoprotein, hemagglutinin and neuraminidase was observed when N_2 gas plasma was used for influenza A and B viruses inactivation[37]. In addition, the injury of viral RNA genome and the inactivation of hemagglutination were observed after N_2 gas plasma treatment. It was concluded that these changes were possibly due to changes in the viral envelope because of modification of the lipid content. They also concluded that oxidation may be the most important factor in the inactivation, degradation and modification of influenza virus by N_2 gas plasma.

Studies on decontamination of viruses using NTPs

Noroviruses: Noroviruses are frequently implicated in human gastroenteritis. Noroviruses spread directly from one person to another and via surfaces, often in crowded facilities. Disinfection of surfaces that come into contact with infected humans is essential for the prevention of cross-contamination and further transmission of the virus. The use of atmospheric pressure, nonthermal plasmas is a promising approach to sterilization and/or disinfection of both viable and nonviable surfaces. The virucidal efficacy of atmospheric pressure, nonthermal plasma jet operated at varying helium/oxygen feed gas concentrations against MS2 bacteriophage, which is widely employed as a convenient surrogate for human norovirus, has been investigated[5]. In this study, the log reductions in MS2 viability after 3 min of the plasma exposure were 3

$\log_{10}$ (99.9%) and the reductions exceeded 7 $\log_{10}$ after 9 min exposure.

The ability of non-thermal plasma to inactivate human enteric virus surrogates on stainless steel surfaces has been investigated[40]. During the experimental procedure, cultivable human norovirus surrogates, feline calicivirus (FCV-F9) and murine norovirus (MNV-1) and bacteriophage MS2 at ~7 log plaque-forming units (PFU)/ml were inoculated and dried on sterile stainless steel coupons. These coupons were treated with the one atmosphere uniform glow discharge plasma for 0, 1, 2, 5 and10 min. FCV-F9 exhibited reduction of 2.34 and 3.55 log PFU after 1 and 2 min respectively and to non-detectable levels after 5 and 10 min. MNV-1 was reduced by 0.56, 1.61, 1.95 and3.16 log PFU after 1, 2, 5 and 10 min respectively. And, MS2 was reduced by 2.03 and 5.46 log PFU after 2 and 5 min respectively and to non-detectable levels after 10 min[40].

The impact of cold atmospheric pressure plasma (CAPP) on the inactivation of a clinical human outbreak norovirus (NoV), GII.4, has been investigated[2]. In this study, NoV-positive stool sample at three different dilutions was prepared and subsequently treated with CAPP for various lengths of time, up to 15 min. Increased NoV reduction was observed with the increase of CAPP treatment time. CAPP reduced the initial quantity of 2.36×10^4 genomic equivalents/ml sample by 1.23 $\log_{10}$ and 1.69 $\log_{10}$ genomic equivalents/ml after 10 and 15 min exposure respectively ($P<0.01$). CAPP treatment of surfaces carrying a lower viral load reduced NoV by at least 1 $\log_{10}$ after CAPP exposure for 2 min ($P<0.05$) and 1 min ($P<0.05$) respectively. The results suggest that NoV can be inactivated by CAPP treatment.

Human norovirus is one of the leading causes of viral foodborne illnesses. NTPs have been used to combat norovirus contamination in food. In a study, inactivation effect of atmospheric pressure plasma (APP) jets against murine norovirus (MNV-1), as a norovirus (NoV) surrogate, associated with three types of fresh meats-beef loin, pork shoulder and chicken breast, was investigated by Bae et al[6]. The reduction in MNV-1 titers [initial inoculums of 10^7 plaque-forming units (PFU)] was >2 $\log_{10}$ PFU/ml in the three types of meat following the treatment with APP jets for 5–20 min. Under 5 min treatment time, there were no significant differences ($P>0.05$) in the L*, a* and b* values and the water content (%) value between untreated and APP jet-treated samples. Although the TBARS values, an indicator of meat rancidity, gradually increased with increase of APP jet treatment times, they were below 1.0 mg MA/kg. The results of the study indicate that 5 min of APP jet treatment was effective in >99% reduction of MNV-1 titer without concomitant changes in meat quality.

In another study, the *in vitro* virucidal activity of radio frequency atmospheric pressure plasma jet against feline calicivirus (FCV), a surrogate of human norovirus, was demonstrated[1]. Exposure of FCV to 1.0, 1.5, 2.0, 2.5 and 3 W Ar plasma for 15 to 180 s led to gradual reductions in the FCV titer ranging from 0.33 to 2.66, 0.66 to 4.00, 0.88 to 4.66, 0.99 to 5.55 and1.11 to 5.55 $\log_{10}$ $TCID_{50}$/0.1 ml respectively. More than 99.999% of FCV was inactivated (more than 5 $\log_{10}$ $TCID_{50}$/ 0.1 ml reduction) after exposure to 2.5 and 3 W plasma for 120 s. Additionally, virucidal effects of four combinations of plasma gas mixtures (Ar, Ar plus 1% O_2, Ar plus 1% dry air and Ar plus 0.27% water) were studied. Of these, Ar plus 1% O_2 plasma treatment showed the highest virucidal effect: more than 6.0 $\log_{10}$ units of the virus after 15 s of exposure [1].

Hepatitis A and B: Hepatitis A virus (HAV) is a small, foodborne, environmentally stable, single-stranded RNA containing non-enveloped virus that causes enteric infections in humans. Atmospheric pressure plasma (APP) jets were found effective against HAV associated with fresh meats. After 5–20 min treatment with APP jets, the reduction in HAV titers (initial inoculums of 10^6 PFU) were >1 $\log_{10}$ PFU/ml in the three types of meat (beef loin, pork shoulder and chicken breast) [6].

Hepatitis B is a viral infection that attacks the liver and can cause both acute and chronic disease. Hepatitis B virus (HBV) is relatively stable in the environment and remains viable for at least 7 days on environmental surfaces at room temperature[9]. Shi et al[39] evaluated the effectiveness of low-temperature plasma (LTP) induced by dielectric barrier discharge (DBD) for HBV deactivation. LTP was used to treat HBV in the blood (serum) of hepatitis B patients with HBsAg, HBeAg and anti-HBc positive at time intervals of 10, 20, 30 and 40 s. A 100 μL of diluted HBV serum was spread evenly on cover glass for each experiment which is operated in atmospheric air with the room temperature of ~20 ◦C and the relative humidity of ~60%. They found a gradual decrease of the copy numbers of HBV DNA with the increase in plasma exposure time. After the 40-s LTP treatment, a five-order magnitude decrease in the copy number of HBV DNA, from the original 1.33×10^7 IU/ml to 0.74×10^2 IU/ml was noted.

Newcastle disease virus (NDV) and avian influenza virus (AIV): Newcastle disease (ND) in many species of birds is commonly caused by highly pathogenic NDV which can result in 100% mortality[4]. Avian influenza (AI), also called bird flu, is an infectious viral disease of birds caused by avian influenza virus (AIV). Outbreaks of high-pathogenicity AI have been reported as a threat to both humans and animals[21]. These are two of the most important pathogens in poultry. In a study, for the purpose of vaccine preparation, an alternating current (AC) atmospheric pressure non-thermal plasma (NTP) jet with $Ar/O_2/N_2$ as the operating gas was used to inactivate a Newcastle disease virus (NDV, LaSota) strain and H9N2 avian influenza virus (AIV, A/Chicken/Hebei/WD/98)[44]. The results showed that complete inactivation could be

achieved with 2 min of NTP treatment for both NDV and AIV.

Adenoviruses: Adenoviruses usually, depending on the serotype, cause mild diseases ranging from respiratory tract to gastrointestinal infections. They are double-stranded DNA viruses without envelope and are physically stable due to the protein capsid. They can tolerate deviations from neutral pH, moderate increases in heat and are relatively resistant to UVC. For disinfection, chlorine bleach or autoclaving (20 min at 121 °C at 1 bar) is used[49]. Experiments with cold atmospheric plasma (CAP) to inactivate adenovirus have been performed. A surface micro-discharge in air was used as the plasma source. Within 240 s of CAP treatment, inactivation of up to 6 decimal log levels was achieved[49]. The results indicate that the inactivation of adenovirus was achieved by a synergetic effect of all possible species produced (apart from ozone) in the non-equilibrium plasma chemistry–electrons, charged and uncharged particles, excited atoms and molecules, reactive species and UV light.

Herpes Simplex Virus: Herpes keratitis (HK) is a viral infection of the eye caused by the herpes simplex virus (HSV). HSV is the common cause of cornea-derived blindness and infection-associated blindness in developed nations. Although acyclovir and its derivatives have been successful in HK patients, the virus prevalence and emergence of acyclovir-resistant strains of herpes simplex virus (HSV) are becoming a challenge[25, 32]. Therefore, for suppressing HSV infection in the cornea, development of novel nonpharmacologic methods may be of therapeutic interest. In a study, Alekseev et al[3] have investigated the antiviral properties of liquids treated with nonthermal dielectric barrier discharge (DBD) plasma. In this study, herpes simplex virus type 1 (HSV-1) infected human corneal epithelial cells and explanted corneas were exposed to culture medium treated with nonthermal DBD plasma.

As a result, a dose-dependent reduction of viral genome replication, the cytopathic effect and the overall production of infectious viral progeny were observed. Genome replication was inhibited more than 90% at the 40-sec treatment intensity. And, no detrimental effects in explanted human corneas were reported due to the DBD plasma treatments which were confirmed by toxicity studies[3]. The study results confirmed that nonthermal DBD plasma can potentially be used to suppress corneal HSV-1 infection in vitro and ex vivo without causing pronounced toxicity.

Influenza and paramyxo viruses: Virus-induced respiratory infections are major causes of upper and lower respiratory tract infections. Influenza viruses and paramyxoviruses are the major pathogens involved in such infections. The mode of transmission is mainly airborne i.e. by direct transmission through droplets from infected cases. Systems that can control virus transmission will reduce the burden of these infections. A new process for the generation of a cold oxygen plasma (COP) by subjecting air to high-energy deep-UV light with an effective radiation spectrum between 180 nm and 270 nm has been developed by Biozone Scientific Technology. The efficiency of COP against different airborne respiratory viruses, namely respiratory syncytial virus (RSV), human parainfluenza virus type 3 (hPIV-3) and Influenza A (H5N2), was evaluated. A reduction of 6.5, 3.8 and 4 log (10) TCID50/ml of the titre of the hPIV-3, RSV and influenza virus A (H5N2) suspensions respectively was noted[42]. Therefore, it has been concluded that the COP technology is an efficient and innovative strategy to control airborne virus dissemination.

Another study showed that N_2 gas plasma generated by a high-voltage pulse using a static induction (SI) thyrister power supply effectively inactivated influenza virus[37]. In this study, influenza virus (A/PR/8/34)-infected allantoic fluid dried on a cover glass was subjected to treatment with N_2 gas plasma (1.5 kilo pulses per second; 0, 1, 5 min). Samples were collected with pure water and injected into embryonated eggs. After incubation for 48 h, no nucleoprotein of influenza virus was detected in fluid from embryonated eggs that had been treated with N_2 gas plasma for 5 min. It has been concluded that influenza virus was inactivated within 5 min of N_2 gas plasma treatment.

Bacteriophages: Antimicrobial activity of the PlasmaSol nonthermal plasma sterilizer apparatus (PlasmaSol Corporation, Hoboken, NJ, USA) against temperate λ bacteriophage C-17 (ATCC 23724-B1) and lytic bacteriophage (Rambo; Microphage) was examined by Venezia et al[43]. Exposure of the both phages at concentrations of 10^6 $PFUml^{-1}$ had resulted in at least 4–6 log_{10} reduction in viability following 10 min of exposure. The early stage inactivation of bacteriophage lambda (λ phage) in the presence of atmospheric pressure cold plasma was demonstrated by Yasuda et al[48]. In this study, a DBD device which generates typical atmospheric cold plasma was employed to treat the PET film containing λ phage particles, under neutral pH and near the room temperature. After 20 s discharge treatment, the number of infectious phages decreased quickly and 6-orders of magnitude inactivation was achieved. The time required for one log_{10} reduction of phages (*D* value) was about 3 s[48].

In another study, the inactivation effect of atmospheric-pressure cold plasma (APCP) against MS2 bacteriophages was examined. Airborne MS2 bacteriophages were exposed to APCP produced using the power levels of 20, 24 and 28 W and gas carriers [ambient air, Ar-O_2 (2%, vol/vol) and He-O_2 (2%, vol/vol)] for subsecond time intervals. The APCP treatment, wherein ambient air was used as the gas carrier at 28 W for 0.12 s, inactivated more than 95% (1.3-log reduction) of the viruses in the air[46]. However, about the same level of inactivation was achieved for waterborne MS2 viruses with an exposure time of less than 1 min when

they were directly subjected to the APCP treatment for up to 3 min.

Conclusion

All these studies clearly indicate the virucidal effect of NTPs. Researchers so far have focused on preliminary studies of inactivation of viruses using NTPs by randomly choosing clinically-important viruses. However, more systematic studies are needed to evaluate the relative susceptibility of the different groups of viruses to NTPs. The inactivation studies indicate that the degree of inactivation of a particular virus is completely dependent on the type of plasma being used, length of plasma exposure and other experimental conditions. Also, mechanism of inactivation of the same virus with two different NTPs seems to vary with the composition of plasma reactive species. As the number of studies is limited regarding the inactivation of viruses using NTPs, more studies are warranted. Future studies need to give more emphasis to proof-of-mechanism for NTPs-induced inactivation.

References

1. Aboubakr H.A., Williams P., Gangal U., Youssef M.M., El-Sohaimy S.A.A., Bruggeman P.J. and Goyal S.M., Virucidal effect of cold atmospheric gaseous plasma on feline calicivirus, a surrogate for human norovirus, *Appl. Environ. Microbiol.*, **81**, 3612–3622 **(2015)**

2. Ahlfeld B., Li Y., Boulaaba A., Binder A., Schotte U., Zimmermann J.L., Morfill G. and Klein G., Inactivation of a foodborne norovirus outbreak strain with nonthermal atmospheric pressure plasma, *MBio,* **6**, e02300–14 **(2015)**

3. Alekseev O., Donovan K., Limonnik V. and Azizkhan-Clifford J., Nonthermal dielectric barrier discharge (DBD) plasma suppresses herpes simplex virus type 1 (HSV-1) replication in corneal epithelium, *Trans. Vis. Sci. Tech.*, **3(2)**, 2 **(2014)**

4. Alexander D., Newcastle disease and other avian paramyxoviruses, *Revue. Sci. Tech.*, **19**, 443–462 **(2000)**

5. Alshraiedeh N.H., Alkawareek M.Y., Gorman S.P., Graham W.G. and Gilmore B.F., Atmospheric pressure, nonthermal plasma inactivation of MS2 bacteriophage: effect of oxygen concentration on virucidal activity, *J. Appl. Microbiol.,* **115**, 1420-1426 **(2013)**

6. Bae S.C., Park S.Y., Choe W. and Ha S.D., Inactivation of murine norovirus-1 and hepatitis A virus on fresh meats by atmospheric pressure plasma jets, *Food Res. Int.,* **76**, 342–347 **(2015)**

7. Baert L., Debevere J. and Uyttendaele M., The efficacy of preservation methods to inactivate foodborne viruses, *Int. J. Food Microbiol.,* **131**, 83–94 **(2009)**

8. Baxter C.S., Hofmann R., Templeton M.R., Brown M. and Andrews R.C., Inactivation of adenovirus types 2, 5 and 41 in drinking water by UV light, free chlorine and monochloramine, *J. Environ. Eng*., **133**, 95−103 **(2007)**

9. Bond W.W., Favero M.S., Petersen N.J., Gravelle C.R., Ebert J.W. and Maynard J.E., Survival of hepatitis B virus after drying and storage for one week, *Lancet*, **1**, 550-1 **(1981)**

10. Boudam M.K., Moisan M., Saoudi B., Popovici C., Gherardi N. and Massines F., Bacterial spore inactivation by atmospheric-pressure plasmas in the presence or absence of UV photons as obtained with the same gas mixture, *J. Phys. D: Appl. Phys.,* **39**, 3494-3507 **(2006)**

11. Cáceres V.M., Kim D.K., Bresee J.S., Horan J., Noel J.S., Ando T., Steed C.J., Weems J.J., Monroe S.S. and Gibson J.J., A viral gastroenteritis outbreak associated with person-to-person spread among hospital staff, *Infect. Cont. Hosp. Ep.,* **19**, 162-167 **(1998)**

12. Chau T.T., Kao K.C., Blank G. and Madrid F., Microwave plasmas for low temperature dry sterilization, *Biomaterials*, **17**, 1273-1277 **(1996)**

13. Chun H., Kim J., Chung K., Won M. and Song K.B., *Listeria monocytogenes*, *Salmonella enterica* serovar Typhimurium and *Campylobacter jejuni* in ready-to-eat sliced ham using UV-C irradiation, *Meat Sci.*, **83**, 599–603 **(2009)**

14. Cromeans T.L., Kahler A.M. and Hill V.R., Inactivation of adenoviruses, enteroviruses and murine norovirus in water by free chlorine and monochloramine, *Appl. Environ. Microbiol.,* **76**, 1028−1033 **(2010)**

15. Dobrynin D., Fridman G., Friedman G. and Fridman A., Physical and biological mechanisms of direct plasma interaction with living tissue, *New J. Phys.,* **11**, 115020 **(2009)**

16. Feng K., Divers E., Ma Y. and Li J., Inactivation of a human norovirus surrogate, human norovirus virus-like particles and vesicular stomatitis virus by gamma irradiation, *Appl. Environ. Microbiol.*, **77**, 3507–3517 **(2011)**

17. Fridman A., Plasma Chemistry, Cambridge University Press, New York **(2008)**

18. Hati S., Mandal S., Vij S., Minz P.S., Basu S., Khetra Y., Yadav D. and Dahiya M., Nonthermal plasma technology and its potential applications against foodborne microorganisms, *J. Food Process Pres.*, **36**, 518–524 **(2012)**

19. Herrmann H.W., Henins I., Park J. and Selwyn G.S., Decontamination of chemical and biological warfare, (CBW) agents using an atmospheric pressure plasma jet (APPJ), *Phys. Plasmas,* **6**, 2284-2289 **(1999)**

20. Hirneisen K.A., Black E.P., Cascarino J.L., Fino V.R., Hoover D.G. and Kniel K.E., Viral inactivation in foods: A review of traditional and novel food-processing technologies, *Compr. Rev. Food. Sci. F.*, **9**, 3–20 **(2010)**

21. Horimoto T. and Kawaoka Y., Influenza: lessons from past pandemics, warnings from current incidents, *Nat. Rev. Microbiol.*, **3**, 591–600 **(2005)**

22. Kelly-Wintenberg K., Montie T.C., Brickman C., Roth J.R., Carr A.K., Sorge K., Wadsworth L.C. and Tsai P.P.Y., Room temperature sterilization of surfaces and fabrics with a one

atmosphere uniform glow discharge plasma, *J. Ind. Microbiol. Biotechnol.*, **20**, 69-74 **(1998)**

23. Kong M.G., Kroesen G., Morfill G., Nosenko T., Shimizu T., van Dijk J. and Zimmermann J.L., Plasma medicine: an introductory review, *New J. Phys.*, **11**, 115012 **(2009)**

24. Kuzmichev A.I., Soloshenko I.A., Tsiolko V.V., Kryzhanovsky V.I., Bazhenov V.Y., Mikhno I.L. and Khomich V.A., Feature of sterilization by different type of atmospheric pressure discharges, 7th International Symposium on High Pressure Low Temperature Plasma Chemistry - Hakone VII, Greifswald (Germany), 402-406 **(2001)**

25. Laibson P.R., Resistant herpes simplex keratitis, *Clin. Exp. Ophthalmol.,* **38**, 227–228 **(2010)**

26. Laroussi M., Low temperature plasma-based sterilization: Overview and state-of-the-art, *Plasma Process Polym*., **2**, 391-400 **(2005)**

27. Laroussi M., Nonthermal decontamination of biological media by atmospheric pressure plasmas: Review, analysis, and prospects. *IEEE T. Plasma Sci.,* **30**, 1409-1415 **(2002)**

28. Laroussi M., Sterilization of contaminated matter with an atmospheric pressure plasma, *IEEE T. Plasma Sci.*, **24**, 1188-1191 **(1996)**

29. Mendis D.A., Rosenberg M. and Azam F., A note on the possible electrostatic disruption of bacteria, *IEEE T. Plasma Sci.,* **28**, 1304-1306 **(2000)**

30. Moreau M., Orange N. and Feuilloley M.G.J., Non-thermal plasma technologies: New tools for bio-decontamination, *Biotechnol. Adv.*, **26**, 610–617 **(2008)**

31. Morent R. and De Geyter N., Inactivation of Bacteria by Non-Thermal Plasmas, Biomedical Engineering - Frontiers and Challenges, Prof. Reza Fazel, ed., In Tech, 25-54 **(2011)**

32. Piret J. and Boivin G., Resistance of herpes simplex viruses to nucleoside analogues: mechanisms, prevalence and management, *Antimicrob. Agents Ch.,* **55**, 459–472 **(2011)**

33. Pirtle E.C. and Beran G.W., Virus survival in the environment, *Rev. Sci. Tech. Off. Int. Epiz.,* **10**, 733-748 **(1991)**

34. Richards G.P., Enteric virus contamination of foods through industrial practices: a primer on intervention strategies, *J. Ind. Microbiol. Biotechnol.,* **27**, 117–125 **(2001)**

35. Richardson J.P., Dyer F.F., Dobbs F.C., Alexeff I. and Laroussi M., On the use of the resistive barrier discharge to kill bacteria: Recent results, 27th IEEE International Conference on Plasma Science - ICOPS2000, New Orleans (USA), 109-109 **(2000)**

36. Rossi F., Kylian O., Rauscher H., Hasiwa M. and Gilliland D., Low pressure plasma discharges for the sterilization and decontamination of surfaces, *New J. Phys.*, **11**, 115017 **(2009)**

37. Sakudo A., Misawa T., Shimizu N. and Imanishi Y., N_2 gas plasma inactivates influenza virus mediated by oxidative stress, *Front. Biosci.*, **6**, 69-79 **(2014)**

38. Sakudo A., Onodera T. and Tanaka Y., Inactivation of viruses, In Sakudo A. and Shintani H., ed., Sterilization and Disinfection by Plasma, Chapter 2.4, Nova Scientific, 49-60 **(2010)**

39. Shi X.M., Zhang G.J., Wu X.L., Peng Z.Y., Zhang Z.H., Shao X.J. and Chang Z.S., Effect of low-temperature plasma on deactivation of hepatitis B virus, *IEEE T. Plasma Sci.*, **40**, 2711-2716 **(2012)**

40. Su X., Golden D.A. and D'Souza D.H., Inactivation of Human Enteric Virus Surrogates on Stainless Steel Surfaces by Non-thermal Plasma, International Association for Food Protection, Annual Meeting, Charlotte, NC **(2013)**

41. Tendero C., Tixier C., Tristant P., Desmaison J. and Leprince P., Atmospheric pressure plasmas: A review, *Spectrochim. Acta B,* **61**, 2-30 **(2006)**

42. Terrier O., Essere B., Yver M., Barthélémy M., Bouscambert-Duchamp M., Kurtz P., VanMechelen D., Morfin F., Billaud G., Ferraris O., Lina B., Rosa-Calatrava M. and Moules V., Cold oxygen plasma technology efficiency against different airborne respiratory viruses, *J. Clin. Virol.,* **45**, 119-124 **(2009)**

43. Venezia R.A., Orrico M., Houston E., Yin S.M. and Naumova Y.Y., Lethal activity of nonthermal plasma sterilization against microorganisms, *Infect. Cont. Hosp. Ep.*, **29**, 430–436 **(2008)**

44. Wang G. et al, Non-thermal plasma for inactivated-vaccine preparation, *Vaccine*, http://dx.doi.org/10.1016/j.vaccine. 2015.10.099 **(2016)**

45. Wigginton K.R., Pescon B.M., Sigstam T., Bosshard F. and Kohn T., Virus inactivation mechanisms: impact of disinfectants on virus function and structural integrity, *Environ. Sci. Technol.*, **46**, 12069–12078 **(2012)**

46. Wu Y., Liang Y., Wei K., Li W., Yao M., Zhang J. and Grinshpun S.A., MS2 virus inactivation by atmospheric-pressure cold plasma using different gas carriers and power levels, *Appl. Environ. Microbiol.*, **81**, 996-1002 **(2015)**

47. Yardimci O. and Setlow P., Plasma sterilization: opportunities and microbial assessment strategies in medical device manufacturing, *IEEE T. Plasma Sci.,* **38**, 973–981 **(2010)**

48. Yasuda H., Miura T., Kurita H., Takashima K. and Mizuno A., Biological evaluation of DNA damage in bacteriophages inactivated by atmospheric pressure cold plasma, *Plasma Process Polym.*, **7**, 301–308 **(2010)**

49. Zimmermann J.L., Dumler K., Shimizu T., Morfill G.E., Wolf A., Boxhammer V., Schlegel J., Gansbacher B. and Anton M., Effects of cold atmospheric plasmas on adenoviruses in solution, *J. Phys. D: Appl. Phys.,* **44**, 505201 **(2011)**.

(Received 29th January 2016, accepted 15th February 2016)

*****

Journal Pre-proof

Cold plasma, a new hope in the field of virus inactivation

Arijana Filipić, Ion Gutierrez-Aguirre, Gregor Primc, Miran Mozetič, David Dobnik

PII: S0167-7799(20)30108-6

DOI: https://doi.org/10.1016/j.tibtech.2020.04.003

Reference: TIBTEC 1923

To appear in: *Trends in Biotechnology*

Please cite this article as: A. Filipić, I. Gutierrez-Aguirre, G. Primc, et al., Cold plasma, a new hope in the field of virus inactivation, *Trends in Biotechnology* (2020), https://doi.org/10.1016/j.tibtech.2020.04.003

Cold plasma, a new hope in the field of virus inactivation

Arijana Filipić[1,2,*@], Ion Gutierrez-Aguirre[1], Gregor Primc[3], Miran Mozetič[3], David Dobnik[1]

[1]Department of Biotechnology and Systems Biology, National Institute of Biology, Večna pot 111, 1000 Ljubljana, Slovenia[@]

[2]Jožef Stefan International Postgraduate School, Jamova cesta 39, 1000 Ljubljana, Slovenia

[3]Department of Surface Engineering and Optoelectronics, Jožef Stefan Institute, Jamova cesta 39, 1000 Ljubljana, Slovenia[@]

*Correspondence: arijana.filipic@nib.si (A. Filipić)

[@]Twitter accounts: @ArijanaFilipic, @NIB_FITO_SI, @DepartmentF4

Keywords: Virus, virus inactivation, cold plasma, reactive oxygen and nitrogen species

Abstract

Viruses can infect all cell-based organisms, from bacteria to humans, animals, and plants. They are responsible for numerous cases of hospitalization, many deaths, and widespread crop destruction, which all result in an enormous medical, economical, and biological burden. Each of the currently used decontamination methods have important drawbacks. Cold plasma has entered this field as a novel, efficient, and clean solution for virus inactivation. Here, we present the recent developments in this promising field of cold-plasma-mediated virus inactivation, and describe the applications and mechanisms of the inactivation. This is a particularly relevant subject as viral pandemics, such as the COVID-19 pandemic, expose the need for alternative viral inactivation methods to replace, complement or upgrade existing ones.

When viruses meet plasma

Viruses are the most abundant and diverse microbes on our planet. They have inhabited the Earth for billions of years [1], so they have adapted to various environments and are now found across all ecosystems. Viruses have contributed to the evolution of life on Earth, and can be beneficial for preserving ecosystems and important natural Earth cycles, such as the carbon cycle in the sea [2]. On the other hand, pathogenic viruses cause tens to hundreds of millions of plant, animal and human infections annually, which result in high crop losses and numerous deaths (Box 1). Therefore, inactivating harmful viruses is crucial for better quality of life.

Viruses can be transmitted directly from one infected individual to another, or indirectly via contaminated intermediates, such as surfaces, objects, air, food, and water. Transmission via contaminated surfaces and aerosols has shown to be of great importance in the COVID-19 pandemic, caused by severe acute respiratory syndrome coronavirus 2 (SARS-CoV-2) [3]. Water is also becoming an increasingly important transmission route for pathogenic viruses. This has arisen from global climate change and the continued increasing water demand, combined with inefficient virus removal by traditional water treatments, and with re-use of wastewater for irrigation purposes [4,5]. Pathogenic waterborne viruses are important contributors to one of the most important global risks we are facing today, the scarcity of potable water [6]. Various inactivation methods are used to prevent viral spread in different matrices but unfortunately, the ideal method has yet to be discovered (Box 1). Thus, there is an urgent need for an environmentally friendly treatment that produces neither waste nor toxic by-products, does not use toxic chemicals, is easy and safe to work with, and is also efficient in terms of viral

inactivation. The emergence of cold plasma (CP) treatments for virus inactivation aims to provide a solution to all of these features.

Plasma is the fourth state of matter. It is a partially or fully ionized gas where the atoms and/or molecules are stripped of their outer-shell electrons (Box 2) [7]. Among its complex constituents, ultraviolet (UV) radiation and **reactive oxygen and/or nitrogen species (RONS)** (see Glossary) provide the most important antimicrobial properties [8]. UV can damage nucleic acids [9], while RONS can oxidize nucleic acids, proteins, and lipids, with different affinities that depend on the species [10]. These inherent properties of plasma, and more specifically of CP, have motivated extensive studies on the use of CP for inactivation of various pathogenic microorganisms. Here, the main target has been bacteria, with investigations across different fields, such as food production [11], medicine, and dentistry [12]. These have even extended to oncotherapy applications, where cancer cells are targeted instead of pathogenic microorganisms [13].

The scientific niche of plasma-mediated virus inactivation is a relatively young field of research (for reviews, see [14,15]), which started only about 20 years ago [16]. This is despite the decades-old knowledge that ozone that is usually synthesized from O_2 subjected to plasma conditions can inactivate viruses [17]. However, over the last few years, the number of publications in the CP-virus field has doubled, and the research has expanded from only defining the virucidal properties of plasma to describing its modes of inactivation.

This review offers a comprehensive overview of the latest progress and achievements in the CP-virus field. It also describes and discusses the modes of CP-mediated virus inactivation, and the reactive species responsible for it.

Cold plasma inactivation of viruses

Almost every study on CP inactivation of viruses is unique, as they either use a specific plasma source (e.g. **dielectric barrier discharge** [**DBD**], **plasma (micro)jet**) (Figure 1) with different characteristics (e.g. power, gas, treatment time), or they deal with the treatment of different liquid volumes (from microliters to several milliliters), matrices (e.g. water, other solutions, surfaces, cells), and viruses (surrogates of human viruses, human, animal and plant viruses). Such wide diversity makes it difficult to directly compare these studies and to define the mechanistic conclusions or any universal inactivation parameters. To simplify these complexities, we will consider here the individual types of viruses that have been subjected to CP treatments. For a complete list of the treatments published to date, please see Tables S1 and S2.

Human viruses

Enteric viruses

CP treatments have been often focused on **enteric viruses**, such as norovirus, adenovirus, and hepatitis A virus. These are the leading causes of **acute gastroenteritis**, the second most common infectious disease worldwide, which is responsible for high levels of hospitalization and deaths [18]. Working with human viruses can pose serious health hazards, thus such studies require specialized laboratories and equipment. Moreover, infectivity assessments of important enteric viruses, such as norovirus, have been limited due to a lack of cultivation methods [19]. For these reasons, these viruses are often replaced by surrogate viruses.

Animal viruses such as feline calicivirus (FCV), murine norovirus (MNV), and Tulane virus (TV) have been used as surrogates for norovirus due to their similar sizes,

morphologies and genetic material. Furthermore, these surrogate viruses are easy to culture/reproduce, and are safe to work with [19]. Opinions are divided over which of these surrogate viruses best resembles the stability of norovirus, and the final choice strongly depends on the inactivation method used and the environmental properties [13–15]. In addition to animal viruses, bacteriophages (viruses that infect bacteria), can be used as surrogates for enteric viruses, and for other human pathogens (Box 3).

Enteric viruses and their surrogates have been successfully treated in aqueous solutions [20–22] and other liquid media [23], and also on the surfaces of food [24–26], stainless-steel [25,27], and glass [28,29]. Three of these studies have reported on the comparative use of both surrogates and enteric viruses [23,25,27]. It was shown that the inactivation of a chosen surrogate virus is more efficient than that of the target enteric virus [23,27], suggesting that the effects of CP on such surrogates might not always mirror their effects on the enteric virus counterparts, and should thus be interpreted with caution.

Norovirus is one of the most, if not the most, problematic enteric virus. Its inactivation in comparison to FCV as its surrogate has been investigated using CP for diluted stool samples on a stainless-steel surface and lettuce leaves. As no infectivity assays are available to date for norovirus, the inactivation was determined using **ethidium-monoazide-coupled reverse-transcriptase quantitative real-time PCR (EMA-RT-qPCR)** [25]. A decrease of ~2.6 log units of gene copies was observed after 5 min treatment with DBD on both of these surfaces. Here, the inactivation of the surrogate FCV measured by EMA-RT-qPCR in the same medium on the stainless-steel surface was similar to that of norovirus, although the cell-culture-based infectivity assays showed complete FCV inactivation after 3 min (also

confirmed in [20]). The underestimation of FCV inactivation based on EMA-RT-qPCR in comparison with the infectivity assay might also indicate underestimation of norovirus inactivation. Since FCV and norovirus were similarly affected by the CP treatment, FCV can be considered as an appropriate surrogate. However, it still needs to be determined if this would also apply when using different treatment conditions.

FCV was inactivated by DBD plasma torch also on a glass surface [28], indicating that both this device, and the previously mentioned DBD, have a good potential to inactivate enteric viruses on the objects of various surfaces. On the other hand, the inactivation of adenovirus on a glass surface with a pulsed high-voltage source that sustains plasma at 0.5 bar was not as successful and would thus not be as suitable as DBDs for this purpose [29].

One of the most successful inactivation in liquid medium, including the work on bacteriophages (Box 3), was achieved by 15 s treatment of FCV using plasma jet [21,22]. This extremely short treatment time indicates that such plasma jet could be an important tool for enteric virus inactivation in liquids, however based on its present configuration, it would be limited to treatment of smaller objects contaminated with potentially infected droplets.

Different CP sources were also applied on the surfaces of various foods, such as blueberries [24], lettuce [25,26], and meat [30], where viruses were successfully inactivated without altering the appearance of the treated food. It was also shown that DBD could be used to treat packaged food [26], however, inactivation was not as good as in case of non-packaged food and therefore this process would require further improvements before its implementation. Application of CP in food industry

for decontamination has multiple advantages over the most widely used thermal processing of food, as it can sustain freshness and quality of food with minimal impact on the environment due to shorter treatment times and energy requirements [11]. One must be careful when using CP for treating sensitive material such as food, as despite CP is in general at room temperature at the point of application, the temperatures can rise in some cases due to the specific CP generation conditions. To prevent thermal damage during treatments of sensitive materials, the CP discharge needs to be placed far enough from the treated material [24] and/or have additional cooling provided. Another option is to use indirect treatments with plasma-activated liquids.

Respiratory viruses

Treatments of the respiratory viruses influenza A and B (for review, see [14]) and respiratory syncytial virus (RSV) [31] have only been performed with the already mentioned pulsed high-voltage CP source. RSV is the most frequent causative agent of lower respiratory tract infections in infants, and it is one of the most important viruses in pediatric medicine, particularly as it spreads easily through contact with contaminated surfaces [32]. Even though CP treatment completely inactivated RSV on a glass surface after 5 min [31], a simpler and more portable plasma configuration would be needed for efficient decontamination of hospital surfaces, while the previously described one would be practical only for decontamination of tools and smaller objects. Some respiratory viruses can also remain stable as aerosols for longer periods of time, such as SARS-CoV-2, and in order to stop their spread, it is crucial to treat the air, not just surfaces (see section Animal viruses and Box 3).

Sexually transmitted viruses

Human immunodeficiency virus (HIV) is one of the most important sexually transmitted pathogens, and one of the greatest challenges to public health in general (https://www.who.int/news-room/facts-in-pictures/detail/hiv-aids). Three shots for a total of 45 s with a plasma jet were applied to macrophages prior to their infection with HIV [33]. Upon infection, this treatment reduced the viral reverse-transcriptase activity by over two-thirds, and it impaired the other steps required for successful virus infection, without any cytotoxic effects on the macrophages. In contrast, another study reported the increasing cytotoxicity of the treated cells with the decrease of virus concentration [34].

Despite these promising results, there are some limitations for deploying such strategy in real-life scenarios, including the extraction of macrophages from the sick individual in order to treat them by CP, and their delivery back into the body. Such issues will need to be solved before CP is to be considered as an alternative HIV treatment option in the future.

Animal viruses

Three important animal pathogens have been treated by CP: avian influenza virus (AIV), Newcastle disease virus (NDV), and porcine reproductive and respiratory syndrome virus (PRRSv). All three viruses pose a significant threat to global food security and economic stability. Some strains of AIV viruses can cause up to 100% mortality in chickens (https://www.cdc.gov/flu/avianflu/influenza-a-virus-subtypes.htm), and some strains of NDV can cause up to 100% mortality in different avian species [35]. This is why prevention of their spread by vaccination is essential. Vaccines for both viruses would benefit from the improvements that would allow them to be more cost-effective, provide higher immune protection and decrease the

risks of disease development, by ensuring complete viral inactivation without affecting the antigens responsible for inducing the immune response [36,37]. For this purpose, CP was used as a possible inactivation step in vaccine preparation [35]. Complete inactivation was achieved after a 2-min treatment with a plasma jet. This was shown to be a perfect time for vaccine preparation, as longer treatment times can alter the antigen determinants responsible for immunogenicity. Both vaccines have been used to successfully induce the production of specific antibodies, and the NDV vaccine induced even higher antibody titers compared to the traditionally inactivated vaccines. Additional prevention method to stop the spread of these viruses would be decontamination of surfaces and tools that are in contact with potentially infected poultry by using CP-activated disinfection solutions. It has been shown that at specific ratios, CP- activated distilled water, 0.9% NaCl and 0.3% H_2O_2 completely inactivated viruses, and the chicken embryos attained 100% survival [38].

PRRSv is economically one of the most important pathogens in the pork industry that can be transmitted as aerosols and stay infective after travelling long distances, making it a potential threat even to distant barns [39,40]. Most commonly used methods for air treatment in general rely on either physically limiting virus transmission (such as various filters) or on lowering virus infectivity (such as UV-radiation). CP could potentially achieve both goals, stopping the viral spread and abolishing virus infectivity, by charge-driven filtration and RONS, respectively [39–41]. Aerosolized PRRSv has been treated in two studies by different DBDs [39,40]. Promising results with complete virus inactivation (~3.5 log reduction), were achieved by one DBD system [39], while the other system was only partially successful [40] and authors have suggested potential improvements that would increase inactivation efficiency. Based on these and the results on bacteriophages

(Box 3), we can conclude that CP has great potential to be used for direct air disinfection, which could also be utilized in the fight against COVID-19-like outbreaks. Nevertheless, issues such as the high ozone production (Box 3) will have to be addressed and solved before such treatment becomes a part of a regular practice.

Plant viruses

Plant viruses were the first viruses to be discovered [42]. Although most virus-to-plant transmission occurs via insects [42], the increasing re-use of untreated wastewater and the use of closed irrigation systems as an answer to water scarcity are promoting viral spread. Plant viruses can result in tremendous economic losses that have been estimated at approximately 30 billion US dollars annually [43]. Despite this, there are only two reports on their deactivation by CP treatments. Inactivation of the most important potato viral pathogen, potato virus Y (PVY), in water samples was achieved using plasma jet [7]. This water-transmissible virus [44] was successfully inactivated in polluted and clean water with treatments of only 5-min and 1-min, respectively. Other economically relevant plant viruses that are highly stable, resistant to classic inactivation methods, and water-transmissible are the members of the genus *Tobamovirus*, such as tobacco mosaic virus (TMV). Despite the inherent stability of TMV, a 10-min treatment by DBD was shown to be enough to inactivate it [45].

Since enormous quantities of water are being used for irrigation (up to 70% of global water usage), closed irrigation systems or reuse of wastewater are being increasingly utilized, enabling the spread of plant pathogens and high crop losses. Based on the results on efficient inactivation of important resilient plant viral

pathogens by CP, we believe that the use of plasma as a decontamination tool in agriculture has a high potential and deserves additional attention, especially in the upcoming global warming scenario.

Proposed mechanisms of inactivation

An understanding of the underlying mechanisms of virus inactivation by CP is crucial to be able to fine-tune CP treatments before their deployment in industrial, medical, and agricultural environments, and to more easily predict all possible outcomes, which include potential formation of undesired by-products that do not contribute to the inactivation.

Reactive species responsible for inactivation

The main consensus between the diverse studies to date is that the formation of ROS and/or RNS is the main feature of CP that contributes to viral inactivation, while UV radiation and temperature changes remain as minor contributors or have no effect at all. Different methods have been used to measure and identify the RONS (Table 1), which is a challenging task due to their short life span.

Singlet O_2 ($^1O_2$) was shown to be the most important ROS for inactivation of FCV [21,22,28] and phage T4 [46]. $^1O_2$ causes oxidative modification of histidine residues and a shift in molecular mass of methionine residues [21]. It also reacts with cysteine, tyrosine, and tryptophan, and oxidizes guanine [46]. Ozone (O_3) has been used as the main [20] or an additional inactivation factor [21,22] in FCV treatment, and it was proposed to also have roles in the inactivation of MS2 [41] and adenovirus [47]. Hydrogen peroxide (H_2O_2) has been suggested to be crucial for inactivation of RSV [31] and influenza A virus [48], but to have a secondary role in inactivation of FCV [22], PVY [7], and adenovirus [29]. RNS have been proposed as the principal

inactivation factors only in studies with FCV, where the main RNS species were ONOOH (in an acidic environment) [22,28], $ONOO^-$ [28], or NO_x [20]. Other groups have measured increases in different RONS during CP treatments [7,33,35,45,49] (Table 1), but these studies did not expand their research to determine the precise involvement of each of the RONS in virus inactivation.

In summary, RONS are the main contributors to CP-mediated virus inactivation; however, the particular reactive species that have the essential roles vary and are highly dependent on the experimental conditions, such as the gas used for the CP generation, the matrix, the virus treated and the method used for RONS determination. Increased availability and development of more accurate methods for measurement of RONS and UV intensity will enable determination of the exact CP properties that are crucial for viral inactivation. In addition to determination of the CP properties that contribute the most to viral inactivation, for a better mechanistic understanding of the inactivation process, it is also important to explore which virus component is disrupted.

Modes of virus inactivation

The viral capsid, or envelope, is the first contact point with the host, and for efficient recognition of a virus by the cell receptors, it is important that their outer structure is more or less intact. Once in the cells, the viral genome takes over the process of replication. Therefore, these two components are the most important ones for the evaluation of virus inactivation (Table 1).

Capsid protein damage and nucleic acid degradation were reported for bacteriophages T4 [46], MS2 [49] and λ [50], as well as NDV [38] and FCV [21]. In the case of the enveloped virus influenza A, in addition to capsid and nucleic acid

damage, changes in lipid components from the envelope have been reported [48]. Only in the case of bacteriophage λ [50] and FCV [21] has it been shown that the main mode of inactivation was degradation of the capsid proteins, which preceded the degradation of nucleic acids. In other studies, it was not possible to determine which degradation path contributed more to the decay in viral infectivity. The beforementioned detailed study of FCV [21] identified primary targets of the CP oxidation, which included specific amino acids in different regions of the capsid protein, and specific functional peptide residues in the capsid protein region that were responsible for virus attachment and entry into the host cell. CP treatments resulted in nucleic acid degradation for FCV [28] and PVY [7], for which protein degradation was not measured, and for adenovirus [29], RSV [31], and TMV [45], where nucleic-acid degradation was indicated as the only mode of inactivation (the viral proteins or their subunits stayed intact).

It is evident that the high oxidative power of CP derivatives can disrupt virus integrity at both the structural and genomic levels by affecting both proteins and nucleic acids. Minor disruption or conformational changes of the capsid proteins (or the lipid envelope when present) caused by RONS can result in loss of viral infectivity, due to disruption of the virus binding to the receptors on the host-cell surface. In cases where the genomic nucleic acids are damaged, viruses will no longer be infective, as an intact genetic material is needed for virus genome translation and replication. Even in cases where the damage was shown to be inflicted only to nucleic acids, it is likely that the RONS had also damaged or disrupted the outer protein layer to a certain extent, as otherwise it would not be possible for the RONS to penetrate the virus and reach the genetic material.

One of the challenges for the study of the modes of viral inactivation is the selection of the appropriate method. Methods used for determination of protein degradation are either not as sensitive as the molecular methods used to determine nucleic acid degradation, or they target only specific protein subunits, and hence can sometimes overlook other changes to the proteins. Future studies using combinations of the state-of-the-art methods to assess both types of damage will help with more accurate interpretation of how the damage occurs. These include cryo-electron microscopy, mass spectrometry, and long-read sequencing, along with methods based on nucleic acid amplification, like quantitative PCR and digital PCR.

Concluding Remarks

Diverse CP sources can completely inactivate or significantly reduce the infectivity of numerous human, animal and plant pathogenic viruses on or in various matrices (Figure 2, Key Figure). However, as indicated from various studies (Table S1), virus inactivation is highly dependent on the treatment properties, so the optimal parameters need to be chosen on a case-by-case basis.

Based on the recent developments in the CP-virus field described here, we anticipate that CP will be one of the most effective and environmentally friendly tools for inactivation of different viruses in the near future. Ultimately, its use should lead to reduced human, animal and plant infections, and along with this, lower economic and biological burdens. We believe that one of the fields of virus inactivation where plasma can represent a more significant breakthrough is water decontamination. It could inactivate problematic enteric viruses and resilient plant viruses for either human consumption and/or for agricultural purposes. In any case, it will first be necessary to evaluate the potential adverse genotoxic and cytotoxic effects of

plasma-activated water on humans and plants. Additionally, a field of CP application that may gain relevance as a response to viral outbreaks (like SARS-CoV-2), would in our opinion be CP-mediated air purification and incorporation of CP in protective masks and respirators (Box 3), which could help to palliate the sanitary burden caused by any future outbreaks. There is also potential in decontaminating small-surface objects, such as tools and food. Even with the promising initial results, using CP in medicinal treatments or vaccine preparation would still require significant research before their actual implementation.

Despite the high efficiency of virus inactivation, the exact modes of action and the plasma functionality in scaled-up systems remain largely unexplored (see Outstanding Questions), and further research needs to be focused in this direction. This insufficient knowledge of plasma/virus interaction presents the biggest obstacle in the expansion of this field. To understand this interaction, it is important to know the flux of reactive species (RONS or radiation) on the surface of the virus, the probability for the reaction of a particular type of reactive species with the virus, and any synergetic effects between different reactive species for viral deactivation. None of these parameters are currently understood completely. Another issue to be dealt with is how to scale up CP reactors without altering the composition and amount of reactive species achieved at small scale. This could be overcome by a scale-out approach, where several small-scale reactors could be used in parallel, increasing the amount of treated material but maintaining the desired plasma composition. Such an approach would also abolish the need for specialized equipment for characterizing plasma chemistry in scaled-up systems, as they would be the same as the ones already characterized at laboratory scale.

In view of environment protection, novel environmentally friendly decontamination methods are needed. We think that CP should replace current chemical decontamination practices, as it does not produce excessive waste and can efficiently inactivate viruses in or on different media and surfaces. CP usage will likely spread in different directions to help coping with upcoming global challenges, such as the scarcity of clean water and the detrimental effects of future viral epidemics or pandemics like COVID-19. CP in combination with other existing technologies could help to improve virus inactivation through synergistic effects, thus providing an ultimate decontamination tool.

Acknowledgements

This work was financially supported by the Slovenian Research Agency (research core funding No P4 – 0407, project No. L4-9325 and program for young researchers in the accordance with »agreement on (co) financing research activity in 2019« No. 1000-18-0105), Ministry of Agriculture, Forestry and Food and wastewater treatment plant JP Centralna Čistilna Naprava Domžale-Kamnik d.o.o. We want to thank Assoc. Prof. Dr. Jana Žel for her valuable input on the manuscript.

References

1 Nasir, A. and Caetano-Anollés, G. (2015) A phylogenomic data-driven exploration of viral origins and evolution. *Sci. Adv.* 1, e1500527

2 Wilhelm, S.W. and Suttle, C.A. (1999) Viruses and nutrient cycles in the sea aquatic food webs. *Bioscience* 49, 781–788

3 van Doremalen, N. *et al*. (2020) Aerosol and Surface Stability of SARS-CoV-2 as Compared with SARS-CoV-1. *N. Engl. J. Med.* DOI:10.1056/NEJMc2004973

4 Shrestha, S. *et al.* (2018) Virological quality of irrigation water sources and pepper mild mottle virus and tobacco mosaic virus as index of pathogenic virus contamination level. *Food Environ. Virol.* 10, 107–120

5 Mehle, N. and Ravnikar, M. (2012) Plant viruses in aqueous environment - Survival, water mediated transmission and detection. *Water Res.* 46, 4902–4917

6 World Economic Forum. (2020). *The Global Risks Report 2020 15th Edition. Insight Report.* Geneva.

7 Filipić, A. *et al.* (2019) Cold atmospheric plasma as a novel method for inactivation of potato virus Y in water samples. *Food Environ. Virol.* 11, 220–228

8 Guo, J. *et al.* (2015) Bactericidal effect of various non-thermal plasma agents and the influence of experimental conditions in microbial inactivation: A review. *Food Control* 50, 482–490

9 USEPA. (2006). *Ultraviolet disinfection guidance manual for the final long term 2 enhanced surface water treatment rule.* Washington, DC.

10 Mittler, R. (2017) ROS Are Good. *Trends Plant Sci.* 22, 11–19

11 Bourke, P. *et al.* (2018) The potential of cold plasma for safe and sustainable food production. *Trends Biotechnol.* 36, 615–626

12 Sakudo, A. *et al.* (2019) Disinfection and sterilization using plasma technology: fundamentals and future perspectives for biological applications. *Int. J. Mol. Sci.* 20, 5216

13 Dai, X. *et al.* (2018) The emerging role of gas plasma in oncotherapy. *Trends Biotechnol.* 36, 1183–1198

14 Puligundla, P. and Mok, C. (2016) Non-thermal plasmas (NTPs) for inactivation of viruses in abiotic environment. *Res. J. Biotechnol.* 11, 91–96

15 Weiss, M. *et al.* (2017) Virucide properties of cold atmospheric plasma for future clinical applications. *J. Med. Virol.* 89, 952–959

16 Kelly-Wintenberg, K. *et al.* (1999) Use of a one atmosphere uniform glow discharge plasma to kill a broad spectrum of microorganisms. *J. Vac. Sci. Technol. A* 17, 1539–1544

17 Burleson, G.R. *et al.* (1975) Inactivation of viruses and bacteria by ozone, with and without sonication. *Appl. Microbiol.* 29, 340–4

18 McMinn, B.R. *et al.* (2017) Bacteriophages as indicators of faecal pollution and enteric virus removal. *Lett. Appl. Microbiol.* 65, 11–26

19 Cromeans, T. *et al.* (2014) Comprehensive comparison of cultivable norovirus surrogates in response to different inactivation and disinfection treatments. *Appl. Environ. Microbiol.* 80, 5743–5751

20 Nayak, G. *et al.* (2018) Reactive species responsible for the inactivation of feline calicivirus by a two-dimensional array of integrated coaxial microhollow dielectric barrier discharges in air. *Plasma Process. Polym.* 15, 1–12

21 Aboubakr, H.A. *et al.* (2018) Cold argon-oxygen plasma species oxidize and disintegrate capsid protein of feline calicivirus. *PLoS One* 13, e0194618

22 Aboubakr, H.A. *et al.* (2016) Inactivation of virus in solution by cold atmospheric pressure plasma: identification of chemical inactivation pathways. *J. Phys. D. Appl. Phys.* 49, 1–17

23 Takamatsu, T. *et al.* (2015) Microbial inactivation in the liquid phase induced by multigas plasma jet. *PLoS One* 10, e0132381

24 Lacombe, A. *et al.* (2017) Nonthermal inactivation of norovirus surrogates on blueberries using atmospheric cold plasma. *Food Microbiol.* 63, 1–5

25 Aboubakr, H.A. *et al.* (2020) În situ inactivation of human norovirus GII.4 by cold plasma: Ethidium monoazide (EMA)-coupled RT-qPCR underestimates virus reduction and fecal material suppresses inactivation. *Food Microbiol.* 85, 103307

26 Min, S.C. *et al.* (2016) Dielectric barrier discharge atmospheric cold plasma inhibits Escherichia coli O157:H7, Salmonella, Listeria monocytogenes, and Tulane virus in Romaine lettuce. *Int. J. Food Microbiol.* 237, 114–120

27 Park, S.Y. and Ha, S. Do (2018) Assessment of cold oxygen plasma technology for the inactivation of major foodborne viruses on stainless steel. *J. Food Eng.* 223, 42–45

28 Yamashiro, R. *et al.* (2018) Key role of singlet oxygen and peroxynitrite in viral RNA damage during virucidal effect of plasma torch on feline calicivirus. *Sci. Rep.* 8, 17947

29 Sakudo, A. *et al.* (2016) Nitrogen gas plasma generated by a static induction thyristor as a pulsed power supply inactivates adenovirus. *PLoS One* 11, e0157922

30 Bae, S.C. *et al*. (2015) Inactivation of murine norovirus-1 and hepatitis A virus on fresh meats by atmospheric pressure plasma jets. *Food Res. Int*. 76, 342–347

31 Sakudo, A. *et al.* (2017) Crucial roles of reactive chemical species in modification of respiratory syncytial virus by nitrogen gas plasma. *Mater. Sci. Eng. C* 74, 131–136

32 Toivonen, L. *et al.* (2019) Respiratory syncytial virus infections in children 0–24 months of age in the community. *J. Infect* 80, 69-75

33 Volotskova, O. *et al.* (2016) Cold atmospheric plasma inhibits HIV-1 replication in macrophages by targeting both the virus and the cells. *PLoS One* 11, e0165322

34 Amiran, M.R. *et al.* (2016) In vitro assessment of antiviral activity of cold atmospheric pressure plasma jet against the human immunodeficiency virus (HIV). *J Med Microbiol Infec Dis* 4, 62–67

35 Wang, G. *et al.* (2016) Non-thermal plasma for inactivated-vaccine preparation. *Vaccine* 34, 1126–1132

36 Dimitrov, K.M. *et al*. (2017) Newcastle disease vaccines—A solved problem or a continuous challenge? *Vet. Microbiol.* 206, 126–136

37 Jang, H. *et al*. (2018) Efficacy and synergy of live-attenuated and inactivated influenza vaccines in young chickens. *PLoS One* 13, e0195285

38 Su, X. *et al.* (2018) Inactivation efficacy of nonthermal plasma-activated solutions against Newcastle disease virus. *Appl. Environ. Microbiol.* 84, e02836-17

39 Nayak, G. *et al.* (2020) Rapid inactivation of airborne porcine reproductive and respiratory syndrome virus using an atmospheric pressure air plasma. *Plasma Process. Polym*. DOI: 10.1002/ppap.201900269

40 Xia, T. *et al.* (2020) Inactivation of airborne porcine reproductive and respiratory syndrome virus (PRRSv) by a packed bed dielectric barrier discharge non-thermal plasma. *J. Hazard. Mater*. 393, 122266

41 Xia, T. *et al.* (2019) Inactivation of airborne viruses using a packed bed non-thermal plasma reactor. J. Phys. D. Appl. Phys. 52, 255201

42 Lefeuvre, P. *et al.* (2019) Evolution and ecology of plant viruses. *Nat. Rev. Microbiol.* 17, 632-644

43 Nicaise, V. (2014) Crop immunity against viruses: Outcomes and future challenges. *Front. Plant Sci.* 5, 1–18

44 Mehle, N. *et al.* (2014) Survival and transmission of potato virus Y, pepino mosaic virus, and potato spindle tuber viroid in water. *Appl. Environ. Microbiol.* 80, 1455–1462

45 Hanbal, S.E. *et al.* (2018) Atmospheric - pressure plasma irradiation can disrupt tobacco mosaic virus particles and RNAs to inactivate their infectivity. *Arch. Virol.* 163, 2835–2840

46 Guo, L. *et al.* (2018) Mechanism of virus inactivation by cold atmospheric-pressure plasma and plasma-activated water. *Appl. Environ. Microbiol.* 84, 1–10

47 Zimmermann, J.L. *et al.* (2011) Effects of cold atmospheric plasmas on adenoviruses in solution. *J. Phys. D. Appl. Phys.* 44, 505201

48 Sakudo, A. *et al.* (2014) N2 gas plasma inactivates influenza virus mediated by oxidative stress. *Front. Biosci.* 6, 69–79

49 Wu, Y. *et al.* (2015) MS2 virus inactivation by atmospheric-pressure cold plasma using different gas carriers and power levels. *Appl. Environ. Microbiol.* 81, 996–1002

50 Yasuda, H. *et al.* (2010) Biological evaluation of DNA damage in bacteriophages inactivated by atmospheric pressure cold plasma. *Plasma Process. Polym.* 7, 301–308

51 Koonin, E. V. and Starokadomskyy, P. (2016) Are viruses alive? The replicator paradigm sheds decisive light on an old but misguided question.

Stud. Hist. Philos. Sci. Part C Stud. Hist. Philos. Biol. Biomed. Sci. 59, 125–134

52 Roossinck, M.J. and Baz, E.R. (2017) Symbiosis: Viruses as Intimate Partners. *Annu. Rev. Virol.* 4, 123-139

53 Milone, M.C. and O'Doherty, U. (2018) Clinical use of lentiviral vectors. *Leukemia* 32, 1529–1541

54 Wang, D. *et al.* (2019) Adeno-associated virus vector as a platform for gene therapy delivery. *Nat. Rev. Drug Discov.* 18, 358–378

55 Mehle, N. *et al.* (2018) Water-Mediated Transmission of Plant, Animal, and Human Viruses. In *Advences in virus research* (Malmstrom, C. M., ed), pp. 85–128, Academic Press

56 Staggemeier, R. *et al.* (2015) Animal and human enteric viruses in water and sediment samples from dairy farms. *Agric. Water Manag.* 152, 135–141

57 Zhang, T. *et al.* (2006) RNA viral community in human feces: Prevalence of plant pathogenic viruses. *PLoS Biol.* 4, 0108–0118

58 Lyon, B.A. *et al.* (2014) Integrated chemical and toxicological investigation of UV-chlorine/ chloramine drinking water treatment. *Environ. Sci. Technol.* 48, 6743–6753

59 Machala, Z. and Pavlovich, M.J. (2018) A New Phase in Applied Biology. *Trends Biotechnol*. 36, 577–578

60 Mozetič, M. *et al.* (2019) Introduction to Plasma and Plasma Diagnostics. In *Non-thermal plasma technology for polymeric materials: applications in composites, nanostructured materials and biomedical fields* (Thomas, S., Mozetic M., Cvelbar U., Spatenka P., Praveen K.M., eds), pp. 23-65, Elsevier

61 Ehlbeck, J. *et al.* (2011) Low temperature atmospheric pressure plasma sources for microbial decontamination. *J. Phys. D. Appl. Phys*. 44, 013002

62 Bruggeman, P.J. *et al.* (2016) Plasma–liquid interactions: a review and roadmap. *Plasma Sources Sci. Technol*. 25, 053002

63 Labay, C. *et al*. (2019) Production of reactive species in alginate hydrogels for cold atmospheric plasma-based therapies. *Sci. Rep.* 9, 1–12

64 McMinn, B.R. *et al.* (2017) Bacteriophages as indicators of faecal pollution and enteric virus removal. *Lett. Appl. Microbiol.* 65, 11–26

65 Machala, Z. *et al.* (2019) Chemical and antibacterial effects of plasma activated water: correlation with gaseous and aqueous reactive oxygen and

nitrogen species, plasma sources and air flow conditions. *J. Phys. D. Appl. Phys.* 52, 034002

66 Alekseev, O. *et al.* (2014) Nonthermal dielectric barrier discharge (DBD) plasma suppresses herpes simplex virus type 1 (HSV-1) replication in corneal epithelium. *Transl. Vis. Sci. Technol.* 3, 2

67 Jakober, C. and Phillips, T (California Environmental Protection Agency, Air Resources Board). (2008) *Evaluation of ozone emissions from portable indoor air cleaners: electrostatic precipitators and ionizers.* Sacramento, CA

Figure legends

Figure 1: Examples of the most used plasma sources for virus inactivation in different matrices. These include some different types of (micro)jets **(a)** and dielectric barrier discharges **(b)**, and various matrices that have been inoculated with viruses and treated using cold plasma (**c**: left to right: meat, blueberries, lettuce, glass, stainless steel, water, buffer or other liquid medium, air, cells).

Figure 2, Key Figure: Inactivation of viruses using cold plasma. (a) Morphologically different viruses under treatment with cold plasma. **(b)** Close-up of the cold-plasma properties that are responsible for viral inactivation. The most essential particles in virus inactivation are reactive oxygen and/or nitrogen species (RONS), although UV radiation and charged particles (e.g. ions, electrons) can also have some role. Molecules in the ground state are neutral and do not have any effects on virus inactivation. Cold plasma can target both the viral proteins and their nucleic acids (or even the virus envelope, when present). **(c)** After the cold-plasma treatment, the virus particles and nucleic acids are partially or completely degraded to non-infective particles that cannot cause any harm to their hosts.

Table 1. Mechanisms of viral inactivation by plasma.

Virus	Reactive oxygen and/or nitrogen species involved in	Mode of virus inactivation		Methods for identification of virus inactivation		Methods used for cold-plasma characterization[b]	Ref.
		Protein	DNA/RNA	Protein degradat	DNA/RNA		

	inactivation[a]	degradation	Aggregation	ion	degradation		
Bacteriophage							
λ	NA	Yes	Yes	SDS-PAGE alone, or in combination with *in-vitro* packaging	Agarose gel electrophoresis alone, or in combination with *in-vitro* packaging	Optical emission spectroscopy	[50]
MS2[c]	↑O	Yes	Yes	SDS-PAGE	RT-PCR, agarose gel electrophoresis	Optical emission spectroscopy	[49]
MS2	O_3[f]	NA	No	Not measured	RT-qPCR	Ozone sensor	[41]
T4	$^1O_2$[g]	Yes	Yes	SDS-PAGE	Agarose gel	H_2O_2/peroxidase assay kit,	[4

					electrophoresis	nitrite/nitrate colorimetric assay kit, electron spin resonance	6]
Animal surrogate of enteric virus							
FCV[d]	$^1O_2$ or ONOOH (in acidic conditions)[g], O_3[h], H_2O_2, NO_2^-[f].	Yes	NA	SDS-PAGE, LC-MS/MS	Not measured	Colorimetric assay with titanium sulfate, Griess assay, LC/MS equipped with electrospray ionization ion source, fluorescence probe, spectrophotometry	[22]
FCV	$^1O_2$ and $ONOO^-$ or ONOOH (acidic conditions)[g]	NA	Yes	Not measured	RT-qPCR	Optical emission spectroscopy, UV test strips, Griess assay, H_2O_2 test strips	[28]
FCV	$^1O_2$[g], O_3[h]	Yes	Yes	EMA-RT-qPCR, EMA-RT-PCR, SDS-PAGE	RT-PCR, RT-qPCR, sequencing	Indirect measurements with LC-MS/MS	[21]
FCV	NO_x, O_3[g]	NA	NA	Not measured	Not measured	UV light meter, UV absorption spectroscopy, Griess	[20]

						assay	]
Human virus							
Adenovirus	H_2O_2[f]	No	Yes	Immuno-chromatography and Western blotting	PCR, qPCR	H_2O_2, nitrite and nitrate test strips	[29]
Adenovirus	O_3[f]	NA	NA	Not measured	Not measured	Optical spectrometer, UV-Power meter, photometric ozone analyzer	[47]
Influenza A and B virus[e]	H_2O_2[g]	Yes	Yes	Hemagglutination assays, ELISA, Western blotting	RT-qPCR	Chemical indicator strips, multichannel spectrophotometer, gas detector	[48]
RSV	H_2O_2[g]	No	Yes	Immunochromatography kits	RT-PCR, RT-qPCR	Active O_2 test strips	[31]
HIV	↑O_2^+, O, NO, N_2 (second positive), N_2^+	NA	Yes	Not measured	qPCR	Optical emission spectroscopy	[33]
Animal virus							

NDV	↑Oxidation/ reduction potential, H_2O_2, $OH^{\cdot}$, $NO^{\cdot}$	Yes	Yes	Bradford protein assay kits	Agilent 2100 bioanalyzer	Oxidation/reduction potential probe, H_2O_2 assay kit, electrical conductivity meter, electron spin resonance	[38]
NDV, AIV	↑Oxidation/ reduction potential, O, NO, OH	NA	NA	Not measured	Not measured	Oxidation/reduction potential probe, optical emission spectroscopy	[35]
Plant virus							
TMV	↑H_2O_2, NO_3^-, HNO_2, N_2O_2, NO_2^-	No	Yes	Western blotting	RT-PCR	Optical absorption spectroscopy, chemical probe	[45]
PVY	H_2O_2[f]. ↑OH, O	NA	Yes	Not measured	RT-PCR	Optical emission spectroscopy, H_2O_2 test strips	[7]

[a] ↑: In case where the increase of reactive oxygen and/or nitrogen species was only measured but their importance in inactivation was not determined

[b] Measurements of pH and temperature are excluded as are scavenger experiments and other methods used for indirect identification of RONS

[c] Methods to determine modes of viral inactivation were applied only for treated solutions

[d] Methods to determine modes of viral inactivation were applied only for plasma ignited in 99% Ar and 1% O_2

[e] The only group that noticed degradation of viral envelope using Fourier-Transform InfraRed (FT-IR) spectrophotometer. ELISA was done only for Influenza B, Western blotting, RT-qPCR, hemagglutination and FT-IR only for Influenza A

[f] Some role in the inactivation, it is not defined how important it is

[g] The main role in the inactivation

[h] Very important but does not have the main role in the inactivationAbbreviations: ELISA, enzyme-linked immunosorbent assay; EMA, ethidium monoazide; LC-MS, liquid chromatography-mass spectrometry; MS/MS, tandem mass spectrometry; NA, not applicable; PCR, polymerase chain reaction; RT-PCR, Reverse transcription PCR; RT-qPCR, Reverse transcription real-time PCR; SDS-PAGE, sodium dodecyl sulfate-polyacrylamide gel electrophoresis

Box 1. Viruses and methods for their disinfection.

Viruses are microscopic agents that can infect all existing forms of cellular life. Their classification as living organisms has historically been a question of interesting, almost philosophical debate, but what it is definitely unquestionable is that they are one of the most powerful engines of evolution on the planet [51]. Most viruses are not harmful, and some of them are even beneficial for their hosts [52]. In recent years, viruses have been increasingly used towards human wellbeing. For example, lentiviruses [53] and adeno-associated viruses [54] are being genetically engineered to formulate state-of-the-art gene therapies. Nevertheless, viruses have a bad reputation as causative agents of various human, animal and plant diseases. This is no surprise, as they were the main players in numerous epidemics and pandemics throughout history (https://www.who.int/emergencies/diseases/managing-epidemics/en/). Several viral agents have contributed to the well-deserved ‘biohazard’ fame of viruses, including influenza, Ebola, HIV and coronavirus SARS-

CoV-2 that causes COVID-19 disease. Despite not being such ‘viral celebrities’, waterborne viruses pose increasingly serious health and economic burdens in the present era that is threatened by climate change and scarcity of potable water.

Different physical and chemical treatments have been traditionally applied for inactivation of viruses. Chlorine, alcohols, acids, alkalis, and bleach are examples of chemical disinfectants, while UV radiation, filtration, pressure and temperature are among the physical ones [55]. The method of choice depends greatly on the matrix to be disinfected and on the virus targeted for inactivation. Waterborne viruses, including enteric viruses [56] and plant tobamoviruses [57], are among the most stable of the viruses. To inactivate such stable viruses in such a delicate matrix, the disinfection method needs to be strong enough to inactivate the virus, and at the same time it needs to be non-toxic to maintain the quality and properties of the water. It is now known that chlorination, a traditionally used method for water disinfection, is not efficient enough for inactivation of certain viruses, and in the long term, it can pose a risk to human health due to release of toxic by-products [58]. In more recent years, novel waterborne viral inactivation technologies have been developed, such as membrane filtration, reverse osmosis, UV and ozone treatments, and hydrodynamic cavitation, each of which has their own pros and cons. The frequent disadvantages of these technologies are cost inefficiency, scalability problems, and unsustainable power usage. Laboratory scale studies suggest that cold plasma has the potential to overcome these problems, but actual confirmation will only arrive with studies focused on pilot or industrial scale deployment of plasma-based disinfection devices.

Box 2. Let's talk about plasma

Plasma is the most abundant state of matter in the visible universe, as it comprises 99% of it. The sun and other stars, nebulae, solar winds, lightning, and aurora borealis are all in plasma state. Plasma TVs, neon and fluorescent lights are the best-known man-made uses of plasma. Generally, plasma contains free electrons, atoms, and molecules in neutral, ionized and/or excited states (including reactive oxygen and nitrogen species). Plasma of many gases represents an extensive source of ultraviolet and vacuum ultraviolet radiation [59]. The possibility to use a particular or a combination of constituents makes plasma a unique material-treatment technique.

On a rough scale, plasma can be divided into thermal or equilibrium plasma, where all particles have roughly the same temperature (average kinetic energy of random motion), and non-thermal, non-equilibrium, or cold plasma, where light electrons have much higher temperatures compared to heavy atoms and molecules, which often remain close to room temperature. In other words, cold plasma is at the point of application at room temperature, and as such, it is suitable for treating any biological material, be it solid, liquid, or an aerosol. Cold plasma can be further classified into low pressure and atmospheric pressure. The latter is limited to the volume where there are large electric fields, while low-pressure plasma spreads in a large volume [60]. Cold plasma is usually sustained with an electrical discharge. The gas temperature usually remains almost unaffected, but the chemical reactivity is huge comparing to the source gas due to the presence of reactive species. In most cases of virus inactivation, the atmospheric-pressure plasma has been used, for practical considerations (for more information on various plasma sources used in microbial decontamination, see [61]).

Plasmas are used in various industries, mainly for tailoring surfaces of solids (e.g. oxidation, cleaning, nanostructuring, binding different atom/ molecule groups), including destruction of microorganisms such as viruses. Plasma can also be used for treatment of liquids, however, inactivation of viruses in liquid media is much more challenging, compared to surfaces, as plasma cannot be sustained in liquids, but only in gaseous bubbles inside the liquid or above the liquid surface. Depending on the place of their generation, RONS interact with either the surface of bubbles or the surface of liquid, where many dissolve. They can then diffuse within the liquid, and might eventually interact with the virus. Furthermore, UV radiation penetrates liquids with a penetration depth that depends enormously on the wavelength, and the concentration and type of impurities [62]. There are various techniques for measuring both long- and short-lived RONS in liquids [63], but they are not used frequently by authors working on the destruction of viruses. Many authors state the discharge parameters (voltage, current, power) rather than plasma parameters (concentration of reactive species), which are necessary to compare various plasma sources. The plasma-virus scientific niche is therefore in its infancy at present.

Box 3. Bacteriophages as surrogates and an alternative cold plasma treatment

Bacteriophages are the first choice in many studies to establish proof of concept for virus inactivation methods, due to their many advantages. They are relatively inexpensive to culture/produce, easy and safe to work with, they can be produced in large quantities, and plaque-based infectivity assays are time efficient [64]. However, care must be taken when interpreting the results, as they might not always correlate with the response of the actual virus to the inactivation method.

The very first study that triggered the expansion of the plasma-virus field was conducted on bacteriophages [16]. In recent years, bacteriophages have been used to test the use of CP for air purification [41,49], and to study CP effects on waterborne viral pathogens [46,49].

Bacteriophages have been successfully inactivated in water, where almost complete inactivation of MS2 was obtained after 3 min using a plasma microjet [49]. Waterborne MS2, T4 and ⌽174 were treated directly with surface DBD or indirectly with CP-activated water [46]. All three of these phages were successfully inactivated with both of these treatments, but with shorter treatment times needed for inactivation of ⌽174 and MS2, compared to T4 (Table S1). In general, CP-activated liquids are gaining a lot of attention [65], as they can be produced in more controlled ways compared to direct CP treatments. Such a strategy is likely to be a better choice when working with irregular and very sensitive samples, as CP-activated liquids can be applied evenly and can reduce potentially unwanted mechanical changes in a treated material [66].

Airborne human viral pathogens pose a serious threat to human health. In two studies, aerosolized MS2 bacteriophages were successfully inactivated by CP after

only 0.12 s [49] or 0.25 s [41] of contact time of the aerosol with the plasma. Although these are very promising results, one of the biggest concerns when using plasma for air purification is the production of ozone, as it can be hazardous at high concentrations. Every future application of plasma should consider this, and thus aim to lower ozone concentrations below the recommended limit [67]. Another plasma-based alternative to protect against aerosolized pathogenic viruses would be using a protective mask equipped with a miniature plasma source. Such a mask would have the potential to stop the spread of various viruses, like SARS-CoV-2, that are transmitted by droplets, as droplets are ideal for dissolution of radicals due to the large surface-to-volume ratio. Here, the problem again arises from the fact that the radicals like ozone and nitric oxides would be inhaled so a mask would have to include a radical catalyzer, or even better, a two-membrane mask, where the first plasma membrane would inactivate the virus, while the second membrane would serve as a catalyzer for unhealthy plasma created species. We believe that such innovative mask configuration could be highly beneficial in future outbreaks.

Glossary

Acute gastroenteritis: Inflammation of the gastrointestinal tract that is mainly caused by viruses, especially rotavirus and norovirus. The most common symptoms are vomiting, diarrhea, and abdominal pain.

Dielectric barrier discharge (DBD): Plasma is created when the processing gas is guided between an insulator with electrodes on the opposite side.

Ethidium-monoazide-coupled reverse-transcriptase qPCR (EMA-RT-qPCR): This method combines the nucleic acid intercalating dye that polymerizes nucleic acid upon exposure to light (ethidium monoazide), which prevents the targeted part of the genome from PCR amplification. As a result, the EMA-RT-qPCR method should only detect infectious viruses with an intact capsid after treatment. This has been proposed to be used instead of infectivity assays.

Enteric viruses: A very diverse group of human viruses that are most commonly transmitted via the fecal-oral route (including contaminated food and water), including norovirus, rotavirus, hepatitis A, sapovirus, astrovirus and adenovirus. They infect the gastrointestinal tract, where they replicate and are then excreted in high concentrations. They can cause illness at low doses, and they can survive in the environment for long periods of time, as they are resistant to physiological changes like pH and temperature.

Polymerase chain reaction (PCR): A method frequently used in molecular biology for amplification of targeted parts of nucleic acids. Different versions of PCR can be used qualitatively and/or quantitively. The most often quantitative methods used are real-time PCR (qPCR) and the more advanced version, digital PCR (dPCR).

Plasma (micro)jet: Plasma is created by blowing a gas next to or through an electrode.

Plaque-forming units (PFUs): A measure of the number of viral particles that form plaques in a certain volume of a sample under examination.

Reactive oxygen and nitrogen species (RONS): ROS (e.g. O_3, O, O_2*, H_2O_2, $OH^{\cdot}$, $^1O_2$) are partially reduced or excited forms of oxygen, and RNS (e.g. N, N_2*, NO, NO_2, NO_2^-, NO_3^-, $ONOO^-$, ONOOH) are the most common nitrogen- and nitric-

oxide-derived compounds. RONS have crucial and versatile roles in the maintenance of normal functions of different cells in most organisms.

Virus inactivation: To decrease the infection of a host by a virus. The most reliable method to determine the inactivation efficiency is an infectivity assay, in which appropriate hosts (e.g. bacterial or eukaryotic cells, plants, chicken embryos) are inoculated with a virus. The inoculation is followed by the observation/ measurement of different factors, such as the formation of plaques, cytopathic effects and symptoms in plants, survival of the embryos or the integrity of viral nucleic acids.

Outstanding questions

1. What cold plasma source conditions will enable optimal efficiency of targeted virus inactivation in terms of the required treatment times and energy consumption?
2. Which reactive oxygen and/or nitrogen species are the most relevant for inactivation of a given virus in a given matrix, how to optimize production of such relevant RONS, and which methods should be used for their accurate determination?
3. Does ultraviolet radiation have a synergetic effect with reactive oxygen and/or nitrogen species in virus inactivation?
4. What are the main viral components that are affected by different cold plasma-mediated virus inactivation strategies, and which viral characterization methods should be used in each experiment to get a precise answer? Should a standardized protocol be developed for this purpose?
5. What is the scale-up potential of cold-plasma treatments?
6. Can cold plasma cause cytotoxic or genotoxic damage when used for virus inactivation in specific matrices that will come in contact with human, plant, and animal tissues?
7. Would the combination of cold plasma with already established methods, such as chlorine treatment, or some new environmentally friendly methods such as cavitation, have a synergistic effect on the virus inactivation? Would such synergy contribute to shorter treatment times, lower energy consumption and decreased environmental burden?

Highlights

- Pathogenic viruses are becoming an increasing burden for health, agriculture and the global economy. Classic disinfection methods have some downsides, so innovative solutions for virus inactivation are urgently needed.
- Cold plasma can be used as an environmentally friendly tool for virus inactivation. It can inactivate different human, animal, and plant viruses in various matrices.
- When using cold plasma for virus inactivation it is important to set up the right parameters and to choose treatment durations that allow particles to interact with the contaminated material.
- Reactive oxygen and/or nitrogen species have been shown to be responsible for virus inactivation through effects on capsid proteins and/or nucleic acids. Development of more accurate methods will provide information on which plasma particles are crucial in each experiment, and how exactly do they affect viruses.

Journal of Hazardous Materials 393 (2020) 122266

Contents lists available at ScienceDirect

Journal of Hazardous Materials

journal homepage: www.elsevier.com/locate/jhazmat

Inactivation of airborne porcine reproductive and respiratory syndrome virus (PRRSv) by a packed bed dielectric barrier discharge non-thermal plasma

T. Xia[a,*], M. Yang[b], I. Marabella[c], E.M. Lee[d], B. Olson[c], D. Zarling[c], M. Torremorell[b], H.L. Clack[a]

[a] Civil and Environmental Engineering, University of Michigan, Ann Arbor, MI, United States
[b] Veterinary Population Medicine, University of Minnesota, St. Paul, MN, United States
[c] Mechanical Engineering, University of Minnesota, Minneapolis, MN, United States
[d] Mechanical, Materials and Aerospace Engineering, Illinois Institute of Technology, Chicago, IL, United States

GRAPHICAL ABSTRACT

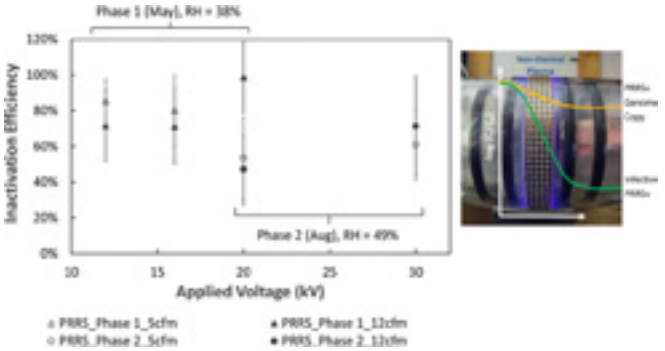

ARTICLE INFO

Keywords:
Non-thermal plasma
Airstream inactivation
PRRSv
$TCID_{50}$
qPCR

ABSTRACT

Porcine reproductive and respiratory syndrome virus (PRRSv) is one of the most significant airborne viruses impacting the pork industry in the US. Non-thermal plasmas (NTPs) are electrical discharges comprised of reactive radicals and excited species that inactivate viruses and bacteria. Our previous experiments using a packed bed NTP reactor demonstrated effective inactivation of bacteriophage MS2 as a function of applied voltage and power. The present study examined the effectiveness of the same reactor in inactivating aerosolized PRRSv. A PRRSv solution containing $\sim 10^5$ $TCID_{50}$/ml of PRRSv VR2332 strain was aerosolized at 3 ml/min by an air-jet nebulizer and introduced into 5 or 12 cfm air flow followed by NTP exposure in the reactor. Twin impingers upstream and downstream of the reactor collected samples of the virus-laden air flow for subsequent $TCID_{50}$ assay and qPCR analyses. An optical particle sizer measured upstream and downstream aerosol size distributions, giving estimates of aerosol filtration by the reactor. The results showed that PRRSv was inactivated to a similar degree as MS2 at the same conditions, with the maximum 1.3-log inactivation of PRRSv achieved at 20 kV and 12 cfm air flow rate. The results demonstrate the potential of properly optimized NTPs in controlling PRRSv transmission.

* Corresponding author at: M6075 SPH II, 1415 Washington Heights, Ann Arbor, MI, 48109, United States.
E-mail address: xiatian@umich.edu (T. Xia).

https://doi.org/10.1016/j.jhazmat.2020.122266
Received 13 October 2019; Received in revised form 4 February 2020; Accepted 8 February 2020
Available online 10 February 2020
0304-3894/

1. Introduction

Airborne transmission of livestock or zoonotic diseases such as Newcastle disease, avian influenza, foot-and-mouth disease, and porcine reproductive and respiratory syndrome (PRRS), just to name a few, greatly threaten global food security, agricultural industry and public health by causing significant losses in production, high mortality, decrease in productivity, stoppage of exports, etc.. This is particularly significant in the face of ongoing climate change, especially for pathogens whose efficiency of airborne transmission through the atmosphere may change in counterintuitive ways. In addition, animals can experience a greater degree of exposure to ambient atmospheric conditions or unconditioned outdoor air compared to humans. Foot and mouth disease is considered as the top foreign animal disease threat to US agriculture (Colby, 2013), and the 2014–2015 outbreak of highly pathogenic avian influenza in the US caused an average of 50,000 bird losses per operation for turkeys and over 1 million bird losses per operation for table-egg laying chickens where the disease was confirmed (Ramos et al., 2017).

In the case of the pork industry, porcine reproductive and respiratory syndrome virus (PRRSv), an enveloped virus that appeared in the US in the 1980s (Keffaber, 1989), has drawn increasing research attention due to its significant impact on pork production and ability to be transmitted in air over kilometers. It was estimated that in 2011 the outbreaks of PRRSv in the US national breeding- and growing-pig herd overall cost $664 million annually due to productivity losses, 45 % of which occurred in the breeding herd (Holtkamp et al., 2013). Outbreaks of PRRSv in China caused great economic losses and gained public concern due to the emergence of highly pathogenic strains. In 2006, a highly pathogenic PRRSv disease outbreak emerged in China, with its clinical signs being prolonged high fever, red discoloration of the body, and blue ears associated with high mortality of infected pigs. It quickly spread to 12 provinces and significantly impacted the country's pork industry (Tian et al., 2007). In 2014, another novel NADC30-like strain of PRRSv emerged in China (Zhou et al., 2015), which was virulent to pigs but is less pathogenic than the highly virulent PRRSv discovered in 2006 (Sun et al., 2016). Since late 1990s, research has shown that PRRSv can survive in aerosols and be transmitted through airborne pathways. PRRSv can be released in aerosols from infected pig barns and has been found in aerosols generated when swine manure collection tanks are pumped out (Millerick-May et al., 2016). Once released, the virus can be transmitted in ambient air over several kilometers (up to 9.1 km as reported) from the source (Otake et al., 2010) and can potentially cause outbreaks in distant barns. The airborne transmission of PRRSv can be affected by many environmental factors, such as aerosol concentration, aerosol size distribution, ambient temperature, relative humidity (RH), and solar radiation. It is reported that PRRSv can survive longer in aerosols at lower ambient temperature and lower relatively humidity (Hermann et al., 2007). Open-air factors with unidentified chemical nature (Hood, 2009) may also have adverse effects to the survival of viruses in aerosols. In 2019, Arruda et al. gave a detailed and comprehensive literature review on the previous research projects, findings and current knowledge gaps of PRRSv aerosols and airborne PRRSv transmission (Arruda et al., 2019).

The most commonly applied technologies to control airborne pathogens in both human-occupied buildings and animal confinements are the collection of bioaerosols on filters, such as HEPA, MERV 14 and MERV 16 filters, and UV germicidal irradiation (UVGI). HEPA filtration has been proven to be very effective in removal of bioaerosols from airstreams. (Farnsworth et al. (2006)) reported 96.5 ± 1.5 % bacterial collection efficiency of B. subtilis by HEPA filtration. The study also examined HEPA filtration of three virus species, and reported no viable virus recovered from the downstream sampler. A study by (Dee (2011)) found that new PRRSv outbreaks were recorded at 20 % of farms with ventilation air filters installed as compared to 92 % of farms without such filters in the control group. The use of HEPA filters comes with several limitations, including high filter replacement costs; high pressure drops, and the associated increase in energy consumption of the HVAC system to maintain desired ventilation rate. In the case of agricultural buildings, there are also high reconstruction costs to achieve an air-tight building envelope and eliminate potential air infiltration (Pitkin et al., 2009a). Lastly, collection of bioaerosols on HEPA filters does not actually inactivate the pathogens, with the possibility of re-emitting more environmentally resilient pathogens into the ambient air during filter replacement and disposal processes (Miaskiewicz-Peska and Lebkowska, 2012). Effective UVGI disinfection requires a sufficiently high light intensity, achieved through a combination of a number of bulbs and exposure time in a carefully designed ventilation system. UV inactivation efficiency is also to some degree influenced by the susceptibility of the pathogen (Bolashikov and Melikov, 2009). UVGI has been shown to diminish the transmission of Mycobacterium tuberculosis from patients occupying hospital wards to guinea pigs raised in an exposure chamber (Riley, 1961), and prevent the spread of rubella within army barracks (Wheeler et al., 1945). The application of UVGI in indoor air disinfection is limited by the need to avoid the adverse health effects of UV on humans and livestock. In the indoor environment, UV lights can be installed in the upper regions of the room near the ceiling to avoid exposing the occupants to UV light. The process, however, is passive in nature and can only inactivate pathogens transported by upward air currents into the UVGI treatment zone. In many cases, UV radiation alone is not effective enough in instantaneous air disinfection, and is often applied in conjunction with HEPA filters: airborne pathogens are collected on filter surfaces and inactivated by UV radiation (Memarzadeh et al., 2010). However, UV light is unable to penetrate deeply into HEPA filters, where collected pathogens may survive and re-enter the air flow. The energy consumption of the UV system is also significant, and broken bulbs should be detected and replaced periodically. In all, of the two defining characteristics of infectious aerosols - transport and infectivity (Pitkin et al., 2009b) - particulate filters only address transport and UVGI mainly addresses infectivity. Non-thermal plasmas (NTPs) address both characteristics by 1) electrostatic removal of larger particles (> 1 μm approx.) and 2) sterilization of the remaining smaller particles by direct plasma exposure. NTPs are stable electrical discharges containing excited and ionized species and radicals that are orders of magnitude more reactive than ozone (O_3) (Xiao et al., 2014), the more familiar, less effective, and more persistent oxidant used by indoor air cleaners. Radicals and excited species are thought to vigorously attack the bacterial cell membrane or virus capsid, leading to damage that causes a loss in structural integrity and eventual pathogen inactivation. NTPs have already been proven for surface disinfection, inactivating biological pathogens on the surfaces of food products (Perni et al., 2008; Noriega et al., 2011) and treatment of skin diseases (Heinlin et al., 2010). NTPs have also been thoroughly studied for destruction of gaseous pollutants, the radicals and excited species having been shown to destroy a wide variety of gaseous volatile hydrocarbons such as those emitted from industrial processes (Xiao et al., 2014) as well as gaseous pollutants such as nitrous and sulfurous oxides (NO_x and SO_x) emitted from combustion (McAdams, 2001). However, the intersection of these two established applications of NTPs - disinfection of an air stream - is substantially complicated by the fact that viruses and bacteria act as charged aerosols suspended in the gas stream, both the aerosols and the gas responding separately to the electric fields and flow of charged ions that form the foundation of NTPs. Another concern of applying NTP inactivation in animal confinements is that the elevated concentrations of chemically reducing species such as NH_3 and H_2S, common emissions from urine and manure in animal confinements, have the potential to react with the plasma-generated oxidative species, possibly reducing the inactivation efficiency of NTP.

Our previous research (Xia et al., 2019) has developed a packed bed NTP reactor and demonstrated inactivation of airborne bacteriophage MS2 by the reactor as a function of applied voltage and power with a

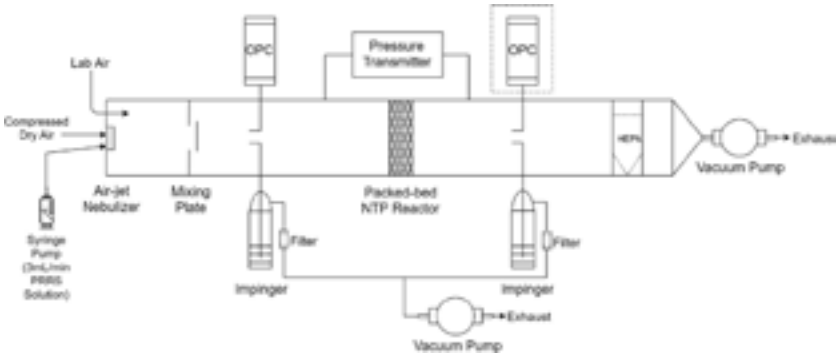

Fig. 1. Schematic of the small-scale wind tunnel setup at University of Minnesota with the NTP reactor mounted in the middle test section. One OPC is indicated with a dashed box since only one OPC instrument was available, its location alternated between upstream and downstream sampling probes during each test.

maximum inactivation of 2-log at 30 kV peak-to-peak voltage and 2.08 W (734 J/m^3 at 170 LPM)). The objective of the present study is to measure the inactivation of aerosolized PRRSv by the same packed bed NTP reactor and compare the results with our previous bacteriophage MS2 inactivation results to investigate if the packed bed NTP reactor has different performance inactivating an enveloped airborne virus (PRRSv) versus a non-enveloped virus (bacteriophage MS2). Using virus stocks and wind tunnel facilities provided by the University of Minnesota, the packed bed NTP reactor was tested for effectiveness in inactivating aerosolized PRRSv.

2. Materials and methods

2.1. Experimental apparatus

The tests of PRRSv inactivation by NTP were conducted using a small-scale non-recirculating wind tunnel located at the University of Minnesota. A schematic of the experimental setup is shown in Fig. 1. The wind tunnel has an inside duct diameter of 3.5″, an overall length of 96″ and can operate in a volumetric flow rate range from approximately 3–30 cfm. An induced draft (ID) fan is connected at the outlet of the wind tunnel and the volumetric flow rate is maintained by measuring the pressure drop (OMEGA Differential Pressure Transmitter P X 653-10D5V) across a calibrated orifice meter installed near the tunnel exit and applying the necessary voltage to the vacuum pump downstream of the tunnel. Temperature and relative humidity in the tunnel and absolute pressure are measured and taken into account in the volumetric flow rate measurements. The flow rate is calculated and maintained using Proportional-Integral-Derivative (PID) feedback control in LabView. Data acquisition by the LabView software is facilitated by a National Instruments USB-6001 DAQ. A HEPA filter is installed at the exit of the tunnel to prevent contamination or release of the PRRSv into the laboratory.

The packed bed NTP reactor was mounted in the test section of the wind tunnel (shown in Fig. 1) and was tested at volumetric flow rates of 5 and 12 cfm. The design and schematic of the dielectric barrier discharge (DBD) packed bed NTP reactor are described in detail in our previous paper (Xia et al., 2019a). The Plexiglas tube wall serves as the dielectric barrier which would promote microdischarge generation. Two grounded electrodes, compressing 500 inert borosilicate glass beads (0.25-inch diameter) in between, formed the packed bed setup which can further enhance the microdischarge by partial discharges at the contact points between the glass beads for more effective plasma species-viral aerosol interactions.

An air-jet large particle generator (LPG) atomizer was installed at the entrance of the tunnel and used to generate PRRSv challenge aerosols. A PRRSv solution from a 65 ml syringe was feed into the LPG atomizer using a syringe pump set (New Era Pump Systems Inc. NE-300) at a constant liquid feed rate of 3 mL/min. Dry and filtered dispersion air at a volumetric flow rate of 1.5 L per minute (LPM) was directed into the dispersion air inlet of the atomizer to help aerosolize the virus solution reaching the atomizer nozzle. After aerosolization, the PRRSv aerosols were diluted and dried with lab air drawn into the wind tunnel, and the air was mixed thoroughly using a downstream orifice mixing plate, which generates turbulence to achieve uniform aerosol distribution in the air flow. Isokinetic probes were installed upstream and downstream of the packed bed NTP reactor to extractively sample from the wind tunnel flow at 2.8 LPM, and the droplet number concentrations in the sampled air were measured by a portable optical particle counter (OPC, TSI AeroTrak model 9306-V2). An aerosol diluter was used to prevent coincidence errors in the OPC. Two additional isokinetic probes were installed as well upstream and downstream of the packed bed NTP reactor at the same locations as the OPC probes, which extractively sampled the wind tunnel air flow at a nominal volumetric flow rate of 9 LPM. The sampled air was drawn by a vacuum pump through two identical liquid impingers (Ace Glass, Inc. 125 mL 24/25 Impinger), leading to collection of infectious and inactivated PRRSv aerosols in the 20 mL impinger collection fluid (Dulbecco's Modified Eagle Medium (DMEM)). The pressure drop across the NPT reactor was measured by another differential pressure transmitter (Omega P X 653-03D5V).

2.2. Experimental procedure

2.2.1. NTP inactivation testing procedure

The tests of airborne PRRSv inactivation by the packed bed NTP reactor took place in two phases, in May and August 2017, over the course of four months to allow time for samples collected in the first phase to be analyzed by the Veterinary Diagnostic Lab at Univ. of Minnesota. The two-phase tests were designed because there was initial concern that the sensitivity of PRRSv titration, which is limited by the initial titer of infective PRRSv that is aerosolized, might lead to a situation where no infective virus was detected downstream of the reactor, resulting in uncertainty as to whether such a result represented a 100 % inactivation or evidence of reaching the lower detection limit. As a result, Phase 1 employed the lowest voltages to make sure to the extent possible that as little of the virus was inactivated. Test conditions in the second phase employed higher voltages after analyses showed the results of Phase 1 yielded partial inactivation.

In the first phase (May data), the NTP reactor was operated at voltages of 12, 16, and 20 kV, and the highest NTP discharge power was 0.56 W achieved at 20 kV. In the second phase (August data), voltages of 30 kV were applied in the reactor using a second power supply, resulting in about 2.08 W discharge power in the NTP reactor (Xia et al., 2019a). For each voltage setting, the PRRSv inactivation by the packed bed NTP reactor was examined under two air flow rates (5 cfm and 12 cfm), and all tests were conducted in triplicate. In both Phase 1 and Phase 2 (May and August), two control tests, either with the reactor

deactivated (no voltage supplied) or with the reactor removed from the wind tunnel, were also conducted in duplicate. At the beginning of each test, the vacuum pump downstream of the sampling train was turned on to reach a constant desired flow rate though the wind tunnel, after which the syringe pump and compressed air supplied to the air-jet nebulizer were turned on to initiate PRRSv aerosolization. When consistent mist was observed emitting from the nebulizer, the packed bed NTP reactor was activated (for reactor-on tests only), and the sampling pumps downstream of the impingers were turned on to start the 20-minute impinger sampling. Only one OPC was available for this study, which was switched between upstream and downstream sampling probes, consecutively making a 5-minute upstream particle size distribution (PSD) measurement, a 5-minute downstream PSD measurement, and then another 5-minute upstream PSD measurement during the 20-minute testing period. The two 5-minute upstream PSD data were averaged as an estimation of the synchronous upstream PSD when the downstream PSD was actually measured. The OPC had six particle size bins (set to 0.3 µm, 0.5 µm, 1 µm, 3 µm, 5 µm and 10 µm) and was set to report the differential particle number concentrations between adjacent bin sizes. It was assumed that the log-average of the two adjacent bin sizes was the average droplet size for the corresponding measured differential number concentrations.

2.2.2. PRRS virus preparation, aerosolization and collection

PRRSv VR2332 reference strain was propagated in MARC-145 cells and titrated to 10^5 $TCID_{50}$/mL (50 % Tissue Culture Infectious Dose per milliliter). The virus was aliquoted and frozen at −80 °C until used. For each test, a syringe was filled with 65 mL of PRRSv at 10^5 $TCID_{50}$/mL, placed into a New Era pump system, model NE-1000 multi-phaser, and aerosolized into the testing chamber at 3 mL/min via an air-jet nebulizer for 20 min. Room temperature and relative humidity (RH) level were measured during each test by a portable humidity/temperature pen (Traceable 4093). During each test, air samples were collected with twin impingers, placed upstream and downstream of NTP reactor, for 20 min. Each impinger was filled with 20 mL of DMEM supplemented with 1.5 mg/mL of bovine serum albumin fraction V 7.5 %, 1X antibiotic-antimycotic, 0.0015 mg/mL of Trypsin-TPCK, and 0.05 mg/mL of gentamicin. After 20 min sampling time, the volume of supplemented DMEM in each impinger was measured, recorded, aliquoted into 3 tubes and frozen at −80 °C until tested. The collected impinger samples were submitted to the Veterinary Diagnostic Lab at the University of Minnesota for quantitative RT-PCR analysis and $TCID_{50}$ assay analysis.

2.2.3. Quantitative RT-PCR (RT-qPCR)

Samples were quantified for PRRSv using quantitative RT-PCR as previously described (Cho et al., 2006). A standard curve based on transcript RNA with a quantitative linear range from 1×10^3 copies/µL to 1×10^6 copies/µL was used to determine the RNA copy number/mL. The copy number/mL results were consecutively converted to copies/m^3 of air. The detection limit of PRRSv quantitative RT-qPCR is approximately 1000 copies/mL, which is equivalent to approximately 8×10^4 copies/m^3 of air in this study.

2.2.4. Sample titration

Samples were serially diluted 5-fold. 100 u L of the serial dilution was plated onto 96-wells plates containing MARC-145 cells in 4 replicates. Plated samples were incubated for 7 days at 37 °C with 5 % CO_2. At day 7, plates were removed and cytophatic effect (CPE) was read and recorded. $TCID_{50}$/mL was calculated using the Spearman-Karber method and consecutively converted to $TCID_{50}$/m^3 of air. The detection limit of PRRSv $TCID_{50}$ is 1.43 $TCID_{50}$/100 µL, which is equivalent to approximately 1200 $TCID_{50}$/m^3 of air in this study.

2.2.5. Testing the effects of liquid accumulation on NTP performance

During the experiment, it was observed that compared with the previous bacteriophage MS2 inactivation tests (Xia et al., 2019a), more virus solution droplets (mainly DMEM in this study) reached and impacted on the packed bed and accumulated in the reactor between the glass beads, likely due to higher RH conditions of the supplied air, shorter distance between the atomizer and the packed bed NTP reactor, and potentially larger droplets produced by the air-jet large particle generator. The accumulated virus solution may have promoted virus aerosol filtration by the packed bed, but could also have led to re-emission of viral aerosols from the reactor into the region downstream. In addition, increase of RH and accumulation of liquid inside the packed bed may change the NTP discharge scenario, serve as a protective reservoir for suspended viruses, and affect reactive species formation by the reactor. To examine the effects of accumulated DMEM solutions, another set of tests was conducted at the University of Michigan using bacteriophage MS2 as the target virus. 5 mL and 10 mL DMEM solution were sprayed directly into the packed bed before each test and the reduction of airborne infectious MS2 from upstream to downstream of the DMEM-soaked packed bed NTP reactor were examined with the reactor powered by the 20 kV power supply at 170 LPM air flow rate. The setup of the sampling line, the methodology of MS2 ultrasonic atomization, and the virus sample analysis methods were described in detail in our previous paper (Xia et al., 2019a).

3. Results and discussion

3.1. Droplet size distribution

For all powered-reactor tests, particle size distributions (PSD) were measured both upstream and downstream of the packed bed NTP

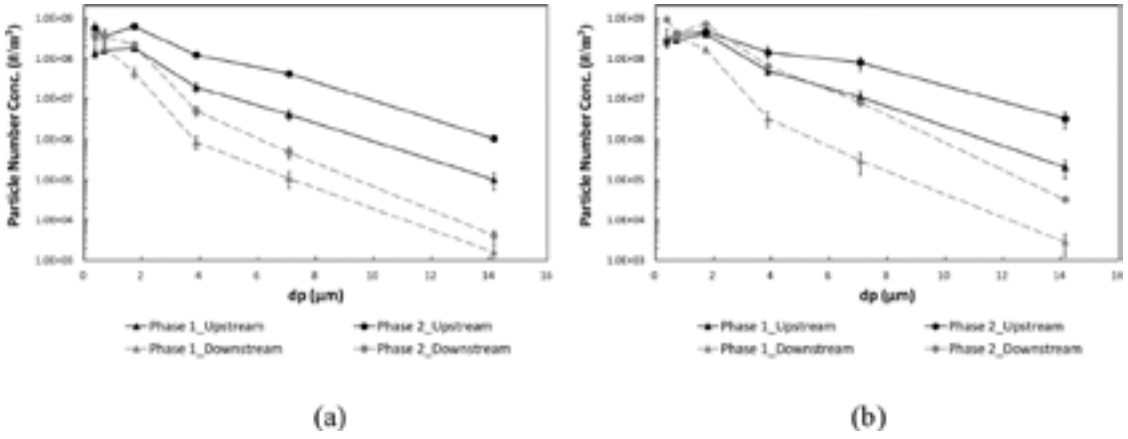

Fig. 2. Average droplet size distributions both upstream and downstream of the reactor in each test program phase (Phase 1 and Phase 2) for wind tunnel flow rates of (a) 12 cfm and (b) 5 cfm.

reactor under two flow rates, and the results were averaged for each phase of the test program and each flow rate (Fig. 2). From Fig. 2 it is evident that the OPC measurements were quite consistent with small confidence intervals, indicating that the virus solution aerosolization process was repeatable and the packed bed had relatively consistent filtration efficiencies regardless of the applied voltage level (which is proved by PSD data comparison between different applied voltages in the same test program phase with the same flow rate). The PSD plots confirm that aerosols generated by air-jet nebulizers are polydisperse in size with large proportions of droplets over 5 μm in diameter, which agrees with other reports on aerosol PSDs generated by air-blast atomization (Lorenzetto and Lefebvre, 1977; Steckel and Eskandar, 2003). The upstream sampling probe was installed about 40″ (101.6 cm) downstream of the air-jet nebulizer, which was only about a quarter of the distance between the ultrasonic atomizer and upstream sampling port (144″, 365.8 cm) in our previous bacteriophage MS2 inactivation setup (Xia et al., 2019a). The shorter distance led to more incomplete aerosol evaporation, and as a result more coarse droplets (with droplet diameter d_p ranging from 2.5–10 μm) would reach the reactor where they would be filtered by the packed bed and accumulate as a bulk liquid in the reactor. This inference was proved by experimental observations: during all PRRSv inactivation tests in both test program phases, bulk virus solution was found accumulating between the glass beads in the packed bed NTP reactor, while for all MS2 tests conducted in University of Michigan, no liquid accumulation was found with an ultrasonic atomizer expected to generate aerosols with smaller and more uniform size distribution (Steckel and Eskandar, 2003) and using a dry (RH typically < 10 %) compressed air supply. It should be noted in interpreting the results that the accumulated virus solution is undesirable since it may cause reemission of aerosols from the packed bed, change the NTP discharge phenomena, serve as a protective reservoir for suspended viruses, and impact reactive species formation by the reactor.

The two plots in Fig. 2 illustrate how virus solution aerosolization and packed bed filtration would change with changing flow rate and flow relative humidity. In the same test program phase, the upstream droplet number concentration is generally higher at 5 cfm (Fig. 2b) than that at 12 cfm flow rate (Fig. 2a), due to reduced dilution and slower droplet evaporation at lower air flow rate. The average RH of the ambient room air (which was the major air source of the wind tunnel flow) in Phase 2 was 49 %, higher than the ambient condition in Phase 1 (38 %), while the air temperature remained relatively constant (22.2 ℃ in Phase 1 and 23.2 ℃ in Phase 2). Higher inlet RH in Phase 2 caused slower droplet evaporation, and as a result more droplets in all sizes were found upstream of the reactor in Phase 2 in both Fig. 2a and 2b. Comparison between upstream and downstream PSD in both plots provides a measure of the packed bed filtration effects on various size droplets. Fig. 2a showed that the number concentrations of droplets larger than 1 μm reduced significantly from upstream to downstream of the reactor, which should be mainly due to filtration by the packed bed and size reduction through evaporation, and larger droplets had more significant decreases in number concentration due to their low mobility and large surface area and thus rapid evaporation. Concentrations of submicron droplets (droplets smaller than 1 μm), however, increased from upstream to downstream of the reactor, potentially due to re-aerosolization of virus solutions accumulated in the packed bed, and evaporation of super micron droplets to submicron sizes. Fig. 2b showed similar droplet number concentration changing trends, while concentrations of droplets between 1 μm and 7 μm, especially in Phase 2, showed less reduction compared with the 12 cfm data. This should be due to slower evaporation of droplets larger than 7 μm to this size range at 5 cfm. At 12 cfm, these droplets may evaporate faster and fall into the submicron region before reaching the downstream sampling probe. These observations and hypotheses are confirmed by comparing droplet penetration (downstream concentration divided by upstream concentration) in the two phases at two flow rates (Fig. 3). From Fig. 3, it is

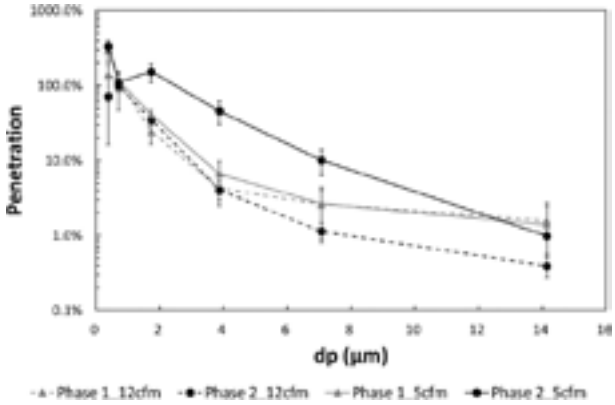

Fig. 3. Penetration of particles (downstream number concentration / upstream number concentration) in each OPC size bin measured at two flow rates in the two test program phases.

evident that in Phase 1 droplets had similar penetration through the reactor at both flow rates, and 1 μm–5 μm droplets had slightly higher penetration at 5 cfm. In Phase 2 at 12 cfm, the penetration of droplets smaller than 4 μm had similar values as the Phase 1 data, while droplets larger than 4 μm had less penetration, likely due to the increased amount of virus solution accumulated in the packed bed at higher RH. At 5 cfm in Phase 2, the penetration curve was quite different from the other three, with significantly higher droplet penetration in the range 2 μm–7 μm. It is likely that at this air-to-water mass flow ratio, the RH in the wind tunnel exceeded the critical RH predicted by our previous droplet evaporation numerical model (Xia et al., 2020), which prevented rapid liquid evaporation and led to more 2 μm–7 μm droplets reaching the downstream sampling probe. Based on the OPC data and assuming spherical droplets, the average volumetric droplet penetration through the packed bed was 10.6 % in Phase 1 at 12 cfm, 13.7 % in Phase 1 at 5cfm, 6.2 % in Phase 2 at 12 cfm, and 22.2 % in Phase 2 at 5 cfm.

3.2. PRRSv filtration and inactivation by the packed-bed NTP

In this study, $TCID_{50}$ analysis of the twin upstream and downstream impinger samples collected in each test provided a measure of the reduction in viable PRRSv for all mechanisms. qPCR analysis of the upstream and downstream samples was performed with $TCID_{50}$ analysis and provided a measure of the reduction in the PRRSv genome irrespective of changes in viability caused by NTP exposure; in the context of the present study, reductions in the abundance of the PRRSv genome were interpreted as packed bed filtration. Such filtration effects could also be inferred from $TCID_{50}$ analyses showing reductions in viable PRRSv between the upstream and downstream impinger samples collected when the reactor was not powered. The latter method, however, were not applied in this study since it can yield greater uncertainties with two groups of tests (reactor-on and reactor-off) conducted separately, which might have experienced different RH conditions, varied virus solution aerosolization and evaporation phenomena, or have different viable PRRSv concentration in the initial solution filled into the syringe pump. In addition, the previous bacteriophage MS2 inactivation study used qPCR data as the indication of packed bed filtration, so it is preferable to apply the same analytical method in order to compare results between the two studies. Reductions in viable PRRSv from $TCID_{50}$ analyses, after correcting for packed bed filtration according to the qPCR data, yielded the inactivation of PRRSv by the reactor solely due to NTP exposure.

Table 1 summarizes the measured abundance of PRRSv genome copies (in RNA copies/m^3) and abundance of infective PRRSv (in $TCID_{50}/m^3$) in the tunnel air flow before- (upstream, U) and after- (downstream, D) NTP treatment. Averages of 8.1–73.5 × 10^{10} RNA

Table 1
Summary of the measured abundance of PRRSv genome copies (in RNA copies/m^3) and abundance of infective PRRSv (in $TCID_{50}/m^3$) in the tunnel air flow before- (upstream, U) and after- (downstream, D) NTP treatment.

Phase	Voltage (kV)	Tunnel air flow Rate (cfm)	Replicates	Acceptable Replicates		10^{10} RNA copies/m^3	SD	10^5 $TCID_{50}/m^3$	SD
1	20	12	3	1	U	8.10	——	167.62	——
					D	1.87	——	0.53	——
1	16	12	3	3	U	12.32	5.65	5.42	2.92
					D	1.88	1.78	0.20	0.15
1	12	12	3	1	U	16.73	——	8.73	——
					D	5.96	——	0.88	——
1	20	5	3	2	U	73.47	69.43	108.10	146.73
					D	6.19	2.70	1.27	0.59
1	16	5	3	1	U	36.90	——	11.48	——
					D	9.11	——	0.57	——
1	12	5	3	2	U	28.87	1.45	44.47	2.96
					D	8.71	3.33	2.02	1.51
2	30	12	3	2	U	14.57	2.31	26.20	26.46
					D	0.70	0.05	0.19	0.03
2	20	12	6	3	U	8.67	2.91	20.53	19.45
					D	0.62	0.11	0.35	0.20
2	30	5	3	1	U	18.57	——	16.62	——
					D	1.95	——	0.68	——
2	20	5	6	3	U	18.38	4.02	22.05	21.24
					D	3.37	0.83	1.54	1.41

(SD: standard deviation; U: upstream; D: downstream).

copies/m^3 were detected in the air flow upstream of NTP treatment, and 0.6–9.1 × 10^{10} RNA copies/m^3 were detected downstream. In terms of infective PRRSv concentration, 5.4–167.6 × 10^5 $TCID_{50}/m^3$ were detected upstream of NTP and 0.2–2.0 × 10^5 $TCID_{50}/m^3$ were detected in the downstream flow. Comparing the $TCID_{50}$ results with qPCR at the upstream location, there was ~5-log inactivation of PRRSv in the aerosols before reaching the reactor, which is comparable with our previous research (Xia et al., 2019a) and should be due to the evaporation of droplets and intensive air-jet nebulization (Niven et al., 1995). Three to six replicates were conducted for each applied voltage and tunnel flow rate combination, however, only one to three replicates yielded physical results. The rejected replicates yielded unphysical results with either the abundance of infective PRRSv or the number of genome copies higher at the downstream location than at the upstream location. Degradation of the airborne PRRSv by attack from reactive species within the non-thermal plasma would not be expected to result in either an increase in $TCID_{50}$ or an increase in the number of PRRSv genome copies at the downstream sampling location. The increase in $TCID_{50}$ or PRRSv genome copies data could be due to sampling or analysis errors or accumulation of virus solution in the packed bed and the resulting potential re-aerosolization of PRRSv into the downstream flow. Repeating tests may not reduce these errors with the present experimental design, since each replicated test may experience different RH conditions, varied virus solution aerosolization and evaporation phenomena, or have different viable PRRSv concentration in the initial solution filled into the syringe pump. As shown in Table 1, tests with two to three replicates may result in average values with relatively large standard deviations and thus fail to reduce the uncertainty level. The inherent errors and uncertainties of this study is acknowledged in the following discussions and figures.

The PRRSv inactivation efficiency by NTP was calculated based on the ratio of downstream to upstream abundance of viable PRRSv, normalized by the ratio of downstream to upstream abundance of PRRSv genome copies determined by qPCR. The results are plotted in Fig. 4. For data acquired in Phase 1 (May), the figure illustrates the increasing trend in inactivation efficiency with increasing applied voltage, as expected, and the generally lower inactivation efficiency at the higher air flow rate (12 cfm) as compared to the lower air flow rate (5 cfm). These trends are as expected and agree with those observed in previous results involving inactivation of bacteriophage MS2 conducted at University of Michigan (Xia et al., 2019a). The measured PRRSv inactivation levels

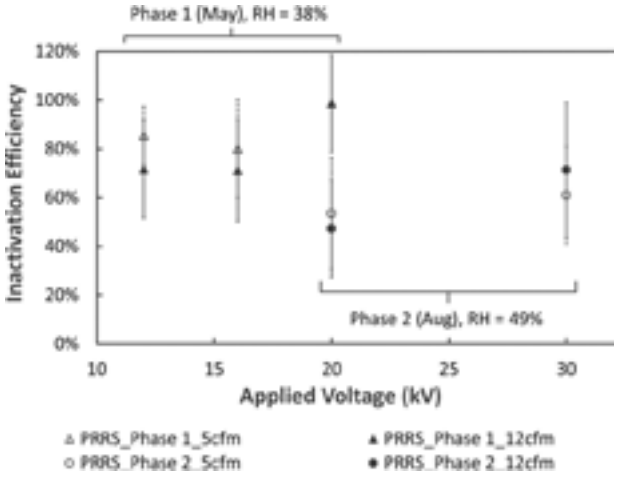

Fig. 4. Comparison of Phase 1 (May) and Phase 2 (August) PRRSv inactivation by NTP treatment at two air flow rates (5cfm and 12 cfm) and four voltages (12, 16, 20, and 30 kV).

by NTP are close to the relevant NTP inactivation levels reported by other research groups using different NTP reactor designs inactivating different bioaerosol species (Vaze et al., 2010; Wu et al., 2015). Vaze et al. constructed a 28 kV 600 µs pulse dielectric barrier grating discharge NTP reactor, which achieved 29 %–97 % inactivation (0.15–1.5 log) of aerosolized *E. coli* during the 10 s treatment time (Vaze et al., 2010). Wu et al. applied 14 kV 10 kHz AC power to a miniature wire-cylinder DBD reactor, and the reactor achieved ~80 % inactivation (0.9 log) of aerosolized bacteriophage MS2 during a 0.12 s treatment time (with 20 W power) (Wu et al., 2015). Evident from the Phase 1 data presented in Fig. 4 is the fact that under similar experimental conditions, the effectiveness of the NTP in inactivating PRRSv aerosols was somewhat higher than the demonstrated effectiveness for inactivating MS2 with the same device at the same conditions; however, the large uncertainty in the results as indicated by the large confidence intervals allows only for a conclusion that the two viruses were likely inactivated comparably. Data acquired in Phase 2 (August), however, showed reduced inactivation efficiency. With 20 kV supplied voltage, the measured inactivation efficiency at both flow rates in Phase 2 was 30 %–50 % lower than the values acquired in Phase 1 or in the MS2 inactivation

study (Xia et al., 2019a). When the supplied voltage was increased from 20 kV to 30 kV, and the estimated discharge power was increased from 0.56 W at 20 kV (237 J/m^3 at 5 cfm) to 2.08 W at 30 kV (881 J/m^3 at 5 cfm), the packed bed NTP reactor showed increased PRRSv inactivation efficiencies at both flow rates, which were still lower than the values acquired with 20 kV power supply in Phase 1 or during the MS2 inactivation study (Xia et al., 2019a). It was found in our previous study that the bacteriophage MS2 inactivation by the packed bed NTP reactor with 30 kV power supply can lead to at least 2-log (99 %) viable MS2 reduction (Xia et al., 2019a), which was significantly higher than the 30 kV results presented in Fig. 4. It is likely that the reduced NTP inactivation efficiency observed in Phase 2, as well as the large confidence intervals for all PRRSv inactivation results in both phases of the PRRSv test program, were due to increased accumulation of bulk virus solution (in this study DMEM) in the packed bed.

As discussed in previous paragraphs, incomplete evaporation of the PRRSv-laden droplets of DMEM was consistent throughout both Phase 1 and Phase 2 tests, while prior tests involving MS2 inactivation achieved complete or near complete droplet evaporation after several modifications to the experimental apparatus: lengthening the distance between the introduction of the droplets into the airstream and the NTP reactor; supplementing ambient air with dry compressed air (RH $<$ 10 %), and thereby lowering relative humidity and speeding evaporation; and producing smaller droplets via an ultrasonic atomizer. These remedies were not available or not possible for the current project. As a result, the significant unanswered question regarding the present results is the impacts, if any, of the persistent presence of liquid DMEM in fine droplets exposed to the non-thermal plasma and accumulating in the NTP reactor itself. DMEM is a solution of glucose in water. One hypothesis is that residual DMEM on aerosols or as aerosols passing through the NTP reactor may have the effect of protecting PRRSv from oxidation by the reactive species generated by the plasma. Whereas H_2O alone, when dissociated, produces additional reactive species in the form of H^+ and OH^-,hydrocarbons would act more as a sink for the plasma-generated species, consuming them in the course of their complete oxidation. There exists a separate branch of plasma environmental remediation that involves using plasmas to oxidize chemical contaminants in water supplies or wastewater. Support for this hypothesis came from preliminary tests prior to Phase 1. Prior testing at University of Michigan using MS2 phage determined that ozone (O_3) produced by the NTP reactor had the potential to accumulate in the downstream impinger fluid, a phosphate buffered saline (PBS) consisting of small amounts of sodium and phosphorous salts dissolved in water. The dissolved ozone was found to continuously inactivate MS2 phage in the impinger during and after testing, potentially leading to a high bias in inactivation efficiency results. To compensate for this, sodium sulfite was routinely added to the PBS during MS2 testing, serving to consume O_3 and prevent inactivation of MS2 phage while in the impinger. However, when similar tests were conducted exposing PRRSv in DMEM to dissolved O_3, the results showed no inactivation of PRRSv in DMEM by O_3, suggesting that O_3 was consumed by oxidation reactions with the hydrocarbons in DMEM and therefore unavailable to chemically attack the PRRSv in solution. A second potential effect of residual DMEM could be in influencing the electrical properties of the packed bed and the strength or distribution of the plasma therein. In the packed bed, the plasma exists in the voids between the beads where the electric field increases above the threshold where electrical breakdown occurs in air. Accumulation of DMEM (approximate conductivity $\sigma = 1.4$ S/m (Chen et al., 2009)) in these spaces could provide a conductive electrical pathway that prevents such electric fields from forming. This, too, would be expected to reduce the apparent inactivation efficiency of tests involving DMEM as compared to tests in which evaporation of the liquid phase was more complete.

In order to test these hypotheses and the potential effects of accumulated DMEM, experiments were conducted after Phase 2 in which the packed bed NTP reactor was pre-soaked with known amounts of DMEM (5 mL or 10 mL), and the inactivation of MS2 aerosols by the "wet" reactor was measured. Fig. 5 shows the results of these tests in the form of viable MS2 reduction, comprising both physical filtration and NTP inactivation (with 20 kV), comparing samples collected at the upstream pre-treatment location against those collected at the downstream post-treatment location. The degree of viable MS2 reduction induced by the 20 kV reactor when dry was acquired from the previous bacteriophage MS2 inactivation study. With 5 mL DMEM sprayed into the packed bed, the viable MS2 reduction decreased from 88 % (dry reactor) to 79 %, and with 10 mL DMEM added, the viable MS2 reduction was further reduced to 46 %. The figure proves that increasingly accumulated DMEM in the packed bed would reduce viable MS2 reduction from upstream to downstream locations of the packed bed NTP reactor, potentially by quenching reactive plasma species or preventing electric field build up for NTP discharge. With regard to the electrical effects, it seemed that the residual DMEM in the packed bed NTP reactor can increase the amplitude of transmitted current without changing the amplitude and waveform of the applied voltage. With 20 kV applied to the dry packed bed NTP reactor, the current had an amplitude of 0.40 mA. The addition of 5 ml of MEM to the packed bed increased the current amplitude to 0.48 mA, and the addition of 10 ml of MEM to the packed bed further increased the current amplitude to 0.56 mA. This was reasonable since the accumulation of liquid in the packed bed could reduce the overall resistance of the reactor and thus increasing the transmitted current. This discharge environment, however, may not be favorable for plasma generation, since more current would pass through the conductive liquid without ionizing air in the packed bed.

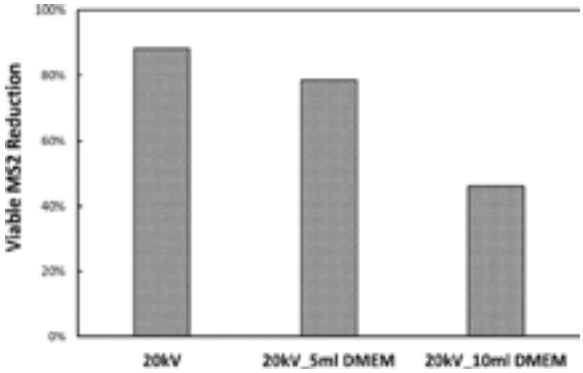

Fig. 5. Reduction (filtration + inactivation) of viable bacteriophage MS2 in response to 5 ml and 20 ml of DMEM added to and held within the NTP packed bed.

4. Conclusion

In summary, this study provides the first demonstration of NTP inactivation of an airborne pathogen relevant to livestock. Both the non-enveloped bacteriophage MS2, and the enveloped PRRS virus were likely inactivated to comparable degrees. The highest PRRSv inactivation efficiency was 98.6 % achieved in Phase 1 (May) with 20 kV voltage supplied to the packed bed NTP reactor at the wind tunnel flow rate of 12 cfm. However, size, composition of DMEM droplets and relative humidity were all likely contributors to variability in measured inactivation. Accumulated DMEM bulk liquid in the packed bed can reduce the reactor's efficiency on viable PRRSv reduction, potentially through quenching reactive plasma species or preventing electric field build up for NTP discharge. Future studies with improved virus aerosolization methods and more consistent and dryer inlet air supply should be conducted to further examine how non-enveloped and enveloped viruses react to NTP inactivating environment. Overall, the results show promising results to inactivate airborne PRRSv by NTP and offer potential alternatives to pork producers to enhance their

biosecurity practices.

Supporting information

None.

Funding sources

This project is funded by the National Pork Board, under award # 16-098. The MS2-related work is supported by the National Institute of Food and Agriculture, U.S. Department of Agriculture, under award # 2016-67030-24892.

CRediT authorship contribution statement

T. Xia: Methodology, Investigation, Formal analysis, Writing - original draft, Writing - review & editing, Visualization. **M. Yang:** Methodology, Investigation, Formal analysis. **I. Marabella:** Methodology, Investigation. **E.M. Lee:** Methodology, Investigation. **B. Olson:** Methodology. **D. Zarling:** Methodology. **M. Torremorell:** Conceptualization, Funding acquisition, Writing - review & editing. **H.L. Clack:** Conceptualization, Funding acquisition, Writing - review & editing.

Declaration of Competing Interest

EML and HLC are affiliated with Taza Aya LLC; HLC is co-founder and CTO. TX, MY, IM, BO, DZ, and MT all declare no competing financial interest.

Acknowledgements

This project is funded by the National Pork Board, under award # 16-098. The MS2-related work is supported by the National Institute of Food and Agriculture, U.S. Department of Agriculture, under award # 2016-67030-24892. Any opinions, findings, conclusions, or recommendations expressed in this publication are those of the author(s) and do not necessarily reflect the view of the U.S. Department of Agriculture. The authors thank Minmeng Tang for helping in the experimental setup and Prof. Krista R. Wigginton and Yinyin Ye (Univ. of Michigan) for helping us with the MS2 inactivation test. The authors also thank Prof. John Foster and Selman Mujovic (Univ. of Michigan) for helping in the design and power consumption measurements of the packed bed NTP reactor used in this research.

References

Arruda, A.G., Tousignant, S., Sanhueza, J., Vilalta, C., Poljak, Z., Torremorell, M., Alonso, C., Corzo, C.A., 2019. Aerosol detection and transmission of porcine reproductive and respiratory syndrome virus (PRRSV): what is the evidence, and what are the knowledge gaps? Viruses 11 (8), 712.

Bolashikov, Z.D., Melikov, A.K., 2009. Methods for air cleaning and protection of building occupants from airborne pathogens. Build. Environ. 44 (7), 1378–1385.

Chen, M.-T., Jiang, C., Vernier, P.T., Wu, Y.-H., Gundersen, M.A., 2009. Two-dimensional nanosecond electric field mapping based on cell electropermeabilization. PMC Biophys. 2 (1), 9.

Cho, J.G., Dee, S.A., Deen, J., Guedes, A., Trincado, C., Fano, E., Jiang, Y., Faaberg, K., Collins, J.E., Murtaugh, M.P., 2006. Evaluation of the effects of animal age, concurrent bacterial infection, and pathogenicity of porcine reproductive and respiratory syndrome virus on virus concentration in pigs. Am. J. Vet. Res. 67 (3), 489–493.

Colby, M.M., 2013. DHS S&T's Agricultural Defense Program Overview. National Center for Foreign Animal and Zoonotic Disease Defense (FAZD).

Dee, S., 2011. An Assessment of Air Filtration for Reducing the Risk of PRRSV Infection in Large Breeding Herds in Swine Dense Regions. NPB #09-209. .

Farnsworth, J.E., Goyal, S.M., Kim, S.W., Kuehn, T.H., Raynor, P.C., Ramakrishnan, M., Anantharaman, S., Tang, W., 2006. Development of a method for bacteria and virus recovery from heating, ventilation, and air conditioning (HVAC) filters. J. Environ. Monit. 8 (10), 1006–1013.

Heinlin, J., Morfill, G., Landthaler, M., Stolz, W., Isbary, G., Zimmermann, J.L., Shimizu, T., Karrer, S., 2010. Plasma medicine: possible applications in dermatology. JDDG 8 (12), 968–976.

Hermann, J., Hoff, S., Muñoz-Zanzi, C., Yoon, K.-J., Roof, M., Burkhardt, A., Zimmerman, J., 2007. Effect of temperature and relative humidity on the stability of infectious porcine reproductive and respiratory syndrome virus in aerosols. Vet. Res. 38 (1), 81–93.

Holtkamp, D.J., Kliebenstein, J.B., Neumann, E.J., Zimmerman, J.J., Rotto, H.F., Yoder, T.K., Wang, C., Yeske, P.E., Mowrer, C.L., Haley, C.A., 2013. Assessment of the economic impact of porcine reproductive and respiratory syndrome virus on United States pork producers. J. Swine Health Prod. 21 (2), 72–84.

Hood, A., 2009. The effect of open-air factors on the virulence and viability of airborne Francisella tularensis. Epidemiol. Infect. 137 (6), 753–761.

Keffaber, K., 1989. Reproductive failure of unknown etiol-ogy. Am. Assoc. Swine Pract. Newsl 1, 1–9.

Lorenzetto, G., Lefebvre, A.H., 1977. Measurements of drop size on a plain-jet airblast atomizer. Aiaa J. 15 (7), 1006–1010.

McAdams, R., 2001. Prospects for non-thermal atmospheric plasmas for pollution abatement. J. Phys. D Appl. Phys. 34 (18), 2810.

Memarzadeh, F., Olmsted, R.N., Bartley, J.M., 2010. Applications of ultraviolet germicidal irradiation disinfection in health care facilities: effective adjunct, but not stand-alone technology. Am. J. Infect. Control 38 (5), S13–S24.

Miaskiewicz-Peska, E., Lebkowska, M., 2012. Comparison of aerosol and bioaerosol collection on air filters. Aerobiologia 28 (2), 185–193.

Millerick-May, M.L., Ferry, E., Benjamin, M., May, G.A., 2016. Routine Manure Removal From Swine Operations: a Potential Mechanism for Pathogen Dispersion. *Michigan Pork Symposium*, Lansing, Michigan.

Niven, R.W., Ip, A.Y., Mittelman, S., Prestrelski, S., Arakawa, T., 1995. Some factors associated with the ultrasonic nebulization of proteins. Pharm. Res. 12 (1), 53–59.

Noriega, E., Shama, G., Laca, A., Díaz, M., Kong, M.G., 2011. Cold atmospheric gas plasma disinfection of chicken meat and chicken skin contaminated with Listeria innocua. Food Microbiol. 28 (7), 1293–1300.

Otake, S., Dee, S., Corzo, C., Oliveira, S., Deen, J., 2010. Long-distance airborne transport of infectious PRRSV and Mycoplasma hyopneumoniae from a swine population infected with multiple viral variants. Vet. Microbiol. 145 (3-4), 198–208.

Perni, S., Liu, D.W., Shama, G., Kong, M.G., 2008. Cold atmospheric plasma decontamination of the pericarps of fruit. J. Food Prot. 71 (2), 302–308.

Pitkin, A., Otake, S., Dee, S., Acvm, D.M.P.D., 2009a. Biosecurity Protocols for the Prevention of Spread of Porcine Reproductive and Respiratory Syndrome Virus. Swine Disease Eradication Center. University of Minnesota College of Veterinary Medicine, pp. 1–17.

Pitkin, A., Deen, J., Dee, S., 2009b. Use of a production region model to assess the airborne spread of porcine reproductive and respiratory syndrome virus. Vet. Microbiol. 136 (1-2), 1–7.

Ramos, S., MacLachlan, M., Melton, A., 2017. Impacts of the 2014-2015 Highly Pathogenic Avian Influenza Outbreak on the US Poultry Sector.

Riley, R.L., 1961. Airborne pulmonary tuberculosis. Bacteriol. Rev. 25 (3), 243.

Steckel, H., Eskandar, F., 2003. Factors affecting aerosol performance during nebulization with jet and ultrasonic nebulizers. Eur. J. Pharm. Sci. 19 (5), 443–455.

Sun, Z., Wang, J., Bai, X., Ji, G., Yan, H., Li, Y., Wang, Y., Tan, F., Xiao, Y., Li, X., 2016. Pathogenicity comparison between highly pathogenic and NADC30-like porcine reproductive and respiratory syndrome virus. Arch. Virol. 161 (8), 2257–2261.

Tian, K., Yu, X., Zhao, T., Feng, Y., Cao, Z., Wang, C., Hu, Y., Chen, X., Hu, D., Tian, X., 2007. Emergence of fatal PRRSV variants: unparalleled outbreaks of atypical PRRS in China and molecular dissection of the unique hallmark. PLoS One 2 (6), e526.

Vaze, N.D., Gallagher, M.J., Park, S., Fridman, G., Vasilets, V.N., Gutsol, A.F., Anandan, S., Friedman, G., Fridman, A.A., 2010. Inactivation of bacteria in flight by direct exposure to nonthermal plasma. IEEE Trans. Plasma Sci. 38 (11), 3234–3240.

Wheeler, S., Ingraham, H., Hollaender, A., Lill, N., Gershon-Cohen, J., Brown, E., 1945. Ultra-violet light control of air-borne infections in a naval training center: preliminary report. Am. J. Public Health Nations Health 35 (5), 457–468.

Wu, Y., Liang, Y., Wei, K., Li, W., Yao, M., Zhang, J., Grinshpun, S.A., 2015. MS2 virus inactivation by atmospheric-pressure cold plasma using different gas carriers and power levels. Appl. Environ. Microbiol. 81 (3), 996–1002.

Xia, T., Kleinheksel, A., Lee, E., Qiao, Z., Wigginton, K., Clack, H., 2019. Inactivation of airborne viruses using a packed bed non-thermal plasma reactor. J. Phys. D Appl. Phys. 52 (25), 255201.

Xia, T., Kleinheksel, A., Wigginton, K.R., Clack, H.L., 2020. Suspending Viruses in an Airstream Using a Consumer-grade Ultrasonic Humidifier. In preparation. .

Xiao, G., Xu, W., Wu, R., Ni, M., Du, C., Gao, X., Luo, Z., Cen, K., 2014. Non-thermal plasmas for VOCs abatement. Plasma Chem. Plasma Process. 34 (5), 1033–1065.

Zhou, L., Wang, Z., Ding, Y., Ge, X., Guo, X., Yang, H., 2015. NADC30-like strain of porcine reproductive and respiratory syndrome virus, China. Emerging Infect. Dis. 21 (12), 2256.

ALLEGATO 13.2

ARTICOLI SCIENTIFICI SU
RIMOZIONE CONTAMINANTI INORGANICI

Wen-Jun Liang, H.-P. F.-X.-Q. (2011). Performance of non-thermal DBD plasma reactor during the removal of hydrogen sulfide. Journal of Electrostatics Volume 69, Issue 3, 206-213.

Journal of Electrostatics 69 (2011) 206–213

Contents lists available at ScienceDirect

Journal of Electrostatics

journal homepage: www.elsevier.com/locate/elstat

Performance of non-thermal DBD plasma reactor during the removal of hydrogen sulfide

Wen-Jun Liang*, Hong-Ping Fang, Jian Li, Feng Zheng, Jing-Xin Li, Yu-Quan Jin

College of Environmental & Energy Engineering, Beijing University of Technology, No.100 Ping Le Yuan, Chaoyang District, Beijing 100124, PR China

ARTICLE INFO

Article history:
Received 4 January 2010
Received in revised form
11 September 2010
Accepted 25 March 2011
Available online 9 April 2011

Keywords:
Non-thermal plasma
Dielectric barrier discharge
Lissajous diagram
Specific energy density
Hydrogen sulfide

ABSTRACT

Destruction of hydrogen sulfide using dielectric barrier discharge plasma in a coaxial cylindrical reactor was carried out at atmospheric pressure and room temperature. Three types of DBD reactor were compared in terms of specific energy density (SED), equivalent capacitances of the gap (Cg) and the dielectric barrier (Cd), energy yield (EY), and H_2S decomposition. In addition, byproducts during the decomposition of H_2S and destruction mechanism were also investigated. SED for all the reactors depended almost linearly on the voltage. In general, Cg decreased with increasing voltage and with the existence of pellet material, while Cd displayed the opposite trend. The removal efficiency of H_2S increased substantially with increasing AC frequency and applied voltage. Longer gas residence times also contributed to higher H_2S removal efficiency. The choice of pellet material was an important factor influencing the H_2S removal. The reactor filled with ceramic Raschig rings had the best H_2S removal performance, with an EY of 7.30 g/kWh. The likely main products in the outlet effluent were H_2O, SO_2, and SO_3.

1. Introduction

There is a growing concern that malodorous pollution at sewage and industrial wastewater treatment plants is not only a nuisance in the ambient environment but may also produce adverse health effects in humans. The odors are mainly caused by sulfurous compounds such as hydrogen sulfide (H_2S), which has an extremely low odor threshold, is highly toxic and has a characteristic rotten-egg smell [1]. Prolonged exposure to a concentration of 300 ppm of H_2S in the air has caused death, and concentrations exceeding 2000 ppm can be fatal to humans are exposed for only a few minutes [2]. Therefore, the effective removal of these sulfur compounds from air is highly desired.

Traditional methods to control the emissions of gaseous odor-causing materials into the atmosphere include absorption (wet scrubbing), adsorption, incineration (either thermal or catalytic), masking and biofiltration [3–10]. Unfortunately, all these technologies may have limitations when removing odor-causing substances from gas streams. Absorption and adsorption transfer odor-causing materials from the gas phase to scrubbing liquids or solid adsorbents, potentially causing other forms of pollution while resolving the odor problems. Incineration can be effective in controlling odor-causing substances. However, the possibility of generating other air pollutants such as NOx, potential poisoning of the catalyst, and relatively high cost associated with this technology should be taken into account. The technical and economic limitations of traditional odor control methods are particularly important for low concentration odor abatement. Nowadays, some new oxidation technologies such as microwave discharge [11] and photocatalytic oxidation [12–14] are also used to remove odor gases.

Due to some unique advantages (rapid reaction at ambient temperature under atmospheric pressure and achievement of high electron energies within a short residence time) as well as ease of operation, non-thermal plasma (NTP) processing has received considerable attention. Recent progress in applying NTP technology to the control of polluting gases such as acidifying components (SO_2 [15,16], NOx [17,18]) and volatile organic compounds [19–22] is very encouraging. While plasma technology has been used to remove H_2S [18,23–26], in our opinion, the combination of plasma and pellets in the reactor is likely to be more effective. There are also opportunities for further work – very few studies have been carried out using AC of 100–400 Hz, and reports on the byproducts formed during H_2S decomposition in dielectric barrier discharge (DBD) systems are few. Many literatures reported the pollutants removal with plasma reactor, in which the spherical ceramic pellets were filled.

* Corresponding author. Tel.: +86 10 67392080.
E-mail address: liangwenj1978@hotmail.com (W.-J. Liang).

0304-3886/$ – see front matter © 2011 Elsevier B.V. All rights reserved.
doi:10.1016/j.elstat.2011.03.011

In the present paper, we present a new DBD plasma reactor, filled with glass beads or ceramic Raschig rings as "pellets". The main objective of this study is to compare the decomposition of H_2S with and without the pellets. The electrical parameters during the discharge process and the energy efficiency for H_2S removal were investigated at the same time. The byproducts during the decomposition of H_2S were also evaluated, enabling destruction mechanisms to be discussed.

2. Experimental setup

2.1. Experimental apparatus

The schematic diagram of the experimental setup for the present study is shown in Fig. 1. The setup consisted of a DBD plasma reactor, an AC power supply (0–100 kV, 50–500 Hz, sine wave), a continuous flow gas supply system and electric and gaseous analytical systems. H_2S (99.9%, Beijing Zhaoge Special Gas Co.) was mixed with compressed air through a mixing chamber and then introduced into the DBD reactor. The flow rate and H_2S concentration were adjusted by mass flow controllers (MFC). The coaxial cylindrical DBD reactor was made of PMMA with an inner diameter of 28 mm and wall thickness of 2 mm wrapped with an iron mesh, 20 cm long, which acted as a ground electrode. The inner discharge electrode was a tungsten wire, 1.25 mm diameter, placed on the axis of the reactor. The relative humidity in the reactor was controlled at 30% with a thermohygrometer. Ceramic Raschig rings or glass pellets were chosen as pellets and were packed randomly packed into the DBD reactor. When a sufficiently high voltage was applied to the reactor, micro-discharges began, initiating a series of chemical reactions.

2.2. Analyses and procedures

The concentrations of H_2S before and after plasma treatment were determined by a spectrophotometric method. H_2S in the gas stream was absorbed by a solution of N,N-dimethyl-p-phenylenediamine in acid, to which $FeCl_3$ was added afterward to form methylene blue. H_2S was then determined by measuring absorbance at 665 nm with a spectrophotometer (UV/vis 2000, Shanghai Precision & Scientific Instrument CO., LTD, China). A typical standard curve relating absorbance to the mass of H_2S in solution is shown in Fig. 2. A linear relationship between absorbance and mass of H_2S in solution was observed with a correlation coefficient of 0.999. The initial concentration of H_2S was 30 ppm and the gas flow rate in the reactor was 8–18 L/min.

The H_2S removal efficiency is calculated as:

$$\eta_{H_2S}(\%) = \frac{C_{in} - C_{out}}{C_{in}} \times 100 \quad (1)$$

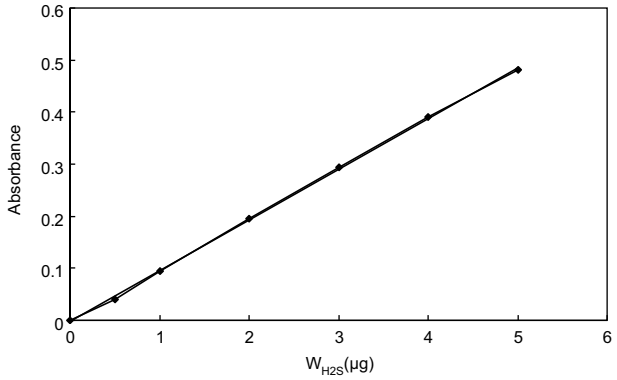

Fig. 2. Typical standard curve for light absorbance with the mass of H_2S.

where C_{in} and C_{out} denote the inlet and outlet concentrations (mg/m^3) of H_2S respectively.

The products of the reaction were detected by GC–MS (Trace DSQ, USA). Intermediate product analysis was done using EI mode, 70 eV and full scan. The byproducts were also analyzed by an ion chromatography (IC) (Metrohm 861, Switzerland).

The surface areas of the pellets used in the experiment were measured using gas adsorption principles (Detected by Micromeritics, NOVA 1000, USA).

2.3. Electrical measurements

The plasma was generated at atmospheric pressure and room temperature. The voltage and current waves were measured by an oscilloscope (Tektronix 2014). To investigate the electric characteristics of the discharge, the voltage applied to the reactor was sampled by a 12500:1 voltage divider. The current was determined from the voltage drop across a shunt resistor ($R3 = 10\ k\Omega$) connected in series with the ground electrode. In order to obtain the total charge and discharge power simultaneously, a capacitor ($Cm = 2\ \mu F$) was inserted between the reactor and the ground. The electrical power provided to the discharge was measured using the V-Q Lissajous diagram [27]. The discharge power is directly proportional to the area of the parallelogram in the diagram, and can be calculated according to the relation:

$$P = f \cdot C_m \cdot S \quad (2)$$

where C_m is the 2 μF measuring capacitance, f is the frequency and S is the area of the parallelogram.

In addition to energy consumption, the equivalent capacitance during the discharge process is an important parameter. The two gradients of the parallelogram of the V-Q Lissajous diagram

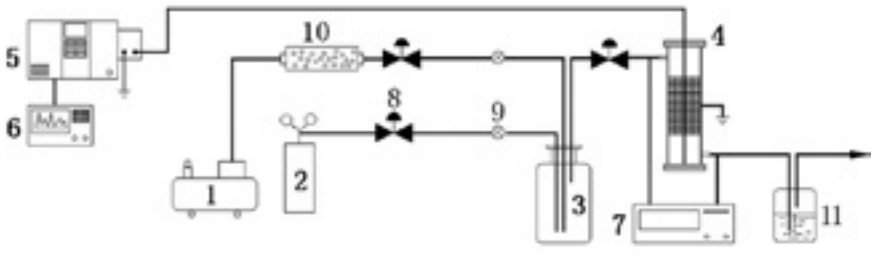

Fig. 1. Schematic diagram of the experimental setup 1. Air compressor 2. H_2S gas cylinder 3. Mixing chamber4. DBD reactor 5. AC power supply 6. Oscillograph 7. Spectrophotometer 8. MFC 9. Needle valve 10. Gas filtration system 11. Absorbent.

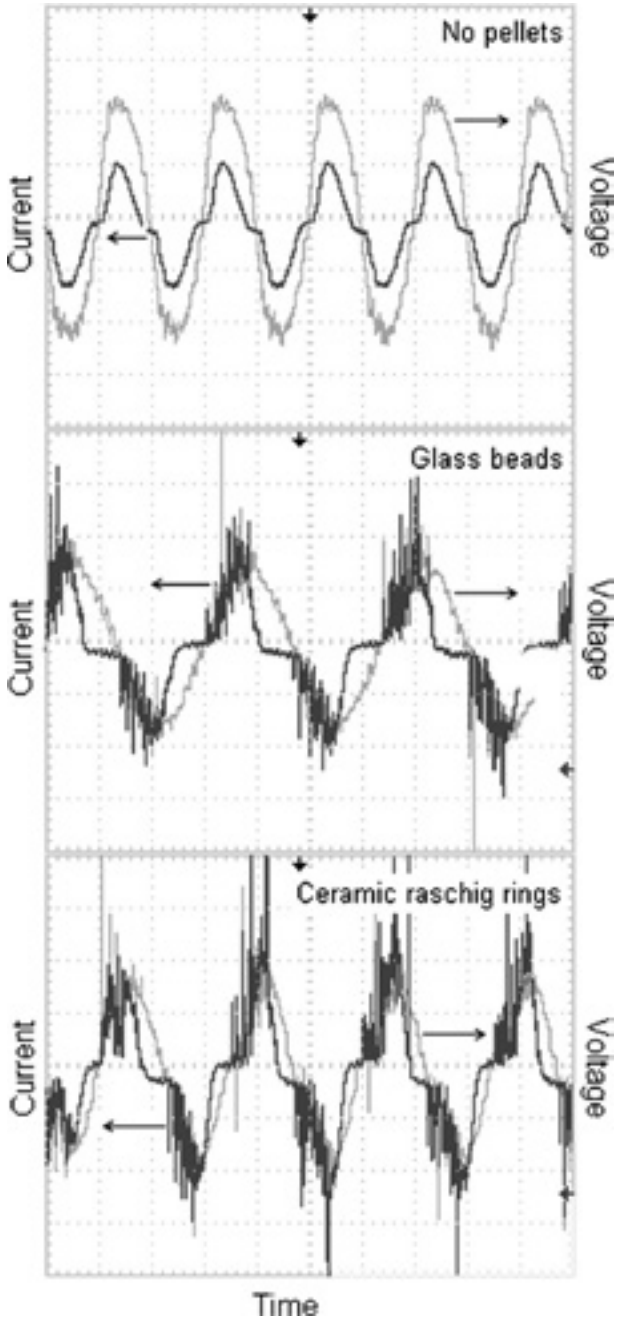

Fig. 3. Waveforms of applied voltage and discharge current (13 kV applied voltage, 300 Hz frequency).

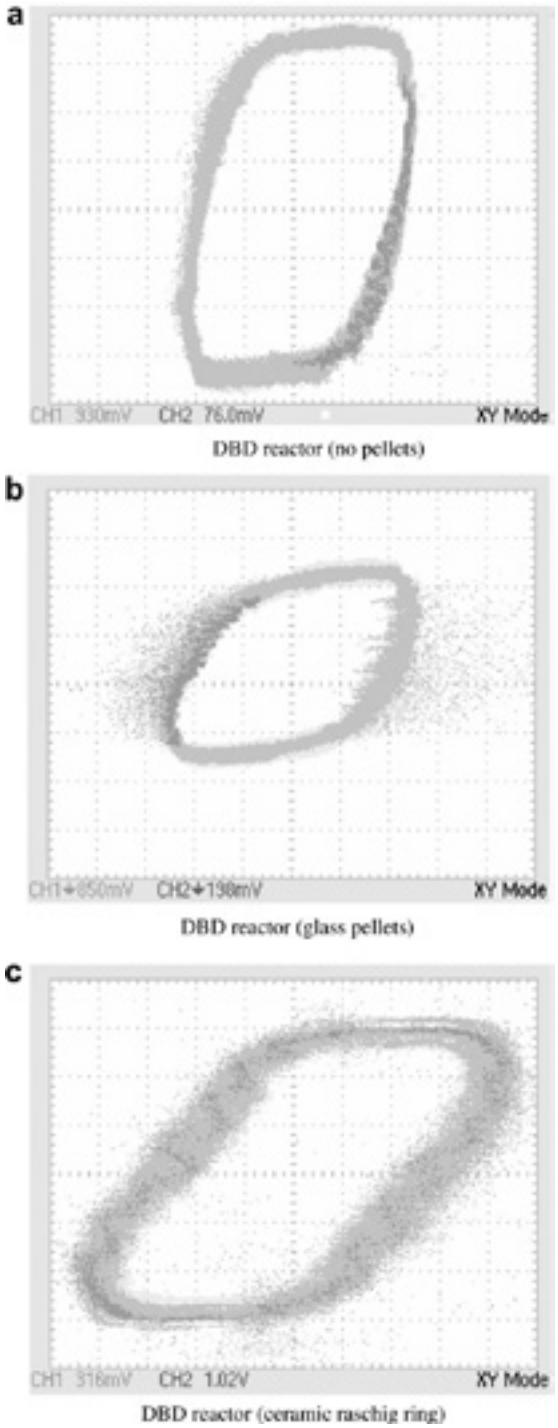

Fig. 4. Typical Lissajous figures for three kinds of dielectric barrier discharge (13 kV applied voltage, 300 Hz frequency).

represent the capacitances in the equivalent circuit of the reactor. In this paper, *C*, *Cd*, and *Cg* denote the total equivalent capacitance, the equivalent capacitance of the dielectric barrier and the equivalent capacitance of the gap, respectively. The relationship between them can be expressed as:

$$C = \frac{Cd \times Cg}{Cd + Cg} \tag{3}$$

The specific energy density (SED) was defined as the average power dissipated in the discharge, divided by the total gas flow rate:

$$\mathrm{SED}\left(J/l\right) = \frac{P(W)}{\mathrm{Q}\left(l/\mathrm{min}\right)} \times 60 \tag{4}$$

where *P* and *Q* denote the discharge power (*W*) and gas flow rate (*l*/min).

As a measure of the energy efficiency, the energy yield (EY) was defined:

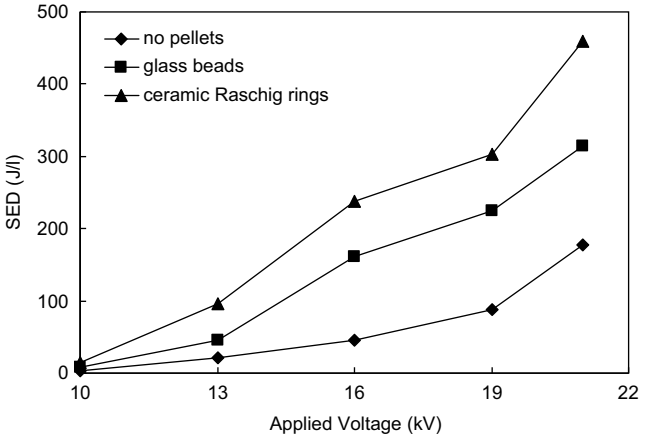

Fig. 5. Variation of SED as a function of applied voltage.

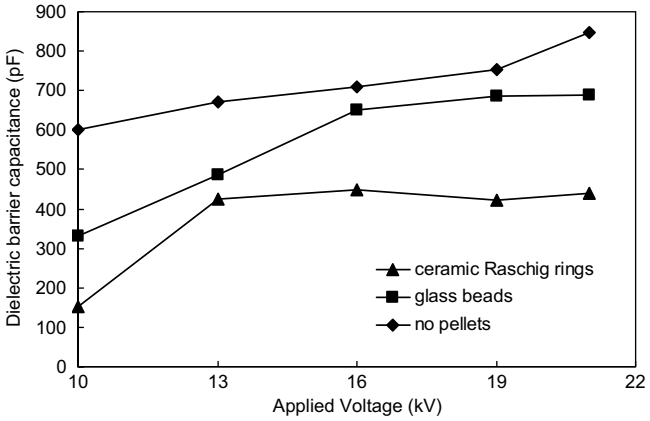

Fig. 7. Variation of dielectric barrier capacitance as a function of applied voltage.

$$\mathrm{EY}\left(\mathrm{g/kWh}\right) = \frac{C_{\mathrm{in}} - C_{\mathrm{out}}}{\mathrm{SED}} \times 3.6 \tag{5}$$

where C_{in} and C_{out} denote the inlet and outlet concentrations ($\mathrm{mg/m^3}$) of H_2S respectively.

3. Results and discussion

3.1. Electrical discharge characteristics

Typical applied voltage and discharge current waveforms for various reactors are shown in Fig. 3. The applied voltage was 13 kV (300 Hz, sinusoidal waveform), and was slightly distorted by the microdischarge current, especially when the reactor contained pellets. These micro-discharges, which were uniformly distributed over the surface of the dielectric, were of nanosecond duration and generated radicals, excited atomic or molecular species that initiate plasma chemical reactions. Obviously, the number of micro-discharge pulses in the presence of pellets was much larger than without pellets. The number of microdischarge is directly related to the pollutant decomposition via non-thermal plasma. The discharge voltage and current showed typical barrier discharge waveforms; that is, the microdischarge current appeared when the applied voltage passed through certain values (discharge onset voltages) to the positive or negative maximum, which is in agreement with the literature [27]. Typically, the voltage charge Lissajous figure of the three kinds of reactors was shaped like a parallelogram, as shown in Fig. 4. The area of this parallelogram was equal to the energy dissipated during one period of the voltage [28]. Fig. 5 shows the variation in SED as a function of applied voltage in the presence and absence of pellets. The SED values for reactors with different pellets were generally in the order: ceramic Raschig rings reactor > glass beads reactor > no pellets reactor under the same experimental conditions. When the applied voltage was below 13 kV, the SED of the ceramic Raschig rings reactor was slightly higher than that of the glass beads reactor and the no pellets reactor. At an applied voltage of 13 kV, the SEDs for the three reactors were 21 J/l (no pellets), 45 J/l (glass beads) and 96 J/l (ceramic Raschig rings). This order was maintained with further increase in voltage, as the SED increased substantially for all reactors, particularly those containing pellets. As the applied voltage increased from 13 to 21 kV, the SED of the reactors increased from 21 J/l to 178 J/l (no pellets), 45 J/l to 315 J/l (glass beads), and 96 J/l to 459 J/l (ceramic Raschig rings). In an electric field, materials such as ceramics and glass are able to store energy. The relative dielectric constants of the ceramic and glass at normal temperature and pressure were 9.16 and 4.10, which meant that the energy storage ability of the ceramic was higher than that of glass. At low applied voltage, there was little effect of the materials in the electric field, and the plasma was mainly of the type referred to as corona discharge, which occurs in regions of high electric field near electrically stressed wire edges. When the voltage was high enough, dielectric barrier discharge began to occur, and the pellets

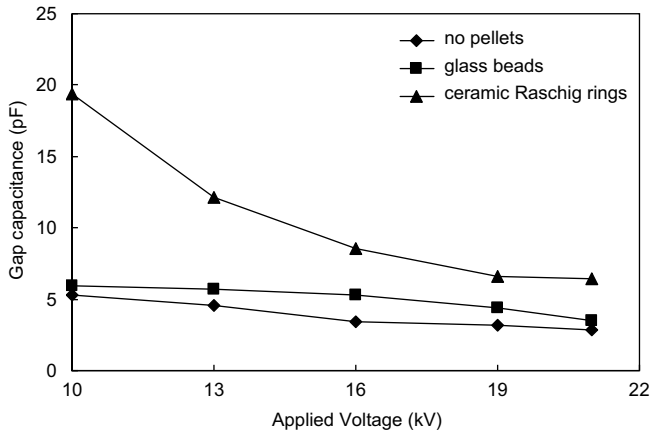

Fig. 6. Variation of gap capacitance as a function of applied voltage.

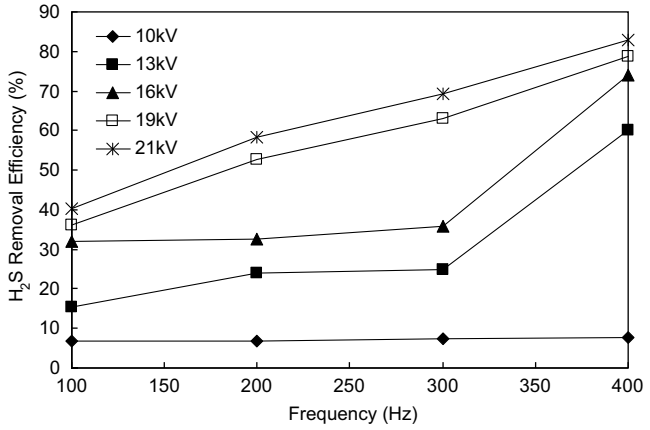

Fig. 8. H_2S removal as a function of frequency under different applied voltage inlet concentration was 30 ppm; gas flow rate was 0.25l/s, and residence time was 0.8 s.

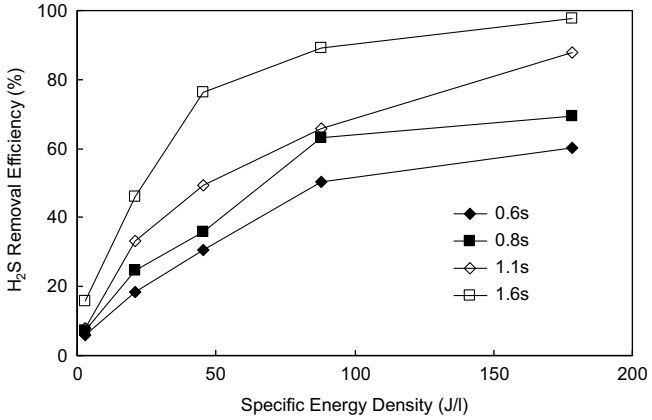

Fig. 9. H_2S removal as a function of SED under different gas residence time inlet concentration was 30 ppm; and frequency was 300 Hz.

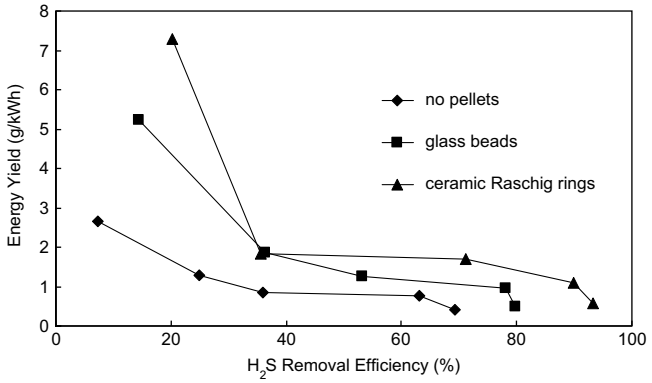

Fig. 11. Relationship between energy yield and H_2S removal Inlet concentration was 30 ppm; gas residence time was 0.8 s; and frequency was 300 Hz.

stored more energy as the electric field strength increased. More micro-discharges appeared under these electric fields, which resulted in initiation of chemical reactions between H_2S molecules, radicals and electrons.

For DBD plasma, the plasma reactor can be regarded as equivalent to a capacitive load, so the equivalent capacitance of the gap (Cg) and the equivalent capacitance of the dielectric barrier (Cd) are important parameters. In accordance with methods in literature [29,30], Cg and Cd for our experiments were calculated using V-Q Lissajous diagrams. Fig. 6 shows the equivalent gap capacitance (Cg) as a function of applied voltage for the different kinds of DBD reactor. In general, Cg decreased gradually with increasing applied voltage. At the same time, Cg of the DBD reactor with ceramic Raschig rings decreased sharply when the applied voltage was 10–16 kV. For the reactor with ceramic Raschig rings, when the applied voltage increased from 10 to 21 kV, Cg decreased from 19 pF to 6 pF. This is consistent with the observations reported by Takaki et al. [30].

The equivalent capacitance of the dielectric barrier (Cd, obtained by V-Q Lissajous diagrams) as a function of applied voltage is shown in Fig. 7. All the reactors displayed the same general trend, with Cd increasing with higher applied voltage. Cd values for the various reactors were in the order: no pellets reactor > glass beads reactor > ceramic Raschig rings reactor. When the applied voltage increased from 10 kV to 21 kV, the Cd values changes as follows: no pellets reactor increased from 600 pF to 847 pF; ceramic Raschig rings reactor increased from 151 pF to 441 pF; glass beads reactor increased from 330 pF to 690 pF. According to the investigation by Takaki et al. [30], a small capacitance of the reactor has some advantages: 1) the capacity of the power supply required to drive the DBD reactor can be reduced and 2) the dielectric loss in the barrier can be decreased. In summary, the DBD reactor with ceramic Raschig rings had the best discharge characteristics of the three reactors investigated.

3.2. H_2S decomposition in the plasma

3.2.1. Effect of applied frequency on H_2S decomposition

Experiments were conducted to determine the dependence of H_2S removal efficiency on AC frequency and applied voltage, as shown in Fig. 8. Both the number and average energy of electrons and active radicals apparently increased with increasing applied voltage and AC frequency, leading to higher H_2S removal efficiency. When the frequency was lower than 300 Hz, H_2S removal efficiency increased slowly with frequency, while it increased sharply when frequency was higher than 300 Hz. The dependence of η_{H_2S} on applied voltage was similar to the dependence on frequency. An increase in AC frequency from 100 Hz to 400 Hz, resulted in an increase in H_2S removal efficiency from 6.8% to 7.8% with for an applied voltage of 10 kV, and a very significant increase from 40.4% to 82.8% was observed when the applied voltage was 21 kV. When the amplitude of the applied voltage is low, the voltage across the discharge gap is not high enough to ignite the plasma. Once the voltage was high enough to cause breakdown of the gas, the charge was phase shifted with respect to the voltage due to resistive losses in the charge [29].

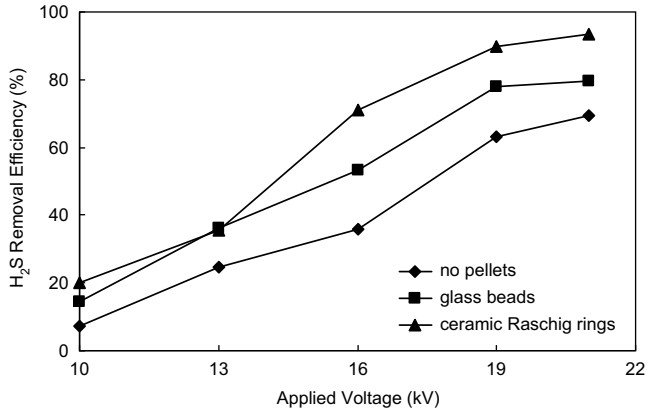

Fig. 10. H_2S removal as a function of applied voltage for different reactors inlet concentration was 30 ppm; gas residence time was 0.8 s; and frequency was 300 Hz.

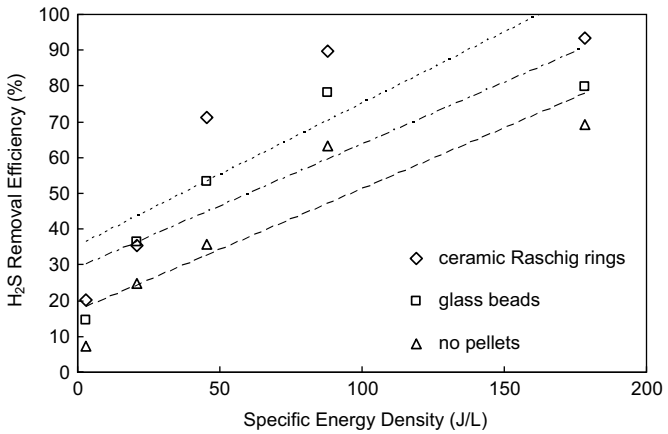

Fig. 12. Relationship between η and SED and linear fits for different reactors.

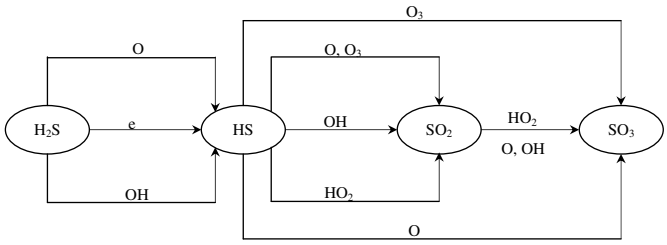

Fig. 13. Dominant pathways leading to the destruction of H_2S molecules.

These resistive losses arise as free electrons or radicals transfer all or part of their kinetic energy to the target molecules through inelastic collisions, leading to destruction of the target molecule.

According to the investigation by Xia et al. [17], when their plasma system was operated for a long enough time, the temperature of the whole plasma zone was observed to increase from 150 °C to 250 °C with peak voltage rising from 3 kV to 9 kV and fixed frequency of 20 kHz. In our experiment, during the course of plasma discharge, the temperature of the plasma zone was only 5–8 °C higher than room temperature.

3.2.2. Effect of gas residence time on H_2S decomposition

Fig. 9 presents the influence of gas residence time and SED on H_2S decomposition. Similar trends were observed for different gas residence times. It is found that the effect of increasing the gas residence time depends on the SED – a sharp increase in removal efficiency was observed when the SED was lower than 87.9 J/l while only a slight increase resulted when the SED was higher than 87.9 J/l. Longer gas residence times result in a larger probability of collisions between H_2S molecules and electrons and radicals, and hence enhance the removal of H_2S. Furthermore, with increasing SED, the energy throughout the entire discharge volume was increasing, leading to micro-discharges throughout the reactor and stimulating the chemical reactions between H_2S molecules and electrons and radicals. Similar experiment results were obtained by Xia et al. [11,17].

3.2.3. Effect of pellets on H_2S removal

Fig. 10 represents the H_2S removal process for DBD reactors containing different pellets as a function of applied voltage. The H_2S removal efficiencies followed the same trend, that is, η_{H_2S} was enhanced with increasing applied voltage. The H_2S removal efficiency of three reactors was in the order ceramic Raschig rings reactor > glass beads reactor > no pellets reactor for the same experimental conditions. For example, at 10 kV applied voltage, the efficiency values were: 20.2% (ceramic Raschig rings reactor), 14.5% (glass beads reactor) and 7.4% (no pellets reactor), while at 21 kV applied voltage, the values were 93.3%, 79.7% and 69.3% respectively. Durme et al. [31] indicated that packing pellets are helpful for expanding the discharge region because the streamers (or micro-discharges) are apt to propagate along the solid surfaces. Our experiment results demonstrate that the packing material is an important factor influencing H_2S removal. In our experiment, the BET surface areas of the ceramic Raschig rings and glass beads were 0.2461 m^2/g and 0.0353 m^2/g. This implies that more H_2S molecules, electrons and radicals could react with one another on the ceramic pellet surface than on the glass pellet surface. And both reactors with pellets had higher H_2S decomposition ability than the no pellets reactor. As mentioned above in Fig. 5, we observed that the SED values of the different pellet reactors were in the order ceramic Raschig rings reactor > glass beads reactor > no pellets reactor under the same experimental conditions, which means more energetic electrons and radicals were generated in the ceramic Raschig rings reactor than the other reactors, which is consistent with the observed higher H_2S removal efficiency.

3.3. Energy efficiency for H_2S removal

We have used the energy yield (EY) to characterize the H_2S removal ability of each plasma reactor. From Equation (5), it can be seen that EY is inversely proportional to SED. Fig. 11 illustrates the relationship between EY and H_2S removal efficiency for the three reactors. Obviously, as the H_2S removal efficiency increased, the energy yield decreased for all reactors. The highest EY was 7.30 g/kWh for the ceramic Raschig rings reactor. Once the removal efficiency ratio for the glass beads reactor and ceramic Raschig rings reactor exceeded 35%, the EY stabilized at about 1.8 g/kWh, double the energy efficiency of the no pellets reactor.

The decomposition rate of H_2S molecules depends on both the concentration of H_2S itself and the concentrations of the active species generated in the reactor. The concentrations of active

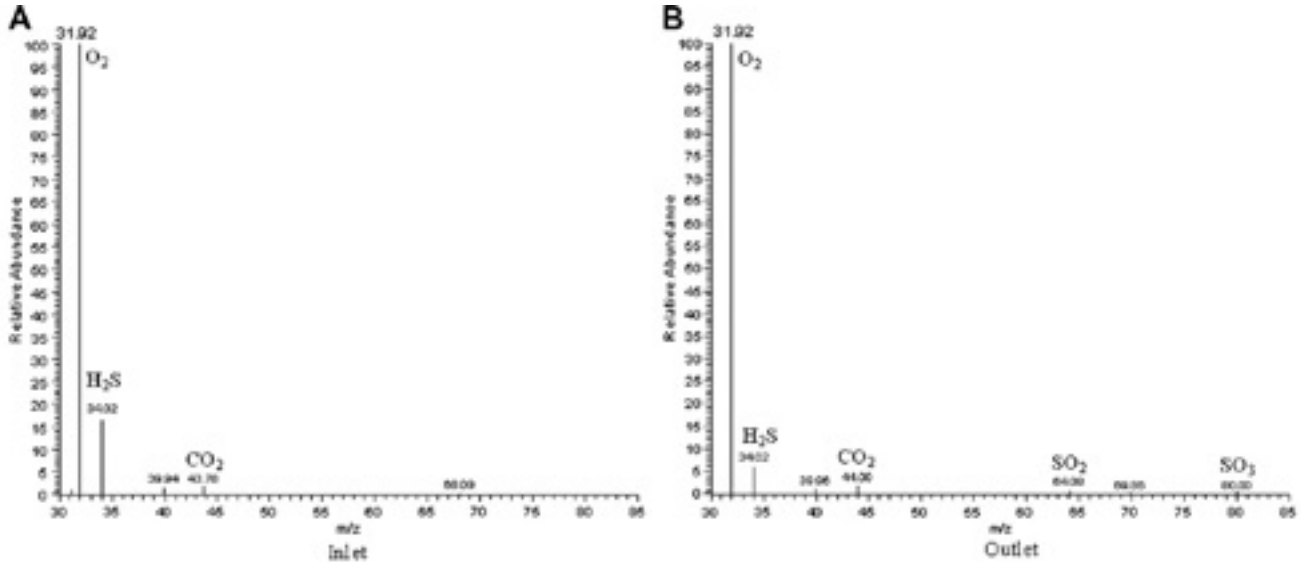

Fig. 14. Mass spectrogram of inlet and outlet products.

species generated are proportional to the discharge power. This leads to the important relationship between H_2S removal and discharge power, as shown in Equation (6).

$$\eta = \mathrm{SED} \times K_d + b \tag{6}$$

where K_d is the reaction rate constant, and b is the intercept.

Variation in η as a function of SED is given in Fig. 12. The reaction rate constants for ceramic, glass and no pellet reactors were 0.3982, 0.3453 and 0.3397, respectively. The ceramic Raschig rings reactor had the best H_2S decomposition capability of all the reactors.

3.4. Destruction mechanism for H_2S and analysis for by-products

A DBD plasma generates electrons with sufficient energy to cause the formation of gas-phase radicals, thereby driving the reactions of decomposition and oxidation of H_2S to form end products including H_2O, SO_2, and SO_3. The removal of H_2S probably depends on two mechanisms: (a) direct removal caused by the collision of electrons and (b) reaction between H_2S molecules and gas-phase radicals (indirect gas-phase radical reaction). Gas-phase radicals may consist of O•, OH•, $HO_2^{\bullet}$ and O_3. Suggested reactions at normal temperature and pressure are shown in Equations (7)–(18) [11,14–16,25,26].

$$H_2S + e \rightarrow H^{\bullet} + HS^{\bullet} \tag{7}$$

$$H_2S + OH^{\bullet} \rightarrow HS^{\bullet} + H_2O \tag{8}$$

$$H_2S + O^{\bullet} \rightarrow HS^{\bullet} + OH^{\bullet} \tag{9}$$

$$HS^{\bullet} + OH^{\bullet} \rightarrow SO_2 + H^{\bullet} \tag{10}$$

$$HS^{\bullet} + O^{\bullet} \rightarrow SO_2 + H^{\bullet} \tag{11}$$

$$HS^{\bullet} + O_3 \rightarrow SO_2 + OH^{\bullet} \tag{12}$$

$$HS^{\bullet} + HO_2^{\bullet} \rightarrow SO_2 + H^{\bullet} \tag{13}$$

$$HS^{\bullet} + O^{\bullet} \rightarrow SO_3 + H^{\bullet} \tag{14}$$

$$HS^{\bullet} + O_3 \rightarrow SO_3 + H^{\bullet} \tag{15}$$

$$SO_2 + O^{\bullet} \rightarrow SO_3 \tag{16}$$

$$SO_2 + OH^{\bullet} \rightarrow SO_3 + H^{\bullet} \tag{17}$$

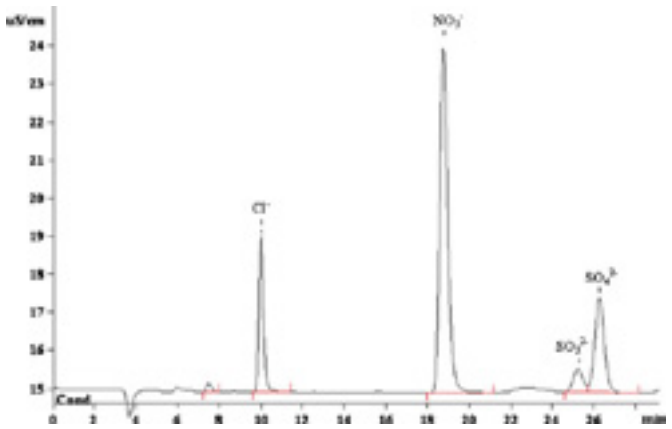

Fig. 15. Products in inlet and outlet gas.

$$SO_2 + HO_2^{\bullet} \rightarrow SO_3 + OH^{\bullet} \tag{18}$$

It can be seen from these reactions that generation of HS radicals is a very important step resulting in further oxidation and removal of H_2S molecules. The dominant pathways for the removal of H_2S are described in Fig. 13.

In our experiments, the contents of both the inlet gas and outlet effluent were confirmed through GC-MS. From the mass spectrograms of inlet and outlet gases in Fig. 14A and B, we could determine that the main components of the inlet gas were O_2, H_2S and CO_2, while in the outlet gas, the main products were O_2, less H_2S, CO_2, SO_2 and SO_3. The assignment of the peaks at $m/z = 39.94, 68.09$ and 69.86 requires further investigation.

To confirm the products of H_2S decomposition, the gas products were sampled into distilled water and the ion chromatography (IC) technique was employed to analyze products qualitatively. As shown in Fig. 15, the main anions were Cl^-, NO_3^-, SO_3^{2-} and SO_4^{2-}, and no other anions were detected in the sample using IC. The SO_2 and SO_3 in outlet gas are the products of H_2S decomposition, while the NO_3^- is assumed to result from nitrogen oxides in the effluent. The origin of Cl^- is unclear at this stage.

4. Conclusions

The abatement of H_2S with non-thermal DBD plasma was experimentally investigated in a coaxial cylindrical reactor. The main results are that the efficiencies (as measured by the SED) for reactors containing different pellets were in the order: ceramic Raschig rings reactor > glass beads reactor > no pellets reactor under the same experimental conditions. Cg generally decreased gradually with increasing applied voltage, but Cd increased with higher applied voltage. Both the number and average energy of the electrons and active radicals increased with increased applied voltage or AC frequency, which led to higher H_2S removal efficiency. Longer gas residence times (which result in greater collision probability between H_2S molecules and electrons and radicals) enhanced the removal of H_2S, as did the choice of pellet material. The highest EY was 7.30 g/kWh for the ceramic Raschig rings reactor. The likely major products in the outlet effluent were H_2O, SO_2, and SO_3.

Acknowledgment

This work was supported by the Youth Scientific Research Fund of BJUT(X1005013200802).

References

[1] B. Mills, Review of methods of odor control, Filtr. Sep. 32 (1995) 146–152.
[2] M. Tomar, T.H.A. Abdullah, Evaluation of chemicals to control the generation of malodorous hydrogen sulfide in waste water, Water Res. 28 (1994) 2545–2552.
[3] D. Gabriel, M.A. Deshusses, Retrofitting existing chemical scrubbers to biotrickling filters for H_2S emission control, Proc. Natl. Acad. Sci. U S A 100 (2003) 6308–6312.
[4] M.A. Daley, C.L. Mangun, J.A.D. Barr, S. Riha, A. Lizzio, G. Donnals, J. Economy, Adsorption of SO_2 onto oxidized and heat-treated activated carbon fibers (ACFs), Carbon 35 (1997) 411–417.
[5] A. Bagreev, S. Katikaneni, S. Parab, T.J. Bandosz, Desulfurization of digester gas: prediction of activated carbon bed performance at low concentrations of hydrogen sulfide, Catal. Today 99 (2005) 329–337.
[6] D.N. Thanh, K. Block, T.J. Bandosz, Adsorption of hydrogen sulfide on montmorillonites modified with iron, Chemosphere 59 (2005) 343–353.
[7] M.N. Bae, M.K. Song, Y. Kim, K. Seff, The catalytic activity of vanadium pentoxide film modified electrode on the electrochemical oxidation of hydrogen sulfide in alkaline solutions, Micropor. Mesopor. Mater. 63 (2003) 21–31.
[8] X.H. Wang, T.H. Sun, J. Yang, L. Zhao, J.P. Jia, Low-temperature H_2S removal from gas streams with SBA-15 supported ZnO nanoparticles, Chem. Eng. J. 142 (2008) 48–55.
[9] L.A. Fenouil, S. Lynn, Study of calcium-based sorbents for high-temperature H_2S removal. 1. Kinetics of H_2S sorption by uncalcined limestone, Ind. Eng. Chem. Res. 34 (1995) 2324–2333.

[10] L.A. Fenouil, S. Lynn, Study of calcium-based sorbents for high-temperature H_2S removal. 2. Kinetics of H_2S sorption by calcined limestone, Ind. Eng. Chem. Res. 34 (1995) 2334–2342.
[11] L.Y. Xia, D.H. Gu, J. Tan, W.B. Dong, H.Q. Hou, Photolysis of low concentration H_2S under UV/VUV irradiation emitted from microwave discharge electrodeless lamps, Chemosphere 71 (2008) 1774–1780.
[12] R. Portela, B. Sánchez, J.M. Coronado, R. Candal, S. Suárez, Selection of TiO_2-support: UV-transparent alternatives and long-term use limitations for H_2S removal, Catal. Today 129 (2007) 223–230.
[13] R. Portela, M.C. Canela, B. Sánchez, F.C. Marques, A.M. Stumbo, R.F. Tessinari, J.M. Coronado, S. Suárez, H_2S photodegradation by TiO_2/M-MCM-41 (M = Cr or Ce): deactivation and by-product generation under UV-A and visible light, Appl. Catal. B 84 (2008) 643–650.
[14] E. Subramanian, J.O. Baeg, S.M. Lee, S.J. Moon, K.J. Kong, Dissociation of H_2S under visible light irradiation ($\lambda \geq 420$ nm) with $FeGaO_3$ photocatalysts for the production of hydrogen, Int. J. Hydrogen Energy 33 (2008) 6586–6594.
[15] M.D. Bai, Z.T. Zhang, M.D. Bai, C.W. Yi, X.Y. Bai, Removal of SO_2 from gas streams by oxidation using plasma-generated hydroxyl radicals, Plasma Chem. Plasma Process 26 (2006) 177–186.
[16] M.B. Chang, J.H. Balbach, M.J. Rood, M.J. Kushner, Removal of SO_2 from gas streams using a dielectric barrier discharge and combined plasma photolysis, J. Appl. Phys. 69 (1991) 4409–4417.
[17] L.Y. Xia, L. Huang, X.H. Shu, R.X. Zhang, W.B. Dong, H.Q. Hou, Removal of ammonia from gas streams with dielectric barrier discharge plasmas, J. Hazard. Mater. (2007). doi:10.1016/j.jhazmat.2007.06.070.
[18] M.B. Chang, T.D. Tseng, Gas-phase removal of H_2S and NH_3 with dielectric barrier discharges, J. Environ. Eng. 122 (1996) 41–46.
[19] C.L. Chang, T.S. Lin, Decomposition of toluene and acetone in packed dielectric barrier discharge reactors, Plasma Chem. Plasma Process 25 (2005) 227–243.
[20] H.H. Kim, H. Kobara, A. Ogata, S. Futamura, Comparative assessment of different non-thermal plasma reactors on energy efficiency and aerosol formation from the decomposition of gas-phase benzene, IEEE Trans. Ind. Appl. 41 (2005) 206–214.
[21] Z.L. Ye, Y.N. Zhang, P. Li, L.Y. Yang, R.X. Zhang, H.Q. Hou, Feasibility of destruction of gaseous benzene with dielectric barrier discharge, J. Hazard. Mater. 156 (2008) 356–364.
[22] M.B. Chang, J.S. Chang, Abatement of PFCs from semiconductor manufacturing processes by nonthermal plasma technologies: a critical review, Ind. Eng. Chem. Res. 45 (2006) 4101–4109.
[23] V. Dalaine, J.M. Cormier, S. Pellerin, P. Lefaucheux, H_2S destruction in 50 Hz and 25 kHz gliding arc reactors, J. Appl. Phys. 84 (1998) 1215–1221.
[24] J.J. Ruan, W. Li, Y. Shi, Y. Nie, X. Wang, T.E. Tan, Decomposition of simulated odors in municipal wastewater treatment plants by a wire-plate pulse corona reactor, Chemosphere 59 (2005) 327–333.
[25] D.J. Helfritch, Pulsed corona discharge for hydrogen sulfide decomposition, IEEE Trans. Ind. Appl. 29 (1993) 882–886.
[26] H.B. Ma, P. Chen, R. Ruan, H_2S and NH_3 removal by silent discharge plasma and ozone combo-system, Plasma Chem. Plasma Process 21 (2001) 611–624.
[27] K. Takaki, K. Urashima, J.S. Chang, Ferro-electric pellet shape effect on C_2F_6 removal by a packed-bed-type nonthermal plasma reactor, IEEE Trans. Plasma Sci. 32 (2004) 2175–2183.
[28] M. Kraus, B. Eliasson, U. Kogelschatz, A. Wokaun, CO_2 reforming of methane by the combination of dielectric-barrier discharges and catalysis, Phys. Chem. Chem. Phys. 3 (2001) 294–300.
[29] M. Magureanu, N.B. Mandache, V.I. Parvulescu, Ch. Subrahmanyam, A. Renken, L. Kiwi-Minsker, Improved performance of non-thermal plasma reactor during decomposition of trichloroethylene: optimization of the reactor geometry and introduction of catalytic electrode, Appl. Catal. B 74 (2007) 270–277.
[30] K. Takaki, M. Shimizu, S. Mukaigawa, T. Fujiwara, Effect of electrode shape in dielectric barrier discharge plasma reactor for NOx removal, IEEE Trans. Plasma Sci. 32 (2004) 32–38.
[31] J.V. Durme, J. Dewulf, C. Leys, H. Langenhove, Combining non-thermal plasma with heterogeneous catalysis in waste gas treatment: a review, Appl. Catal. B 78 (2008) 324–333.

ALLEGATO 13.3

ARTICOLI SCIENTIFICI SU
RIMOZIONE CONTAMINANTI ORGANICI (VOC)

Osman Karatum, M. A. (2016). A comparative study of dilute VOCs treatment in a non-thermal plasma reactor. Chemical Engineering Journal 294, 308–315.

J. Karuppiaha, E. Linga Reddya, P. Manoj Kumar Reddya, B. Ramarajua, R. Karvembub, Ch. Subrahmanyama (2012) - Abatement of mixture of volatile organic compounds (VOCs) in a catalytic non-thermal plasma reactor. Journal of Hazardous Materials 237– 238 (2012) 283– 289

Carlos M. Nunez, G. H. (2012). Corona Destruction: An Innovative Control Technology for VOCs and Air Toxics. Waste, 242-247.

Shijie Lia, Xiaoqing Danga, Xin Yua, Ghulam Abbasb, Qian Zhanga, Li Cao (2020) - The application of dielectric barrier discharge non-thermal plasma in VOCs abatement: A review - Chemical Engineering Journal 388 (2020) 124275

Chemical Engineering Journal 294 (2016) 308–315

Contents lists available at ScienceDirect

Chemical Engineering Journal

journal homepage: www.elsevier.com/locate/cej

A comparative study of dilute VOCs treatment in a non-thermal plasma reactor

Osman Karatum [1], Marc A. Deshusses *

Department of Civil and Environmental Engineering, Duke University, United States

HIGHLIGHTS

- The treatment of 7 dilute VOCs vapors in air using non-thermal plasma was investigated.
- Very fast degradation rates were obtained.
- Benzene and MEK were most difficult to degrade while hexane was the easiest.
- Large residual ozone concentrations were observed.
- Tar-like deposits was observed when treating ethylbenzene and toluene.

GRAPHICAL ABSTRACT

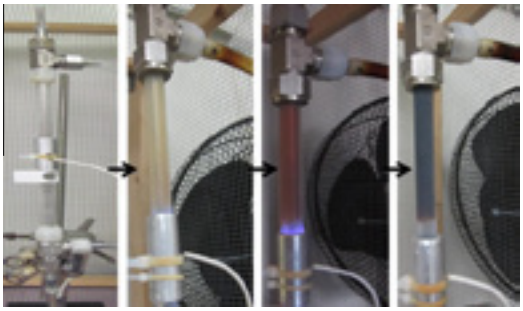

ARTICLE INFO

Article history:
Received 13 January 2016
Received in revised form 29 February 2016
Accepted 1 March 2016
Available online 5 March 2016

Keywords:
Non-thermal plasma
Dielectric barrier discharge
Deposits
VOCs removal
Air pollution control

ABSTRACT

Non-thermal plasma (NTP) is an emerging technology for the treatment of volatile organic compounds (VOCs) in polluted point source air streams. Here, a dielectric barrier discharge NTP was used to evaluate the treatment efficiency of several common VOCs at constant experimental conditions (gas residence time of 0.016 s in the plasma zone, 95–100 ppm_v average inlet VOC concentration in air). When treated as single pollutant with a specific input energy (SIE) of 350 J L^{-1}, the removal efficiency of the VOC followed the following sequence: methyl ethyl ketone (50%), benzene (58%), toluene (74%), 3-pentanone (76%), methyl tert-butyl ether (80%), ethylbenzene (81%), and n-hexane (90%). The effects of pollutant structure on VOC removal efficiency were investigated. The highest removal efficiencies were observed for compounds with the highest percentage of hydrogen in their molecular structures. During treatment of toluene and ethylbenzene vapors, a dark brown, tar-like deposit formed inside the plasma reactor. The deposit formation rate depended on both treated VOCs as well as on experimental conditions such as VOC concentration, and SIE.

1. Introduction

The emission of volatile organic compounds (VOCs) from anthropogenic sources is an important factor associated with human and environmental health, and has both local and global impacts. For example, benzene emissions have been linked to childhood leukemia in Houston, TX [1], a high correlation between VOC emissions and some types of cancer (i.e., brain, endocrine system, and skin) has been reported [2] and many VOCs are precursors to ozone formed by photochemical reactions leading to increased asthma [3].

Different technologies have been used for controlling VOCs, including adsorption, incineration, condensation and biological treatment [4–6]. Adsorption is generally cost-effective only for low concentrations of VOCs, whereas incineration and condensation are best used for high VOC concentrations [7]. For air streams

* Corresponding author at: Dept. of Civil and Environmental Engineering, 127C Hudson Hall, Box 90287, Duke University, Durham, NC 27708-0287, United States. Tel.: +1 919 660 5480; fax: +1 919 660 5219.

E-mail addresses: osman.karatum@duke.edu (O. Karatum), marc.deshusses@duke.edu (M.A. Deshusses).

[1] Dept. of Civil and Environmental Engineering, 121 Hudson Hall, Box 90287, Duke University, Durham, NC 27708-0287, United States. Tel.: +1 919 265 8248; fax: +1 919 660 5219.

http://dx.doi.org/10.1016/j.cej.2016.03.002
1385-8947/

with medium to low concentrations of VOCs, biological treatment methods (e.g., biofiltration) have proven to be effective, however biofiltration is only applicable to the treatment of biodegradable pollutants [4].

An emerging air pollution control technology is non-thermal plasma (NTP) which has the potential to treat high flows for both low (<100 ppm_v) to high (>1000 ppm_v) concentrations of pollutants [8–11]. In particular, NTP or cold plasma has been used to treat air contaminated with elemental mercury, H_2S, SO_2, NO_x, odors, and VOCs such as toluene, benzene, acetone, and trichloroethylene [12–19].

In NTP, electrons and their surroundings are not in thermal equilibrium. Electric discharges in the gas heat the electrons instead of the gas itself, and the resulting high energy electrons, active radicals and ions promote numerous chemical reactions in the ionized zones thus produced. While NTP is a very promising development for a variety of applications [20,21], it also has some drawbacks, notably low energy efficiency, incomplete oxidation of the pollutants undergoing treatment, and the formation of undesired by-products [22–24]. For example, the low selectivity of the oxidation reactions can lead to toxic by-product formation such as CO, NO_x, and O_3 [25,26] and typical values for VOC conversion to CO_2 are only 30–70% [27,28]. In light of this, the original motivation for the present study was to explore and demonstrate the feasibility of combining NTP treatment with a biotrickling filter, as a possible means for effective treatment of low concentrations of selected VOCs (including recalcitrant ones such as hexane) in air. The vision was that NTP would only provide partial breakdown of the VOC and that incompletely oxidized by-products would subsequently be removed biologically in a biotrickling filter. This would capitalize on the high efficiency of NTP for initial breakdown of hard to biodegrade VOCs and rely on effective biotreatment for completing treatment similar to other studies combining advanced oxidation with biological treatment [29,30]. Thus, experiments were conducted with a NTP operated at a very short gas residence time and treating selected VOCs vapors. However, these experiments revealed that the treated VOCs were preferably converted to all the way to CO_2 without the formation of partially oxidized volatile intermediates suggesting that the NTP as used was unsuitable as a pretreatment to a biotrickling filter. On the other hand, a significant amount of solid was found to deposit inside our NTP reactor, and thus the focus of the study was shifted toward characterizing the fate of common VOCs while undergoing treatment and understanding NTP's critical limitations.

2. Materials and methods

2.1. NTP reactor, conditions, and analytical

NTP was generated using a dielectric discharge barrier (DBD) consisting of a cylindrical quartz tube (9 mm inner diameter, 266 mm length, 3.5 mm thick) fitted with an aluminum cylindrical sleeve (5 cm long, 3.2 mm thick) serving as the external electrode. The internal high voltage electrode was a stainless steel rod (6.32 mm outer diameter, 40 cm long) positioned in the center of the quartz tube running along the axial direction of the reactor. Thus, the discharge gap was 1.34 mm, and the total volume of the plasma zone in the reactor was 1.6 mL. Note that the plasma reactor did not include any catalyst or packing materials. A schematic of the experimental setup is shown in Fig. 1. The excitation frequency for the DBD was kept constant at 22 kHz and the voltage was varied ranging from 7 to 10 kV using a PVM500 dielectric barrier corona driver (Information Unlimited, Amherst, NH).

The synthetic VOC-laden air stream (6.6 L min^{-1}) was produced using compressed air from our central laboratory air system which produces dry and oil-free compressed air from ambient air. A metered stream of compressed air was passed through the headspace of a 500 mL flask containing small vials filled with the selected VOC. This VOC-laden stream was then diluted with another metered stream of compressed air at room temperature to the prescribed VOC concentration (95 ppm_v or 100 ppm_v). For experiments with humid air, the main air stream was split prior to being mixed with the VOC vapor and part of it was sparged in a container filled with deionized water. The dry and moist air streams were combined such that the resulting air reached the target relative humidity of 30% at 20–22 °C.

The VOC concentrations at the inlet and outlet of the plasma reactor were determined using a GC (Shimadzu 2014, Kyoto, Japan) equipped with flame ionization detector (FID). The concentrations of CO_2 in the reactor influent and effluent were determined using a non-dispersive infrared portable CO_2 meter (Vaisala Carbon Dioxide Meter-GMP70, Louisville, CO). Carbon monoxide effluent concentrations were determined using Dräeger tubes (Sugarland, TX), and the ozone concentration was measured by the iodometric method (Iodometric Method, Standardized Procedure 001/96, International Ozone Association) after absorption of a metered air stream into solutions of KI. Elemental analysis of the deposits was conducted by the Duke Environmental Stable Isotope Laboratory using a Carlo Erba Elemental Analyzer. The temperature of the

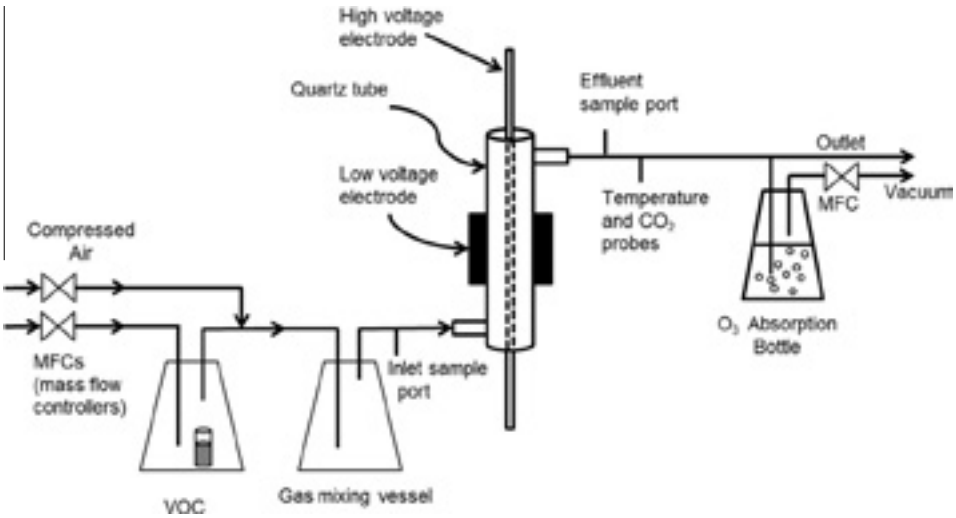

Fig. 1. General schematic of the experimental set up (see Figs. SM-1 and SM-2 for power monitoring setup).

discharge zone was measured with a surface mounted K-type thermocouple attached to the outer electrode. Another thermocouple was placed in the effluent air downstream of the plasma reactor. The thermocouples were connected to a data logger to record temperature at 5-s intervals. Average temperatures were reported.

2.2. Electrical measurements

One of the most important parameters for assessing plasma reactors for air or gas treatment is the specific input energy (SIE), which is the power dissipated in the plasma divided by the gas flow rate and thus has units of J L^{-1}. The SIE was determined using Eq. (1) [31].

$$\text{SIE (J L}^{-1}) = \frac{\text{Power (W)}}{\text{Flow Rate (L s}^{-1})} \quad (1)$$

The discharge power was determined using the charge (Q) accumulated on a non-inductive capacitor (C = 0.22 μF) calculated (using $V = Q/C$) from the voltage measured using a high frequency data acquisition (Nationals Instruments, NI, USB-5132) (see Fig. SM-1 in supplementary information). Plotting Q vs. the voltage measured across the capacitor allows calculation of the power (i.e., the so-called Q–V Lissajous method). The multiplication of frequency with the area of the parallelogram formed by Q vs. V is equal to the discharge power in the DBD reactor (Fig. SM-2). Real-time calculation of the discharge power was carried out by a custom LabView (National Instruments, Austin, TX) code using Matlab sub-routines.

2.3. Experimental protocol

All experiments were carried out at room temperature (20–22 °C) and atmospheric pressure. The selected VOCs were toluene, benzene, ethylbenzene, methyl ethyl ketone (MEK), methyl tert-butyl ether (MTBE), 3-pentanone, and n-hexane. These VOCs were selected to determine the effect of the molecular structure (e.g., aromatics, ketones, or alkanes) on the removal of these VOCs in the NTP reactor and because of their frequent occurrence as air pollutants. Experiments were conducted at a constant air flow rate (6.6 L min^{-1} corresponding to a contact time of 0.016 s in the plasma zone) and a constant inlet concentration of VOCs (95 ppm_v). Determination of the VOC removal, effluent CO_2, O_3 concentrations, and mass of deposit was performed at selected SIEs ranging from 50 to 300 J L^{-1}. Subsequently, VOCs that caused the formation of deposits inside the plasma reactor were tested at a constant inlet concentration (100 ppm_v), flow rate (6.6 L min^{-1}), and SIE (360 J L^{-1}) in order to determine the relationship between VOC removal, the rate of deposit formation, and the time until reactor clogging.

3. Results and discussion

3.1. Influence of SIE on VOC removal efficiency

The effect of SIE on the removal efficiency (RE) of VOCs was investigated first. Many studies have reported that when keeping the SIE constant, increasing the VOC concentration and/or the air flow rate decreased the RE, and that increasing the SIE at a constant air flow rate and inlet pollutant concentration increased pollutant removal [7,32]. As will be discussed in more details in Section 3.4, the VOCs were primarily converted to CO_2 and some unaccounted fraction (possibly CO), and no partially degraded volatile organics were detected by GC. The absence of partially oxidized by-products had been explained by Nunez et al. [14] by the fact that once the reaction is initiated, the heat of the reaction is generally sufficient to sustain the completion of the oxidation to CO_2. Fig. 2 shows the removal efficiency of the seven VOCs tested as a function of SIE. Clearly, the RE increased proportionally with SIE, however, both the removal of the VOCs and the effect of the SIE depended on the specific compound being treated. Selected results of this study are summarized and compared to others in Table 1. Holzer et al. [28] investigated the treatment of MTBE and toluene vapors; the addition of a catalyst in their NTP system resulted in much higher removal efficiencies (⩾90%) even at very high inlet concentrations (240 and 450 ppm_v). Delagrange et al. [24] reported that the oxidation of high concentrations of toluene required higher SIEs in the absence of a catalyst. In non-catalyst applications, Mista and Kacprzyk [33] focused on the removal of toluene using a direct current (DC) back corona discharge reactor at room temperature and found very low RE (15%), despite using relatively high SIE (400 J L^{-1}). One likely reason for the lower removal may be the additional electrode (described as a passive electrode used for the back-ionization process), which could have resulted in non-homogenous distribution of energetic electrons. Differences in experimental conditions can also cause differences in reactor performance, hence the interest in systematic studies like

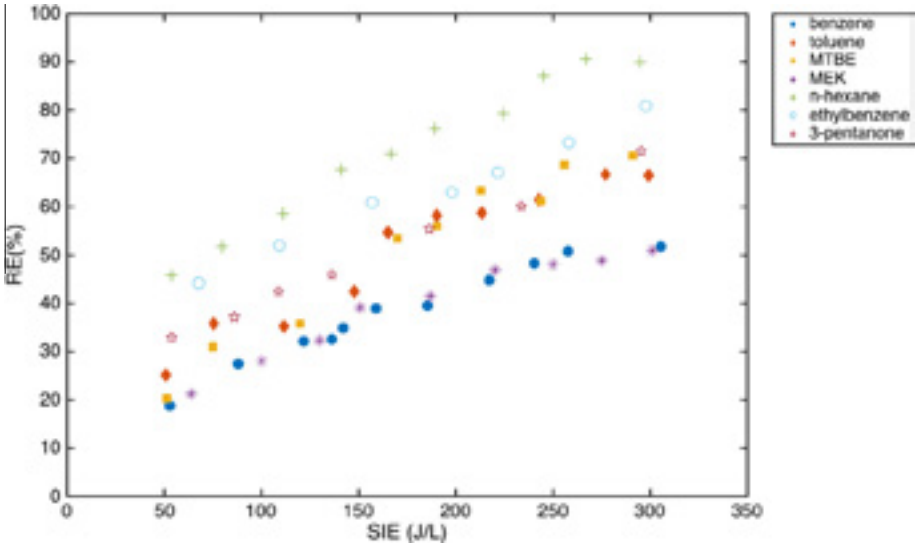

Fig. 2. Removal efficiencies (REs) of selected VOCs as a function of applied specific input energy (SIE) for a flow rate of 6.6 L min^{-1} and an inlet VOCs concentration of 95 ppm_v.

Table 1
Comparison of selected removal efficiencies (RE) for this and other studies (some using a catalyst). C_{in} = inlet concentration, RE = removal efficiency, SIE = specific input energy, V = voltage, ND = no data.

VOCs	C_{in} (ppm_v)	RE (%)	SIE ($J\,L^{-1}$)	Gap (mm)	V (kV)	Catalyst	g VOC removed/kW h	References
Toluene	95	74	360	1.3	7–10	None	2.6	This study
Toluene	200	15	400	ND	12 (DC)	None	1.0	[33]
Toluene	50	95.9	756	8.0	30	MnO_2	0.86	[34]
Toluene	450	90	2400	1.5–10	0–35	$BaTiO_3$ and $LaCoO_3$	2.3	[28]
Toluene	240	55	172	6.0	0–40	MnO_2/AC	10.4	[24]
MTBE	95	80	360	1.3	7–10	None	2.7	This study
MTBE	200	~100	1300	1.5–10	0–35	$BaTiO_3$ and $LaCoO_3$	2.0	[28]

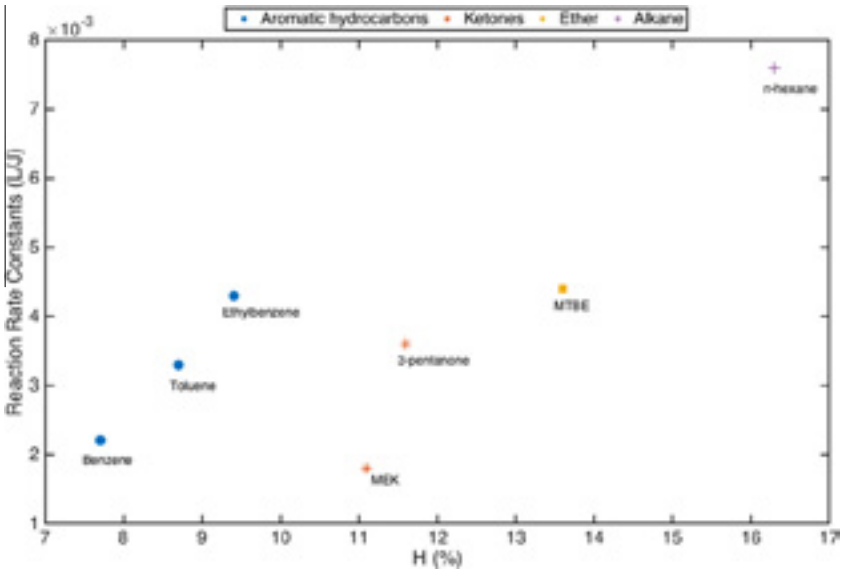

Fig. 3. Calculated reaction rate constants of the VOCs as a function of the hydrogen weight fraction H% (w/w) for the tested VOCs for a constant inlet concentration (95 ppm_v in dry air) and SIE (360 $J\,L^{-1}$).

ours for comparison purposes. Guo et al. [34] reported that higher oxygen content in the gas stream resulted in slightly lower removal of toluene. Overall, our removal data seem to indicate yields better than most (but not all) of the selected NTP studies (see the column (g VOC removed per kWh) in Table 1), although in absolute terms, the energy demand for VOC treatment in NTP remains quite high. One possible explanation for the lower yield is that significant amounts of ozone were formed in our experiments as discussed below, and that parasitic discharges occurred on the outer electrode (in some instances, ozone could be detected in the laboratory). Both account for some of the energy input not converted into beneficial reactions.

3.2. Determination of the overall reaction rate constants

Knowing the overall reaction rate constant is important to compare systems and to predict the removal of VOCs in NTP reactors. A previously published first-order kinetic model was used [35,36]. This model (Eqs. (2) and (3)) is semi-empirical and does not attempt to describe the detailed chemistry occurring in the plasma reactor. Instead, it lumps all processes into a simple equation that often provides an adequate overall kinetic relationship. The model has been shown to be generally applicable when the VOC removal does not exceed 95% [37].

$$\dot{O} + [VOC] \xrightarrow{k} \text{products} \tag{2}$$

$$\frac{[\text{VOC}]}{[\text{VOC}]_0} = e^{-\text{SIE}/\beta} \tag{3}$$

where $\dot{O}$ represents the oxygen radicals produced in the discharge zone of the plasma, and $[VOC]_0$ is the inlet concentration of the VOC. The β ($J\,L^{-1}$) parameter is thus determined by regression of the natural logarithm of VOC/VOC_0 vs. SIE. The slope of the straight line ($-1/\beta$) is (minus) the reaction rate constant k ($L\,J^{-1}$). The k and β values obtained for the seven VOCs that were tested (for the dry air condition) are reported in Table SM-1. Similar reaction rate constants values were reported for some of the VOCs by others ([23,38]). The reaction rate values reported in Table SM-1 allow direct comparison of the reactivity of the tested VOCs since all conditions were kept the same. The results highlight that important differences exist in the reactivity of the VOCs that were selected in our study, allowing some examination of structure-activity relationships.

It has been suggested that the hydrogen weight fraction of the pollutant undergoing treatment is an important factor affecting the reactivity of VOCs in NTP reactors [39]. This is believed to be because molecules with a greater number of methyl groups tend to be more reactive, with a proton lost or gained at the methyl group [14]. In Fig. 3, the reaction rate constant for each VOC was plotted vs. the hydrogen weight fraction. Indeed, the trend shows that a greater hydrogen fraction generally resulted in a greater reaction rate (in particular k for hexane far exceeded all others). This trend and proposed mechanism might explain why simple hydrocarbons are better removed compared to aromatics or ketones. In addition, removal of aromatic compounds (e.g., ethylbenzene, toluene and benzene) seem to follow their own trend with respect to the their hydrogen fractions. Overall, this was not unexpected. For example, Cho et al. found that molecules

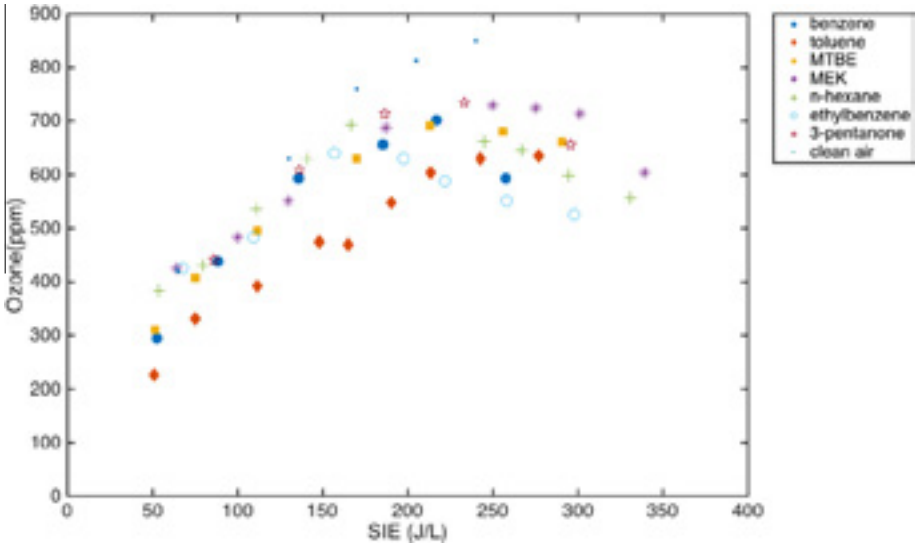

Fig. 4. SIE impact on effluent ozone concentration at a flow rate of 6.6 L min^{-1}. Typical standard deviations for the ozone measurements were 40–60 ppm_v.

with oxygen or chlorine lead to formation of volatile products in the plasma, which in turn enhanced the decomposition of VOCs [39]. Another correlation was attempted between *k* and the ionization potentials as a measure of how easily the electrons in a molecule respond to a perturbation. The results are shown in Fig. SM-3 did not lead to any obvious trend adding further evidence that reaction mechanisms are complex. Clearly, in order to develop better predictive models based on chemical structures, many more VOCs should be tested in a systematic and quantitative manner.

3.3. Influence of SIE on ozone production

Ozone production was quite important, with outlet concentrations ranging from 300 to 900 ppm_v depending on the specific conditions (Fig. 4). Production of O_3 was greater in the absence of VOCs at higher SIE (>200 J L^{-1}) because ozone is consumed by the oxidation of VOCs. Using this logic, one would expect ozone concentrations to be lower when treating pollutants that are well removed, but this was not the case, highlighting the fact that degradation of the VOC vapor follows complex mechanisms. A similar decrease in ozone concentration during VOC treatment was reported by Holzer et al. [28], while Oda [23] observed that presence of VOC (i.e., TCE) first decreased the ozone concentration (4000 ppm_v–1000 ppm_v), and then remained constant. Two likely reasons for the difference between studies are (1) the different types of high voltage rods (bolt type or coil type) and/or (2) that a lower SIE could cause different trends in ozone production and consumption. These different types of electrodes (e.g., wire, rod or a bold) in barrier discharge reactors might change the stability of the discharge from the electrode to the dielectric wall (barrier). Here, as expected, ozone production increased with increasing SIE up to 200 J L^{-1} (Fig. 4), but at higher SIE (>200 J L^{-1}), ozone production decreased. This decrease may be caused by different mechanisms. One possible explanation is that the temperature in the NTP increased (by about 10 °C; temperature in discharge zone was 40 ± 6 °C) with greater SIEs, and ozone is known to decompose faster at higher temperatures [23]. Another possible explanation proposed by Liang et al. [40] is that at higher SIE, a greater density of high energy electron reacts with ozone thereby lowering its concentrations. Finally, it is possible that NO_x (in particular NO_2) were formed at high SIE as was described by several authors (see e.g., Shin and Yoon, 2013) [41]. Unfortunately, NO_x were not measured in the reactor effluent. In any case, detailed studies would be needed to confirm and quantify the contribution of each of these mechanisms. Obviously, both NO_x and ozone are unwanted in the effluent of an air pollution control device and their formations also reduce the energy efficiency of the process. One approach to lower ozone generation is to use a catalyst in situ or post plasma applications. For example, using a MnO_x/SMF catalyst in-situ decreased ozone formation from 800 ppm_v to 500 ppm_v [32]. Another study also concluded that MnO_2 catalyst (this time post-plasma) decreased ozone production while increasing the removal of benzene vapors [15].

3.4. Formation of deposit

The treatment of toluene and ethylbenzene vapors resulted in a deposit forming inside the plasma zone, whereas no deposit was observed during the treatment of the other five VOCs tested. Deposits were observed first as color changes (yellow–brown) to solid surfaces (electrodes, outlet tubing) as well as a significant amount of small dark brown particles accumulating at the exit port of the plasma reactor (see Graphical Abstract, Figs. SM-4 and SM-5). These deposits were dark brown in color and gave off a petroleum- or tar-like odor. This came as a surprise, since the NTP published literature is relatively silent on the formation of such deposits. Only a few papers [34,42,43] briefly mention similar observations, but thorough and quantitative determinations are lacking. Guo et al. [34] reported that a yellow product was observed after the treatment of toluene vapors in a DBD, and described it as an aromatic polymer. A few reports exist on deposit formation after the treatment of VOCs with non-thermal plasma and catalyst hybrid systems [44–46]. They generally described the deposits as polymeric substances, or carbonaceous deposits, some were identified as benzoic acid crystals. Deposit formation increased with decreasing flow rate or reducing the SIE. Another study by Demidiouk et al. [42] found that solid particles formed during the treatment of toluene vapors, but not during butyl acetate. These papers only focused on the qualitative aspects of the deposits.

Thus, an important question was to determine what percentage of the treated pollutant was transformed into these deposits. The carbon content in the deposit was determined to be 54 ± 1% by mass and nitrogen was 2.9 ± 0.1%. As shown in Fig. 5, between 1% and 3% (as carbon) of the toluene or ethylbenzene fed to the reactor was recovered as deposit. This number still leaves a fairly

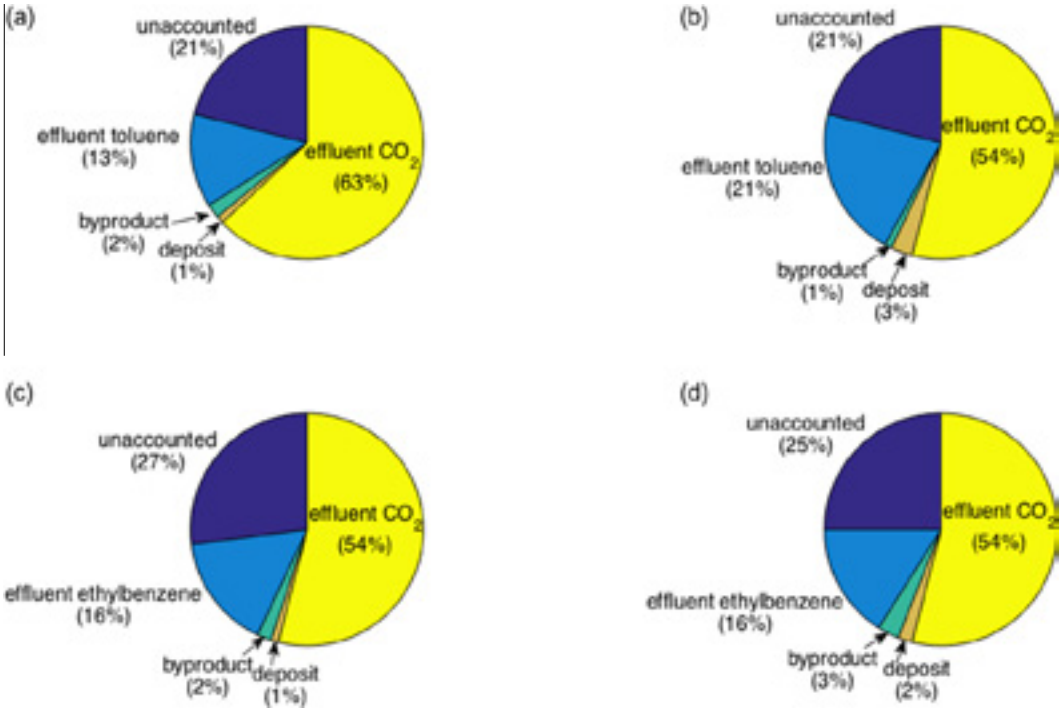

Fig. 5. Fate of influent pollutant (as carbon mass fraction) during VOC treatment under dry and humid air conditions. (a) Toluene, dry air; (b) toluene, 30% RH; (c) ethylbenzene, dry air; (d) ethylbenzene, 30% RH. Experimental conditions: constant inlet concentration (100 ppm_v), flow rate (6.6 L min^{-1}), and SIE (360 J L^{-1}).

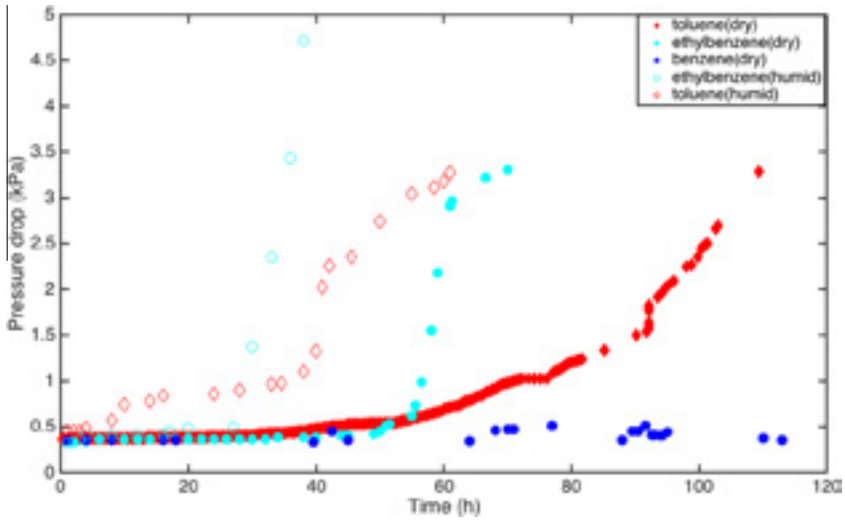

Fig. 6. Pressure drop determined as a function of time. Experimental conditions were 360 J L^{-1} SIE, a gas flow rate of 6.6 L min^{-1}, and 100 ppm_v inlet concentration.

large fraction of the carbon unaccounted; it is quite possible that some semi- or non-volatiles left via the exhaust instead of being deposited, and thus could be part of the carbon labeled as "unaccounted". It was reported that higher concentrations of treated VOCs (i.e., 1000 ppm_v styrene) produced more (60–70%) deposits inside a plasma reactor [35]. In our experiments, the CO concentration in the exhaust was measured, but was always below our detection limit of 20 ppm_v. It is only in selected experiments (not shown) conducted at SIE >700 J L^{-1} that CO in the exhaust rose to about 50 ppm_v. Because of the relatively high detection limit of CO, CO could well be a major fraction of the carbon unaccounted for in Fig. 5. If this was indeed the case, it would be consistent with the large amount of CO observed by Yu-fang et al. [47].

The time required for the deposit to cause significant clogging was determined by measuring the pressure drop over the reactor (Fig. 6). An increase in the pressure drop across the reactor could cause serious malfunctions, leakages, or fractures in the dielectric tubes. As shown in Fig. 6, a greater deposit formation was observed in humid conditions while no deposit was observed with benzene. This contrasts with Cal et al. [48] who reported deposit formation during benzene vapor treatment and could easily dissolve it with a small amount of water. Here, the deposit was different in nature from that of Cal et al.; it was not water soluble, and required an organic solvent (ethanol or methanol) to remove it. In addition to the greater amount of deposit yield in humid conditions, the structure and visual aspects of the deposit in humid conditions

was different than in dry conditions. Under humid air condition, the deposit formed a more compact than under dry air conditions and some (unidentified) crystals could be seen (see Fig. SM5). The results of Fig. 6 show that when deposits occur, they can cause reactor malfunction if not managed properly. Solutions can include special reactor designs and/or specific operating procedures. For example, Zhang et al. [49] demonstrated that increasing the volume of the discharge zone and placing additional dielectric tube (i.e., double tube dielectric barrier discharge reactor) could overcome the solid deposit accumulation inside the plasma zone.

4. Conclusions

In this study, the treatment of selected volatile organic vapors in a DBD-type non-thermal plasma reactor was evaluated. Experiments conducted at the same operating conditions for all VOCs allowed to determine how the treatment performance was affected by the nature of the pollutant and by the SIE.

The main findings can be summarized as follows:

(i) Removal of 95 ppm_v of the tested VOCs at 350 J L^{-1} followed the following sequence: methyl ethyl ketone (50%), benzene (58%), toluene (74%), 3-pentanone (76%), methyl tert-butyl ether (80%), ethylbenzene (81%), and *n*-hexane (90%). The treated VOCs were primarily oxidized to CO_2.

(ii) The solid deposits that formed when treating toluene and ethylbenzene vapors can be problematic. About 1–3% of the total inlet carbon was recovered as a deposit for the treatment of 100 ppm_v ethylbenzene and toluene at 360 J L^{-1}. When humid air was treated, a greater fraction of the treated pollutant was recovered as deposit and reactor clogging happened sooner. However, deposits from treating benzene were minor and did not clog the reactor within the duration of the experiments.

(iii) Deposits also accumulated downstream the dielectric tube. They did not change the reactor's removal efficiency, but caused clogging problems over time.

(iv) The hydrogen content of the molecules undergoing treatment was a reasonable predictor for the trends in VOC reaction rate constants (k). Molecules with a greater hydrogen content were more reactive and better removed.

(v) As a by-product, effluent ozone concentrations increased with the SIE, but leveled off or decreased at high SIEs (>200 J L^{-1}). The high outlet ozone concentrations (200–900 ppm_v) decrease the process's energy efficiency and need further consideration.

Appendix A. Supplementary data

Supplementary data associated with this article can be found, in the online version, at http://dx.doi.org/10.1016/j.cej.2016.03.002.

References

[1] S.R. Hanna, R. Paine, D. Heinold, E. Kintigh, D. Baker, Uncertainties in air toxics calculated by the dispersion models AERMOD and ISCST3 in the Houston ship channel area, J. Appl. Meteorol. Climatol. 46 (2007) 1372–1382.
[2] M.L. Boeglin, D. Wessels, D. Henshel, An investigation of the relationship between air emissions of volatile organic compounds and the incidence of cancer in Indiana counties, Environ. Res. 100 (2006) 242–254.
[3] S.I.V. Sousa, M.C.M. Alvim-Ferraz, F.G. Martins, Health effects of ozone focusing on childhood asthma: what is now known–a review from an epidemiological point of view, Chemosphere 90 (2013) 2051–2058.
[4] J.S. Devinny, M.A. Deshusses, T.S. Webster, Biofiltration for Air Pollution Control, Lewis Publishers, New York, 1998.
[5] D. Gabriel, H.H.J. Cox, M.A. Deshusses, Conversion of full-scale wet scrubbers to biotrickling filters for H_2S control at publicly owned treatment works, J. Environ. Eng. 130 (2004) 1110–1117.
[6] Q. Hu, C. Wang, K. Huang, Biofiltration performance and characteristics of high temperature gaseous benzene, hexane and toluene, Chem. Eng. J. 279 (2015) 689–695.
[7] G. An, Y. Sun, T. Zhu, X. Yan, Degradation of phenol in mists by a non-thermal plasma reactor, Chemosphere 84 (2011) 1296–1300.
[8] B.M. Penetrante, S.E. Schultheis, Non-thermal plasma techniques for pollution control: part A–overview, fundamentals and supporting technologies and part B–electron beam and electrical discharge processing, NATO ASI Ser Ser G 84 (2011) 1296–1300.
[9] B.M. Penetrante, M.C. Hsiao, J.N. Bardsley, B.T. Merritt, G.E. Vogtlin, A. Kuthi, C. P. Burkhart, J.R. Bayless, Identification of mechanisms for decomposition of air pollutants by non-thermal plasma processing, Plasma Sources Sci. Technol. 6 (1997) 251–259.
[10] S. Schmid, M.C. Jecklin, R. Zenobi, Degradation of volatile organic compounds in a non-thermal plasma air purifier, Chemosphere 79 (2010) 124–130.
[11] S. Lu, L. Chen, Q. Huang, L. Yang, C. Du, X. Li, J. Yan, Decomposition of ammonia and hydrogen sulfide in simulated sludge drying waste gas by a novel non-thermal plasma, Chemosphere 117 (2014) 781–785.
[12] A. Mizuno, J.S. Clements, R.H. Davis, A method for the removal of sulfur dioxide from exhaust gas utilizing pulsed streamer corona for electron energization, IEEE Trans. Ind. Appl. 3 (1986) 516–522.
[13] T. Yamamoto, K. Ramanathan, P. Lawless, D.S. Ensor, J.R. Newsome, N. Plaks, G. H. Ramsey, Control of volatile organic compounds by an ac energized ferroelectric pellet reactor and a pulsed corona reactor, IEEE Trans. Ind. Appl. 28 (1992) 528–534.
[14] C.M. Nunez, G.H. Ramsey, W.H. Ponder, J.H. Abbott, L.E. Hamel, P.H. Kariher, Corona destruction: an innovative control technology for VOCs and air toxics, J. Air Waste Manage. Assoc. 43 (1993) 242–247.
[15] S. Futamura, A. Zhang, H. Einaga, H. Kabashima, Involvement of catalyst materials in nonthermal plasma chemical processing of hazardous air pollutants, Catal. Today 72 (2002) 259–265.
[16] Y. Byun, D.J. Koh, D.N. Shin, Removal mechanism of elemental mercury by using non-thermal plasma, Chemosphere 83 (2011) 69–75.
[17] L. Huang, L. Xia, X. Ge, H. Jing, W. Dong, H. Hou, Removal of H_2S from gas stream using combined plasma photolysis technique at atmospheric pressure, Chemosphere 88 (2012) 229–234.
[18] T. Zhu, R. Chen, N. Xia, X. Li, X. He, W. Zhao, T. Carr, Volatile organic compounds emission control in industrial pollution source using plasma technology coupled with F-TiO2/γ-Al2O3, Environ. Technol. 36 (2015) 1405–1413.
[19] J. Liu, J. Wang, X. Cao, R. Zhang, H. Hou, Decomposition of gaseous toluene using a continuous flow discharge plasma reactor with new configurations, Environ. Technol. 36 (2015) 3084–3093.
[20] C.A. Aggelopoulos, P. Svarnas, M.I. Klapa, C.D. Tsakiroglou, Dielectric barrier discharge plasma used as a means for the remediation of soils contaminated by non-aqueous phase liquids, Chem. Eng. J. 270 (2015) 428–436.
[21] K.B. Andersen, J.A. Beukes, A. Feilberg, Non-thermal plasma for odour reduction from pig houses – a pilot scale investigation, Chem. Eng. J. 223 (2013) 638–646.
[22] K. Urashima, J.S. Chang, Removal of volatile organic compounds from air streams and industrial flue gases by non-thermal plasma technology, IEE Trans. Dielectr. Electr. Insul. 7 (2000) 602–614.
[23] T. Oda, Non-thermal plasma processing for environmental protection: decomposition of dilute VOCs in air, J. Electrostat. 57 (2003) 293–311.
[24] S. Delagrange, L. Pinard, J.M. Tatibouet, Combination of a non-thermal plasma and a catalyst for toluene removal from air: manganese based oxide catalysts, Appl. Catal. B 68 (2006) 92–98.
[25] U. Roland, F. Holzer, F.D. Kopinke, Improved oxidation of air pollutants in a non-thermal plasma, Catal. Today 73 (2002) 315–323.
[26] R. Zhu, Y. Mao, L. Jiang, J. Chen, Performance of chlorobenzene removal in a nonthermal plasma catalysis reactor and evaluation of its byproducts, Chem. Eng. J. 279 (2015) 463–471.
[27] D.E. Tevault, Carbon monoxide production in silent discharge plasmas of air and air-methane mixtures, Plasma Chem. Plasma Process. 7 (1987) 231–242.
[28] F. Holzer, F.D. Kopinke, U. Roland, Influence of ferroelectric materials and catalysts on the performance of non-thermal plasma (NTP) for the removal of air pollutants, Plasma Chem. Plasma Process. 25 (2005) 595–611.
[29] Z. Runye, K. Christian, C. Zhuowei, L. Lichao, Y. Jianming, C. Jianmeng, Styrene removal in a biotrickling filter and a combined UV-biotrickling filter: steady- and transient-state performance and microbial analysis, Chem. Eng. J. 275 (2015) 168–178.
[30] Y. Jianming, L. Wei, C. Zhuowei, J. Yifeng, C. Wenji, C. Jianmeng, Dichloromethane removal and microbial variations in a combination of UV pretreatment and biotrickling filtration, J. Hazard. Mater. 268 (2014) 14–22.
[31] T.C. Manley, The electric characteristics of the ozonator discharge, Trans. Electrochem. Soc. 84 (1943) 83–96.
[32] C. Subrahmanyam, M. Magureanu, A. Renken, L. Kiwi-Minsker, Catalytic abatement of volatile organic compounds assisted by non-thermal plasma: Part 1. A novel dielectric barrier discharge reactor containing catalytic electrode, Appl. Catal. B. 65 (2006) 150–156.
[33] W. Mista, R. Kacprzyk, Decomposition of toluene using non-thermal plasma reactor at room temperature, Catal. Today 137 (2008) 345–349.
[34] Y.F. Guo, D.Q. Ye, K.F. Chen, J.C. He, W.L. Chen, Toluene decomposition using a wire-plate dielectric barrier discharge reactor with manganese oxide catalyst in situ, J. Mol. Catal. A Chem. 245 (2006) 93–100.
[35] G.K. Anderson, H. Snyder, J. Coogan, Oxidation of styrene in a silent discharge plasma, Plasma Chem. Plasma Process. 19 (1999) 131–151.

[36] T. Zhang, Q. Li, Y. Liu, Y. Duan, W. Zhang, Equilibrium and kinetics studies of fluoride ions adsorption CeO_2/Al_2O_3 composites pretreated with non-thermal plasma, Chem. Eng. J. 168 (2011) 665–671.
[37] L.A. Rosocha, R.A. Korzekwa, Advanced oxidation and reduction processes in the gas phase using non-thermal plasmas, J. Adv. Oxid. Technol. 4 (1999) 247–264.
[38] L.A. Rosocha, G.K. Anderson, L.A. Bechtold, J.J. Coogan, H.G. Heck, M. Kang, W.H. McCulla, R.A. Tennant, P.J. Wantuck, Treatment of hazardous organic wastes using silent discharge plasmas, Non-Thermal Plasma Techniques for Pollution Control, NATO ASI Series, Springer, Berlin 34 (1993) 281–308.
[39] D.L. Cho, D.C. Chung, G.S. Kim, Decomposition and solidification of hazardous volatile organic compounds through plasma chemical reactions, J. Ind. Eng. Chem. 13 (2007) 287–291.
[40] W.J. Liang, L. Ma, H. Liu, J. Li, Toluene degradation by non-thermal plasma combined with a ferroelectric catalyst, Chemosphere 92 (2013) 1390–1395.
[41] H.H. Shin, W.S. Yoon, Hydrocarbon effects on the promotion of non-thermal plasma NO–NO_2 conversion, Plasma Chem. Plasma Process. 23 (2003) 681–704.
[42] V. Demidiouk, S.I. Moon, J.O. Chae, Toluene and butyl acetate removal from air by plasma-catalytic system, Catal. Commun. 4 (2003) 51–56.
[43] M.S. Gandhi, A. Ananth, Y.S. Mok, J.I. Song, K.H. Park, Time dependence of ethylene decomposition and byproducts formation in a continuous flow dielectric-packed plasma reactor, Chemosphere 91 (2013) 685–691.
[44] M. Magureanu, D. Piroi, N.B. Mandache, V.I. Parvulescu, V. Parvulescu, B. Cojocaru, C. Cadigan, R. Richards, In situ study of ozone and hybrid plasma Ag–Al catalysts for the oxidation of toluene: evidence of the nature of the active sites, Appl. Catal. B. 104 (2011) 84–90.
[45] H.L. Chen, H.M. Lee, S.H. Chen, M.B. Chang, S.J. Yu, S.N. Li, Removal of volatile organic compounds by single-stage and two-stage plasma catalysis systems: a review of the performance enhancement mechanisms, current status, and suitable applications, Environ. Sci. Technol. 43 (2009) 2216–2227.
[46] M. Magureanu, N.B. Mandache, Toluene oxidation in a plasma-catalytic system, J. Appl. Phys. 99 (2006) 123301–123304.
[47] G. Yu-fang, Y. Dai-qi, T. Ya-feng, C. Ke-fu, Humidity effect on toluene decomposition in a wire-plate dielectric barrier discharge reactor, Plasma Chem. Plasma Process. 26 (2006) 237–249.
[48] M.P. Cal, M. Schluep, Destruction of benzene with non-thermal plasma in dielectric barrier discharge reactors, Environ. Prog. 20 (2001) 151–156.
[49] H. Zhang, K. Li, C. Shu, Z. Lou, T. Sun, J. Jia, Enhancement of styrene removal using a novel double-tube dielectric barrier discharge (DDBD) reactor, Chem. Eng. J. 265 (2014) 107–118.

Journal of Hazardous Materials 237–238 (2012) 283–289

Contents lists available at SciVerse ScienceDirect

Journal of Hazardous Materials

journal homepage: www.elsevier.com/locate/jhazmat

Abatement of mixture of volatile organic compounds (VOCs) in a catalytic non-thermal plasma reactor

J. Karuppiah [a], E. Linga Reddy [a], P. Manoj Kumar Reddy [a], B. Ramaraju [a], R. Karvembu [b], Ch. Subrahmanyam [a,*]

[a] Energy and Environmental Research Laboratory, Department of Chemistry, Indian Institute of Technology, Hyderabad 502205, India
[b] Department of Chemistry, National Institute of Technology, Tiruchirappalli 620015, India

HIGHLIGHTS

- Oxidation of mixture of VOCs in a catalytic dielectric barrier discharge reactor.
- Synergy effect on integration of catalyst to plasma.
- Positive effect of water vapor during removal of mixture of VOCs.
- Best activity of AgO_x/MnO_x under humid conditions.

GRAPHICAL ABSTRACT

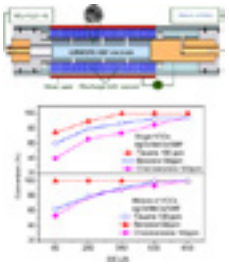

ARTICLE INFO

Article history:
Received 29 May 2012
Received in revised form 17 August 2012
Accepted 18 August 2012
Available online 24 August 2012

Keywords:
VOC abatement
SMF
Ozone
Non-thermal plasma
Synergy

ABSTRACT

Total oxidation of mixture of dilute volatile organic compounds was carried out in a dielectric barrier discharge reactor with various transition metal oxide catalysts integrated in-plasma. The experimental results indicated the best removal efficiencies in the presence of metal oxide catalysts, especially MnO_x, whose activity was further improved with AgO_x deposition. It was confirmed water vapor improves the efficiency of the plasma reactor, probably due to the formation of hydroxyl species, whereas, in situ decomposition of ozone on the catalyst surface may lead to nascent oxygen. It may be concluded that non-thermal plasma approach is beneficial for the removal of mixture of volatile organic compounds than individual VOCs, probably due to the formation of reactive intermediates like aldehydes, peroxides, etc.

1. Introduction

Volatile organic compounds (VOCs) are one of the major contributors to the atmospheric pollution and may have adverse effects on human health [1]. Technical VOC mixtures of different chemical character such as aromatic hydrocarbons, alkanes, alcohols, acetates and ketones are utilized for commercial and industrial applications such as paints, chemical plants, and printing industries. Exposure to VOCs has implications in a number of human diseases, including cancer, cardiovascular and several insusceptible diseases [2]. As some of the VOCs are carcinogenic more rigorous environmental regulations have to be followed in order to reduce the VOCs emission [1–3]. There are many conventional methods for VOCs reduction including adsorption, absorption, catalytic oxidation and thermal incineration. These techniques are not effective, especially for dilute concentrations (<1000 ppmv), where non-thermal plasma (NTP) generated at atmospheric pressure may be energy saving due to fast ignition response and generation of highly energetic electrons that may contribute to plasma chemistry reactions [2–6]. Further, a synergy

* Corresponding author. Tel.: +91 40 23016050; fax: +91 40 23016032.
E-mail address: csubbu@iith.ac.in (Ch. Subrahmanyam).

0304-3894/$ – see front matter © 2012 Elsevier B.V. All rights reserved.
http://dx.doi.org/10.1016/j.jhazmat.2012.08.040

between NTP and catalytic action is expected with suitable catalyst integration with plasma in order to overcome the low selectivity problems of NTP [4–6]. As the typical industrial emissions comprise a blend of VOCs, an effective technology for the oxidative decomposition of VOCs is desirable [7,8]. Catalytic NTP technique has often been tested for the removal of various single component VOCs, but reports on VOCs mixture are limited [9,10]. During the present study, a mixture of VOCs of different nature was tested with NTP combined with MnO_x and AgO_x/MnO_x catalysts and results were compared with NTP alone. Influence of various parameters like design of the reactor, catalyst, presence of water vapor, concentration of VOCs, nature of the by-products formed and ozone formation inside the NTP reactor has been studied.

2. Experimental set-up

2.1. Materials

Toluene (TOL), benzene (BZ) chlorobenzene (CB), manganese acetate tetrahydrate and silver nitrate were also purchased from Merck (Germany). All the solutions were prepared with deionized water. Sintered metal fiber (SMF) filters made of stainless steel consisting of thin uniform metal fibers of diameter 30 μm, wetness capacity of ~30 wt% and porosity of ~80% were acquired, Southwest Screens and Filters SA, Belgium.

2.2. Catalyst supported SMF preparation

Manganese oxide and silver supported manganese oxide on SMF were prepared by wet chemical route. The SMF was first oxidized at 873 K for 3 h, followed by impregnation with manganese acetate aqueous solutions of desired concentration. Then it was dried at room temperature followed by calcination in air at 773 K for 5 h to obtain MnO_x/SMF, whereas, AgO_x/MnO_x/SMF were prepared by deposition of $AgNO_3$ and drying at room temperature followed by calcination at 773 K for 5 h. Finally, SMF filters were subjected to an electrical hot press to shape them into cylindrical form giving the desired discharge gap of 2.5 mm.

2.3. Experimental procedure

A detailed description of the reactor has been given elsewhere [11]. Briefly, the dielectric discharge was generated in a cylindrical quartz tube with an inner diameter of 18.5 mm. One end of the SMF electrode was connected through a stainless steel rod to AC high voltage, whereas the other end was connected to the inlet gas stream through a Teflon tube. The gas after passing the discharge zone diffuses through the SMF and was analyzed with a gas chromatograph at the outlet. The discharge length was 10 cm and discharge gap was fixed at 2.5 mm during the destruction of VOCs. V-Q Lissajous method was used to determine the discharge power (W) from which specific input energy (SIE) was calculated by dividing power (W) with flow rate (l/s). SIE in the present study was varied in between 60 and 650 J/l by changing the amplitude of AC high voltage (14–22 kV/50 Hz). The VOCs BZ, CB and TOL were introduced with a motor driven syringe pump and were mixed with air at a flow rate of 250 ml/min at standard temperature and pressure and were fed into the plasma reactor with a Teflon tube. Conversion at each voltage was measured after 30 min. The concentration of VOCs at the outlet of reactor was measured with a gas chromatograph (Varian 450) equipped with a flame ionization detector and a VF1 capillary column (50 m length, 0.25 mm thickness), whereas an on-line GC–MS (Thermo Fisher Scientific) was used to identify the by-products formed. The formation of CO_2 and CO was simultaneously monitored with an online infrared gas analyser (Analyser Instruments Company, India), whereas ozone formed in the plasma reactor was measured with UV absorption ozone monitor (API-450 NEMA). As the volume change due to chemical reactions is negligible, global selectivity of CO_2 and CO_x was defined as follows:

$$\text{Conversion of CB } (\%) = \frac{[CB]_{in} - [CB]_{out}}{[CB]_{in}} \times 100\%$$

$$\text{Conversion of TOL } (\%) = \frac{[TOL]_{in} - [TOL]_{out}}{[TOL]_{in}} \times 100\%$$

$$\text{Conversion of BZ } (\%) = \frac{[BZ]_{in} - [BZ]_{out}}{[BZ]_{in}} \times 100\%$$

$$\text{Global selectivity of CO } S_{CO} = \frac{[CO]_{out}}{6 \times ([BZ]_{in} - [BZ]_{out}) + 7 \times ([TOL]_{in} - [TOL]_{out}) + 6 \times ([CB]_{in} - [CB]_{out})} \times 100\%$$

$$\text{Global selectivity of } CO_2\ S_{CO_2} = \frac{[CO_2]_{out}}{6 \times ([BZ]_{in} - [BZ]_{out}) + 7 \times ([TOL]_{in} - [TOL]_{out}) + 6 \times ([CB]_{in} - [CB]_{out})} \times 100\%$$

$$S_{CO_x} = S_{CO} + S_{CO_2}$$

where all concentrations are in ppmv.

3. Results and discussion

The present study has been aimed at the removal of mixture of VOCs of different nature. However, in order to understand the oxidation behavior of VOCs in a mixture, initial experiments were carried out with single component VOCs over MnO_x/SMF, AgO_x/MnO_x/SMF and SMF and the results are presented in Fig. 1. As seen in Fig. 1a, SMF showed least conversion compared to modified catalysts. At 60 J/l, MnO_x/SMF showed conversion of 30, 50 and 60%, respectively for CB, BZ and TOL and with increasing SIE to 650 J/l, conversion increased up to 90, 90 and 100%, respectively. Interestingly, AgO_x/MnO_x/SMF catalyst showed higher conversion compared to MnO_x/SMF in the entire SIE range. Even at 60 J/l, AgO_x/MnO_x/SMF showed 45, 60 and 75% for CB, BZ and TOL. Even though, during the decomposition of VOCs total oxidation is desired, in general, NTP leads to the formation of undesired products and the selectivity to CO_2 may not be 100%. As seen in Fig. 1b, selectivity to CO_x ($CO + CO_2$) was never 100%, indicating the formation of by products along with carbonaceous deposits on the walls of the reactor. For the VOCs tested in the present study, the selectivity to CO_2 followed the order SMF < MnO_x < AgO_x/MnO_x/SMF.

3.1. Plasma-catalytic oxidation of mixture of VOCs

The performance of various catalytic electrodes during the destruction of 200 ppm of mixture of VOCs (50 ppm CB, 100 ppm BZ and 50 ppm TOL) in the SIE range of 60–650 J/l was tested. As seen in Fig. 2a, SMF without any modification showed ~100% conversion

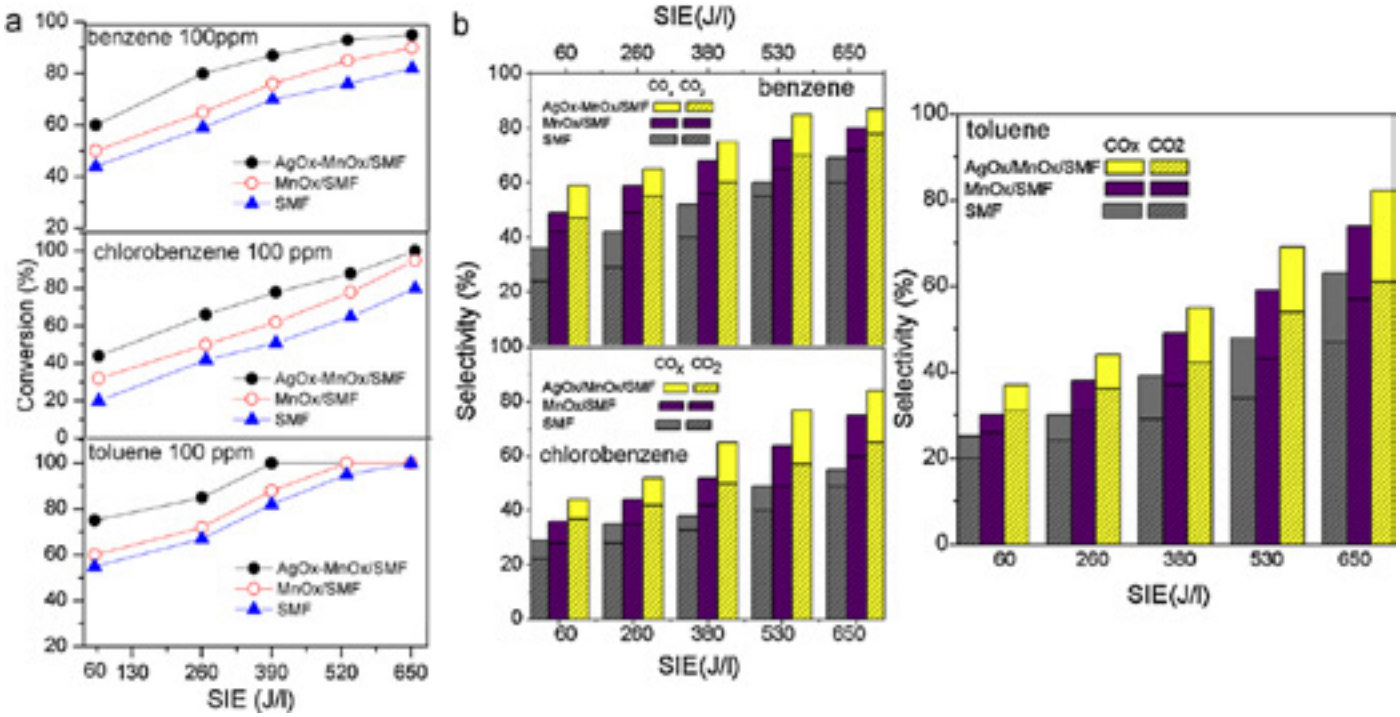

Fig. 1. Influence of SIE and SMF modification during the destruction of VOCs. (a) Conversion and (b) selectivity (SIE 60–650 J/l and 100 ppm of VOCs).

of TOL even at 60 J/l, whereas, under the same input energy conversion of BZ and CB was only around 65%. Nearly the same results were observed for MnO_x/SMF, whereas, AgO_x/MnO_x/SMF showed better performance than SMF and MnO_x/SMF, where the conversion of BZ and CB increased to 70 and 80%, respectively. SMF showed complete conversion of BZ and CB only at 530 J/l, whereas, with AgO_x/MnO_x/SMF the same result was obtained even at 400 J/l. AgO_x/MnO_x/SMF showed better activity over SMF and MnO_x/SMF throughout the range of the present study. Among all electrodes, AgO_x/MnO_x/SMF under dry condition showed the high activity for all the VOCs. Interesting observation is that AgO_x/MnO_x/SMF under humid conditions showed 100% conversion of the mixture of VOCs at 300 J/l, whereas, relatively high energy (420 J/l) was needed with unmodified SMF.

Fig. 2b presents the global selectivity of CO_x ($CO + CO_2$) for various catalysts during the destruction of 200 ppm of VOCs mixture. As seen in Fig. 2b, increasing SIE leads to higher CO_x selectivity and among the catalysts studied, AgO_x/MnO_x electrodes showed best selectivity (up to ~85–95%), whereas, SMF showed only 65% even at 650 J/l. Fig. 2b also presents the CO_2 selectivity that also followed a similar trend to that of conversion, where AgO_x/MnO_x/SMF showed the highest selectivity of close to 80% under dry condition. Hence, for the mixture of VOCs, SMF showed poor carbon balance for VOCs mixture. During the present study trace amounts of by products (aldehyde, aromatic acids, alcohol etc.) were detected at the reactor outlet.

Most of the industrial oxidation processes produce flue gases containing water vapor, thus the effect of water vapor on VOC oxidation process always needs careful investigation [12,13]. The effect of water vapor on oxidation of VOCs mixture has been examined by employing a feed gas containing 50–100 ppm of each VOC in 2% of water vapor (20,000 ppmv). Fig. 2a and b shows the conversion and selectivity to CO_x as a function of SIE. As seen from Fig. 2, AgO_x/MnO_x/SMF under humid conditions showed ~85–90% conversion even at 60 J/l, especially for CB and BZ, against 70 and 80% conversion under dry conditions. The complete conversion was achieved with AgO_x/MnO_x/SMF/humid air at SIE of 280 J/l. CO_x and CO_2 selectivity was always high under humid conditions over AgO_x/MnO_x/SMF. For example at 650 J/l, AgO_x/MnO_x/SMF showed ~95% selectivity to CO_2 under humid conditions, whereas for dry mixture, it was around 80%. A similar trend was earlier reported by Gerasimov and Kim during the destruction of VOCs, where on addition of water vapor conversion increased due to in situ formation of OH radicals [5,12].

3.2. Decomposition of ozone on metal oxide catalysts

During the present study, SMF electrode modified by transition metal oxides shifted the product distribution toward total oxidation. It was generally believed that ozone decomposition on the metal oxide surface may lead to the formation of a strong oxidant atomic oxygen that may improves the selectivity to total oxidation [11,14–19]. In order to understand the role of ozone during the oxidation of mixture of VOCs, its concentration at the outlet was measured. It has been observed that 850, 450 and 350 ppm of ozone formed at 260 J/l (Fig. 3) with SMF, MnO_x/SMF and AgO_x/MnO_x/SMF, respectively, whereas under humid conditions ozone concentration with AgO_x/MnO_x/SMF catalyst was zero. This decrease in the ozone concentration under humid air suggests the formation of atomic oxygen [Eqs. (3) and (4)] on the catalyst surface that may improve the CO_2 selectivity [12,20].

$$H_2O \xrightarrow{e^-} H_2O^* \rightarrow H^\bullet + HO^\bullet \quad (1)$$

$$H^\bullet + O_3 \rightarrow HO^\bullet + O_2 \quad (2)$$

$$HO^\bullet + O_3 \rightarrow HO_2^\bullet + O_2 \quad (3)$$

$$HO_2^\bullet + O_3 \rightarrow HO^\bullet + 2O_2 \quad (4)$$

Also, even in dry conditions, MnO_x and AgO_x/MnO_x/SMF decreased ozone conversion, which is in agreement with the better performance over SMF, which changed the product distribution toward the total oxidation of mixture (Fig. 3). Even though MnO_x facilitates the ozone decomposition leading to formation of atomic

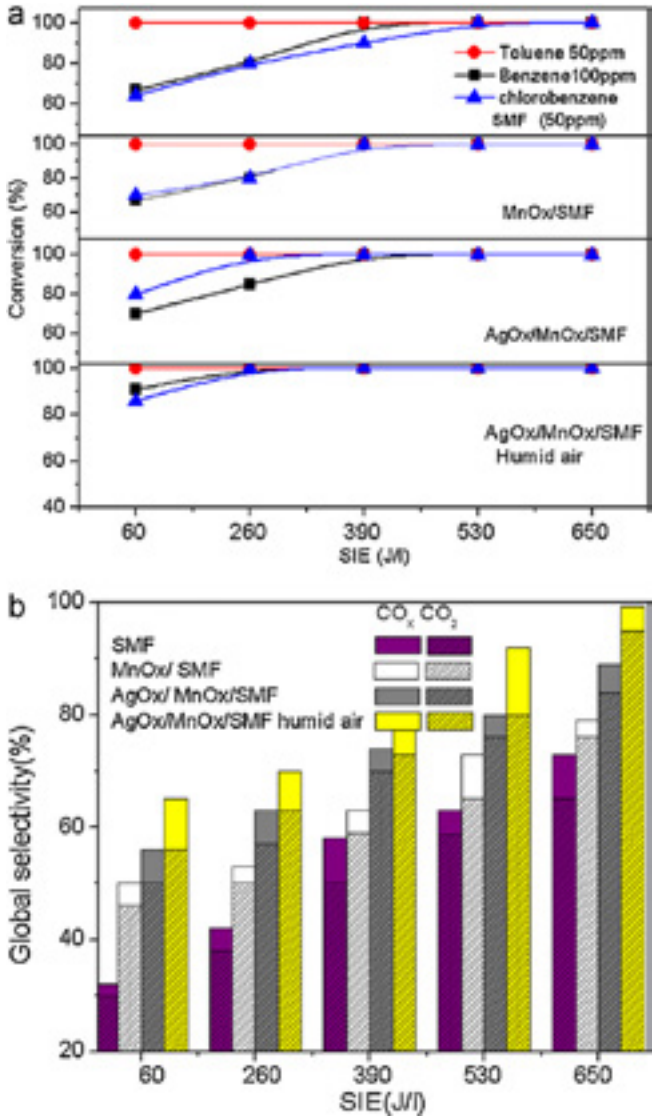

Fig. 2. Influence of SIE and SMF modification during the destruction dry and humid air of mixture VOCs. (a) Conversion and (b) selectivity (SIE 60–650 J/l and 200 ppm of VOCs).

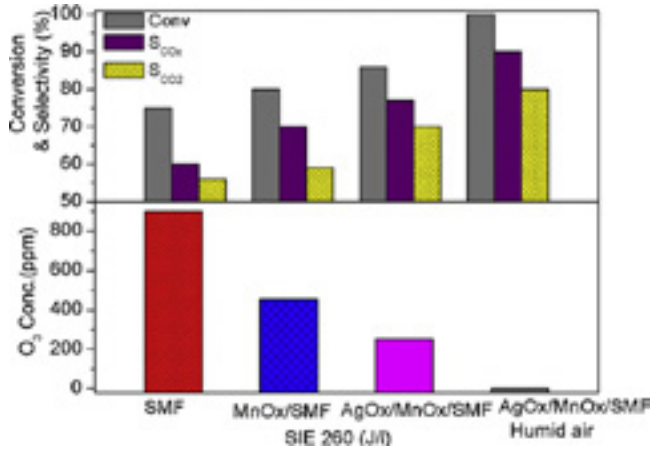

Fig. 3. Activity of SMF electrodes in plasma reactor during ozone decomposition with dry and humid air and influence of ozone concentration in the reactor on decomposition of mixture of VOCs at 260 J/l.

oxygen, AgO_x/MnO_x on humid conditions destroyed ozone completely and showed the best performance.

Some transition-metal oxides may deactivate in NTP due to the poisoning effect of carbonaceous deposit, whereas, during the present study, the reactivity of AgO was stable. The oxygen species produced on Ag may be remarkably active in the oxidative process compared with other transition-metal oxides. Reactions (5) and (6) are envisaged to proceed via the dissociative adsorption of O_3 on AgO, which decomposes to atomic oxygen [21,22]:

$$2Ag + O_3 \rightarrow Ag_2O + O_2 \quad (5)$$

$$Ag_2O + O_3 \rightarrow Ag^{I}Ag^{III}O_2 + O_2 \quad (6)$$

$$O_3 \rightarrow O_2 + O_{ads} \quad (7)$$

The distribution of oxygen atom on Ag surface followed by the formation of chemisorbed oxygen is thermodynamically favored over bulk oxide [22]. The heat of adsorption of oxygen on Ag ($\Delta H = -177.2\ kJ\ mol^{-1}\ O_2$) is larger than the enthalpy of formation of silver oxides ($\Delta H = -60.6\ kJ\ mol^{-1}\ O_2$) [21]. Once the surface is completely covered, the formation of silver oxides from ozone decomposition becomes thermodynamically favored as shown in Eq. (6). Exposure of oxide catalysts to water vapor results in adsorption of H_2O molecules that may then dissociates into OH^- and H^+, forming surface hydroxyl group.

3.3. Performance of the reactor on individual and mixture of VOCs decomposition

In order to understand the nature of individual VOCs (100 ppm) and its presence in the mixture (100 ppm each) was tested in the SIE range 60 and 650 J/l with SMF electrode modified with AgO_x/MnO_x and the results are presented in Fig. 4a and b. The experiment was performed under dry conditions. Interesting observation is that conversion of any individual VOC is less than that in the mixture. For example conversion of TOL was 75% at 60 J/l, whereas it was close to 100% in the mixture at the same input energy. A similar trend was observed for BZ and CB where higher conversion was observed in the mixture. At 60 J/l, the removal efficiencies for the mixture was 100, 60 and 50%, whereas, for individual VOCs it was only 75, 60 and 40%, respectively for TOL, BZ and CB. Selectivity to the CO_x was shown in Fig. 4b. As seen from Fig. 4b, selectivity to CO_x for individual VOC was around 80% at 650 J/l, against ~95% for the mixture. Hence, during the destruction of individual and mixture of VOCs, individual VOC demands high energy than mixture. A single component VOC may generate reactive intermediates. However, number of such reactive species generated in a mixture may be more, hence a higher probability to form reaction intermediates/radicals. As seen from the data presented in the manuscript; conversion of any VOC was higher in a mixture when compared to individual one. Hence, it may be concluded that treatment of VOCs mixture may enhance the utilization efficiency of active species generated in NTP like high energy electrons and or radicals. This may be due to the possible reactions taking place with excited and/or partially decomposed molecules in the mixture.

In order to understand the observed phenomena, two fundamental types of chemisorption processes on the catalyst surface can be proposed namely, molecular or associative chemisorption, in which all bonds of the adsorbate molecules are retained. Whereas, dissociative chemisorption proceeds via cleavage of adsorbate molecules and fragmented species will be adsorbed on the catalyst surface. As the dissociative chemisorption is always exothermic, the reaction enthalpy is large and positive. Similar observation was made by some authors that the VOCs can be easily activated in a mixture [23–25]. Piotrowska and Syczewska found that the oxidation of n-butyl acetate was high in a mixture of aromatics and alcohols [25]. These activations are probably due to the exothermic

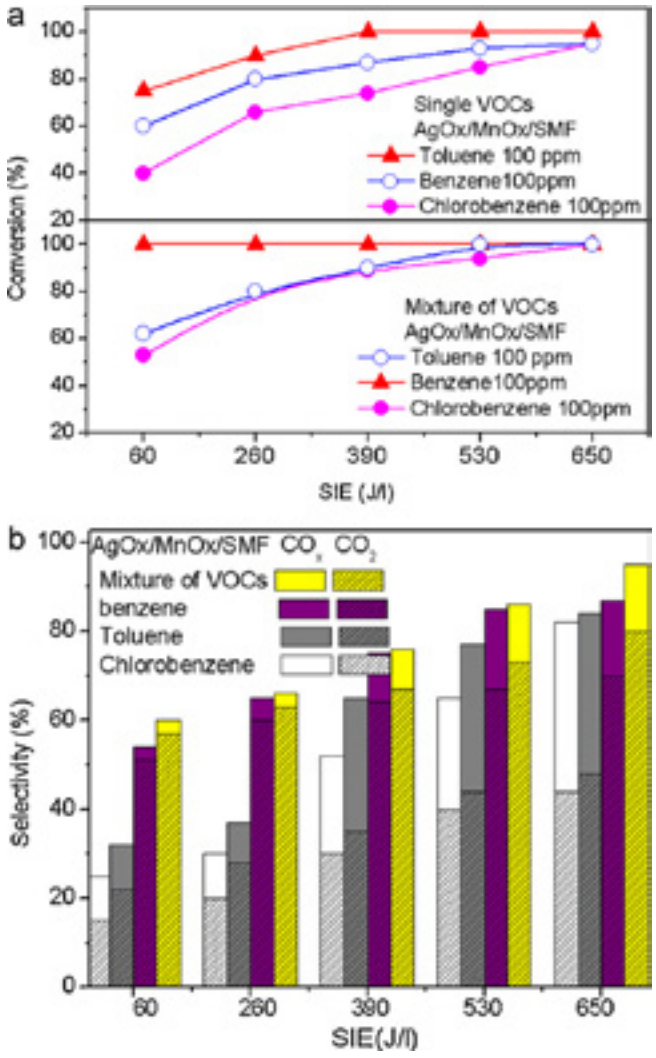

Fig. 4. Influence of single VOCs and mixture of VOCs on AgO_x–MnO_x/SMF electrode. (a) Conversion and (b) selectivity to CO_x and CO_2.

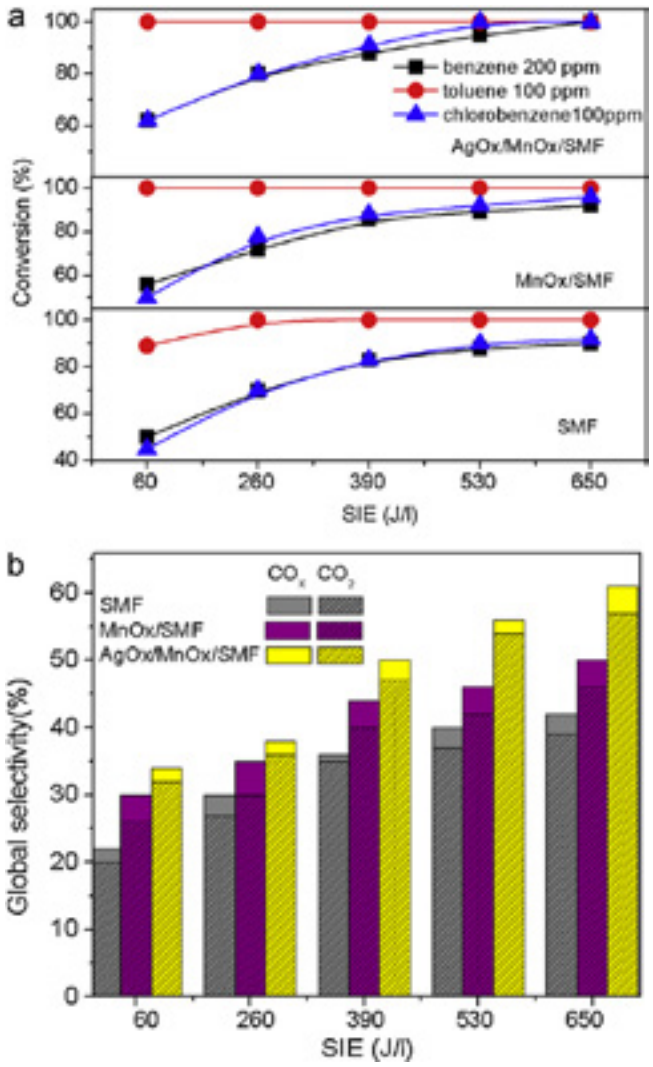

Fig. 5. Activity of SMF electrodes for higher VOC concentrations. (a) Conversion and (b) selectivity to CO_x and CO_2.

character of the complete oxidation reaction, which would raise locally the surface temperature of the catalyst [24]. Conversion at each voltage was recorded only after 30 min and the surface area of 5 wt% of catalyst on SMF was less than 10 m^2/g, hence the activation of VOCs in NTP is due to exothermic nature of the oxidation reactions.

3.4. Performance of the reactor for conversion of VOCs at higher initial concentrations

During the present study, concentration of VOCs mixture was changed from 200 to 400 ppm in order to understand the performance of the reactor at higher concentration of VOCs. The experiment was performed under dry conditions. Fig. 5a presents the activity of various catalytic electrodes during the conversion of 400 ppm of VOCs mixture in the SIE range 60–650 J/l. As seen in Figs. 2a and 5a, with increasing the mixture of VOCs concentration from 200 to 400 ppm, the conversion of CB decreased from 80 to 60% at SIE of 60 J/l with AgO_x/MnO_x/SMF. However, as seen from Fig. 5a SMF modification with MnO_x and AgO_x/MnO_x showed slightly better conversion than unmodified SMF. For 400 ppm of VOCs mixture the activity of the studied catalysts followed the trend AgO_x/MnO_x/SMF > MnO_x/SMF > SMF. Selectivity to the CO_x was shown in Fig. 5b. As seen from Figs. 2b and 5b, for 400 ppm of VOC mixture ~40% selectivity to CO_x was observed at 260 J/l, whereas under the same conditions, for 200 ppm of VOCs mixture, selectivity to CO_x was around 70% for AgO_x/MnO_x/SMF. Hence, during the destruction of 200 ppm of VOC mixture, at any SIE, selectivity to CO_x and CO_2 was high. For 400 ppm of VOCs mixture, SMF showed ~35% selectivity to CO_2 at 260 J/l, whereas AgO_x/MnO_x/SMF showed around 40% CO_2 selectivity even at 260 J/l and reached 65% at 650 J/l. A similar trend was observed on MnO_x/SMF. Hence, selectivity toward total oxidation of VOCs mixture increases with metal oxide integrated NTP reactor and among the catalysts, AgO_x/MnO_x/SMF under humid conditions showed improved performance toward total oxidation.

3.5. Reaction products and mechanism of mixture of VOCs decomposition

The chromatogram and GC–MS spectra for the identification of intermediate products during the degradation of mixture of VOCs are given in the supporting information. All detected compounds were identified using the NIST98 library database with fit values higher than 35–95% probability (Table S1 in the supporting information).

Catalytic oxidation of mixture of VOCs was studied over modified SMF catalysts and it was observed that carbon balance was not 100%. High removal efficiencies not always accompanied by high CO_x or CO_2 selectivity and formation of by-products like NO_x, ozone, partially fragmented products (benzaldehyde, ethyl benzene, aromatic or higher aliphatic hydrocarbons, aliphatic acids, aromatic acids and alcohols) were observed by GC–MS. Little amounts of polymeric deposits are formed on the walls of the plasma reactor and on the inner electrode, however, they were not analyzed. MnO_x and AgO_x/MnO_x catalysts integration to plasma not only increased the selectivity to CO_2, but also decreased the by-products like aromatic and aliphatic acids and alcohols. Besides these by-products, the formation of HCl and Cl_2 is also expected from chlorobenzene [26,27]. Close to 60 ppm of NO was detected under dry conditions at SIE of 260 J/l, whereas, under humid conditions it increased to ~150 ppm. With increasing SIE to >400 J/l, NO concentration approached zero, probably due to chemical reactions of NO with active species like O, OH radicals and O_3 that may lead to the formation of HNO_3. Nitric acid formation was confirmed by acid–base titration of the water after bubbling gas stream for 4 h. It has been reported that in NTP process, NO molecules may be oxidized to NO_2 and finally to HNO_3 [14,28].

Concerning the reaction mechanism responsible for the removal of VOCs mixture in plasma, decomposition by direct electron impact is unlikely, due to the low concentration of mixture of VOCs in air. Urashima and Chang, and Vandenbroucke et al. suggested that VOCs oxidation takes place by either radicals, negative or positive ions [2,29]. It is proposed that the initial steps of VOCs decomposition differ depending on the plasma regime applied, however, it is generally accepted that ionic reaction may be favored in both dry and humid conditions. The presence of mixture has a beneficial effect on the amount and type of undesired side products, notably ozone and NO_x. Thus, VOC mixture reduces the formation of ozone and promotes the conversion of NO_x to HNO_3. The formation of nitric acid, a desirable side product which is more readily disposed than the NO_x is favored. NO_2 is formed from oxidation of NO coupled to the conversion of organic peroxyradicals ($ROO^\bullet$) to the corresponding oxy radicals ($RO^\bullet$) and may promote the VOC oxidation to CO_2 [2,29,30].

In the same context, MnO_x and AgO_x facilitate the formation of atomic oxygen by ozone decomposition. As observed from the data presented, AgO_x/MnO_x on humid conditions destroyed ozone completely and showed the best performance. Hence, a possible decomposition mechanism expected to be VOC derived radicals such organic radicals ($R^\bullet$) generated during plasma reactions are trapped by molecular oxygen (via ozone decomposition on catalytic oxide surface) to form a peroxy radical ($ROO^\bullet$) and oxyradical ($RO^\bullet$) [31–36]. The reactions of such radicals either via hydrogen abstraction by molecular oxygen and/or fragmentation lead to carbonyl derivatives, notably aldehydes and ketones. These carbonyl intermediates may form the ultimate oxidation products, CO_2 and water [37,38]. Earlier studies found that the catalytic oxidation and degree of destruction for a compound may also depend on VOCs mixture [38–41].

4. Conclusions

In this work, the enhanced removal of mixture of VOCs in air using a DBD reactor operating at ambient conditions was reported. The present study reveals that NTP is an energy-efficient technology for complete diminution of dilute VOCs of different nature. It also reveals that plasma catalytic approach not only enhances the conversion of mixture of VOCs, but also improves the product selectivity to total oxidation. The experimental results during the oxidation of dilute VOCs mixture indicated that the removal efficiencies of mixture of VOCs enhanced significantly in the presence of metal oxide catalysts, especially MnO_x, whose activity was further improved with AgO_x deposition. Water vapor may facilitate the formation of strong oxidant hydroxyl radical on the catalyst surface. It may be concluded that NTP assisted removal of VOCs from a mixture appeared to be beneficial than the individual VOCs, probably due to the formation of reactive intermediates like aldehydes, peroxides, etc. However, the selectivity to total oxidation needs further improvement. These findings implied that NTP is a promising technique for the removal of mixture of VOCs with MnO_x and AgO_x/MnO_x catalysts integration.

Acknowledgements

This work was supported by the Department of Science and Technology (DST) - New Delhi, India under SERC scheme. The authors gratefully acknowledge the generous support by Profs. Albert Renken and Kiwi-Minsker, EPFL, Switzerland.

Appendix A. Supplementary data

Supplementary data associated with this article can be found, in the online version, at http://dx.doi.org/10.1016/j.jhazmat.2012.08.040.

References

[1] A.P. Jones, Indoor air quality and health, Atmos. Environ. 33 (1999) 4535–4564.
[2] A.M. Vandenbroucke, R. Morent, N.D. Geyter, C. Leys, Non-thermal plasmas for non-catalytic and catalytic VOC abatement, J. Hazard. Mater. 195 (2011) 30–54.
[3] S. Schmid, M.C. Jecklin, R. Zenobi, Degradation of volatile organic compounds in a non-thermal plasma air purifier, Chemosphere 79 (2010) 124–130.
[4] A.M. Harling, D. Glover, J.C. Whitehead, K. Zhang, Novel method for enhancing the destruction of environmental pollutants by the combination of multiple plasma discharges, Environ. Sci. Technol. 42 (2008) 4546–4550.
[5] G. Gerasimov, Modelling study of electron-beam polycyclic and nitro-polycyclic aromatic hydrocarbons treatment, Radiat. Phys. Chem. 76 (2007) 27–36.
[6] H.L. Chen, H.M. Lee, S.H. Chen, M.B. Chang, S.J. Yu, S.N. Li, Removal of volatile organic compounds by single-stage and two-stage plasma catalysis systems: a review of the performance enhancement mechanisms, current status, and suitable applications, Environ. Sci. Technol. 43 (2009) 2216–2227.
[7] C. Fitzsimmons, F. Ismail, J.C. Whitehead, J.J. Wilman, The chemistry of dechloromethane destruction in atmospheric-pressure gas streams by a dielectric packed-bed plasma reactor, J. Phys. Chem. A 104 (2000) 6032–6038.
[8] L.Y. Jin, R.H. Ma, J.J. Lin, L. Meng, Y.J. Wang, M.F. Luo, Bifunctional Pd/Cr_2O_3–ZrO_2 catalyst for the oxidation of volatile organic compounds, Ind. Eng. Chem. Res. 50 (2011) 10878–10882.
[9] H. Wang, D. Li, Y. Wu, L. Jie, G. Li, Removal of four kinds of volatile organic compounds mixture in air using silent discharge reactor driven by bipolar pulsed power, J. Electrostat. 67 (2009) 547–553.
[10] Z. Yue, L.I. Duan, W. Hongchang, Removal of volatile organic compounds (VOCs) mixture by multi-pin-mesh corona discharge combined with pulsed high-voltage, Plasma Sci. Technol. 12 (2010) 702–707.
[11] Ch. Subrahmanyam, A. Renken, L. Kiwi-Minsker, Catalytic abatement of volatile organic compounds assisted by non-thermal plasma: Part 1. A novel dielectric barrier discharge reactor containing catalytic electrode, Appl. Catal. B: Environ. 65 (2006) 150–156.
[12] J.C. Kim, Factors affecting aromatic VOC removal by electron beam treatment, Radiat. Phys. Chem. 65 (2002) 429–435.
[13] L.F. Liotta, Catalytic oxidation of volatile organic compounds on supported noble metals, Appl. Catal. B: Environ. 100 (2010) 403–412.
[14] J. Karuppiah, R. Karvembu, Ch. Subrahmanyam, The catalytic effect of MnO_x and CoO_x on the decomposition of nitrobenzene in a non-thermal plasma reactor, Chem. Eng. J. 180 (2012) 39–45.
[15] Ch. Subrahmanyam, M. Magureanu, D. Laub, A. Renken, L. Kiwi-Minsker, Non-thermal plasma abatement of trichloroethylene enhanced by photocatalysis, J. Phys. Chem. C 111 (2007) 4315–4318.
[16] H. Einaga, A. Ogata, Benzene oxidation with ozone over supported manganese oxide catalysts: effect of catalyst support and reaction conditions, J. Hazard. Mater. 164 (2009) 1236–1241.
[17] H. Einaga, A. Ogata, Catalytic oxidation of benzene in the gas phase over alumina-supported silver catalysts, Environ. Sci. Technol. 44 (2010) 2612–2617.
[18] U. Roland, F. Holzer, F.D. Kopinke, Improved oxidation of air pollutants in a non-thermal plasma, Catal. Today 73 (2002) 315–323.

[19] A.M. Harling, D.J. Glover, J.C. Whitehead, K. Zhang, The role of ozone in the plasma-catalytic destruction of environmental pollutants, Appl. Catal. B: Environ. 90 (2009) 157–161.
[20] S. Imamura, M. Ikebata, Decomposition of ozone on a silver catalyst, Ind. Eng. Chem. Res. 30 (1991) 217–221.
[21] F. Besenbacher, J.K. Norskov, Oxygen chemisorption on metal surfaces: general trends for Cu, Ni and Ag, Prog. Surf. Sci. 44 (1993) 5–66.
[22] C.I. Carlisle, T. Fujimoto, W.S. Sim, D.A. King, Atomic imaging of the transition between oxygen chemisorption and oxide film growth on Ag{1 1 1}, Surf. Sci. 470 (2000) 15–31.
[23] D.M. Papenmeier, J.A. Rossin, Catalytic-oxidation of dichloromethane, chloroform, and their binary-mixtures over a platinum alumina catalyst, Ind. Eng. Chem. Res. 33 (1994) 3094–3103.
[24] N. Burgos, M. Paulis, M.M. Antxustegi, M. Montes, Deep oxidation of VOC mixtures with platinum supported on Al_2O_3/Al monoliths, Appl. Catal. B: Environ. 38 (2002) 251–258.
[25] A.M. Piotrowska, K. Syczewska, Destruction of volatile organic mixtures by catalytic combustion, Environ. Prot. Eng. 15 (1989) 115–125.
[26] H.R. Snyder, G.K. Anderson, Effect of air and oxygen content on the dielectric barrier discharge decomposition of chlorobenzene, IEEE Trans. Plasma Sci. 26 (1998) 1695–1699.
[27] M. Dilmeghani, K.O. Zahir, Kinetics and mechanism of chlorobenzene degradation in aqueous samples using advanced oxidation processes, J. Environ. Qual. 30 (2001) 2062–2070.
[28] L. Xia, L. Huang, Shu, R. Zhang, W. Dong, H. Hou, Removal of ammonia from gas stream with dielectric barrier discharge plasmas, J. Hazard. Mater. 152 (2008) 113–119.
[29] K. Urashima, J.S. Chang, Removal of volatile organic compounds from air streams and industrial flue gases by non-thermal plasma technology, IEEE Trans. Dielect. Elect. Insul. 7 (2000) 602–614.
[30] M.J. Kirkpatrick, W.C. Finney, B.R. Locke, Plasma-catalyst inter-actions in the treatment of volatile organic compounds and NO_x with pulsed corona discharge and reticulated vitreous carbon Pt/Rh-coated electrodes, Catal. Today 89 (2004) 117–126.
[31] M. Schiorlin, E. Marotta, M. Rea, C. Paradisi, Comparison of toluene removal in air at atmospheric conditions by different corona discharges, Environ. Sci. Technol. 43 (2009) 9386–9392.
[32] Y. Xi, C. Reed, Y.K. Lee, S.T. Oyama, Acetone oxidation using ozone on manganese oxide catalysts, J. Phys. Chem. B 109 (2005) 17587–17596.
[33] B. Dhandapani, S.T. Oyama, Gas phase ozone decomposition catalysts, Appl. Catal. B: Environ. 11 (1997) 129–166.
[34] K. Genov, V. Georgiev, T. Batakliev, D.K. Sarker, Ozone decomposition over silver-loaded perlite, Int. J. Civil Environ. Eng. 3 (2011) 202–205.
[35] H. Einaga, S. Futamura, T. Ibusuki, Complete oxidation of benzene in gas phase by platinized titania photocatalysts, Environ. Sci. Technol. 35 (2001) 1880–1884.
[36] J. Ma, N.J.D. Graham, Degradation of atrazine by manganese-catalalyzed ozonation: influence of humic substances, Water Res. 33 (1999) 785–793.
[37] L. Yang, C. Hu, Y. Nie, J. Qu, Catalytic ozonation of selected pharmaceuticals over mesoporous alumina-supported manganese oxide, Environ. Sci. Technol. 43 (2009) 2525–2529.
[38] R.K. Sharma, B. Zhou, S. Tong, K.T. Chuane, Catalytic destruction of volatile organic compounds using supported platinum and palladium hydrophobic catalysts, Ind. Eng. Chem. Res. 34 (1995) 4310–4317.
[39] S.K. Gangwal, M.E. Mullins, J.J. Spivey, P.R. Caffrey, B.A. Tichenor, Kinetics and selectivity of deep catalytic oxidation of n-hexane and benzene, Appl. Catal. 36 (1988) 231–247.
[40] B.A. Tichenor, M.A. Palazzolo, Destruction of volatile organic compounds via catalytic incineration, Environ. Prog. 6 (1987) 172–176.
[41] J.J. Spivey, Complete catalytic oxidation of volatile organics, Ind. Eng. Chem. Res. 26 (1987) 2165–2180.

Air & Waste

ISSN: 1073-161X (Print) (Online) Journal homepage: https://www.tandfonline.com/loi/uawm19

Corona Destruction: An Innovative Control Technology for VOCs and Air Toxics

Carlos M. Nunez , Geddes H. Ramsey , Wade H. Ponder , James H. Abbott , Larry E. Hamel & Peter H. Kariher

To cite this article: Carlos M. Nunez , Geddes H. Ramsey , Wade H. Ponder , James H. Abbott , Larry E. Hamel & Peter H. Kariher (1993) Corona Destruction: An Innovative Control Technology for VOCs and Air Toxics, Air & Waste, 43:2, 242-247, DOI: 10.1080/1073161X.1993.10467131

To link to this article: https://doi.org/10.1080/1073161X.1993.10467131

Published online: 06 Mar 2012.

Corona Destruction: An Innovative Control Technology for VOCs and Air Toxics

Carlos M. Nunez, Geddes H. Ramsey, Wade H. Ponder and James H. Abbott
Air and Energy Engineering Research Laboratory
Environmental Protection Agency
Research Triangle Park, North Carolina

Larry E. Hamel and Peter H. Kariher
Acurex Corporation
Research Triangle Park, North Carolina

This paper discusses the work and results to date leading to the demonstration of the corona destruction process at pilot scale. The research effort in corona destruction of volatile organic compounds (VOCs) and air toxics has shown significant promise for providing a valuable contribution to critical U.S. Environmental Protection Agency and national goals of reducing the health effects associated with exposures to hazardous air pollutants. The corona destruction technology could be especially useful in future years in helping industry meet the residual risk requirements of the Clean Air Act Amendments of 1990.

Since 1988, EPA has conducted research in the area of corona destruction of VOCs and air toxics. EPA's interest in corona destruction of molecular species started with modeling of a point-plane reactor for destroying toxic organic compounds. EPA's goal is to develop a technology capable of controlling low concentration streams at low capital and operating costs. The purpose of this work is to develop an industrial scale corona reactor capable of efficiently and cost-effectively destroying VOCs and air toxics at ambient temperature and pressure. Results show that corona destruction is a promising control technology for many VOC-contaminated air streams, especially at low concentrations. Cost comparisons are presented for corona destruction and conventional control devices, carbon adsorption, catalytic incineration and thermal incineration.

The research effort in corona destruction of volatile organic compounds (VOCs) and air toxics has shown significant promise for providing a valuable contribution to critical EPA and national goals of reducing the health effects associated with exposures to hazardous air pollutants. The corona destruction technology could be especially useful in future years in helping industry meet the residual risk requirements of the Clean Air Act Amendments of 1990.

Since 1988, EPA's Air and Energy Engineering Research Laboratory has conducted research in the area of corona destruction of VOCs and air toxics. EPA's interest in corona destruction of molecular species started with modeling of a point-plane reactor for destroying toxic organic compounds.[1] The emerging concern for excessive concentrations of ambient ozone, for which many VOCs are precursors, the need to develop technology to control low concentration streams, and the economic advantages of ambient temperature operation provided impetus for the work on high intensity corona reactor devices.

The purpose of this work is to develop an industrial scale corona reactor capable of efficiently and cost-effectively destroying VOCs and air toxics at ambient temperature and pressure.

The work and results to date leading to the demonstration of the corona destruction process at pilot scale are presented in this paper.

Background

The initial work at EPA involved investigating the viability of corona destruction as an effective device for VOCs. The initial tests were run with toluene and were very successful. The next phase of the research program involved developing the destruction mechanism and prediction theory for destruction of other hydrocarbons. Even though corona destruction was able to destroy toluene, an understanding of the reaction mechanisms, both chemically and electrically, is necessary before larger systems can be successfully designed. Thus, a series of experiments was conducted using 10 compounds, and the destruction efficiency and ionization potential of each compound was examined to determine the possible existence of a statistical correlation. The compounds tested were benzene, cyclohexane, ethanol, hexane, hexene, methane, methylene chloride, methyl ethyl ketone, styrene and toluene. Preliminary results indicate that a relationship exists between ionization potential and ease of destruction for VOCs, the lower the ionization potential, the easier the compounds are destroyed.

Corona destruction has several advantages over conventional control devices as shown in Table I. The compounds that we have tested have been oxidized to carbon dioxide, carbon monoxide, and water, plus, in the case of chlorinated compounds, chlorine and hydrochloric acid. The exhaust streams have been analyzed thoroughly with a gas chromatograph/flame ionization detector (GC/FID) and gas chromatograph/mass spectroscopy (GC/MS), and no intermediate compounds have been found. Since the contami-

Table I. Benefits of corona destruction over conventional technologies.

- Performs effectively and economically at very low concentrations
- Operates at ambient temperature
- Eliminates disposal or treatment problems associated with carbon adsorption
- Eliminates sensitivity to poisoning by sulfur or halogen containing compounds
- Requires no auxiliary fuel
- Requires low maintenance

nants are destroyed, the problem of disposing of collected toxins is avoided.

Two corona destruction processes have been evaluated for their potential in destroying VOCs and air toxics. One of the corona destruction processes uses high dielectric barium titanate pellets in a packed-bed reactor across which a high voltage alternating current (AC) is applied. The microelectric fields developed in the interstitial spaces between the pellets form a multiplicity of corona sites which generate electrons. These electrons initiate the reactions that lead to destruction of the challenge gas species. The second process consists of a wire-in-tube reactor which is energized by high voltage nanosecond pulses. These techniques have the potential of generating very energetic electrons without wasting power by accelerating ions.

The corona processes operate at ambient temperature. The corona is generated in the packed-bed of barium titanate pellets or along the wire in the pulsed reactor. The necessity of heating the contaminated air streams to the temperature required for a catalyst or for thermal incineration to work is avoided.

The corona destruction processes were also evaluated as a means to control very low concentrations of contaminants in air streams. Experiments with contaminant streams using 10 ppmv single component VOCs in air demonstrated the ability to destroy the contaminant beyond the detection limit of our analytical equipment (< 10 ppbv). Corona destruction may be an alternative control technology for low concentration streams where conventional control devices such as catalytic incineration and carbon adsorption have disadvantages, either economical or technical. Preliminary power estimates for the corona process indicate that the power requirement for VOC destruction is approximately 3 W/ft^3 (106 J/sec/m^3). As shown in Figure 1, the annual operating costs of corona destruction fall below the costs of catalytic incineration and thermal incineration.[2] The annual operating costs for these technologies are based on a contaminated air stream at ambient conditions with a flowrate of 3000 acfm and an organic concentration of less than 100 ppmv. For these reasons, corona destruction may be well suited to destroy VOCs and air toxics in the outlet stream from operations such as the ones shown in Table II.

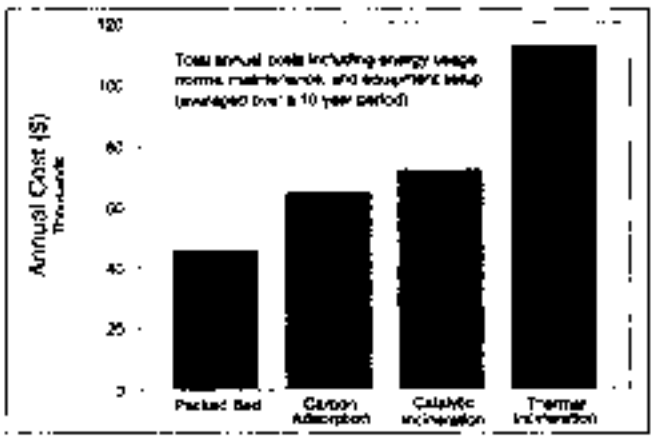

Figure 1. Estimated costs of corona process and conventional VOC control technologies

Table II. Potential source categories for the application of corona destruction.

Industrial
- Painting and coating operations
- Semiconductor and electric component manufacture
- Food and pharmaceutical processing
- Site remediation

Commercial
- Commercial paint operations (body shops)
- Furniture manufacturers
- Dry cleaning establishments
- Restaurants

One of our current program objectives is to test the corona reactor on a larger scale. Experiments are currently underway to prove the feasibility of the packed-bed reactor on a 20 to 50 cfm (0.57 to 1.42 m^3/min) stream. At this stage, the reactor design can be optimized as to dimensions and power requirements. Other program objectives include demonstration of this technology on an industrial scale and commercialization of corona destruction as a VOC control alternative.

The purpose of this work is to determine if VOCs can be destroyed in these high intensity corona reactors. In setting up the original feasibility-of-concept experiments, an attempt was made to relate the work to the greatest extent possible to current problems threatening the environment. For these experiments both non-halogenated and halogenated compounds were evaluated.

Theory of Corona Destruction

Although several theoretical concepts are still being evaluated to describe the destruction pathways for several families of hydrocarbons, the following discussion provides some of the most likely mechanisms for VOC destruction in a corona process.

Electrons undergo both elastic and inelastic collisions as they travel through energy fields. In an elastic collision, the electron retains the majority of its kinetic energy. Under the influence of the strong electric field, free electrons are accelerated. They undergo an elastic collision at the end of each free path length. The electrons continue to increase in energy until the energy becomes high enough to allow the electrons to undergo an inelastic collision. During an inelastic collision the electron transfers all or part of its kinetic energy to the particle with which it has collided. Inelastic collisions result in a change to the target particle or molecule such as ionization, dissociation or excitation.[3] In an inelastic collision, significant amounts of energy are transferred from an electron to the target species. Examples of these inelastic collisions are:

- Electron attachment by electronegative gases to form negative ions.
- Dissociation of molecular species into smaller fragments including formation of free radicals.
- Excitation of molecular and elemental species.
- Ionization to form positive ions and additional free electrons (a Townsend avalanche develops under favorable circumstances, generating many additional free electrons).

- Breaking down of molecular species into their elemental components.

The amount of energy required for the above events varies by type of event and molecular/elemental species. Energy requirements for different types of events are less than 5 eV for electron attachment and 5 to 25 eV to form positive ions by electron removal.[4] An electron volt (eV) is defined as the energy that an electron acquires (or loses) in passing through a 1 V change in potential. The electron volt is a particularly useful unit of measurement for this work because it allows an easy comparison of electrical energy input required for destruction of the target molecules. The probability of one of the above events occurring is expressed by the collision cross section which is mainly a function of concentration. The probability that the event will occur is dependent on the electron's having achieved the energy level needed for the event.

At atmospheric pressure and ambient temperatures, an electron's energy level can increase by a fraction of 1 eV in one mean free path length, if the mean free path length is parallel to an electric field of 20 to 30 kV/cm. At atmospheric pressure and ambient temperature a mean free path length is about 1×10^{-7} m.

In addition to the above effects of inelastic electron collisions, there are also photoelectric effects (ionization, dissociation, excitation, etc.) which are either activated by or result in the emission of a photon. The events that can occur are very much interrelated.

In summary, the picture that is presented is one of high complexity when the possibility of electron collisions and the effects of photons are considered. The energy distribution in a swarm of energetic electrons ranges from very low to very high, with the majority centered around some median value. Therefore, electrons having a wide range of energies will undergo various types of inelastic collisions such as attachment, excitation and ionization. For a mixture of gases the picture becomes even more complex.

The power input to the bench-scale packed-bed reactor was measured, allowing the calculation of the energy introduced for a unit of time. For a typical toluene concentration of about 200 ppmv the energy introduced per toluene molecule was about 400 eV (9300 kcal/g-mole). The carbon byproducts were CO_2 and CO. The ratio of CO_2 to CO was about 2:1.

A number of reaction mechanisms are possible in the corona destruction of aromatic hydrocarbons. Three of the reactions are presented and discussed. The first reaction mechanism involves initial attack of the hydrocarbon molecule with an energized oxygen molecule. The other two reaction mechanisms, which involve breaking a C-C bond in the ring or removing a hydrogen from one of the carbons in the ring, have a lower probability.[5]

A mechanism likely to occur in the destruction of toluene is the oxidation of the methyl group of the molecule. Toluene has a resonance structure where a proton is lost or gained at the methyl group which should result in a more reactive site. The methyl group serves as an electron donor to the phenyl group. An excited oxygen molecule would attack the methyl group and the following reaction would proceed:

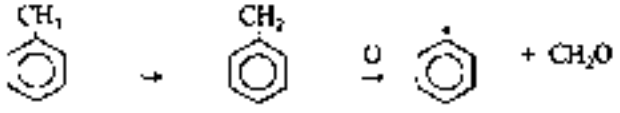

The CH_2O radical rapidly reacts to form a CHO radical which goes to CO. The benzene radical reacts as follows:

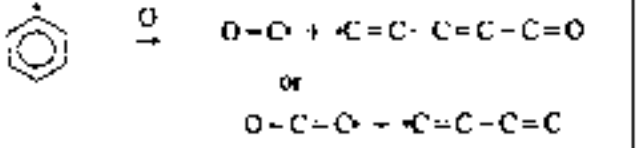

The O=C or O=C=C radical reacts with oxygen to form CO_2. The other radical oxidizes rapidly to CHO and then to CO.[5] Although the reaction to form CO rather than CO_2 is favored at low temperatures, high temperatures may be generated at the pellets, which would explain the favored formation of CO_2. A CO_2 molecule is formed when the ring breaks, but the CO reaction is favored in the remainder of bond destruction reactions. This accounts for the approximately 1.7:1 ratio of CO_2 to CO observed experimentally.

The energies of bond formation/destruction are:[5]

C-C	3.6 eV
C=C	6.3 eV
C=C (in ring)	5.5 eV
C-H	4.3 eV
C-O	3.7 eV
C=O	7.7 eV
C=O (in CO_2)	8.3 eV
C-Cl	3.5 eV

During the destruction of a toluene molecule, energy is required to break a C-H bond by an electron or by reaction with oxygen. The radical formed will react with an excited oxygen molecule, e.g., singlet oxygen ($^1\Sigma_g^+$ and $^1\Delta_g$) to form a C-O bond.[6] The energy released when the C-O bond forms is more than enough to break the adjacent C-C bonds. Therefore, the energy for the reaction once past the initiation energy must come from the oxidation of the toluene itself.[7] Because 20 percent of the gas is oxygen and since the oxygen molecule is one of the easiest to excite, the excitation of the oxygen molecule is consequently the most likely mechanism occurring in the process. The potential energies for the ground state and the first four electronically excited states of oxygen are shown in Table III.

The addition of energy greater than 7 eV causes dissociation of the oxygen molecule to one atom in the ground state and one in the 1st excitation state.[8] Many other excited states of oxygen are possible inside the corona destruction reactor.

The benzene molecule should react similarly to the toluene molecule, but slightly more energy would be required to initiate the benzene reaction. Instead of the excited oxygen attacking the methyl group of the toluene molecule, the point of attack in the benzene molecule would have to be the ring structure or a C-H bond. The bond energies would favor an attack of the C-H bond (4.3 eV for the C-H bond compared to 5.5 eV for the C=C bond). This is slightly

Table III. The potential energies for the excited state of oxygen.

State of Oxygen Molecule	Energy Required eV	Comments
Ground state	0	
1st excitation	0.98	Forbidden transition
2nd excitation	1.63	Allowed; half-life of about 10 seconds; collisionally relaxing to 1g; excitation state
3rd excitation	4.25	Theoretically forbidden
4th excitation	6.00	Allowed; creates two oxygen atoms in the ground state via a non-radiative transition

higher than the C-C bond energy which would be the point of attack in the toluene molecule (3.6 eV for the C-C bond). Therefore, since a higher energy is required to initiate the reaction of the benzene molecule, destruction of benzene should be lower than toluene under similar conditions. This was confirmed by our laboratory results.

The second possible reaction is the breaking of a C-C bond in the chain by a sufficiently energetic electron. This reaction is of the type:

$$AB + e^- \rightarrow [AB] + e^-$$

in which [AB] is a radical. For the toluene molecule, the ring structure has a greater affinity for an electron than does the methyl group. The energy required to break a C-C bond in the toluene ring is 5.3 eV (123 kcal/g-mole). For toluene, cleavage of an arbitrary C-C bond would be:

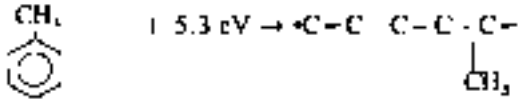

The fragment on the right-hand side of the above reaction equation is a radical. The energy required for the ionization of toluene is 8.5 eV (195 kcal/g-mole). Consequently, the collision cross section for the C-C bond cleavage is considerably less than that for the ionization.

Once a C-C bond is broken and the free radical is formed, the free radical is able to react with oxygen. The heat of oxidation of toluene is 39 eV (901 kcal/g-mole) when going to CO_2 and 22 eV (497 kcal/mole) when going to CO.[3] Either pathway will supply sufficient energy to sustain the oxidation of all carbon molecules once the reaction starts.

For this second reaction to occur, electrons would have to achieve 5.3 eV to sever a C-C bond. Many electrons do achieve the higher energy levels, but not all.

A final reaction possibility is removing a hydrogen from the ring structure by electron collision. The energy required to break a C-H bond is about 4.3 eV. Once the C-H bond is broken the reaction will proceed by the same mechanism as the primary reaction suggested above. This mechanism would also account for the CO/CO_2 formation.

The intermediate steps in the oxidation require the attachment of an oxygen to a severed carbon bond or to a site where a hydrogen was removed. The energy released by attachment of the oxygen is sufficient to break an adjacent C-C bond, which provides the site for the next oxygen attachment. The most likely intermediate byproduct is the radical CHO which is favored at low temperatures. The CHO radical leads to the formation of CO; higher temperature reactions favor the formation of CO_2. Note that once a C-C bond in the ring is severed, the radical that is formed has two active ends for attachment of an oxygen.

In all the suggested mechanisms, once the reaction of the individual molecule is initiated, the destruction of the molecule proceeds to completion since no other lower molecular weight species are found during analysis. If the molecule were not completely oxidized, other hydrocarbon byproducts would appear in the exhaust stream. The absence of other hydrocarbons has been confirmed by GC/MS. For operating conditions in which less than 100 percent destruction is deliberately achieved, the unreacted toluene molecules remain intact, which is evident in GC/MS.

Results and Discussion

The packed-bed corona reactor makes use of a bed of ferroelectric pellets across which an AC electric field is impressed. A total of 10 hydrocarbons (benzene, cyclohexane, ethanol, hexane, hexene, methane, methylene chloride, methyl ethyl ketone, styrene and toluene) were tested in the bench-scale packed-bed reactor. The bench-scale packed-bed reactor is depicted in Figure 2.

The pellets must be made of a material with a high dielectric constant. In this case the material is barium titanate with a dielectric constant ranging from 15 to 12,000.[9] The dielectric constant for barium titanate varies due to temperature, bead size and impurities. The barium titanate pellets are energized by an AC voltage applied through porous stainless steel plates. Corona appears at the contact points of the pellets when an AC electric field is generated as low as about 1 kV/cm. Sparking across the bed occurs for fields of 5 to 8 kV/cm, depending upon the size of the pellets. The reactor obviously uses more energy during sparking; however, the reactor performance is not improved proportionally to the increased amount of power applied during sparking. The most efficient operating point will be below sparking conditions.

The work required to remove a given electron from its atomic orbit and place it at rest at an infinite distance, is called the ionization potential.[9] Since all the compounds evaluated in the laboratory were not destroyed equally in the packed-bed corona reactor, the first method attempted to predict the destruction efficiency was based on ionization potential (see Table IV). Other parameters evaluated were heat of combustion, size of molecule, molecule bonding energy, Gibbs free energy and enthalpy. From the parameters evaluated to estimate the destruction of compounds in the packed-bed corona reactor, the ionization potential was the value that best correlated with destruction efficiency, i.e., the higher the ionization potential, the lower the destruction at constant operating conditions. As shown in Figure 3, factors other than ionization potential may explain the deviations from the predicted destruction efficiencies. In addition to the great ionization power of electrons, they also have the property of attaching to many molecular and atomic species to form negative gas ions. Electron attachment is greatest for atoms in the upper right-hand region of the periodic table. For example, methylene chloride has

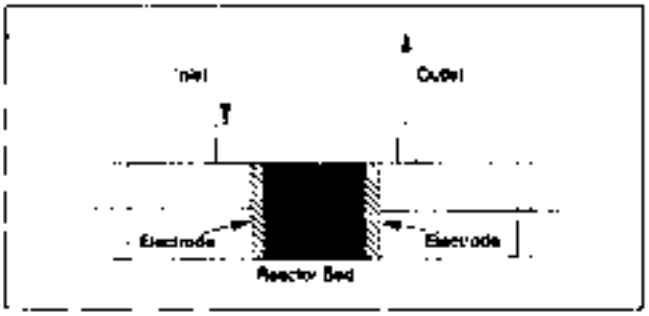

Figure 2. Bench-scale packed-bed corona destruction reactor.

Table IV. Ionization energies of selected molecules, eV.

Nitrogen	15.6	Formaldehyde	10.9
Hydrogen	15.4	Methanol	10.9
Carbon Monoxide	14.0	Hexane	10.2
Carbon Dioxide	13.8	Nitrogen Dioxide	9.8
Methane	13.0	Methyl Ethyl Ketone	9.5
Nitrous Oxide	12.9	Hexene	9.4
Ozone	12.8	Cyclohexane	9.4
Water	12.6	Benzene	9.3
Oxygen	12.1	Nitric Oxide	9.3
Methylene Chloride	11.3	Toluene	8.8
		Naphthalene	8.1

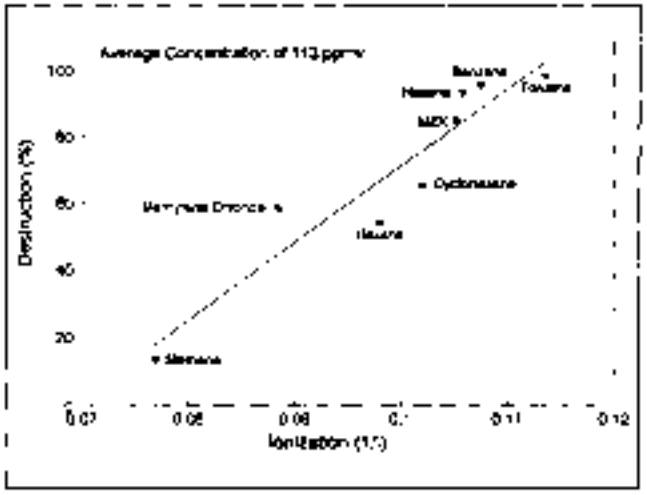

Figure 3. Destruction of VOCs as a function of ionization potential.

a higher ionization potential than hexane; however, the destruction efficiency is higher. This is probably due to the high electronegativity of the chlorine atom which will increase the chance of electron attachment to the chlorine atom.

A test matrix consisting of three sets of eight runs for a total of 24 runs was performed using toluene in the bench scale corona reactor. This test matrix was designed to support the calculation of material and energy balances, characterize wall effects, and determine the magnitude of systematic and random errors. Two reactor sizes (diameters of 2.23 and 3.18 cm), two face velocities (1.8 and 5.3 cm/sec), two residence times (0.48 and 1.43 seconds), and two toluene concentrations (50 and 250 ppmv) were used for the test matrix. The reactor length was 2.5 cm. The reactors were placed in an oven at 50 °C to maintain a constant temperature. Before each block of eight runs was initiated, the reactors were disassembled, the pellets were replaced by an equal weight of unused pellets, and the reactors were reassembled. Figures 4 and 5 show the outlet concentration of toluene, CO_2 and CO obtained during these experiments for toluene inlet concentrations of 50 and 250 ppmv, respectively. Each reactor performance was controlled by the gas flowrate (face velocity and residence time). The product of face velocity and residence time was maintained at about 2.5 cm for both reactors (R_1 and R_2). The carbon balance for the test matrix varied from 102 to 105 percent.

In Figure 6, the effect of voltage on reactor performance for the large reactor (R_2) and for a toluene concentration of 50 ppmv is shown. For voltages over 15 kV complete destruction of toluene was obtained.

The electric power for these experiments was measured using a digital oscilloscope connected to the corona reactor. The circuitry used to measure both voltage and amperage is depicted in Figure 7. Since the current signal is not of a sinusoidal form, ei cos θ was not used to estimate power consumption. Power was calculated by integrating the area under the power curve using Simpson's rule. The power curve is the result of multiplying each data point of the current curve with the corresponding data point of the voltage curve. The voltage and amperage for one cycle (16.7 ms) was analyzed using a customized spreadsheet program. Figure 8 is an example of the graphical output from the power curve analysis.

Conclusions

The packed-bed corona destruction process shows significant promise as an alternative control method for re-

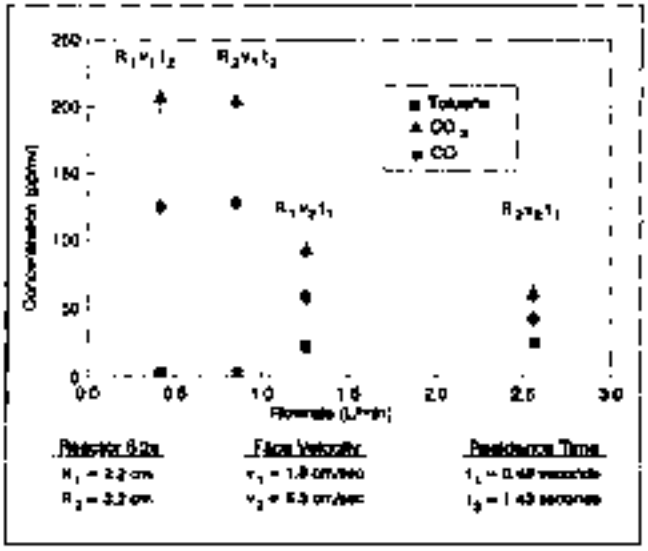

Figure 4. Outlet concentration of toluene, CO_2, and CO at various flowrates (toluene inlet concentration of 50 ppmv).

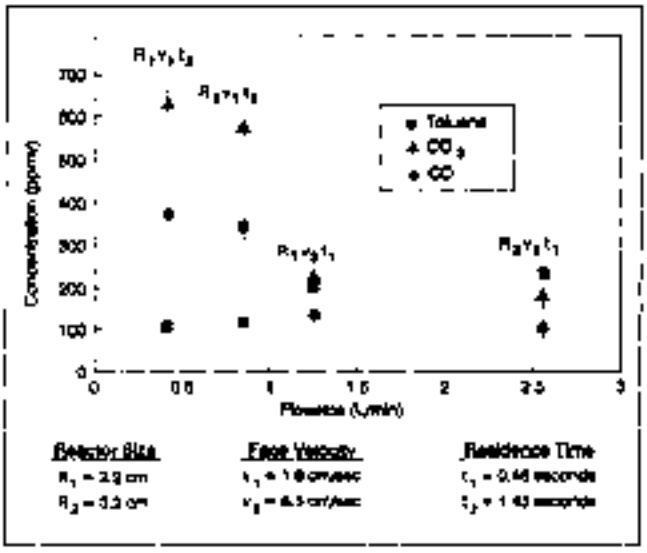

Figure 5. Outlet concentration of toluene, CO_2, and CO at various flowrates (toluene inlet concentration of 250 ppmv).

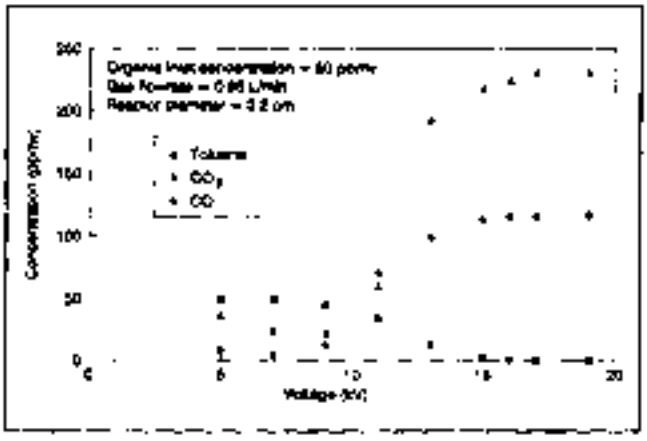

Figure 6. Toluene, CO_2, and CO outlet concentration as a function of voltage.

ducing VOC and air toxics emissions from industrial and commercial operations. Preliminary data show that this technology is technically and economically feasible. When the corona destruction process is compared to conventional control technologies such as carbon adsorption, catalytic

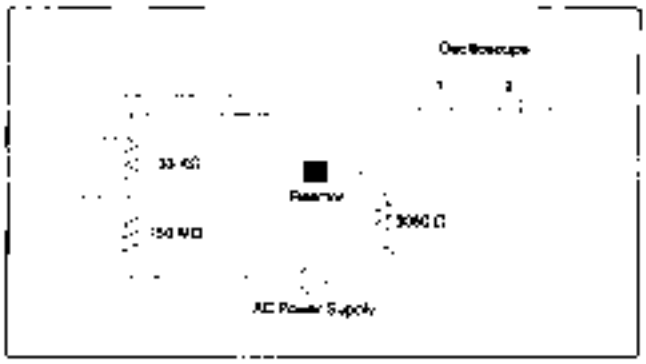

Figure 7. Voltage and current measurement system.

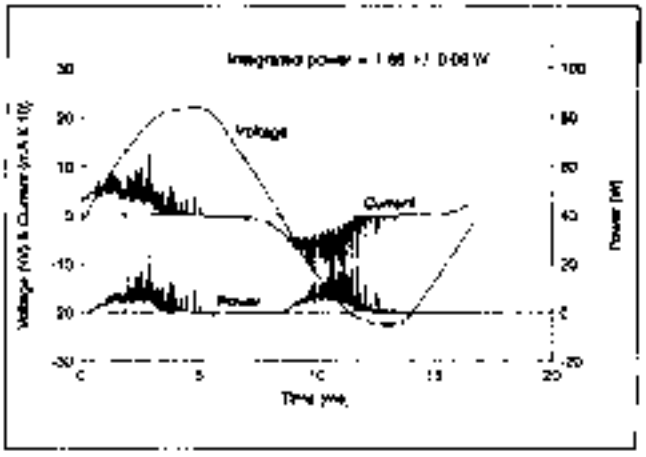

Figure 8. Power curve for the bench-scale packed-bed corona reactor.

incineration, and thermal incineration, the corona process demonstrates several significant advantages over the conventional control methods. These advantages are listed in Table I.

Conventional control technologies usually fail either technically or economically in effectively controlling VOC and air toxics at very low concentrations. In the corona destruction process, the lower the concentration the lower the power required to achieve excellent performance. Based on the durability of the bed packing material, ease of assembly, and simplicity of the hardware required, packed-bed corona destruction requires very little maintenance.

In catalytic and thermal incineration systems, relatively high temperatures are required to obtain the desired performance. This usually translates to a high cost of operation. In addition, when the inlet organic concentration is low, auxiliary fuel is needed to maintain proper incineration of the pollutants. However, the corona destruction process operates at ambient temperature, thus substantially reducing operating costs. Unlike catalytic systems, the corona process is not sensitive to poisoning by sulfur or halogen containing compounds.

Corona destruction also eliminates the problem associated with the treatment and disposal of the adsorbent used in carbon adsorption. Although the use of carbon adsorption in recovering VOCs may be cost-effective at high adsorbate concentrations, its performance dramatically declines when the adsorbate concentration is low. The application of carbon adsorption at low concentrations then becomes prohibitive.

Corona destruction is an effective alternative control method for a variety of VOCs and air toxics. Its destruction efficiency for VOCs such as benzene, cyclohexane, ethanol, hexane, hexene, methane, methylene chloride, methyl ethyl ketone, styrene and toluene may be predicted from the ionization potential and types of bonds in the molecules.

During the tests of destruction of VOCs and air toxics by the corona process, no products of incomplete reaction are formed. When the compounds were treated with the corona, molecules either were completely destroyed or passed through the reactor unaffected. More complex compounds and mixtures will have to be tested to determine if these promising results hold true in practical applications. The percentage of molecules destroyed can be predicted and controlled by appropriate reactor design and specification of operational parameters.

The performance of the corona destruction system can be enhanced by either increasing the power input or adjusting the residence time in the reactor to achieve a high degree of destruction for VOCs.

References

1. G.H. Ramsey, N. Plaks, C.A. Vogel, et al., "The destruction of volatile organic compounds by an innovative corona technology," Presented at *The Eighth Symposium on the Transfer and Utilization of Particulate Control Technology*, San Diego, CA, March 20-23, 1990.
2. S. Moore, *HAP-PRO User's Manual*, Version 1.0, EPA-600/8-91-211a (NTIS PB92-135904) (manual), EPA-600/8-91-211b (diskettes), October 1991.
3. H.J. White, *Industrial Electrical Precipitation*, Addison-Wesley Publishing Co., Reading, MA, 1963.
4. G.C. Pimentel, R.D. Spratley, *Chemical Bonding Clarified Through Quantum Mechanics*, Holden-Day, Inc., San Francisco, CA, January 1970.
5. J.A. Miller, G.A. Fisk, "Combustion chemistry," *Chem. Engineer. News* 65:22 (1987).
6. *Advances in Environmental Sciences*, Volume 1, J.N. Pitts, R.L. Metcalf, Eds., Wiley and Sons, New York, 1969, p. 310.
7. R.J. Heinsohn, P.M. Becker, "Effects of Electric Fields on Flames," in *Combustion Technology: Some Modern Developments*, Academic Press, New York, 1974.
8. B.J. Finlayson-Pitts, J.N. Pitts, Jr., *Atmospheric Chemistry: Fundamentals and Experimental Techniques*, John Wiley & Sons, New York, 1986, p. 220-225.
9. *CRC Handbook of Chemistry and Physics*, R.C. Weast, Ed., CRC Press, Inc., Cleveland, OH, 1975, p. F-60.

About the Authors

C.M. Nunez, G.H. Ramsey, W.H. Ponder and J.H. Abbott are with the Air and Energy Engineering Research Laboratory, U.S. Environmental Protection Agency, Research Triangle Park, NC 27711. L.E. Hamel and P.H. Kariher are with Acurex Corporation, P.O. Box 13109, Research Triangle Park, NC 27709. This manuscript was submitted for peer review on April 17, 1992. The revised manuscript was received on November 19, 1992.

Chemical Engineering Journal 388 (2020) 124275

Contents lists available at ScienceDirect

Chemical Engineering Journal

journal homepage: www.elsevier.com/locate/cej

Review

The application of dielectric barrier discharge non-thermal plasma in VOCs abatement: A review

Shijie Li[a], Xiaoqing Dang[a,*], Xin Yu[a], Ghulam Abbas[b], Qian Zhang[a,*], Li Cao[a]

[a] School of Environment & Municipal Engineering, Xi'an University of Architecture & Technology, Xi'an 710055, China
[b] Department of Chemical Engineering and Technology, University of Gujrat, Gujrat 50700 Pakistan

HIGHLIGHTS

- The history, microdischarge formation and application of DBD were presented.
- The effect of reactor structure, power supplies, packing materials and gas properties on VOCs removal were described.
- The discussion of the above factors was based on discharge behaviors, VOCs removal and mineralization rate, and by-products.
- The practical implementation of DBD in VOCs abatement were examined.
- Future trends on DBD for VOCs treatment were given.

GRAPHICAL ABSTRACT

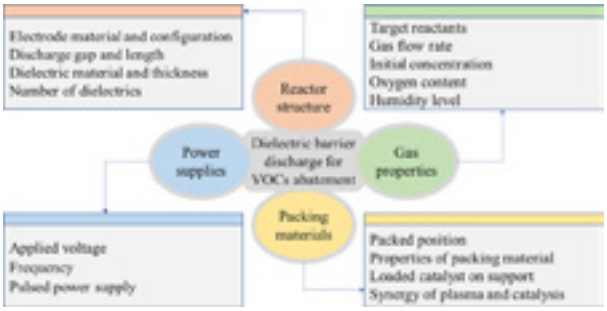

ARTICLE INFO

Keywords:
Dielectric barrier discharge
Volatile organic compounds
Reactor structure
Power supplies
Packing material
Gas properties
Practical application

ABSTRACT

This review describes the history and current status of dielectric barrier discharge (DBD) non-thermal plasma (NTP) for volatile organic compounds (VOCs) abatement. Firstly, the history of DBD, the formation of microdischarge and its environmental applications were presented. Next, the status quo of DBD for VOCs removal was discussed in detail from four aspects: reactor structure (include electrode material and configuration, discharge gap and length, dielectric material and thickness, and number of dielectrics), power supplies (include applied voltage, frequency and pulsed power supply), packing materials (include packed position, properties of packing material, loaded catalyst on support and synergy of plasma and catalysis) and gas properties (include target reactants, gas flow rate, initial concentration, oxygen content and humidity level). The description of these factors is mainly based on their effects on discharge characteristics and VOCs decomposition in DBD. Subsequently, a number of aspects related to the practical implementation of DBD for VOCs treatment were described. Finally, future trends were suggested based on the existing research works.

1. Introduction

As the pollution of particulate matter, SOx and NOx gradually decreases, the abatement of volatile organic compounds (VOCs) emitted from various industries is becoming a matter of wider concern for researchers and environmentalist. Most VOCs have high photochemical reactivity and react easily with NOx to form ozone [1,2]. Meanwhile VOCs are key precursor of secondary organic aerosols, which are significant components of fine particulate matter [3–5]. In addition to the adverse effects on the environment, VOCs also have hazards for human

* Corresponding authors.
E-mail addresses: xiaoqingdang@hotmail.com (X. Dang), zhangqian2018@xauat.edu.cn (Q. Zhang).

https://doi.org/10.1016/j.cej.2020.124275
Received 14 October 2019; Received in revised form 8 January 2020; Accepted 28 January 2020
Available online 30 January 2020
1385-8947/

health. Many VOCs are carcinogenic, affecting the central nervous system, causing respiratory diseases [6–8], etc.

In order to reduce the emission of VOCs, three techniques have been developed, namely source, process and terminal control. Although the first two techniques can decrease the production or emission of VOCs, end-of-pipe solution is still essential. End-of-pipe techniques include the recovery and destruction of VOCs. The former refers to the transfer or concentration of VOCs from exhaust gas, including adsorption [9,10], condensation [11], absorption [12] and membrane separation [13]. The latter means decomposing VOCs into harmless substances such as CO_2 and H_2O, including thermal oxidation [14], biological treatment [15,16], catalytic oxidation [17–19], photocatalysis [20–22], thermal plasma [23] and non-thermal plasma [24,25]. Recent reviews have highlighted the benefits and drawbacks of different techniques available for VOCs removal [26–29]. Among these techniques, adsorption and thermal oxidation are the most widely applied ones in the industrial sector. However, for the adsorption, the saturated adsorbents need to be desorbed and the desorbed gas requires further treatment, and thermal oxidation is high in energy consumption by heating a large amount of gas [30]. Alternatively, non-thermal plasma (NTP) is widely deemed to have the following merits: (1) Its energy efficiency is higher than that of thermal oxidation. (2) It operates at atmospheric pressure and room temperature. (3) It can be easily integrated with various packing materials. (4) It can be quickly switched on/off [31–33].

Although Francis Hauksbee created the first gas discharge in 1705 and Siemens invented the first silent discharge (also referred to as dielectric barrier discharge) device for producing ozone in 1857 [34], until 1928, the term 'plasma' was proposed by Irving Langmuir to describe a 'region containing balanced charges of ions and electrons [35]. In other words, plasma is a partially or fully ionized gas consisting of electrons, atoms, ions and ground state, metastable and excited molecules. It is worth noting that not all balanced charges of ionized gas are plasma. In plasma, the spatial scale of the 'region' should be much larger than Debye length (λ_D) and the density of charged species should be sufficiently large. The term of temperature is commonly used to quantitatively describe plasma. In thermal plasma, the temperature of heavy particles (ions, atoms, molecules and radicals) and electrons is similar, indicating that almost all its species are at thermal equilibrium. In non-thermal plasma, the temperature is beyond thermal equilibrium, and the temperature of electrons (10^4-10^5 K) is much higher than heavy particles (300–1000 K) due to the differences in their mass [36]. For environmental pollution control, thermal plasma processes are used for the decontamination of solids like sludge, filter ash, municipal waste and hospital waste [37], while non-thermal plasma is mainly applied to the control of gaseous pollutants like SOx, NOx and VOCs [38].

Accelerated in an electric field, electrons in NTP reach a temperature of 10000 K to 250000 K (1–20 eV) due to their light mass [39]. Bombarded by these high-energy electrons, the ground state molecules (e.g. N_2, O_2) become metastable (N_2^m, O_2^m) or excited (N_2^*, O_2^*). These metastable and excited state particles collide with each other and with ground state molecules or are again bombarded by electrons, and processes such as ionization, dissociation and Penning dissociation occur in the electric field. Through these multi-step physical and chemical reactions, free radicals and ions are formed. These free radicals (e.g. ·O, ·OH) are ideal oxidants that react with gaseous contaminants and intermediates generated from the collision of electrons and precursors to form harmless products like CO_2 and H_2O. These chemical changes can be realized in NTP at low temperature, while they are only possible in combustion systems and thermal discharge at much higher temperature (> 1000 K) [36]. NTP can be produced through various ways, including dielectric barrier discharge [40–42], pulsed/AC/DC corona discharge [43,44], electron-beam [45,46], gliding arc discharge [47,48], microwave plasma [49,50], etc. Among them, DBD (include silent, surface and dielectric packed bed discharge) reactor is considered to have the following advantages: (1) Its geometrical configuration is very simple; (2) It can be scaled up for industrial application without additional difficulties; (3) It is available to get reliable, efficient and affordable power supplies; (4) It requires no vacuum chambers with delicate windows like electron beam; (5) The plasma conditions in DBD are stable and reproducible [51,52]. Theoretically, DBD plasma has lower energy efficiency compared to other types of plasma such as gliding arc. However, this demerit can be compensated by optimizing reactor configuration and packing the reactor with suitable catalysts. In addition, most of the current researchers on VOCs removal by NTP use DBD reactors, especially in the presence of catalysts. However, there are few reviews focusing on the application of DBD in VOCs abatement. Therefore, it is necessary to pay special attention to DBD rather than various discharge types to gain insight into VOCs removal by NTP.

This review presents an overview of the applications of dielectric barrier discharge NTP in VOCs abatement. In the first part, an introduction of DBD is given, including the history, microdischarge formation and environmental applications of DBD. In the next four parts, the influence of reactor structure (including electrode material and configuration, discharge gap and length, dielectric material and thickness, and number of dielectrics), power supplies (including applied voltage, frequency and pulsed power supply), packing materials (including packed position, properties of packing material, loaded catalyst on support and synergy of plasma and catalysis) and gas properties (including target reactants, gas flow rate, initial concentration, oxygen content and humidity level) on discharge characteristics and VOCs removal in DBD reactor are discussed. Subsequently, a number of aspects associated to the practical application of DBD for VOCs abatement are discussed. In the last part, conclusions and future trends for this promising technique are described.

2. What is dielectric barrier discharge?

2.1. History

It has been over 150 years since the invention of dielectric barrier discharge by W. Siemens in 1857 [53]. The first DBD device focused on the ozone generation and it was the earliest environmental application of an NTP. As presented in Fig. 1, the device consists of two coaxial cylindrical glass tubes and high voltage and ground electrodes, which were attached on the inner surface of the inner tube and the outer surface of the outer tube, respectively. Air or oxygen passed through a narrow annular gap between two glass tubes, where discharge happened. Since then, DBD was primarily applied to generate ozone for water disinfection. In addition to industrial application, the processes of ozone and nitrogen oxide formation in DBD became a significant research area for many decades [54]. An important work was made by K. Buss (1932), who photographed the traces of current filaments on dielectric plates (as depicted in Fig. 2) and pointed out that air breakdown occurs in these filaments [55]. Then, a lot of works on these

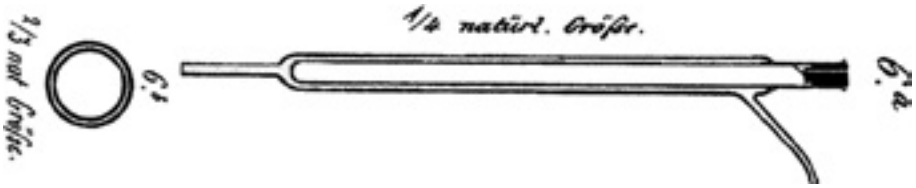

Fig. 1. Historic ozonator of W. Siemens, 1857 [53].

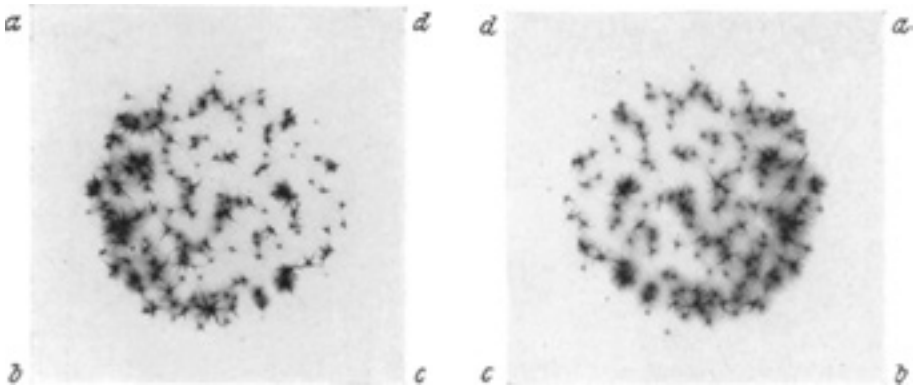

Fig. 2. Photographic footprints of current filaments [55].

current filaments was documented. Another considerable step was taken in 1943 by T. C. Manley, who proposed a method for determining the dissipated power in DBD by measuring closed Lissajous figures [56]. Around 1970, extensive studies were conducted to better understand the physical and chemical processes in DBD. These research efforts not only improved the performance of ozone generator, but also promoted the application of DBD in other fields, including surface modification, excimer UV lamps, CO_2 lasers, plasma display panels, contamination control and greenhouse gas recycling and utilization [57]. The abatement of VOCs with DBD began around 1990. More details about the history of DBD can be found in Kogelschatz's reviews [51,57–60].

2.2. Micro-discharge formation

Dielectric barrier discharge is characterized by inserting one or more dielectrics between the high voltage and the ground electrode. As illustrated in Fig. 3, there are two common DBD reactor configurations, namely panel and cylinder. Since DC cannot pass through insulating dielectric, the power applied to a DBD should be AC or pulsed high voltage power. The gas discharge characteristics between the two electrodes will change due the presence of the dielectric. An intact dielectric can limit the amount of accumulated charge and avoid spark or arc in the discharge gap. The material commonly used as a dielectric barrier is glass or silica glass, and in some special cases ceramics or polymer layers are also used.

When the electric field strength of the discharge gap is large enough to cause breakdown, the electron density at certain regions reaches a critical value, and a large number of independent short-lived current filaments (i.e. micro-discharge) are produced. The common appearance of micro-discharges in a DBD at atmospheric pressure is shown in Fig. 4.

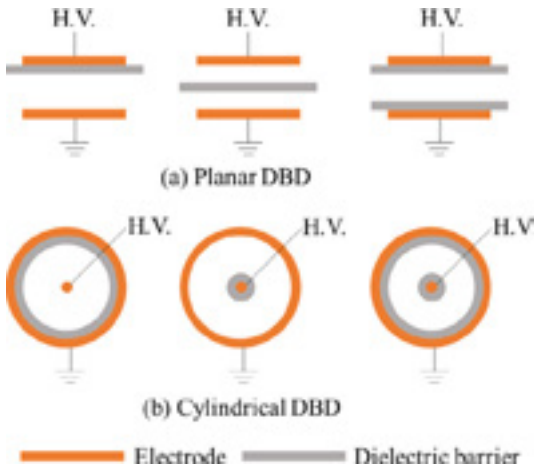

Fig. 3. Illustrations of various DBD reactors.

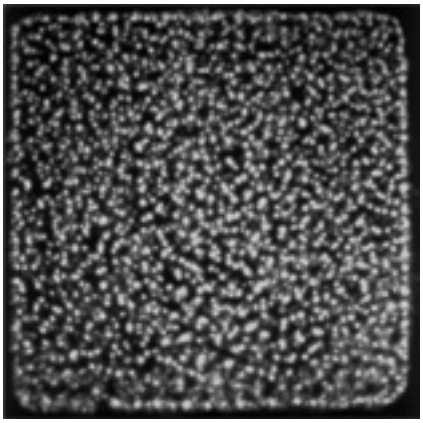

Fig. 4. End-on view of microdischarges in atmospheric-pressure air [51].

Each micro-discharge has an approximately cylindrical plasma channel with a radius about 100 μm. A single micro-discharge develops rapidly in few nanoseconds to tens of nanoseconds and propagates at the dielectric surface to form a surface discharge, which has a larger radius than the original current filaments channel. As a result, the transferred charge accumulates on the surface and decreases the electric field strength. As the electric field is further weakened, the micro-discharge extinguished when the attachment of electrons exceeded ionization. Every time the polarity of the AC voltage changes, a new micro-discharge is created at the original position. Fig. 5 depicts the model of an individual micro-discharge. The charges transported by a single micro-

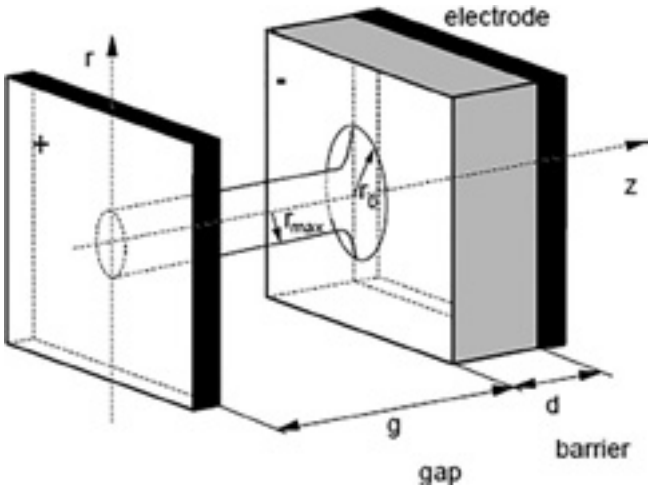

Fig. 5. The shape of a single microdischarge [64] .

discharge are in the order of 100 pC and the energies are in order of μJ [61].

It is noteworthy that filamentary discharge is not the only form of discharge in DBD. There are various discharge types such as filamentary, regularly patterned or diffuse, laterally homogeneous discharges that can exist in DBD [62]. In the study by Starostin et al. [63], different types of DBD were observed, including stationary filaments, Townsend discharge, non-stationary microdischarges and glow. They investigated the pathways of formation and temporal evolution of the diffuse glow-like DBD at atmosphere pressure by means of optical (fast imaging camera) and electrical diagnostics.

2.3. Environmental application

Ozone production: Since 1857, ozonizer has been the most widely used application of DBD. The formation of ozone involves two steps. First, the oxygen was bombarded by electrons and dissociated into oxygen atoms, and then oxygen reacts with these atoms to form ozone. Usually, a third collision partner like O_2, N_2 will participate in the latter reaction. The time scale for ozone formation during atmospheric discharge is about 10 μs in oxygen and 100 μs in air. The yield of ozone is affected by the feed gas composition, supply voltage, gas temperature, dielectric thickness and electrode configuration [65,66]. Since the low stability of ozone requires operation at low temperatures, an effective cooling system is necessary in an ozonizer. The development of power supply units and process control has greatly contributed to the improvement of ozonizer performance. For example, at a fixed input power, the use of high frequency power makes it possible to operate at a lower voltage. Recently, a substantial progress in an effective ozone generation was achieved by a pulse discharge usage [67,68]. As the fundamental physical and chemical processes of DBD are similar, some research results on ozonizer can inspire other environmental applications.

Air pollution control: The application of DBD on air pollution control primarily involves the abatement of gaseous contaminants like NOx, SO_2, H_2S and VOCs. Depending on the chemical process, there are two strategies for removing NOx: oxidation and reduction. Whether it is a stationary source (e.g. coal-fired fuel gas) or a mobile source (e.g. diesel and gasoline exhaust), the most widely used technique of removing NOx at present is selective catalyst reduction (SCR). However, activation of the SCR catalyst requires high temperature conditions (about 300°C). Instead, DBD can be operated at room temperature without heating bulk gas. In addition, the possibility of ammonia leakage, catalyst poisoning or blockage and the construction of solution stations will affect the use of SCR [69–71]. For a stationary source like coal-fired power plants, the SCR and wet flue gas desulfurization (WFGD) could effectively eliminate NOx and SOx. However, the separate treatment system has the demerit of complicated treatment process, large construction space and high investment cost [72]. Non-thermal plasma is a promising technique for simultaneous removal of SO_2 and NOx. Recent studies have shown that DBD can effectively remove SO_2 and NOx simultaneously at low energy consumption [73–75]. DBD can also be applied to remove H_2S, which emit from sewage industrial wastewater treatment plants [76,77].

Unlike SO_2, NOx and H_2S, VOCs involve many kinds of organic substances and their molecular structure are usually more complex. Using DBD for VOCs abatement starts from around 1990, because the concern for the pollution of VOCs was realized later than SO_2 and NOx. Table 1 gives an overview of researches on the degradation of VOCs by DBD in past 30 years. In the early years, packed bed reactor meant packing a dielectric material in an AC corona discharge reactor and it can be considered as a special dielectric barrier discharge. Before 2000, most of the experiments on DBD degradation of VOCs were without packing materials or catalyst, and the removal efficiency was used as the main evaluation index of reactor performance. Subsequently, combining the catalyst with DBD opened a new window for the research of VOCs abatement. In the past two decades, extensive research on catalysts in DBD has been carried out, such as different packing materials and metal supported catalysts, the location of the catalyst, and the like. In addition to its combination with catalysts, some researchers have focused their attention on configuration improvements in DBD reactor and the destruction of mixture of various VOCs. Since organic by-products are unavoidable in the degradation process of VOCs, it is necessary to use mineralization rate (also refers to as COx selectivity) and CO_2 selectivity rather than just removal efficiency as evaluation index. The type of organic by-products generated during VOCs degradation has not been discussed detailly in this review, as it is mainly used to speculate about the VOCs decomposition pathways. It is also worth noting that some pilot scale experiments have been carried with gas flow rates of several hundred m^3/h, which is of great significance for the practical application of DBD.

2.4. Summary

Dielectric barrier discharge was invented some 150 years ago, i.e., over a century earilier than its application in VOCs abatement. In the past 100 years, the physical characteristics and chemical processes of DBD have been extensively investigated, and tremendous achievements were obtained. The chemical reaction channels in DBD are provided by a large number of current filaments (micro-discharges) and their formation process and physical characteristics have been clarified. However, filamentary discharge is not the only discharge mode in DBD. In fact, DBD can be operated in the form of filamentary, regularly patterned or diffuse, laterally homogeneous discharges. Studying how VOCs are degraded in discharge forms other than filamentary discharge may provide a new window for VOCs removal in DBD. Although VOCs abatement is an emerging field in DBD application, there are a large number of experimental and theoretical studies on DBD itself or on ozone generation, which are available in history for reference. Therefore, while focusing on the status quo and looking into the future, we should also review history, and there may be some serendipity can be found. On the other hand, there is also a lot of research on SOx and NOx removal as well as energy applications (e.g. CO_2 conversion [78], dry reforming of methane [79,80] and ammonia synthesis [81,82]) in DBD, which may provide inspiration for VOCs abatement.

3. 3. Effect of reactor structure

3.1. Electrode material and configuration

The material and structure of the high voltage and ground electrodes directly affect the discharge characteristics of DBD reactor, thereby affecting the degradation performance of VOCs. The high voltage electrode can be made of stainless steel [115], tungsten [116], molybdenum [94], copper [117], nickel [118], brass [119], iron, metallic oxide [120], sintered metal fiber [121] or MWNTs (Multi-walled carbon nanotubes)/sponge [122] with a structure of wire [123], rod [124], bolt [125] and coil [126]. The discharge current and electrical field distribution of plasma reactor is directly affected by work function and secondary electron emission of the cathode [127]. Jin et al. [128] used a plasma reactor with different high voltage electrodes (tungsten, copper and steel) to degrade toluene and xylene, indicating that the removal efficiency of VOCs is positively correlated with the secondary electron emission coefficient of electrodes. Jahanmiri et al. [119] investigated the influence of electrode material on naphtha cracking through a pulsed DBD plasma reactor and found that process energy efficiency was in the order of: steel > Al ≫brass > Fe > Cu. Yao et al. [120] observed a remarkable discharge currents increase in the reactor with MgO/NiO/Ni cathode and NiO/Ni cathode than the one with Ni cathode and discharges with oxide cathodes displayed better toluene decomposition performance than the one with Ni cathode. The geometry of inner electrode affects the formation of micro-discharge

Table 1
An overview of researches on the degradation of VOCs by DBD.

Reactor type	Power supply	Flow rate /residence time	Packing materials	Target pollutant (ppm)	RE	MR/S_{CO2}	Ref.	Year
Packed bed	60 Hz	0.2,0.8 L/min	$BaTiO_3$	Toluene (23–235)	100		[83]	1992
		7.9 s		CH_2Cl_2 (500,1000)	95			
		7.9 s		CFC-113 (500,1000)	67			
Silent discharge	4.5 kHz	10 L/min		TEC (500)	~90		[84]	1993
Surface discharge	5,10 kHz, 6,8 kV	1.5, 3.6, 8.0 s		CFC-22(1000)	90		[85]	1993
				CFC-113(100)	99			
DBD	60 Hz, 16–19 kV	1.0–2.0 L/min		Formaldehyde (40–120)	97		[86]	1995
Dielectric & surface discharge	50 Hz, 5–50 kHz, 4.5–30 kV	0.35 L/min, 2.7 s		Trichloroethylene (1000)	99		[87]	1996
Packed bed	60 Hz, 18 kHz, 3–16.4 kV	0.2 L/min	$BaTiO_3$	Toluene (57–234)	100		[88]	1996
		0.3–1 L/min		o-xylene (200)	100			
		0.3–1 L/min		TCE (200)	98.1			
Silent discharge	15–19 kV	3 L/min, 3–12 s		Toluene (50–400)	80		[89]	1997
				MEK (125)	80			
Packed bed	50 Hz, 5–8 kV	0.5–1.5 L/min, 3.0–8.9 s	$BaTiO_3$	Butane (1000)	94		[90]	1998
Packed bed, sequential	50 Hz, 3–11 W	0.2 L/min	$BaTiO_3$, Al_2O_3, Ag,Co,Cu,Ni/ Al_2O_3	Benzene (200)			[91]	1999
Double DBD & packed bed	10–27 kV	1 L/min	$BaTiO_3$	Benzene (500), Toluene (480), Xylene (480), Cumene (450),	95		[92]	1999
				Diethylether (500, 800), Dichlormethane (460)	80			
Packed bed	50 Hz	0.2 L/min	$BaTiO_3$, Al_2O_3	Benzene (200)	97		[93]	2000
Packed bed DBD	60 Hz, 12–21 kV	1.0–2.0 L/min	γ-Al_2O_3	Acetaldehyde (1000)	99		[94]	2001
Packed bed DBD, PPC & IPC	50 Hz, 12.5 kV	0.1 L/min	γ-Al_2O_3, α-Al_2O_3, silica gel, quartz powder	n-eicosane	100		[95]	2002
				p-terphenyl	69			
				Toluene (200)		63		
DBD	14–16 kV	0.5–1.5 L/min		p-xylene (0–500)	100	95	[96]	2003
Packed bed DBD	100–600 Hz	4 L/min	Ag/TiO_2	Benzene (203–210)	~85	76 (S_{CO2})	[97]	2004
Packed bed DBD	50 Hz	0.5 L/min	NaY, HY, Ferrierite, HMordenite	Toluene (200)	87		[98]	2005
DBD, catalytic electrode	12.5–22.5 kV, 200– 450 Hz	0.5 L/min	MnOx, CoOx/Sintered metal fiber	Toluene (100–1000)	100	~80	[99]	2006
Packed bed DBD, PPC & IPC	16.5–17.5 kV, 10.25–13.25 kHz	1 L/min	$BaTiO_3$, γ-Al_2O_3,Ag_2O, MnO_2/ Al_2O_3	Toluene (500)	100		[100]	2007
Packed bed DBD, sequential	9–12 kV, 2 kHz	0.6 L/min (ad), 0.06 L/min (de)	Ag/HZSM-5	Benzene (7.6 μmol)	~100	~100	[101]	2009
Packed bed DBD, PPC & IPC	1 kHz	0.5 L/min	Ba–CuO–Cr_2O_3/Al_2O_3	Toluene (200)	~97		[102]	2010
				Dichloromethane (200)	~70			
DBD, catalytic electrode	50 Hz, 14–22 kV	0.25 L/min	MnOx, AgOx/Sintered metal fiber	Toluene (1 0 0)	100	~82	[103]	2012
				Benzene (1 0 0)	90	~85		
				Chlorobenzene (100)	90	~82		
Packed bed DBD	15–20 kV, 50–500 Hz	8.7 L/min	$BaTiO_3$, TiO_2/ Al_2O_3	Toluene (243)	~75		[104]	2013
Packed bed DBD	50 Hz, 0–15 kV	0.3 L/min	MnxOy/SBA-15	Toluene (1 0 0)	94	~82	[105]	2014
Packed bed DBD	5–9 kV, 10 kHz	3–15 s	CeO_2/HZSM-5, CuO/MnO_2, Ag/ TiO_2	Chlorobenzene (50–250)	~99	61.7	[106]	2015
DBD	7–10 kV, 22 kHz	6.6 L/min		Toluene, benzene, ethylbenzene, methyl ethyl ketone, methyl tert-butyl ether, 3-pentanone, and n-hexane (95)	50–90	54–63 (S_{CO2})	[107]	2016
DBD	0–30 kV, 50 Hz	250–500 m^3/ h		Isovaleraldehyde (2–10)		5–35	[108]	2016
Packed bed DBD	15–24 W	0.13–0.4 L/min	CeO_2-MnOx	Toluene (500–2500)	95.94	90.73 (S_{CO2})	[109]	2017
Sliding DBD	0–60 kV	0.3 L/min		Toluene (100)	~62	~80 (S_{CO2})	[110]	2018
TiO_2/UV-DBD	30 kV, 50 Hz	1, 2 m^3/h	TiO_2	Butyraldehyde (11–90)	40	72	[111]	2018
				Ammonia (11–90)	83			
Packed bed DBD	11 kV, 350–750 Hz	1000 m^3/h	Halloysite	VOCs from compost plant (13.1–21.5)	62.9		[112]	2018
Packed bed DBD	10.1 kHz	1 L/min	$LaMO_3$ (M: Mn, Fe, Co)	Ethyl acetate (1 0 0)	98.8	78.6	[113]	2019

(*continued on next page*)

Table 1 (*continued*)

Reactor type	Power supply	Flow rate /residence time	Packing materials	Target pollutant (ppm)	RE	MR/S_{CO2}	Ref.	Year
Packed bed DBD, sequential	10 kHz	0.5 L/min (ad), 0.5–1.2 L/min (de)	Ag/ZSM-5	Toluene (61.35 μmol)	100	96.83	[114]	2019

RE: removal efficiency, MR: mineralization rate, S_{CO2}: selectivity of CO_2

and the discharge gap. For example, the sharp edge of bolt electrode can distort the surrounding electric field, resulting in more high-energy electrons than the rod and wire one [129]. The coil electrode exhibits lower gap capacitance than rod and bolt electrodes, indicating that the dielectric loss in the barrier can be decreased by coil electrode [130]. As the diameter of inner electrode increases, the discharge gap reduces, thereby increasing the average electric filed strength, resulting in more active species. Also, a large diameter means a large surface area, resulting in more secondary electron emission [131].

The materials that make up the ground electrodes are similar to the high voltage electrodes, but the structure is different, especially for cylindrical reactors. Typically, the ground electrode is a wire, tape, sheet or mesh that wrapped around the surface of dielectric. Some researchers also used silver paste as a ground electrode [132,133]. Bahri et al. [134] investigated the effect of ground electrode configuration on ozone production. The results showed that Ag_{paste} has higher energy yield than Al_{foil} and stainless-$steel_{mesh}$. There is no secondary electron emission at ground electrode, so the difference between various electrodes is mainly due to its structure rather than material. When a foil or mesh used as ground electrode, streamers or corona discharges are formed in the void between electrode and dielectric [97]. The energy used to ionize air in the outer of dielectric can be considered as "wasted energy", meaning that it does not contribute to the degradation of VOCs or the production of ozone. Using sliver paste as ground electrode, the gap between electrode and dielectric barrier can be eliminated [133,135]. Thereby more energy is used to ionize the gas inside reactor, resulting in higher energy yield and better degradation of VOCs.

3.2. Discharge gap and length

A suitable discharge gap is significant for VOCs abatement in DBD. On the one hand, increasing the discharge gap increases the gas residence time, which facilitates the removal of VOCs. On the other hand, increasing the discharge gap reduces the average electric field strength, which is detrimental to the abatement of VOCs. In addition, if the discharge gap is changed by changing the diameter of cathode, the secondary electron emission of the cathode also affects the degradation of VOCs. The discharge gap of DBD reactor in laboratory usually ranges from 1 to about 15 mm. Magureanu et al. [136] compared the removal efficiency of trichloroethylene (TCE) for various discharge gap in the range of 1–5 mm. The results showed that shorter gap (1–3 mm) is more favorable for the conversion of TCE. However, in the dry reforming of methane experiments conducted by Khoja et al [137], the conversion of methane and CO_2 increased first and then decreased with the increase of discharge gap (1–5 mm). A higher power density can be achieved at a constant discharge power, and current filaments are more likely to cover the entire discharge volume with a small gap [138]. But if the gap is too short, arc or spark discharge may occur, and the interaction between target contamination molecule and active species might be limited due to a short residence time. Therefore, to obtain a good performance of DBD for VOCs abatement, both discharge gap and the residence time should be considered.

The discharge length also plays a significant role in DBD degradation of VOCs. By increasing the effective discharge length, lower voltage is required to achieve the plasma ignition. An increase of the discharge length leads to a higher effective electrode surface, resulting in more micro-discharge inside the reactor, which increases the probability of gas breakdown [134]. In addition, increasing the discharge length will increase the residence time of VOCs in the plasma zone, which is advantageous for the decomposition of VOCs due to the increased chance of collision between VOCs molecule and energetic electrons and other reactive species. Chang et al. [139] investigated the degradation of styrene with various discharge length (10, 20, 30, 40, 50, 60 cm) and found that the input power increased linearly with discharge lengths. The selectivity of CO_2 also improved with the increase of discharge length. The same experimental results were

obtained by Zhang et al. [140]. However, at a fixed input power, a long discharge length means a smaller power density due to the enlarged plasma region. Moreover, increasing the discharge length results in higher energy loss due to heat dissipation of dielectric barrier [141]. As a result, increasing the discharge length may reduce energy efficiency.

3.3. Dielectric material and thickness

The insulating dielectric material in DBD reactor can be glass [142], quartz [143], plexiglas [144], pyrex [145], alumina [146], mullite [147], ceramics [148], polytef [149], polyethylene therephtalate [150], teflon and epoxy resin [151]. Among these materials, quartz is the most widely used due to its moderate price and commercial availability. The dielectric permittivity affects the discharge characteristics of DBD, which affects the degradation of VOCs. Since the dielectric capacitance and the gas gap capacitance are connected in series in the circuit, increasing the dielectric capacitance increases the electric field strength of the discharge gap which results in more micro-discharge. Zhu et al. [152] investigated the influence of dielectric material on toluene removal and found that the discharge current and toluene removal rate of the 99-ceramic reactor were higher than that of quartz reactor. They attributed this difference to the higher relative permittivity of 99-ceramic (5–10) than quartz (3.5–4.5). In the study of Khoja et al. [137], it was observed that the conversion of methane and CO_2 of aluminum dielectric reactor were slightly higher than that of quartz. They believe this is because the surface of aluminum reactor is porous and rough, which increases the gas residence time. Therefore, the longer residence time in aluminum reactor allowed more collision between gas molecules and energetic electrons due to its porous peculiarity. Moreover, Meiners et al. [153] found that the reactor with MgO dielectric has higher electron densities than that of aluminum reactor at the same input energy. They attributed this to the higher secondary electron emission of MgO (0.11) than that of alumina (0.099).

The performance of the DBD reactor is also affected by the thickness of dielectric barrier, which typically ranges from 1 to 3 mm. As the thickness of the dielectric barrier increases, the required plasma ignition voltage increases and the current pulses reduces [153]. Mei et al. [138] investigated the influence of dielectric material thickness on CO_2 conversion and they pointed out that increasing the thickness of the quartz dielectric reduced the conversion of CO_2 at a fixed specific energy input due to a decreased transferred charge. Interestingly, Ozkan et al. [147] observed the opposite results. In their study, a thick dielectric is more conducive to CO_2 conversion due to the formation of more micro-discharge. Therefore, the influence of dielectric thickness on the performance of DBD reactor is not certain, but it is related to other conditions of the system. In addition, the thickness of the dielectric barrier cannot be chosen at will. Because most dielectric material are fragile, electrical breakdown may occur if it is too thin.

3.4. Number of dielectrics

Although most of the current DBD reactors contain only one dielectric, the first DBD reactor created by Siemens consisted of two dielectrics. An important reason why double dielectric barrier discharge (DDBD) is less of concern is that its structure is more complicated than single dielectric barrier discharge (SDBD). The electric field strength of discharge gap is uniform in planar DBD, whereas in cylindrical DBD it is related with the distance to high voltage electrode. As a result, the difference between DDBD and SDBD is more remarkable for cylindrical reactor than for planar reactor. Therefore, the DDBD discussed later is mainly used for cylindrical reactors. As depicted in Fig. 6, there are two different configurations of DDBD reactors, one of which is that the high voltage electrode is separated from inner dielectric barrier and the other is closely attached. For latter, both electrodes are not in contact with plasma, so the electrodes can be protected from plasma corrosion and etching. However, the former contains two different discharge

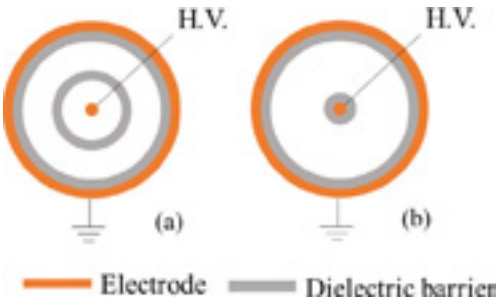

Fig. 6. Configuration of DDBD reactors.

regions, which may be more advantageous for the decomposition of VOCs. In the study by Jiang et al. [130], it was demonstrated that benzene could be degraded in both discharge regions and the highest benzene removal efficiency could be obtained while utilizing two regions simultaneously.

Some studies have shown that VOCs can be efficiently removed in DDBD [154,155], but there are not many studies comparing DDBD with traditional SDBD. Fig. 7 presented the current and voltage waveforms of DDBD and SDBD. Obviously, the current pulses in SDBD are more than DDBD, which means more micro-discharges are formed in SDBD. Since micro-discharge is developed from the cathode, the inner dielectric barrier of DDBD will prevent the advancement of micro-discharge to the inner surface of the outer dielectric. As a result, SDBD consumes much more power than DDBD (Fig. 8). However, a large input power does not mean that the removal efficiency of VOCs is destined to be higher. Because there is a lot of energy that is dissipated in the form of heat, which heats the gas and dielectric barrier. Zhang et al. [156] used DBD to degrade styrene and found that DDBD has higher mineralization rate and energy utilization efficiency than SDBD. In fact, since DDBD has a strong and a weak discharge zone with one power supply, it can be considered as a special two-stage reactor that achieves high mineralization of VOCs and inhibits the generation of by-product like ozone and NOx. Much of the information about VOCs removal in DDBD is still not clear enough and further research is needed.

3.5. Summary

Although the geometry of DBD reactor is simple, its specific structure is diverse. Various structural features, such as electrode material and configuration, discharge gap and length, dielectric material and thickness, and number of dielectrics will affect the discharge characteristic of DBD, and thus influence VOCs removal performance. In most case, optimization of these structures will result in enhanced electric field or increased discharge current, which will increase the removal and mineralization rate of VOCs. However, by-products such as residual O_3 and NOx will also increase without a suitable catalyst. Exceptionally, in double dielectric barrier discharge (DDBD) reactor, the discharge current will be significantly reduced compared with a single barrier reactor, but the VOCs removal efficiency may be increased. This could be due to a change in discharge type in DDBD reactor. Actually, in the area of VOCs abatement by DBD, there is not much research on the optimization of reactor structure compared with plasma-catalysis. Moreover, most of these existing studies do not explain explicitly how the discharge characteristics are altered by these factors. This is largely due to the lack of electrical diagnostics for discharge behaviors and the complexity of gas discharges. In the near future, the application of advanced plasma diagnostics (such as intensified charge coupled device (ICCD) imaging) and fluid modeling will provide new opportunities for investigating how these reactor structures affect VOCs removal.

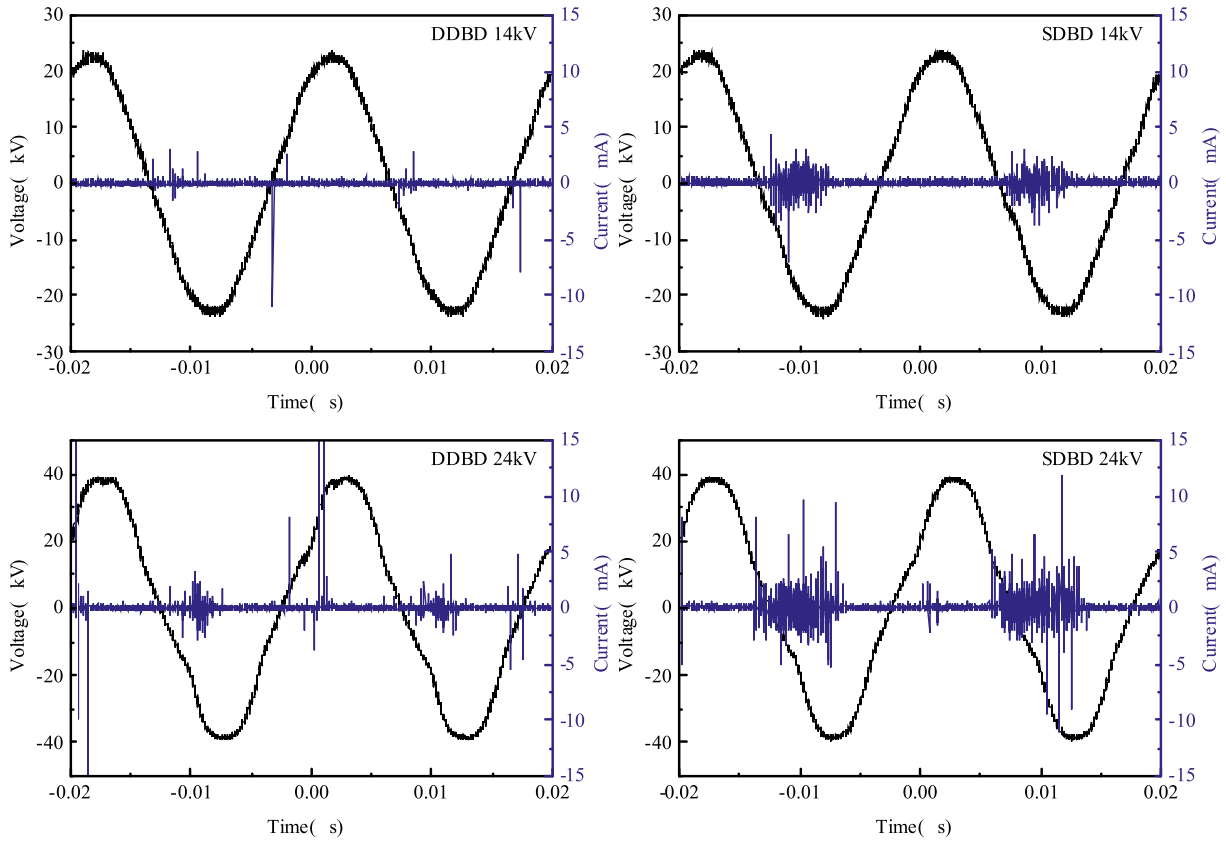

Fig. 7. Voltage and current waveform of DDBD and SDBD.

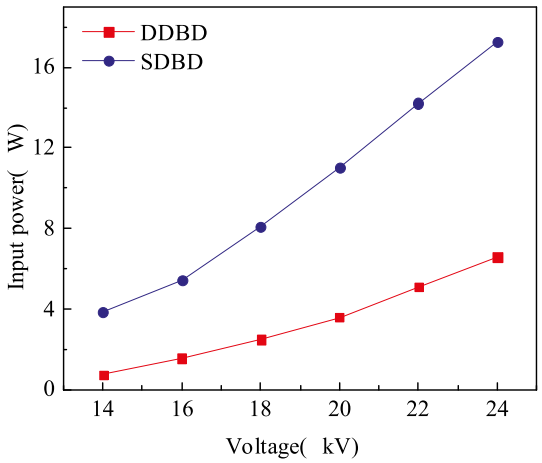

Fig. 8. The input power of DDBD and SDBD.

4. Effect of power supplies

4.1. Applied voltage

The applied voltage is one of the most significant parameters for DBD removal of VOCs. The voltage applied to DBD reactor is in the range of few kV to around 30 kV. At a fixed discharge gap, a high applied voltage means a strong electric field strength. Therefore, an increase in voltage causes an increase in the kinetic energy of free electrons, causing an increase in the collision cross section of electrons with other particles, meaning that the gaseous molecule or atom is more susceptible to ionization and dissociation. As depicted in Fig. 7, both the number and intensity of current pluses increase with rising voltage, which means more micro-discharges are formed at a high voltage. Therefore, VOCs are more easily removed at high voltages. Because the chemical bonds of VOCs molecules are more easily destroyed by higher energy electrons, and a large number of actives species means that VOCs can be more fully decomposed. Although enhancing the applied voltage can increase the removal efficiency and mineralization rate of VOCs, however, it is not the case that the higher the voltage the better. Firstly, a high voltage means more ozone and nitrogen oxides [157,158], which are considered as undesirable by-products in the exhaust. Secondly, if the voltage is too high, arc or spark discharge may occur [159], and the dielectric barrier may be broken down. Finally, a high voltage causes more energy to be dissipated as thermal energy by heating a large amount of gas and dielectric barrier, which may result in reduced energy efficiency of VOCs removal [160–162]. Hence, choosing a suitable voltage is significant for the abatement of VOCs in DBD.

4.2. Frequency

The frequency of AC applied to DBD for removing VOCs ranges from several tens of Hz to several tens of kHz. The same number of identical micro-discharges is produced in each period. Therefore, a higher frequency means that more micro-discharges are generated in a fixed time [51]. Therefore, a higher frequency means that more micro-discharges are generated in a fixed time, which is beneficial to the decomposition of VOCs. At a frequency of 200 to 450 Hz, Subrahmanyam et al. [163] found that the COx selectivity of toluene destruction increased with elevating frequency. In the study by Liang et al. [131], the removal efficiency of toluene raised with increasing frequency from 10 to 35 kHz, but the energy yield decreased. However, Ozkan et al. [164] used DBD to split carbon dioxide and observed that the conversion of CO_2 decreased slightly with increasing frequency (16.2–28.6 kHz). They thought this may be due to a drop in the electron density involved in CO_2 splitting. In each half-cycle, the number of current pulses at low

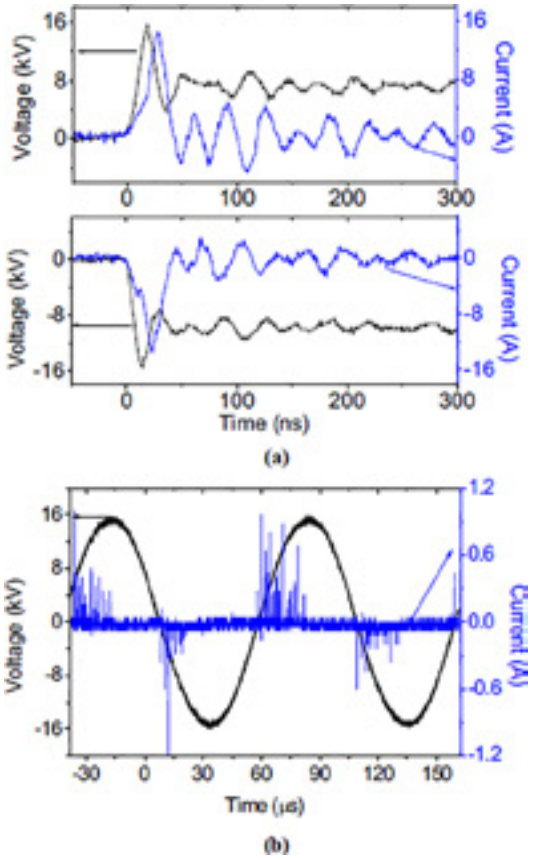

Fig. 9. Typical voltage and current waveforms of (a) nanosecond pulsed discharge and (b) AC discharge [173].

frequency is more than higher frequency [164–166]. At high frequencies, multiple breakdowns do not occur during discharge due to insufficient time in between the voltage cycles [166]. Moreover, the formation of micro-discharge may be choked if the electron transit time is longer than voltage cycle. Therefore, the input power is positively correlated with frequency but not proportional. In addition, the energy efficiency of VOCs abatement reduces with elevating frequency [131]. Another notable feature of high frequencies is that it can reduce the breakdown voltage at a fixed input power. Because by operating at high frequencies, the DBD discharge exhibits a high memory voltage due to the accumulation of charge on the surface of dielectric [167]. In summary, the choice of a suitable frequency is important and it may also refer to the applied voltage.

4.3. Pulsed power supply

In addition to sinusoidal alternating current, pulsed high voltage power can also be applied in DBD reactors to generate non-thermal plasma at atmospheric pressure. The typical voltage and current waveform of AC and pulse discharges is significantly different (Fig. 9). For AC discharge, many comb-like filaments (also known as localized micro-discharge) appear on the edge of the voltage polarity reversal, indicating that AC discharge is filamentary mode. The discharges mainly occur at the first peaks of both positive and negative pulse voltage, this means that only the first peaks are effective for discharge. However, the peak current of pulsed discharge is much higher than that of AC discharge at the same applied voltage. As a result, the deposition power of pulse discharge is much higher than that of AC discharge at the same repetition rates and applied voltage [168]. Although the threshold voltage of discharge is relatively low for AC DBD, but its discharges are inhomogeneous and consist of some bright spots [169]. In contrast, for pulsed DBD, the discharge is homogeneous and without any bright spot or irregular distribution mode. In [170], Yuan et al. reported that both ·OH formation and energy efficiency of bipolar pulse power were superior than those driven by AC power. Wang et al. [171] investigated the effect of power supply mode on removal of benzene and found that at the same input power, the removal efficiency and CO_2 selectivity of benzene of bipolar pulsed power were higher than those of AC power. For pulsed discharge DBD, in addition to applied voltage and frequency, pulse rise time, pulse-forming capacitance and pulsed modes also affect its discharge characteristics. Chirumamilla et al. [172] investigated the influence of microsecond (ms) and nanosecond (ns) pulse on NO abatement and observed that the nanosecond is more efficient for NO conversion. The energy transfer efficiency is closed related with the pulse-forming capacitor (*C*p). In [149], Jiang et al. reported that the toluene decomposition efficiency increases and the energy yield reduces with the increase of *C*p. Jiang et al. [110] also researched the effect of pulsed modes on toluene destruction, indicating that the removal efficiency and energy yield decrease is in the order of: ± pulse > +pulse > − pulse. Although pulsed DBD seems to be superior to AC DBD in VOCs abatement, AC power supply is widely applied due to economic reasons.

4.4. Summary

The power supply has a significant effect on VOCs removal in a given DBD reactor. Generally, increasing the applied voltage amplitude will increase the removal and mineralization rate of VOCs, but more by-products (O_3 and N_2O) will be generated. In addition, a high voltage amplitude can also lead to low energy efficiency. Increasing the frequency will result in more micro-discharges in a fixed time, leading an increase in removal and mineralization rate of VOCs, but also a raise in residual O_3 and NOx formation and a decrease in energy efficiency. Therefore, it is imperative to choose a proper applied voltage amplitude and frequency to trade off removal efficiency, mineralization rate, by-products formation, and energy yield. Compared with AC power, a much higher pulsed current can be obtained in a short time for pulsed power at the same applied voltage. In addition, the discharge is more homogeneous in pulsed DBD than AC DBD. Although pulsed DBD exhibits good VOCs abatement performance, it is not widely used for economic reasons. In the future, using DBD to remove VOCs may benefit from the development of new power supplies.

5. Effect of packing materials

In order to improve the removal efficiency of VOCs by DBD, several approaches have been developed, such as optimizing the reactor configuration, electrode or power supplies. However, most of these approaches increase VOCs removal efficiency at the expense of producing more undesired by-products (O_3 and NOx), which hinder the industrial application of DBD. In addition to the above approaches, packed bed DBD has also been extensively investigated and it is considered to be the most promising method because it can simultaneously increase removal efficiency of VOCs and suppress by-products at low energy consumption. In packed bed DBD reactors, a packing material is positioned in plasma zone or downstream of plasma zone. In the former case, there are synergistic effects between plasma and packing material, which promotes the degradation of VOCs. The electrical and morphological properties and the loaded catalyst of packing material all influence the characteristics of plasma and thus affect VOCs removal efficiency as well as by-product production.

5.1. Packed position

As illustrated in Fig. 10, the common types of packed bed DBD reactor include one- and two-stage configurations. In one-stage system (a) (also referred to as in plasma catalysis-IPC), the packing material is

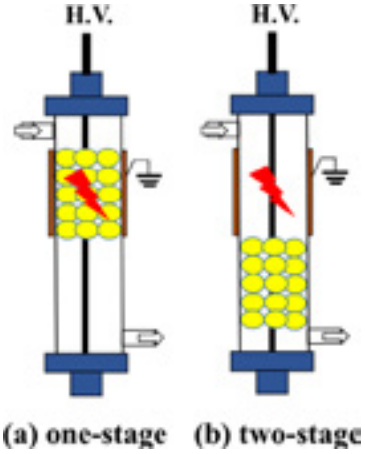

Fig. 10. Types of packed bed DBD reactors according to packing material position.

positioned in the plasma region of DBD reactor. In contrast, packing material is located in the downstream of plasma zone in two-stage system (b) (also referred to as post plasma catalysis-PPC). In PPC configuration, only long-lived species like O_3 and metastable particles can reach the packing region, while short-lived species such as electrons and radicals are quenched before interacting with packing material. Conversely, for an IPC system, both short-lived and long-lived species will interact with the packing material and, more importantly, the packing material will influence the discharge characteristic of DBD reactor. As a result, there is the chance of contributions from electron- and photon-induced processes, surface discharge, radicals and excited species [174], which are significant for VOCs degradation. There is no doubt that the PPC system has an advantage in ozone suppression for VOCs abatement. However, as concerned for the removal efficiency of VOCs, it is difficult to assert which configuration is better. Although in most cases, IPC configuration is superior to PPC in VOCs removal [100,157,175–180], some studies have shown that PPC system is better than IPC [102,181]. Moreover, in the research by Durme et al. [182], IPC or PPC system is better related to the type of catalyst.

Besides the location of packing material, operational process is another important basis for packed bed DBD reactor classification. According to whether the plasma is turned on when VOCs-containing gas enters the reactor, there are continuous and sequential processes. In a sequential operating system, VOCs are first adsorbed onto the packing material and then plasma is switched on to degrade adsorbed VOCs. A significant advantage of sequential process is that its energy efficiency is higher than for continuous operation [183]. A fact that cannot be ignored is that both IPC and PPC configuration can be operated continuously or sequentially. Therefore, the packed bed DBD reactor includes four systems, namely continuous IPC (CIPC), continuous PPC (CPPC), sequential IPC (SIPC) and sequential PPC (SPPC). In a CPPC system, VOCs are partially decomposed and then reach the downstream packing region if the VOCs-containing gas stream passes through discharge zone. For the SPPC system, VOCs are only degraded in the packed area since VOCs have been adsorbed before plasma is turned on. In some studies of CPPC system [102,181], the VOCs-containing gas stream is in parallel with the gas stream through DBD reactor, and the two gas streams were mixed and then passed through packed zone. Hence, in CPPC system and SPPC system with parallel gas flow, the DBD reactor acts as an ozone generator.

Anyhow, the combination of plasma and catalyst exhibits multiple advantages in terms of removal efficiency, mineralization rate and energy efficiency of VOCs abatement. In an IPC configuration, a better understanding of the interaction between plasma and catalyst is significantly important for further optimization of a given system. Therefore, the discussion of the next few sections is based on the IPC system.

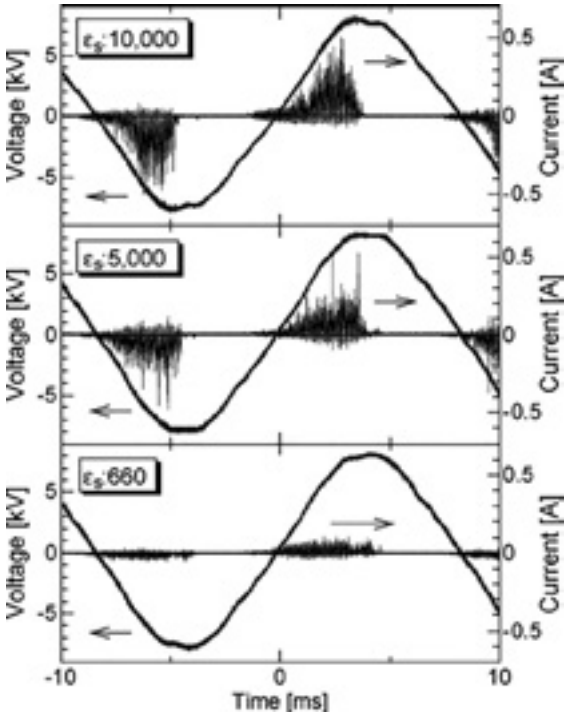

Fig. 11. Waveforms of voltage and current for various dielectric constant of sphere pellet at 14 kVpp applied voltage [190].

5.2. Properties of packing material

Usually the materials packed in DBD reactor include ferroelectrics ($BaTiO_3$, $CaTiO_3$, $SrTiO_3$), metal oxides (CeO_2, γ-Al_2O_3, MnOx), semiconductors (TiO_2, WO_3) and zeolites (ZSM, HY, 13X, SBA, MCM). These materials can be filled alone in the reactor or after loading with metal catalyst. The electrical, surface and morphological properties of these materials significantly affect the discharge characteristics of DBD and the performance of VOCs decomposition.

Dielectric constant: DBD reactor is actually a capacitor in which the capacitance of the dielectric and the gas are connected in series in an equivalent circuit. The introduction of a packing material means that a new capacitor is added to the series circuit. Since the packing material generally has a dielectric constant greater than that of air, a packed bed reactor can store more energy than DBD alone during a single discharge. At the same applied voltage, there is a greater discharge current when DBD is packed with a material with a high permittivity, as illustrated in Fig. 11. In addition, material with high permittivity reduce breakdown voltage and enhance local electric field strength, thereby increasing VOCs removal efficiency [184]. In [185], benzene conversion increased with increasing dielectric constant (20 to 1100), but the conversion is not obviously affected when the permittivity is in the range of 1600–15000. Gallon et al. [186] pointed out that the effect of permittivity in the range of less than 100 plays a very minor role in the reduction of breakdown voltage in DBD. Therefore, dielectric constant of packing material will only have a significant effect on the performance of DBD under a certain range. Recently, some fluid model studies have provided more information for understanding the discharge characteristics of packed bed DBD. In a fluid model investigation by Laer et al. [187], the results indicated that the enhancement of permittivity on electric is limited to a certain value of permittivity, being 9 for a micro-gap and 100 for a mm-gap. Also, the enhanced electric field results in a higher electron temperature, but a lower electron density. In [188], Zhang et al. reported that smaller pore sizes only yield enhanced

ionization for smaller dielectric constants (i.e., up to ε_r = 200, 150, and 50 for pore sizes of 50, 30, and 10 μm). This means that plasma is more easily formed inside pores of low permittivity materials. Hence, the porosity of packing material cannot be neglected when investigating the influence of permittivity on VOCs removal. Moreover, the dielectric constant of packing material is affected by temperature and humidity, both of which are variable in DBD. As the temperature increases, the packing material becomes more resistive rather than capacitive [189], which is confirmed by the fact that the shape of V-Q Lissajous figure changes from a parallelogram to an ellipse [51]. Therefore, an increase in temperature lowers dielectric constant, which may result in a decrease of VOCs removal efficiency.

Surface properties: DBD reactor packed with porous material is more favorable for the decomposition of VOCs than with non-porous materials because porous material has a strong adsorption capacity, and micro-discharge may be formed in its inner pores. Gandhi et al. [191] examined the performance of porous and nonporous α-alumina (α-Al_2O_3) for the degradation of ethylene in a DBD reactor and the results indicated that the decomposition efficiency obtained with the porous α-alumina was higher than that with the nonporous one. For porous packing materials, their surface properties such as specific surface area and pore size play a significant role in VOCs decomposition by DBD. The surface area of material is directly related to its adsorption capacity for VOCs, which affects the residence time of VOCs in reactor and the probability of collision between VOCs and active species. As the S_{BET} of flake-like HZSM-5 decreased from 366 to 341 m^2/g, the carbon balance of toluene removal reduced significantly from 81.9% to 65.8% [118]. In study by Wang et al. [109], the highest removal efficiency of toluene and CO_2 selectivity were obtained in a catalyst (Ce1Mn1) with the largest surface area (84.1 m^2/g). However, a high surface area does not necessarily mean a high VOCs removal performance. For example, ZSM-5 (306.6 m^2/g) has a larger surface area than γ-Al_2O_3 (175.1 m^2/g), but γ-Al_2O_3 has a higher toluene mineralization rate than ZSM-5 [192]. This is because γ-Al_2O_3 has a higher dielectric constant than ZSM-5 and thus has a better discharge performance. Moreover, the surface area is reduced after metal is loaded on the support, but VOCs removal efficiency is improved [193,194]. Wang et al. [195] investigated toluene degradation over different MnO_2 polymorphs and found that α-MnO_2 showed the best toluene conversion, but its surface area is lower than γ-MnO_2 and δ-MnO_2. Therefore, in addition to surface area, the dielectric constant and crystal structure of packing material and the presence of metal catalyst all significantly affect the degradation of VOCs.

Porous material is more susceptible to adsorbing molecules that are smaller in size than its pore size. Compared to ferrierite, benzene is more easily assimilated into the micropore in HY [132]. Because the molecular size of benzene is 5.9 Å, which is smaller than the pore size of HY (7.4 Å) but greater than ferrierite (4.3–5.3 Å). As the pore size of HZSM-5 decreased from 0.533 to 0.522 nm, the equilibrium adsorption capacity of toluene decreased from 39.70 to 30.32 mg/g, and removal efficiency decreased from 84.9% to 79.8% [118]. In contrast, the pore size of γ-Al_2O_3 is larger than that of 13X zeolite, but the adsorption capacity of γ-Al_2O_3 is poor [143]. Therefore, the pore size of packing material should not be too large nor too small, and pore size slightly larger than the target molecular size is preferable. Considering that both discharge enhancement and adsorption capacity are important for VOCs removal, combining materials with different properties may give a better performance. After mechanically mixing ZSM-5 and γ-Al_2O_3, TiO_2 or $BaTiO_3$, the mineralization of toluene is significantly improved compared to ZSM-5 alone [115]. In addition, the shape of pores will also influence the electric field enhancement and thus the plasma properties. In the study by Zhang et al. [196], the strongest electric field enhancement occurs at the opening and bottom corners of the conical pore with small opening, at the bottom of the conical pore with large opening and at the bottom corners of cylindrical pore.

Size and shape: Since the micro-discharge mainly occurs near the contact point of packing material, increasing the size of packing material decreases the number of contact points and causes a decrease in the number of micro-discharges. However, the amount of charge transferred by a single micro-discharge will be intensified [197]. Ogata et al. [185] studied the influence of $BaTiO_3$ pellets size on benzene degradation and the result indicated that the benzene decomposition efficiency was: 1 mm ≈ 2 mm > 3 mm. For a given pellet size, the total contact points between packing material will be affected by the reactor size. Therefore, the optimum packing material size may vary for different reactors. In addition, it should be noted that these low particle sizes may be optimal at lab scale conditions but not adequate to pilot or industrial scaled system due to the higher gas velocities.

Although spherical particles are the most widely used packing materials, they are not morphologically advantageous for enhancing discharge. Because a strong local electric field is more likely to appear near sharp edges. In the study by Chang et al. [198], three different shapes were tested for $BaTiO_3$. The discharge current has a relationship of the order: small hollow > large hollow > cylinder > sphere, which indicates that reactor filled with hollow $BaTiO_3$ may be more efficient for VOCs removal. Takaki et al. [190] researched the influence of $BaTiO_3$ shapes on C_2F_6 degradation. The sequence of discharge current was as follows: hollow cylinder > cylinder > sphere. As a result, the energy efficiency for C_2F_6 abatement in the reactor with hollow cylinder and sphere were 3.7 and 2.5 g/kWh, respectively. Furthermore, the pressure drops of the reactor with hollow cylindrical is lower than that with sphere [198], which is advantageous for industrial applications.

5.3. Loaded catalyst on support

Although most packing material can improve the removal of VOCs by discharge enhancement and/or adsorption, metal catalysts are still necessary to obtain desired performance, such as suppressing residual ozone. An important part of plasma catalyzed removal of VOCs is to find a suitable combination of metal (e.g.: Ag, Co, Ni, Fe, Mn, Ce and Cu) and support. Fig. 12 illustrated a plausible pathway of VOCs degradation in a plasma-driven catalysts system. According to Kim [126], the VOCs decomposition process occurs primarily on the surface of packing material rather than on the loaded metal catalyst. However, the supported metal catalyst facilitates further oxidation of CO and carbon balance.

The type, loading amount, shape and size of supported metal catalyst will affect VOCs abatement. Although there has been a lot of research on plasma catalytic abatement of VOCs, it has not been concluded so far which catalyst is the best for a given target pollutant. Table 2 gives an overview of VOCs removal by different catalysts in plasma. It is clear that the sequence of catalyst for VOCs degradation is not consistent in different studies. For example, for the decomposition of benzene, Ag is superior to Cu in [144] but the opposite result was obtained in [178]. This means that the performance of catalyst in plasma in not only related to the target pollutant, but also to the reactor configuration, packing position, type of support and the like. The difference between various metal catalysts at a given condition depends primarily on their ability to decompose ozone in to oxygen radicals (O^{2-}, O_2^{2-}, O^-), which are indispensable in the degradation of VOCs. Ozone molecules are adsorbed and decomposed in oxygen vacancies, which are electron-deficient as Lewis acid sites [199].

The loading amount of metal catalyst has an optimum value. Below this value, the increase in the amount is beneficial to VOCs degradation, and greater than this value is unfavorable. This is because a large loading amount can provide more active sites, however, an amount above a certain value will reduce the surface area of the catalyst. In [144], the benzene removal efficiency increased with the increase of Ag loading in the range of 4–15 wt%, and then decreased at higher loading amount. Wu et al. [201] investigated the effect of Ni loading of NiO/γ-Al_2O_3 on toluene abatement and the result indicated that 5 wt% is the optimum value. When the loading of Ni exceeded a certain value,

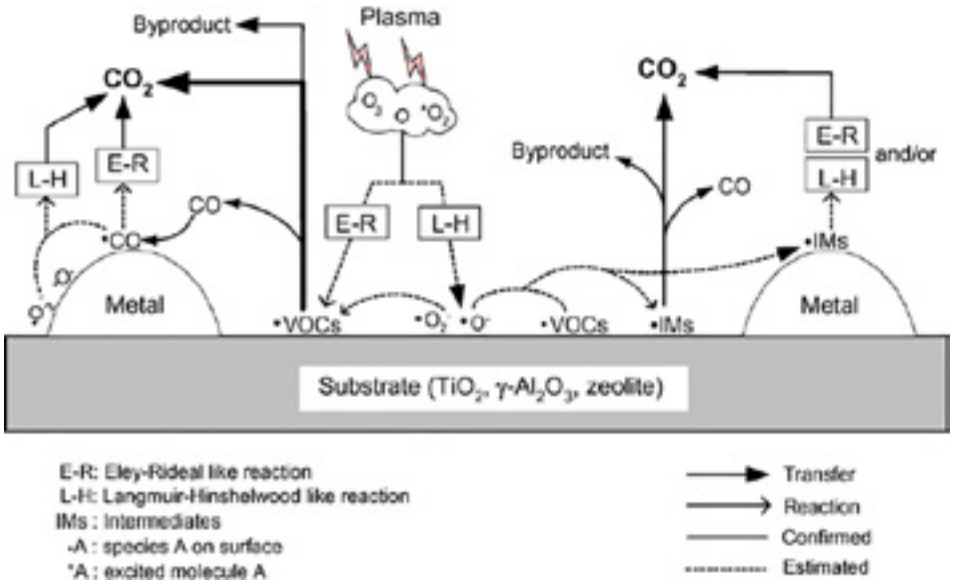

Fig. 12. Plausible mechanism for the plasma-driven catalysis of VOCs [126].

multilayer or bulk NiO may occur, resulting in a decrease of active component area exposed to air.

In the study by Peng et al. [203], the shape effect of Pt/CeO_2 catalysts on catalytic oxidation of toluene was elucidated. The immobilized Pt particles on nanorods, nanoparticles, and nanocubes CeO_2. Pt/CeO_2-rods achieved the best catalytic performance due to its best reducibility and highest concentration of surface oxygen vacancies. Further, they found the size effect of Pt nanoparticles in the range of 1.3 to 2.5 nm [204]. Due to the optimum balance of Pt dispersion and concentration of oxygen vacancy in CeO_2, Pt/CeO_2-1.8 exhibited the best catalytic activity. Although the two studies applied catalytic oxidation, the results are useful for plasma-catalytic process.

Recently, some studies have shown that more effective degradation of VOCs can be obtained by combining two different metal catalysts such as Mn–Co [160,205], Ag-Mn [117,123,193], Mn–Ce [109,193,202,205,206], Mn-Cu [202], Ag–Ce [207], Cu–Ce [208]. The molar ratio of two metals will significantly affect the activity of catalyst. The optimum molar ration of Ag-Mn was 1:2 for xylene abatement in [117], which is due to the higher proportion of surface-adsorbed O and better reducibility through the synergy between Ag and Mn. In [109], the best ratio of Ce-Mn was 1:1 for toluene destruction. This is because Ce1Mn1 catalyst has higher surface area, more oxygen vacancies and higher mobility of oxygen species. In addition to mixing ratio, the impregnation sequence of different metals will also affect the degradation of VOCs if catalyst is prepared by impregnation method. For example, when Mn is first impregnated [Ag-Mn(F)/ γ-Al_2O_3], a longer breakthrough time and better mineralization rate of toluene was observed compared to first Ag impregnation and co-impregnation [209]. This is attributed to the larger amount of Ag^+ on catalyst surface and the better promotion of surface-active oxygen migration in Ag-Mn(F)/ γ-Al_2O_3.

5.4. Synergy of plasma and catalysis

Effect of catalyst on plasma. The discharge characteristics of DBD reactor are obviously changed after the introduction of catalytic/non-catalytic packing materials in plasma region. In a fully packed bed DBD, the discharge mode partially changes from bulk streamers to more intense surface streams that is distributed along the surface of packing material. This phenomenon has been confirmed by Kim et al. [210–212] through ICCD imaging and several numerical investigations [213,214]. The formation of micro-discharge will also be affected. The propagation of micro-discharge will be limited between the voids of packing material particles rather than the entire discharge gap. As a result, the number and intensity of micro-discharges increase, which leads to an elevation in the average energy of electrons and thus promoting the degradation of VOCs. Since most packing materials are porous, it is possible for micro-discharges to form in these pores. Holzer et al. [95] demonstrated the formation of short-lived active species in intra-particle volume by comparing the degradation of VOCs in porous and non-porous alumina. Moreover, Zhang et al. [215] investigated micro-discharge formation inside catalyst pore by a fluid model and believed that plasma species can be formed in micron-sized pores. Packing material also reduces the breakdown voltage, thereby increasing energy efficiency. In was observed that the breakdown voltage decreased from 3.3 to 0.75 kV with the addition of Ni/Al_2O_3 catalyst in a DBD reactor [216]. In addition to physical properties, the chemical characteristics of plasma are also altered by the presence of catalyst. For

Table 2
VOCs removal by different type of catalyst.

Reactor	Target pollutant	Support	Catalyst performance	Reference
CIPC	Ethyl acetate		$LaCoO_3$ > $LaMnO_3$ > $LaFeO_3$ (MR)	[113]
CPPC	Benzene	γ-Al_2O_3	AgOx > MnOx > CuOx > FeOx (RE)	[144]
CIPC	Acetone	γ-Al_2O_3	CuOx > MnOx ≈ CoOx > NiOx > CeOx (RE)	[200]
SPPC	Toluene	HZSM-5	Ag–Mn > Ce–Mn > Mn > Ag > Ce (MR)	[193]
CIPC	Toluene	γ-Al_2O_3	NiO > MnO_2 > CeO_2 > Fe_2O_3 > CuO (RE)	[201]
CIPC/CPPC	Toluene	Al_2O_3	Au > Ag > Cu > Co (RE)	[177]
SIPC/SPPC	Benzene	HZ	Ce > Cu > Zn > Ag > Fe > Mn > Ni > Co (MR)	[178]
CPPC	Methanol	γ-Al_2O_3	Mn-Cu > Mn-Ce > Mn > Cu ≥ Ce (RE)	[202]

Here MR and RE refer to mineralization rate and removal efficiency, respectively.

instance, ozone is easily decomposed by catalysts to produce oxygenated radicals, which have higher oxidation activity, thus enhancing the decomposition of VOCs [109,217].

Effect of plasma on catalyst: Since NTP can be applied as a material surface modification technique, in can also be used for catalyst preparation. When the catalyst is exposed to plasma, active sites will be more uniform and particle size will be decreased, thereby increasing the activity and stability of catalyst [39,218]. Smaller Pt particle size and higher dispersion of nanoparticles were observed on Pt/CeO_2 after plasma treatment [219]. In addition, a change in the concentration of oxygen vacancies and Ce^{3+} in Pt/CeO_2 indicates that the oxidation state of catalyst can be changed by plasma. After 8 h of plasma process, parent Ti–O bonds in TiO_2 was reduced [174]. The energy of the Pd–support bond increases during plasma treatment, causing a rise in the degree of dispersion and sintering resistance of Pd, thereby a higher stability [220]. The adsorption behavior of catalyst in plasma is different from conventional thermal catalytic process. Compared to molecules, atoms and radicals are more susceptible to adsorption by catalysts due to their lower energy barriers. For thermal catalysis, atoms and radicals can only be produced by dissociative chemisorption of stable precursors. However, in plasma catalyst, a large amount of radicals and atoms around the boundary layer can be directly adsorbed with a low energy [36]. Therefore, plasma catalysis will provide new reaction pathways, which leads to reduced activation energy and higher reaction rate [189]. In addition to affecting the process of adsorption and surface reactions, plasma also promotes the desorption of products by electron and ion bombardment. The gas temperature in NTP is typically less than 400 K, which generally does not result in thermocatalytic activation. However, hotspots can be created between corners of adjacent pellets and sharp edges due to local intense electric fields [39]. Furthermore, the metal particles dispersed on the support have a high electrical conductivity, and Joule heating is generated as discharge spreads along the surface [221]. Hence, VOCs may be degraded partially through thermal catalysis.

5.5. VOCs decomposition mechanisms

In order to verify the degradation pathway of VOCs in packed-bed DBD, various surface analysis techniques such as gas chromatography-mass spectrometry (GC–MS), X-ray photoelectron spectroscopy (XPS), Raman and infrared were used to identify the species that are present on catalytic surface during plasma processing. However, these analyses were performed when the catalyst was removed from the DBD reactor. Therefore, some weakly adsorbed intermediates may have been lost before detection, so that only limited information on the catalyst surface can be obtained. The application of in-situ detection technique will provide more real and detailed information about the intermediates. Xu et al. [222] used an in-situ FT-IR spectroscopy to evaluate toluene abatement process in continuous and sequential systems with NiO/Al_2O_3 packed. The results indicated that toluene was gradually removed and organic intermediates were mostly destructed after 90 min reaction in sequential system, while the types of organic by-products accumulated on catalyst surface in continuous system, and eventually impeded the further steps of toluene decomposition. In order to investigate the difference in degradation of adsorbed toluene in IPC and PPC systems, Jia et al. [175] used two complementary in situ diagnostics (diffuse reflectance infrared fourier transform spectroscopy (DRIFTS) and transmission fourier transform infrared spectroscopy using Sorbent track (ST) device) to dynamically probing toluene surface coverage and adsorbed intermediates on CeO_2. As depicted in Fig. 13 (a), for PPC system, the toluene surface coverage decreased as soon as the plasma was turned on and the surface concentrations of benzyl alcohol and benzaldehyde gradually increased until plateau was reached. Different from benzyl alcohol and benzaldehyde, the production of surface benzoic acid started beyond 500 s. Compared to PPC system, some similar trends were observed in IPC configuration (Fig. 13 (b)). However, the

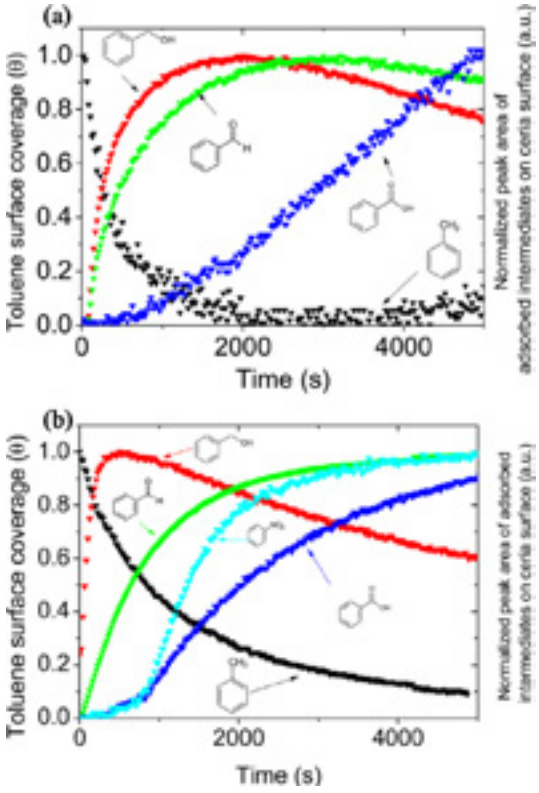

Fig. 13. Evolution of toluene and adsorbed intermediates surface coverage on CeO_2 as a function of post situ (a) and in situ (b) NTP exposure time [175].

concentration of benzyl alcohol in IPC increased faster than that in PPC and the formation of nitrobenzene in IPC was observed. In addition, IPC showed a higher reaction rate of toluene decomposition than PPC system. This was attributed to the fact that the toluene on catalytic surface is simultaneously exposed to long- and short-lived species in IPC, while only long-lived species contributed to toluene degradation.

Although in situ detection can provide more reliable and detailed information about the intermediates on catalyst surface, it is still hard to sketch the real map of VOCs degradation. Based on these experimental results, using computational chemistry to obtain the reaction pathways can lead to a better understanding of reaction dynamics in plasma-catalysis systems. To our best knowledge, there is currently no research on the application of computational chemistry to plasma-catalyzed oxidation of VOCs. However, in other fields of plasma catalysis, some studies can be referenced. Shirazi et al. [223] conducted a density functional theory (DFT) study of Ni-catalyzed plasma dry for methane reforming. They inspected many activation barriers, from the early stage of adsorption of major chemical fragments derived from CH_4 and CO_2 molecules up to the formation of value-added chemicals at the surface. The results indicated that the hydrogenation of a chemical fragment on the hydrogenated crystalline surface is energetically favored compared to the simple hydrogenation of the chemical fragment at the bare Ni (1 1 1) surface. The surface-bound H atoms and the remaining chemical fragments at the crystalline surface will facilitate the catalytic conversion of the fragments generated from CH_4 and CO_2. They believed that the retention of methane fragments, especially CH_3, in the presence of surface bound H atoms can be regarded as an identifier for the choice of a suitable catalyst.

5.6. Summary

Plasma catalysis is considered as the most promising way to improve the performance of DBD in VOCs abatement due to its excellent capability in the enhancement of mineralization rate and energy

efficiency as well as the suppression of by-products. There are four types of packed-bed DBD system according to the catalyst packing position and operation process, namely CIPC, CPPC, SIPC and SPPC. For an IPC system, the properties of packing material (such as dielectric constant, surface properties, size and shape) will directly affect the discharge characteristics of DBD and VOCs decomposition performance. These effects can be partially confirmed by measuring the discharge characteristics, represented by the current–voltage waveforms and Lissajous figures obtained by an oscilloscope. Recently, the application of ICCD imaging and fluid modeling has made it possible to gain a deeper insight of discharge characteristics. It is foreseeable that effects such as packing material shape on discharge characteristics will be explored by these advanced methods. Since temperature plays a significant role in plasma catalyst system, investigating the change and distribution of temperature in packed-bed DBD through fluid modeling may yield some vital findings. The loading of metal catalyst on packing material will further improve VOCs removal performance, which is affected by the type, loading amount, shape and size of supported metal catalyst. In a plasma catalysis system, there are synergistic effects between the catalyst and plasma. However, the fundamental physical and chemical processes of the interactions between plasma and catalyst are still not well understood. As a result, the selection of catalyst and operating conditions in plasma process is still based on trial and error approach. The dynamically monitoring of intermediates on catalyst surface through in situ detection technique can provide a deeper understanding about VOCs decomposition mechanism in plasma catalysis system. Combined with the results from in situ analysis, computational chemistry makes it possible to tailor the catalyst for a specific chemical reaction process. More details about the synergy of plasma and catalyst can be accessed in recent reviews [34,36,39,61,79,189,218,224–230].

6. Effect of gas properties

6.1. Target pollutants

There are > 100 kinds of VOCs emitted from various industrial processes, which is a major difficulty in VOCs abatement. Table 3 summarizes the abatement of different common VOCs as well as odors (such as dimethylamine, dimethyl sulfide, acetaldehyde) by DBD reactor. According to the difference in chemical structure, these VOCs include aromatics, ketones, aldehydes, alcohols, esters, alkanes, alkenes and halocarbons. The degree of difficulty for various VOCs decomposition in DBD may be related to its chemical structure, ionization potential and hydrogen content (mass percentage). Karatum et al. [107] chose methyl ethyl ketone, benzene, toluene, 3-pentanone, methyl *tert*-butyl ether, ethylbenzene, and n-hexane as target reactants to degrade in a DBD reactor. The results showed that the molecule (n-hexane) with the highest hydrogen content has the highest removal efficiency (90%). The reaction rate constants of different VOCs are significantly positively correlated with their hydrogen weight fraction. Moreover, aromatic compounds follow their own trend with respect to their hydrogen content. In [231], a higher hydrogen content results in higher removal efficiency for aromatic hydrocarbons (benzene, toluene and xylene), ketones (propanone, 2-butanone and 2-pentanone) and esters (ethyl acetate, ethyl propionate and ethyl butyrate) but the results were in the reverses order for alkanes (n-pentane, n-hexane and cyclohexane). However, there is no obvious relationship between removal efficiency and hydrogen content when considering all four types of VOCs. Hence, the relationship between hydrogen content and removal efficiency may only be applicable to different VOCs with similar chemical structures. Further, the lower the ionization potential, the higher the reactivity of VOCs and radicals, which gives rise to the higher degradation efficiency of VOCs. In addition, the three alkanes deviate from the main trend due to their inclusion of more single bonds, which are more easily destructed in NTP. In the study by Kim et al. [232], no correlation between the ionization potential and VOCs degradation was observed in plasma driven catalyst reactor, which indicates that the decomposition mechanism of VOCs in packed bed reactor is different from NTP alone. Moreover, the effect of chemical structure on removal rate is not negligible, e.g., the presence of double or triple bonds of CC are beneficial for initial activation during VOCs destruction [233]. In terms of total energy demand, single bonds are cracked more easily than double bonds. However, the second bond of a double bond needs low energy levels to be activated and, afterwards, transformation of the activated single bonded compounds is preferred in comparison to the non-activated single bond compound. Hill et al. found that at an input energy of 100 J/ L, the removal rates were 16% and 68% for propane and propene, respectively [234]. This is due to the limited number of available pathways to initiate propane removal. The influence of functional groups is also noteworthy. For example, the reason why the toluene removal rate is greater than that of benzene is more likely due to the presence of methyl group in toluene than its higher hydrogen content.

6.2. Gas flow rate

The gas flow rate significantly affects the performance of VOCs

Table 3
Overview of various VOCs degraded by DBD.

Classification	VOCs	Reference
Aromatics	Toluene	[33,109,114,118,143,149,157,161,235–239]
	Benzene	[101,129,178,207,240–243]
	Styrene	[116,139,140,156,232,244]
	Xylene	[96,117,232,245–247]
Ketones	Acetone	[41,200,248–250]
Aldehydes	Formaldehyde	[86,179,208,251,252]
	Acetaldehyde	[94,145,253]
Alcohols	Methanol	[42,202,206,254]
	Ethanol	[255,256]
Esters	Ethyl acetate	[113,154,231]
Alkanes	Methane	[155,180,257,258]
	Propane	[234,259–264]
Alkenes	Ethylene	[176,191,265]
	Propene	[234,258,259,266]
Halocarbons	Dichloromethane	[267–271]
	Tetrachloromethane	[272–274]
	Chlorobenzene	[103,106,133,205,275,276]
	Trifluoromethane	[148,277–279]
	Trichloroethylene (TCE)	[136,272,280–285]
Odors	Dimethylamine, dimethyl sulfide, acetaldehyde, ammonia, dimethyl sulphide, thiols, hydrothion	[112,233,286–290]

degradation in DBD reactor. A higher gas flow rate means that more VOCs molecules pass through the reaction zone per unit time, resulting in a reduction in the number of active species available for each molecule. In addition, a higher gas flow rate results in a shorter residence time, which reduces the probability of collision between VOCs molecules and active particles. As a result, increasing the gas flow rate leads to a decrease in VOCs removal efficiency and CO_2 selectivity. For example, in [109], when the gas flow rate varies from 0.13 to 0.4 L/ min, the residence time is reduced from 4.3 s to 1.4 s, the toluene decomposition efficiency is reduced from 93.39% to 80.84%, and the CO_2 selectivity is lowered from to 92.53% to 72.18%. However, increasing the gas flow rate significantly enhances the energy efficiency for a given system [206], as the active species can be more fully utilized at a high gas flow rate. If VOCs are decomposed by a sequential processing, the effect of gas flow rate will be different from continuous processing. In sequential treatment, VOCs are first adsorbed on packing material and then degraded by plasma. On the one hand, if the discharge gas flow rate is too low, there may be insufficient oxygen active species to react with the adsorbed VOCs, resulting in a decrease in mineralization rate and CO_2 selectivity. On the other hand, as the discharge gas flow rate increases, the specific input energy and residence time are reduced, which is detrimental to the degradation of VOCs. In [114], the toluene mineralization rate and CO_2 selectivity with discharge gas flow rate of 1.0 L/min are higher than that of 0.5 and 1.2 L/min. Interestingly, in [291], as the discharge gas flow rate (0.025, 0.05, 0.1 and 0.2 L/min) increases, the CO_2 selectivity increases while the CO selectivity decreases, and the mineralization rate (or COx selectivity) remains constant. Therefore, the effect of gas flow rate on VOCs degradation in sequential treatment is dependent on the specific experimental conditions.

6.3. Initial concentration

DBD is primarily applied to treat low concentration VOCs, typically less than 1000 ppm. Under a given operating condition, the amount of active species such as high-energy electrons and radicals generated in the DBD reactor is constant. Therefore, increasing the initial concentration of VOCs leads to a decrease in the number of active species that react with each molecule, resulting in a decrease in removal efficiency and mineralization rate of VOCs. In [161], the initial toluene concentration increased from 25 to 125 ppm, the removal efficiency and mineralization rate decreased from 70.58% to 39.32% and from 19.60% to 6.68%, respectively. However, increasing the initial concentration will increase the amount of VOCs removed [106], thereby increasing energy efficiency. This is because the probability of collision between VOCs active species is higher when a higher number of VOCs are introduced into the reactor per unit time. In [248], the energy efficiency increased from 0.56 to 1.18 g/kWh when the initial concentration of acetone increased from 100 to 300 ppm. For sequential processing, the performance of VOCs removal is related to the amount of stored VOCs rather than the initial concentration. In [114], as the toluene storage increased from 53.17 to 65.44 μmol, the carbon balance decreased from 98.26% to 92.36%, and the energy efficiency increased from 1.925 to 2.369 g/kWh. The reason for this result is similar to the influence of initial concentration on VOCs decomposition in continuous treatment. In addition, increasing the concentration or adsorbed amount of VOCs will cause more active species to contribute to VOCs decomposition. As a result, the formation of O_3 and NOx is suppressed.

6.4. Oxygen content

Since oxygen plays a significant role in the degradation of VOCs in DBD, the oxygen content in the discharge gas significantly affects the performance of VOCs abatement. For DBD process alone, the degradation efficiency of VOCs generally increases first and then decreases with the increase of oxygen content. In pure nitrogen, VOCs are removed by collision with electrons and active metastable nitrogen atoms and molecules. After adding oxygen, the active oxygen atoms and molecules as well as OH radicals participate in the decomposition of VOCs, thereby enhancing the removal efficiency of VOCs [268]. However, when the oxygen content exceeds a certain value, the formation of NOx and O_3 begins to prevail, which consumes a large amount of active species derived from oxygen and nitrogen, resulting in less degradation of VOCs. In addition, the reaction rate of O_3 towards VOCs is too small to contribute to VOCs degradation.

Several studies have reported the dependence of VOCs decomposition on oxygen content in DBD and the maximum efficiency was obtained at 5% O_2 for toluene [292], 4% for dichloromethane [268], 2% for trifluoromethane [148], 3–5% for benzene [126], 5% for p-xylene [96]. The influence of oxygen content on COx selectivity is different from VOCs removal efficiency. In [293], the selectivity of CO_2 and COx increased with the increase of oxygen concentration, but according to Kim [126], the selectivities of CO and CO_2 were much less affected by the partial pressure of O_2 compared with decomposition efficiency. Unlike DBD alone, a high oxygen content enhances VOCs decomposition in packed bed reactor. After introducing catalyst, reactive oxygen species (such as ·O, O^{2-} and O^-) can be produced from lattice oxygen and interaction with ozone. As the oxygen concentration increases, a large amount of ozone is formed, most of which is decomposed into active oxygen species on the surface of catalyst, thereby increasing the decomposition efficiency and COx selectivity of VOCs. In [126], the increase of O_2 concentration elevated both the degradation efficiency of benzene and CO_2 selectivity regardless of the type of catalysts (TiO_2, γ-Al_2O_3, zeolites). If the target reactant contains oxygen atoms, the effect of oxygen content on VOCs decomposition may differ from the above results. In [249], the removal efficiency of acetone is decreased with increasing oxygen concentration with or without packing materials (γ-Al_2O_3, α-Al_2O_3 and glass beads). This is because acetone is less reactive with oxygen species than other VOCs such as toluene and benzene.

6.5. Humidity level

Since industrial VOCs containing exhaust gases usually contain water vapors, the effect of humidity on the degradation of VOCs in DBD is not negligible. The presence of water vapor cannot be neglected in VOCs removal by NTP since it can be decomposed into ·OH , which has a stronger oxidation power than other active species such as oxygen atoms and metastable nitrogen molecules and atoms. In a DBD reactor with photo-catalytic electrode (SMF/TiO_2), the concentration of ·OH at a relative humidity (RH) of 80% is approximately three times than that at 10% RH [294]. The discharge characteristics of DBD are affected by the presence of water. Water vapor may cover the surface of the dielectric, resulting in reduced surface resistance and increased dielectric capacitance, which leads to decline of total transferred discharge [295].

Similar to oxygen, the addition of suitable water may facilitate the decomposition of VOCs due to the high oxidizing power of ·OH. However, if too much water is introduced, the high-energy electrons will be quenched by the electronegative water molecules, so that the density and average energy of electrons are lowered, resulting in a decrease in the number of active species. Many studies have reported that the highest VOCs removal efficiency can be obtained at a suitable humidity level. For example, at 20% RH for toluene [296], at 30% for benzene [207], at 70% for ethanethiol [297]. In other studies [93,181,201,298,299], the decomposition of VOCs is decreased with the increase of humidity level. The difference in these findings may be due to the variety of VOCs and experimental conditions. Fan et al. [300], found that different VOCs have different sensitivity to water vapor. Humidity suppressed benzene removal, while toluene decomposition was slightly enhanced by increasing RH from 30% to 50–80% and p-xylene conversion was insensitive to water vapor. In packed bed DBD reactor, the presence of water vapor may poison the catalyst by covering a portion of active sites, which are available for VOCs and O_3

adsorption [299]. Therefore, the resistance to water should be considered when choosing a catalyst.

As for the influence of water vapor on COx selectivity, the results reported by various studies are also different. In [161] and [207], the highest COx yield and CO_2 selectivity were obtained at 30% RH, which is consistent with the effect of humidity on decomposition efficiency. In other studies [93,240,296], increasing humidity enhances CO_2 selectivity due to the further oxidation of intermediates by ·OH. The presence of catalyst affects the influence of humidity on CO_2 selectivity. In [300], the CO_2 selectivity by DBD alone increased while that by packed bed DBD decreased with the increase of RH. The humidity level also affects the formation of O_3 and NOx. Generally, an increase in humidity results in a decrease in O_3 concentration due to the quench of high energy electrons by water molecular, which led to the decrease of atomic oxygen, and then decreased the amount of ozone in the plasma [201]. Intriguingly, Jiang et al. observed a reverse trend in a PPC system and they attributed it to the competitive adsorption between H_2O and O_3 molecules on the catalyst [207]. For NO_2, its concentration decreases with increasing humidity level in both NTP alone and PPC systems [207]. This was because high water vapor in discharge plasma tends to induce electron attachment reaction and thereby reduce the energetic electron density and mean electron energy, resulting in a decreased total production of active species.

6.6. Summary

In a given DBD reactor, VOCs removal performance is affected by various gas properties, such as the type of target pollutants, gas flow rate, initial concentration, oxygen content and humidity level. The degree of difficulty for different VOCs decomposition in DBD may be related to its chemical structure, functional groups, ionization potential and hydrogen content. In continuous systems, an increase in gas flow rate will reduce the gas retention time, which lead to a reduction in VOCs removal and mineralization rates, but will increase energy efficiency. In sequential systems, the influence of gas flow rate on VOCs removal is dependent on specific experimental conditions. Similarly, increasing the initial concentration leads to a decrease in removal and mineralization rate of VOCs, but an increase in energy efficiency. For sequential processing, what matters is the amount of stored VOCs rather than the initial concentration. A appropriate level of oxygen content and water vapor will facilitate the decomposition of VOCs due to the formation of highly oxidizing species (such as ·O and ·OH). An increase in oxygen content will lead to an increase in ozone, which is hard to oxidize VOCs but is easily decomposed into strong oxidizing species by catalyst. In contrast, too much water vapor will cover the active sites of the catalyst, thereby poising the catalyst. These results about the effect of gas properties on VOCs abatement are of great significance for the practical application of DBD. However, most of these results were obtained from laboratory-scale experiments. In the future, more efforts should focus on using DBD to remove VOCs-containing gases which are close to industrial conditions.

7. Practical application

Although DBD exhibits various merits for VOCs abatement, its commercial implementation is still scarce. There are barriers that need to be addressed, such as the formation of stable organic by-products, residual O_3 and NOx, and the sensibility to humidity. Theoretically, the presence of suitable catalysts can alleviate these problems, which has been confirmed in many laboratory experiments. However, the performance of plasma catalysis for the treatment of industrial VOCs-containing exhaust gas is still uncertain. Therefore, before the industrial application of DBD (with or without catalyst) for VOCs removal, a large number of pilot experiments should be performed. Table 4 presents some scale-up experiments on DBD removal of VOCs. In these experiments, VOCs-containing exhaust gas come from industrial processes or

Table 4
Scaled-up experiments of DBD system for VOCs abatement.

Equipment	Power supply	Flow rate m^3/h	RH	Pollutant	RE	Reference
DBD (10 tubes)	3–10.5 kV, 1.12–3.4 kW	509	50	Benzene (2050.8–3243 mg/m^3)	40.5–59.2	[301]
DBD + post catalyst	7–8 kV, 350–400 Hz,0.3–0.6 kW	196	–	Emissions of water treatment plants(odor 96300–265100 OU/m^3)	57–90	[290]
DBD (40 tubes)	25–100 kV,1 kHz	100	–	Toluene 100 mg/m^3	~25–90	[303]
DBD	10 kV, 1 kHz, 150 W	2.5–5	40	Oil shale processing plant:butyl acetate (30–110 ppm)	~26–71	[305]
DBD + photocatalyst	0–30 kV, 50 Hz	350	53	Animal quartering centers: isobutyraldehyde, isovaleraldehyde,2-methylbutyraldehyde,and dimethyl disulfide, 30 mg /m^3(total)	65,55,75,25	[302]
DBD + zeolite + Biotrickling filter	11 kV, 520 Hz, 1.5–1.6 kW	1000	25–80	Emissions of sludge centrifugation(odor 200–1400 OU/m^3)	~95	[233]

laboratories, and in most cases the gas flow rate is about several hundred cubic meters. These industrial waste gases are emitted from water treatment plants, oil shale processing plant, animal quartering centers and sludge centrifugation. Most of these experiments were conducted in the bypass of the emission duct during the industrial process. Unlike laboratory, the conditions of the process gases to be treated were varying (fluctuation of pollutants concentration, humidity and flow rate). As a result, the performance of DBD may be poorer than the results obtained from laboratory, in which the gas conditions are carefully controlled and are generally single-component. Nevertheless, it is not difficult to meet the local legislative limitations since the inlet gas concentration is usually relatively low. In addition, multiple DBD systems can be arranged in series to improve VOCs removal efficiency. In the study by Ye et al. [301], the removal rates of benzene increased from 58.2% with one DBD system to 92.7% with three DBD system in series at 10.5 kV. Surely, this was achieved at the expense of increasing constructional and operational costs.

Upon inspection of these scale-up experiments, DBD system appeared to exhibit high potential for odor elimination. Over 90% of odor abatement were achieved in several studies [233,290], in which DBD system was combined with other techniques such as catalyst, adsorber and biotrickling filter. At the same time, the destruction of methane [233] and dimethyl disulfide (DMDS) [302] was unsatisfactory, which is consistent with the results obtained from laboratory experiments. For the degradation of different VOCs in laboratory and in the case of real gases, the degree of difficulty should be the same. In other words, the results gained in laboratory are significant for the treatment of industrial VOCs despite the different gas conditions.

During the scale-up experiment, some unpredictable situations may occur due to the changes in operating conditions. Therefore, the comparison of lab-scale and pilot-scale test is imperative. Liang et al. [303] evaluated the performance of toluene decomposition in two DBD reactors with different scale. They found that the toluene removal rate in lab-scale reactor was higher than that in pilot-scale reactor at the same applied voltage. This was due to the fact that the discharge gap of pilot-scale reactor (6 mm) is larger than that of lab-scale reactor (2.5 mm). However, the pilot-scale reactor exhibited a higher energy efficiency than lab-scale reactor at the same amount of exhaust gas. They attributed this to the much weaker wall effect in pilot-scale reactor compared to lab-scale reactor. Assadi et al. [108] investigated the capacities of isovaleraldehyde (3-methylbutanal) removal in laboratory scale (planar and cylindrical reactor) and pilot scale reactors and they believed that the plasma reactor scale-up for pollutant removal can be feasible.

The feasibility of industrial application for DBD to remove VOCs is not only relates to pollutants degradation performance, but also depends on its construction and operational costs. Ye et al. [301] calculated the treatment cost of benzene destruction in DBD (509 m^3/h, RH = 50%) and concluded that the cost ranged from 0.24 to 0.52 \$/10^3 m^3 at the voltage of 6–10.5 kV. Dobslaw et al. [233] estimated the construction and operational costs of using the combined NTP-mineral adsorber – biotrickling filter process to treat waste gas from sludge centrifugation in a waste water treatment plan. For treatment of 20,000 m^3/h of waste gas at an annual operation time of 8000 h, the construction and operational costs were 11.17 \$/(m^3/h) and 0.53 \$/10^3 m^3, respectively. Martini et al. [304] have made hypotheses on fixed and variable costs for a Q = 50,000 m^3/h BDB system and concluded that the DBD fixed cost and the annual variable cost were 33.99 \$/(m^3/h) and 0.0112 \$/10^3 m^3, respectively. The costs in the above two studies were calculated based on original data and the exchange rate of € and \$ (1€ =1.1175\$). It should be pointed out that Dobslaw's research included the construction and operational costs of adsorber and biotrickling filter, which was not considered in Martini's economic analysis. Even if the two costs are added in Martini's study, the results of the two economic analyses are still very different, which may be correlated to the balance between fixed and variable costs. Currently, economic data on the application of DBD for VOCs abatement is scarce. Therefore, more research is needed to illustrate the economic viability of DBD.

Based on the above-mentioned pilot scale studies, the prospects for the application of DBD in VOCs abatement are clearer. There are a number of aspects which are correlated to the practical use and targets for DBD systems can be discussed.

Adaptability to gas conditions The real gas conditions are more complicated than those in laboratories. Since many industrial waste gases contain fine particles or aerosols, so a filter for dust retention is necessary before the gas enters DBD reactors. In the industrial process, the pollutant concentration, moisture and flow rate of the exhaust gas fluctuate randomly. Hence, the DBD equipment's capability for pollutants treatment should be able to adjust as the gas conditions change. This can be achieved by adjusting the applied voltage. Specifically, when the pollutant load is at a low level, the DBD can work at a lower voltage to save energy and prevent over oxidation, which results in a large amount of O_3 and NOx formation. Similarly, the voltage should be raised with the increase of pollutant load to ensure removal rate. Various industrial processes such as printing and painting are operated intermittently, which means that the waste gas is not continuously generated. Therefore, VOCs treating equipment should be able to be turned on and off at any time. For DBD, this requirement is easily met because there is no warm-up stage.

Acceptable construction and operational cost Construction costs mainly include pipes, DBD casing, DBD stacks, DBD power supply and ventilator. Among these fixed costs, DBD stacks and power supply account for the majority. The operational cost will be dictated predominately by electricity cost, which consists of power supply and ventilator consumption. For plasma catalysis systems, the cost of catalyst purchase and disposal needs to be considered. The price of commercially viable catalysts ranges from several \$ to hundreds \$ per kg. Therefore, in practical applications, there should be a compromise between the cost and efficiency of the catalyst. In addition, the disposal of deactivated catalyst after a long period of use cannot be ignored. For commercial applications, with or without a catalyst, the total cost of DBD for VOCs abatement should be comparable to thermal oxidation technique.

By-products formation The formation of undesired by-products is inevitable during the degradation of VOCs in DBD. The mineralization rate of VOCs in DBD is generally less than 50% in the absence of catalysts. This means that more than half of initial pollutants are converted into organic by-products. Some of these by-products are emitted in a gaseous form, and the rest are deposited in the form of aerosols on dielectric barrier surface or electrodes. The long-term accumulation of these aerosols will inevitably affect the normal operation of DBD and may even cause accidents. Hence, these deposited by-products should be cleaned in due course of time. The presence of catalysts can reduce but cannot eliminate the formation of organic by-products. As a result, the catalyst may be deactivated by the gradual deposition of by-products. Currently, there are few studies related to the deactivation of catalysts during VOCs removal in DBD. Although ozone is an oxidant, it hardly reacts with VOCs in the absence of catalysts. This is why a large amount of ozone can be detected in the exhaust gas while the mineralization rate is low. Depending on the reactor configuration and applied voltage, the residual ozone concentration ranges from tens to thousands of ppm. Nevertheless, the residual ozone can be easily decomposed if a suitable catalyst is located downstream of the discharge zone in both IPC and PPC systems. As for nitrogen oxides, they can also be reduced by appropriate catalysts.

Safety The security risks in the operation of DBD equipment cannot be ignored. Firstly, the concentration of VOCs to be treated should be below the explosion limit. Secondly, fine particles such as oil or paint mist should be effectively filtered before the exhaust gas enters DBD. These particles can be deposited on the electrode or the dielectric surface and may cause accidents during discharge. Thirdly, insulators on the high-voltage input should be protected from contamination and

condensation to avoid creepage and creeping discharge. Lastly, the organic by-products deposited in the equipment should be cleaned in due course of time. These deposits may be ignited by local high temperature during discharge and cause accidents. Most of these deposits can be cleaned by alcohol. Therefore, maintenance and cleaning of the DBD equipment during VOCs treatment are significant for its safe operation.

Modularity DBD reactor can be easily scaled up based on actual demands. In order to treat high gas flows, several modules can be used in series or in parallel, which provides a high degree of flexibility. The number of modules required depends on the gas volume and the treatment capacity of single modules. The connection mode of each module can be determined according to the space of the site. Other benefits of modularity include the flexibility of transportation and high utilization of space.

These benefits, requirements and associated issues are helpful in identifying the applicability of DBD for VOCs abatement and smooth operation of DBD equipment in industrial setting.

8. Conclusions and perspectives

The application of dielectric barrier discharge non-thermal plasma in VOCs abatement was discussed along with the history, micro-discharge formation and environmental application of DBD. Subsequently, the effect of reactor configuration, power supplies, packing materials and gas properties on discharge characteristics and VOCs degradation in DBD were presented. A desirable DBD reactor should have high VOCs removal efficiency and mineralization rate, as well as low by-products. In order to achieve this goal, various aspects, such as optimization of reactor structure, application of advanced power supply and the introduction of catalysts need to be considered. In addition, investigating the influence of gas properties such as initial concentration, flow rate and humidity level on VOCs abatement can provide an important reference for the industrial applications of DBD. Based on several pilot scale experiments, a number of aspects associated to the practical implementation and targets for DBD systems were discussed.

In the past three decades, a huge number of researches have been implemented and great achievements have been made, which paved for the practical application of DBD in VOCs abatement. However, the mechanisms behind these experimental results are still veiled, and commercial applications of DBD on VOCs removal are still scarce. Therefore, future work should be carried out from both theoretical and practical aspects.

In terms of theory, it mainly lies in the understanding of the discharge process and the degradation pathways of VOCs in the presence or absence of a catalyst. In the early days, the discharge process information such as consumed power was mainly obtained through oscilloscopes. Recently, the application of fast imaging technique has made it possible to directly observe the discharge behavior such as the propagation of streamers on catalyst surface. Further, the information about variation and distribution of the temperature and density of electrons during discharge can be gained through fluid modeling. Through these advanced means, a better insight into the discharge behavior could be obtained, such as electric field enhancement in packed bed DBD reactors, plasma streamer propagation in packed bed DBD reactors and plasma streamer penetration in catalyst pores. In the near future, the discharge mechanism of packed bed DBD will be more fully understood. Unexpectedly, few researchers have focused on the impact of reactor structure on discharge behavior through these advanced means and methods.

About VOCs decomposition mechanisms, most of them were speculated from the information obtained by ex situ detection techniques. To date, the underlying physical and chemical processes of VOCs degradation with or without catalyst are still not clear enough. This is mainly because the survival time of reactive species such as radicals and electrons in plasma and the intermediates generated from VOCs are too short to be detected. Recently, the application of direct in situ detection has provided more information for understanding the mechanism for VOCs decomposition. Further, the results obtained by in situ measurements can be used in conjunction with computational chemistry such as DFT (Density Functional Theory) to gain a better insight into the reaction pathways of packed-bed DBD systems.

Although a deep insight into the mechanisms of discharge and VOCs degradation can provide theoretical guidance for reactor optimization and catalyst tailoring, it is a difficult task to unveil these mechanisms due to the complexity of plasma behavior, especially in the presence of catalysts. Therefore, in addition to theoretical research, we can also focus on practical aspects to promote the industrial application of DBD in VOCs abatement through process improvement and scale-up experiments. The possible research areas that needs to be explored are as follows:

1) Since real exhaust gas contains many types of VOCs, it is useful to investigate the performance of DBD on mixed VOCs removal.

2) Many studies have shown that sequential DBD process (adsorption with plasma off and oxidation with plasma on) exhibits high energy efficiency. Therefore, it is necessary to undertake research work in this field to testify the practical performance of this operation process.

3) It is promising to combine DBD with other waste air treatment techniques to develop more energy efficient systems. For instance, DBD can be operated as a pre-treatment stage to decompose VOCs into hydrophilic substances, which can be effectively removed by a subsequent biological treatment. More research efforts are needed to identify the potential of these combined systems.

4) In most case, high mineralization rates can be obtained in IPC systems, while PPC system is effective for the suppression of residual ozone. The addition of a downstream catalyst to an IPC system may provide a pragmatic solution to treat VOCs efficiently while ensuring a low residual ozone level. On the other hand, it may be difficult for a single catalyst to effectively remove various types of VOCs simultaneously. A multistage arrangement with different catalysts may be a valid option to address this issue. Therefore, the investigation of multistage catalytic systems is crucial in terms of both residual ozone elimination and complex VOCs mixtures treatment.

5) At present, pilot-scale experiments on industrial VOCs removal by DBD are scarce, which has led to insufficient information and guidance for its practical implementation. In order to promote the commercial application of DBD in VOCs abatement, more scale-up experiments and economic analysis need to be performed in the future.

Declaration of Competing Interest

The authors declare that they have no known competing financial interests or personal relationships that could have appeared to influence the work reported in this paper.

Acknowledgments

This work was financially supported by National Key R&D Program of China (No. 2017YFC0212204), Shaanxi Key R&D Program (No. 2018ZDCXL-SF-02-04), Youth Talents Lifting Project of Science and Technology Association in Shaanxi Provinces Universities and Colleges (No. 20190703), Special Research Project of Education Department of Shaanxi Province (No. 19JK0453), Key Research and Development Program of Shaanxi Province (No. 2018-ZDXM3-01).

References

[1] Z. Tan, K. Lu, M. Jiang, R. Su, H. Dong, L. Zeng, S. Xie, Q. Tan, Y. Zhang, Exploring ozone pollution in Chengdu, southwestern China: A case study from radical chemistry to O_3-VOC-NOx sensitivity, Sci. Total. Environ. 636 (2018) 775–786.

[2] Y. Yan, L. Peng, R. Li, Y. Li, L. Li, H. Bai, Concentration, ozone formation potential and source analysis of volatile organic compounds (VOCs) in a thermal power station centralized area: A study in Shuozhou, China, Environ. Pollut. 223 (2017)

295–304.
[3] L. Hui, X. Liu, Q. Tan, M. Feng, J. An, Y. Qu, Y. Zhang, N. Cheng, VOC characteristics, sources and contributions to SOA formation during haze events in Wuhan, Central China, Sci. Total. Environ. 650 (2019) 2624–2639.
[4] W. Wei, Y. Li, Y. Wang, S. Cheng, L. Wang, Characteristics of VOCs during haze and non-haze days in Beijing, China: Concentration, chemical degradation and regional transport impact, Atmos. Environ. 194 (2018) 134–145.
[5] R.J. Huang, Y. Zhang, C. Bozzetti, K.F. Ho, J.J. Cao, Y. Han, K.R. Daellenbach, J.G. Slowik, S.M. Platt, F. Canonaco, P. Zotter, R. Wolf, S.M. Pieber, E.A. Bruns, M. Crippa, G. Ciarelli, A. Piazzalunga, M. Schwikowski, G. Abbaszade, J. Schnelle-Kreis, R. Zimmermann, Z. An, S. Szidat, U. Baltensperger, I. El Haddad, A.S. Prevot, High secondary aerosol contribution to particulate pollution during haze events in China, Nature 514 (2014) 218–222.
[6] R. Hu, G. Liu, H. Zhang, H. Xue, X. Wang, Levels, characteristics and health risk assessment of VOCs in different functional zones of Hefei, Ecotox. Environ. Safe. 160 (2018) 301–307.
[7] M.A. Bari, W.B. Kindzierski, Ambient volatile organic compounds (VOCs) in Calgary, Alberta: Sources and screening health risk assessment, Sci. Total. Environ. 631–632 (2018) 627–640.
[8] D. Wang, L. Nie, X. Shao, H. Yu, Exposure profile of volatile organic compounds receptor associated with paints consumption, Sci. Total. Environ. 603–604 (2017) 57–65.
[9] X. Zhang, B. Gao, A.E. Creamer, C. Cao, Y. Li, Adsorption of VOCs onto engineered carbon materials: A review, J. Hazard. Mater. 338 (2017) 102–123.
[10] H. Wang, B. Wang, J. Li, T. Zhu, Adsorption equilibrium and thermodynamics of acetaldehyde/acetone on activated carbon, Sep. Purif. Technol. 209 (2019) 535–541.
[11] B. Belaissaoui, Y.L. Moullec, E. Favre, Energy efficiency of a hybrid membrane/condensation process for VOC (Volatile Organic Compounds) recovery from air: A generic approach, Energy 95 (2016) 291–302.
[12] A.S.R. Castillo, P.F. Biard, S. Guihéneuf, L. Paquin, A. Amrane, A. Couvert, Assessment of VOC absorption in hydrophobic ionic liquids: Measurement of partition and diffusion coefficients and simulation of a packed column, Chem. Eng. J. 360 (2019) 1416–1426.
[13] W. Yang, H. Zhou, C. Zong, Y. Li, W. Jin, Study on membrane performance in vapor permeation of VOC/N_2 mixtures via modified constant volume/variable pressure method, Sep. Purif. Technol. 200 (2018) 273–283.
[14] X. Hao, R. Li, J. Wang, X. Yang, Numerical simulation of a regenerative thermal oxidizer for volatile organic compounds treatment, Environ. Eng. Res. 23 (2018) 397–405.
[15] H. Wu, H. Yan, Y. Quan, H. Zhao, N. Jiang, C. Yin, Recent progress and perspectives in biotrickling filters for VOCs and odorous gases treatment, J. Environ. Manage. 222 (2018) 409–419.
[16] D. Dobslaw, J. Schöller, D. Krivak, S. Helbich, K.H. Engesser, Performance of different biological waste air purification processes in treatment of a waste gas mix containing tert-butyl alcohol and acetone: A comparative study, Chem. Eng. J. 355 (2019) 572–585.
[17] Z. Zhang, Z. Jiang, W. Shangguan, Low-temperature catalysis for VOCs removal in technology and application: A state-of-the-art review, Catal. Today 264 (2016) 270–278.
[18] C. Yang, G. Miao, Y. Pi, Q. Xia, J. Wu, Z. Li, J. Xiao, Abatement of various types of VOCs by adsorption/catalytic oxidation: A review, Chem. Eng. J. 370 (2019) 1128–1153.
[19] J. Guo, C. Lin, C. Jiang, P. Zhang, Review on noble metal-based catalysts for formaldehyde oxidation at room temperature, Appl. Surf. Sci. 475 (2019) 237–255.
[20] W. Zou, B. Gao, Y.S. Ok, L. Dong, Integrated adsorption and photocatalytic degradation of volatile organic compounds (VOCs) using carbon-based nanocomposites: A critical review, Chemosphere 218 (2019) 845–859.
[21] Z. Shayegan, C.S. Lee, F. Haghighat, TiO_2 photocatalyst for removal of volatile organic compounds in gas phase – A review, Chem. Eng. J. 334 (2018) 2408–2439.
[22] A.H. Mamaghani, F. Haghighat, C.S. Lee, Photocatalytic oxidation technology for indoor environment air purification: The state-of-the-art, Appl. Catal. B: Environ. 203 (2017) 247–269.
[23] S.H. Chen, O. Živný, A. Mašláni, S.W. Chau, Abatement of fluorinated compounds in thermal plasma flow, J. Fluorine Chem. 217 (2019) 41–49.
[24] J.C. Whitehead, Plasma catalysis: A solution for environmental problems, Pure Appl. Chem. 82 (2010) 1329–1336.
[25] S.K.P. Veerapandian, N.D. Geyter, J.M. Giraudon, J.F. Lamonier, R. Morent, The Use of Zeolites for VOCs Abatement by Combining Non-Thermal Plasma, Adsorption, and/or Catalysis: A Review, Catalysts 9 (2019).
[26] A.K.G.F.I. Khan, Removal of Volatile Organic Compounds from polluted air, J. Loss Prevent. Proc. 13 (2000) 527–545.
[27] G.R. Parmar, N.N. Rao, Emerging Control Technologies for Volatile Organic Compounds, Crit. Rev. Env. Sci. Tec. 39 (2008) 41–78.
[28] A. Luengas, A. Barona, C. Hort, G. Gallastegui, V. Platel, A. Elias, A review of indoor air treatment technologies, Rev. Environ. Sci. Bio. 14 (2015) 499–522.
[29] C. Dai, Y. Zhou, H. Peng, S. Huang, P. Qin, J. Zhang, Y. Yang, L. Luo, X. Zhang, Current progress in remediation of chlorinated volatile organic compounds: A review, J. Ind. Eng. Chem. 62 (2018) 106–119.
[30] K.H. Kim, J.E. Szulejko, P. Kumar, E.E. Kwon, A.A. Adelodun, P.A.K. Reddy, Air ionization as a control technology for off-gas emissions of volatile organic compounds, Environ. Pollut. 225 (2017) 729–743.
[31] F. Thevenet, L. Sivachandiran, O. Guaitella, C. Barakat, A. Rousseau, Plasma–catalyst coupling for volatile organic compound removal and indoor air treatment: a review, J. Phys. D: Appl. Phys. 47 (2014).
[32] A. Bogaerts, E.C. Neyts, Plasma Technology: An Emerging Technology for Energy Storage, ACS Energy Lett. 3 (2018) 1013–1027.
[33] B. Lee, D.W. Kim, D.W. Park, Dielectric barrier discharge reactor with the segmented electrodes for decomposition of toluene adsorbed on bare-zeolite, Chem. Eng. J. 357 (2019) 188–197.
[34] E.C. Neyts, K.K. Ostrikov, M.K. Sunkara, A. Bogaerts, Plasma Catalysis: Synergistic Effects at the Nanoscale, Chem. Rev. 115 (2015) 13408–13446.
[35] R.N. Franklin, N.S.J. Braithwaite, 80 Years of Plasma, Plasma Sources Sci. T. 18 (2009).
[36] J.C. Whitehead, Plasma–catalysis: the known knowns, the known unknowns and the unknown unknowns, J. Phys. D: Appl. Phys. 49 (2016).
[37] T. Hammer, Application of Plasma Technology in Environmental Techniques, Contrib. Plasma Phys. 39 (1999) 441–462.
[38] R. McAdams, Prospects for non-thermal atmospheric plasmas for pollution abatement, J. Phys. D: Appl. Phys. 34 (2001) 2810–2821.
[39] A.M. Vandenbroucke, R. Morent, N.D. Geyter, C. Leys, Non-thermal plasmas for non-catalytic and catalytic VOC abatement, J. Hazard. Mater. 195 (2011) 30–54.
[40] W.A. Saoud, A.A. Assadi, M. Guiza, S. Loganathan, A. Bouzaza, W. Aboussaoud, A. Ouederni, S. Rtimi, D. Wolbert, Synergism between non-thermal plasma and photocatalysis: Implicationsin the post discharge of ozone at a pilot scale in a catalytic fixed-bed reactor, Appl. Catal. B: Environ. 241 (2019) 227–235.
[41] X. Li, T. Guo, Z. Peng, L. Xu, J. Dong, P. Cheng, Z. Zhou, Real-time monitoring and quantification of organic by-products and mechanism study of acetone decomposition in a dielectric barrier discharge reactor, Environ. Sci. Pollut. Res. Int. 26 (2019) 6773–6781.
[42] C. Norsic, J.M. Tatibouët, C.B. Dupeyrat, E. Fourré, Methanol oxidation in dry and humid air by dielectric barrier discharge plasma combined with MnO_2–CuO based catalysts, Chem. Eng. J. 347 (2018) 944–952.
[43] X. Zhang, F. Feng, S. Li, X. Tang, Y. Huang, Z. Liu, K. Yan, Aerosol formation from styrene removal with an AC/DC streamer corona plasma system in air, Chem. Eng. J. 232 (2013) 527–533.
[44] J.V. Durme, J. Dewulf, W. Sysmans, C. Leys, H.V. Langenhove, Abatement and degradation pathways of toluene in indoor air by positive corona discharge, Chemosphere 68 (2007) 1821–1829.
[45] J.H. Park, J.W. Ahn, K.H. Kim, Y.S. Son, Historic and futuristic review of electron beam technology for the treatment of SO_2 and NOx in flue gas, Chem. Eng. J. 355 (2019) 351–366.
[46] Y.S. Son, T.H. Kim, C.Y. Choi, J.H. Park, J.W. Ahn, T.V. Dinh, Treatment of toluene and its by-products using an electron beam/ultra-fine bubble hybrid system, Radiat. Phys. Chem. 144 (2018) 367–372.
[47] F. Zhu, X. Li, H. Zhang, A. Wu, J. Yan, M. Ni, H. Zhang, A. Buekens, Destruction of toluene by rotating gliding arc discharge, Fuel 176 (2016) 78–85.
[48] H. Zhang, F. Zhu, X. Li, R. Xu, L. Li, J. Yan, X. Tu, Steam reforming of toluene and naphthalene as tar surrogate in a gliding arc discharge reactor, J. Hazard. Mater. 369 (2019) 244–253.
[49] Y. Qin, G. Niu, X. Wang, D. Luo, Y. Duan, Status of CO_2 conversion using microwave plasma, J. CO_2 Util. 28 (2018) 283–291.
[50] A.G. Zherlitsyn, V.P. Shiyan, P.V. Demchenko, Microwave plasma torch for processing hydrocarbon gases, Resource Efficient Technol. 2 (2016) 11–14.
[51] U. Kogelschatz, Dielectric-barrier Discharges Their History, Discharge Physics, and Industrial Applications, Plasma Chem. Plasma P. 23 (2003) 1-46.
[52] Plasma Chem Plasma Process 34 (5) (2014) 1033–1065, https://doi.org/10.1007/s11090-014-9562-0.
[53] W. Siemens, Ueber die elektrostatische Induction und die Verzögerung des Stroms in Flaschendrähten, Ann. Phys. Chem. 178 (1857) 66–122.
[54] B. Eliasson, M. Hirth, U. Kogelschatz, Ozone synthesis from oxygen in dielectric barrier discharges, J. Phys. D: Appl. Phys. 20 (1987) 1421–1437.
[55] K. Buss, Die elektrodenlose Entladung nach Messung mit dem Kathodenoszillographen, Archiv für Elektrotechnik 26 (1932) 261–265.
[56] T.C. Manley, The Electric Characteristics of the Ozonator Discharge, J. Electrochem. Soc. 84 (1943) 83–96.
[57] U. Kogelschatz, B. Eliasson, W. Egli, Dielectric-Barrier Discharges. Principle and, Applications, J. PHYS IV FRANCE 4 (1997) 46–66.
[58] B. Eliasson, U. Kogelschatz, Modeling and Applications of Silent Discharge Plasmas, IEEE T. Plasma Sci. 19 (1991) 309–323.
[59] U. Kogelschatz, B. Eliasson, W. Egli, From ozone generators to flat television screens: history and future potential of dielectric-barrier discharges, Pure Appl. Chem. 71 (1999) 1819–1828.
[60] U. Kogelschatz, Fundamentals and applications of dielectric-barrier, discharges (2000).
[61] Plasma Chem Plasma Process 36 (1) (2016) 185–212, https://doi.org/10.1007/s11090-015-9662-5.
[62] U. Kogelschatz, Collective phenomena in volume and surface barrier discharges, J. Phys. Conf. Series 257 (2010).
[63] S.A. Starostin, P.A. Premkumar, M. Creatore, E.M. van Veldhuizen, H. de Vries, R.M.J. Paffen, M.C.M. van de Sanden, On the formation mechanisms of the diffuse atmospheric pressure dielectric barrier discharge in CVD processes of thin silica-like films, Plasma Sources Sci. Technol. 18 (2009).
[64] H.E. Wagner, R. Brandenburg, K.V. Kozlov, A. Sonnenfeld, P. Michel, J.F. Behnke, The barrier discharge: basic properties and applications to surface treatment, Vacuum 71 (2003) 417–436.
[65] Y. Sun, F. Zhang, Investigation of influencing factors in ozone generation using dielectric barrier discharge, Proceedings of the 9th International Conference on Properties and Applications of Dielectric Materials, 2009, pp. 614–617.
[66] K. Takaki, Y. Hatanaka, K. Arima, S. Mukaigawa, T. Fujiwara, Influence of electrode configuration on ozone synthesis and micro-discharge property in dielectric

barrier discharge reactor, Vacuum 83 (2008) 128–132.
[67] S. Jodzis, M. Zięba, Energy efficiency of an ozone generation process in oxygen, Analysis of a pulsed DBD system, Vacuum 155 (2018) 29–37.
[68] L.S. Wei, D.K. Yuan, Y.F. Zhang, Z.J. Hu, G.P. Dong, Experimental and theoretical study of ozone generation in pulsed positive dielectric barrier discharge, Vacuum 104 (2014) 61–64.
[69] P. Talebizadeh, M. Babaie, R. Brown, H. Rahimzadeh, Z. Ristovski, M. Arai, The role of non-thermal plasma technique in NOx treatment: A review, Renew. Sust. Energ. Rev. 40 (2014) 886–901.
[70] Z. Adnan, S. Mir, M. Habib, Exhaust gases depletion using non-thermal plasma (NTP), Atmos. Pollut. Res. 8 (2017) 338–343.
[71] M. Babaie, P. Davari, P. Talebizadeh, F. Zare, H. Rahimzadeh, Z. Ristovski, R. Brown, Performance evaluation of non-thermal plasma on particulate matter, ozone and CO_2 correlation for diesel exhaust emission reduction, Chem. Eng. J. 276 (2015) 240–248.
[72] S. Ma, Y. Zhao, J. Yang, S. Zhang, J. Zhang, C. Zheng, Research progress of pollutants removal from coal-fired flue gas using non-thermal plasma, Renew. Sust. Energ. Rev. 67 (2017) 791–810.
[73] S. Cui, R. Hao, Dong Fu, Integrated method of non-thermal plasma combined with catalytical oxidation for simultaneous removal of SO_2 and NO, Fuel 246 (2019) 365–374.
[74] S. Cui, R. Hao, D. Fu, An integrated system of dielectric barrier discharge combined with wet electrostatic precipitator for simultaneous removal of NO and SO_2: Key factors assessments, products analysis and mechanism, Fuel 221 (2018) 12–20.
[75] B.M. Obradovic, G.B. Sretenovic, M.M. Kuraica, A dual-use of DBD plasma for simultaneous NO(x) and SO_2 removal from coal-combustion flue gas, J. Hazard. Mater. 185 (2011) 1280–1286.
[76] W.J. Liang, H.P. Fang, J. Li, F. Zheng, J.X. Li, Y.Q. Jin, Performance of non-thermal DBD plasma reactor during the removal of hydrogen sulfide, J. Electrostat. 69 (2011) 206–213.
[77] X. Dang, J. Huang, L. Kang, T. Wu, Q. Zhang, Research on Decomposition of Hydrogen Sulfide Using Nonthermal Plasma with Metal Oxide Catalysis, Energy Procedia 16 (2012) 856–862.
[78] R. Snoeckx, A. Bogaerts, Plasma technology - a novel solution for CO_2 conversion? Chem. Soc. Rev. 46 (2017) 5805–5863.
[79] A.H. Khoja, M. Tahir, N.A.S. Amin, Recent developments in non-thermal catalytic DBD plasma reactor for dry reforming of methane, Energ. Convers. Manage. 183 (2019) 529–560.
[80] W.C. Chung, M.B. Chang, Review of catalysis and plasma performance on dry reforming of CH_4 and possible synergistic effects, Renew. Sust. Energ. Rev. 62 (2016) 13–31.
[81] P. Peng, P. Chen, C. Schiappacasse, N. Zhou, E. Anderson, D. Chen, J. Liu, Y. Cheng, R. Hatzenbeller, M. Addy, Y. Zhang, Y. Liu, R. Ruan, A review on the non-thermal plasma-assisted ammonia synthesis technologies, J. Clean. Prod. 177 (2018) 597–609.
[82] J. Hong, S. Prawer, A.B. Murphy, Plasma Catalysis as an Alternative Route for Ammonia Production: Status, Mechanisms, and Prospects for Progress, ACS Sustain. Chem. Eng. 6 (2017) 15–31.
[83] T. Yamamoto, K. Ramanathan, P.A. Lawless, D.S. Ensor, J.R. Newsome, N. Plaks, G.H. Ramsey, C.A. Vogel, L. Hammel, Control of Volatile Organic Compounds by an ac Energized Ferroelectric Pellet Reactor and a Pulsed Corona Reactor, IEEE Trans. Ind. Appl. 28 (1992) 528–534.
[84] D. Evans, L.A. Rosocha, G.K. Anderson, J.J. Coogan, M.J. Kushner, Plasma remediation of trichloroethylene in silent discharge plasmas, J. Appl. Phy. 74 (1993) 5378–5386.
[85] T. Oda, T. Takahashi, H. Nakano, S. Masuda, Decomposition of Fluorocarbon Gaseous Contaminants by Surface Discharge-Induced Plasma Chemical Processing, IEEE Trans. Ind. Appl. 29 (1993) 787–792.
[86] M.B. Chang, C.C. Lee, Destruction of Formaldehyde with Dielectric Barrier Discharge Plasmas, Environ. Sci. Techno. 29 (1995) 181–186.
[87] T. Oda, R. Yamashita, T. Takahasi, S. Masuda, Atmospheric Pressure Discharge Plasma Processing for Gaseous Air Contaminants, IEEE Trans, Ind. Appl. 32 (1996) 227–232.
[88] T. Yamamoto, J.S. Chang, A.A. Berezin, H. Kohno, S. Honda, A. Shibuya, Decomposition of Toluene, o-Xylene, Trichloroethylene, and Their Mixture Using a $BaTiO_3$ Packed-Bed Plasma Reactor, J. Adv. Oxid. Technol. 1 (1996) 67–78.
[89] M.B. Chang, C.C. Chang, Destruction and Removal of Toluene and MEK from Gas Streams with Silent Discharge Plasmas, Aiche J. 43 (1997) 1325–1330.
[90] S. Futamura, A. Zhang, G. Prieto, T. Yamamoto, Factors and Intermediates Governing Byproduct Distribution for Decomposition of Butane in Nonthermal Plasma, IEEE Trans. Ind. Appl. 34 (1998) 967–974.
[91] A. Ogata, K. Yamanouchi, K. Mizuno, S. Kushiyama, T. Yamamoto, Decomposition of Benzene Using Alumina-Hybrid and Catalyst-Hybrid Plasma Reactors, IEEE T. Ind. Appl. 35 (1999) 1289–1295.
[92] J. Chae, S. Moon, H. Sun, K. Kim, V.A. Vassiliev, E.M. Mikholap, A Study of Volatile Organic Compounds Decomposition with the Use of Non-Thermal Plasma, KSME Int. J. 13 (1999) 647–655.
[93] A. Ogata, N. Shintani, K. Yamanouchi, S. Kushiyama, K. Mizuno, T. Yamamoto, Effect of Water Vapor on Benzene Decomposition Using a Nonthermal-Discharge Plasma Reactor, Plasma Chem. Plasma P. 20 (2000) 453-467.
[94] M.B. Chang, H.M. Lee, Gas-Phase Removal of Acetaldehyde via Packed-Bed Dielectric Barrier Discharge Reactor, Plasma Chem. Plasma P. 21 (2001) 329-343.
[95] F. Holzer, U. Roland, F.D. Kopinke, Combination of non-thermal plasma and heterogeneous catalysis for oxidation of volatile organic compounds Part 1. Accessibility of the intra-particle volume, Appl. Catal. B: Environ. 38 (2002) 163–181.
[96] H.M. Lee, M.B. Chang, Abatement of Gas-phase p-Xylene via Dielectric Barrier Discharges, Plasma Chem. Plasma P. 23 (2003) 541-558.
[97] H.H. Kim, S.M. Oh, A. Ogata, S. Futamura, Decomposition of benzene using $AgTiO_2$ packed plasma-driven catalyst reactor influence of electrode configuration and Ag-loading amount, Catal. Lett. 96 (2004) 189–194.
[98] S.M. Oh, H.H. Kim, A. Ogata, H. Einaga, S. Futamura, D.W. Park, Effect of zeolite in surface discharge plasma on the decomposition of toluene, Catal. Lett. 99 (2005) 101–104.
[99] C. Subrahmanyam, M. Magureanu, A. Renken, L. Kiwi-Minsker, Catalytic abatement of volatile organic compounds assisted by non-thermal plasma, Appl. Catal. B: Environ. 65 (2006) 150–156.
[100] Vladimir Demidyuk, J. Christopher Whitehead, Influence of temperature on gas-phase toluene decomposition in plasma-catalytic system, Plasma Chem. Plasma Process 27 (1) (2007) 85–94, https://doi.org/10.1007/s11090-006-9045-z.
[101] H.Y. Fan, C. Shi, X.S. Li, D.Z. Zhao, Y. Xu, A.M. Zhu, High-efficiency plasma catalytic removal of dilute benzene from air, J. Phy. D Appl. Phy. 42 (2009) 1–5.
[102] Atsushi Ogata, Keiichi Saito, Hyun-Ha Kim, Masami Sugasawa, Hirofumi Aritani, Hisahiro Einaga, Performance of an Ozone Decomposition Catalyst in Hybrid Plasma Reactors for Volatile Organic Compound Removal, Plasma Chem Plasma Process 30 (1) (2010) 33–42, https://doi.org/10.1007/s11090-009-9206-y.
[103] J. Karuppiah, E.L. Reddy, P.M. Reddy, B. Ramaraju, R. Karvembu, C. Subrahmanyam, Abatement of mixture of volatile organic compounds (VOCs) in a catalytic non-thermal plasma reactor, J. Hazard. Mater. 237–238 (2012) 283–289.
[104] W.J. Liang, L. Ma, H. Liu, J. Li, Toluene degradation by non-thermal plasma combined with a ferroelectric catalyst, Chemosphere 92 (2013) 1390–1395.
[105] Plasma Chem Plasma Process 34 (5) (2014) 1141–1156, https://doi.org/10.1007/s11090-014-9556-y.
[106] R. Zhu, Y. Mao, L. Jiang, J. Chen, Performance of chlorobenzene removal in a nonthermal plasma catalysis reactor and evaluation of its byproducts, Chem. Eng. J. 279 (2015) 463–471.
[107] O. Karatum, M.A. Deshusses, A comparative study of dilute VOCs treatment in a non-thermal plasma reactor, Chem. Eng. J. 294 (2016) 308–315.
[108] A.A. Assadi, A. Bouzaza, D. Wolbert, Comparative study between laboratory and large pilot scales for VOC's removal from gas streams in continuous flow surface discharge plasma, Chem. Eng. Res. Des. 106 (2016) 308–314.
[109] B. Wang, C. Chi, M. Xu, C. Wang, D. Meng, Plasma-catalytic removal of toluene over CeO_2 -MnOx catalysts in an atmosphere dielectric barrier discharge, Chem. Eng. J. 322 (2017) 679–692.
[110] N. Jiang, L. Guo, C. Qiu, Y. Zhang, K. Shang, N. Lu, J. Li, Y. Wu, Reactive species distribution characteristics and toluene destruction in the three-electrode DBD reactor energized by different pulsed modes, Chem. Eng. J. 350 (2018) 12–19.
[111] W.A. Saoud, A.A. Assadi, M. Guiza, A. Bouzaza, W. Aboussaoud, I. Soutrel, A. Ouederni, D. Wolbert, S. Rtimi, Abatement of ammonia and butyraldehyde under non-thermal plasma and photocatalysis: Oxidation processes for the removal of mixture pollutants at pilot scale, Chem. Eng. J. 344 (2018) 165–172.
[112] D. Dobslaw, O. Ortlinghaus, C. Dobslaw, A combined process of non-thermal plasma and a low-cost mineral adsorber for VOC removal and odor abatement in emissions of organic waste treatment plants, J. Environ. Chem. Eng. 6 (2018) 2281–2289.
[113] Y. Cai, X. Zhu, W. Hu, C. Zheng, Y. Yang, M. Chen, X. Gao, Plasma-catalytic decomposition of ethyl acetate over $LaMO_3$ (M = Mn, Fe, and Co) perovskite catalysts, J. Ind. Eng. Chem. 70 (2019) 447–452.
[114] Mohammad Sharif Hosseini, Hassan Asilian Mahabadi, Rasoul Yarahmadi, Removal of Toluene from Air Using a Cycled Storage-Discharge (CSD) Plasma Catalytic Process, Plasma Chem Plasma Process 39 (1) (2019) 125–142, https://doi.org/10.1007/s11090-018-9938-7.
[115] C. Qin, H. Guo, P. Liu, W. Bai, J. Huang, X. Huang, X. Dang, D. Yan, Toluene abatement through adsorption and plasma oxidation using ZSM-5 mixed with γ-Al2O3, TiO2 or BaTiO3, J. Ind. Eng. Chem. 63 (2018) 449–455.
[116] H. Zhang, K. Li, L. Li, L. Liu, X. Meng, T. Sun, J. Jia, M. Fan, High efficient styrene mineralization through novel NiO-TiO_2-Al_2O_3 packed pre-treatment/treatment/post-treatment dielectric barrier discharge plasma, Chem. Eng. J. 343 (2018) 759–769.
[117] N. Jiang, C. Qiu, L. Guo, K. Shang, N. Lu, J. Li, Y. Zhang, Y. Wu, Plasma-catalytic destruction of xylene over Ag-Mn mixed oxides in a pulsed sliding discharge reactor, J. Hazard. Mater. 369 (2019) 611–620.
[118] W. Xu, K. Lin, D. Ye, X. Jiang, J. Liu, Y. Chen, Performance of Toluene Removal in a Nonthermal Plasma Catalysis System over Flake-Like HZSM-5 Zeolite with Tunable Pore Size and Evaluation of Its Byproducts, Nanomaterials (Basel) 9 (2019).
[119] A. Jahanmiri, M.R. Rahimpour, M.M. Shirazi, N. Hooshmand, H. Taghvaei, Naphtha cracking through a pulsed DBD plasma reactor: Effect of applied voltage, pulse repetition frequency and electrode material, Chem. Eng. J. 191 (2012) 416–425.
[120] X. Yao, N. Jiang, J. Li, N. Lu, K. Shang, Y. Wu, An improved corona discharge ignited by oxide cathodes with high secondary electron emission for toluene degradation, Chem. Eng. J. 362 (2019) 339–348.
[121] J. Karuppiah, R. Karvembu, C. Subrahmanyam, The catalytic effect of MnOx and CoOx on the decomposition of nitrobenzene in a non-thermal plasma reactor, Chem. Eng. J. 180 (2012) 39–45.
[122] Y. Zhang, J. Nie, C. Yuan, Y. Long, M. Chen, J. Tao, Q. Wang, Y. Cong, CuO@Cu/Ag/MWNTs/sponge electrode-enhanced pollutant removal in dielectric barrier discharge (DBD) reactor, Chemosphere 229 (2019) 273–283.
[123] C. Qin, X. Dang, J. Huang, J. Teng, X. Huang, Plasma-catalytic oxidation of

adsorbed toluene on Ag–Mn/γ-Al_2O_3: Comparison of gas flow-through and gas circulation treatment, Chem. Eng. J. 299 (2016) 85–92.
[124] M. Bahri, F. Haghighat, S. Rohani, H. Kazemian, Metal organic frameworks for gas-phase VOCs removal in a NTP-catalytic reactor, Chem. Eng. J. 320 (2017) 308–318.
[125] M.S. Gandhi, Y.S. Mok, S.B. Lee, H. Park, Effect of various parameters for butane decomposition under ambient temperature in a dielectric barrier discharge non-thermal plasma reactor, J. Taiwan Inst. Chem. E. 44 (2013) 786–794.
[126] H.H. Kim, A. Ogata, S. Futamura, Oxygen partial pressure-dependent behavior of various catalysts for the total oxidation of VOCs using cycled system of adsorption and oxygen plasma, Appl. Catal. B: Environ. 79 (2008) 356–367.
[127] H. Baránková, L. Bárdos, Effect of the electrode material on the atmospheric plasma conversion of NO in air mixtures, Vacuum 84 (2010) 1385–1388.
[128] X. Jin, Y. Zhang, X. Jiang, R. Wang, Analysis of electrode material effect on organic exhaust gas decomposition by pulse plasma, China Environ. Sci. 18 (1998) 213–217.
[129] N. Jiang, N. Lu, J. Li, Y. Wu, Degradation of Benzene by Using a Silent-Packed Bed Hybrid Discharge Plasma Reactor, Plasma Sci. Technol. 14 (2012) 140–146.
[130] N. Jiang, N. Lu, K. Shang, J. Li, Y. Wu, Effects of electrode geometry on the performance of dielectric barrier/packed-bed discharge plasmas in benzene degradation, J. Hazard. Mater. 262 (2013) 387–393.
[131] W. Liang, J. Li, J. Li, Y. Jin, Abatement of toluene from gas streams via ferroelectric packed bed dielectric barrier discharge plasma, J. Hazard. Mater. 170 (2009) 633–638.
[132] H.H. Kim, A. Ogata, S. Futamura, Effect of different catalysts on the decomposition of VOCs using flow-type plasma-driven catalysis, IEEE T. Plasma Sci. 34 (2006) 984–995.
[133] L. Sivachandiran, J. Karuppiah, C. Subrahmanyam, DBD plasma reactor for oxidative decomposition of Chlorobenzene, Int. J. Chem. React. Eng. 10 (2012).
[134] M. Bahri, F. Haghighat, S. Rohani, H. Kazemian, Impact of design parameters on the performance of non-thermal plasma air purification system, Chem. Eng. J. 302 (2016) 204–212.
[135] H.H. Kim, S.M. Oh, A. Ogata, S. Futamura, Decomposition of gas-phase benzene using plasma-driven catalyst (PDC) reactor packed with Ag/TiO_2 catalyst, Appl. Catal. B: Environ. 56 (2005) 213–220.
[136] M. Magureanu, N.B. Mandache, V.I. Parvulescu, C. Subrahmanyam, A. Renken, L. Kiwi-Minsker, Improved performance of non-thermal plasma reactor during decomposition of trichloroethylene Optimization of the reactor geometry and introduction of catalytic electrode, Appl. Catal. B: Environ. 74 (2007) 270–277.
[137] A.H. Khoja, M. Tahir, N.A.S. Amin, Dry reforming of methane using different dielectric materials and DBD plasma reactor configurations, Energ. Convers. Manage. 144 (2017) 262–274.
[138] D. Mei, X. Tu, Conversion of CO_2 in a cylindrical dielectric barrier discharge reactor: Effects of plasma processing parameters and reactor design, J. CO_2 Util. 19 (2017) 68–78.
[139] Chung-Liang Chang, Hsunling Bai, Shu-Jen Lu, Destruction of Styrene in an Air Stream by Packed Dielectric Barrier Discharge Reactors, Plasma Chem Plasma Process 25 (6) (2005) 641–657, https://doi.org/10.1007/s11090-005-6818-8.
[140] H. Zhang, K. Li, T. Sun, J. Jia, Z. Lou, L. Feng, Removal of styrene using dielectric barrier discharge plasmas combined with sol–gel prepared TiO2 coated γ-Al_2O_3, Chem. Eng. J. 241 (2014) 92–102.
[141] B. Wang, W. Yan, W. Ge, X. Duan, Methane conversion into higher hydrocarbons with dielectric barrier discharge micro-plasma reactor, J. Energ. Chem. 22 (2013) 876–882.
[142] U. Roland, F. Holzer, F.D. Kopinke, Combination of non-thermal plasma and heterogeneous catalysis for oxidation of volatile organic compounds, Appl. Catal. B: Environ. 58 (2005) 217–226.
[143] C. Qin, H. Guo, W. Bai, J. Huang, X. Huang, X. Dang, D. Yan, Kinetics study on non-thermal plasma mineralization of adsorbed toluene over γ-Al_2O_3 hybrid with zeolite, J. Hazard. Mater. 369 (2019) 430–438.
[144] N. Jiang, C. Qiu, L. Guo, K. Shang, N. Lu, J. Li, Y. Wu, Post Plasma-Catalysis of Low Concentration VOC Over Alumina-Supported Silver Catalysts in a Surface/Packed-Bed Hybrid Discharge Reactor, Water Air Soil Poll. 228 (2017) 113.
[145] A.S. Chiper, N.B. Simiand, F. Jorand, S. Pasquiers, G. Popa, C. Postel, Influence of water vapour on acetaldehyde removal efficiency by DBD, J. Optoelectron. Adv. M. 8 (2006) 208–212.
[146] J.H. Byeon, J.H. Park, Y.S. Jo, K.Y. Yoon, J. Hwang, Removal of gaseous toluene and submicron aerosol particles using a dielectric barrier discharge reactor, J. Hazard. Mater. 175 (2010) 417–422.
[147] A. Ozkan, T. Dufour, A. Bogaerts, F. Reniers, How do the barrier thickness and dielectric material influence the filamentary mode and CO_2 conversion in a flowing DBD? Plasma Sources Sci. T. 25 (2016).
[148] M.S. Gandhi, Y.S. Mok, Decomposition of trifluoromethane in a dielectric barrier discharge non-thermal plasma reactor, J. Environ. Sci. 24 (2012) 1234–1239.
[149] Nan Jiang, Cheng Qiu, Lianjie Guo, Kefeng Shang, Na Lu, Jie Li, Yan Wu, Improved Performance for Toluene Abatement in a Continuous-Flow Pulsed Sliding Discharge Reactor Based on Three-Electrode Configuration, Plasma Chem Plasma Process 39 (1) (2019) 227–240, https://doi.org/10.1007/s11090-018-9939-6.
[150] A.S. Chiper, A. Nastuta, G. Rusu, G. Popa, Electrical characterisation of a double DBD in He at atmospheric pressure used for surface treatments, J. Optoelectron. Adv. M. 9 (2007) 2926–2931.
[151] H. Ma, P. Chen, M. Zhang. X. Lin, R. Ruan, Study of SO2 Removal Using Non-thermal Plasma Induced by Dielectric Barrier Discharge (DBD), Plasma Chem. Plasma P. 22 (2002) 239-254.
[152] T. Zhu, J. Li, W.J. Liang, Y.Q. Jin, Experimental Research on Toluene Decomposition with High Frequency DBD, High Voltage Eng. 35 (2009) 359–363.
[153] A. Meiners, M. Leck, B. Abel, Efficiency enhancement of a dielectric barrier plasma discharge by dielectric barrier optimization, Rev. Sci. Instrum. 81 (2010) 113507.
[154] M.F. Mustafa, X. Fu, Y. Liu, Y. Abbas, H. Wang, W. Lu, Volatile organic compounds (VOCs) removal in non-thermal plasma double dielectric barrier discharge reactor, J. Hazard. Mater. 347 (2018) 317–324.
[155] M.F. Mustafa, X. Fu, W. Lu, Y. Liu, Y. Abbas, H. Wang, M.T. Arslan, Application of non-thermal plasma technology on fugitive methane destruction: Configuration and optimization of double dielectric barrier discharge reactor, J. Clean. Prod. 174 (2018) 670–677.
[156] H. Zhang, K. Li, C. Shu, Z. Lou, T. Sun, J. Jia, Enhancement of styrene removal using a novel double-tube dielectric barrier discharge (DDBD) reactor, Chem. Eng. J. 256 (2014) 107–118.
[157] K.L. Pan, M.B. Chang, Plasma catalytic oxidation of toluene over double perovskite-type oxide via packed-bed DBD, Environ. Sci. Pollut. Res, Int, 2019.
[158] Z. Bo, H. Hao, S. Yang, J. Zhu, J. Yan, K. Cen, Vertically-oriented graphenes supported Mn_3O_4 as advanced catalysts in post plasma-catalysis for toluene decomposition, Appl. Surf. Sci. 436 (2018) 570–578.
[159] H. Zhang, K. Li, T. Sun, J. Jia, X. Yang, Y. Shen, J. Wang, Z. Lou, The removal of styrene using a dielectric barrier discharge (DBD) reactor and the analysis of the by-products and intermediates, Res. Chem. Intermediat. 39 (2012) 1021–1035.
[160] T. Chang, Z. Shen, Y. Huang, J. Lu, D. Ren, J. Sun, J. Cao, H. Liu, Post-plasma-catalytic removal of toluene using MnO_2–Co_3O_4 catalysts and their synergistic mechanism, Chem. Eng. J. 348 (2018) 15–25.
[161] T. Chang, J. Lu, Z. Shen, Y. Huang, D. Lu, X. Wang, J. Cao, R. Morent, Simulation and optimization of the post plasma-catalytic system for toluene degradation by a hybrid ANN and NSGA-II method, Appl. Catal. B: Environ. 244 (2019) 107–119.
[162] T. Zhu, Y.D. Wan, J. Li, X.W. He, D.Y. Xu, X.Q. Shu, W.J. Liang, Y.Q. Jin, Volatile organic compounds decomposition using nonthermal plasma coupled with a combination of catalysts, Int. J. Environ. Sci. Tech. 8 (2011) 621–630.
[163] C. Subrahmanyam, A. Renken, L. Kiwi-Minsker, Catalytic abatement of volatile organic compounds assisted by non-thermal plasma, Appl. Catal. B: Environ. 65 (2006) 157–162.
[164] A. Ozkan, T. Dufour, T. Silva, N. Britun, R. Snyders, A. Bogaerts, F. Reniers, The influence of power and frequency on the filamentary behavior of a flowing DBD—application to the splitting of CO_2, Plasma Sources Sci. T. 25 (2016) 025013.
[165] I. Radu, R. Bartnikas, M.R. Wertheimer, Frequency and voltage dependence of glow and pseudoglow discharges in helium under atmospheric pressure, IEEE T. Plasma Sci. 31 (2003) 1363–1378.
[166] S. Gadkari, S. Gu, Numerical investigation of co-axial DBD: Influence of relative permittivity of the dielectric barrier, applied voltage amplitude, and frequency, Phys. Plasmas 24 (2017) 053517.
[167] R.V. Barrientos, J.P. Sotelo, M.P. Pacheco, J.S.B. Read, R.L. Callejas, Analysis and electrical modelling of a cylindrical DBD configuration at different operating frequencies, Plasma Sources Sci. T. 15 (2006) 237–245.
[168] J.M. Williamson, D.D. Trump, P. Bletzinger, B.N. Ganguly, Comparison of high-voltage ac and pulsed operation of a surface dielectric barrier discharge, J. Phys. D: Appl. Phys. 39 (2006) 4400–4406.
[169] H. Jiang, T. Shao, C. Zhang, Z. Niu, Y. Yu, P. Yan, Y. Zhou, Comparison of AC and Nanosecond-Pulsed DBDs in Atmospheric Air, IEEE T. Plasma Sci. 39 (2011) 2076–2077.
[170] D. Yuan, S. Tang, J. Qi, N. Li, J. Gu, H. Huang, Comparison of hydroxyl radicals generation during granular activated carbon regeneration in DBD reactor driven by bipolar pulse power and alternating current power, Vacuum 143 (2017) 87–94.
[171] H. Wang, D. Li, Y. Wu, J. Li, G. Li, Effect of Power Supply Mode on Removal of Benzene by DBD-Catalysis, High Voltage Eng. 35 (2009) 2759–2763.
[172] V.R. Chirumamilla, W.F.L.M. Hoeben, F.J.C.M. Beckers, T. Huiskamp, E.J.M. Van Heesch, A.J.M. Pemen, Experimental Investigation on the Effect of a Microsecond Pulse and a Nanosecond Pulse on NO Removal Using a Pulsed DBD with Catalytic Materials, Plasma Chem Plasma Process 36 (2) (2016) 487–510, https://doi.org/10.1007/s11090-015-9670-5.
[173] S. Zhang, W. Wang, P. Jiang, D. Yang, L. Jia, S. Wang, Comparison of atmospheric air plasmas excited by high-voltage nanosecond pulsed discharge and sinusoidal alternating current discharge, J. Appl. Phys. 114 (2013) 163301.
[174] A.E. Wallis, J.C. Whitehead, K. Zhang, Plasma-assisted catalysis for the destruction of CFC-12 in atmospheric pressure gas streams using TiO_2, Catal. Lett. 113 (2007) 29–33.
[175] Z. Jia, X. Wang, F. Thevenet, A. Rousseau, Dynamic probing of plasma-catalytic surface processes: Oxidation of toluene on CeO_2, Plasma Process. Polym. 14 (2017) 1600114.
[176] Q.H. Trinh, Y.S. Mok, Effect of the adsorbent/catalyst preparation method and plasma reactor configuration on the removal of dilute ethylene from air stream, Cataly. Today 256 (2015) 170–177.
[177] H.T. Quoc An, T. Pham Huu, T. Le Van, J.M. Cormier, A. Khacef, Application of atmospheric non thermal plasma-catalysis hybrid system for air pollution control: Toluene removal, Cataly. Today 176 (2011) 474–477.
[178] Hong-Yu Fan, Xiao-Song Li, Chuan Shi, De-Zhi Zhao, Jing-Lin Liu, Yan-Xia Liu, Ai-Min Zhu, Plasma Catalytic Oxidation of Stored Benzene in a Cycled Storage-Discharge (CSD) Process: Catalysts, Reactors and Operation Conditions, Plasma Chem Plasma Process 31 (6) (2011) 799–810, https://doi.org/10.1007/s11090-011-9320-5.
[179] X. Fan, T. Zhu, Y. Sun, X. Yan, The roles of various plasma species in the plasma and plasma-catalytic removal of low-concentration formaldehyde in air, J. Hazard. Mater. 196 (2011) 380–385.
[180] T.P. Huu, S. Gil, P.D. Costa, A.G. Fendler, A. Khacef, Plasma catalytic hybrid

reactor Application to methane removal, Cataly. Today 257 (2015) 86–92.
[181] H. Huang, D. Ye, X. Guan, The simultaneous catalytic removal of VOCs and O_3 in a post-plasma, Cataly. Today 139 (2008) 43–48.
[182] J. Van Durme, J. Dewulf, W. Sysmans, C. Leys, H. Van Langenhove, Efficient toluene abatement in indoor air by a plasma catalytic hybrid system, Appl. Catal. B: Environ. 74 (2007) 161–169.
[183] L. Sivachandiran, F. Thevenet, A. Rousseau, Isopropanol removal using Mn_XO_Y packed bed non-thermal plasma reactor: Comparison between continuous treatment and sequential sorption/regeneration, Chem. Eng. J. 270 (2015) 327–335.
[184] S. Veerapandian, C. Leys, N. De Geyter, R. Morent, Abatement of VOCs Using Packed Bed Non-Thermal Plasma Reactors: A Review, Catalysts 7 (2017).
[185] A. Ogata, N. Shintani, K. Mizuno, S. Kushiyama, T. Yamamoto, Decomposition of Benzene Using a Nonthermal Plasma Reactor Packed with Ferroelectric Pellets, IEEE T. Ind. Appl. 35 (1999) 753–759.
[186] H.J. Gallon, X. Tu, J.C. Whitehead, Effects of Reactor Packing Materials on H_2 Production by CO_2 Reforming of CH_4 in a Dielectric Barrier Discharge, Plasma Process. Polym. 9 (2012) 90–97.
[187] K.V. Laer, A. Bogaerts, Influence of Gap Size and Dielectric Constant of the Packing Material on the Plasma Behaviour in a Packed Bed DBD Reactor A Fluid Modelling Study, Plasma Process. Polym. 14 (2017) 1600129.
[188] Y.R. Zhang, E.C. Neyts, A. Bogaerts, Influence of the Material Dielectric Constant on Plasma Generation inside Catalyst Pores, J. Phys. Chem. C 120 (2016) 25923–25934.
[189] Hyun-Ha Kim, Yoshiyuki Teramoto, Atsushi Ogata, Hideyuki Takagi, Tetsuya Nanba, Plasma Catalysis for Environmental Treatment and Energy Applications, Plasma Chem Plasma Process 36 (1) (2016) 45–72, https://doi.org/10.1007/s11090-015-9652-7.
[190] K. Takaki, K. Urashima, J.S. Chang, Ferro-Electric Pellet Shape Effect on C_2F_6 Removal by a Packed-Bed-Type Nonthermal Plasma, Reactor, IEEE T. Plasma Sci. 32 (2004) 2175–2183.
[191] M.S. Gandhi, A. Ananth, Y.S. Mok, J. Song, K.H. Park, Effect of porosity of a-alumina on non-thermal plasma decomposition of ethylene in a dielectric-packed bed reactor, Res. Chem. Intermed. 40 (2014) 1483–1493.
[192] S. Li, X. Yu, X. Dang, H. Guo, P. Liu, C. Qin, Using non-thermal plasma for decomposition of toluene adsorbed on γ-Al_2O_3 and ZSM-5: Configuration and optimization of a double dielectric barrier discharge reactor, Chem. Eng. J. 375 (2019) 122027.
[193] W. Wang, H. Wang, T. Zhu, X. Fan, Removal of gas phase low-concentration toluene over Mn, Ag and Ce modified HZSM-5 catalysts by periodical operation of adsorption and non-thermal plasma regeneration, J. Hazard. Mater. 292 (2015) 70–78.
[194] W. Xu, X. Xu, J. Wu, M. Fu, L. Chen, N. Wang, H. Xiao, X. Chen, D. Ye, Removal of toluene in adsorption–discharge plasma systems over a nickel modified SBA-15 catalyst, RSC Advances 6 (2016) 104104–104111.
[195] T. Wang, S. Chen, H. Wang, Z. Liu, Z. Wu, In-plasma catalytic degradation of toluene over different MnO_2 polymorphs and study of reaction mechanism, Chinese J. Catal. 38 (2017) 793–803.
[196] Y.R. Zhang, E.C. Neyts, A. Bogaerts, Enhancement of plasma generation in catalyst pores with different shapes, Plasma Sources Sci. T. 27 (2018).
[197] H.L. Chen, H.M. Lee, S.H. Chen, M.B. Chang, Review of Packed-Bed Plasma Reactor for Ozone Generation and Air Pollution Control, Ind. Eng. Chem. Res. 47 (2008) 2122–2130.
[198] J.S. Chang, A. Chakrabart, K. Urashima, M. Arai, The Effects of Barium Titanate Pellet Shapes on the Gas Discharge Characteristics of Ferroelectric Packed Bed Reactors, Proc. Conf. Electr. Insul. Dielectr. Phenom. (1998).
[199] J. Li, H. Na, X. Zeng, T. Zhu, Z. Liu, In situ DRIFTS investigation for the oxidation of toluene by ozone over Mn/HZSM-5, Ag/HZSM-5 and Mn–Ag/HZSM-5 catalysts, Appl. Surf. Sci. 311 (2014) 690–696.
[200] X. Zhu, X. Gao, X. Yu, C. Zheng, X. Tu, Catalyst screening for acetone removal in a single-stage plasma-catalysis system, Cataly. Today 256 (2015) 108–114.
[201] J. Wu, Y. Huang, Q. Xia, Z. Li, Decomposition of Toluene in a Plasma Catalysis System with NiO, MnO2, CeO2, Fe2O3, and CuO Catalysts, Plasma Chem. Plasma P. 33 (2013) 1073–1082.
[202] C. Norsic, J.M. Tatibouët, C.B. Dupeyrat, E. Fourré, Non thermal plasma assisted catalysis of methanol oxidation on Mn, Ce and Cu oxides supported on γ-Al_2O_3, Chem. Eng. J. 304 (2016) 563–572.
[203] R. Peng, X. Sun, S. Li, L. Chen, M. Fu, J. Wu, D. Ye, Shape effect of Pt/CeO_2 catalysts on the catalytic oxidation of toluene, Chem. Eng. J. 306 (2016) 1234–1246.
[204] R. Peng, S. Li, X. Sun, Q. Ren, L. Chen, M. Fu, J. Wu, D. Ye, Size effect of Pt nanoparticles on the catalytic oxidation of toluene over Pt/CeO_2 catalysts, Appl. Catal. B: Environ. 220 (2018) 462–470.
[205] H. Song, F. Hu, Y. Peng, K. Li, S. Bai, J. Li, Non-thermal plasma catalysis for chlorobenzene removal over CoMn/TiO_2 and CeMn/TiO_2: Synergistic effect of chemical catalysis and dielectric constant, Chem. Eng. J. 347 (2018) 447–454.
[206] X. Zhu, S. Liu, Y. Cai, X. Gao, J. Zhou, C. Zheng, X. Tu, Post-plasma catalytic removal of methanol over Mn–Ce catalysts in an atmospheric dielectric barrier discharge, Appl. Catal. B: Environ. 183 (2016) 124–132.
[207] N. Jiang, J. Hu, J. Li, K. Shang, N. Lu, Y. Wu, Plasma-catalytic degradation of benzene over Ag–Ce bimetallic oxide catalysts using hybrid surface/packed-bed discharge plasmas, Appl. Catal. B: Environ. 184 (2016) 355–363.
[208] X. Zhu, X. Gao, R. Qin, Y. Zeng, R. Qu, C. Zheng, X. Tu, Plasma-catalytic removal of formaldehyde over Cu–Ce catalysts in a dielectric barrier discharge reactor, Appl. Catal. B: Environ. 170–171 (2015) 293–300.
[209] C. Qin, X. Huang, X. Dang, J. Huang, J. Teng, Z. Kang, Toluene removal by sequential adsorption-plasma catalytic process: Effects of Ag and Mn impregnation sequence on Ag-Mn/gamma-Al_2O_3, Chemosphere 162 (2016) 125–130.
[210] H.J. Gallon, H.H. Kim, X. Tu, J.C. Whitehead, Microscope–ICCD Imaging of an Atmospheric Pressure CH_4 and CO_2 Dielectric Barrier Discharge, IEEE T. Plasma Sci. 39 (2011) 2176–2177.
[211] H.H. Kim, Y. Teramoto, T. Sano, N. Negishi, A. Ogata, Effects of Si/Al ratio on the interaction of nonthermal plasma and Ag/HY catalysts, Appl. Catal. B: Environ. 166–167 (2015) 9–17.
[212] H.H. Kim, A. Ogata, Nonthermal plasma activates catalyst: from current understanding and future prospects, Eur. Phys. J. Appl. Phys. 55 (2011) 13806.
[213] W. Wang, H.H. Kim, K.V. Laer, A. Bogaerts, Streamer propagation in a packed bed plasma reactor for plasma catalysis applications, Chem. Eng. J. 334 (2018) 2467–2479.
[214] S. Gadkari, S. Gu, Influence of catalyst packing configuration on the discharge characteristics of dielectric barrier discharge reactors: A numerical investigation, Phys. Plasmas 25 (2018) 063513.
[215] Y.R. Zhang, K. Van Laer, E.C. Neyts, A. Bogaerts, Can plasma be formed in catalyst pores? A modeling investigation, Appl. Catal. B: Environ. 185 (2016) 56–67.
[216] X. Tu, H.J. Gallon, M.V. Twigg, P.A. Gorry, J.C. Whitehead, Dry reforming of methane over a Ni/Al_2O_3catalyst in a coaxial dielectric barrier discharge reactor, J. Phy. D: Appl. Phy. 44 (2011) 274007.
[217] Z. Wu, Z. Zhu, X. Hao, W. Zhou, J. Han, X. Tang, S. Yao, X. Zhang, Enhanced oxidation of naphthalene using plasma activation of TiO2/diatomite catalyst, J. Hazard. Mater. 347 (2018) 48–57.
[218] B. Wang, X. Xu, W. Xu, N. Wang, H. Xiao, Y. Sun, H. Huang, L. Yu, M. Fu, J. Wu, L. Chen, D. Ye, The Mechanism of Non-thermal Plasma Catalysis on Volatile Organic Compounds Removal, Catal. Surv. Asia 22 (2018) 73–94.
[219] B. Wang, B. Chen, Y. Sun, H. Xiao, X. Xu, M. Fu, J. Wu, L. Chen, D. Ye, Effects of dielectric barrier discharge plasma on the catalytic activity of Pt/CeO_2 catalysts, Appl. Catal. B: Environ. 238 (2018) 328–338.
[220] A.S. Pribytkov, G.N. Baeva, N.S. Telegina, A.L. Tarasov, A.Y. Stakheev, A.V. Tel'nov, V.N. Golubeva, Effect of electron irradiation on the catalytic properties of supported Pd catalysts, Kinet. Catal. 47 (2006) 765–769.
[221] S. Kameshima, K. Tamura, Y. Ishibashi, T. Nozaki, Pulsed dry methane reforming in plasma-enhanced catalytic reaction, Cataly. Today 256 (2015) 67–75.
[222] W. Xu, N. Wang, Y. Chen, J. Chen, X. Xu, L. Yu, L. Chen, J. Wu, M. Fu, A. Zhu, D. Ye, In situ FT-IR study and evaluation of toluene abatement in different plasma catalytic systems over metal oxides loaded γ-Al_2O_3, Catal. Commun. 84 (2016) 61–66.
[223] M. Shirazi, E.C. Neyts, A. Bogaerts, DFT study of Ni-catalyzed plasma dry reforming of methane, Appl. Catal. B: Environ. 205 (2017) 605–614.
[224] E.C. Neyts, A. Bogaerts, Understanding plasma catalysis through modelling and simulation—a review, J. Phy. D: Appl. Phy. 47 (2014).
[225] H.H. Kim, Y. Teramoto, N. Negishi, A. Ogata, A multidisciplinary approach to understand the interactions of nonthermal plasma and catalyst: A review, Cataly. Today 256 (2015) 13–22.
[226] E.C. Neyts, K. Ostrikov, Nanoscale thermodynamic aspects of plasma catalysis, Cataly. Today 256 (2015) 23–28.
[227] X. Feng, H. Liu, C. He, Z. Shen, T. Wang, Synergistic effects and mechanism of a non-thermal plasma catalysis system in volatile organic compound removal: a review, Catal. Sci. Technol. 8 (2018) 936–954.
[228] H.L. Chen, H.M. Lee, S.H. Chen, M.B. Chang, S.J. Yu, S.N. Li, Removal of Volatile Organic Compounds by Single-Stage and Two-Stage Plasma Catalysis Systems: A Review of the Performance Enhancement Mechanisms, Current Status, and Suitable Applications, Environ. Sci. Technol. 43 (2009) 2216–2227.
[229] H. Puliyalil, D. Lašič Jurković, V.D.B.C. Dasireddy, B. Likozar, A review of plasma-assisted catalytic conversion of gaseous carbon dioxide and methane into value-added platform chemicals and fuels, RSC Adv. 8 (2018) 27481–27508.
[230] W.C. Chung, D.H. Mei, X. Tu, M.B. Chang, Removal of VOCs from gas streams via plasma and catalysis, Catal. Rev. 61 (2018) 270–331.
[231] X. Zhao, X. Liu, J. Liu, J. Chen, S. Fu, F. Zhong, The effect of ionization energy and hydrogen weight fraction on the non-thermal plasma volatile organic compounds removal efficiency, J. Phy. D: Appl. Phy. 52 (2019).
[232] H.H. Kim, A. Ogata, S. Futamura, Atmospheric plasma-driven catalysis for the low temperature decomposition of dilute aromatic compounds, J. Phy. D: Appl. Phy. 38 (2005) 1292–1300.
[233] D. Dobslaw, A. Schulz, S. Helbich, C. Dobslaw, K.-H. Engesser, VOC removal and odor abatement by a low-cost plasma enhanced biotrickling filter process, J. Environ. Chem. Eng. 5 (2017) 5501–5511.
[234] S.L. Hill, H.H. Kim, S. Futamura, J.C. Whitehead, The Destruction of Atmospheric Pressure Propane and Propene Using a Surface Discharge Plasma Reactor, J. Phys. Chem. A 112 (2008) 3953–3958.
[235] J. Li, H. Zhang, D. Ying, Y. Wang, T. Sun, J. Jia, In Plasma Catalytic Oxidation of Toluene Using Monolith CuO Foam as a Catalyst in a Wedged High Voltage Electrode Dielectric Barrier Discharge Reactor: Influence of Reaction Parameters and Byproduct Control, Int. J. Environ. Res. Public Health 16 (2019).
[236] X. Yao, J. Zhang, X. Liang, C. Long, Plasma-catalytic removal of toluene over the supported manganese oxides in DBD reactor: Effect of the structure of zeolites support, Chemosphere 208 (2018) 922–930.
[237] B. Wang, S. Yao, Y. Peng, Y. Xu, Toluene removal over TiO_2-$BaTiO_3$ catalysts in an atmospheric dielectric barrier discharge, J. Environ. Chem. Eng. 6 (2018) 3819–3826.
[238] B. Dou, D. Liu, Q. Zhang, R. Zhao, Q. Hao, F. Bin, J. Cao, Enhanced removal of toluene by dielectric barrier discharge coupling with Cu-Ce-Zr supported ZSM-5/TiO_2/Al_2O_3, Catal. Commun. 92 (2017) 15–18.
[239] X. Xu, P. Wang, W. Xu, J. Wu, L. Chen, M. Fu, D. Ye, Plasma-catalysis of metal loaded SBA-15 for toluene removal: Comparison of continuously introduced and

adsorption-discharge plasma system, Chem. Eng. J. 283 (2016) 276–284.
[240] L. Mao, Z. Chen, X. Wu, X. Tang, S. Yao, X. Zhang, B. Jiang, J. Han, Z. Wu, H. Lu, T. Nozaki, Plasma-catalyst hybrid reactor with CeO_2/γ -Al_2O_3 for benzene decomposition with synergetic effect and nano particle by-product reduction, J. Hazard. Mater. 347 (2018) 150–159.
[241] S. Hamada, H. Hojo, H. Einaga, Effect of catalyst composition and reactor configuration on benzene oxidation with a nonthermal plasma-catalyst combined reactor, Cataly, Today, 2018.
[242] J. Hu, N. Jiang, J. Li, K. Shang, N. Lu, Y. Wu, Degradation of benzene by bipolar pulsed series surface/packed-bed discharge reactor over MnO_2 –TiO_2/zeolite catalyst, Chem. Eng. J. 293 (2016) 216–224.
[243] X. Dang, C. Qin, J. Huang, J. Teng, X. Huang, Adsorbed benzene/toluene oxidation using plasma driven catalysis with gas circulation: Elimination of the byproducts, J. Ind. Eng. Chem. 37 (2016) 366–371.
[244] X. Zhang, Y. Huang, Z. Liu, K. Yan, Aerosol emission and collection in styrene-contaminated air remediation with a multi-stage plasma system, J. Electrostat. 76 (2015) 31–38.
[245] T. Shou, N. Xu, Y. Li, G. Sun, M.T. Bernards, Y. Shi, Y. He, Mechanisms of Xylene Isomer Oxidation by Non-thermal Plasma via Paired Experiments and Simulations, Plasma Chem, Plasma P, 2019.
[246] Plasma Chem Plasma Process 36 (6) (2016) 1501–1515, https://doi.org/10.1007/s11090-016-9741-2.
[247] T. Kuroki, K. Hirai, R. Kawabata, M. Okubo, T. Yamamoto, Decomposition of Adsorbed Xylene on Adsorbents Using Nonthermal Plasma With Gas Circulation, IEEE T. Ind. Appl. 46 (2010) 672–679.
[248] X. Zhu, X. Tu, D. Mei, C. Zheng, J. Zhou, X. Gao, Z. Luo, M. Ni, K. Cen, Investigation of hybrid plasma-catalytic removal of acetone over CuO/γ-Al_2O_3 catalysts using response surface method, Chemosphere 155 (2016) 9–17.
[249] C. Zheng, X. Zhu, X. Gao, L. Liu, Q. Chang, Z. Luo, K. Cen, Experimental study of acetone removal by packed-bed dielectric barrier discharge reactor, J. Ind. Eng. Chem. 20 (2014) 2761–2768.
[250] H.Q. Trinh, Y.S. Mok, Plasma-catalytic oxidation of acetone in annular porous monolithic ceramic-supported catalysts, Chem. Eng. J. 251 (2014) 199–206.
[251] K. Saulich, S. Müller, Removal of formaldehyde by adsorption and plasma treatment of mineral adsorbent, J. Phy. D: Appl. Phy. 46 (2013).
[252] D.Z. Zhao, X.S. Li, C. Shi, H.Y. Fan, A.M. Zhu, Low-concentration formaldehyde removal from air using a cycled storage–discharge (CSD) plasma catalytic process, Chem. Eng. Sci. 66 (2011) 3922–3929.
[253] C. Klett, X. Duten, S. Tieng, S. Touchard, P. Jestin, K. Hassouni, A. Vega-Gonzalez, Acetaldehyde removal using an atmospheric non-thermal plasma combined with a packed bed: role of the adsorption process, J. Hazard. Mater. 279 (2014) 356–364.
[254] D.H. Lee, T. Kim, Effect of Catalyst Deactivation on Kinetics of Plasma-Catalysis for Methanol Decomposition, Plasma Process. Polym. 11 (2014) 455–463.
[255] S. Lovascio, N. Blin-Simiand, L. Magne, F. Jorand, S. Pasquiers, Experimental Study and Kinetic Modeling for Ethanol Treatment by Air Dielectric Barrier Discharges, Plasma Chem Plasma Process 35 (2) (2015) 279–301, https://doi.org/10.1007/s11090-014-9601-x.
[256] I. Aouadi, J.-M. Tatibouët, L. Bergaoui, MnOx/TiO_2 Catalysts for VOCs Abatement by Coupling Non-thermal Plasma and Photocatalysis, Plasma Chem Plasma Process 36 (6) (2016) 1485–1499, https://doi.org/10.1007/s11090-016-9740-3.
[257] H. Lee, D.H. Lee, Y.H. Song, W.C. Choi, Y.K. Park, D.H. Kim, Synergistic effect of non-thermal plasma–catalysis hybrid system on methane complete oxidation over Pd-based catalysts, Chem. Eng. J. 259 (2015) 761–770.
[258] T.P. Huu, L. Sivachandiran, P. Da Costa, A. Khacef, Methane, Propene and Toluene Oxidation by Plasma-Pd/γ-Al_2O_3 Hybrid Reactor: Investigation of a Synergetic Effect, Top. Catal. 60 (2016) 326–332.
[259] Tarryn Blackbeard, Vladimir Demidyuk, Sarah L. Hill, J. Christopher Whitehead, The Effect of Temperature on the Plasma-Catalytic Destruction of Propane and Propene: A Comparison with Thermal Catalysis, Plasma Chem Plasma Process 29 (6) (2009) 411–419, https://doi.org/10.1007/s11090-009-9189-8.
[260] J. Tang, W. Zhao, Y. Duan, In-Depth Study on Propane-Air Combustion Enhancement With Dielectric Barrier Discharge, IEEE T. Plasma Sci. 38 (2010) 3272–3281.
[261] P.V. Julien Jarrige, Plasma-enhanced catalysis of propane and isopropyl alcohol at ambient temperature on a MnO_2-based catalyst, Appl. Catal. B: Environ. 90 (2009) 74–82.
[262] C. Trionfetti, A. Ağıral, J.G.E. Gardeniers, L. Lefferts, K. Seshan, Oxidative Conversion of Propane in a Microreactor in the Presence of Plasma over MgO-Based Catalysts An Experimental Study, J. Phys. Chem. C 112 (2008) 4267–4274.
[263] Olivier Aubry, Jean-Marie Cormier, Improvement of the Diluted Propane Efficiency Treatment Using a Non-thermal Plasma, Plasma Chem Plasma Process 29 (1) (2009) 13–25, https://doi.org/10.1007/s11090-008-9161-z.
[264] A. Ağıral, C. Trionfetti, L. Lefferts, K. Seshan, J.G.E. Gardeniers, Propane Conversion at Ambient Temperatures C-C and C-H Bond Activation Using Cold Plasma in a Microreactor, Chem. Eng. Technol. 31 (2008) 1116–1123.
[265] Q.H. Trinh, S.B. Lee, Y.S. Mok, Removal of ethylene from air stream by adsorption and plasma-catalytic oxidation using silver-based bimetallic catalysts supported on zeolite, J. Hazard. Mater. 285 (2015) 525–534.
[266] T. Pham, H. Bui, A. Khacef, Oxidation of propene from air by atmospheric plasma-catalytic hybrid system, J. Serbian Chem. Soc. 83 (2018) 641–649.
[267] V. Gaikwad, E. Kennedy, J. Mackie, C. Holdsworth, S. Molloy, S. Kundu, M. Stockenhuber, B. Dlugogorski, Reaction of dichloromethane under non-oxidative conditions in a dielectric barrier discharge reactor and characterisation of the resultant polymer, Chem. Eng. J. 290 (2016) 499–506.
[268] Z.A. Allah, J.C. Whitehead, P. Martin, Remediation of dichloromethane (CH_2Cl_2) using non-thermal, atmospheric pressure plasma generated in a packed-bed reactor, Environ. Sci. Technol 48 (2014) 558–565.
[269] A.E. Wallis, J.C. Whitehead, K. Zhang, The removal of dichloromethane from atmospheric pressure nitrogen gas streams using plasma-assisted catalysis, Appl. Catal. B: Environ. 74 (2007) 111–116.
[270] A.E. Wallis, J.C. Whitehead, K. Zhang, The removal of dichloromethane from atmospheric pressure air streams using plasma-assisted catalysis, Appl. Catal. B: Environ. 72 (2007) 282–288.
[271] C. Fitzsimmons, F. Ismail, J.C. Whitehead, J.J. Wilman, The Chemistry of Dichloromethane Destruction in Atmospheric-Pressure Gas Streams by a Dielectric Packed-Bed Plasma Reactor, J. Phys. Chem. A 104 (2000) 6032–6038.
[272] B. Ulejczyk, Decomposition of Halocarbons in the Pulsed Dielectric Barrier Discharge, International Conference on Optimization of Electrical & Electronic Equipment (2014) 1053–1059.
[273] K. Krawczyk, B. Ulejczyk, H.K. Song, A. Lamenta, B. Paluch, K. Schmidt-Szałowski, Plasma-catalytic Reactor for Decomposition of Chlorinated Hydrocarbons, Plasma Chem Plasma Process 29 (1) (2009) 27–41, https://doi.org/10.1007/s11090-008-9159-6.
[274] A.A. Gushchin, V.I. Grinevich, T.V. Izvekova, E.Yu. Kvitkova, K.A. Tyukanova, V.V. Rybki, The Destruction of Carbon Tetrachloride Dissolved in Water in a Dielectric Barrier Discharge in Oxygen, Plasma Chem, Plasma P, 2019.
[275] L. Jiang, G. Nie, R. Zhu, J. Wang, J. Chen, Y. Mao, Z. Cheng, W.A. Anderson, Efficient degradation of chlorobenzene in a non-thermal plasma catalytic reactor supported on CeO_2/HZSM-5 catalysts, J. Environ. Sci. (China) 55 (2017) 266–273.
[276] F.G. Shahna, A. Bahrami, I. Alimohammadi, R. Yarahmadi, B. Jaleh, M. Gandomi, H. Ebrahimi, K.A. Abedi, Chlorobenzene degeradation by non-thermal plasma combined with EG-TiO_2/ZnO as a photocatalyst: Effect of photocatalyst on CO_2 selectivity and byproducts reduction, J. Hazard. Mater. 324 (2017) 544–553.
[277] D.H. Kim, Y.S. Mok, S.B. Lee, Effect of temperature on the decomposition of trifluoromethane in a dielectric barrier discharge reactor, Thin Solid Films 519 (2011) 6960–6963.
[278] D.B. Nguyen, W.G. Lee, Effects of ambient gas on cold atmospheric plasma discharge in the decomposition of trifluoromethane, RSC Adv. 6 (2016) 26505–26513.
[279] D.H. Kim, Y.S. Mok, S.B. Lee, S.M. Shin, Nonthermal Plasma Destruction of Trifluoromethane Using a Dielectric- Packed Bed Reactor, J. Adv. Oxid. Technol. 13 (2010) 36–42.
[280] S. Sultana, A.M. Vandenbroucke, M. Mora, C. Jiménez-Sanchidrián, F.J. Romero-Salguero, C. Leys, N. De Geyter, R. Morent, Post plasma-catalysis for trichloroethylene decomposition over CeO_2 catalyst: synergistic effect and stability test, Appl. Catal. B: Environ. 253 (2019) 49–59.
[281] A.M. Vandenbroucke, M.T. Nguyen Dinh, N. Nuns, J.M. Giraudon, N. De Geyter, C. Leys, J.F. Lamonier, R. Morent, Combination of non-thermal plasma and Pd/$LaMnO_3$ for dilute trichloroethylene abatement, Chem. Eng. J. 283 (2016) 668–675.
[282] M.T. Nguyen Dinh, J.M. Giraudon, A.M. Vandenbroucke, R. Morent, N. De Geyter, J.F. Lamonier, Manganese oxide octahedral molecular sieve K-OMS-2 as catalyst in post plasma-catalysis for trichloroethylene degradation in humid air, J. Hazard. Mater. 314 (2016) 88–94.
[283] M.T.N. Dinh, J.M. Giraudon, A.M. Vandenbroucke, R. Morent, N. De Geyter, J.F. Lamonier, Post plasma-catalysis for total oxidation of trichloroethylene over Ce–Mn based oxides synthesized by a modified “redox-precipitation route”, Appl. Catal. B: Environ. 172–173 (2015) 65–72.
[284] S. Sultana, Z. Ye, S.K.P. Veerapandian, A. Löfberg, N. De Geyter, R. Morent, J.-M. Giraudon, J.-F. Lamonier, Synthesis and catalytic performances of K-OMS-2, Fe/K-OMS-2 and Fe-K-OMS-2 in post plasma-catalysis for dilute TCE abatement, Cataly. Today 307 (2018) 20–28.
[285] A.M. Vandenbroucke, M. Mora, C. Jiménez-Sanchidrián, F.J. Romero-Salguero, N. De Geyter, C. Leys, R. Morent, TCE abatement with a plasma-catalytic combined system using MnO_2 as catalyst, Appl. Catal. B: Environ. 156–157 (2014) 94–100.
[286] F. Holzer, F.D. Kopinke, U. Roland, Non-thermal plasma treatment for the elimination of odorous compounds from exhaust air from cooking processes, Chem. Eng. J. 334 (2018) 1988–1995.
[287] J. Chen, J. Yang, H. Pan, Q. Su, Y. Liu, Y. Shi, Abatement of malodorants from pesticide factory in dielectric barrier discharges, J. Hazard. Mater. 177 (2010) 908–913.
[288] T. Kuwahara, M. Okubo, T. Kuroki, H. Kametaka, T. Yamamoto, Odor removal characteristics of a laminated film-electrode packed-bed nonthermal plasma reactor, Sensors (Basel) 11 (2011) 5529–5542.
[289] C.W. Park, J.H. Byeon, K.Y. Yoon, J.H. Park, J. Hwang, Simultaneous removal of odors, airborne particles, and bioaerosols in a municipal composting facility by dielectric barrier discharge, Sep. Purif. Technol. 77 (2011) 87–93.
[290] M. Hołub, R. Brandenburg, H. Grosch, S. Weinmann, B. Hansel, Plasma Supported Odour Removal from Waste Air in Water Treatment Plants: An Industrial Case Study, Aerosol Air Qual. Res. 14 (2014) 697–707.
[291] J.S. Youn, J. Bae, S. Park, Y.K. Park, Plasma-assisted oxidation of toluene over Fe/zeolite catalyst in DBD reactor using adsorption/desorption system, Catal. Commun. 113 (2018) 36–40.
[292] Y.F. Guo, D.Q. Ye, K.F. Chen, J.C. He, W.L. Chen, Toluene decomposition using a wire-plate dielectric barrier discharge reactor with manganese oxide catalyst in situ, J. Mol. Catal. A: Chem. 245 (2006) 93–100.
[293] M. Lu, R. Huang, J. Wu, M. Fu, L. Chen, D. Ye, On the performance and mechanisms of toluene removal by FeOx/SBA-15-assisted non-thermal plasma at atmospheric pressure and room temperature, Cataly. Today 242 (2015) 274–286.
[294] J. Chen, Z. Xie, J. Tang, J. Zhou, X. Lu, H. Zhao, Oxidation of toluene by dielectric barrier discharge with photo-catalytic electrode, Chem. Eng. J. 284 (2016)

166–173.
[295] Z. Falkenstein, J.J. Coogan, Microdischarge behaviour in the silent discharge of nitrogen - oxygen and water - air mixtures, J. Phys. D: Appl. Phys. 30 (1997) 817–825.
[296] H.P. Nguyen, M.J. Park, S.B. Kim, H.J. Kim, L.J. Baik, Y.M. Jo, Effective dielectric barrier discharge reactor operation for decomposition of volatile organic compounds, J. Clean. Prod. 198 (2018) 1232–1238.
[297] Chengzhu Zhu, Ying Liu, Jun Lu, Zhe Yang, Yunxia Li, Tianhu Chen, Decomposition of Ethanethiol Using Dielectric Barrier Discharge Combined with 185 nm UV-Light Technique, Plasma Chem Plasma Process 35 (2) (2015) 355–364, https://doi.org/10.1007/s11090-014-9609-2.
[298] H. Huang, D. Ye, D.Y.C. Leung, Abatement of Toluene in the Plasma-Driven Catalysis: Mechanism and Reaction Kinetics, IEEE T. Plasma Sci. 39 (2011) 877–882.
[299] J. Wu, Q. Xia, H. Wang, Z. Li, Catalytic performance of plasma catalysis system with nickel oxide catalysts on different supports for toluene removal: Effect of water vapor, Appl. Catal. B: Environ. 156–157 (2014) 265–272.
[300] X. Fan, T. Zhu, Y. Wan, X. Yan, Effects of humidity on the plasma-catalytic removal of low-concentration BTX in air, J. Hazard. Mater. 180 (2010) 616–621.
[301] Z. Ye, Y. Zhang, P. Li, L. Yang, R. Zhang, H. Hou, Feasibility of destruction of gaseous benzene with dielectric barrier discharge, J. Hazard. Mater. 156 (2008) 356–364.
[302] A.A. Assadi, A. Bouzaza, I. Soutrel, P. Petit, K. Medimagh, D. Wolbert, A study of pollution removal in exhaust gases from animal quartering centers by combining photocatalysis with surface discharge plasma: From pilot to industrial scale, Chem. Eng. Process. 111 (2017) 1–6.
[303] P. Liang, W. Jiang, L. Zhang, J. Wu, J. Zhang, D. Yang, Experimental studies of removing typical VOCs by dielectric barrier discharge reactor of different sizes, Process Saf. Environ. 94 (2015) 380–384.
[304] L.M. Martini, G. Coller, M. Schiavon, A. Cernuto, M. Ragazzi, G. Dilecce, P. Tosi, Non-thermal plasma in waste composting facilities: From a laboratory-scale experiment to a scaled-up economic model, J. Clean. Prod. 230 (2019) 230–240.
[305] M. Schmidt, I. Jõgi, M. Hołub, R. Brandenburg, Non-thermal plasma based decomposition of volatile organic compounds in industrial exhaust gases, Int. J. Environ. Sci. Te. 12 (2015) 3745–3754.

JONIX
pure living

NON THERMAL PLASMA E VIRUS

PAPER

Inactivation of airborne viruses using a packed bed non-thermal plasma reactor

To cite this article: T Xia *et al* 2019 *J. Phys. D: Appl. Phys.* **52** 255201

IOP Publishing
Journal of Physics D: Applied Physics
J. Phys. D: Appl. Phys. **52** (2019) 255201 (12pp)
https://doi.org/10.1088/1361-6463/ab1466

Inactivation of airborne viruses using a packed bed non-thermal plasma reactor

T Xia[1,3], A Kleinheksel[1], E M Lee[2], Z Qiao[1], K R Wigginton[1] and H L Clack[1]

[1] Department of Civil and Environmental Engineering, University of Michigan, Ann Arbor, MI, United States of America
[2] Department of Mechanical, Materials, and Aerospace Engineering, Illinois Institute of Technology, Chicago, IL, United States of America

E-mail: xiatian@umich.edu

Received 28 November 2018, revised 25 March 2019
Accepted for publication 28 March 2019
Published 23 April 2019

Abstract

Outbreaks of airborne infectious diseases such as measles or severe acute respiratory syndrome can cause significant public alarm. Where ventilation systems facilitate disease transmission to humans or animals, there exists a need for control measures that provide effective protection while imposing minimal pressure differential. In the present study, viral aerosols in an airstream were subjected to non-thermal plasma (NTP) exposure within a packed-bed dielectric barrier discharge reactor. Comparisons of plaque assays before and after NTP treatment found exponentially increasing inactivation of aerosolized MS2 phage with increasing applied voltage. At 30 kV and an air flow rate of 170 standard liters per minute, a greater than 2.3 log reduction of infective virus was achieved across the reactor. This reduction represented ~2 log of the MS2 inactivated and ~0.35 log physically removed in the packed bed. Increasing the air flow rate from 170 to 330 liters per minute did not significantly impact virus inactivation effectiveness. Activated carbon-based ozone filters greatly reduced residual ozone, in some cases down to background levels, while adding less than 20 Pa pressure differential to the 45 Pa differential pressure across the packed bed at the flow rate of 170 standard liters per minute.

Keywords: non-thermal plasma, bioaerosol inactivation, bacteriophage MS2, ozone, plaque assay, qPCR

Supplementary material for this article is available online

(Some figures may appear in colour only in the online journal)

Introduction

Airborne infectious disease outbreaks such as measles, tuberculosis, and severe acute respiratory syndrome (SARS) can cause risk of infection by the essential and involuntary action of respiration. Airborne disease transmission, the processes governing it, and the development of protective measures against it, are less understood than transmission via water, food, arthropod vectors, and direct contact with infected individuals. Disease transmission among humans and animals often involves either direct contact with an infected individual or transport across very short distances; however, pathogen transmission over longer distances can also occur. The SARS outbreak within the Amoy Gardens housing complex in Hong Kong [1] was spread between apartments by sewer main gases drawn in by improperly sized ventilation fans and poorly maintained drains.

Livestock diseases such as Newcastle disease, avian influenza, hoof-and-mouth disease, porcine reproductive and respiratory syndrome (PRRS), and African swine flu are potential threats to global food security. In pork and poultry production, biosecurity measures for preventing the introduction of pathogens into animal confinement buildings primarily protect against disease spread through direct contact between animals and from pathogen-contaminated surfaces. PRRS and avian

[3] Author to whom any correspondence should be addressed.

1361-6463/19/255201+12$33.00

and porcine influenza are two examples of high impact diseases for which biosecurity measures have been implemented to prevent airborne transmission. The virus that causes PRRS is understood to survive transmission through the atmosphere in greater numbers when atmospheric conditions are cool, damp, or cloudy [2]. Long-term changes in climate and their influences on infectious disease outbreaks vary by route of transmission and are highly uncertain [3]. While increasing vector populations with increasing annual average temperature and precipitation could increase vector-borne transmission, the influences of changing meteorological conditions on airborne transmission of pathogens are unclear.

In contexts where humans or animals move freely, the potential for disease transmission through direct contact is greater, reducing the importance of airborne transmission and greatly limiting the utility of airborne pathogen inactivation. However, where airborne transmission is or is suspected of being an important transmission route, few mitigation technologies exist. Disinfection by UV irradiation requires UV doses involving a combination of radiative fluxes and exposure times that have been established [4], which are difficult to implement in air. Upper-room UV irradiation relies on natural air circulation patterns within a room to transport airborne pathogens into the illumination zone of a wall-mounted, upward facing UV fixture near the ceiling. Upper room UV was proven effective in reducing TB transmission in hospital wards [5] and rubella transmission within army barracks [6]. UV germicidal irradiation (UVGI) directs UV radiation onto conventional particulate filters within ventilation systems to inactivate bacteria and viruses captured on the filter surfaces [7]; however, viruses and bacteria that migrate into the filter media or that are shielded from the UV source as subsequent particles are collected, are inactivated with lower efficiencies [7]. The US EPA concludes that there is insufficient evidence, and no standard test procedures, for assessing UVGI performance and that UVGI provides virtually no additional protection over the use of conventional HEPA filtration alone [8]. Conventional filtration presents several drawbacks, including the low fluid permeability needed for high particle collection efficiency, which inherently increases the differential pressure across the filter and promotes infiltration of untreated air into indoor spaces at partial vacuum. In buildings not constructed to an air-tight standard, this can lead to high costs of building reconstruction and retrofit.

Two factors govern the potential for disease transmission of airborne pathogens such as viruses and bacteria: aerosol *transport* and aerosol *infectivity* [9]. UV radiation alone only addresses aerosol infectivity and particle filtration only addresses aerosol transport. Unlike filtration and UV irradiation, non-thermal plasmas (NTPs) can address *both* transport (by charge-driven filtration) *and* infectivity (by reaction with reactive plasma species) of airborne pathogens. NTP is a result of electrical discharges within a neutral gas under atmospheric conditions and mainly consists of electrons, ions, and radicals. Unlike thermal plasma, where all constituents are in thermal equilibrium, a NTP in comparison is always in a state of non-equilibrium because the electrons with very light masses can reach higher temperatures (10^4–2.5×10^5 K) and attain higher kinetic energy (1–20 eV) than the rest of the NTP constituents, which are heavier and at lower temperatures [10]. On these bases, an NTP is also known as non-equilibrium plasma or cold plasma. A commonly applied NTP reactor type is the dielectric barrier discharge (DBD) reactor. DBD or silent discharge refers to the electrical discharge through a dielectric barrier, such as glass, quartz, or alumina. A high voltage AC source is commonly used in a DBD reactor, because the changing polarity of AC is essential to sustain the electrical discharge in a DBD reactor. The dominant electrical discharge mode in a DBD reactor is microdischarge, which is in a form of filaments with nanosecond lifespan. When the microdischarge reaches a dielectric barrier, the dielectric surface allows for the spreading and accumulation of the charges and thus reduces the electric field until the field is completely quenched. The use of an AC source repeats the cycle by generating microdischarge with a different electrical polarity. In studying the effectiveness of removing air pollutants such as methyl tert-butyl ether (MTBE) by NTP, Holzer *et al* [11] utilized a gaseous plasma generated by a DBD reactor using different dielectric barriers including glass, Al_2O_3, and TiO_2. Kuwahara *et al* [12] developed a DBD reactor using polyester-laminated electrodes to evaluate the removal characteristics of odorous compounds, including NH_3 and NH_3 mixed with CH_3CHO, by NTP. In studying oil mist-to-gas conversion, Park *et al* [13] developed a DBD reactor using thin copper electrodes (0.05 mm thickness) where each electrode was sandwiched in between by two dielectric plates made of alumina (1 mm thickness).

A packed-bed reactor provides a more efficient way of treating trace air pollutants by adding pellets between the electrodes in a corona reactor or a DBD reactor. A typical air pollutant has a concentration in the range of parts per million by volume (ppmv), so direct interactions between the electrons and air pollutants are usually negligible under ambient conditions [10]. In a packed-bed reactor, the electron-impact reactions serve as the main plasma chemistry for air pollutant decomposition [14]. By packing the pellets, electron generation takes place through partial discharges at the pellet contact points within a packed-bed reactor. More specifically, an external electric field applied between the pellets and the electrodes enables polarization, which in turn induces partial discharges and subsequently the electron-impact reactions. While a packed-bed arrangement can provide evenly distributed flows, it can also lead to a higher pressure drop across the packed-bed. Perovskite pellets, such as $BaTiO_3$ and Al_2O_3 are commonly used dielectric materials for packed-bed reactors. The addition of catalytically active materials can further improve the selectivity of a packed-bed reactor. Mizuno *et al* [15, 16] discovered that a ferroelectric pellet packed-bed reactor was not only capable of collecting particles, but also destroying yeast cells. In studying organic solvents (e.g. MTBE, toluene, and acetone), Holzer *et al* [11] evaluated three packed-bed materials (i.e. glass beads, $BaTiO_3$, and $PbZrO_3$–$PbTiO_3$) and one catalyst (i.e. $LaCoO_3$) using various cylindrical DBD reactors designs, which showed that the ferroelectric packed-bed reactor using $BaTiO_3$ pellets significantly increased the conversion of MTBE and toluene to CO_x. Kuwahara *et al* [12] used a ferroelectric packed-bed reactor

to study the decomposition of odorous compounds (i.e. NH_3) by adding $BaTiO_3$ pellets to the previously developed DBD reactor, which used polyester-laminated electrodes. The results showed that the DBD reactor with ferroelectric packed-bed pellets could decompose NH_3 at a much faster rate than the DBD reactor alone.

Researchers [17, 18] have reported reductions in infective airborne pathogen concentrations as a result of NTP treatment, results that included confounding effects of extended exposure of viral aerosols to ozone [17] or loss of viral aerosols by charge-driven filtration [18]. In one study, a DBD NTP reactor with 10 s plasma exposure and a very high air flow rate (25 l s^{-1}) resulted in 97% *Escherichia coli* inactivation [17]. The research group found that the synergetic action of short-living plasma agents, such as hydroxyl radicals, and plasma-generated ozone, achieved the previously measured 97% in-flight inactivation of aerosolized *E. coli* [19]. Another research group constructed a 12 mm diameter DBD NTP device and reported >95% inactivation of bacteria and 85%–98% inactivation of fungal species with a 24 W reactor energy output and a flow rate of 28.3 LPM (liters per minute) [20]. That same team examined NTP inactivation of MS2 and reported over 95% MS2 airstream inactivation with a 28 W reactor energy output at 12.5 LPM flow rate [18]. None of these research, however, examined the airstream inactivation performance of a reactor with a pack-bed feature.

In this study, we describe the development and performance of a packed-bed NTP in-flight airstream disinfection process. A DBD NTP reactor was constructed to treat an air stream seeded with viral aerosols. Aerosols of bacteriophage MS2 were generated by the evaporation of fine mists produced by ultrasonic atomization. Plaque assay and quantitative polymerase chain reaction (qPCR) analyses were conducted to determine the abundance of infective and total MS2 aerosols, respectively, in the pre- and post-treatment samples. Ultimately, the ability to remove residual ozone with carbon filters was assessed. A maximum of 2.3 log reduction of infective MS2 virus was achieved by the reactor, demonstrating NTP is a viable technology for in-flight disinfection and the prevention of airborne virus transmission.

Materials and methods

Experimental setup

The experimental apparatus (figure 1) for NTP inactivation of viral aerosols includes: (1) an induced draft (ID) fan, (2) a DBD reactor, (3) an aerosol generator, (4) a digital oscilloscope, (5) a high voltage amplifier, and (6) a digital function generator. The aerosol generator is a modified consumer-grade cool-mist humidifier (Vicks V5100-N) that piezoelectrically atomizes virus buffer solution containing MS2, a single-stranded RNA bacteriophage. A 10.2 cm (4-inch) ID fan at the end of the apparatus draws ambient air (25%–36% RH) into a flexible duct (8.9 cm (3.5-inch) ID and 4 m (13-ft) length), where mixing occurs between the air and the droplets, allowing for droplet evaporation and thus bioaerosol generation. The droplet evaporation process is further enhanced by the addition of a facility-supplied stream of dry compressed air (<10% RH; figure 1). The DBD reactor is powered by one of the two AC voltage amplifiers, namely a variable 0 to 20 kV (peak-to-peak) high voltage amplifier (Trek Model-610E) and a 30 kV neon transformer (France 15030 P5G-2UE ServiceMaster). The variable 0 to 20 kV high voltage amplifier is coupled with a digital function generator (BK Precision Model-4052), which outputs 60 Hz sinusoidal AC voltage. The amplifier can output applied voltage (U) signals at 1 V/1000 V and two current (I) signals, total current and return current, at 1 V/200 μA, which can be monitored directly by a digital oscilloscope (BK Precision Model-2190D). For the 30 kV neon transformer, a high voltage probe (Cal Test Electronics CT2700, 1 V/1000 V) and a Pearson current coil (Model 6585, 1V/1A) are connected to one of the power supply's high voltage electrodes (the schematic is illustrated in figure S1 in the supplementary information, available online (stacks.iop.org/JPhysD/52/255201/mmedia)), whose output signals are monitored by the digital oscilloscope. The power (P) of the reactor was therefore calculated according to the equation:

$$P = \frac{1}{T}\int_T U \times I dt \quad (1)$$

where T is the period of the AC voltage. A honeycomb-structured ozone filter (figure 1; Burnett Process Inc. BP-4810) is located downstream of the reactor to remove ozone from the exhaust. Two impingers installed upstream and downstream (figure 1) of the reactor enabled the quantification of virus inactivation by the NTP reactor.

NTP and reactor design

The NTP reactor developed in the present study utilizes the characteristics of DBD and packed-bed discharge for the application of viral aerosol inactivation. Figure 2 is a close-up schematic of the DBD packed-bed reactor. The reactor is composed of one larger Plexiglas tube (10.2 cm (4-inch) OD, 9.5 cm (3.75-inch) ID, 20.3 cm (8-inch) length) and two smaller tubes (8.9 cm (3.5-inch) OD, 7.6 cm (3-inch) ID, 30.5 cm (12-inch) length). The smaller tubes slide freely relative to the larger tube due to a clearance of 0.3 cm (0.125-inch). Two rubber O-rings, which sit in the grooves on the OD of the smaller tube permit an air-tight sliding mechanism. As indicated in figure 2, a circular perforated brass plate is installed at the end of each sliding tube to serve as the ground electrode and to evenly distribute the inlet and outlet flow of the reactor. The design of the sliding electrode allows for packed bed depth adjustment ranging between 0.6 and 12.7 cm (0.25 and 6 inches). A brass ring (0.9 mm (0.035-inch) thickness, 2.5 cm (1-inch) width) adhered to the OD of the larger Plexiglas tube serves as the high voltage electrode for the AC high voltage supply. Two flow plugs made of styrofoam (6.35 cm (2.5-inch) OD) are positioned at the center of the reactor to direct the airflow with viral aerosols through an annular region in which the plasma is concentrated (figure 2). The DBD reactor utilizes the microdischarge generated through a dielectric barrier made of Plexiglas. The packed-bed, consisting of 500 inert borosilicate glass beads (0.6 cm (0.25-inch) diameter), further

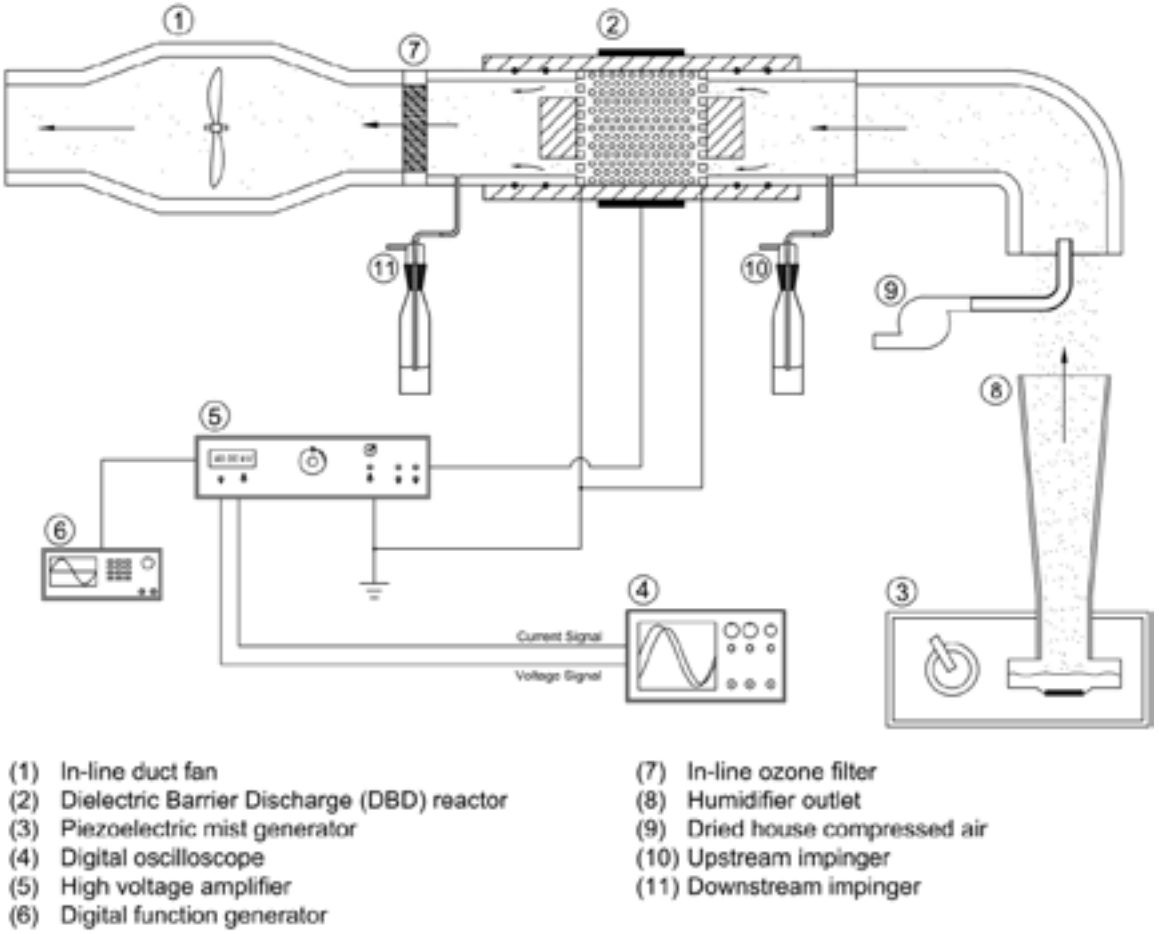

Figure 1. Experimental setup for the inactivation of viral aerosols with the 0–20 kV variable amplifier.

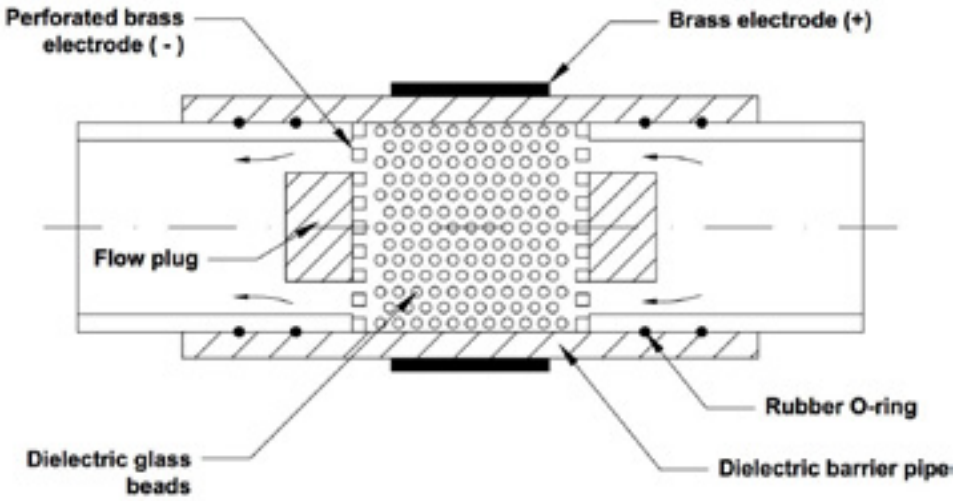

Figure 2. Schematic of the DBD packed-bed reactor.

enhances the microdischarge by partial discharges at the contact points between the glass beads for effective electron-viral aerosol collisions and inactivation process.

Experimental procedure

During the virus inactivation tests, a consumer-grade ultrasonic humidifier was used to generate MS2 viral aerosols from the original virus solution. Each inactivation test involved adding 300 ml (for a 60 min test) or 200 ml (for a 30 min test) of MS2 solution consisting of ~1×10^8 pfu ml^{-1} in phosphate-buffered saline (PBS; 0.78 g NaH_2PO_4/L, 0.58 g NaCl/L, pH of 7.5) into the ultrasonic humidifier reservoir. The humidifier was set to built-in power level 2 (labeled as H2) and the atomization rate was approximately 117 ml h^{-1} over a 30 min experimental period [21]. The air flow rate through

the sampling train was maintained by the ID fan with a viable transformer (Staco Energy 3PN221B). In each test, the ID fan and humidifier were turned on for five minutes until reaching steady state. Then the packed-bed NTP reactor was activated by the selected high voltage supply. An electric vacuum pump (McMaster–Carr model #4176K11) was turned on to draw samples from the air stream near the inner wall of the pipe through the impingers (ACE Glass 7533-13) upstream and downstream of the reactor at 1 LPM, leading to collection of MS2 aerosols in the 20 ml impinger collection fluid (PBS).

For inactivation tests with the reactor powered by the 0–20 kV variable amplifier, the sampling time was 30 min. For tests with the 30 kV transformer, the sampling time was 60 min in order to collect a higher number of viable viruses within the impinger installed downstream of the reactor (figure 1). Virus samples were also collected directly from the ultrasonic humidifier reservoir before each trial. Plaque assays and reverse transcriptase quantitative polymerase chain reaction (RT-qPCR) assays, both described in detail below, were performed on each sample to determine the concentration of infectious MS2 plaque forming units (pfu/ml) and the concentration of MS2 genome copies (gc/ml) in the PBS collecting solution. To compare the humidifier reservoir samples with impinger samples, all of the acquired infectious MS2 concentrations in aqueous PBS solutions were converted to concentrations in the air stream using the following two mass balance equations:

$$C_{8,air} = \dot{V} \times \frac{C_3}{\dot{Q}_{air}} \tag{2}$$

$$C_{10,air} = \frac{V_{impinger} C_{10}}{\dot{Q}_{sample} t_{sample}};\ C_{11,air} = \frac{V_{impinger} C_{11}}{\dot{Q}_{sample} t_{sample}} \tag{3}$$

where $\dot{V}$ is the average ultrasonic atomization rate (117 ml h^{-1}), C_3 is the measured infective MS2 concentrations in samples acquired from the humidifier reservoir (position 3 in figure 1) immediately before each test. C_{10} and C_{11} are the infective MS2 concentrations in the impingers (positions 10 and 11 in figure 1 respectively). $C_{8,air}$, $C_{10,air}$ and $C_{11,air}$ are converted infectious MS2 concentrations in the airstream at the humidifier outlet and at the upstream and downstream sampling points, respectively. $\dot{Q}_{air}$ is the air flow rate through the apparatus, $V_{impinger}$ is the volume of PBS in each of the impingers (20 ml), and $\dot{Q}_{sample}$ and t_{sample} are, respectively, air flow rates through the impingers (1 LPM) and the standard elapsed time allowed for sampling (30 or 60 min). It should be noted that the MS2 inactivation in the reservoir during atomization is not considered in the calculation of $C_{8,air}$, so the calculated results should be good approximations rather than true values. According to our previous study, there may be a 0.3 log reduction of viable MS2 concentration in the humidifier reservoir during the 30 min test, but this inactivation would not affect the estimation of the NTP reactor inactivation efficiency as long as viable MS2 are measured in the upstream impinger [21]. Similarly, total virus genome concentrations (both infective and inactivated) were assessed with qPCR and measured as genome copies per milliliter of solution (gc/ml), corrected with equations (2) and (3), and reported as genome copies per liter of air.

MS2 propagation and enumeration. Bacteriophage MS2 (ATCC 15597-B1) and its corresponding *E. coli* host ATCC 15597 was purchased from American Type Culture Collection (ATCC). MS2 was propagated and assayed in its *E. coli* host using previously published methods [22, 23]. The virus stocks were purified using an Econo Fast Protein Liquid Chromatography system (Bio-Rad, USA) with a HiPrep Sephacryl S-400 HR column (GE, USA). The purified virus fractions were concentrated with 100 kDa Amicon ultracentrifugal filters (Millipore, USA), and finally filter-sterilized with 0.22 μm PES membrane filters. The final MS2 stocks (~10^{11} pfu ml^{-1} were stored in phosphate buffer (5 mM NaH_2PO_4 and 10 mM NaCl, pH 7.5) at 4 °C. In the experiments, the detection limit was 10 pfu ml^{-1} since only 100 μl of a sample was used for each plate.

RT-qPCR. Viral RNA was extracted from 200 μl MS2 virus samples using Maxwell 16 Viral Total Nucleic Acid Purification Kits (Promega, Madison, WI) according to the manufacturer's instructions. Extracted RNA was eluted using 50 μl of nuclease-free water. The forward primer (5′-CCGCTACCTTGCCCTAAAC-3′) and reverse primer (5′-GACGACAACCATGCCAAAC-3′) were designed with the Primer3free software (http://primer3.sourceforge.net/) and purchased from ThermoFisher Scientific (Grand Island, NY). Extracted MS2 RNA samples and RNA standards were reverse transcribed and amplified in parallel in an Eppendorf Mastercycler ep realplex Real-time PCR System (Eppendorf, Hauppauge, NY). Each reverse transcription-qPCR reaction was run in 20 μl of total volume comprising 10 μl of GoTaq 1-Step Master Mix, 0.4 μl of RT mix, 0.6 μl each of 10 μM forward and reverse primers, 6.4 μl of nuclease-free water and 2 μl of RNA sample (Promega, Madison, WI). The following thermocycling conditions were used: 15 min at 40 °C; 10 min at 95 °C; and 45 cycles of 95 °C for 15 s, 60 °C for 30 s and 72 °C for 40s, followed by a melting ramp from 68 to 95 °C, with the temperature held for 45 s at 60 °C and for 5 s at all subsequent temperatures.

Measurements of system performance. During the experiment, a portable humidity/temperature pen (Traceable 4093) measured the temperature and relative humidity (RH) inside the sampling train upstream of the reactor. An insertable anemometer (Extech 407123) measured the air stream radial velocity profile ~30.5 cm (12-inch) downstream of the reactor. The pressure drops across the packed-bed NTP reactor and the ozone filter were measured by a low-pressure differential gauge (Magnehelic 2300-0). When the reactor was powered by the 0–20 kV variable amplifier, an oscilloscope (BK Precision Model-2190D) monitored the applied voltage and current to the packed-bed NTP reactor, from which the input and discharge power can be calculated. When the reactor was powered by the fixed 30kV transformer, the total input power consumption of the transformer was measured by an electricity power meter (P3 International P4460), and the discharge power was measured by a high voltage probe and a Pearson coil, as discussed in the experimental setup section. To ensure that collected MS2 would not be inactivated in the impinger

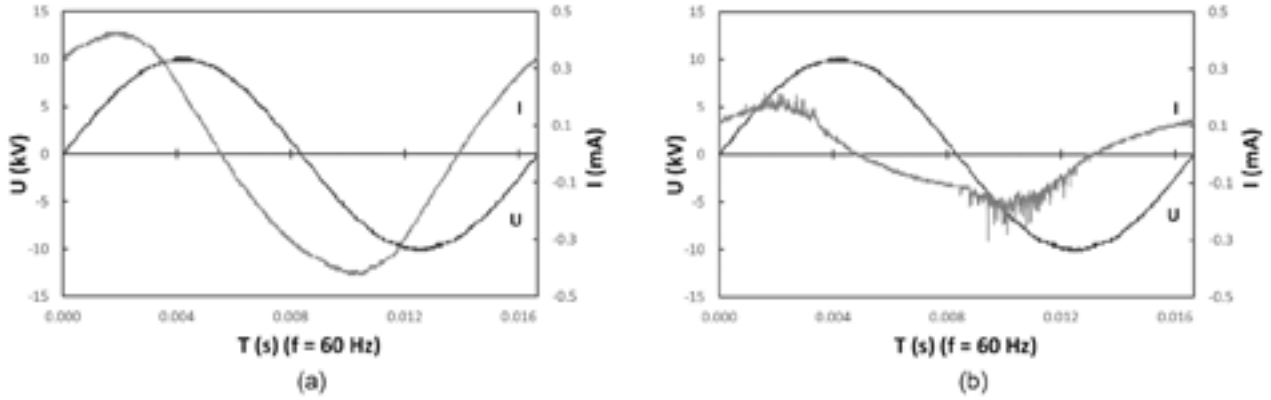

Figure 3. Applied voltage and (a) total current or (b) return current waveform acquired by the oscilloscope with 20 kV peak-to-peak voltage.

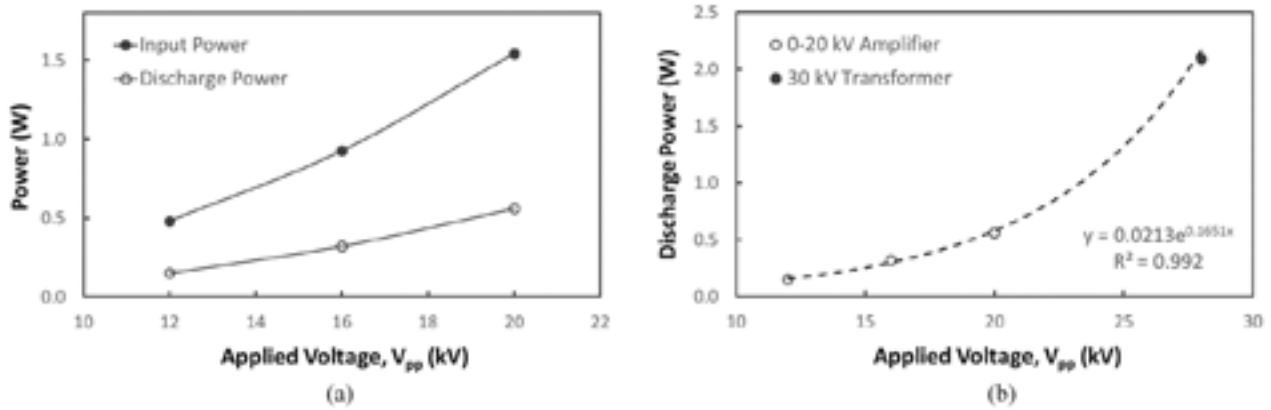

Figure 4. (a) Input and discharge power of the reactor at 12 kV, 16 kV and 20 kV applied voltage with the 0–20 kV variable amplifier; (b) estimated discharge power showed a strong exponential correlation with the applied voltage with both high voltage power supplies.

liquid during sampling, 20 ml of 1×10^6 pfu ml^{-1} MS2-PBS solution was added into the downstream impinger, which was then connected to the downstream sampling port. The packed-bed NTP reactor was either inactivated or activated by the 20 kV voltage supply, and the effluent gas from the reactor was bubbled through the impinger liquid for 15, 30 and 45 min, after which the infectious MS2 concentrations in the impinger were assayed. Ozone generated by the packed-bed NTP reactor when energized had the potential to dissolve into sampling liquid in the downstream impinger and inactivate MS2 during and after sample collection. To quench the ozone in solution, 50 mM of anhydrous sodium sulfite (Na_2SO_3, Fisher Scientific BP355-500) was added into the downstream 20 ml impinger collection liquid. An ozone sensor (EcoSensors A-21ZX) measured the ozone concentration either upstream of the ozone filter (downstream of the reactor) or downstream of the filter to determine the amount of ozone generated by the packed-bed NTP reactor at various power and flow rate levels and to examine the removal efficiency of ozone by the ozone filter.

Results and discussion

Operating conditions

In this study, the overall air flow rate through the sampling train was estimated to be 170 LPM at 30% voltage setting of the ID fan and 330 LPM at 60% voltage setting, by integrating the measured air velocity profile along the pipe radius. The pressure difference upstream and downstream of the NTP DBD packed bed measured at the 170 LPM flow rate was 45 Pa, a reasonably low difference due to the high porosity of the packed bed. The ozone filter was also quite porous, with a honeycomb structure that produced a pressure drop of 20 Pa at the flow rate of 170 LPM. The total pressure drop across the system was about 65 Pa at the flow rate of 170 LPM, or 0.38 Pa/LPM. It was estimated that at 170 LPM, the virus exposure time to NTP species was about 0.25 s.

Typical applied voltage and current waveforms measured by the oscilloscope are presented in figure 3, and all voltage and current waveforms at all voltage setups (12 kV, 16 kV, 20 kV and 30 kV) can be found in the supporting information. Two current waveforms were measured: the total current represented the current supplied into the system and was used to calculate input power; the return current represented the current returned to the supply from the ground electrode, and was used to calculate NTP discharge power. When applied voltage increased from 12 kV to 20 kV, the input power increased from 0.5 W to 1.5 W and the discharge power increased from 0.2 W to 0.6 W, 31%–36% of the input power (figure 4(a)). Kuwahara *et al* [12] reported similar differences (76%) between input and discharge power, and two other research reported that 20%–27% of the input power was converted to

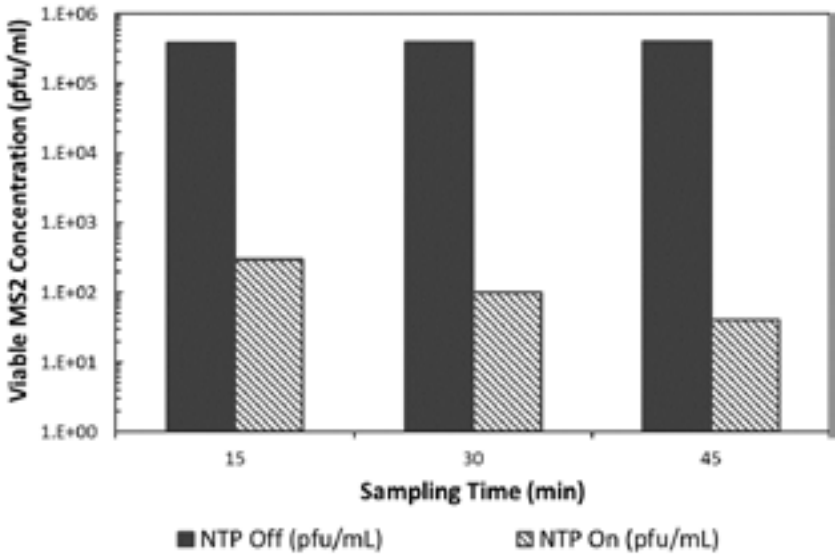

Figure 5. Change of infectious MS2 concentration in the downstream impinger with either ozone-free air (reactor off) or ozone-loaded air (reactor activated by 20 kV) bubbling through the impinger liquid.

plasma discharge power in their NTP reactor [24, 25]. With the 0–20 kV variable amplifier, the maximum discharge power in the reactor was 0.56 W (198 J m^{-3} at 170 LPM) at 20 kV. With the fixed 30 kV neon transformer, the actual peak-to-peak voltage applied to the reactor was 28 kV and the total input power consumption was ~21 W measured by the commercial power meter. The estimated discharge power was 2.08 W (734 J m^{-3} at 170 LPM), 10% of the input power, according to the high voltage probe and Pearson coil measurements. The estimated discharge power showed a strong exponential correlation with the applied peak-to-peak voltage, no matter which power supply is used (figure 4(b)). In future, the V–Q Lissajous method can be applied to more accurately estimate the discharge power with both the 0–20 kV variable amplifier and the 30 kV neon transformer.

When ambient air was supplemented with dry compressed air, the initial temperature and RH of the air stream inside the sampling train were 20 °C and 30%, respectively. The addition of water mist from the humidifier into the air stream can induce evaporative cooling, in which the air temperature would be reduced, and the RH would be increased. According to the measurement data, at 170 LPM air flow rate and the humidifier power level 2 (H2; atomization rate of 117 ml h^{-1}), both the temperature and RH reached steady state values of 16.5 °C and 60%, respectively, after 30 min.

Control tests were conducted during which 20 ml of an MS2 solution (1×10^6 pfu ml^{-1} in PBS) was added into the downstream impinger and the effluent gas from the reactor was bubbled through the impinger liquid. The concentration of infective viruses when the NTP reactor was off proved that bubbling ozone-free air through the impinger for 45 min did not inactivate the MS2 (figure 5). When the reactor was on, a 3 log reduction in the infective MS2 concentration was observed in the impinger solution over the first 15 min. This indicated that when the reactor was activated by 20 kV, the generated ozone dissolved in the impinger liquid and inactivated the sampled MS2. As the goal of these experiments was to inactivate viruses within the reactor and not in the sampling liquid downstream of the reactor, the ozone that dissolved in the downstream impinger liquid was quenched with 50 mM of anhydrous sodium sulfite. According to the measured ozone concentration and the calculated equilibrium dissolved ozone concentration in the impinger liquid (based on Henry's Law), the added sodium sulfite should be sufficient to quench all of the dissolved ozone during the packed-bed NTP inactivation tests. Control experiments proved that the sodium sulfite did not inactivate MS2 within the experimental timeframe.

MS2 Inactivation

The decrease in infective MS2 particles and total MS2 particles across the reactor were assayed by taking samples from the atomizer reservoir and samples from impingers both upstream and downstream of the NTP treatment. Although plaque assay results are normally reported in pfu per ml of solution and qPCR results are reported as gene copies (gc) per ml of solution, our reported concentrations are in pfu or gc per liter of air, which correspond to the overall air flow rate for the case of gross concentrations entering the sampling train, and to the 1 LPM air sampling rate through the impingers.

When the volumetric air flow rate was maintained at 170 LPM and the reactor was off, a ~2.6 log decrease in infective MS2 concentrations from the humidifier outlet to the upstream impinger was observed, as was a ~0.35 log decrease between the upstream and downstream impingers (figure 6). The qPCR results, which reflect the total number of viruses, suggested a decrease of ~1 log between the humidifier outlet and the upstream impinger and a decrease of ~0.35 log between the upstream and downstream impingers (figure 6). The ~1 log decrease in gene copy concentrations from the humidifier outlet (position 8) to the upstream impinger (position 10), which indicates the loss of total (infectious and inactivated) viruses during atomization, may have several causes, including wall losses along the four-meter-long duct. These impacts are discussed in greater detail in Xia *et al* [21]. The additional 1.6 log reduction in infectious MS2 concentrations

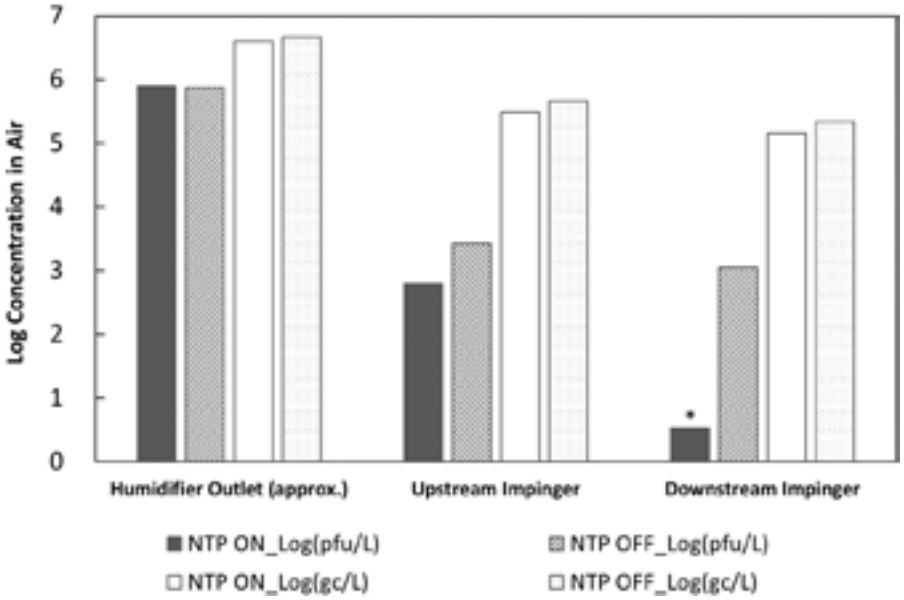

Figure 6. Concentrations of viruses in air measured with plaque assays and RT-qPCR in the NTP reactor powered by 30kV AC supply at a 170 LPM air flow rate (*: detection limit).

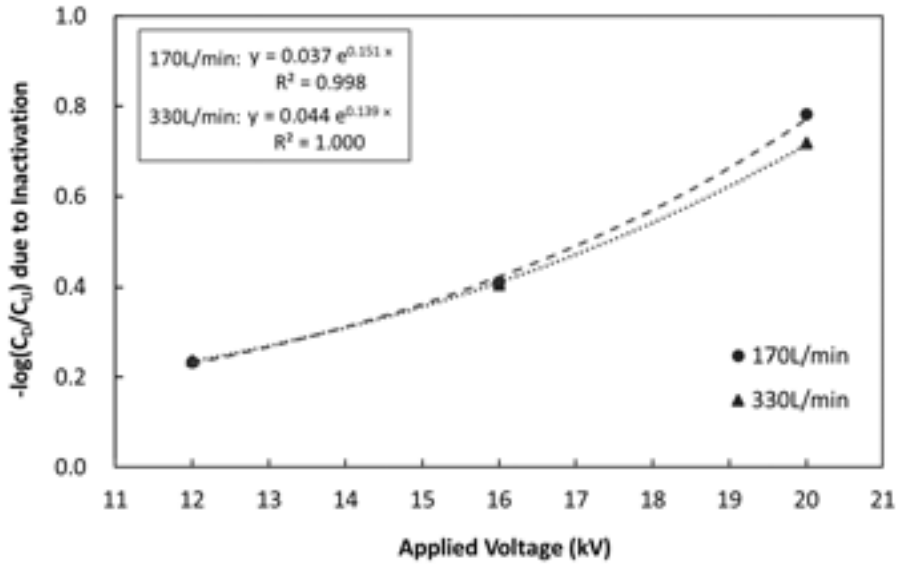

Figure 7. Log-reduction of infectious MS2 in airstream due to inactivation of the packed-bed NTP reactor activated by the variable voltage amplifier at 12 kV, 16 kV and 20 kV (C_D and C_U represent the downstream and upstream concentrations in air, respectively).

was most likely caused by inactivation during the evaporation process of the atomized MS2-PBS droplets. Based on the qPCR results, the 0.35 log decrease of infectious viruses through the packed bed when the reactor was off was not due to inactivation of viruses in the aerosols and was likely due to physical filtration of the virus by the packed bed.

When the reactor was powered with the 30 kV neon transformer, samples collected post-NTP treatment contained infective virus concentrations below our plaque assay limit of quantification (10 pfu ml^{-1}). Consequently, the reactor caused a decrease of more than 2.3 log infective MS2 (2 log inactivation if excluding the 0.35 log filtration discussed above) (figure 6). In contrast, the nearly constant reduction in gene copy concentrations with and without power to the reactor suggests that the virus was inactivated, and not removed physically (figure 6). In Xia *et al* [21], we discuss the likely mechanisms responsible for the nearly three log reduction in infective MS2 concentration between the introduction of the aerosol at position 8 to the upstream impinger at position 10 (figure 1).

MS2 inactivation was measured over a range of lower voltages (12, 16, and 20 kV) and two air flow rates (170 LPM and 330 LPM). Increasing the voltage resulted in an exponential increase in MS2 inactivation by the reactor (figure 7), when the packed-bed filtration effect (an average of 0.14 log) was subtracted. At an air flow rate of 170 LPM and 12 kV, an infective virus inactivation reduction across the reactor of 0.23 log was observed. This increased to a 0.78 log reduction at

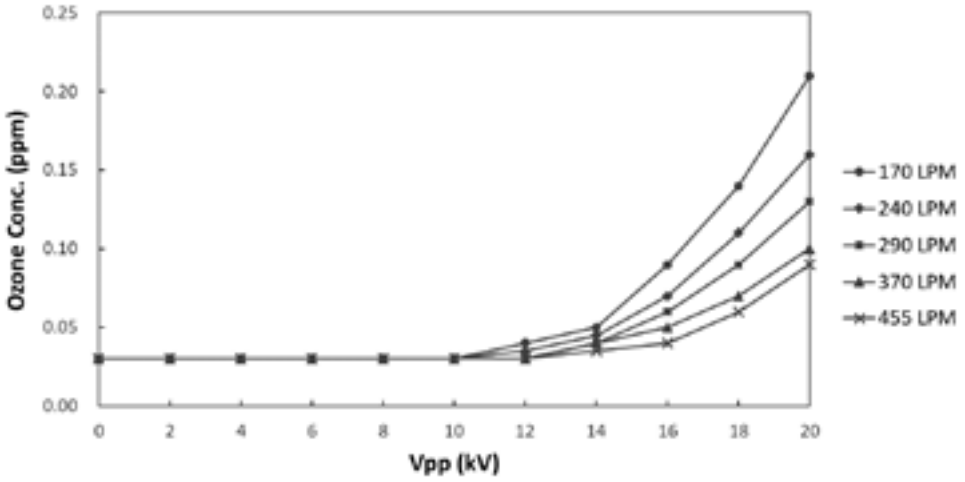

Figure 8. Measured ozone concentrations upstream of the ozone filter as a function of V_{pp} and air flow rate.

20 kV. Inactivation of infectious agents by chemical oxidants generally follows a Chick–Watson model, as illustrated by the equation below [26, 27]:

$$\ln\left(\frac{C_D}{C_U}\right) = -kC_{inact}^{n}t \qquad (4)$$

where C_D and C_U are downstream and upstream infectious virus concentrations respectively, C_{inact} is the concentration of the inactivating agent generated by NTP, n is the coefficient of dilution (usually assumed to be 1), t is duration of treatment, and k is a kinetic constant. When the NTP reactor is operating at steady state under steady applied AC voltage, C_{inact} and treatment time t should remain constant. Increasing applied voltage to the NTP reactor increases the concentration of reactive ions and electrons (C_{inact}) in the plasma, and according to figure 7 and equation (4), C_{inact} should increase exponentially with increasing applied voltage. This assertion, however, needs to be justified in future plasma species measurements and analysis. Increasing the flow rate to 330 LPM, and consequently reducing the treatment time by approximately 50%, had a small impact on inactivation (figure 7), which indicates that the amount of treated air by the reactor can be increased without having a major impact on inactivation efficiency. This may be because that the predominant species inactivating aerosolized MS2 in this study were short-lived radicals rather than long-lived ozone, whose lifetime is at the scale of nanoseconds [28] and would not be affected by the change of second-scale exposure time. Wu *et al* [18] reported similar limited impact of treatment time on NTP inactivation efficiency. Specifically, the study showed that doubling the treatment time would only cause a 2%–4% further inactivation of waterborne MS2 by plasma gas. Extrapolating the results obtained at 12–20 kV and 170 LPM to 30 kV according to the trendline would yield an estimated 3.5 log reduction, in agreement with the greater than 2 log reduction obtained with the fixed 30 kV neon transformer.

In this study, at the flow rate of 170 LPM, the virus exposure time to NTP species was about 0.25 s, and the steady state ozone concentration downstream of the reactor was measured as 0.21 ppm at 20 kV and 2.08 ppm at 30 kV. The ozone dose received by aerosolized MS2 was thereby estimated as 0.0017 min mg m^{-3} at 20 kV and 0.017 min mg m^{-3} at 30 kV (assuming room temperature and pressure). According to Tseng and Li [29], 90% (1 log) inactivation of airborne MS2 required an ozone dose of 1.28 min mg m^{-3}, which is 75–750 times of the ozone dose provided in this study. It was therefore concluded that ozone acted as a secondary inactivating reagent in this study and that aerosolized MS2 was predominantly inactivated by radicals and other reactive oxygen species (ROS) generated by the packed-bed NTP reactor over the short exposure time.

Our MS2 inactivation results (figures 6 and 7) are comparable with the previous studies. For example, Vaze *et al* applied 28 kV 600 μs pulse discharges to generate NTP, and the reactor achieved 97% inactivation of *E. coli* (1.5 log reduction) during the 10 s treatment time [17]. When the plasma generation area was reduced by 25%, the reactor's *E. coli* inactivation efficiency reduced significantly to 29% (0.16 log reduction) [19]. Wu *et al* applied a 14 kV 10 kHz AC power supply, and at 20 W power level, the reactor achieved ~80% MS2 inactivation (0.9 log reduction) in room air during a 0.12 s treatment time [18]. Both of these studies, however, only reported the reductions of viable bioaerosol concentration after the NTP treatment, and did not separate the inactivation effect of the active plasma species from the physical electrostatic precipitation or filtering effect of the reactor.

Ozone generation by the NTP reactor

One major concern for NTP-based airstream disinfection is the production of ozone in ventilation air, which can have detrimental impacts on human and animal health [30]. In California, state environmental regulations [31] require that indoor air cleaning devices intended for use in occupied spaces should not produce ozone concentrations greater than 0.05 ppm in treated air streams. We therefore adapted consumer-grade activated carbon honeycomb filters, normally installed over exhaust vents of photocopiers and laser printers, for use as a post-NTP treatment ozone filter.

The ozone concentrations were measured in the airstream upstream of the ozone filter (downstream of the packed bed

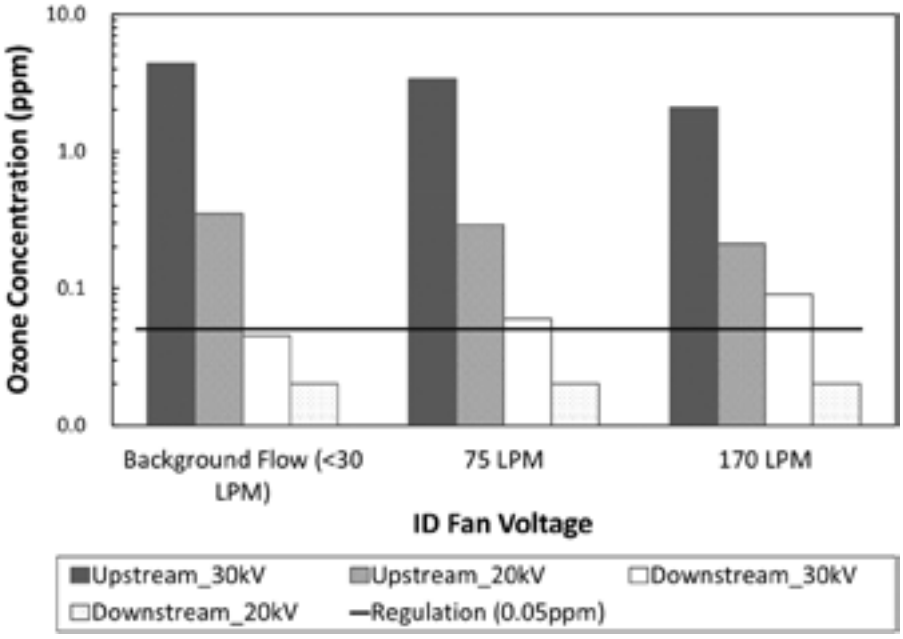

Figure 9. Measured ozone concentration upstream and downstream of the single layer ozone filter with either 20 kV or 30 kV power supply at varied air flow rates. The dashed line represents the ozone standard for indoor air cleaners set by the state of California [31].

section of the reactor), as a function of peak-to-peak voltage (V_{pp}) applied by the Trek high voltage power supply (figure 8). The baseline ozone concentration in the room air was 0.03 ppm. Results suggest that plasma was not established in the reactor and no ozone was produced until the applied V_{pp} exceeded 10 kV (figure 8). Above 10 kV, the ozone concentration downstream of the packed bed and upstream of the ozone filter increased with increasing V_{pp} and decreased due to reduction of NTP discharge energy density (discharge energy per unit volume of the air flow) with increasing air flow rate, as set by the ID fan. When 20 kV AC voltage was applied to the packed-bed NTP reactor and at the 170 LPM flow rate, the highest ozone concentration downstream of the reactor was 0.21 ppm.

Ozone concentrations were measured upstream and downstream of a single, centimeter-thick ozone filter under reactor-on conditions at 20 kV (discharge power of 0.56 W) and 30 kV (discharge power of 2.08 W) over a range of air flow rates (figure 9). Increasing air flow rates corresponded with decreasing upstream ozone concentrations due to reduction of NTP discharge energy density, and increasing downstream ozone concentrations, likely due to increasing space velocity (defined as volumetric flow rate normalized by filter volume) and thus decreasing filter performance. The much higher supplied power of the 30 kV power supply, as compared to the 20 kV power supply, also produced more ozone, approximately ten times higher at all three flow rate conditions (figure 9). This was likely a result of greater oxygen atom radical (O) production at the higher power, which reacted with the available O_2 to form more O_3 [32, 33]. At 170 LPM and 30 kV, the single layer of the activated carbon filter reduced upstream ozone concentrations by 96%; however, the downstream O_3 concentration (0.09 ppm) still exceeded the 0.05 ppm California standard. The addition of a second filter would very likely reduce concentrations below the California standard, with little increase in the pressure drop across the filter (20 Pa at the flow rate of 170 LPM).

Conclusion

In this study, we successfully designed and constructed a packed-bed DBD NTP reactor that was effective at inactivating bacteriophage MS2 in aerosols with minimal pressure drop across the reactor. Ozone generated by the active plasma was effectively reduced to meet regulation standards by the insertion of commercial ozone filters without significant pressure drop. In future applications, the packed-bed depth, the dielectric material, and the air flow rate through the sampling train can be modified to achieve improved performance at various flow conditions.

Associated content

Acknowledgment

This article is based upon work that is supported by the National Institute of Food and Agriculture, US Department of Agriculture, under Award No. 2016-67030-24892. Any opinions, findings, conclusions, or recommendations expressed in this publication are those of the author(s) and do not necessarily reflect the view of the US Department of Agriculture. The authors thank Minmeng Tang and Yinyin Ye (University of Michigan) for helping in the experimental setup and plaque assay analysis respectively. The authors also thank Professor John Foster and Selman Mujovic (University of Michigan) for helping in the design and power consumption measurements of the packed-bed NTP reactor used in this research.

Supporting information

Please see the supplementary material document, available online.

Author contributions

The manuscript was written through contributions from all authors. All authors have given approval to the final version of the manuscript.

Funding sources

This article is based upon work that is supported by the National Institute of Food and Agriculture, US Department of Agriculture, under Award No. 2016-67030-24892.

Notes

E M L and H L C are affiliated with Taza Aya LLC; H L C is co-founder and CEO. T X, A K, Z Q, and K R W all declare no competing financial interest.

ORCID iDs

T Xia https://orcid.org/0000-0002-0601-0467

References

[1] McKinney K R, Gong Y Y and Lewis T G 2006 Environmental transmission of SARS at Amoy Gardens *J. Environ. Health* **68** 26
[2] Hermann J, Hoff S, Muñoz-Zanzi C, Yoon K-J, Roof M, Burkhardt A and Zimmerman J 2007 Effect of temperature and relative humidity on the stability of infectious porcine reproductive and respiratory syndrome virus in aerosols *Vet. Res.* **38** 81–93
[3] Ostfeld R S 2009 Climate change and the distribution and intensity of infectious diseases *Ecology* **90** 903–5
[4] Kowalski W J, Bahnfleth W P, Witham D L, Severin B F and Whittam T S 2000 Mathematical modeling of ultraviolet germicidal irradiation for air disinfection *Quant. Microbiol.* **2** 249–70
[5] Riley R L 1961 Airborne pulmonary tuberculosis *Bacteriol. Rev.* **25** 243
[6] Wheeler S M, Ingraham H S, Hollaneder A, Lill N D, Gershon-Cohen J and Brown E W 1945 Ultra-violet light control of air-borne infections in a naval training center: preliminary report *Am. J. Public Health Nation's Health* **35** 457–68
[7] Memarzadeh F, Olmsted R N and Bartley J M 2010 Applications of ultraviolet germicidal irradiation disinfection in health care facilities: effective adjunct, but not stand-alone technology *Am. J. Infect. Control* **38** S13–24
[8] USEPA 2018 *Air Cleaners and Air Filters in the Home* (Washington, DC: EPA Office of Radiation and Indoor Air, Indoor Environments Division)
[9] Pitkin A, Deen J and Dee S 2009 Use of a production region model to assess the airborne spread of porcine reproductive and respiratory syndrome virus *Vet. Microbiol.* **136** 1–7
[10] Kim H H 2004 Nonthermal plasma processing for air-pollution control: a historical review, current issues, and future prospects *Plasma Process. Polym.* **1** 91–110
[11] Holzer F, Kopinke F and Roland U 2005 Influence of ferroelectric materials and catalysts on the performance of non-thermal plasma (NTP) for the removal of air pollutants *Plasma Chem. Plasma Process.* **25** 595–611
[12] Kuwahara T, Okubo M, Kuroki T, Kametaka H and Yamamoto T 2011 Odor removal characteristics of a laminated film-electrode packed-bed nonthermal plasma reactor *Sensors* **11** 5529–42
[13] Park S S, Kang M S and Hwang J 2015 Oil mist collection and oil mist-to-gas conversion via dielectric barrier discharge at atmospheric pressure *Sep. Purif. Technol.* **151** 324–31
[14] Vandenbroucke A M, Morent R, De Geyter N and Leys C 2011 Non-thermal plasmas for non-catalytic and catalytic VOC abatement *J. Hazard. Mater.* **195** 30–54
[15] Mizuno A, Yamazaki Y, Ito H and Yoshida H 1989 AC energized ferroelectric pellet bed precipitator for sterilization and gas clean up *IEEE Industry Applications Society Annual Meeting* pp 2148–53
[16] Mizuno A, Yamazaki Y, Ito H and Yoshida H 1992 AC energized ferroelectric pellet bed gas cleaner *IEEE Trans. Ind. Appl.* **28** 535–40
[17] Vaze N D, Arjunan K P, Gallagher M J, Vasilets V N, Gutsol A, Fridman A and Anandan S 2007 Air and water sterilization using non-thermal plasma *16th IEEE Int. Pulsed Power Conf.* (IEEE) pp 1231–5
[18] Wu Y, Liang Y, Wei K, Li W, Yao M, Zhang J and Grinshpun S A 2015 MS2 virus inactivation by atmospheric-pressure cold plasma using different gas carriers and power levels *Appl. Environ. Microbiol.* **81** 996–1002
[19] Vaze N D, Gallagher M J, Park S, Fridman G, Vasilets V N, Gutsol A F, Anandan S, Friedman G and Fridman A A 2010 Inactivation of bacteria in flight by direct exposure to nonthermal plasma *IEEE Trans. Plasma Sci.* **38** 3234–40
[20] Liang Y, Wu Y, Sun K, Chen Q, Shen F, Zhang J, Yao M, Zhu T and Fang J 2012 Rapid inactivation of biological species in the air using atmospheric pressure nonthermal plasma *Environ. Sci. Technol.* **46** 3360–8
[21] Xia T, Kleinheksel A, Wigginton K R and Clack H L 2019 Suspending viruses in an airstream using a consumer-grade ultrasonic humidifier *Aerosol Sci. Technol.* in preparation
[22] Pecson B M, Martin L V and Kohn T 2009 Quantitative PCR for determining the infectivity of bacteriophage MS2 upon inactivation by heat, UV-B radiation, and singlet oxygen: Advantages and limitations of an enzymatic treatment to reduce false-positive results *Appl. Environ. Microbiol.* **75** 5544–54
[23] United States Environmental Protection Agency 2001 *Environmental Protection Agency Method 1601: Male-Specific (f+) and Somatic Coliphage in Water by Two-Step* (Washington, DC: US EPA Office of Water)
[24] Harling A M, Glover D J, Whitehead J C and Zhang K 2009 The role of ozone in the plasma-catalytic destruction of environmental pollutants *Appl. Catal.* B **90** 157–61
[25] Ogata A, Mizuno K, Kushiyama S and Yamamoto T 1998 Methane decomposition in a barium titanate packed-bed nonthermal plasma reactor *Plasma Chem. Plasma Process.* **18** 363–73
[26] Chick H 1908 An investigation of the laws of disinfection *J. Hygiene* **8** 92–158
[27] Watson H 1908 A note on the variation of the rate of disinfection with change in the concentration of the disinfectant *J. Hygiene* **8** 536–42

[28] Eliasson B and Kogelschatz U 1991 Nonequilibrium volume plasma chemical processing *IEEE Trans. Plasma Sci.* **19** 1063–77
[29] Tseng C-C and Li C-S 2006 Ozone for inactivation of aerosolized bacteriophages *Aerosol Sci. Technol.* **40** 683–9
[30] Lippmann M 1989 Health effects of ozone. A critical review *JAPCA* **39** 672–95
[31] Jakober C and Phillips T 2008 *Evaluation of Ozone Emissions From Portable Indoor Air Cleaners: Electrostatic Precipitators and Ionizers* (Sacramento, CA: California Environmental Protection Agency, Air Resources Board)
[32] Yehia A and Mizuno A 2013 Ozone generation by negative direct current corona discharges in dry air fed coaxial wire-cylinder reactors *J. Appl. Phys.* **113** 183301
[33] Penetrante B, Hsiao M, Bardsley J, Merritt B, Vogtlin G, Kuthi A, Burkhart C and Bayless J 1997 Identification of mechanisms for decomposition of air pollutants by non-thermal plasma processing *Plasma Sources Sci. Technol.* **6** 251–9

JONIX
pure living

NOTE

JONIX
pure living

NOTE

JONIX
pure living

NOTE

JONIX
pure living

NOTE

JONIX
pure living

NOTE

JONIX
pure living

NOTE

JONIX
pure living

NOTE

JO**NIX** S.p.A.
Società Benefit

Sede Legale
viale Spagna 31-33,
35020 Tribano (PD) - Italy

Sede Centrale
via dell'Artigianato 1,
35020 San Pietro Viminario
(PD) - Italy

Laboratorio Ricerca Scientifica
via Tegulaia 10/B,
56121 Pisa - Italy

Sede Operativa
via Luciano Romagnoli 12/A,
40010 Bentivoglio (BO) - Italy

jonixair.com
info@jonixair.com

Dossier r05 - Dicembre 2021

JONIX

pure living